BU-HEPP-19-03, CERN-TH-2019-061, CP3-19-22, DESY 19-072, FR-PHENO-2019-005, IFIC/19-23, IFT-UAM/CSIC-19-058, IPhT-19-050, IPPP/19/32, KW 19-003, LTH 1203, MPP-2019-84, TTK-19-19, TTP19-008, TUM-HEP-1200/19, ZU-TH 22/19

Theory report on the 11^{th} FCC-ee workshop*

8-11 January 2019, CERN, Geneva

A. Blondel[1], J. Gluza[†,2,3], S. Jadach[4], P. Janot[5], T. Riemann[2,6] (eds.), S. Abreu[7], J.J. Aguilera-Verdugo[8], A.B. Arbuzov[9], J. Baglio[10], S.D. Bakshi[11], S. Banerjee[12], C. Bobeth[13], C. Bogner[14], S.G. Bondarenko[9], S. Borowka[5], S. Braß[15], C.M. Carloni Calame[16], J. Chakrabortty[11], M. Chiesa[17], M. Chrzaszcz[4], D. d'Enterria[5], F. Domingo[18], J. Dormans[19], F. Driencourt-Mangin[8], Ya.V. Dydyshka[20], F. Febres Cordero[19,21], J.A. Gracey[22], Zhi-Guo He[23], G. Heinrich[24], S. Heinemeyer[25,26,27], I. Hönemann[14], H. Ita[19], S. Jahn[24], F. Jegerlehner[6,28], S. P. Jones[5], L.V. Kalinovskaya[20], A. Kardos[29], M. Kerner[30], W. Kilian[15], S. Kluth[24], B. A. Kniehl[23], A. Maier[6], P. Maierhöfer[19], G. Montagna[31,16], O. Nicrosini[16], T. Ohl[17], B. Page[32], S. Paßehr[33], S.K. Patra[11], R. Pittau[34], F. Piccinini[16], W. Placzek[35], J. Plenter[8], S. Ramírez-Uribe[8], J. Reuter[36], G. Rodrigo[8], V. Rothe[36], L.A. Rumyantsev[20,37], R.R. Sadykov[20], J. Schlenk[38], G. F. R. Sborlini[8], A. Schweitzer[39], C. Schwinn[40], M. Skrzypek[4], G. Somogyi[41], M. Spira[42], P. Stienemeier[43], R. Szafron[13], K. Tempest[43], W. J. Torres Bobadilla[8], S. Tracz[8], Z. Trócsányi[41,44], Z. Tulipánt[41], J. Usovitsch[45], A. Verbytskyi[24], B.F.L. Ward[46], Z. Was[4], G. Weiglein[36], C. Weiland[47], S. Weinzierl[48], V.L. Yermolchyk[20] S.A. Yost[49], J. Zurita[50,51]

[1] *DPNC University of Geneva, Switzerland*
[2] *Institute of Physics, University of Silesia, 40-007 Katowice, Poland*
[3] *Faculty of Science, University of Hradec Králové, Czech Republic*
[4] *Institute of Nuclear Physics, PAN, 31-342 Kraków, Poland*
[5] *CERN, CH-1211 Geneva 23, Switzerland*
[6] *Deutsches Elektronen–Synchrotron, DESY, 15738 Zeuthen, Germany*
[7] *Center for Cosmology, Particle Physics and Phenomenology (CP3), Université Catholique de Louvain, 1348 Louvain-La-Neuve, Belgium*
[8] *Instituto de Física Corpuscular, Universitat de València – Consejo Superior de Investigaciones Científicas, Parc Científic, E-46980 Paterna, Valencia, Spain*
[9] *Bogoliubov Laboratory of Theoretical Physics, JINR, Dubna, 141980 Russia*
[10] *Institut für Theoretische Physik, Eberhard Karls Universität Tübingen, Auf der Morgenstelle 14, D-72076 Tübingen, Germany,*
[11] *Indian Institute of Technology, Kanpur, India*
[12] *University of Louisville, Louisville, KY 40292 USA*
[13] *Physik Department T31, Technische Universität München, Garching, Germany*
[14] *Institut für Physik, Johannes Gutenberg-Universität Mainz, D-55099 Mainz, Germany,*
[15] *Department Physik, Universität Siegen, Walter-Flex-Str. 3, 57068 Siegen Germany*
[16] *Istituto Nazionale di Fisica Nucleare, Sezione di Pavia, via A. Bassi 6, 27100 Pavia, Italy*
[17] *Fakultät für Physik und Astronomie, Universität Würzburg, Emil-Hilb-Weg 22, 97074 Würzburg Germany*
[18] *Bethe Center for Theoretical Physics & Physikalisches Institut der Universität Bonn, Nußallee 12, 53115 Bonn, Germany*

*https://indico.cern.ch/event/766859/

†Corresponding editor, E-mail: janusz.gluza@cern.ch

[19] *Physikalisches Institut, Albert-Ludwigs-Universität Freiburg, Hermann-Herder-Str. 3, D-79104 Freiburg, Germany*
[20] *Dzhelepov Laboratory of Nuclear Problems, JINR, Dubna, 141980 Russia*
[21] *Physics Department, Florida State University, 77 Chieftan Way, Tallahassee, FL 32306, U.S.A.*
[22] *Theoretical Physics Division, Department of Mathematical Sciences, University of Liverpool, P.O. Box 147, Liverpool, L69 3BX, United Kingdom,*
[23] *Institut für Theoretische Physik, Universität Hamburg, Luruper Chaussee 149, 22761 Hamburg, Germany*
[24] *Max Planck Institute for Physics, Föhringer Ring 6, 80805 München, Germany*
[25] *Instituto de Física Teórica (UAM/CSIC), Universidad Autónoma de Madrid, Cantoblanco, 28049 Madrid, Spain*
[26] *Instituto de Física de Cantabria (CSIC-UC), 39005 Santander, Spain*
[27] *Campus of International Excellence UAM+CSIC, Cantoblanco, 28049, Madrid, Spain*
[28] *Humboldt–Universität zu Berlin, Institut für Physik, Newtonstrasse 15, D–12489 Berlin, Germany,*
[29] *Institute of Physics, University of Debrecen, 4010 Debrecen, PO Box 105, Hungary,*
[30] *Physik-Institut, Universität Zürich, Winterthurerstrasse 190, 8057 Zürich, Switzerland,*
[31] *Dipartimento di Fisica, Università di Pavia, via A. Bassi 6, 27100 Pavia, Italy*
[32] *Institut de Physique Théorique, CEA, CNRS, Université Paris-Saclay, F-91191 Gif-sur-Yvette cedex, France*
[33] *Sorbonne Université, CNRS, Laboratoire de Physique Théorique et Hautes Énergies (LPTHE), 4 Place Jussieu, 75252 Paris CEDEX 05, France*
[34] *Departamento de Física Teórica y del Cosmos and CAFPE, Universidad de Granada, Campus Fuentenueva s.n., E-18071 Granada, Spain*
[35] *Marian Smoluchowski Institute of Physics, Jagiellonian University, Cracow, Poland*
[36] *Deutsches Elektronen–Synchrotron, DESY, Notkestraße 85, 22607 Hamburg, Germany*
[37] *Institute of Physics, Southern Federal University, Rostov-on-Don, 344090 Russia*
[38] *Institute for Particle Physics Phenomenology, University of Durham, Durham DH1 3LE, UK*
[39] *Institute for Theoretical Physics, ETH Zürich, Wolfgang-Pauli-Str. 27, 8093 Zürich, Switzerland*
[40] *Institut für Theoretische Teilchenphysik und Kosmologie, RWTH Aachen University, Sommerfeldstraße 16, 52056 Aachen, Germany*
[41] *MTA-DE Particle Physics Research Group, University of Debrecen, 4010 Debrecen, PO Box 105, Hungary*
[42] *Paul Scherrer Institut, CH-5232 Villigen PSI, Switzerland*
[43] *Department of Physics, University of Toronto, 60 St George St., Toronto, Ontario, M5S 1A7, Canada*
[44] *Institute for Theoretical Physics, Eötvös Loránd University, Pázmány Péter 1/A, H-1117 Budapest, Hungary*
[45] *School of Mathematics, Trinity College Dublin, The University of Dublin, Ireland*
[46] *Baylor University, Waco, TX, USA*
[47] *Pittsburgh Particle physics, Astrophysics, and Cosmology Center, Department of Physics and Astronomy, University of Pittsburgh, 3941 O'Hara St., Pittsburgh, PA 15260, USA*
[48] *PRISMA Cluster of Excellence, Inst. für Physik, Johannes Gutenberg-Universität, 55099 Mainz, Germany*
[49] *The Citadel, Charleston, SC, USA*
[50] *Institute for Nuclear Physics (IKP), Karlsruhe Institute of Technology, Hermann-von-Helmholtz-Platz 1, D-76344 Eggenstein-Leopoldshafen, Germany*
[51] *Institute for Theoretical Particle Physics (TTP), Karlsruhe Institute of Technology, Engesserstraße 7, D-76128 Karlsruhe, Germany*

Copyright Statement

"Theory report on the 11^{th} FCC-ee workshop", 8-11 January 2019, CERN, Geneva, Switzerland, https://indico.cern.ch/event/766859/

S. Abreu, J.J. Aguilera-Verdugo, A.B. Arbuzov, J. Baglio, S.D. Bakshi, S. Banerjee, A. Blondel, C. Bobeth, C. Bogner, S. Bondarenko, S. Borowka, S. Braß, C.M. Carloni Calame, J. Chakrabortty, M. Chiesa, M. Chrzaszcz, D. d'Enterria, F. Domingo, J. Dormans, F. Driencourt-Mangin, Ya. Dydyshka, F. Febres Cordero, J. Gluza, J.A. Gracey, Zhi-Guo He, G. Heinrich, S. Heinemeyer, I. Hönemann, H. Ita, S. Jadach, S. Jahn, F. Jegerlehner, S. P. Jones, L. Kalinovskaya, A. Kardos, M. Kerner, W. Kilian, S. Kluth, B. A. Kniehl, A. Maier, P. Maierhöfer, G. Montagna, O. Nicrosini, T. Ohl, B. Page, S. Paßehr, S.K. Patra, F. Piccinini, R. Pittau, W. Placzek, J. Plenter, S. Ramírez-Uribe, J. Reuter, T. Riemann, G. Rodrigo, V. Rothe, L. Rumyantsev, R. Sadykov, J. Schlenk, G. F. R. Sborlini, A. Schweitzer, C. Schwinn, M. Skrzypek, G. Somogyi, M. Spira, P. Stienemeier, R. Szafron, K. Tempest, W. J. Torres Bobadilla, S. Tracz, Z. Trócsányi, Z. Tulipánt, J. Usovitsch, A. Verbytskyi, B.F.L. Ward, Z. Was, G. Weiglein, C. Weiland, S. Weinzierl, V. Yermolchyk, S.A. Yost, J. Zurita

Abstract

The FCC at CERN, a proposed 100-km circular facility with several colliders in succession, culminates with a 100 TeV proton-proton collider. It offers a vast new domain of exploration in particle physics, with orders of magnitude advances in terms of Precision, Sensitivity and Energy. The implementation plan published in 2018 foresees, as a first step, an Electroweak Factory electron-positron collider. This high luminosity facility, operating between 90 and 365 GeV centre-of-mass energy, will study the heavy particles of the Standard Model, Z, W, Higgs, and top with unprecedented accuracy. The physics programme offers great discovery potential: (i) through exquisite precision measurements, (ii) through sensitive searches for symmetry violations, forbidden or extremely rare decays, and (iii) through the search for direct observation of new particles with extremely small couplings. The Electroweak Factory e^+e^- collider constitutes a real challenge to the theory and to precision calculations, triggering the need for the development of new mathematical methods and software tools. A first workshop in 2018 had focused on the first FCC-ee stage, the Tera-Z, and confronted the theoretical status of precision Standard Model calculations on the Z-boson resonance to the experimental demands.

The second workshop in January 2019, which is reported here, extended the scope to the next stages, with the production of W-bosons (FCC-ee-W), the Higgs boson (FCC-ee-H) and top quarks (FCC-ee-tt). In particular, the theoretical precision in the determination of the crucial input parameters, $\alpha_{\rm QED}$, $\alpha_{\rm QCD}$, M_W, m_t at the level of FCC-ee requirements is thoroughly discussed. The requirements on Standard Model theory calculations were spelled out, so as to meet the demanding accuracy of the FCC-ee experimental potential. The discussion of innovative methods and tools for multi-loop calculations was deepened. Furthermore, phenomenological analyses beyond the Standard Model were discussed, in particular the effective theory approaches.

Editors' Note

Understanding the origins of the Universe and how it works and evolves is the present mission of a large community of physicists of many nations and specialities. It calls for a large scale vision, involving general relativity, astrophysics and cosmology, together with the detailed, basic understanding provided by particle physics; these disciplines work hand in hand, with the help of several other research fields. Particle physics is presently at an important moment of its history. With the discovery of the Higgs boson, the matrix of interactions and elementary particles that is called the "Standard Model" (SM), is complete. Yet the Higgs boson itself, and how it breaks the electroweak symmetry, remain a fascinating subject requiring verification at the next order of precision, typically at percent or even per mil accuracy. Furthermore, several experimental facts are not accounted for by the SM; let us mention: (i) the baryon asymmetry of the Universe, (ii) the nature and origin of dark matter, and (iii) the origin of neutrino masses; these have no unique, if any, explanation in the SM and yet will require answers from particle physics.

Particle physics exploration must continue ... but we no longer have a guiding scale.

How can this exploration be carried out? Which next tool is needed? Going to higher and higher energies is an obvious idea. It has worked well for the Standard Model particles so far, because they all have roughly the same strong and electro-weak couplings. It is far from evident, however, that the new phenomena or particles, required to explore the above questions, will behave in the same way – the opportunity to explore much smaller couplings or much higher scales must be kept in mind. Here the role of precision measurements, the search for extremely rare decays of known particles, for small violations of the SM symmetries, and for direct production of super-weakly coupled objects is in order. A broad strategy of search is thus needed.

With this in mind, and armed with the recommendation of the European Strategy in 2013 that Europe should be in a position to "propose an ambitious post-LHC accelerator project at CERN", the FCC collaboration has elaborated a strategy of circular colliders fitting in a new facility of 100 km circumference. It will start with a high luminosity e^+e^- Electroweak Factory, FCC-ee, and culminate with a proton collider, FCC-hh, of more than 100 TeV collision energy. Additional options of heavy ion collisions and e-p scattering are foreseen and, possibly, muon collisions. This strategy offers, by way of synergy and complementarity, a thorough study of the Higgs boson. As well as unmatched capabilities of high energy exploration, precision measurements, and sensitive rare process searches [1]. The FCC Conceptual Design Report (CDR) has been prepared and released [2–4]. This powerful exploratory project will, right from its first step as a Z-factory, explore completely uncharted territory in terms of precision and sensitivity. And it constitutes an extraordinary challenge for theory. The theoretical community has responded with enthusiasm to the challenge and already several workshops have gathered an increasing number of contributions.

In this report, we collect theory contributions to the 11^{th} FCC-ee meeting held in January 2019 at CERN [5], completed by a few invited guest contributions. The volume follows the report [6] on the FCC-ee workshop in January 2018 [7], which focused on the theory needs for the Tera-Z, the first stage of the FCC-ee, working in the Z-boson energy range. The purpose is to document existing and also to motivate future theoretical studies enabling by their predictions

to fully explore the experimental potential of the FCC-ee.

It has become evident that a serious amount of work has to be accomplished, both in multi-loop calculations in the Standard Model and also in Beyond Standard Model projects. A documentation of these requirements became highly desirable to complement the submitted Conceptual Design Report. The present report exemplifies both the well-advanced status of phenomenology for the FCC-ee and, at the same time, the need for further mathematically well-founded deepening of the technologies for precision predictions. In this respect, it is a necessary add-on of the FCC CDR.

From a scientific point of view, the FCC is the most challenging collider project for the next decades [8]. We see it as our duty and pleasure to prepare such a frontier project and to sustain CERN's leading role in basic research worldwide. The goals must be set as high as possible, i.e. at the level of the statistical uncertainties because *this precision genuinely equates discovery potential.*

We thank all participants of the workshop for their engagement with presentations and in the discussions during the workshop, and the authors of the report for writing excellent contributions. The exploratory potential of the FCC-ee can be fully exploited only if the talent and efforts of accelerator builders and experimenters is met by theory. The message is: we are working on it.

From this quest for the unknown, driven by curiosity, history shows there is a return to all of us, scientists or not [9–11].

The Editors.

References

[1] FCC - Future Circular Collider, https://fcc.web.cern.ch.

[2] The FCC CDR, the four volumes of the FCC CDR and the contributions to the European Strategy can be found on the FCC-CDR webpage https://fcc-cdr.web.cern.ch/.

[3] M. Benedikt, A. Blondel, O. Brunner, M. Capeans Garrido, F. Cerutti, J. Gutleber, P. Janot, J. M. Jimenez, V. Mertens, A. Milanese, K. Oide, J. A. Osborne, T. Otto, Y. Papaphilippou, J. Poole, L. J. Tavian, F. Zimmermann, Future Circular Collider, Tech. Rep. CERN-ACC-2018-0057, CERN, Geneva, submitted for publication to Eur. Phys. J. ST. (Dec 2018).
URL http://cds.cern.ch/record/2651299

[4] A. Abada, et al., Future Circular Collider: Vol. 1 "Physics opportunities", http://inspirehep.net/record/1713706/files/CERN-ACC-2018-0056.pdf.

[5] A. Blondel, C. Grojean, J. Gluza, M. McCullough, P. Janot (org.), *11th FCC-ee workshop: Theory and Experiments*, 8-11 January 2019, CERN, Geneva, Switzerland, webpage https://indico.cern.ch/event/766859/.

[6] A. Blondel, J. Gluza, S. Jadach, P. Janot, T. Riemann (eds.), Standard Model Theory for the FCC-ee: The Tera-Z, report on the mini workshop on precision EW and QCD calculations for the FCC studies: methods and techniques, CERN, Geneva, Switzerland, January 12-13, 2018; subm. as CERN Yellow Report. arXiv:1809.01830.

[7] A. Blondel, J. Gluza, P. Janot (org.), Mini workshop: *Precision EW and QCD calculations for the FCC studies: methods and tools*, 12-13 January 2018, CERN, Geneva, Switzerland,

webpage https://indico.cern.ch/event/669224/.

[8] A. Blondel, A. Freitas, J. Gluza, T. Riemann, S. Heinemeyer, S. Jadach, P. Janot, Theory Requirements and Possibilities for the FCC-ee and other Future High Energy and Precision Frontier Lepton Colliders, Input 101 to the update of the European Strategy for Particle Physics, https://indico.cern.ch/event/765096/contributions/3295742/. arXiv:1901.02648.

[9] CERN webpage *Why fundamental science?*, https://public-archive.web.cern.ch/public-archive/en/About/Fundamental-en.html (29 April 2019).

[10] *No final frontier*, Editorial (3 April 2019), Nature Reviews Physics 1(2019)231, https://doi.org/10.1038/s42254-019-0052-4.

[11] E. Elsen, F. Bordry, *The case for future colliders* (8 April 2019), https://home.cern/news/opinion/physics/case-future-colliders.

Contents

Executive Summary

The main theoretical issues of the FCC-ee studies discussed in this report may be summarized as follows:

1. In order to adjust the precision of theory predictions to the experimental demands from the FCC-ee, an update of existing software and the development of new, independent software will be needed. It should include in first instance solutions to the following issues:
   (i) Factorization to infinite order of multi-photon soft-virtual QED contributions;
   (ii) Resummations in Monte Carlo generators;
   (iii) Disentangling of QED and EW corrections beyond one-loop, with soft-photon factorization/resummation;
   (iv) Proper implementation of higher loop effects, as Laurent series around the Z peak;
   (v) Further progress in methods and tools for multi-loop calculations and Monte Carlo generators.
   Some discussions have been initiated in the 2018 report [1], here they are extended in the Introduction and through Chapters B and C.

2. In order to meet the experimental precision of the FCC-ee Tera-Z for ElectroWeak Pseudo-Observables (EWPOs), even 3-loop EW calculations of the $Zf\bar{f}$-vertex will be needed, comprising the loop orders $\mathcal{O}(\alpha\alpha_s^2), \mathcal{O}(N_f\alpha^2\alpha_s), \mathcal{O}(N_f^2\alpha^3)$, and also the corresponding QCD 4-loop terms.
   This was mainly a subject of the 2018 report [1].

3. To decrease the α_{QED} error by a factor 5 to 10, to the level $(3 \div 5) \cdot 10^{-5}$, will require improvements in low energy experiments. Alongside, the pQCD prediction of the Adler-function must be improved by a factor of two, accomplished with better error estimates for m_c and m_b. The next mandatory improvements required are:
   (i) 4-loop massive pQCD calculation of the Adler function;
   (ii) Improved α_s in the low Q^2 region above the τ mass;
   (iii) A better control and understanding of $\Delta\alpha^{(5)}_{\rm had}(M_Z^2)$ in terms of R-data;
   (iv) Different methods should be used for directly accessing $\alpha(M_Z^2)$, e.g. the muon forward-backward asymmetry, or for calculating α_{QED} either based on a radiative return experiment, e.g. at the FCC-ee Tera-Z, or using lattice QCD methods.
   This is discussed in Chapter B.

4. FCC-ee precision measurements require many improvements on the theoretical QCD side. These include (i) higher-order pQCD fixed order calculations; (ii) higher-order logarithmic resummations; (iii) permille precision extractions of the α_s coupling; and (iv) an accurate control of nonperturbative QCD effects (such as e.g. colour reconnection, hadronization), both analytically and as implemented in the Monte Carlo generators.
   These issues are discussed in Chapter B.

5. The reduction of the theoretical uncertainty of the total W-pair production cross section to the level of $\sim 0.01\%$ at the FCC-ee-W requires at least the calculation of $\mathcal{O}(\alpha^2)$ and dominant $\mathcal{O}(\alpha^3)$ corrections to double-resonant diagrams. Estimates within an EFT approach show that the theory-induced systematic error of the mass measurement from

a threshold scan can be at the level of $\Delta M_{\rm W} = (0.15 - 0.60)$ MeV. The lower value results from assuming that the non-resonant corrections are under control. In addition, it is also essential to reduce the uncertainty from ISR corrections and QCD corrections for hadronic final states to the required accuracy. This is discussed in Chapter B.

6. Predictions for H decay widths and branching ratios are known with sufficient accuracy for the LHC. At the FCC-ee the Higgs mass can be measured with a precision below 0.05 GeV. The dependence of EWPOs on M_H is mild, $\propto \alpha \log(M_H/M_W)$, and an accuracy of 0.05 GeV of M_H will not affect their determination. The main improvements in Higgs boson studies will be connected with a better determination of branching ratios and self-couplings.
   More on related issues is discussed in the Introduction and in Chapter B.

7. The top-pair line shape for centre-of-mass energies close to the $t\bar{t}$ production threshold is highly sensitive to the mass of the top-quark, which allows its determination with unprecedented precision. The statistical uncertainty of the measurement (~ 20 MeV) is projected to be significantly below the current theory error. It is crucial to continuously improve the theoretical prediction. The most sensitive observable is the total production cross section for $b\bar{b}W^+W^-X$ final states near the top-pair production threshold. A very precise knowledge of the strong coupling constant from other sources will be crucial in order to meaningfully constrain the top Yukawa coupling.
   These issues are discussed in Chapter B.

8. Proper truncation of the ultraviolet scale Λ depends on the experimental precision of the observables and SMEFT theories must be adjusted to FCC-ee experimental conditions, e.g. in construction of appropriate complete operator bases and Wilson coefficients for BSM theories.
   This issue is discussed in Chapter D.

9. FCC in its -ee and -hh options will be sensitive to BSM physics and exotic massive states reaching tens of TeVs and/or very weak couplings. It is proposed to use the SMEFT framework and constrain the Higgs triple coupling by analyzing precision measurements. For these studies, but also exotic Higgs decays, important will be to combine the LHC and HL-LHC data with an analysis at FCC-ee.
   These issues are discussed in Chapter E.

References

[1] A. Blondel, J. Gluza, S. Jadach, P. Janot, T. Riemann (eds.), Standard Model Theory for the FCC-ee: The Tera-Z, report on the mini workshop on precision EW and QCD calculations for the FCC studies: methods and techniques, CERN, Geneva, Switzerland, January 12-13, 2018; subm. as CERN Yellow Report. arXiv:1809.01830.

Chapter A

Introduction and Overview

Authors: A. Blondel, J. Gluza, S. Jadach, P. Janot, T. Riemann
Corresponding Author: Janusz Gluza [janusz.gluza@cern.ch]

This report includes a collection of studies devoted to a discussion of (i) the status of theoretical efforts towards the calculation of higher order Standard Model (SM) corrections needed for the FCC-ee precision measurement program, (ii) the possibility of detecting possible physics by means of these precision measurements, and (iii) methods and tools which must be developed to guarantee precision calculations of the observables to be measured. This report originates from presentations at the *11th FCC-ee workshop: Theory and Experiments*, 8-11 January 2019, CERN, Geneva [1] with 117 registered participants and 42 theory talks.

1 FCC-ee as Electroweak Factory

In the 2018 report [2] we focused on theoretical issues of the FCC-ee Tera-Z, which will be a e^+e^- collider working at the Z-resonance energy region. However, the FCC-ee collider project will work as several energy regions, making it a complete **Electroweak Factory**, covering the direct production of all massive bosons of the SM and the top quark. This plan is summarized in Table A.1.

Table A.1: Run plan for FCC-ee in its baseline configuration with two experiments. The WW event numbers are given for the entirety of the FCC-ee running at and above the WW threshold.

Phase	Run duration (years)	Center-of-mass Energies (GeV)	Integrated Luminosity (ab^{-1})	Event Statistics
FCC-ee-Z	4	88-95	150	$3 \cdot 10^{12}$ visible Z decays
FCC-ee-W	2	158-162	12	10^8 WW events
FCC-ee-H	3	240	5	10^6 ZH events
FCC-ee-tt	5	345-365	1.7	10^6 $t\bar{t}$ events

The exceptional precision of FCC-ee comes from several features of the program. The exceptional precision of FCC-ee comes from several features of the program.

- Extremely high statistics of 5×10^{12} Z decays, 10^8 WW, 10^6 ZH, and 10^6 $t\bar{t}$ events;
- High-precision (better than 100 keV) absolute determination of the centre-of mass energies at the Z pole and WW threshold, thanks to the availability of transverse polarization and the resonant depolarization. This is a unique feature of the circular lepton colliders, e^+e^- and $\mu^+\mu^-$. At higher energy, WW, ZZ and Zγ production can be used to constrain the

centre-of-mass energy with precisions of 2 and 5 MeV, at the ZH cross-section maximum and at the $t\bar{t}$ threshold respectively. At all energies, $e^+e^- \to \mu^+\mu^-$ events, which at the Z pole occur at a rate in excess of 3 kHz, provide by themselves in matters of minutes the determination of the centre-of mass energy spread, the residual difference between the energies of e^+ and e^- beams and a (relative) centre-of-mass energy monitoring with a precision that is more than sufficient for the precision needs of the program.

– The clean environmental conditions and an optimized run plan allow a complete program of ancillary measurements of presently precision-limiting input quantities for the precision EW tests. This is the case of the top quark mass from the scan of the $t\bar{t}$ production threshold; of the unique, direct, measurement of the QED running coupling constant at the Z mass from the Z-γ interference; of the strong coupling constant by measurements of the hadronic to leptonic branching fractions of the Z, the W and the τ lepton; and of course of the Higgs and Z masses themselves.

For the reader's convenience we also from the CDR the Table A.2 showing some of the most significant FCC-ee experimental accuracies compared with those of the present measurements. More on the experimental precision of the FCC-ee can be found in the CDR documents, volumes 1 and 2 [3, 4]. The experimenters are working hard to reduce systematics by devising dedicated methods and ancillary measurements, the task of the theoretical community will be to ensure that the SM predictions will precise enough so as to not not spoil the best foreseeable experimental accuracies, i.e. the statistical errors.

If future theory uncertainties match the FCC-ee experimental precision, the many different measurements from the FCC-ee will provide capability to exhibit and decipher signs of new physics. Here are two examples: the EFT analysis searching for signs of heavy physics with SM couplings shows the potential to exhibit signs of new particles up to around 70 TeV; with a very different but characteristic pattern, observables involving neutrinos would show a significant deviation if these neutrinos were mixed with a heavy counterpart at the level of one part in 100,000, even if those were too heavy to be directly produced.

Table A.2 shows that FCC-ee has the potential to achieve (at least) a 20-100 times higher precision or better in Electroweak precision measurements over the present state-of-the-art situation. This includes input quantities such as the Z, Higgs and top masses, and the strong and QED coupling constants at the Z scale. This extremely favourable situation will require leap-jumps in the precision of the theoretical computations for Standard Model phenomena, for all quantities given in Table A.2. The theory calculation must also be able to include the improved input parameters [2, 5], which in the particular case of FCC-ee, will be measured within the experimental program.

The quantities listed in this table A.2 are called *Electroweak precision observables*, (EWPO) and encapsulate experimental data after extraction of well-known and controllable QED and QCD effects, in a model-independent manner. They provide a convenient bridge between real data and the predictions of the SM, or of the SM plus New Physics. Contrary to raw experimental data (like differential cross sections), EWPOs are also well suited for archiving and long term use. Archived EWPOs can be exploited over long periods of time for comparisons with steadily improving theoretical calculations of the SM predictions, and for validations of the New Physics models beyond the SM. They are also useful for comparison and combination of results from different experiments. However, removing trivial but sizable QED or QCD effects from EWPOs might induces additional sources of uncertainty. The work to do is well known

Table A.2: Measurement of selected electroweak observables (EWPO) at the FCC-ee, compared with the present precision. The systematic uncertainties are initial estimates and might improve with further examination. This set of measurements, together with those of the Higgs properties, achieves indirect sensitivity to new physics up to a scale Λ of 70 TeV in a description with dim 6 operators, and possibly much higher in some specific new physics models.

Observable	present value ± error	FCC-ee Stat.	FCC-ee Syst.	Comment and dominant exp. error
m_Z (keV)	91186700 ± 2200	4	100	From Z line shape scan Beam energy calibration
Γ_Z (keV)	2495200 ± 2300	7	100	From Z line shape scan Beam energy calibration
R_ℓ^Z ($\times 10^3$)	20767 ± 25	0.06	0.2-1	ratio of hadrons to leptons acceptance for leptons
$\alpha_s(m_Z)$ ($\times 10^4$)	1196 ± 30	0.1	0.4-1.6	from R_ℓ^Z above
R_b ($\times 10^6$)	216290 ± 660	0.3	<60	ratio of bb to hadrons stat. extrapol. from SLD
σ^0_{had} ($\times 10^3$) (nb)	41541 ± 37	0.1	4	peak hadronic cross-section luminosity measurement
$N_\nu(\times 10^3)$	2991 ± 7	0.005	1	Z peak cross sections Luminosity measurement
$\sin^2\theta^{eff}_W(\times 10^6)$	231480 ± 160	3	2 - 5	from $A^{\mu\mu}_{FB}$ from $A^{\mu\mu}_{FB}$ at Z peak Beam energy calibration
$1/\alpha_{QED}(m_Z)(\times 10^3)$	128952 ± 14	4	small	from $A^{\mu\mu}_{FB}$ off peak
$A^b_{FB}, 0$ ($\times 10^4$)	992 ± 16	0.02	1-3	b-quark asymmetry at Z pole from jet charge
$A^{pol,\tau}_{FB}$ ($\times 10^4$)	1498 ± 49	0.15	<2	τ polarisation and charge asymmetry τ decay physics
m_W (MeV)	80350 ± 15	0.5	0.3	From WW threshold scan Beam energy calibration
Γ_W (MeV)	2085 ± 42	1.2	0.3	From WW threshold scan Beam energy calibration
$\alpha_s(m_W)(\times 10^4)$	1170 ± 420	3	small	from R_ℓ^W
$N_\nu(\times 10^3)$	2920 ± 50	0.8	small	ratio of invis. to leptonic in radiative Z returns
m_{top} (MeV/c^2)	172740 ± 500	17	small	From $t\bar{t}$ threshold scan QCD errors dominate
Γ_{top} (MeV/c^2)	1410 ± 190	45	small	From $t\bar{t}$ threshold scan QCD errors dominate
$\lambda_{top}/\lambda^{SM}_{top}$	1.2 ± 0.3	0.10	small	From $t\bar{t}$ threshold scan QCD errors dominate
ttZ couplings	± 30%	0.5 – 1.5%	small	From $E_{CM} = 365$GeV run

for what concerns QED, more significant conceptual work may need to be done for QCD. Let us summarize briefly on the mandatory improvements of the calculations of QED effects in

EWPOs according to analysis in the recent work [6]:

(i) Improving on the calculation of the additional light fermion pair emissions (for Z boson mass and width),
(ii) Better calculation of the Final State Radiation effects in the presence of cut-offs (for R_l^Z),
(iii) Implementation of new QED matrix element in the MC event generator for low angle Bhabha process (for the luminosity determination in view of the measurement of σ^0_{had} and other cross-sections),
(iv) $\mathcal{O}(\alpha^2)$ calculation for $e^+e^- \to Z\gamma$ (for the determination of N_ν),
(v) improved MC simulation of τ decays (for the effective weak mixing angle and tau branching ratio measurements),
(vi) QED effects at the W-pair production threshold (for the measurement of the W mass and width),
(vii) Initial-Final state Interference (e.g. for the Forward-Backward charge asymmetry of lepton pairs around the Z-peak).

For more on the related subject of the separation of QED effects from weak quantities at the FCC-ee precision and generally on the improvements in the definition of EWPOs see recent discussions in [2]. Similar systematic discussion of the QCD effects in EWPOs is in progress, see ref. [2] and Section B.2 in the present report.

For the FCC-ee data analysis, due to the rise of non-factorisable QED effects above the experimental errors, a direct use MC programs might become the standard for fitting EWPOs to the data, even at the Tera-Z stage [2, 6, 7]. New MC event generators will have to provide built-in provisions for an efficient direct fitting of EWPOs to data, which are not present in the LEP legacy MCs. Section C3 of [2] describes possible forms of future EWPOs at FCC-ee experiments and specifies the new required MC software. It is underlined there that due to non-factorisable QED contributions, the factorization of the multiphoton QED effects will have to be done at the amplitude level. Additional quantities available in tau and heavy flavour physics will reach the 10^{-5} precision and are likely to need similar attention.

Very precise determinations of M_W at FCC-ee will rely on the precise measurement of the cross section of the $e^+e^- \to W^+W^-$ process near the threshold. A statistical precision of 0.04% of this cross section translates into 0.6 MeV experimental error on M_W, comparing to present 3 MeV theory error for M_W. Therefore, improved theoretical calculations are required for the generic $e^+e^- \to 4f$ process near the WW threshold with an improvement of one order of magnitude. The most economical solution will be to combine $\mathcal{O}(\alpha^1)$ calculation for $e^+e^- \to 4f$ process with $\mathcal{O}(\alpha^2)$ calculation for the doubly-resonant $e^+e^- \to W^+W^-$ subprocess. The former calculation is already available [8]. The latter will need to be developed; Inclusion of the resummed QED corrections will be mandatory. For details, see Chapter B and a talk [9].

In case of FCC-ee-H, M_H will be obtained from $e^+e^- \to HZ$ process with the precision better of order 10 MeV [4,10]. Theory uncertainties (mainly due to final-state radiation effects) will be subdominant. The main focus will be on calculations of Higgs boson branching ratios and self-couplings. See Chapters B and E.

The anticipated experimental error for m_t measurement at FCC-ee-tt [2] is $\mathcal{O}(20)$ MeV. On the theory side, there are several uncertainty sources: *(i)* The perturbative uncertainty for the calculation of the threshold shape with higher order QCD corrections, *(ii)* the threshold mass definition translated into the $\overline{\rm MS}$ scheme *(iii)* precision of $\alpha_{\rm s}$. Combining these three

error sources, a theory uncertainty close to experimental and less than 50 MeV for m_t appears feasible*. In addition a very accurate determination of the efficiency of experimental acceptances and selection cuts is needed. This task will require the inclusion of higher-order corrections and re-summation results in a Monte-Carlo event generator. NLO QCD corrections for off-shell $t\bar{t}$ production, and matching between these contributions are complementing previous semi-analytic results.

In this report we are especially interested in the discussion of input parameters and of electroweak pseudo-observables (EWPOs) connected with W, H and top production physics. These are masses of heavy SM particles, their couplings, and also $\alpha_{\rm QED}$ and $\alpha_{\rm QCD}$, which as running quantities must be adjusted carefully at the considered high energy regions. These issues will be discussed in next Chapters.

2 What this theory report brings: an overview

The report is divided into four basic chapters. Both the workshop and this report are mainly devoted to precision theoretical calculations. It is a most important subject because the value of most of the FCC-ee experimental analyses relies on the precision of the Standard Model and BSM predictions.

In Chapter B the status and prospects for measurements and determination of α_{QED} and α_s at the FCC-ee are given, but also: issues of QED and QCD resummations, an EFT radiative correction approach to W-bosons production, heavy quarkonia, analysis of the weak mixing angle from data (important as it definitely has non-perturbative effects different from the ones in α), QCD vertex functions beyond two-loops, EFT and QED in flavor physics, top pair production and mass determination, summary for SM precision predictions for partial Higgs decay widths.

In Chapter C numerical and analytical methods for precision multi-loop calculations are presented and recent advances in the field are discussed. The chapter is an add on to the 2018 report [2]. We mentioned already that Monte Carlo generators are very important as they link pure experimental data with theory. Generators for precision e^+e^- simulations, tau, top and W-boson physics, and a section on heritage projects and needs for proper software archivization with Monte Carlo generators are also discussed in Chapter C.

Chapter D consists of only one contribution. SMEFT theory is a bridge between SM physics and analysis of extended gauge models. The chapter is connected with this issue and a specific code is presented. For another discussion, see the talk by J. Blas at the workshop [12].

In the last Chapter E, finally, three contributions are collected, about Higgs models which go beyond the Standard Model theory.

References

[1] A. Blondel, C. Grojean, J. Gluza, M. McCullough, P. Janot (org.), *11th FCC-ee workshop: Theory and Experiments*, 8-11 January 2019, CERN, Geneva, Switzerland, webpage https://indico.cern.ch/event/766859/.

[2] A. Blondel, J. Gluza, S. Jadach, P. Janot, T. Riemann (eds.), Standard Model Theory for the FCC-ee: The Tera-Z, report on the mini workshop on precision EW and QCD

*Examples show that estimations of higher order corrections can differ from actual calculations by factors 3-5 [7, 11].

calculations for the FCC studies: methods and techniques, CERN, Geneva, Switzerland, January 12-13, 2018; subm. as CERN Yellow Report. arXiv:1809.01830.

[3] A. Abada, et al., Future Circular Collider: Vol. 1 "Physics opportunities", http://inspirehep.net/record/1713706/files/CERN-ACC-2018-0056.pdf.

[4] M. Benedikt, A. Blondel, O. Brunner, M. Capeans Garrido, F. Cerutti, J. Gutleber, P. Janot, J. M. Jimenez, V. Mertens, A. Milanese, K. Oide, J. A. Osborne, T. Otto, Y. Papaphilippou, J. Poole, L. J. Tavian, F. Zimmermann, Future Circular Collider, Tech. Rep. CERN-ACC-2018-0057, CERN, Geneva, submitted for publication to Eur. Phys. J. ST. (Dec 2018).
URL http://cds.cern.ch/record/2651299

[5] ALEPH collab., DELPHI collab., L3 collab., OPAL collab., SLD Collaboration, LEP Electroweak Working Group, SLD Electroweak Group, SLD Heavy Flavour Group, S. Schael, et al., Precision electroweak measurements on the Z resonance, Phys. Rept. 427 (2006) 257–454. arXiv:hep-ex/0509008, doi:10.1016/j.physrep.2005.12.006.

[6] S. Jadach, M. Skrzypek, QED challenges at FCC-ee precision measurements. arXiv:1903.09895.

[7] A. Blondel, A. Freitas, J. Gluza, T. Riemann, S. Heinemeyer, S. Jadach, P. Janot, Theory Requirements and Possibilities for the FCC-ee and other Future High Energy and Precision Frontier Lepton Colliders, Input 101 to the update of the European Strategy for Particle Physics, https://indico.cern.ch/event/765096/contributions/3295742/. arXiv:1901.02648.

[8] A. Denner, S. Dittmaier, M. Roth, L. H. Wieders, Electroweak corrections to charged-current e^+e^- to 4 fermion processes: Technical details and further results, Nucl. Phys. B724 (2005) 247–294, [Erratum: Nucl. Phys.B854,504(2012)]. arXiv:hep-ph/0505042, doi:10.1016/j.nuclphysb.2011.09.001,10.1016/j.nuclphysb.2005.06.033.

[9] M. Skrzypek, S. Jadach. KoralW and YFSWW3 - lessons from LEP2 for FCC-ee. Talk held by M. Skrzypek at [1]. https://indico.cern.ch/event/766859/contributions/3252674/attachments/1775305/2970123/FCCeeKoralW_CERN2019_MS.pdf.

[10] The FCC CDR, the four volumes of the FCC CDR and the contributions to the European Strategy can be found on the FCC-CDR webpage https://fcc-cdr.web.cern.ch/.

[11] I. Dubovyk, A. Freitas, J. Gluza, T. Riemann, J. Usovitsch, Complete electroweak two-loop corrections to Z boson production and decayarXiv:1804.10236.

[12] J. de Blas, SM effective field theory fits at the FCC. Talk held at [1].
https://indico.cern.ch/event/766859/contributions/3252636/attachments/1776607/2888696/SMEFT_fits_at_FCC_deBlas.pdf.

Chapter B

Precision calculations in the Standard Model

1 $\alpha_{\rm QED,\,eff}(s)$ for precision physics at the FCC-ee/ILC

Author: Fred Jegerlehner [fjeger@physik.hu-berlin.de]

Discovering "Physics behind precision" at future linear or circular colliders (ILC/FCC projects) requires improved SM predictions based on more precise input parameters. I will review the role $\alpha_{\rm QED,\,eff}$ at future collider energies and report on possible progress based on results from low energy machines.

1.1 $\alpha(M_Z^2)$ in precision physics (precision physics limitations)

Uncertainties of hadronic contributions to the effective fine structure constant $\alpha \equiv \alpha_{\rm QED}$ are a problem for electroweak (EW) precision physics. Presently, we have α, G_μ, M_Z as the most precise input parameters, which together with the top Yukawa y_t and the Higgs self-coupling λ and the strong interaction coupling α_s allow us to make precision predictions for the particle reaction cross sections encompassed by the Standard Model (SM). The cross-section data unfolded form detector and photon radiation resolution effects often are conveniently representable in terms of so-called pseudo-observables like $\sin^2\Theta_f, v_f, a_f, M_W, \Gamma_Z, \Gamma_W, \cdots$ as illustrated in Fig. B.1. Because of the large 6% relative correction between α in the classical limit and the effective value $\alpha(M_Z^2)$ at the Z mass scale, where 50% of the shift is due to non-perturbative hadronic effects, one is loosing about a factor of five orders of magnitude in precision. Nevertheless, for vector-boson Z and W, top-quark and Higgs-boson precision physics possible at future e^+e^- colliders, the best effective input parameters are given by $\alpha(M_Z), G_\mu, M_Z$. The effective $\alpha(s)$ at a process scale $\sqrt{s}$ is given in terms of the photon vacuum polarization (VP) self-energy correction $\Delta\alpha(s)$ by

$$\alpha(s) = \frac{\alpha}{1-\Delta\alpha(s)}\;;\quad \Delta\alpha(s) = \Delta\alpha_{\rm lep}(s) + \Delta\alpha^{(5)}_{\rm had}(s) + \Delta\alpha_{\rm top}(s)\,. \tag{1.1}$$

To be included are the perturbative lepton and top-quark contributions in addition to the non-perturbative hadronic VP shift $\Delta\alpha^{(5)}_{\rm had}(s)$ from the five light quarks and the hadrons they form.

The present accuracies of the corresponding SM input parameter are the following:

$$\begin{array}{rcrcll}
\frac{\delta\alpha}{\alpha} & \sim & 3.6 & \times & 10^{-9}\,, & \\
\frac{\delta G_\mu}{G_\mu} & \sim & 8.6 & \times & 10^{-6}\,, & \\
\frac{\delta M_Z}{M_Z} & \sim & 2.4 & \times & 10^{-5}\,, & \\
\frac{\delta\alpha(M_Z)}{\alpha(M_Z)} & \sim & 0.9 \div 1.6 & \times & 10^{-4} & (\text{present : lost } 10^5 \text{ in precision!})\,, \\
\frac{\delta\alpha(M_Z)}{\alpha(M_Z)} & \sim & 5 & \times & 10^{-5} & (\texttt{FCC}-\texttt{ee/ILC requirement})\,.
\end{array} \tag{1.2}$$

We further note that $\frac{\delta M_W}{M_W} \sim 1.5\times10^{-4}$, $\frac{\delta M_H}{M_H} \sim 1.3\times10^{-3}$, $\frac{\delta M_t}{M_t} \sim 2.3\times10^{-3}$, at present. Evidently, $\alpha(M_Z)$ is the least precise among the basic input parameters $\alpha(M_Z), G_\mu, M_Z$ and

requires a major effort of improvement. As an example, one of the most precisely measured derived observable, the leptonic weak mixing parameter $\sin^2\Theta_{\ell\,\rm eff} = (1 - v_\ell/a_\ell)/4 = 0.23148 \pm 0.00017$ and also the related W mass $M_W = 80.379 \pm 0.012$ GeV are affected by the present hadronic error $\delta\Delta\alpha(M_Z) = 0.00020$ in predictions by $\delta \sin^2\Theta_{\ell\,\rm eff} = 0.00007$ and $\delta M_W/M_W \sim 4.3 \times 10^{-5}$, respectively.

Here one has to keep in mind that besides $\Delta\alpha$ there is a second substantial leading 1-loop correction, which enters the neutral to charged current effective Fermi-couplings ratio $\rho = G_{\rm NC}(0)/G_{\rm CC}(0) = 1 + \Delta\rho$, where $\Delta\rho = \frac{3\sqrt{2}M_t^2\,G_\mu}{16\pi^2}$ is quadratic in the top-quark mass. The mentioned $\frac{\delta M_t}{M_t}$ uncertainty affects the M_W and $\sin^2\Theta_{\ell\,\rm eff}$ predictions as given by

$$\frac{\delta M_W}{M_W} \sim M_W^2/(2M_W^2 - M_Z^2)\cdot\Delta\rho\,\frac{\delta M_t}{M_t} \sim 1.3\times 10^{-2}\,\frac{\delta M_t}{M_t} \simeq 3.0\times 10^{-5}\,, \tag{1.3}$$

$$\frac{\delta\sin^2\Theta_f}{\sin^2\Theta_f} \sim \frac{2\,\cos^2\Theta_f}{\cos^2\Theta_f - \sin^2\Theta_f}\,\Delta\rho\,\frac{\delta M_t}{M_t} \sim 2.7\times 10^{-2}\,\frac{\delta M_t}{M_t} \simeq 6.2\times 10^{-5}\,, \tag{1.4}$$

which are comparable to the present uncertainties from $\delta\Delta\alpha$. Thus an inprovement of δM_t by a factor 5 looks to be as important as an improvement of $\alpha(M_Z)$. We remind that the dependence on M_H is very much weaker because of the custodial symmetry which implies the absence of M_H^2 corrections such that only relatively weak $\log H_M$ effects are remaining.

The input-parameter uncertainties affect most future precision tests and may obscure new physics searches! In order to reduce hadronic uncertainties for perturbative QCD (pQCD) contributions, last but not least, it is very crucial also to improve the precision of QCD parameters $\alpha_s,\ m_c,\ m_b,\ m_t$ which is a big challenge also for lattice-QCD.

The relevance of $\alpha(M_Z^2)$

Understanding precisely even the simplest four fermion, vector boson and Higgs boson production and decay processes, requires very precise input parameters. Unlike in QED and QCD in the SM, a Spontaneously Broken non-Abelian Gauge Theory (SBGT), there are intricate parameter inter-dependences, all masses are related to couplings, only 6 quantities (besides $f \neq t$ fermion masses and mixing parameters) α, G_μ, M_Z in addition to the QCD coupling α_s, the top-quark Yukawa coupling y_t and the Higgs boson self-coupling λ_H are independent. The effective $\alpha(M_Z^2)$ exhibits large hadronic correction that affect prediction like versions of the weak mixing parameter via

$$\sin^2\Theta_i\,\cos^2\Theta_i = \frac{\pi\,\alpha}{\sqrt{2}\,G_\mu\,M_Z^2}\,\frac{1}{1-\Delta r_i}\ ;\ \ \Delta r_i = \Delta r_i(\alpha, G_\mu, M_Z, m_H, m_{f\neq t}, m_t)\,, \tag{1.5}$$

with quantum corrections from gauge boson self-energies, vertex- and box- corrections. Δr_i depends on the definition of $\sin^2\Theta_i$. The various definitions coincide at tree level and hence only differ by quantum effects. From the weak gauge boson masses, the electroweak gauge couplings and the neutral current couplings of the charged fermions we obtain

$$\sin^2\Theta_W = 1 - \frac{M_W^2}{M_Z^2}\,, \tag{1.6}$$

$$\sin^2\Theta_g = e^2/g^2 = \frac{\pi\alpha}{\sqrt{2}\,G_\mu\,M_W^2}\,, \tag{1.7}$$

$$\sin^2\Theta_f = \frac{1}{4|Q_f|}\left(1 - \frac{v_f}{a_f}\right)\ ,\ \ f \neq \nu\,, \tag{1.8}$$

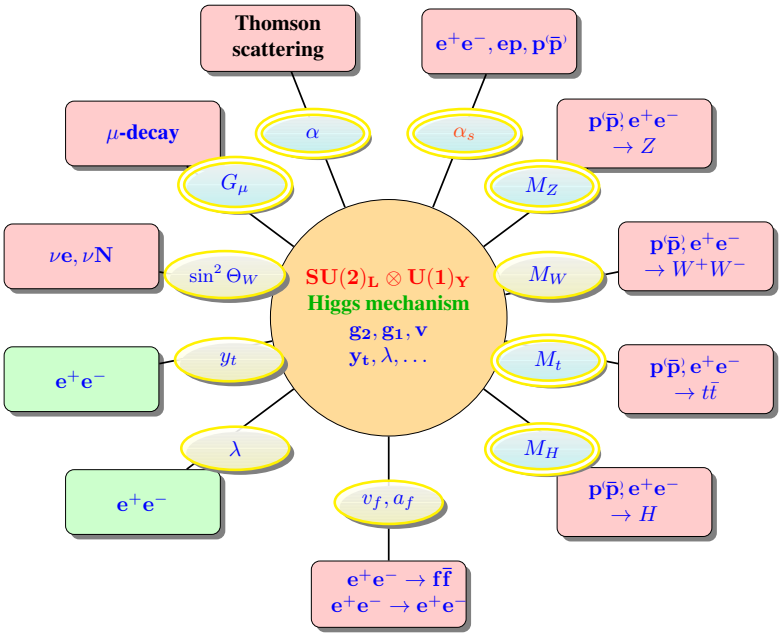

Fig. B.1: Many precisely measurable pseudo-observables associated with scattering-, production- and decay processes are interrelated and predictable in terms of a few independent input parameters.

for the most important cases and the general form of Δr_i reads

$$\Delta r_i \;=\; \Delta\alpha - f_i(\sin^2\Theta_i)\,\Delta\rho + \Delta r_{i\,\rm reminder}\,, \tag{1.9}$$

with a universal term $\Delta\alpha$, which affects the predictions of M_W, A_{LR}, A_{FB}^f, Γ_f, etc. The leading corrections are $\Delta\alpha(M_Z^2) = \Pi'_\gamma(0) - {\rm Re}\Pi'_\gamma({\rm M_Z^2})$ from the running fine structure constant and $\Delta\rho = \frac{\Pi_Z(0)}{M_Z^2} - \frac{\Pi_W(0)}{M_W^2} + 2\,\frac{\sin\Theta_W}{\cos\Theta_W}\,\frac{\Pi_{\gamma Z}(0)}{M_Z^2}$, which is proportional to $G_\mu\,M_t^2$ and therefore large, dominated by the heavy top-quark mass effect, respectively, by the large top Yukawa coupling.

The uncertainty $\delta\Delta\alpha$ implies uncertainties δM_W, $\delta\sin^2\Theta_i$ given by

$$\frac{\delta M_W}{M_W} \;\sim\; \frac{1}{2}\frac{\sin^2\Theta_W}{\cos^2\Theta_W - \sin^2\Theta_W}\,\delta\Delta\alpha \sim 0.23\,\delta\Delta\alpha\,, \tag{1.10}$$

$$\frac{\delta\sin^2\Theta_f}{\sin^2\Theta_f} \;\sim\; \frac{\cos^2\Theta_f}{\cos^2\Theta_f - \sin^2\Theta_f}\,\delta\Delta\alpha \sim 1.54\,\delta\Delta\alpha\,. \tag{1.11}$$

Also affected are the important relationships between couplings and masses like

$$\lambda = 3\sqrt{2}G_\mu\,M_H^2\,(1+\delta_H(\alpha,\cdots))\;;\;\; y_t^2 = 2\sqrt{2}G_\mu\,M_t^2\,(1+\delta_t(\alpha,\cdots)\,, \tag{1.12}$$

which by now offer the only way to determine λ and y_t via the experimentally accessible masses M_H and M_t. The direct measurement of λ and y_t likely will be possible only at future lepton colliders like the FCC-ee.

The parameter relationships between very precisely measurable quantities provide stringent precision tests and at high enough precision would reveal the physics missing within the SM. Presently, the non-perturbative hadronic contribution $\Delta\alpha^{(5)}_{\rm had}(M_Z^2)$ is limiting the precision predictions. Concerning the relevance of quantum corrections and their precision, one

should keep in mind that a 30 SD disagreement between some SM prediction and experiment is obtained when subleading SM corrections are neglected, and only the leading corrections $\Delta\alpha(M_Z^2)$ and $\Delta\rho$ in (1.9) are accounted for. Calculate for example the W and Z mass from $\alpha(M_Z)$, G_μ and $\sin^2\Theta_{\ell\,\rm eff}$: first $\sin^2\Theta_W = 1 - M_W^2/M_Z^2$ is related to $\sin^2\theta_{\ell,\rm eff}(M_Z)$ via

$$\sin^2\theta_{\ell,\rm eff}(M_Z) = \left(1 + \frac{\cos^2\Theta_W}{\sin^2\Theta_W}\,\Delta\rho\right)\sin^2\Theta_W\,,$$

where the leading top quark mass square correction is

$$\Delta\rho = \frac{3\,M_t^2\,\sqrt{2}G_\mu}{16\,\pi^2}\;;\quad M_t = 173 \pm 0.4\ \text{GeV}$$

The iterative solution with input $\sin^2\theta_{\ell,\rm eff}(M_Z) = 0.23148$ is $\sin^2\Theta_W = 0.22426$ while $1 - M_W^2/M_Z^2 = 0.22263$ is what one gets using PDG

$$M_W^{\rm exp} = 80.379 \pm 0.012\ \text{GeV}\;;\quad M_Z^{\rm exp} = 91.1876 \pm 0.0021\ \text{GeV}\,.$$

Predicting then the masses we have

$$M_W = \frac{A_0}{\sin^2\Theta_W}\;;\quad A_0 = \sqrt{\frac{\pi\alpha}{\sqrt{2}G_\mu}}\;;\quad M_Z = \frac{M_W}{\cos\Theta_W}$$

where, including photon VP correction $\alpha^{-1}(M_Z) = 128.953 \pm 0.016$. For the W, Z mass we then get

$$M_W^{\rm the} = 81.1636 \pm 0.0346\ \text{GeV}\;;\quad M_Z^{\rm the} = 92.1484 \pm 0.0264\ \text{GeV}\,.$$

This gives the following SD values:

$$W:\quad 23\,\sigma\;;\quad Z:\quad 36\,\sigma$$

Errors from $\sin^2\theta$, $\alpha(M_z)$, M_t and the experimental ones are added in quadrature. The result is of course scheme-dependent, but illustrates well the sensitivity to taking into account the proper radiative corrections. Actually, including full one-loop and leading two-loop corrections reduces the disagreement below the 2 σ level.

1.2 The ultimate motivation for high precision SM parameters

After the ATLAS and CMS Higgs discovery at the LHC, the Higgs vacuum stability issue is one of the most interesting to be clarified at future e^+e^- facilities. Much more surprising than the discovery of its true existence is the fact that the Higgs boson turned out to exhibit a mass very close to what has been expected from vacuum stability extending up to the Planck scale $\Lambda_{\rm Pl}$ (see Fig. B.2). It looks to be a very tricky conspiracy with other couplings to reach this "purpose". Related is the question of whether the SM allows us to extrapolate it up to Planck scale. So, the central issue for the future is the very delicate "acting together" between SM couplings, which make the precision determination of SM parameters more important than ever. Therefore, higher precise SM parameters g', g, g_s, y_t, λ are mandatory for progress in this direction. Actually, the vacuum stability in controversial at present at the 1.5 σ level between a meta-stable and an stable EW vacuum, which depends on whether λ stays positive up to $\Lambda_{\rm Pl}$ or not. This is illustrated in Fig. B.3. If the SM extrapolates stable to $\Lambda_{\rm Pl}$, obviously the resulting effective parameters affect early cosmology, Higgs inflation, Higgs reheating etc. [3]. The sharp dependence of the Higgs vacuum stability on the SM input parameters and on possible SM extensions and the vastly different scenarios that can result as a consequence of minor shifts in parameter space makes the stable vacuum case a particularly interesting one and it could reveal the Higgs particle as "the master of the universe". After all, it is commonly accepted that dark energy provided by some scalar field is the "stuff" shaping the universe both at very early (inflation) as well as at the late times (accelerated expansion).

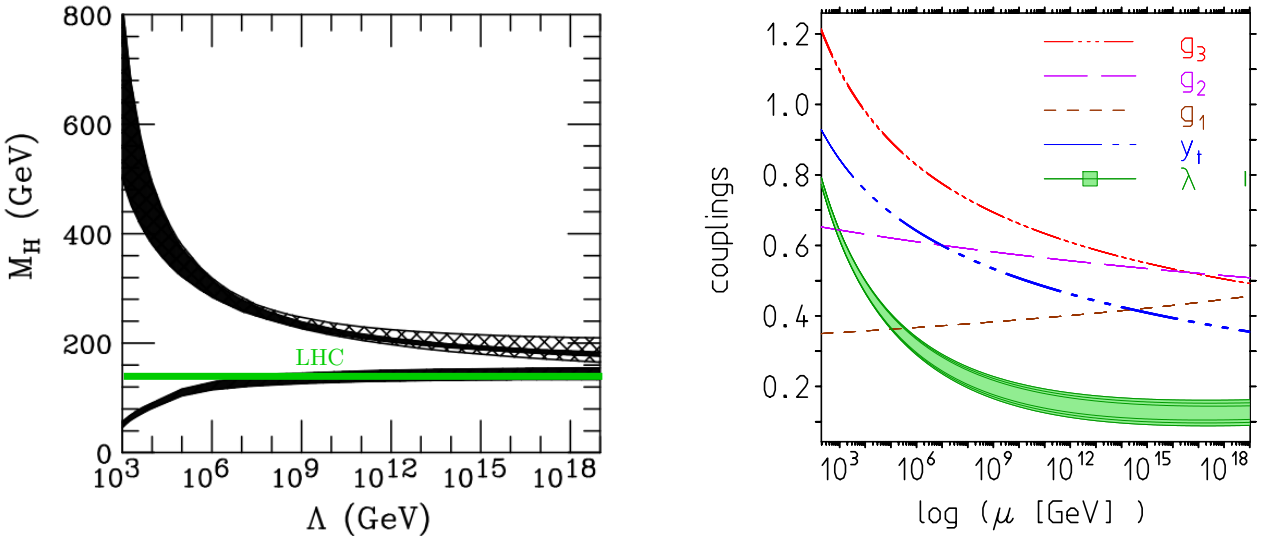

Fig. B.2: Left: Plot by Riesselmann and Hambye in 1996, the first 2-loop analysis after knowing M_t from CDF [1]. Right: the SM dimensionless couplings in the $\overline{\mathrm{MS}}$ scheme as a function of the renormalization scale for $M_H = 124 - 126$GeV, which were obtained in [2–5].

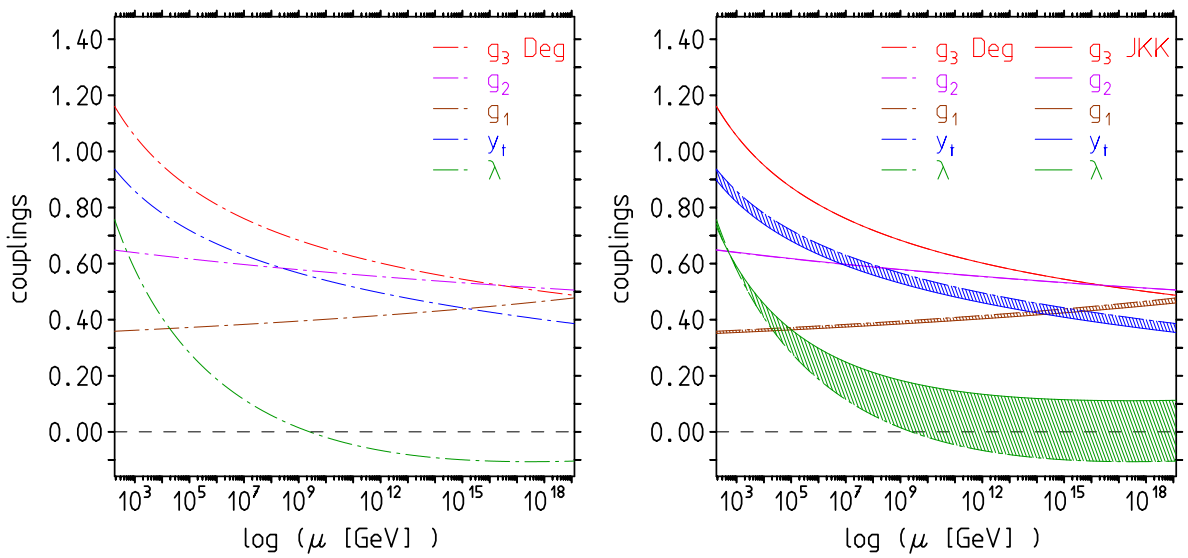

Fig. B.3: Left: Shaposhnikov et al., Degrassi et al. matching [6, 7]. Right: the shaded bands show the difference in the SM parameter extrapolation using the central values of the $\overline{\mathrm{MS}}$ parameters obtained from differences in the matching procedures.

It is very well conceivable that perturbation expansion works up to the Planck scale without a Landau pole or other singularities and Higgs potential remains (meta)stable! The discovery of the Higgs boson for the first time has supplied us with the complete set of SM parameters and for the peculiar SM configuration, revealed that all SM couplings with the exception of the hypercharge g_1 are decreasing with energy. Very surprisingly, this implies that perturbative SM predictions get the better the higher the energy. More specifically the pattern now looks as follows: the gauge coupling related to $U(1)_Y$ is screening (IR free), the ones accociated with $SU(2)_L$ and $SU(3)_c$ are antiscreening (UV free). Thus g_1, g_2, g_3 behave as

expected (standard wisdom). In contrast, the top Yukawa coupling y_t and Higgs self-coupling λ, while screening if standalone (IR free, like QED), as part of the SM, they are transmuted from IR free to UV free. The SM reveals an amazing parameter conspiracy, which reminds us of phenomena often observed in condensed matter systems *"... there is a sudden rapid passage to a totally new and more comprehensive type of order or organization, with quite new emergent properties ..."* [8] i.e. there must be reasons that couplings are as they are. This manifests itself in the QCD dominance within the renormalization group (RG) of the top-Yukawa coupling, which requires $g_3 > \frac{3}{4}\, y_t$ and in the top-Yukawa dominance within the RG of the Higgs-boson coupling, which requires $\lambda < \frac{3\,(\sqrt{5}-1)}{2}\, y_t^2$ in the gaugeless $(g_1, g_2 = 0)$ limit. In the focus is the Higgs self-coupling. Does it stay positive $\lambda > 0$ up to $\Lambda_{\rm Pl}$? A zero $\lambda = 0$ would be essential singularity. The key question/problem concerns the precise size of the top-Yukawa coupling y_t, which decides about the stability of our world! The meta-stability vs. stability controversy will be decided by getting more precise input parameters and by better established EW matching conditions. Most important in this context is the direct measurements of y_t and λ at future e^+e^--colliders. But also the important role that the running gauge couplings are playing, requires substantial progress in obtaining more precise hadronic cross sections in order to reduce hadronic uncertainties in $\alpha(M_Z)$ and $\alpha_2(M_Z)$. A big challenge for low energy hadron facilities. Complementary, progress in lattice QCD simulations of two-point correlators will be important to pin down hadronic effects from first principles. Such improvement in SM precision physics could open the new gate to precision cosmology of the early universe!

1.3 *R*-data evaluation of $\alpha(M_Z^2)$

What we need is a precise calculation of the hadronic photon vacuum polarization function. The non-perturbative hadronic piece from the five light quarks $\Delta\alpha^{(5)}_{\rm had}(s) = -\left(\Pi'_\gamma(s) - \Pi'_\gamma(0)\right)^{(5)}_{\rm had}$ can be evaluated in terms of $\sigma(e^+e^- \to \text{hadrons})$ data via the dispersion integral

$$\Delta\alpha^{(5)}_{\rm had}(s) = -\frac{\alpha\, s}{3\pi}\left(\int\!\!\!\!\!\!-\!\!\!\!\!\!-_{m^2_{\pi_0}}^{E^2_{\rm cut}} {\rm ds'}\, \frac{{\rm R}^{\rm data}_\gamma({\rm s'})}{{\rm s'}({\rm s'}-{\rm s})} + \int\!\!\!\!\!\!-\!\!\!\!\!\!-_{\rm E^2_{cut}}^{\infty} {\rm ds'}\, \frac{{\rm R}^{\rm pQCD}_\gamma({\rm s'})}{{\rm s'}({\rm s'}-{\rm s})} \right), \tag{1.13}$$

where $R_\gamma(s) \equiv \sigma^{(0)}(e^+e^- \to \gamma^* \to \text{hadrons})/\left(\frac{4\pi\alpha^2}{3s}\right)$ measures the hadronic cross-section in units of the tree level $e^+e^- \to \mu^+\mu^-$ cross-section sufficiently above the muon pair production threshold ($s \gg 4m_\mu^2$). The master equation (1.13) is based on analyticity and the optical theorem

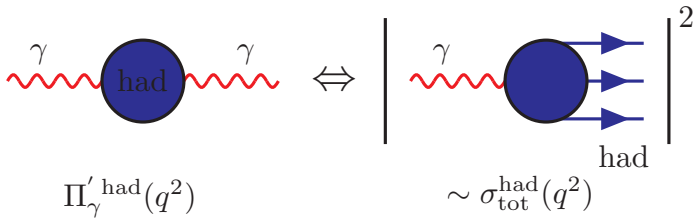

$\Pi'^{\,\rm had}_\gamma(q^2)$ $\qquad\qquad$ $\sim \sigma^{\rm had}_{\rm tot}(q^2)$.

A compilation of the available R-data is shown in Fig. B.4 for the low energy $\pi\pi$ channel and in Fig. B.5 for $R(s)$ above the ρ resonance peak. Since the mid 90's [54] enormous progress has been achieved, also because the new Initial State Radiation (ISR) radiative return approach* provided high statistics data from ϕ- and B-meson factories (see [9–52]). Still, an issue in hadronic vacuum polarization (HVP) is the region 1.2 to 2 GeV, where we have a

*It has been pioneered by the KLOE Collaboration, followed by BaBar and BESIII experiments.

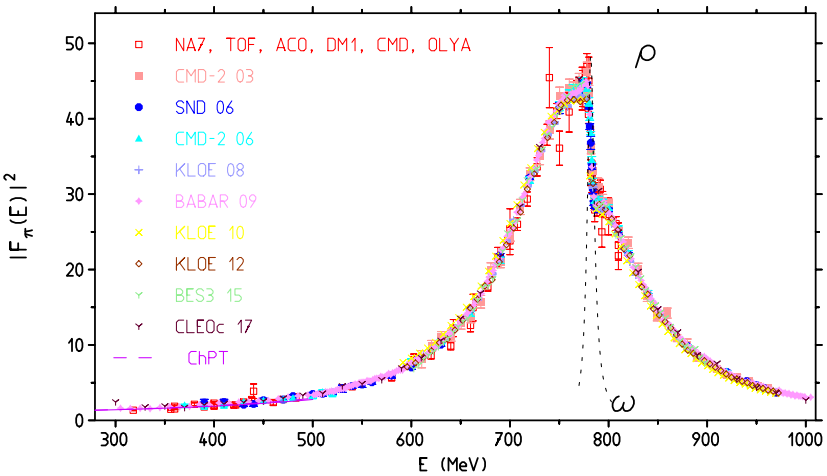

Fig. B.4: The low energy tail of R is provided by $\pi^+\pi^-$ production data. Shown is a compilation of the modulus square of the pion form factor in the ρ meson region. The corresponding $R(s)$ is given by $R(s) = \frac{1}{4}\,\beta_\pi^3\,|F_\pi^{(0)}(s)|^2$, $\beta_\pi = (1-4m_\pi^2/s)^{1/2}$ is the pion velocity ($s = E^2$). Data from CMD-2, SND, KLOE, BaBar, BESIII and CLEOc [9–23] besides some older sets.

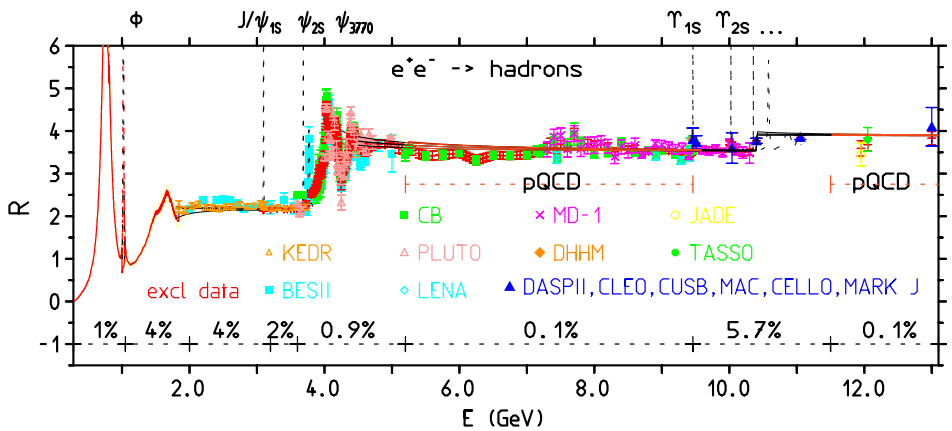

Fig. B.5: The compilation of $R(s)$-data utilized in the evaluation of $\Delta\alpha_{\mathrm{had}}$. The bottom line shows the relative systematic errors within the split regions. Different regions are assumed to have uncorrelated systematics. Data from [24–52] and others. We apply pQCD from 5.2 GeV to 9.46 GeV and above 11.5 GeV using the code of [53].

test-ground for exclusive (more than 30 channels) versus inclusive R measurements, where data taking and/or data analysis is ongoing with CMD-3 and SND detectors [scan] and BaBar and BESIII detector data [radiative return]. The region still contributes about 50% to the uncertainty of the hadronic contribution to the muon $g-2$, as we may learn from Fig. B.8 below. Above 2 GeV fairly accurate BES II data [48–50] are available. Recently, a new inclusive determination of $R_\gamma(s)$ in the range 1.84 to 3.72 GeV has been obtained with the KEDR detector at Novosibirsk [51, 52] (see Fig. B.5). At present the results from the direct and the

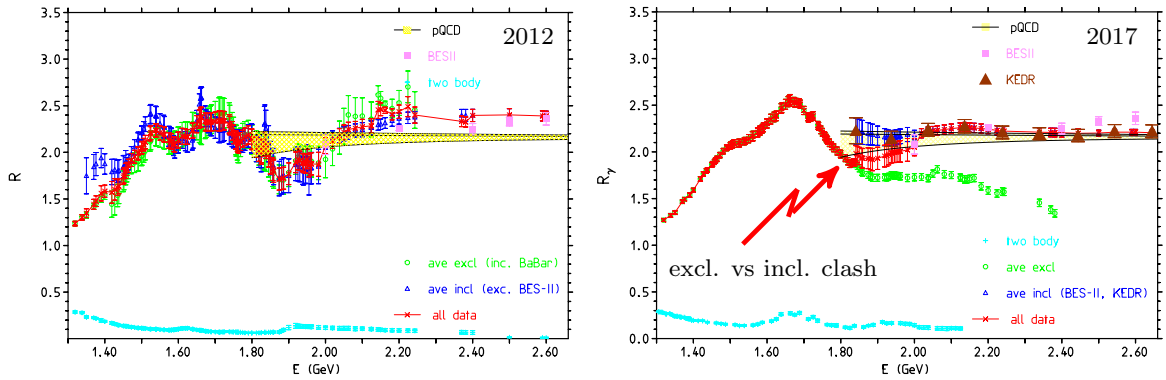

Fig. B.6: Illustrating progress by BaBar and NSK exclusive channel data vs. new inclusive data by KEDR. Why point at 1.84 GeV so high?

Adler function improved approach to be discussed in Sect. 1.4 reads

$$\begin{aligned} \Delta\alpha^{(5)}_{\rm hadrons}(M_Z^2) &= 0.027756 \pm 0.000157 \\ &\quad 0.027563 \pm 0.000120 \quad \text{Adler} \\ \alpha^{-1}(M_Z^2) &= 128.916 \pm 0.022 \\ &\quad 128.953 \pm 0.016 \qquad \text{Adler} \end{aligned} \tag{1.14}$$

In Fig. B.7 we show the effective fine structure constant as a function of the c.m. energy $E = \sqrt{s}$, for the time-like and the space-like region. The question now, what are the possible improvements? Evidently,

• a direct improvement of the dispersion integral requires reducing the error of $R(s)$ to 1% up to above the Υ resonances, likely nobody will do that. One may trust relying on pQCD above 1.8 GeV and refer to quark-hadron duality as in [55]. Then experimental input above 1.8 GeV is not required. But then we are left with questions about where precisely to assume thresholds and what are the mass effects near thresholds. Commonly, pQCD is applied taking into account uncertainties in α_s only. This certainly does not provide a result that can be fully trusted, although the R-data integral in this range is much less precise at present. The problem is that in this theory-driven approach 70% of $\Delta\alpha^{(5)}_{\rm had}(M_Z^2)$ comes from pQCD. Thereby one has to assume that in the time-like region above 1.8 GeV pQCD in average works as precise as the usually adopted $\overline{\rm MS}$ parametrization suggests. Locally, pQCD does not work near thresholds and resonances obviously.

The more promising approach discussed in the following relies on the

• Euclidean split method (Adler-function controlled pQCD), which only requires improved R measurements in the exclusive region from 1 to 2 GeV. Here NSK, BESIII, and Belle II can top what BaBar has achieved. However, in this rearrangement, as important is a substantially more precise calculation of the pQCD Adler-function. Required is an essentially exact massive 4-loop result, which is equivalent to sufficiently high order low- and high-energy expansions, of which a few terms are available already (see [56]).

Because of the high sensitivity to the precise charm and bottom quark values one also needs better parameters m_c and m_b besides α_s. Here one can profit from activities going on anyway and the FCC-ee/ILC projects pose further strong motivation to attempt to reach higher precision for QCD parameters.

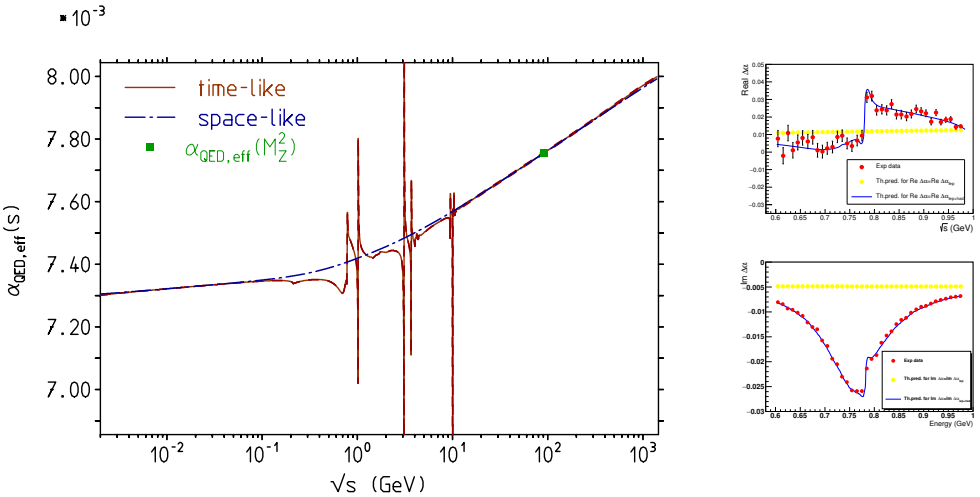

Fig. B.7: Left: the effective $\alpha(s)$ at time-like vs. space-like momentum transfer, showing quark-hadron duality at work. In the time-like region, the effective charge is varying dramatically near resonances but agrees quite well on average with the space-like version. Locally, it is ill-defined near OZI suppressed meson decays $J/\psi, \psi_1, \Upsilon_{1,2,3}$ where Dyson series of self-energy insertions do not converge (see Sect. 5 of [57]). Right: a first experimental determination of the effective charge in the ρ resonance region by KLOE-2 [58], which demonstrates the pronounced variation of the vacuum polarization (charge screening) across a resonance.

$\Delta\alpha_{\rm had}(M_Z^2)$ results from ranges

Table B.1 shows the contributions and errors to $\Delta\alpha^{(5)}_{\rm had}(M_Z)$ for $M_Z = 91.1876$ GeV in units 10^{-4} from different regions. Typically, depending on cuts applied the direct evaluation of the dispersion integral of R yields 43% from data and 57% from perturbative QCD. Here, pQCD is used between 5.2 GeV and 9.5 GeV and above 11.5 GeV. Systematic errors are taken correlated within the different ranges, but taken as independent between the different ranges.

In Fig. B.8 we illustrate the relevance of different energy ranges by comparing the hadronic contribution to the muon $g-2$ with the one to the hadronic shift of the effective charge at M_Z. The point is that the new muon $g-2$ experiments strongly motivate efforts the measure $R(s)$ in the low energy region more precisely. From Fig. B.8 we learn that low energy data alone are not able to substantially improve a direct evaluation of the dispersion integral (1.13). Therefore, in order to achieve the required factor 5 improvement alternative methods to determine $\Delta\alpha^{(5)}_{\rm had}(s)$ at high energies have to be developed.

1.4 Reducing uncertainties via the Euclidean split trick: Adler function controlled pQCD

As we learn from Fig. B.5 it is difficult if not impossible to tell at what precision pQCD can replace data. This especially concerns resonance and threshold effects and to what extent quark-hadron duality can be made precise. This is much simpler to accommodate by comparison in the Euclidean (space-like) region, as it has been suggested by Adler [59] long time ago and has been successfully tested in [60]. As the data pool has been improving a lot since the "experimental" Adler-function is known with remarkable precision by now. Actually, on the experiment side new more precise measurements of $R(s)$ are going on primarily in the low energy range. On the

Table B.1: $\Delta\alpha^{(5)}_{\rm had}(M_Z)$ in terms of e^+e^--data and pQCD. The last two columns list the relative accuracy and the % contribution of the total. The systematic errors (syst) are assumed to be independent among the different energy ranges listed in the table.

final state	range (GeV)	$\Delta\alpha^{(5)}_{\rm had}\times 10^4$ (stat) (syst) [tot]	rel	abs
ρ	(0.28, 1.05)	34.14 (0.03) (0.28)[0.28]	0.8%	3.1%
ω	(0.42, 0.81)	3.10 (0.03) (0.06)[0.07]	2.1%	0.2%
ϕ	(1.00, 1.04)	4.76 (0.04) (0.05)[0.06]	1.4%	0.2%
J/ψ		12.38 (0.60) (0.67)[0.90]	7.2%	31.9%
Υ		1.30 (0.05) (0.07)[0.09]	6.9%	0.3%
had	(1.05, 2.00)	16.91 (0.04) (0.82)[0.82]	4.9%	26.7%
had	(2.00, 3.20)	15.34 (0.08) (0.61)[0.62]	4.0%	15.1%
had	(3.20, 3.60)	4.98 (0.03) (0.09)[0.10]	1.9%	0.4%
had	(3.60, 5.20)	16.84 (0.12) (0.21)[0.25]	0.0%	2.4%
pQCD	(5.20, 9.46)	33.84 (0.12) (0.25)[0.03]	0.1%	0.0%
had	(9.46,11.50)	11.12 (0.07) (0.69)[0.69]	6.2%	19.1%
pQCD	(11.50, 0.00)	123.29 (0.00) (0.05)[0.05]	0.0%	0.1%
data	(0.3,∞)	120.85 (0.63) (1.46)[1.58]	1.0%	0.0%
total		277.99 (0.63) (1.46)[1.59]	0.6%	100.0%

theory side, pQCD calculations for Euclidean two-point current correlators are expected to be pushed further. Advance is also expected from lattice QCD, which also can produce data for the Adler function. As suggested in [61–63] in the Euclidean region a split into a non-perturbative and a pQCD part is self-evident. One may write

$$\alpha(M_Z^2) = \alpha^{\rm data}(-M_0^2) + \Big[\alpha(-M_Z^2) - \alpha(-M_0^2)\Big]^{\rm pQCD} + \Big[\alpha(M_Z^2) - \alpha(-M_Z^2)\Big]^{\rm pQCD}\ , \qquad (1.15)$$

where the space-like offset M_0 is chosen such that pQCD is well under control for $-s < -M_0^2$. The non-perturbative offset $\alpha^{\rm data}(-M_0^2)$ may be obtained integrating $R(s)$ data, by choosing $s = -M_0^2$ in (1.13).

The crucial point is that the contribution from different energy ranges to $\alpha^{\rm data}(-M_0^2)$ is very different form that to $\alpha^{\rm data}(M_Z^2)$. Table B.1 now is replaced by Table B.2 where $\alpha^{\rm data}(-M_0^2)$ is listed for $M_0 = 2$ GeV in units 10^{-4}. Here 94% results using data and only 6% pQCD, applied again between 5.2 GeV and 9.5 GeV and above 11.5 GeV. Of $\Delta\alpha^{(5)}_{\rm had}(M_Z^2)$ 22% data, 78% pQCD! The split point M_0 may be shifted to optimize the uncertainty contributed from the pQCD part and the data based offset value. A reliable estimate of the latter is mandatory and we also have crosschecked its evaluation using the phenomenological effective Lagrangian global fit approach [64, 65], specifically, within the broken Hidden Local Symmetry (BHLS) implementation.

In Fig. B.9 we illustrate the relevance of different energy ranges by comparing the hadronic shift of the effective charge as evaluated at s space-like low energy scale $M_0 = 2$ GeV with the ones at the time-like M_Z scale. The crucial point is that the profile of the offset α at M_0 much more resembles the profile found for the hadronic contribution to a_μ and improving $a_\mu^{\rm had}$ automatically lead to an improvement of $\Delta\alpha^{(5)}_{\rm had}(-M_0^2)$, this is the profit gained from the Euclidean split trick.

What does this have to do with the Adler function? The Adler function is **i)** the monitor to

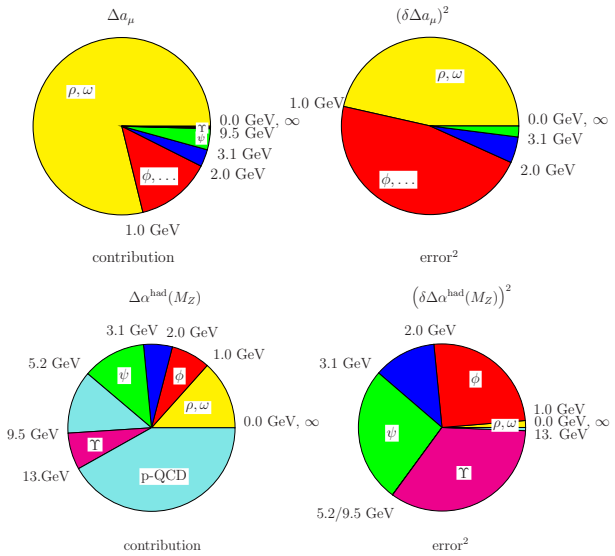

Fig. B.8: A comparison of the weights and square uncertainties between a_μ^{had} and $\Delta\alpha^{(5)}_{\mathrm{had}}(M_Z^2)$ of contributions from different regions. It reveals the importance of the different energy regions. In contrast to the low energy dominated a_μ^{had}, $\Delta\alpha^{(5)}_{\mathrm{had}}(M_Z^2)$ is sensitive to data from much higher energies.

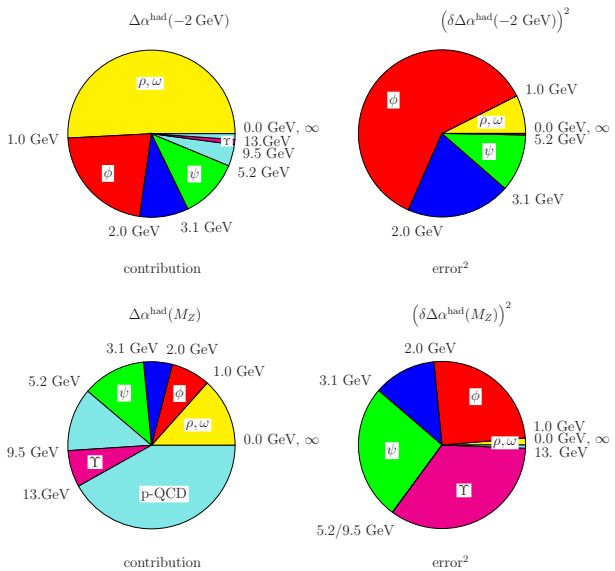

Fig. B.9: Contributions and square errors from e^+e^- data ranges and form pQCD to $\Delta\alpha^{(5)}_{\mathrm{had}}(-M_0^2)$ vs. $\Delta\alpha^{(5)}_{\mathrm{had}}(M_Z^2)$.

Table B.2: $\Delta\alpha^{(5)}_{\rm had}(-M_0^2)$ at $M_0 = 2$ GeV in terms of e^+e^--data and pQCD. Labels as in Table B.1

final state	range (GeV)	$\Delta\alpha^{(5)}_{\rm had}(-M_0^2)\times 10^4$ (stat) (syst) [tot]	rel	abs
ρ	(0.28, 1.05)	29.97 (0.03) (0.24)[0.24]	0.8%	14.3%
ω	(0.42, 0.81)	2.69 (0.02) (0.05)[0.06]	2.1%	0.8%
ϕ	(1.00, 1.04)	3.78 (0.03) (0.04)[0.05]	1.4%	0.6%
J/ψ		3.21 (0.15) (0.15)[0.21]	6.7%	11.2%
Υ		0.05 (0.00) (0.00)[0.00]	6.8%	0.0%
had	(1.05, 2.00)	10.56 (0.02) (0.48)[0.48]	4.6%	56.9%
had	(2.00, 3.20)	6.06 (0.03) (0.25)[0.25]	4.2%	15.7%
had	(3.20, 3.60)	1.31 (0.01) (0.02)[0.03]	1.9%	0.2%
had	(3.60, 5.20)	2.90 (0.02) (0.02)[0.03]	0.0%	0.2%
pQCD	(5.20, 9.46)	2.66 (0.02) (0.02)[0.00]	0.1%	0.0%
had	(9.46,11.50)	0.39 (0.00) (0.02)[0.02]	5.7%	0.1%
pQCD	(11.50, 0.00)	0.90 (0.00) (0.00)[0.00]	0.0%	0.0%
data	(0.3,∞)	60.92 (0.16) (0.62)[0.64]	1.0%	0.0%
total		64.47 (0.16) (0.62)[0.64]	1.0%	100.0%

control the applicability of pQCD and **ii)** the pQCD part $[\alpha(-M_Z^2)-\alpha(-M_0^2)]^{\rm pQCD}$ is favorably calculated by integrating the Adler function $D(Q^2)$. The small remainder $[\alpha(M_Z^2)-\alpha(-M_Z^2)]^{\rm pQCD}$ can be obtained in terms of the VP function $\Pi'_\gamma(s)$. In fact, the Adler function is the ideal monitor for comparing theory and data. The Adler function is defined as the derivative of the VP function:

$$D(-s) \doteq \frac{3\pi}{\alpha}\, s\, \frac{\rm d}{{\rm d}s}\Delta\alpha_{\rm had}(s) = -\left(12\pi^2\right)\, s\, \frac{{\rm d}\Pi'_\gamma({\rm s})}{{\rm d}s} \tag{1.16}$$

and can be evaluated in terms of e^+e^--annihilation data by the dispersion integral

$$D(Q^2) = Q^2\left(\int\limits_{4m_\pi^2}^{E^2_{\rm cut}} {\rm ds}\,\frac{{\rm R(s)^{data}}}{({\rm s}+{\rm Q}^2)^2} + \int_{\rm E^2_{cut}}^{\infty} {\rm ds}\,\frac{{\rm R^{pQCD}(s)}}{({\rm s}+{\rm Q}^2)^2}\right). \tag{1.17}$$

It is a finite object not subject to renormalization and it tends to a constant in the high energies limit, where it is perfectly perturbative. Comparing the direct $R(s)$-based and the $D(Q^2)$-based methods

pQCD $\leftrightarrow$ $R(s)$	pQCD $\leftrightarrow$ $D(Q^2)$
very difficult to obtain in theory	smooth simple function in Euclidean region

we note that in time-like approach pQCD only works well in "perturbative windows" roughly in ranges 3.00 - 3.73 GeV, 5.00 - 10.52 GeV and 11.50 GeV - ∞ (see [53]), while in the space-like approach pQCD works well for $Q > 2.0$ GeV, a clear advantage.

In Fig. B.10 the "experimental" Adler–function is confronted with theory (pQCD + NP). Note that in contrast to most xfR-plots, like Fig. B.5, showing statistical errors only in Fig. B.10 the total error is displayed as the shaded band. We see that while 1-loop and 2-loop predictions

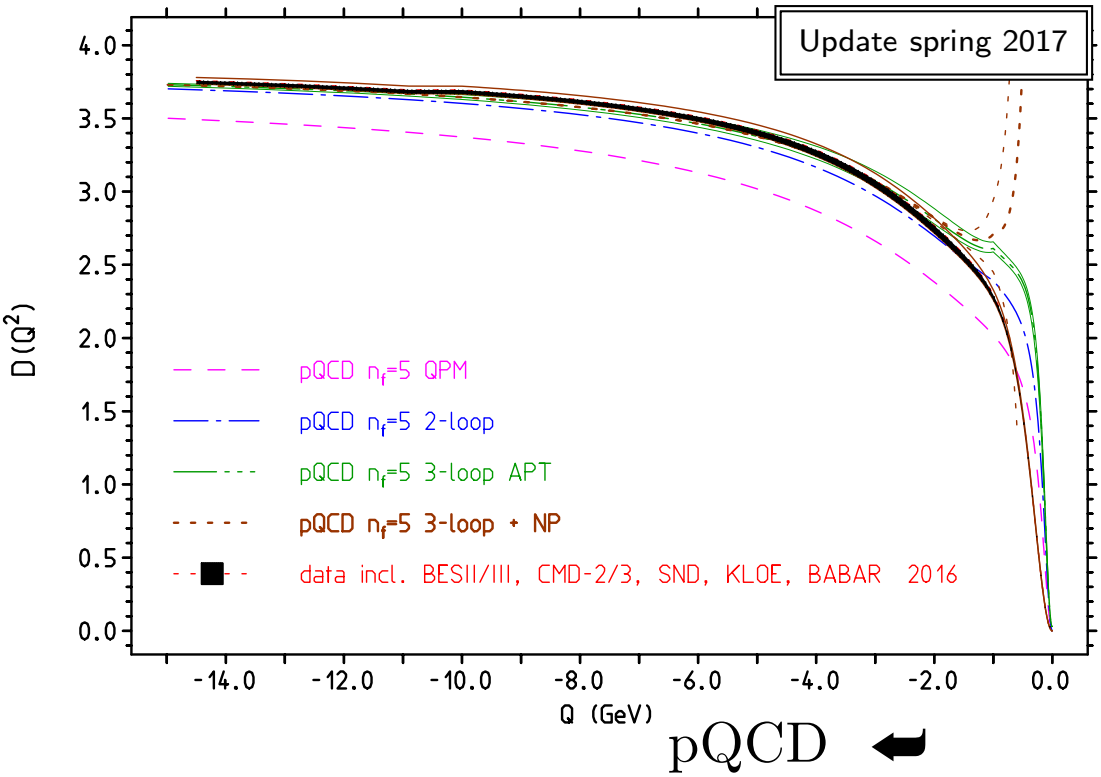

Fig. B.10: Monitoring pQCD vs. data: the pQCD prediction of $D(Q^2)$ works well down to $M_0 = 2.0\,\mathrm{GeV}$, provided full massive QCD at 3- or higher-loop order is employed.

fail clearly to follow the data band, a full massive 3-loop QCD prediction in the gauge invariant background field MOM scheme [66] reproduces the experimental Adler function surprisingly well. This has been worked out in [60] by Padé improvement of the moment expansions provided in [67–69]. The figure also shows that non-perturbative (NP) contributions from the quark and gluon condensates [70, 71][†] start to contribute substantially only at energies where pQCD fails to converge because one is approaching the Landau pole in $\overline{\mathrm{MS}}$ parametrized QCD. Strong coupling constant freezing as in analytic perturbation theory (APT) advocated in [72] or similar schemes actually are not able to improve the agreement in the low energy regime. Coupling constant freezing also contradicts lattice QCD results [73].

From the three terms of (1.15) we already know the low energy offset $\Delta\alpha_{\mathrm{had}}(-M_0^2)$ for $M_0 = 2.0\,\mathrm{GeV}$. The second term we obtain by integrating the pQCD predicted Adler function

$$\Delta_1 = \Delta\alpha_{\mathrm{had}}(-M_Z^2) - \Delta\alpha_{\mathrm{had}}(-M_0^2) = \frac{\alpha}{3\pi}\int_{M_0^2}^{M_Z^2} \mathrm{dQ'^2}\frac{\mathrm{D(Q'^2)}}{\mathrm{Q'^2}}\,, \tag{1.18}$$

based on a complete 3-loop massive QCD analysis. The QCD parameters used are $\alpha_s(M_Z) = 0.1189(20)$, $m_c(m_c) = 1.286(13)[M_c = 1.666(17)]\mathrm{GeV}$, $m_b(m_c) = 4.164(25)[M_b = 4.800(29)]\mathrm{GeV}$. The result obtained is

$$\Delta_1 = \Delta\alpha_{\mathrm{had}}(-M_Z^2) - \Delta\alpha_{\mathrm{had}}(-M_0^2) = 0.021074 \pm 0.000100\ .$$

[†]These are evaluated by means of operator product expansions and the explicit expressions may be found in [60].

This includes a shift +0.000008 from the massless 4-loop contribution included in the high energy tail. The error ±0.000100 will be added in quadrature. Up to three-loops all contributions have the same sign and are substantial. Four- and higher-orders could still add up to non-negligible contribution. An error for missing higher order terms is not included.

The remaining term concerns the link between the space-like and the time-like region at the Z boson mass scale and is given by the difference

$$\Delta_2 = \Delta\alpha^{(5)}_{\rm had}(M_Z^2) - \Delta\alpha^{(5)}_{\rm had}(-M_Z^2) = 0.000045 \pm 0.000002\,,$$

which can be calculated in pQCD. It accounts for the iπ-terms from the logs $\ln(-q^2/\mu^2) = \ln(|q^2/\mu^2|) + {\rm i}\pi$. Since the term is small we can get it as well from direct data integration based on our data compilation. We obtain $\Delta\alpha_{\rm had}(-M_Z^2) = 276.44 \pm 0.64 \pm 1.78$ and $\Delta\alpha_{\rm had}(+M_Z^2) = 276.84 \pm 0.64 \pm 1.90$, and taking into account that errors are almost 100% correlated we have $\Delta\alpha_{\rm had}(M_Z^2) - \Delta\alpha_{\rm had}(-M_Z^2) = 0.40 \pm 0.12$ less precise but in agreement with the pQCD result. We then have

$$\begin{aligned}
\Delta\alpha^{(5)}_{\rm had}(-M_0^2)^{\rm data} &= 0.006409 \pm 0.000063 \\
\Delta\alpha^{(5)}_{\rm had}(-M_Z^2) &= 0.027483 \pm 0.000118 \\
\Delta\alpha^{(5)}_{\rm had}(M_Z^2) &= 0.027523 \pm 0.000119 \quad .
\end{aligned}$$

In order to get $\alpha^{-1}(M_Z^2)$ we have to include also the leptonic piece [74]

$$\Delta\alpha_{\rm lep}(M_Z^2) \simeq 0.031419187418\,, \tag{1.19}$$

and the top-quark contribution. A very heavy top-quark decouples like

$$\Delta\alpha_{\rm top} \simeq -\frac{\alpha}{3\pi}\frac{4}{15}\frac{s}{m_t^2} \to 0$$

when $m_t \gg s$. At $s = M_Z^2$, the top-quark contributes

$$\Delta\alpha_{\rm top}(M_Z^2) = -0.76 \times 10^{-4} \quad . \tag{1.20}$$

Collecting terms, this leads to the result presented in (1.14) above. One should note that the Adler function controlled Euclidean data vs. pQCD split approach is only moderately more pQCD-driven, than the time-like approach adopted by Davier et al. [55] and others as follows from the collection of results shown in Fig. B.11. The point is that the Adler function driven method only uses pQCD where reliable predictions are possible and direct cross checks against lattice QCD data may be carried out. Similarly, possible future direct measurements of $\alpha(-Q^2)$ in μ-e scattering [75] can provide Euclidean HVP data, in particular also for the offset $\Delta\alpha_{\rm had}(-M_0^2)$.

1.5 Prospects for future improvements

The new muon $g-2$ experiments at Fermilab and at JPARC in Japan (expected to go into operation later) trigger the continuation of $e^+e^- \to$ hadrons cross section measurements in the low energy region by CMD-3 and SND at BINP Novosibirsk, by BES III at IHEP Beijing and soon by Belle II at KEK Tsukuba. This automatically helps to improve $\Delta\alpha(-M_0^2)$ and hence

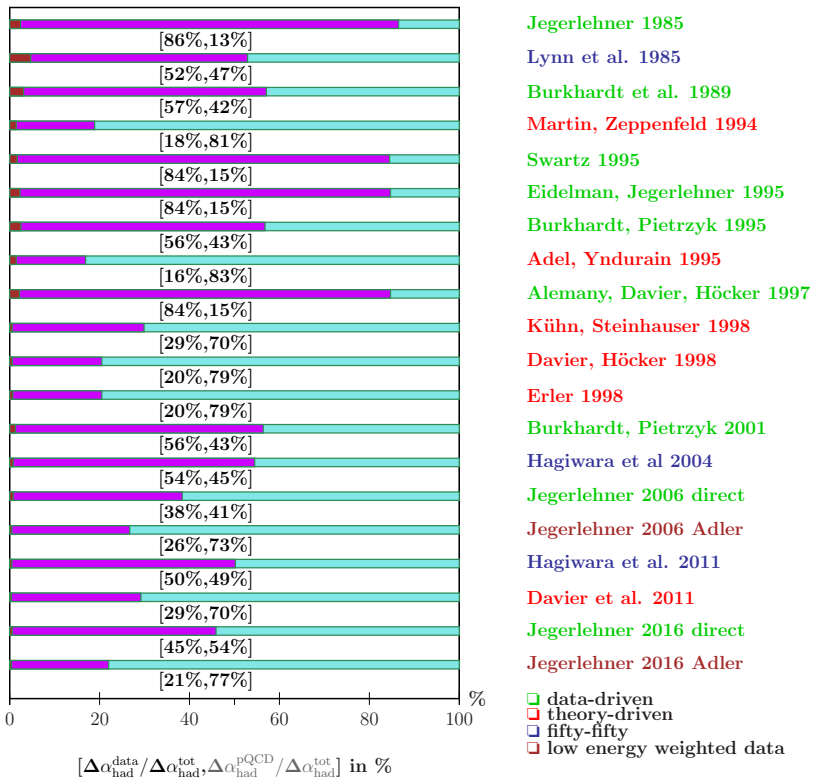

Fig. B.11: How much pQCD? Here a history of results by different authors. It shows that the Adler-function controlled approach to $\Delta\alpha^{(5)}_{\mathrm{had}}(M_Z^2)$ is barely more pQCD driven than many of the standard evaluations. The pQCD piece is 70% in Davier et al. [55] and 77% in our Adler-driven case. With an important difference: in the Adler controlled case, the major part of 71% is based on pQCD in the space-like region and only 6% contributing to the non-perturbative offset value is evaluated in the time-like region, while in the standard theory-driven as well as in the more data-driven approaches pQCD is applied in the time-like region, where it is much harder to be tested against data.

$\alpha(M_Z^2)$ via the Adler function controlled split-trick approach. As important are the results from lattice QCD, which come closer to be competitive with the data-driven dispersive method.

The improvement by a factor 5 to 10 in this case largely relies on improving the QCD prediction of the two-point vector correlator above the 2 GeV scale, which is a well defined comparably simple task. The mandatory pQCD improvements required are:

- 4-loop massive pQCD calculation of Adler function. In practice, this requires the calculation of a sufficient number of terms in the low- and high-momentum series expansions, such that an accurate Padé improvement is possible.
- m_c, m_b improvements by sum rule and/or lattice QCD evaluations.
- improved α_s in low Q^2 region above the τ mass.

Note that the direct dispersion relations (DR) approach requires precise data up to much higher energies or a heavy reliance on the pQCD calculation of the time-like $R(s)$! The virtues of Adler-function approach are obvious:

– no problems with physical threshold and resonances,

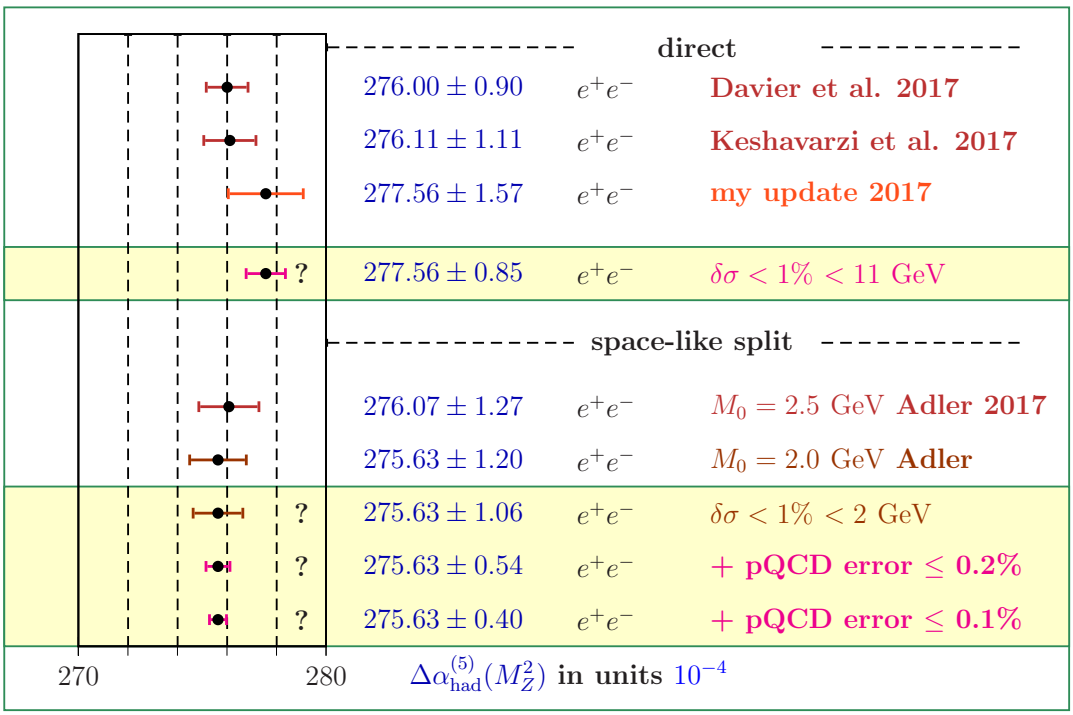

Fig. B.12: Comparison of possible improvements. My "direct" analysis is data-driven adopting pQCD in window $5.2 - 9.5$ GeV and above 11.5 GeV . The Adler-driven results under "space-like split" show the present status for the two offset energies $M_0 = 2.5$ GeV and 2 GeV. The improvement potential is displayed for 3 options: reducing the error of the data offset by a factor two, improving pQCD to a 0.2% precision Adler-function in addition and the same by improving pQCD to a 0.1% precision Adler-function. The direct results are from Refs. [55, 76, 77].

- pQCD is used only where we can check it to work accurately (Euclidean $Q \gtrsim 2.0$ GeV),
- no manipulation of data, no assumptions about global or local duality,
- the non-perturbative "remainder" $\Delta\alpha(-M_0^2)$ is mainly sensitive to low energy data,
- $\Delta\alpha(-M_0^2)$ would be directly accessible in a MUonE experiment (project) [75] or in lattice QCD.

In the direct approach e.g. Davier et al. [55] use pQCD above 1.8 GeV, which means that no error reduction follows from remeasuring cross-sections above 1.8 GeV. Also there is no proof that pQCD is valid at 0.04% precision as adopted. This is a general problem when utilizing pQCD at time-like momenta exhibiting non-perturbative features.

What we can achieve is illustrated in Fig. B.12 and the following tabular on the precision in $\alpha(M_Z^2)$:

present	direct	1.7×10^{-4}	
	Adler	1.2×10^{-4}	
future	Adler QCD 0.2%	5.4×10^{-5}	
	Adler QCD 0.1%	3.9×10^{-5}	
future	via $A_{\rm FB}^{\mu\mu}$ off Z	3×10^{-5}	[78] .

Our analysis shows that the Adler function inspired method is competitive with Patrick Janot's [78] direct near Z pole determination via a measurement of the forward backward asymmetry $A_{\rm FB}^{\mu\mu}$ in $e^+e^- \to \mu^+\mu^-$. The modulus square of the sum of the two tree level diagrams has three terms: the Z-exchange alone $\mathcal{Z} \propto (M_Z^2 G_\mu)^2$, the $\gamma - Z$ interference $\mathcal{I} \propto \alpha(s)\, M_Z^2 G_\mu$ and the γ-exchange only $\mathcal{G} \propto \alpha^2(s)$. The interference term determines the forward-backward (FB) asymmetry, which is linear in $\alpha(s)$. v denotes the vector $Z\mu\mu$ coupling that depends on $\sin^2\Theta_{\ell\,\rm eff}(s)$, while a denotes the axial $Z\mu\mu$ coupling that is sensitive to ρ-parameter (strong M_t dependence). In extracting $\alpha(M_Z^2)$ one is using the v and a couplings as measured at Z-peak directly. At tree level one then has

$$A_{\rm FB}^{\mu\mu} = A_{\rm FB,0}^{\mu\mu} + \frac{3\,a^2}{4\,v^2}\,\frac{\mathcal{I}}{\mathcal{Z}+\mathcal{G}}\;;\quad A_{\rm FB,0}^{\mu\mu} = \frac{3}{4}\,\frac{4v^2a^2}{(v^2+a^2)^2}\,, \tag{1.21}$$

where

$$\mathcal{G} = \frac{c_\gamma^2}{s}\,,\quad \mathcal{I} = \frac{2c_\gamma c_Z\, v^2\,(s-M_Z^2)}{(s-M_Z^2)^2+M_Z^2\Gamma_Z^2}\,,\quad \mathcal{Z} = \frac{c_Z^2\,(v^2+a^2)\,s}{(s-M_Z^2)^2+M_Z^2\Gamma_Z^2}$$

$$c_\gamma = \sqrt{\frac{4\pi}{3}}\,\alpha(s)\,,\quad c_Z = \sqrt{\frac{4\pi}{3}}\,\frac{M_Z^2}{2\pi}\,\frac{G_\mu}{\sqrt{2}}\,,\quad v = (1-4\,\sin^2\Theta_\ell)\,a\,,\quad a = -\frac{1}{2}\,.$$

Note that $M_Z^2 G_\mu = M_W^2 G_\mu/\cos^2\Theta_W = \frac{\pi}{\sqrt{2}}\,\frac{\alpha_2(s)}{\cos^2\Theta_g(s)}$ and $\sin^2\Theta_g(s) = \alpha(s)/\alpha_2(s)$. i.e. all parameters vary more or less with energy depending on the renormalization scheme utilized. The challenges for this direct measurement are precise radiative corrections (see [79, 80] and references therein) and requires dedicated off-Z peak running. Short accounts of the methods proposed for improving $\alpha(M_Z^2)$ may be found in Sects. 8 and 9 of [81].

The Adler-function based method is much cheaper to get, I think, and does not depend on understanding the Z peak region with unprecedented precision. Another very crucial point may be that the dispersive method and the Adler-function modified version provide the effective $\alpha(s)$ for arbitrary c.m. energies, not at $s = M_Z^2$ only; although supposed we are given a very precise $\alpha(M_Z^2)$ one can reliably calculate $\alpha(s) - \alpha(M_Z^2)$ via pQCD for s-values in the perturbative regime, i.e. especially when going to higher energies. In any case the requirements specified above to be satisfied in order to reach a factor 5 improvement looks to be achievable.

1.6 The need for a space-like effective $\alpha(t)$

As a normalization in measurements of cross-sections in e^+e^- collider experiments, small angle Bhabha scattering is the standard choice. This reference process is dominated by the t-channel diagram of the Bhabha scattering process shown in the left of Fig. B.14. In small angle Bhabha scattering we have $\delta_{\rm HVP}\sigma/\sigma = 2\,\delta\alpha(\bar{t})/\alpha(\bar{t})$, and for the FCC-ee luminometer $\sqrt{\bar{t}} \simeq 3.5$ GeV near Z peak and $\simeq 13$ GeV at 350 GeV [82]. The progress achieved after LEP times is displayed in Fig. B.13. What can be achieved for the FCC-ee project is listed in the following tabular:

$\sqrt{s}$	$\sqrt{\bar{t}}$	1996 [83, 84]	present	FCC–ee expected [82]
M_Z	3.5 GeV	0.040%	0.013%	0.6×10^{-4}
350 GeV	13 GeV		1.2×10^{-4}	2.4×10^{-4}

The estimates are based on expected improvements possible for $\Delta\alpha_{\rm had}(-Q^2)$ in the appropriate energy ranges, centered at $\sqrt{\bar{t}}$.

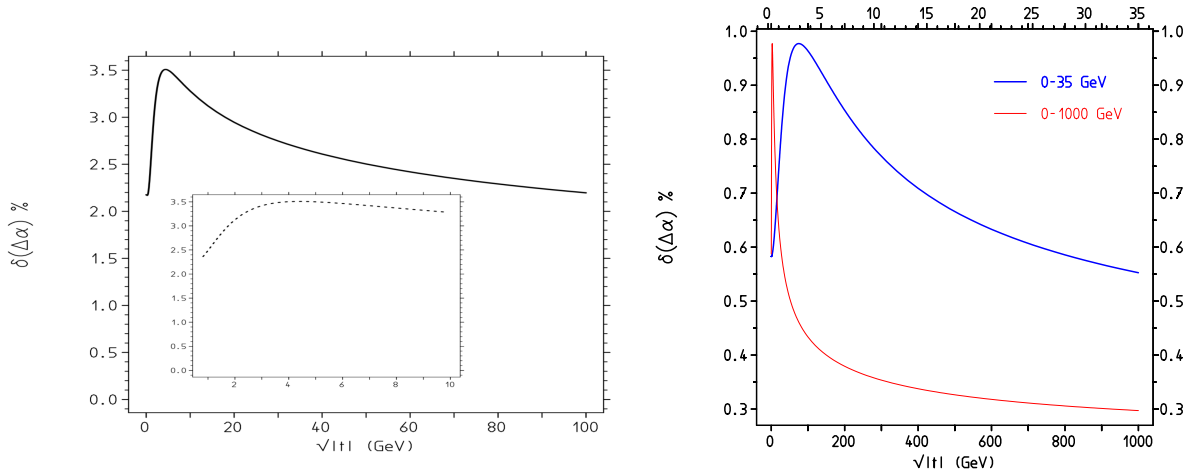

Fig. B.13: Hadronic uncertainty $\delta\Delta\alpha_{\rm had}(\sqrt{t})$. The progress since LEP times 1996 (left) to now (right) is remarkable. Lots of much more precise low energy data $\pi\pi$ etc. are available by now.

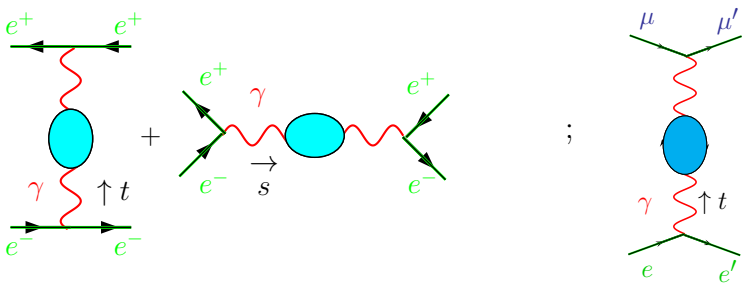

Fig. B.14: t-channel dominated QED processes. Left: VP dressed tree level Bhabha scattering at small scattering angles. Right: the leading VP effect in μe scattering.

A new project: measuring directly the low energy $\alpha(t)$

The possible direct measurement of $\Delta\alpha_{\rm had}(-Q^2)$ follows a very different strategy of evaluating the HVP contribution to the muon $g-2$. There is no VP subtraction issue, there is no exclusive channel separation and recombination, no issue of combining data from very different experiments and controlling correlations. Even a 1% level measurement can provide invaluable independent information. The recent proposal [75] to measure $\alpha(-Q^2)$ via $\mu^- e^-$-scattering (see right part of Fig. B.13) in the `MUonE` projects at CERN is very important for future precision physics. It is based on a cross section measurement

$$\frac{{\rm d}\sigma^{\rm unpol.}_{\mu^-{\rm e}^-\to\mu^-{\rm e}^-}}{{\rm dt}} = 4\pi\,\alpha(t)^2\,\frac{1}{\lambda(s,m_e^2,m_\mu^2)}\left\{\frac{\left(s-m_\mu^2-m_e^2\right)^2}{t^2}+\frac{s}{t}+\frac{1}{2}\right\}\,. \tag{1.22}$$

The primary goal of the project concerns the determination of $a_\mu^{\rm had}$ in an alternative way

$$a_\mu^{\rm had} = \frac{\alpha}{\pi}\int\limits_0^1 {\rm dx}\,(1-{\rm x})\,\Delta\alpha_{\rm had}\left(-{\rm Q}^2({\rm x})\right)\,, \tag{1.23}$$

where $Q^2(x) \equiv \frac{x^2}{1-x} m_\mu^2$ is the space-like square momentum-transfer and

$$\Delta\alpha_{\rm had}(-Q^2) = \frac{\alpha}{\alpha(-Q^2)} + \Delta\alpha_{\rm lep}(-Q^2) - 1 \tag{1.24}$$

directly compares with lattice QCD data and the offset $\alpha(-M_0^2)$ discussed before. We propose to determine very accurately $\Delta\alpha_{\rm had}\,(-Q^2)$ at $Q \approx 2.5$GeV by this method (one single number!) as the non-perturbative part of $\Delta\alpha_{\rm had}\,(M_Z^2)$ as needed in the "Adler-function approach". It also would be of direct use for a precise small angle Bhabha luminometer! Because of the high precision required accurate radiative corrections are mandatory and corresponding calculations are in progress [85–88].

1.7 Conclusions

Reducing the muon $g-2$ prediction uncertainty remains the key issue of high precision physics and strongly motivates more precise measurements of low energy $e^+e^- \to$ hadrons cross sections. Progress is expected from Novosibirsk (VEPP 2000/CMD3,SND), Beijing (BEPCII/BESIII) and Tsukuba (SuperKEKB/BelleII). This helps to improve $\alpha(t)$ in the region relevant for small angle Bhabha scattering and in calculating $\alpha(s)$ at FCC-ee/ILC energies via the Euclidean split-trick method. The latter method requires pQCD prediction of the Adler-function to improve by a factor 2. This also means that we need improved parameters, in particular, m_c and m_b.

One question remains to be asked: Are presently estimated and essentially agreed-on evaluations of $\Delta\alpha^{(5)}_{\rm had}(M_Z^2)$ in terms of R-data reliable? One has to keep in mind that the handling of systematic errors is rather an art than a science. Therefore alternative methods are very important and fortunately are under consideration.

Patrick Janot's approach certainly is an important alternative method directly accessing $\alpha(M_Z^2)$ with very different systematics. A challenging project.

Another interesting option is an improved radiative return measurement of $\sigma(e^+e^- \to$ hadrons) at the GigaZ, allowing for directly improving dispersion integral input, which would include all resonances and thresholds in one experiment!

In any case, on paper, $e^-\mu^+ \to e^-\mu^+$ looks to be the ideal process to perform an unambiguous measurement of $\alpha(-Q^2)$, which determines the LO HVP to a_μ as well as the non-perturbative part of $\alpha(s)$!

Lattice QCD results are very close to becoming competitive here as well. Thus, in the end, we will have alternatives available allowing for important improvements and crosschecks.

The improvement obtained by reducing the experimental error to 1% in the range from ϕ to 3 GeV would allow one to choose a higher cut point e.g. for $\sqrt{M_0} = 3.0$ GeV. One then can balance the importance of data vs. pQCD differently. This would provide further important consolidation of results. For a 3 GeV cut one gets $\Delta\alpha_{\rm had}(-M_0^2) = 82.21 \pm 0.88[0.38]$ in 10^{-4}. The QCD contribution is then smaller as well as safer because the mass effects that are responsible for the larger uncertainty of the pQCD prediction also gets substantially reduced. In view that a massive 4-loop QCD calculation is a challenge, the possibility to optimize the choice of split scale M_0 would be very useful. Therefore the ILC/FCC-ee community should actively support these activities as an integral part of e^+e^--collider precision physics program!

1.8 Addendum: the coupling α_2, M_W and $\sin^2\Theta_f$

Besides α also the $SU(2)$ gauge coupling $\alpha_2 = g^2/(4\pi)$ is running and thereby affected by non-perturbative hadronic effects [77, 89, 90]. Related with the $U_Y(1) \otimes SU_L(2)$ gauge couplings, is the running oft the weak mixing parameter $\sin^2\Theta_f$, which is actually defined by the ratio α/α_2. In [77,89,90] the hadronic effects have been evaluated by means of DRs in terms of e^+e^- data with appropriate flavor separation and reweighting. Commonly, a much simpler approach is adopted in studies of the running of $\sin^2\Theta_f$, namely by using pQCD with effective quark masses [91–94], which have been determined elsewhere.

Given $g \equiv g_2$ and the Higgs VEV v then $M_W^2 = \frac{g^2\,v^2}{4} = \frac{\pi\,\alpha_2}{\sqrt{2}\,G_\mu}$. The running $\sin^2\Theta_f(s)$ relates electromagnetic to weak neutral channel mixing at the LEP scale to low energy $\nu_e e$ scattering as

$$\sin^2\Theta_{\rm lep}(M_Z^2) = \left\{\frac{1-\Delta\alpha_2}{1-\Delta\alpha} + \Delta_{\nu_\mu e,\rm vertex+box} + \Delta\kappa_{e,\rm vertex}\right\}\sin^2\Theta_{\nu_\mu e}(0)\ . \tag{1.25}$$

The first correction from the running coupling ratio is largely compensated by the ν_μ charge-radius, which dominates the second term. The ratio $\sin^2\Theta_{\nu_\mu e}/\sin^2\Theta_{\rm lep}$ is close to 1.002, independent of top and Higgs mass. Note that errors in the ratio $\frac{1-\Delta\alpha_2}{1-\Delta\alpha}$ can be taken to be 100% correlated and thus largely cancel. A similar relation between $\sin^2\Theta_{\rm lep}(M_Z^2)$ and the weak mixing angle appearing in polarized Møller scattering asymmetries has been worked out in [91,92]. It includes specific bosonic contribution $\Delta\kappa_b(Q^2)$ such that

$$\kappa(s=-Q^2) = \frac{1-\Delta\alpha_2(s)}{1-\Delta\alpha(s)} + \Delta\kappa_b(Q^2) - \Delta\kappa_b(0) \tag{1.26}$$

where , in our low energy scheme, we require $\kappa(Q^2) = 1$ at $Q^2 = 0$. Explicitly [91,92], at 1-loop order

$$\begin{aligned}\Delta\kappa_b(Q^2) &= -\frac{\alpha}{2\pi\,s_W}\left\{-\frac{42\,c_W+1}{12}\,\ln c_W + \frac{1}{18} - \left(\frac{r}{2}\,\ln\xi - 1\right)\left[(7-4z)\,c_W\right.\right. \\ &\left.\left. + \frac{1}{6}\,(1+4z)\right] - z\left[\frac{3}{4} - z + \left(z-\frac{2}{3}\right)\,r\,\ln\xi + z\,(2-z)\,\ln^2\xi\right]\right\}, \end{aligned} \tag{1.27}$$

$$\Delta\kappa_b(0) = -\frac{\alpha}{2\pi\,s_W}\left\{-\frac{42\,c_W+1}{12}\,\ln c_W + \frac{1}{18} + \frac{6\,c_W+7}{18}\right\}, \tag{1.28}$$

with $z = M_W^2/Q^2$, $r = \sqrt{1+4z}$, $\xi = \frac{r+1}{r-1}$, $s_W = \sin^2\Theta_W$ and $c_W = \cos^2\Theta_W$. Results obtained in [91, 92] based on one-loop perturbation theory using light quark masses $m_u = m_d = m_s = 100$ MeV are compared with results obtained in our non-perturbative approach in Fig. B.17.

How to evaluate the leading non-perturbative hadronic corrections to α_2? Like in the case of α they are related to quark-loop contributions to gauge-boson self-energies (SE) $\gamma\gamma$, γZ, ZZ and WW, in particular those involving the photon, which exhibit large leading logarithms. In order to disentangle the leading corrections decompose the self-energy functions as follows ($s_\Theta^2 = e^2/g^2$; $c_\Theta^2 = 1 - s_\Theta^2$)

$$\begin{aligned}\Pi^{\gamma\gamma} &= e^2 \quad \hat\Pi^{\gamma\gamma}\,, \\ \Pi^{Z\gamma} &= \tfrac{eg}{c_\Theta} \quad \hat\Pi_V^{3\gamma} \quad - \quad \tfrac{e^2\,s_\Theta}{c_\Theta} \quad \hat\Pi_V^{\gamma\gamma}\,, \\ \Pi^{ZZ} &= \tfrac{g^2}{c_\Theta^2} \quad \hat\Pi_{V-A}^{33} \quad - \quad 2\,\tfrac{e^2}{c_\Theta^2} \quad \hat\Pi_V^{3\gamma} \quad + \quad \tfrac{e^2\,s_\Theta^2}{c_\Theta^2} \quad \hat\Pi_V^{\gamma\gamma}\,, \\ \Pi^{WW} &= g^2 \quad \hat\Pi_{V-A}^{+-}\,, \end{aligned} \tag{1.29}$$

with $\hat{\Pi}(s) = \hat{\Pi}(0) + s\,\Pi'(s)$, we find the leading hadronic corrections

$$\Delta\alpha^{(5)}_{\rm had}(s) = -e^2\left[{\rm Re}\Pi'^{\gamma\gamma}({\rm s}) - \Pi'^{\gamma\gamma}(0)\right], \tag{1.30}$$

$$\Delta\alpha^{(5)}_{2\,\rm had}(s) = -\frac{e^2}{s^2_\Theta}\left[{\rm Re}\Pi'^{3\gamma}({\rm s}) - \Pi'^{3\gamma}(0)\right], \tag{1.31}$$

which exhibit the leading hadronic non-perturbative parts, i.e. the ones involving the photon field via mixing. Besides $\Delta\alpha^{(5)}_{\rm had}(s)$ also $\Delta\alpha^{(5)}_{2\,\rm had}(s)$ can then be obtained in terms of e^+e^--data together with isospin flavor separation of (u,d) and s components

$$\Pi^{3\gamma}_{ud} = \frac{1}{2}\,\Pi^{\gamma\gamma}_{ud}\,;\;\; \Pi^{3\gamma}_{s} = \frac{3}{4}\,\Pi^{\gamma\gamma}_{s} \tag{1.32}$$

and for resonance contributions

$$\begin{aligned}\Pi^{\gamma\gamma} &= \Pi^{(\rho)} + \Pi^{(\omega)} + \Pi^{(\phi)} + \cdots\\ \Pi^{3\gamma} &= \frac{1}{2}\,\Pi^{(\rho)} + \frac{3}{4}\,\Pi^{(\phi)} + \cdots\end{aligned} \tag{1.33}$$

We remind that gauge-boson SE are potentially very sensitive to new physics (oblique corrections) and the discovery of what is missing in the SM may be obscured by non-perturbative hadronic effects. Therefore it is important to reduce the related uncertainties. Interestingly, flavor separation assuming OZI violating terms to be small implies a perturbative reweighting, which however has been shown to disagrees with lattice QCD results [95–98]! Indeed, the "wrong" perturbative flavor weighting

$$\Pi^{3\gamma}_{ud} = \frac{9}{20}\,\Pi^{\gamma\gamma}_{ud}\,;\;\; \Pi^{3\gamma}_{s} = \frac{3}{4}\,\Pi^{\gamma\gamma}_{s}$$

clearly mismatch lattice results, while the replacement $\frac{9}{20} \Rightarrow \frac{10}{20}$ is in good agreement. This also means the OZI suppressed contributions should be at the 5% level and not negligibly small. Actually, if we assume flavor $SU(3)$ symmetry to be an acceptable approximation one obtains

$$\Pi^{3\gamma}_{uds} = \frac{1}{2}\,\Pi^{\gamma\gamma}_{uds}\,,$$

which does not require any flavor separation in the *uds*-sector, i.e. up to the charm threshold at about 3.1 GeV. The Fig. B.15 shows a lattice QCD test of two flavor separation schemes. One labeled "$SU(2)$" denotes the perturbative reweighting advocated in [91–94] and the other one labeled "$SU(3)$" represents the one proposed in [89]. Lattice data clearly disprove pQCD reweighting for the *uds*-sector! This also shows that pQCD-type predictions based on effective quark masses cannot be accurate. This criticism also applies in cases where the effective quark masses have been obtained by fitting $\Delta\alpha^{(5)}_{\rm had}(s)$. Even more so when constituent quark masses are used.

The updated $\sin^2\Theta_W(s)$ is shown in Fig. B.17 for time-like as well as for space-like momentum transfer. Note that $\sin^2\Theta_W(0)/\sin^2\Theta_W(M_Z^2) = 1.02876$ a 3% correction is established at 6.5 σ. Except for the LEP and SLD points (which deviate by 1.8 σ), all existing measurements are of rather limited accuracy, unfortunately. Upcoming experiments will improve results at low space-like Q substantially. We remind that $\sin^2\Theta_{\ell\,\rm eff}$ exhibiting a specific dependence on the gauge boson self-energies is an excellent monitor for New Physics. At pre-LHC times it has

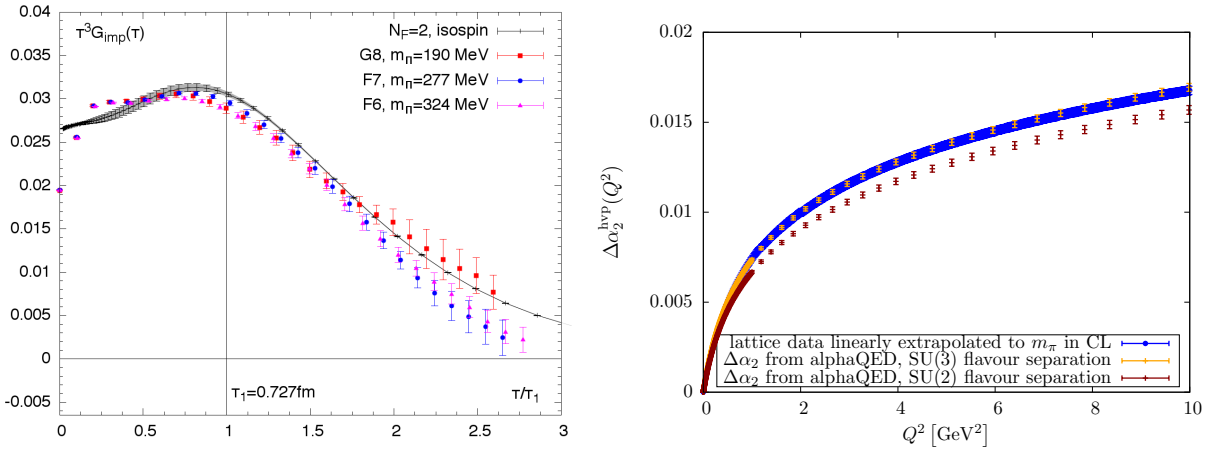

Fig. B.15: Testing flavor separation in lattice QCD. Left: a rough test by checking the Euclidean time correlators clearly favors the flavor separation of (1.33) [95–97], while the pQCD reweighting (not displayed) badly fails. Right: the renormalized photon self-energy at Euclidean Q^2 [98] is in good agreement with the flavor $SU(3)$ limit, while again it fails with the $SU(2)$ case which coincides with perturbative reweighting.

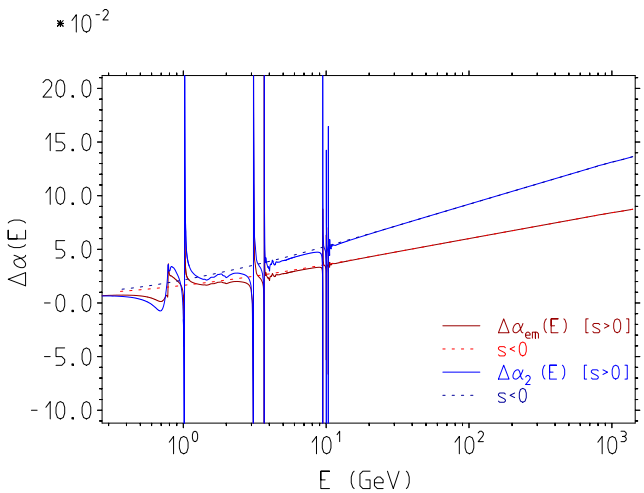

Fig. B.16: $\Delta\alpha_{\rm QED}(E)$ and $\Delta\alpha_2(E)$ as functions of energy E in the time-like and space-like domain. The smooth space-like correction (dashed line) agrees rather well with the non-resonant "background" above the ϕ-resonance (kind of duality). In resonance regions as expected "agreement" is observed in the mean, with huge local deviations.

been the predestinated monitor for virtual Higgs particle effects and a corresponding limiter for the Higgs boson mass.

Acknowledgments

I would like to thank Janusz Gluza and the organizing committee for the invitation to this workshop and for support. Thanks also to Maurice Benayoun, Simon Eidelman and Graziano Venanzoni for collaboration and many useful discussions on the topics presented here.

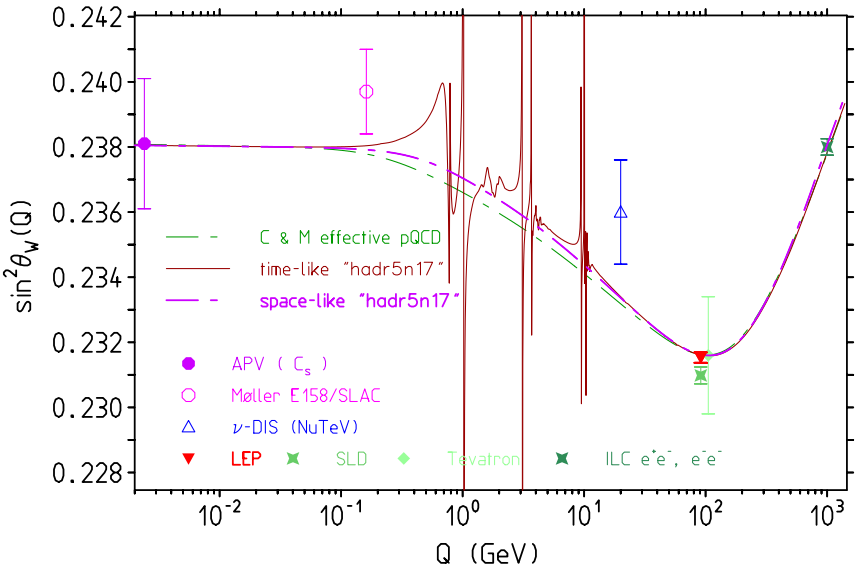

Fig. B.17: $\sin^2\Theta_W(Q)$ as a function of Q in the time-like and space-like region. Hadronic uncertainties are included but barely visible in this plot. Uncertainties from the input parameter $\sin^2\Theta_W(0) = 0.23822(100)$ or $\sin^2\Theta_W(M_Z^2) = 0.23153(16)$ are not shown. Note the substantial difference from applying pQCD with effective quark masses. Future FCC-ee/ILC measurements at 1 TeV would be sensitive to Z', H^{--} etc.

References

[1] T. Hambye, K. Riesselmann, Matching conditions and Higgs mass upper bounds revisited, Phys. Rev. D55 (1997) 7255–7262. arXiv:hep-ph/9610272, doi:10.1103/PhysRevD.55.7255.

[2] F. Jegerlehner, M. Yu. Kalmykov, B. A. Kniehl, On the difference between the pole and the $\overline{MS}$ masses of the top quark at the electroweak scale, Phys. Lett. B722 (2013) 123–129. arXiv:1212.4319, doi:10.1016/j.physletb.2013.04.012.

[3] F. Jegerlehner, The Standard model as a low-energy effective theory: what is triggering the Higgs mechanism?, Acta Phys. Polon. B45 (6) (2014) 1167. arXiv:1304.7813, doi:10.5506/APhysPolB.45.1167.

[4] F. Jegerlehner, Higgs inflation and the cosmological constant, Acta Phys. Polon. B45 (6) (2014) 1215. arXiv:1402.3738, doi:10.5506/APhysPolB.45.1215.

[5] F. Jegerlehner, M. Yu. Kalmykov, B. A. Kniehl, Self-consistence of the Standard Model via the renormalization group analysis, J. Phys. Conf. Ser. 608 (1) (2015) 012074. arXiv:1412.4215, doi:10.1088/1742-6596/608/1/012074.

[6] F. Bezrukov, M. Yu. Kalmykov, B. A. Kniehl, M. Shaposhnikov, Higgs Boson Mass and New Physics, JHEP 10 (2012) 140, [,275(2012)]. arXiv:1205.2893, doi:10.1007/JHEP10(2012)140.

[7] G. Degrassi, S. Di Vita, J. Elias-Miro, J. R. Espinosa, G. F. Giudice, G. Isidori, A. Strumia, Higgs mass and vacuum stability in the Standard Model at NNLO, JHEP 08 (2012) 098. arXiv:1205.6497, doi:10.1007/JHEP08(2012)098.

[8] J. S. Mackenzie, Evolution and ethics. thomas h. huxley, The International Journal of Ethics 4 (1) (1893) 126–127. arXiv:https://doi.org/10.1086/intejethi.4.1.2375721, doi:10.1086/intejethi.4.1.2375721.

URL https://doi.org/10.1086/intejethi.4.1.2375721

[9] R. R. Akhmetshin, et al., Reanalysis of hadronic cross-section measurements at CMD-2, Phys. Lett. B578 (2004) 285–289. arXiv:hep-ex/0308008, doi:10.1016/j.physletb.2003.10.108.

[10] V. M. Aul'chenko, et al., Measurement of the pion form-factor in the range 1.04 GeV to 1.38 GeV with the CMD-2 detector, JETP Lett. 82 (2005) 743–747, [Pisma Zh. Eksp. Teor. Fiz.82,841(2005)]. arXiv:hep-ex/0603021, doi:10.1134/1.2175241.

[11] V. M. Aul'chenko, et al., Measurement of the $e^+e^- \to \pi^+\pi^-$ cross section with the CMD-2 detector in the 370 - 520-MeV c.m. energy range, JETP Lett. 84 (2006) 413–417, [Pisma Zh. Eksp. Teor. Fiz.84,491(2006)]. arXiv:hep-ex/0610016, doi:10.1134/S0021364006200021.

[12] R. R. Akhmetshin, et al., High-statistics measurement of the pion form factor in the rho-meson energy range with the CMD-2 detector, Phys. Lett. B648 (2007) 28–38. arXiv:hep-ex/0610021, doi:10.1016/j.physletb.2007.01.073.

[13] M. N. Achasov, et al., Update of the $e^+e^- \to \pi^+\pi^-$ cross-section measured by SND detector in the energy region 400 MeV $< s^{1/2} <$ 1000 MeV, J. Exp. Theor. Phys. 103 (2006) 380–384, [Zh. Eksp. Teor. Fiz.130,437(2006)]. arXiv:hep-ex/0605013, doi:10.1134/S106377610609007X.

[14] A. Aloisio, et al., Measurement of $\sigma(e^+e^- \to \pi^+\pi^-\gamma)$ and extraction of $\sigma(e^+e^- \to \pi^+\pi^-)$ below 1 GeV with the KLOE detector, Phys. Lett. B606 (2005) 12–24. arXiv:hep-ex/0407048, doi:10.1016/j.physletb.2004.11.068.

[15] F. Ambrosino, et al., Measurement of $\sigma(e^+e^- \to \pi^+\pi^-\gamma(\gamma)$ and the dipion contribution to the muon anomaly with the KLOE detector, Phys. Lett. B670 (2009) 285–291. arXiv:0809.3950, doi:10.1016/j.physletb.2008.10.060.

[16] F. Ambrosino, et al., Measurement of $\sigma(e^+e^- \to \pi^+\pi^-)$ from threshold to 0.85 GeV^2 using Initial State Radiation with the KLOE detector, Phys. Lett. B700 (2011) 102–110. arXiv:1006.5313, doi:10.1016/j.physletb.2011.04.055.

[17] D. Babusci, et al., Precision measurement of $\sigma(e^+e^- \to \pi^+\pi^-\gamma)/\sigma(e^+e^- \to \mu^+\mu^-\gamma)$ and determination of the $\pi^+\pi^-$ contribution to the muon anomaly with the KLOE detector, Phys. Lett. B720 (2013) 336–343. arXiv:1212.4524, doi:10.1016/j.physletb.2013.02.029.

[18] A. Anastasi, et al., Combination of KLOE $\sigma\left(e^+e^- \to \pi^+\pi^-\gamma(\gamma)\right)$ measurements and determination of $a_\mu^{\pi^+\pi^-}$ in the energy range $0.10 < s < 0.95$ GeV^2, JHEP 03 (2018) 173. arXiv:1711.03085, doi:10.1007/JHEP03(2018)173.

[19] G. Venanzoni, From Hadronic Cross Section to the measurement of the Vacuum Polarization at KLOE: a fascinating endeavour, EPJ Web Conf. 166 (2018) 00021. arXiv:1705.10365, doi:10.1051/epjconf/201816600021.

[20] B. Aubert, et al., Precise measurement of the $e^+e^- \to \pi^+\pi^-(\gamma)$ cross section with the Initial State Radiation method at BABAR, Phys. Rev. Lett. 103 (2009) 231801. arXiv:0908.3589, doi:10.1103/PhysRevLett.103.231801.

[21] J. P. Lees, et al., Precise Measurement of the $e^+e^- \to \pi^+\pi^-(\gamma)$ Cross Section with the Initial-State Radiation Method at BABAR, Phys. Rev. D86 (2012) 032013. arXiv:1205.2228, doi:10.1103/PhysRevD.86.032013.

[22] M. Ablikim, et al., Measurement of the $e^+e^- \to \pi^+\pi^-$ cross section between 600 and 900 MeV using initial state radiation, Phys. Lett. B753 (2016) 629–638. arXiv:1507.08188,

doi:10.1016/j.physletb.2015.11.043.

[23] T. Xiao, S. Dobbs, A. Tomaradze, K. K. Seth, G. Bonvicini, Precision Measurement of the Hadronic Contribution to the Muon Anomalous Magnetic Moment, Phys. Rev. D97 (3) (2018) 032012. arXiv:1712.04530, doi:10.1103/PhysRevD.97.032012.

[24] B. Aubert, et al., Study of $e^+e^- \to \pi^+\pi^-\pi^0$ process using initial state radiation with BaBar, Phys. Rev. D70 (2004) 072004. arXiv:hep-ex/0408078, doi:10.1103/PhysRevD.70.072004.

[25] B. Aubert, et al., The $e^+e^- \to \pi^+\pi^-\pi^+\pi^-$, $K^+K^-\pi^+\pi^-$, and $K^+K^-K^+K^-$ cross sections at center-of-mass energies 0.5 GeV - 4.5 GeV measured with initial-state radiation, Phys. Rev. D71 (2005) 052001. arXiv:hep-ex/0502025, doi:10.1103/PhysRevD.71.052001.

[26] B. Aubert, et al., A Study of $e^+e^- \to p\bar{p}$ using initial state radiation with BABAR, Phys. Rev. D73 (2006) 012005. arXiv:hep-ex/0512023, doi:10.1103/PhysRevD.73.012005.

[27] B. Aubert, et al., The $e^+e^- \to 3(\pi^+\pi^-), 2(\pi^+\pi^-\pi^0)$ and $K^+K^-2(\pi^+\pi^-)$ cross sections at center-of-mass energies from production threshold to 4.5 GeV measured with initial-state radiation, Phys. Rev. D73 (2006) 052003. arXiv:hep-ex/0602006, doi:10.1103/PhysRevD.73.052003.

[28] B. Aubert, et al., The $e^+e^- \to 2(\pi^+\pi^-)\pi^0$, $2(\pi^+\pi^-)\eta$, $K^+K^-\pi^+\pi^-\pi^0$ and $K^+K^-\pi^+\pi^-\eta$ Cross Sections Measured with Initial-State Radiation, Phys. Rev. D76 (2007) 092005, [Erratum: Phys. Rev.D77,119902(2008)]. arXiv:0708.2461, doi:10.1103/PhysRevD.77.119902,10.1103/PhysRevD.76.092005.

[29] B. Aubert, et al., Measurements of $e^+e^- \to K^+K^-\eta$, $K^+K^-\pi^0$ and $K^0_sK^\pm\pi^\mp$ cross- sections using initial state radiation events, Phys. Rev. D77 (2008) 092002. arXiv:0710.4451, doi:10.1103/PhysRevD.77.092002.

[30] J. P. Lees, et al., Initial-State Radiation Measurement of the $e^+e^- \to \pi^+\pi^-\pi^+\pi^-$ Cross Section, Phys. Rev. D85 (2012) 112009. arXiv:1201.5677, doi:10.1103/PhysRevD.85.112009.

[31] J. P. Lees, et al., Cross Sections for the Reactions $e^+e^- \to K^+K^-\pi^+\pi^-$, $K^+K^-\pi^0\pi^0$, and $K^+K^-K^+K^-$ Measured Using Initial-State Radiation Events, Phys. Rev. D86 (2012) 012008. arXiv:1103.3001, doi:10.1103/PhysRevD.86.012008.

[32] J. P. Lees, et al., Study of $e^+e^- \to p\bar{p}$ via initial-state radiation at BABAR, Phys. Rev. D87 (9) (2013) 092005. arXiv:1302.0055, doi:10.1103/PhysRevD.87.092005.

[33] J. P. Lees, et al., Precision measurement of the $e^+e^- \to K^+K^-(\gamma)$ cross section with the initial-state radiation method at BABAR, Phys. Rev. D88 (3) (2013) 032013. arXiv:1306.3600, doi:10.1103/PhysRevD.88.032013.

[34] J. P. Lees, et al., Cross sections for the reactions $e^+e^- \to K^0_SK^0_L$, $K^0_SK^0_L\pi^+\pi^-$, $K^0_SK^0_S\pi^+\pi^-$, and $K^0_SK^0_SK^+K^-$ from events with initial-state radiation, Phys. Rev. D89 (9) (2014) 092002. arXiv:1403.7593, doi:10.1103/PhysRevD.89.092002.

[35] J. P. Lees, et al., Study of the reactions $e^+e^- \to \pi^+\pi^-\pi^0\pi^0\pi^0\gamma$ and $\pi^+\pi^-\pi^0\pi^0\eta\gamma$ at center-of-mass energies from threshold to 4.35 GeV using initial-state radiation, Phys. Rev. D98 (11) (2018) 112015. arXiv:1810.11962, doi:10.1103/PhysRevD.98.112015.

[36] M. Davier, e^+e^- results from BABAR and their impact on the muon $g-2$ prediction, Nucl. Part. Phys. Proc. 260 (2015) 102–106. doi:10.1016/j.nuclphysbps.2015.02.021.

[37] M. Davier, A. Hoecker, B. Malaescu, Z. Zhang, Hadron Contribution to Vacuum Polarisation, Adv. Ser. Direct. High Energy Phys. 26 (2016) 129–144. doi:10.1142/9789814733519_0007.

[38] R. R. Akhmetshin, et al., Study of the process $e^+e^- \to 3(\pi^+\pi^-)$ in the c.m.energy range 1.5–2.0 gev with the cmd-3 detector, Phys. Lett. B723 (2013) 82–89. arXiv:1302.0053, doi:10.1016/j.physletb.2013.04.065.

[39] R. R. Akhmetshin, et al., Study of the process $e^+e^- \to p\bar{p}$ in the c.m. energy range from threshold to 2 GeV with the CMD-3 detector, Phys. Lett. B759 (2016) 634–640. arXiv:1507.08013, doi:10.1016/j.physletb.2016.04.048.

[40] E. A. Kozyrev, et al., Study of the process $e^+e^- \to K^0_S K^0_L$ in the center-of-mass energy range 1004–1060 MeV with the CMD-3 detector at the VEPP-2000 e^+e^- collider, Phys. Lett. B760 (2016) 314–319. arXiv:1604.02981, doi:10.1016/j.physletb.2016.07.003.

[41] M. N. Achasov, et al., Study of the process $e^+e^- \to n\bar{n}$ at the VEPP-2000 e^+e^- collider with the SND detector, Phys. Rev. D90 (11) (2014) 112007. arXiv:1410.3188, doi:10.1103/PhysRevD.90.112007.

[42] V. M. Aulchenko, et al., Measurement of the $e^+e^- \to \eta\pi^+\pi^-$ cross section in the center-of-mass energy range 1.22-2.00 GeV with the SND detector at the VEPP-2000 collider, Phys. Rev. D91 (5) (2015) 052013. arXiv:1412.1971, doi:10.1103/PhysRevD.91.052013.

[43] M. N. Achasov, et al., Study of the reaction $e^+e^- \to \pi^0\gamma$ with the SND detector at the VEPP-2M collider, Phys. Rev. D93 (9) (2016) 092001. arXiv:1601.08061, doi:10.1103/PhysRevD.93.092001.

[44] M. N. Achasov, et al., Study of the process $e^+e^- \to \omega\eta\pi^0$ in the energy range $\sqrt{s} < 2$ GeV with the SND detector, Phys. Rev. D94 (3) (2016) 032010. arXiv:1606.06481, doi:10.1103/PhysRevD.94.032010.

[45] M. N. Achasov, et al., Measurement of the $e^+e^- \to \omega\eta$ cross section below $\sqrt{s} = 2$ GeV, Phys. Rev. D94 (9) (2016) 092002. arXiv:1607.00371, doi:10.1103/PhysRevD.94.092002.

[46] M. N. Achasov, et al., Measurement of the $e^+e^- \to K^+K^-$ cross section in the energy range $\sqrt{s} = 1.05 - 2.0$ GeV, Phys. Rev. D94 (11) (2016) 112006. arXiv:1608.08757, doi:10.1103/PhysRevD.94.112006.

[47] M. N. Achasov, et al., Updated measurement of the $e^+e^- \to \omega\pi^0 \to \pi^0\pi^0\gamma$ cross section with the SND detector, Phys. Rev. D94 (11) (2016) 112001. arXiv:1610.00235, doi:10.1103/PhysRevD.94.112001.

[48] J. Z. Bai, et al., Measurement of the total cross-section for hadronic production by e^+e^- annihilation at energies between 2.6 GeV - 5 GeV, Phys. Rev. Lett. 84 (2000) 594–597. arXiv:hep-ex/9908046, doi:10.1103/PhysRevLett.84.594.

[49] J. Z. Bai, et al., Measurements of the cross-section for e^+e^- → hadrons at center-of-mass energies from 2 GeV to 5 GeV, Phys. Rev. Lett. 88 (2002) 101802. arXiv:hep-ex/0102003, doi:10.1103/PhysRevLett.88.101802.

[50] M. Ablikim, et al., R value measurements for e^+e^- annihilation at 2.60 GeV, 3.07 GeV and 3.65 GeV, Phys. Lett. B677 (2009) 239–245. arXiv:0903.0900, doi:10.1016/j.physletb.2009.05.055.

[51] V. V. Anashin, et al., Measurement of $R_{\rm uds}$ and R between 3.12 and 3.72 GeV at the KEDR detector, Phys. Lett. B753 (2016) 533–541. arXiv:1510.02667, doi:10.1016/j.physletb.2015.12.059.

[52] V. V. Anashin, et al., Measurement of R between 1.84 and 3.05 GeV at the KEDR detector, Phys. Lett. B770 (2017) 174–181. arXiv:1610.02827, doi:10.1016/j.physletb.2017.04.073.

[53] R. V. Harlander, M. Steinhauser, rhad: A Program for the evaluation of the hadronic R ratio in the perturbative regime of QCD, Comput. Phys. Commun. 153 (2003) 244–274. arXiv:hep-ph/0212294, doi:10.1016/S0010-4655(03)00204-2.

[54] S. Eidelman, F. Jegerlehner, Hadronic contributions to $g-2$ of the leptons and to the effective fine structure constant $\alpha(M_Z^2)$, Z. Phys. C67 (1995) 585–602. arXiv:hep-ph/9502298, doi:10.1007/BF01553984.

[55] M. Davier, A. Hoecker, B. Malaescu, Z. Zhang, Reevaluation of the hadronic vacuum polarisation contributions to the Standard Model predictions of the muon $g-2$ and $\alpha(m_Z^2)$ using newest hadronic cross-section data, Eur. Phys. J. C77 (12) (2017) 827. arXiv:1706.09436, doi:10.1140/epjc/s10052-017-5161-6.

[56] A. Maier, P. Marquard, Validity of Padé approximations in vacuum polarization at three- and four-loop order, Phys. Rev. D97 (5) (2018) 056016. arXiv:1710.03724, doi:10.1103/PhysRevD.97.056016.

[57] F. Jegerlehner, Leading-order hadronic contribution to the electron and muon $g-2$, EPJ Web Conf. 118 (2016) 01016. arXiv:1511.04473, doi:10.1051/epjconf/201611801016.

[58] A. Anastasi, et al., Measurement of the running of the fine structure constant below 1 GeV with the KLOE Detector, Phys. Lett. B767 (2017) 485–492. arXiv:1609.06631, doi:10.1016/j.physletb.2016.12.016.

[59] S. L. Adler, Some Simple Vacuum Polarization Phenomenology: $e^+e^- \to$ Hadrons: The μ - Mesic Atom x-Ray Discrepancy and $g_\mu - 2$, Phys. Rev. D10 (1974) 3714, [,445(1974)]. doi:10.1103/PhysRevD.10.3714.

[60] S. Eidelman, F. Jegerlehner, A. L. Kataev, O. Veretin, Testing nonperturbative strong interaction effects via the Adler function, Phys. Lett. B454 (1999) 369–380. arXiv:hep-ph/9812521, doi:10.1016/S0370-2693(99)00389-5.

[61] F. Jegerlehner, Hadronic effects in $(g-2)_\mu$ and $\alpha_{\rm QED}(M_Z^2)$: Status and perspectives, in: Radiative corrections: Application of quantum field theory to phenomenology. Proceedings, 4th International Symposium, RADCOR'98, Barcelona, Spain, September 8-12, 1998, 1999, pp. 75–89. arXiv:hep-ph/9901386.

[62] F. Jegerlehner, Hadronic vacuum polarization effects in $\alpha_{\rm em}(M_Z^2)$, in: Electroweak precision data and the Higgs mass. Proceedings, Workshop, Zeuthen, Germany, February 28-March 1, 2003, 2003, pp. 97–112. arXiv:hep-ph/0308117.

[63] F. Jegerlehner, The Running fine structure constant $\alpha(E)$ via the Adler function, Nucl. Phys. Proc. Suppl. 181-182 (2008) 135–140. arXiv:0807.4206, doi:10.1016/j.nuclphysbps.2008.09.010.

[64] M. Benayoun, P. David, L. DelBuono, F. Jegerlehner, Muon $g-2$ estimates: can one trust effective Lagrangians and global fits?, Eur. Phys. J. C75 (12) (2015) 613. arXiv:1507.02943, doi:10.1140/epjc/s10052-015-3830-x.

[65] M. Benayoun, L. DelBuono, F. Jegerlehner, BHLS$_2$, a New Breaking of the HLS Model and its PhenomenologyarXiv:1903.11034.

[66] F. Jegerlehner, O. V. Tarasov, Exact mass dependent two loop $\bar{\alpha}(s)(Q^2)$ in the background MOM renormalization scheme, Nucl. Phys. B549 (1999) 481–498. arXiv:hep-ph/9809485, doi:10.1016/S0550-3213(99)00141-8.

[67] K. G. Chetyrkin, J. H. Kühn, M. Steinhauser, Three loop polarization function and $O(\alpha_s^2)$ corrections to the production of heavy quarks, Nucl. Phys. B482 (1996) 213–240. arXiv:hep-ph/9606230, doi:10.1016/S0550-3213(96)00534-2.

[68] K. G. Chetyrkin, R. Harlander, J. H. Kühn, M. Steinhauser, Mass corrections to the vector current correlator, Nucl. Phys. B503 (1997) 339–353. arXiv:hep-ph/9704222, doi:10.1016/S0550-3213(97)00383-0.

[69] K. G. Chetyrkin, J. H. Kühn, M. Steinhauser, Heavy quark current correlators to $O(\alpha_s^2)$, Nucl. Phys. B505 (1997) 40–64. arXiv:hep-ph/9705254, doi:10.1016/S0550-3213(97)00481-1.

[70] M. A. Shifman, A. I. Vainshtein, V. I. Zakharov, QCD and Resonance Physics. Theoretical Foundations, Nucl. Phys. B147 (1979) 385–447. doi:10.1016/0550-3213(79)90022-1.

[71] M. A. Shifman, A. I. Vainshtein, V. I. Zakharov, QCD and Resonance Physics: Applications, Nucl. Phys. B147 (1979) 448–518. doi:10.1016/0550-3213(79)90023-3.

[72] D. V. Shirkov, I. L. Solovtsov, Analytic model for the QCD running coupling with universal $\alpha_s(0)$ value, Phys. Rev. Lett. 79 (1997) 1209–1212. arXiv:hep-ph/9704333, doi:10.1103/PhysRevLett.79.1209.

[73] M. Bruno, M. Dalla Brida, P. Fritzsch, T. Korzec, A. Ramos, S. Schaefer, H. Simma, S. Sint, R. Sommer, QCD Coupling from a Nonperturbative Determination of the Three-Flavor Λ Parameter, Phys. Rev. Lett. 119 (10) (2017) 102001. arXiv:1706.03821, doi:10.1103/PhysRevLett.119.102001.

[74] M. Steinhauser, Leptonic contribution to the effective electromagnetic coupling constant up to three loops, Phys. Lett. B429 (1998) 158–161. arXiv:hep-ph/9803313, doi:10.1016/S0370-2693(98)00503-6.

[75] G. Abbiendi, et al., Measuring the leading hadronic contribution to the muon g-2 via μe scattering, Eur. Phys. J. C77 (3) (2017) 139. arXiv:1609.08987, doi:10.1140/epjc/s10052-017-4633-z.

[76] A. Keshavarzi, D. Nomura, T. Teubner, Muon $g-2$ and $\alpha(M_Z^2)$: a new data-based analysis, Phys. Rev. D97 (11) (2018) 114025. arXiv:1802.02995, doi:10.1103/PhysRevD.97.114025.

[77] F. Jegerlehner, Variations on Photon Vacuum Polarization, arXiv:1711.06089.

[78] P. Janot, Direct measurement of $\alpha_{QED}(m_Z^2)$ at the FCC-ee, JHEP 02 (2016) 053, [Erratum: JHEP11,164(2017)]. arXiv:1512.05544, doi:10.1007/JHEP02(2016)053,10.1007/JHEP11(2017)164.

[79] A. Blondel, et al., Standard Model Theory for the FCC-ee: The Tera-Z, in: Mini Workshop on Precision EW and QCD Calculations for the FCC Studies : Methods and Tools, CERN, Geneva, Switzerland, January 12-13, 2018, 2018, p. 243pp. arXiv:1809.01830.

[80] I. Dubovyk, A. Freitas, J. Gluza, T. Riemann, J. Usovitsch, Complete electroweak two-loop corrections to Z boson production and decay, Phys. Lett. B783 (2018) 86–94. arXiv:1804.10236, doi:10.1016/j.physletb.2018.06.037.

[81] P. Azzurri, et al., Physics Behind Precision, arXiv:1703.01626.

[82] S. Jadach, W. Płaczek, M. Skrzypek, B. F. L. Ward, S. A. Yost, The path to 0.01% theoretical luminosity precision for the FCC-ee, Phys. Lett. B790 (2019) 314–321. arXiv:1812.01004, doi:10.1016/j.physletb.2019.01.012.

[83] S. Jadach, et al., Event generators for Bhabha scattering, in: CERN Workshop on LEP2 Physics (followed by 2nd meeting, 15-16 Jun 1995 and 3rd meeting 2-3 Nov 1995) Geneva, Switzerland, February 2-3, 1995, 1996, pp. 229–298. arXiv:hep-ph/9602393.

[84] A. Arbuzov, et al., The Present theoretical error on the Bhabha scattering cross-section in the luminometry region at LEP, Phys. Lett. B383 (1996) 238–242. arXiv:hep-ph/

9605239, doi:10.1016/0370-2693(96)00733-2.

[85] P. Mastrolia, M. Passera, A. Primo, U. Schubert, Master integrals for the NNLO virtual corrections to μe scattering in QED: the planar graphs, JHEP 11 (2017) 198. arXiv:1709.07435, doi:10.1007/JHEP11(2017)198.

[86] S. Di Vita, S. Laporta, P. Mastrolia, A. Primo, U. Schubert, Master integrals for the NNLO virtual corrections to μe scattering in QED: the non-planar graphs, JHEP 09 (2018) 016. arXiv:1806.08241, doi:10.1007/JHEP09(2018)016.

[87] M. Fael, Hadronic corrections to μ-e scattering at NNLO with space-like data, JHEP 02 (2019) 027. arXiv:1808.08233, doi:10.1007/JHEP02(2019)027.

[88] M. Alacevich, C. M. Carloni Calame, M. Chiesa, G. Montagna, O. Nicrosini, F. Piccinini, Muon-electron scattering at NLO, JHEP 02 (2019) 155. arXiv:1811.06743, doi:10.1007/JHEP02(2019)155.

[89] F. Jegerlehner, Hadronic Contributions to Electroweak Parameter Shifts: A Detailed Analysis, Z. Phys. C32 (1986) 195. doi:10.1007/BF01552495.

[90] F. Jegerlehner, Electroweak effective couplings for future precision experiments, Nuovo Cim. C034S1 (2011) 31–40. arXiv:1107.4683, doi:10.1393/ncc/i2011-11011-0.

[91] A. Czarnecki, W. J. Marciano, Electroweak radiative corrections to polarized Møller scattering asymmetries, Phys. Rev. D53 (1996) 1066–1072. arXiv:hep-ph/9507420, doi:10.1103/PhysRevD.53.1066.

[92] A. Czarnecki, W. J. Marciano, Polarized Møller scattering asymmetries, Int. J. Mod. Phys. A15 (2000) 2365–2376. arXiv:hep-ph/0003049, doi:10.1016/S0217-751X(00)00243-0, 10.1142/S0217751X00002433.

[93] J. Erler, M. J. Ramsey-Musolf, The Weak mixing angle at low energies, Phys. Rev. D72 (2005) 073003. arXiv:hep-ph/0409169, doi:10.1103/PhysRevD.72.073003.

[94] J. Erler, R. Ferro-Hernández, Weak Mixing Angle in the Thomson Limit, JHEP 03 (2018) 196. arXiv:1712.09146, doi:10.1007/JHEP03(2018)196.

[95] D. Bernecker, H. B. Meyer, Vector Correlators in Lattice QCD: Methods and applications, Eur. Phys. J. A47 (2011) 148. arXiv:1107.4388, doi:10.1140/epja/i2011-11148-6.

[96] A. Francis, G. von Hippel, H. B. Meyer, F. Jegerlehner, Vector correlator and scale determination in lattice QCD, PoS LATTICE2013 (2013) 320. arXiv:1312.0035, doi:10.22323/1.187.0320.

[97] M. Cè, A. Gérardin, K. Ottnad, H. B. Meyer, The leading hadronic contribution to the running of the Weinberg angle using covariant coordinate-space methods, PoS LATTICE2018 (2018) 137. arXiv:1811.08669.

[98] F. Burger, K. Jansen, M. Petschlies, G. Pientka, Leading hadronic contributions to the running of the electroweak coupling constants from lattice QCD, JHEP 11 (2015) 215. arXiv:1505.03283, doi:10.1007/JHEP11(2015)215.

2 Precision Quantum Chromodynamics

Author: David d'Enterria [dde@cern.ch]

The unprecedentedly small experimental uncertainties expected in the electron-positron measurements at the FCC-ee, key to searches for physics beyond the SM up to $\Lambda \approx 50$ TeV, impose exquisitely precise calculations for the corresponding theoretical observables. At the level of theoretical precision required to match that of the FCC-ee experimental measurements, the current relevant QCD uncertainties have to be reduced at least in four different levels:

1. Purely theoretical perturbative uncertainties from missing higher-order (HO) corrections in perturbative QCD (pQCD) calculations of e^+e^- scattering amplitudes and decay processes involving multiple real emissions and/or virtual exchanges of quarks and gluons. Such fixed-order (FO) corrections include pure-QCD, and mixed QCD-QED or QCD-weak terms. Reducing such uncertainties, requires pQCD calculations beyond the state-of-the-art today given often by next-to-next-to-leading order (NNLO) accuracy, pure or mixed with higher-order electroweak terms.

2. Theoretical uncertainties due to incomplete logarithmic resummations of different energy scales potentially appearing in the theoretical calculations. Examples include resummations of (i) soft and collinear logs in final states dominated by jets –either in analytical calculations or (only partially) incorporated into matched parton shower Monte Carlo generators– and (ii) logarithmic terms in the velocity of the produced top quarks in $e^+e^- \to t\bar{t}$ cross sections. Reducing such uncertainties, requires calculations beyond the state-of-the-art today given often by the next-to-next-to-leading-log (NNLL) accuracy.

3. Parametric uncertainties propagated into the final theoretical result due to the dependence of the calculation on the input values of (i) the QCD coupling at the Z pole scale, $\alpha_s(m_Z)$, known today with a relatively poor $\pm 0.9\%$ precision, and (ii) the heavy-quark (charm and bottom) masses m_c and m_b. Theoretical progress in lattice QCD determinations of α_s and $m_{c,b}$ is needed, complemented with much more precise experimental measurements. A permille extraction of $\alpha_s(m_Z)$ is thereby also one of the key axis of the FCC-ee physics programme [1].

4. Non-perturbative uncertainties from final-state hadronic effects linked to power-suppressed infrared phenomena, such as colour reconnection, hadronization, and multi-particle correlations (in spin, colour, space, momenta), that cannot be currently computed from first-principles QCD theory, and that often rely on phenomenological Monte Carlo models. The high precision study of parton hadronization and other non-pQCD phenomena is also an intrinsic part of the FCC-ee physics programme [2].

The examples of key observables where such four sources of QCD uncertainty will have an impact at the FCC-ee, are numerous:

1. Uncertainties from missing HO terms are non-negligible in theoretical predictions for ElectroWeak Precision Observables (EWPOs) at the Z pole, WW and $t\bar{t}$ cross sections, (N)MSSM Higgs cross sections and decays, etc.

2. Uncertainties from missing soft and collinear log resummations, in analytical calculations or in parton shower MC generators, impact all e^+e^- final states with jets – e.g., the

accurate extraction of forward-backward quark asymmetries at the Z pole– as well as precision flavour physics studies via B-meson decays. Similarly, the size of the NNLL corrections (in the $\ln v$ top quark velocity) appears to be as large as that from the FO N^{3}LO terms in $e^+e^- \to t\bar{t}$ cross section calculations.

3. The $\alpha_s(m_Z)$ parametric uncertainty has a significant effect on the determination of all top properties (m_{top}, λ_{top} , Γ_{top}), all hadronic Higgs decay widths ($H \to c\bar{c}, b\bar{b}, q\bar{q}, g\,g$) and associated Yukawa couplings, as well as on the extraction of other similarly crucial SM parameters (m_c, m_b, α_{QED}).

4. Non-perturbative uncertainties, in particular colour reconnection and hadronization effects, impact hadronic final states in $e^+e^- \to WW$ and $e^+e^- \to t\bar{t}$, and forward-backward angular asymmetries of quarks at the Z pole.

In the next subsections, the current status and FCC-ee prospects for these four axes of QCD studies are summarized.

2.1 Higher fixed-order pQCD corrections

Computations of pQCD corrections beyond the N^{2,3}LO accuracy are required for many theoretical FCC-ee observables in order to match their expected experimental precision. New analytical, algorithmic, and numerical concepts and tools are needed to be able to compute HO QCD and mixed QCD+electroweak multi-loop,-legs,-scales corrections for processes involving the heaviest SM particles (W, Z, H, t) to be carefully scrutinized at the FCC-ee. Concrete developments are covered in more detail in various other sections of this report, and summarized here:

- EWPOs: Mixed QCD-electroweak calculations of the $Zf\bar{f}$-vertex will be needed at the FCC-ee at higher order than known today, including the $\mathcal{O}(\alpha\alpha_s^2), \mathcal{O}(N_f\alpha^2\alpha_s), \mathcal{O}(N_f^2\alpha^3)$ loop orders, where N_f^n denotes n or more closed internal fermion loops, plus the corresponding QCD 4-loop terms [3]. The number of QCD diagrams for $Z \to b\bar{b}$ decays at two (three) loops is 98 (10 386) [3]. Section 9 provides e.g., details on the extension of calculations beyond the two-loop QCD off-shell vertex functions, noting that for the triple-gluon vertex there are 2382 (63 992) three- (four-) loop graphs to evaluate. Including massive quarks in 3- and 4-point functions is a further requirement in order to reduce the FO theoretical uncertainties.
- W boson (Section 7): The resonant $e^+e^- \to WW$ cross section contains soft corrections to the Coulomb function analogous to ultrasoft ($m_{top}v^2$) QCD corrections in $t\bar{t}$ production [4]. For the W hadronic decay modes, QCD corrections to the partial decay widths have to be included beyond NNLO to match the corresponding theoretical QED precision given by the counting $\mathcal{O}(\alpha_s^2) \sim \mathcal{O}(\alpha_{QED})$. QCD corrections to W self-energies and decay widths up to $\mathcal{O}(\alpha_{QED}\,\alpha_s^2)$ and $\mathcal{O}(\alpha_s^4)$ are required. Currently, $\mathcal{O}(\alpha_s^4)$ corrections for inclusive hadronic vector-boson decays are known [5], while mixed QCD-EW corrections are known up to $\mathcal{O}(\alpha_{QED}\,\alpha_s)$ [6].
- Higgs boson (Section 12): The pure QCD corrections to Higgs boson decays into quarks, gluons, and photons are known up to N^{4}LO (no mass effects), N^{3}LO (heavy-top limit), and NLO, respectively. Those translate into approximately 0.2%, 3%, and $< 1\%$ scale uncertainties from missing HO corrections. In the case of the (N)MSSM Higgs sector

(Section 3), HO pQCD corrections to the Higgs bosons decays are mostly known at NLO accuracy, and thereby their uncertainty is larger than for the SM Higgs case.

- Top-quark (Section 11): The total cross section for inclusive $e^+e^- \to b\bar{b}W^+W^-X$ production can be computed in a non-relativistic effective field theory with local effective vertices and matching corrections known up to N^{3}LO in pQCD [7]. Those translate into about 3% theoretical scale uncertainties of the threshold $t\bar{t}$ cross sections that propagate into an uncertainty of $\pm$60 MeV in the position of the resonant peak. Although the uncertainty has been reduced by a factor of two going from NNLO to N^{3}LO, perturbative progress is still needed, in particular in the threshold top mass definition translated into the $\overline{\rm MS}$ scheme.
- The extraction of $\alpha_{\rm QED}$ from the R-ratio (Section 1) requires the calculation of the 4-loop massive pQCD calculation of the Adler function (together with better estimates of $\alpha_{\rm s}$ in the low-Q^2 region above the τ mass, as well as of the m_c and m_b masses).

2.2 Higher-order logarithmic resummations

Improvements in the resummations of all-order logarithmic terms from different energy scales, appearing in the theoretical calculations for certain processes, are needed along various directions:

- Soft and collinear parton radiation impacts many e^+e^- observables with jets in the final state. Such uncertainties enter through incomplete N^{n}LL resummations in analytical calculations (e.g., based on soft-collinear effective theory, SCET), or through approximate models of the coherent branching implemented in the parton shower MC generators used to unfold and interpret the experimental data. Among those experimental observables, the measured forward-backward (FB) angular asymmetries of charm and bottom quarks in e^+e^- collisions around the Z pole, directly connected to the weak mixing angle, will need a careful study. The asymmetry value measured at LEP, $(A_{\rm FB}^{0,b})_{\rm exp} = 0.0992 \pm 0.0016$, remains today the electroweak precision observable with the largest disagreement (2.9σ) with respect to the SM prediction, $(A_{\rm FB}^{0,b})_{\rm th} = 0.1038$ [8,9]. Consequently, so does also the effective weak mixing angle derived from it, $\sin^2\theta^f_{\rm eff} = 0.23221 \pm 0.00029$, compared with the $\sin^2\theta^f_{\rm eff} = 0.23154 \pm 0.00003$ world-average [10]. The dominant systematic uncertainties on $(A_{\rm FB}^{0,b})_{\rm exp}$ arise from angular decorrelations induced in the thrust axis by soft and collinear parton radiation and/or parton-to-hadron b-quark hadronization, and were estimated using MC simulations 20 years ago [11]. A recent reanalysis of the QCD corrections to $A_{\rm FB}^{0,b}$ [12], with different modern parton shower models [13–15], indicates propagated uncertainties of about 1% (0.4%) for the lepton (jet) charge-based measurements, slightly smaller but still consistent with the original ones derived at LEP. The measurement of $A_{\rm FB}^{0,b}$ at the FCC-ee will feature insignificant statistical uncertainties, and improvements on the modelling of parton radiation will be required for any high-precision extraction of the associated $\sin^2\theta^f_{\rm eff}$ value.
- Another field of e^+e^- measurements where progress in logarithmic resummations is needed is in the studies of event shapes – such as the thrust T, C-parameter, and jet broadening. All those observables are commonly used to extract the QCD coupling [1]. The theoretical studies of event shapes supplement FO perturbation theory with the resummation of enhanced logarithmic contributions, specifically accounting for terms ranging from $\alpha_{\rm s}^n \ln^{n+1}$ down to $\alpha_{\rm s}^n \ln^{n-2}$, i.e. N^{3}LL [16]. However, the $\alpha_{\rm s}(m_{\rm Z})$ values derived from the T and

C measurements differ and their combination has thereby a final 2.9% systematic uncertainty [10]. This result points to limits in the resummation formalism that (i) holds only for $C, 1-T \ll 1$, where every emission is so soft and collinear that one can effectively neglect the kinematic cross-talk (e.g., energy-momentum conservation) that arises when there are multiple emissions, and (ii) uses a power correction valid only in the 2-jet limit, $1-T \ll 1$ [16].

- High-precision studies of n-jet rates at FCC-ee will also benefit from a reduction of resummation uncertainties. Jet rates in e^+e^- rely on an algorithm to reconstruct them that comes with a parameter ($y_{cut} = k_T^2/s$, in the k_T Durham [17] and Cambridge [18] cases) to define how energetic the emission should be in order to be considered a jet. For $\ln y_{cut} > -4$, the extracted α_s value from 3-jet rates is fairly independent of y_{cut}, whereas the result depends substantially on the choice of y_{cut} below that [19]. This feature points to a breakdown of FO perturbation theory, due to logarithmically enhanced $(\alpha_s \ln^2 y_{cut})^n$ terms. Jet rates at the one-in-a-million level in e^+e^- at the Z pole will be available at the FCC-ee including: 4-jet events up to $k_T \approx 30$ GeV (corresponding to $|\ln y_{cut}| \approx 2$), 5-jet events at $k_T \approx 20$ GeV ($|\ln y_{cut}| \approx 3$), 6-jet events at $k_T \approx 12$ GeV ($|\ln y_{cut}| \approx 4$), and 7-jet events at $k_T \approx 7.5$ GeV ($|\ln y_{cut}| \approx 5$). Such results will be compared to theoretical calculations with accuracy beyond the NNLO+NNLL provided today by the EERAD3 [20], MERCUTIO 2 [21], and CoLoRFulNNLO [22] (NNLO), and ARES [23] (NNLL) codes, thereby leading to α_s extractions with uncertainties well below the current few-percent level. In general, with the envisioned FCC-ee luminosities, jet measurements will extend along the six axes of higher accuracy, finer binning, higher jet resolution scales, larger numbers of resolved final-state objects, more differential distributions, and possibility to place stringent additional cuts to isolate specific interesting regions of the n-jet phase spaces not strongly constrained by LEP measurements [24].
- In top physics studies, the size of the NNLL corrections (in top quark velocity, $\ln v$) in $e^+e^- \to t\bar{t}$ cross section calculations, appears to be as large as that from the FO N^{3}LO terms [7], calling for improved resummation studies for such an observable.
- In the sector of flavour physics (Section 10), new tools based on SCET, developed to study processes with energetic quarks and gluons, can be applied after certain modifications to improve the accuracy of theoretical corrections for B-physics studies at the FCC-ee, in particular for regions of phase space where the perturbative approach breaks down due to the presence of large logarithmic enhancements and where the next-to-soft effects become more important.

2.3 Permille-precision α_s extraction

The strong coupling α_s is one of the fundamental parameters of the Standard Model, and its value not only directly affects the stability of the electroweak vacuum [25] but it chiefly impacts all theoretical calculations of e^+e^- scattering and decay processes involving real and/or virtual quarks and gluons [1]. Known today with a 0.9% precision, making of it the worst known of all fundamental interaction couplings in nature [10], the input value of $\alpha_s(m_Z)$ propagates as a parametric uncertainty into many of the FCC-ee physics observables, chiefly in the Z, Higgs, and top-quark sectors:

- The leading source of uncertainty in the calculation of crucial EWPOs pseudo-observables at the Z pole, such as Γ_Z, R_b, and R_ℓ, is the propagated $\delta\alpha_s$ parametric one [3].

- In the Higgs sector (Section 12), the current $\alpha_s(m_Z)$ parametric uncertainty (combined with those from our imperfect knowledge of m_c and m_b) propagates into total final uncertainties of ∼2% for the BR(H →WW, ZZ) and BR(H → $\tau^+\tau^-, \mu^+\mu^-$) branching ratios, of ∼6–7% for BR(H → gg) and BR(H → $c\bar{c}$), ∼3% for BR(H → $\gamma\gamma$), and ∼7% for BR(H → $Z\gamma$).
- Precise studies of the $e^+e^- \to t\bar{t}$ cross section (Section 11) indicate that it should be possible to extract the top-quark width and mass with an uncertainty around 50 MeV, provided that a precise independent extraction of the strong coupling is available. Such a requirement is in particular crucial to meaningfully constrain the top Yukawa coupling.

The current world-average value, $\alpha_s(m_Z) = 0.1181 \pm 0.0011$, is derived from a combination of six subclasses of approximately-independent observables [10] measured in e^+e^- (hadronic Z boson and τ decays, and event shapes and jet rates), DIS (structure functions and global fits of parton distributions functions), and p-p collisions (top-pair cross sections), as well as from lattice QCD computations constrained by the empirical values of hadron masses and decay constants. In order to enter into the $\alpha_s(m_Z)$ world-average, the experimental (or lattice) results need to have a counterpart pQCD theoretical prediction at NNLO (or beyond) accuracy.

Among the current six $\alpha_s(m_Z)$ extractions entering in the PDG average, the one derived from comparisons of NNLO pQCD predictions to lattice QCD results (Wilson loops, $q\bar{q}$ potentials, hadronic vacuum polarization, QCD static energy) [26], provides today the most precise result: $\alpha_s(m_Z) = 0.1188 \pm 0.0011$. The current ∼0.9% uncertainty is dominated by finite lattice spacing, truncations of the pQCD expansion up to NNLO, and hadron extrapolations. Over the next 10 years, reduction of the statistical uncertainties, at least by a factor of two, can be anticipated with increased computing power, whereas reaching the ∼0.1% uncertainty level will require also the computation of fourth-order pQCD corrections [1].

After the lattice result, the most theoretically and experimentally "clean" extractions of α_s are those based on the hadronic decays of the τ lepton, and W and Z bosons that will be measured with unparalleled accuracies at the FCC-ee. In order to derive $\alpha_s(m_Z)$, the experimental ratios of hadronic to leptonic decays are compared to the corresponding pQCD theoretical prediction, known today up to $\mathcal{O}(\alpha_s^4)$ [5, 27]:

$$R_\ell^{\tau,W,Z}(Q = m_\tau, m_W, m_Z) = \frac{\sigma(e^+e^- \to (\tau, W, Z) \to \text{hadrons})}{\sigma(e^+e^- \to (\tau, W, Z) \to \ell^+\ell^-)} = R_{EW}(Q)\left(1 + \sum_{i=1}^{N=4} c_n(Q)\left(\frac{\alpha_s(Q)}{\pi}\right)^n + \mathcal{O}(\alpha_s^5) + \delta_m + \delta_{np}\right). \quad (2.34)$$

In this equation, Q is the typical momentum transfer in the process used for measuring R_ℓ, c_n are coefficients of the perturbative series that can in practice be calculated up to some finite order $n = N$, and the terms δ_m and δ_{np} correspond, respectively, to mixed QCD+EW higher-order and power-suppressed $\mathcal{O}(\Lambda^p/Q^p)$ non-perturbative corrections, that affect differently the tau lepton and electroweak bosons decays. For $\alpha_s(m_Z) = 0.118$, the size of the QCD term in Eq. (2.34) amounts to a 4% effect, so at least permille measurement accuracies for the R_ℓ ratios are required for a competitive $\alpha_s(m_Z)$ determination [8]. Such an experimental precision has been reached in measurements of τ and Z boson decays, but not for the W boson and that is why the latter does not provide still a precise α_s extraction [28]. Reaching permille uncertainties in α_s determinations based on Eq. (2.34) requires 100 times smaller uncertainties in the experimental τ, W and Z measurements, a situation only reachable at the FCC-ee.

The ratio of hadronic to leptonic tau decays, known experimentally to within ±0.23% ($R_\ell^{\tau,\mathrm{exp}} = 3.4697 \pm 0.0080$), compared to next-to-NNLO ($\mathrm{N^3LO}$) calculations, yields $\alpha_\mathrm{s}(m_\mathrm{Z}) = 0.1192 \pm 0.0018$, i.e., a 1.5% uncertainty, through a combination of results from different theoretical approaches (contour-improved and fixed-order perturbation theory, CIPT and FOPT) with different treatments of non-pQCD corrections [29,30]. The current α_s uncertainty is shared roughly equally between experimental and theoretical systematics. The latter are driven by differences of the CIPT and FOPT results, although the power-suppressed non-perturbative δ_np term in Eq. (2.34), which is of $\mathcal{O}(\Lambda^2/m_\tau^2) \approx 10^{-2}$, is not negligible for the tau at variance with the much heavier W and Z bosons. High-statistics τ spectral functions (e.g., from B-factories now, and FCC-ee in the future), and solving CIPT-FOPT discrepancies (extending the calculations to $\mathrm{N^4LO}$ accuracy and controlling the non-pQCD uncertainties) are required to reduce the relative α_s uncertainty below the ∼1% level.

The current state-of-the-art $\mathrm{N^3LO}$ calculations of W boson decays [6] would allow a theoretical extraction of α_s with a ∼0.7% uncertainty provided that one would have experimental measurements of good enough precision. Unfortunately, the relevant LEP $\mathrm{W^+W^-}$ data are poor, based on $5 \cdot 10^4$ W bosons alone, and result in a QCD coupling extraction, $\alpha_\mathrm{s}(m_\mathrm{Z}) = 0.117 \pm 0.040$, with a huge ∼37% uncertainty today [28]. A determination of α_s with permille uncertainty from W boson decays can only be achieved through the combination of two developments: (i) data samples commensurate with those expected at FCC-ee (10^8 W bosons), and (ii) a significantly reduced uncertainty of the V_{cs} CKM element, which directly enters into the leading $R_\mathrm{EW}(Q)$ prefactor of Eq. (2.34) and propagates into a significant parametric uncertainty on the extracted α_s. Figure B.18 (left) shows the expected $\alpha_\mathrm{s}(m_\mathrm{Z})$ value derived from the R_ℓ^W ratio with 10^8 W bosons at FCC-ee assuming that V_{cs} has a negligible uncertainty (or, identically, assuming CKM matrix unitarity). The extracted QCD coupling would have ∼0.2% propagated experimental uncertainties.

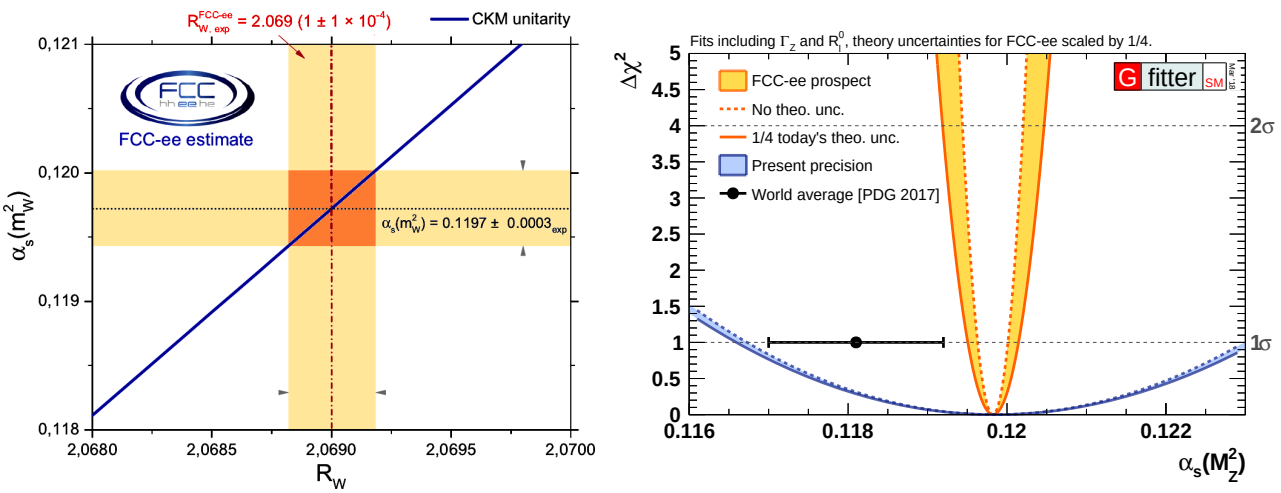

Fig. B.18: Left: Expected α_s determination from the W hadronic-to-leptonic decay ratio (R_ℓ^W) at the FCC-ee (the diagonal blue line assumes CKM matrix unitarity) [28]. Right: Precision on α_s derived from the electroweak fit today (blue band) [31] and expected at the FCC-ee (yellow band, without theoretical uncertainties and with the current theoretical uncertainties divided by a factor of four).

The current QCD coupling extraction based on Z boson hadron decays uses three closely-related pseudo-observables measured at LEP: $R_\ell^0 = \Gamma_\mathrm{had}/\Gamma_\ell$, $\sigma_0^\mathrm{had} = 12\pi/\mathrm{m_Z} \cdot \Gamma_\mathrm{e}\Gamma_\mathrm{had}/\Gamma_\mathrm{Z}^2$, and

Γ_Z, combined with N^{3}LO calculations, to give $\alpha_s(m_Z) = 0.1203 \pm 0.0028$ with a 2.5% uncertainty [10]. Alternatively, fixing all SM parameters to their measured values and letting free α_s in the electroweak fit yields $\alpha_s = 0.1194 \pm 0.0029$ (∼2.4% uncertainty, shallow blue curve in Fig. B.18 right) [31]. At the FCC-ee, with 10^{12} Z bosons providing high-precision measurements with $\Delta m_Z = 0.1$ MeV, $\Delta\Gamma_Z = 0.1$ MeV, $\Delta R^0_\ell = 10^{-3}$ (achievable thanks to the possibility to perform a threshold scan including energy self-calibration with resonant depolarization) reduces the uncertainty on $\alpha_s(m_Z)$ to ∼0.15%. Figure B.18 (right) shows the expected α_s extractions from R^Z_ℓ and Γ^Z at the FCC-ee (yellow band) with the experimental uncertainties listed in Table (A.2), without theoretical uncertainties (dotted red curve) and with the theoretical uncertainties reduced to one-fourth of their current values (solid red curve) [31].

The FCC-ee will not only provide an unprecedented amount of electroweak boson data, but also many orders-of-magnitude more jets than collected at LEP. The large and clean set of accurately-reconstructed (and flavour-tagged) e^+e^- hadronic final-states will provide additional high-precision α_s determinations from studies of event shapes, jets rates, and parton-to-hadron fragmentation functions (FFs) [1]. The existing measurements of e^+e^- event shapes (thrust T, C-parameter) [23,32–34] and n-jet rates [19,35,36], analyzed with N^{2,3}LO calculations matched, in some cases, to soft and collinear N$^{(2)}$LL resummations, yield $\alpha_s(m_Z) = 0.1169 \pm 0.0034$, with a 2.9% uncertainty [10]. This relatively large uncertainty is mostly driven by the span of individual extractions that use different (Monte Carlo or analytical) approaches to account for soft and collinear radiation as well as to correct for hadronization effects. Modern jet substructure techniques [37] can help mitigate the latter corrections. In terms of event shapes, the recent combination of the CoLoRFulNNLO subtraction method [38] with NNLL corrections in the back-to-back region [39], has led to a precise calculation of the energy-energy correlation (EEC) observable in electron-positron collisions, and thereby an accurate NNLO+NNLL extraction of $\alpha_s(m_Z) = 0.1175 \pm 0.0029$ (∼2.5% uncertainty) [40], as discussed in detail in Section 4. Also a very recent analysis of 2-jet rates in e^+e^- collisions at N^{3}LO+NNLL accuracy [41] has provided a new QCD coupling determination with a ∼1% uncertainty: $\alpha_s(m_Z) = 0.11881 \pm 0.00132$. In addition, other sets of observables computed today with a lower degree of accuracy (NLO, or approximately-NNLO, bottom part of Fig. B.19), and thereby not included now in the PDG average, will provide additional constraints [1]. The energy dependence of the low-z FFs provides today $\alpha_s(m_Z) = 0.1205 \pm 0.0022$ (∼2% uncertainty) at NNLO*+NNLL [42, 43], whereas NLO scaling violations of the high-z FFs yield $\alpha_s(m_Z) = 0.1176 \pm 0.0055$ (∼5% uncertainty, mostly of experimental origin) [44]. Also, measurements of the photon structure function $F_2^\gamma(x, Q^2)$, via $e^+e^- \to \gamma\gamma \to$ hadrons, have been employed to derive $\alpha_s(m_Z) = 0.1198 \pm 0.0054$ (∼4.5% uncertainty) at NLO [45]. Extension to full-NNLO accuracy of the FFs and $F_2^\gamma(x, Q^2)$ fits using the much larger e^+e^- data sets available at various center-of-mass energies at the FCC-ee will allow reaching subpercent precision in $\alpha_s(m_Z)$. Figure B.19 presents a comparison of the current $\alpha_s(m_Z)$ results (top), the expected FCC-ee extractions (middle), and the other aforementioned methods based on e^+e^- data not currently included in the world-average.

2.4 High-precision Non-Perturbative QCD

All e^+e^- processes with quarks and gluons in the final state have an intrinsic uncertainty linked to the final nonperturbative conversion of the partons, present in the last stage of the QCD shower, into hadrons. Such a process cannot be computed with first-principles QCD calculations and is described with phenomenological models such as the Lund string [46], as implemented in the PYTHIA MC generator [13], or the cluster hadronization approach [47] typ-

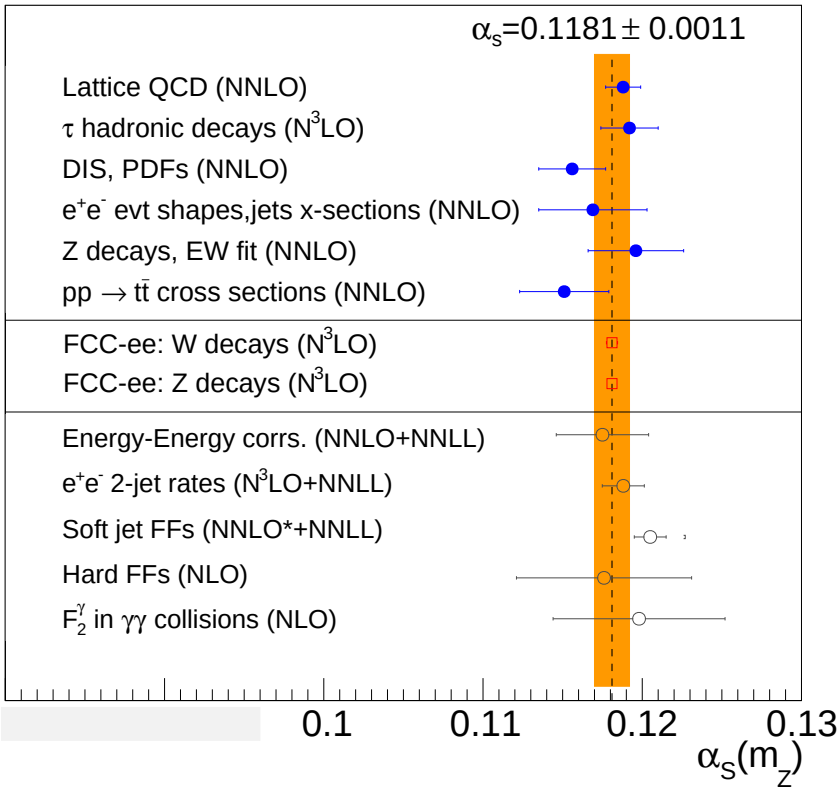

Fig. B.19: Summary of the $\alpha_s(m_Z)$ determinations discussed here. Upper: Subclasses entering in the current PDG world-average (solid dots, orange band) whose numerical value is listed on top [10]. Middle: Expected FCC-ee values via W, Z hadronic decays (open squares). Lower: Other methods based on e^+e^- data not (yet) in the $\alpha_s(m_Z)$ world-average: recent EEC [40] and 2-jet rates [41], plus other extractions at a (currently) lower level of theoretical accuracy.

ical of the HERWIG event generator [48]. The analysis and unfolding of any e^+e^- experimental measurement of hadronic final-states relies on these very same Monte Carlo generators, and therefore the final results are sensitive to their particular implementation of soft and collinear parton radiation (whose MC modelling is equivalent to an approximate-NLL accuracy [49]) and of the hadronization process. Examples of such propagated uncertainties have been discussed above in the context of α_s extractions from various experimental e^+e^- observables. An improved MC reproduction of the experimental hadron data can e.g., help in the possibilities for advanced light-quark and gluon jet tagging in constraints of the Higgs Yukawa couplings to the first and second family of quarks. Controlling the uncertainties linked to hadronization and other final-state partonic effects, such as colour reconnection and multiparticle (spin, momenta, space, etc.) correlations, is therefore basic for many high-precision SM studies. Such effects are optimally studied in the clean environment provided by e^+e^- collisions, without coloured objects in the initial state. Among the FCC-ee goals is therefore to produce truly precise QCD measurements to constrain many aspects of nonperturbative dynamics to the 1% level or better, leaving an important legacy for MC generators for the FCC-eh and FCC-hh physics programme, much as those from LEP proved crucial for the parton shower models used today at the LHC [2]. In particular, the FCC-ee operating at different c.m. energies will enormously help to control resummation and hadronization effects in event-shape distributions reducing, in particular, non-perturbative uncertainties from a 9% effect at $\sqrt{s} = 91.2$ GeV to a 2% at 400

GeV [2, 50].

The modelling of parton hadronization in the current MC event generators has a moderate success, and the LHC data have only further complicated the situation. First, the production of baryons (in particular containing strange quarks) remains poorly understood and is hard to measure in the complicated hadron-hadron environment. Second and most importantly, the LHC measurements have challenged the standard assumption of parton-hadronization universality, i.e., that models developed from e^+e^- data can be directly applied to hadron-hadron collisions. Strong final-state effects, more commonly associated with heavy-ion physics and quark-gluon-plasma formation, such as the "ridge" [51] or the increase of strangeness production in high-multiplicity pp events [52], cannot be accommodated within the standard MC generators. The large statistical samples available at the FCC-ee will allow to control parton hadronization in the QCD vacuum with subpercent uncertainties, and thereby provide a better understanding of any collective final-state effects present in hadron-hadron collisions. Starting with multiple-strange baryons whose total production rates could only be determined with 5–20% accuracy at LEP [53, 54]; and going further to excited [54, 55], exotic, and/or multiple heavy hadrons, with implications for more advanced fragmentation models. For Λ-Λ correlation distributions, where MC generator programs fail today describe the LEP [56] and LHC data, the huge FCC-ee samples of hadronic Z decays will have statistical uncertainties matching the best LEP systematic uncertainties, corresponding to total errors reduced by a factor of ten or more.

In $e^+e^- \to t\bar{t}$, when the top and anti-top quarks decay and hadronize close to each other, interactions and interferences among them, the decay bottoms, and any radiated gluons affect the rearrangement of the colour flow and thereby the kinematic distributions of the final hadronic state. Whereas the perturbative radiation in the process can be in principle theoretically controlled, there is a "cross talk" among the produced hadronic strings, also known as colour reconnection (CR), that can only be modelled phenomenologically [57]. In the pp case, such CR effects can decrease the precision that can be achieved in the extraction of the top mass, and constitute 20 to 40% of its uncertainty [58]. Colour reconnection can also impact limits for CP-violation searches in $H \to W^+W^- \to q_1q_2q_3q_4$ decays [59]. Searches for such effects can be optimally studied in the process $e^+e^- \to W^+W^- \to q_1\bar{q}_2q_3\bar{q}_4$ [59], where CR could lead to the formation of alternative "flipped" singlets $q_1\bar{q}_4$ and $q_3\bar{q}_2$, and correspondingly more complicated string topologies [60]. The combination of results from all four LEP collaborations excluded the no-CR null hypothesis at 99.5% CL [61], but the size of the WW data sample was too small for any quantitative studies. At the FCC-ee, with the W mass determined to better than 1 MeV by a threshold scan, the semileptonic WW measurements (unaffected by CR) can be used to probe the impact of CR in the hadronic WW events [2,62]. Alternative CR constraints at the FCC-ee have been proposed through the study of event shape observables sensitive to string overlap, such as sphericity for different hadron flavours, as described in "rope hadronization" approaches [63, 64].

References

[1] D. d'Enterria, P. Z. Skands (Eds.), Proceedings, High-Precision α_s Measurements from LHC to FCC-ee, CERN, CERN, Geneva, 2015. arXiv:1512.05194.
URL http://lss.fnal.gov/archive/2015/conf/fermilab-conf-15-610-t.pdf

[2] D. d'Enterria, P. Z. Skands (Eds.), Proceedings, Parton Radiation and Fragmentation from LHC to FCC-ee, 2017. arXiv:1702.01329.

[3] A. Blondel, et al., Standard Model Theory for the FCC-ee: The Tera-Z, in: Mini Workshop on Precision EW and QCD Calculations for the FCC Studies : Methods and Techniques CERN, Geneva, Switzerland, January 12-13, 2018, 2018. arXiv:1809.01830.

[4] M. Beneke, Y. Kiyo, Ultrasoft contribution to heavy-quark pair production near threshold, Phys. Lett. B668 (2008) 143–147. arXiv:0804.4004, doi:10.1016/j.physletb.2008.08.031.

[5] P. A. Baikov, K. G. Chetyrkin, J. H. Kuhn, Order α_s^4 QCD Corrections to Z and tau Decays, Phys. Rev. Lett. 101 (2008) 012002. arXiv:0801.1821, doi:10.1103/PhysRevLett.101.012002.

[6] D. Kara, Corrections of Order $\alpha\alpha_s$ to W Boson Decays, Nucl. Phys. B877 (2013) 683–718. arXiv:1307.7190, doi:10.1016/j.nuclphysb.2013.10.024.

[7] M. Beneke, Y. Kiyo, P. Marquard, A. Penin, J. Piclum, M. Steinhauser, Next-to-Next-to-Next-to-Leading Order QCD Prediction for the Top Antitop S-Wave Pair Production Cross Section Near Threshold in e^+e^- Annihilation, Phys. Rev. Lett. 115 (19) (2015) 192001. arXiv:1506.06864, doi:10.1103/PhysRevLett.115.192001.

[8] S. Schael, et al., Precision electroweak measurements on the Z resonance, Phys. Rept. 427 (2006) 257–454. arXiv:hep-ex/0509008, doi:10.1016/j.physrep.2005.12.006.

[9] LEP Electroweak Working Group, Precision Electroweak Measurements and Constraints on the Standard Model, arXiv:1012.2367.

[10] C. Patrignani, et al., Review of Particle Physics, Chin. Phys. C40 (10) (2016) 100001. doi:10.1088/1674-1137/40/10/100001.

[11] D. Abbaneo, P. Antilogus, T. Behnke, S. C. Blyth, M. Elsing, R. Faccini, R. W. L. Jones, K. Monig, S. Petzold, R. Tenchini, QCD corrections to the forward-backward asymmetries of c and b quarks at the Z pole, Eur. Phys. J. C4 (1998) 185–191. doi:10.1007/s100520050196.

[12] D. d'Enterria, C. Yan, Forward-backward b-quark asymmetry at the Z pole: QCD uncertainties redux, in: 53rd Rencontres de Moriond on QCD and High Energy Interactions (Moriond QCD 2018) La Thuile, Italy, March 17-24, 2018, 2018. arXiv:1806.00141.

[13] T. Sjöstrand, S. Ask, J. R. Christiansen, R. Corke, N. Desai, P. Ilten, S. Mrenna, S. Prestel, C. O. Rasmussen, P. Z. Skands, An Introduction to PYTHIA 8.2, Comput. Phys. Commun. 191 (2015) 159–177. arXiv:1410.3012, doi:10.1016/j.cpc.2015.01.024.

[14] W. T. Giele, D. A. Kosower, P. Z. Skands, Higher-Order Corrections to Timelike Jets, Phys. Rev. D84 (2011) 054003. arXiv:1102.2126, doi:10.1103/PhysRevD.84.054003.

[15] N. Fischer, S. Prestel, M. Ritzmann, P. Skands, Vincia for Hadron Colliders, Eur. Phys. J. C76 (11) (2016) 589. arXiv:1605.06142, doi:10.1140/epjc/s10052-016-4429-6.

[16] G. P. Salam, The strong coupling: a theoretical perspective, in: A. Levy, S. Forte, G. Ridolfi (Eds.), From My Vast Repertoire ...: Guido Altarelli's Legacy, 2019, pp. 101–121. arXiv:1712.05165, doi:10.1142/9789813238053_0007.

[17] S. Catani, Y. L. Dokshitzer, M. Olsson, G. Turnock, B. R. Webber, New clustering algorithm for multi - jet cross-sections in e^+e^- annihilation, Phys. Lett. B269 (1991) 432–438. doi:10.1016/0370-2693(91)90196-W.

[18] Y. L. Dokshitzer, G. D. Leder, S. Moretti, B. R. Webber, Better jet clustering algorithms, JHEP 08 (1997) 001. arXiv:hep-ph/9707323, doi:10.1088/1126-6708/1997/08/001.

[19] G. Dissertori, A. Gehrmann-De Ridder, T. Gehrmann, E. W. N. Glover, G. Heinrich, H. Stenzel, Precise determination of the strong coupling constant at NNLO in QCD from

the three-jet rate in electron–positron annihilation at LEP, Phys. Rev. Lett. 104 (2010) 072002. arXiv:0910.4283, doi:10.1103/PhysRevLett.104.072002.

[20] A. Gehrmann-De Ridder, T. Gehrmann, E. W. N. Glover, G. Heinrich, EERAD3: Event shapes and jet rates in electron-positron annihilation at order α_s^3, Comput. Phys. Commun. 185 (2014) 3331. arXiv:1402.4140, doi:10.1016/j.cpc.2014.07.024.

[21] S. Weinzierl, Jet algorithms in electron-positron annihilation: Perturbative higher order predictions, Eur. Phys. J. C71 (2011) 1565, [Erratum: Eur. Phys. J.C71,1717(2011)]. arXiv:1011.6247, doi:10.1140/epjc/s10052-011-1717-z,10.1140/epjc/s10052-011-1565-x.

[22] V. Del Duca, C. Duhr, A. Kardos, G. Somogyi, Z. Trócsányi, Three-Jet Production in Electron-Positron Collisions at Next-to-Next-to-Leading Order Accuracy, Phys. Rev. Lett. 117 (15) (2016) 152004. arXiv:1603.08927, doi:10.1103/PhysRevLett.117.152004.

[23] A. Banfi, H. McAslan, P. F. Monni, G. Zanderighi, A general method for the resummation of event-shape distributions in e^+e^- annihilation, JHEP 05 (2015) 102. arXiv:1412.2126, doi:10.1007/JHEP05(2015)102.

[24] N. Fischer, S. Gieseke, S. Kluth, S. Plätzer, P. Skands, Measurement of observables sensitive to coherence effects in hadronic Z decays with the OPAL detector at LEP, Eur. Phys. J. C75 (12) (2015) 571. arXiv:1505.01636, doi:10.1140/epjc/s10052-015-3766-1.

[25] D. Buttazzo, G. Degrassi, P. P. Giardino, G. F. Giudice, F. Sala, A. Salvio, A. Strumia, Investigating the near-criticality of the Higgs boson, JHEP 12 (2013) 089. arXiv:1307.3536, doi:10.1007/JHEP12(2013)089.

[26] S. Aoki, et al., FLAG Review 2019. arXiv:1902.08191.

[27] P. A. Baikov, K. G. Chetyrkin, J. H. Kuhn, J. Rittinger, Adler Function, Sum Rules and Crewther Relation of Order $O(\alpha_s^4)$: the Singlet Case, Phys. Lett. B714 (2012) 62–65. arXiv:1206.1288, doi:10.1016/j.physletb.2012.06.052.

[28] D. d'Enterria, M. Srebre, α_s and V_{cs} determination, and CKM unitarity test, from W decays at NNLO, Phys. Lett. B763 (2016) 465–471. arXiv:1603.06501, doi:10.1016/j.physletb.2016.10.012.

[29] A. Pich, A. Rodríguez-Sánchez, Determination of the QCD coupling from ALEPH τ decay data, Phys. Rev. D94 (3) (2016) 034027. arXiv:1605.06830, doi:10.1103/PhysRevD.94.034027.

[30] D. Boito, M. Golterman, K. Maltman, S. Peris, Strong coupling from hadronic τ decays: A critical appraisal, Phys. Rev. D95 (3) (2017) 034024. arXiv:1611.03457, doi:10.1103/PhysRevD.95.034024.

[31] J. Haller, A. Hoecker, R. Kogler, K. Moenig, T. Peiffer, J. Stelzer, Update of the global electroweak fit and constraints on two-Higgs-doublet models, Eur. Phys. J. C78 (8) (2018) 675. arXiv:1803.01853, doi:10.1140/epjc/s10052-018-6131-3.

[32] S. Bethke, S. Kluth, C. Pahl, J. Schieck, Determination of the Strong Coupling alpha(s) from hadronic Event Shapes with $O(\alpha_s^3)$ and resummed QCD predictions using JADE Data, Eur. Phys. J. C64 (2009) 351–360. arXiv:0810.1389, doi:10.1140/epjc/s10052-009-1149-1.

[33] R. Abbate, M. Fickinger, A. H. Hoang, V. Mateu, I. W. Stewart, Precision Thrust Cumulant Moments at N^3LL, Phys. Rev. D86 (2012) 094002. arXiv:1204.5746, doi:10.1103/PhysRevD.86.094002.

[34] A. H. Hoang, D. W. Kolodrubetz, V. Mateu, I. W. Stewart, Precise determination of α_s

from the C-parameter distribution, Phys. Rev. D91 (9) (2015) 094018. arXiv:1501.04111, doi:10.1103/PhysRevD.91.094018.

[35] S. Weinzierl, NNLO corrections to 3-jet observables in electron-positron annihilation, Phys. Rev. Lett. 101 (2008) 162001. arXiv:0807.3241, doi:10.1103/PhysRevLett.101.162001.

[36] J. Schieck, S. Bethke, S. Kluth, C. Pahl, Z. Trocsanyi, Measurement of the strong coupling α_s from the three-jet rate in e^+e^- annihilation using JADE data, Eur. Phys. J. C73 (3) (2013) 2332. arXiv:1205.3714, doi:10.1140/epjc/s10052-013-2332-y.

[37] Les Houches 2017: Physics at TeV Colliders Standard Model Working Group Report. arXiv:1803.07977.
URL http://lss.fnal.gov/archive/2018/conf/fermilab-conf-18-122-cd-t.pdf

[38] V. Del Duca, C. Duhr, A. Kardos, G. Somogyi, Z. Szőr, Z. Trócsányi, Z. Tulipánt, Jet production in the CoLoRFulNNLO method: event shapes in electron-positron collisions, Phys. Rev. D94 (7) (2016) 074019. arXiv:1606.03453, doi:10.1103/PhysRevD.94.074019.

[39] D. de Florian, M. Grazzini, The Back-to-back region in e^+e^- energy-energy correlation, Nucl. Phys. B704 (2005) 387–403. arXiv:hep-ph/0407241, doi:10.1016/j.nuclphysb.2004.10.051.

[40] A. Kardos, S. Kluth, G. Somogyi, Z. Tulipánt, A. Verbytskyi, Precise determination of $\alpha_S(M_Z)$ from a global fit of energy–energy correlation to NNLO+NNLL predictions, Eur. Phys. J. C78 (6) (2018) 498. arXiv:1804.09146, doi:10.1140/epjc/s10052-018-5963-1.

[41] A. Verbytskyi, A. Banfi, A. Kardos, P. F. Monni, S. Kluth, G. Somogyi, Z. Szőr, Z. Trócsányi, Z. Tulipánt, G. Zanderighi, High precision determination of α_s from a global fit of jet rates, Submitted to: JHEParXiv:1902.08158.

[42] R. Perez-Ramos, D. d'Enterria, Energy evolution of the moments of the hadron distribution in QCD jets including NNLL resummation and NLO running-coupling corrections, JHEP 08 (2014) 068. arXiv:1310.8534, doi:10.1007/JHEP08(2014)068.

[43] D. d'Enterria, R. Pérez-Ramos, α_s determination at NNLO*+NNLL accuracy from the energy evolution of jet fragmentation functions at low z, in: Proceedings, 50th Rencontres de Moriond, QCD and high energy interactions: La Thuile, Italy, March 21-28, 2015, 2015, p. 117. arXiv:1505.02624.

[44] S. Albino, B. A. Kniehl, G. Kramer, Fragmentation functions for light charged hadrons with complete quark flavor separation, Nucl. Phys. B725 (2005) 181–206. arXiv:hep-ph/0502188, doi:10.1016/j.nuclphysb.2005.07.010.

[45] S. Albino, M. Klasen, S. Soldner-Rembold, Strong coupling constant from the photon structure function, Phys. Rev. Lett. 89 (2002) 122004. arXiv:hep-ph/0205069, doi:10.1103/PhysRevLett.89.122004.

[46] B. Andersson, G. Gustafson, B. Soderberg, A General Model for Jet Fragmentation, Z. Phys. C20 (1983) 317. doi:10.1007/BF01407824.

[47] B. R. Webber, A QCD Model for Jet Fragmentation Including Soft Gluon Interference, Nucl. Phys. B238 (1984) 492–528. doi:10.1016/0550-3213(84)90333-X.

[48] G. Corcella, I. G. Knowles, G. Marchesini, S. Moretti, K. Odagiri, P. Richardson, M. H. Seymour, B. R. Webber, HERWIG 6: An Event generator for hadron emission reactions with interfering gluons (including supersymmetric processes), JHEP 01 (2001) 010. arXiv:hep-ph/0011363, doi:10.1088/1126-6708/2001/01/010.

[49] M. Dasgupta, F. A. Dreyer, K. Hamilton, P. F. Monni, G. P. Salam, Logarithmic accuracy of parton showers: a fixed-order study, JHEP 09 (2018) 033. arXiv:1805.09327, doi:10.1007/JHEP09(2018)033.

[50] G. Bell, A. Hornig, C. Lee, J. Talbert, e^+e^- angularity distributions at NNLL′ accuracy, JHEP 01 (2019) 147. arXiv:1808.07867, doi:10.1007/JHEP01(2019)147.

[51] V. Khachatryan, et al., Observation of Long-Range Near-Side Angular Correlations in Proton-Proton Collisions at the LHC, JHEP 09 (2010) 091. arXiv:1009.4122, doi:10.1007/JHEP09(2010)091.

[52] J. Adam, et al., Enhanced production of multi-strange hadrons in high-multiplicity proton-proton collisions, Nature Phys. 13 (2017) 535–539. arXiv:1606.07424, doi:10.1038/nphys4111.

[53] P. Abreu, et al., Strange baryon production in Z hadronic decays, Z. Phys. C67 (1995) 543–554. doi:10.1007/BF01553980.

[54] G. Alexander, et al., Strange baryon production in hadronic Z0 decays, Z. Phys. C73 (1997) 569–586. doi:10.1007/s002880050349.

[55] R. Akers, et al., Inclusive strange vector and tensor meson production in hadronic Z0 decays, Z. Phys. C68 (1995) 1–12. doi:10.1007/BF01579799.

[56] G. Abbiendi, et al., A Study of parton fragmentation in hadronic Z0 decays using Lambda anti-Lambda correlations, Eur. Phys. J. C13 (2000) 185–195. arXiv:hep-ex/9808031, doi:10.1007/s100520000207,10.1007/s100520050685.

[57] V. A. Khoze, T. Sjostrand, Color correlations and multiplicities in top events, Phys. Lett. B328 (1994) 466–476. arXiv:hep-ph/9403394, doi:10.1016/0370-2693(94)91506-7.

[58] S. Argyropoulos, T. Sjöstrand, Effects of color reconnection on $t\bar{t}$ final states at the LHC, JHEP 11 (2014) 043. arXiv:1407.6653, doi:10.1007/JHEP11(2014)043.

[59] J. R. Christiansen, T. Sjöstrand, Color reconnection at future e^+e^- colliders, Eur. Phys. J. C75 (9) (2015) 441. arXiv:1506.09085, doi:10.1140/epjc/s10052-015-3674-4.

[60] T. Sjöstrand, V. A. Khoze, On Color rearrangement in hadronic W^+W^- events, Z. Phys. C62 (1994) 281–310. arXiv:hep-ph/9310242, doi:10.1007/BF01560244.

[61] S. Schael, et al., Electroweak Measurements in Electron-Positron Collisions at W-Boson-Pair Energies at LEP, Phys. Rept. 532 (2013) 119–244. arXiv:1302.3415, doi:10.1016/j.physrep.2013.07.004.

[62] A. Abada, et al., Future Circular Collider: Vol. 1 "Physics opportunities", http://inspirehep.net/record/1713706/files/CERN-ACC-2018-0056.pdf.

[63] C. Bierlich, G. Gustafson, L. Lönnblad, A shoving model for collectivity in hadronic collisions arXiv:1612.05132.

[64] C. Bierlich, Rope Hadronization and Strange Particle Production, EPJ Web Conf. 171 (2018) 14003. arXiv:1710.04464, doi:10.1051/epjconf/201817114003.

3 Inclusion of mixed QCD-QED resummation effects at higher-orders

Author: German F. R. Sborlini [german.sborlini@ific.uv.es]

In this document, we review some recent results concerning the inclusion of mixed QCD-QED corrections to the computation of physical observables. First, we comment on the extension of the DGLAP equations to deal with the presence of mixed QCD-QED interactions. We describe the calculation of the full set of higher-order corrections to the splitting kernels, through the Abelianization algorithm. This procedure allows to build the functional form of the QCD-QED corrections starting from pure QCD terms. As a practical application of this technique, we also explore the computation of fixed-order corrections to diphoton production, and the inclusion of higher-order mixed QCD-QED resummation effects to Z production. In both cases, we directly apply the Abelianization to the q_T-subtraction/resummation formalism, obtaining the universal ingredients that allow to compute the beforehand mentioned corrections to any process involving colorless and neutral particles in the final state.

3.1 Introduction and motivation

The large amount of data that high-energy experiments are collecting allows to increase notoriously the precision of several measurements. In consequence, theoretical predictions must be pushed forward by including previously neglected small effects. This is the case of electroweak (EW) or QED corrections, which are sub-dominating for collider physics. However, from a naive power-counting, it is easy to notice that $\mathcal{O}(\alpha) \approx \mathcal{O}(\alpha_S^2)$. On top of that, QED interactions (as well as the full set of EW ones) lead to novel effects that could interfere with the well-known QCD signals. Moreover, these effects might play a crucial role in the context of future lepton colliders, such as the FCC-ee. For these reasons, EW and QED higher-order corrections must be seriously studied in a fully consistent framework.

The aim of this brief document is presenting some results related to the impact of QED corrections in the calculation of physical observables for colliders. In Sec. 3.2, we recall the computation of the full set of QCD-QED splitting functions at $\mathcal{O}(\alpha\,\alpha_S)$ and $\mathcal{O}(\alpha^2)$, centering into the Abelianization algorithm and the relevance of the corrections to achieve a better determination of the photon PDF. Then, we apply the Abelianization to the well-established q_T-subtraction/resummation [1, 2] framework. In Sec. 3.3, we show the impact of the NLO QED corrections to diphoton production. After that, we characterize the mixed QCD-QED resummation of soft gluon/photons for Z boson production in Sec. 3.4. The conclusions and future research directions are discussed in Sec. 3.5.

3.2 Splittings and PDF evolution

Splitting functions are crucial to describe the singular collinear behavior of scattering amplitudes. On one side, they are used to build the counter-terms to subtract infrared (IR) singularities from cross-sections. On the other hand, they are the evolution kernels of the integro-differential DGLAP equations [3], which govern the perturbative evolution of PDFs. When taking into account QCD and EW/QED interactions, it is necessary to include photon and lepton PDFs, and this will lead to the presence of new splitting functions. In Refs. [4, 5] we computed the $\mathcal{O}(\alpha\,\alpha_S)$ and $\mathcal{O}(\alpha^2)$ corrections to the DGLAP equations, as well as the associated kernels. The strategy that we adopted was based on the implementation of a universal

algorithm, called *Abelianization*, which aims to explode previously known pure QCD results to obtain the corresponding QCD-QED or QED expressions. Roughly speaking, the key idea behind this method is *transforming gluons into photons*: color factors are replaced by suitable electric charges, as well as symmetry or counting factors.

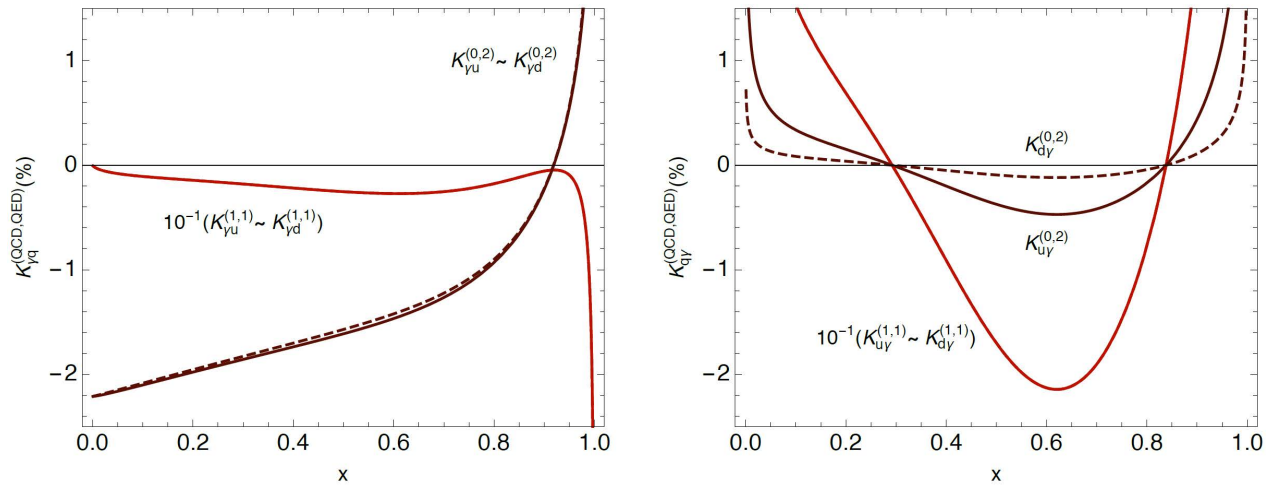

Fig. B.20: Corrections due to the inclusion of QED contributions in the $P_{q\gamma}$ (right) and $P_{\gamma q}$ (left) splitting kernels. We include both $\mathcal{O}(\alpha^2)$ (brown) and $\mathcal{O}(\alpha\,\alpha_S)$ (red) terms. K-ratio is defined using the leading order as normalization. To ease the visual presentation, we re-scaled the $\mathcal{O}(\alpha\,\alpha_S)$ terms by a factor 0.1.

With the purpose of exhibiting the quantitative effects that mixed QCD-QED or $\mathcal{O}(\alpha^2)$ corrections might have, we plot the K-ratio for quark-photon and photon-quark splitting functions in Fig. B.20. It is important to notice that these contributions are not present in pure QCD, which implies that the evolution of photon PDF is noticeably affected by the $\mathcal{O}(\alpha\,\alpha_S)$ splittings or even higher-orders in the mixed QCD-QED perturbative expansion. We would like to highlight that a precise determination of photon distributions is crucial to obtain more accurate predictions for several physical observables.

3.3 Fixed order effects: Application to diphoton production

The q_T-subtraction/resummation formalism [1, 2] is a powerful approach to compute higher-order corrections to physical observables. This formalism has been mainly applied to QCD calculations, and relies on the color-neutrality of the final state particles[‡]. So, we used the Abelianization algorithm to compute the universal coefficients required to implement NLO QED corrections to any process involving only neutral particles in the final state. In this way, we demonstrate that this extension can deal consistently with the cancellation of IR divergences in the limit $q_T \to 0$.

As a practical example, we used the public code `2gNNLO` [8,9], which provides up to NNLO QCD corrections to diphoton production, and we implemented the corresponding NLO QED corrections [10, 11]. We applied the default ATLAS cuts, with 14 TeV center-of-mass energy, and the `NNPDF3.1QED` [12, 13] PDF set. The transverse momentum and invariant mass spectra are shown in Fig. B.21. It is interesting to appreciate that, even if the corrections are small

[‡]An extension to deal with massive or coloured particles in the final state was presented in Refs. [6, 7].

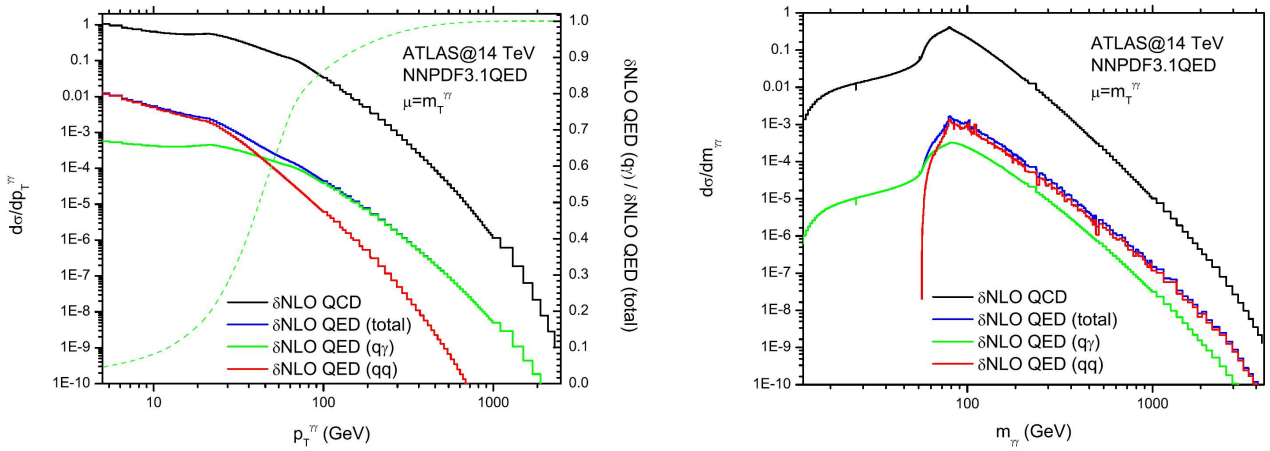

Fig. B.21: Impact of higher-order QED corrections on the transverse momentum (left) and invariant mass (right) distributions for diphoton production. The black (blue) curve shows the total NLO QCD (QED) prediction, without including the LO contribution. The dashed green line indicates the relative contribution of the $q\gamma$-channel to the total NLO QED correction.

compared to the QCD contributions, the QED interactions lead to novel features, such as a dynamical cut in the invariant mass spectrum. This is due to the fact that real radiation in the $q\bar{q}$-channel contains three final state photons, which must be ordered according to their transverse momenta before imposing the selection cuts. Besides that, introducing the QED corrections (or, even better, mixed NLO QCD-QED corrections) will allow to reduce the scale uncertainties and produce more reliable theoretical predictions.

3.4 Mixed resummation effects: Z-boson production

Finally, we studied the impact of including mixed QCD-QED terms within the q_T-resummation formalism. This is equivalent to consider the simultaneous emission of soft/collinear gluons and photons. A detailed description of the formalism is presented in Ref. [14], where we computed the modified Sudakov form factors as well as all the required universal coefficients to reach mixed NLL'+NLO accuracy in the double expansion in α and α_S. Explicitly, we obtained

$$\begin{aligned}\mathcal{G}'_N(\alpha_S,\alpha,L) &= \mathcal{G}_N(\alpha_S,L) + L\, g'^{(1)}(\alpha L) + g'^{(2)}_N(\alpha L) + \sum_{n=3}^{\infty}\left(\frac{\alpha}{\pi}\right)^{n-2} g'^{(n)}_N(\alpha L) \\ &+ g'^{(1,1)}(\alpha_S L,\alpha L) + \sum_{\substack{n,m=1\\ n+m\neq 2}}^{\infty}\left(\frac{\alpha_S}{\pi}\right)^{n-1}\left(\frac{\alpha}{\pi}\right)^{m-1} g'^{(n,m)}_N(\alpha_S L,\alpha L)\ , \end{aligned} \tag{3.35}$$

and

$$\begin{aligned}\mathcal{H}'^{F}_N(\alpha_S,\alpha) &= \mathcal{H}^{F}_N(\alpha_S) + \frac{\alpha}{\pi}\,\mathcal{H}'^{F\,(1)}_N + \sum_{n=2}^{\infty}\left(\frac{\alpha}{\pi}\right)^{n}\mathcal{H}'^{F\,(n)}_N \\ &+ \sum_{n,m=1}^{\infty}\left(\frac{\alpha_S}{\pi}\right)^{n}\left(\frac{\alpha}{\pi}\right)^{m}\mathcal{H}'^{F\,(n,m)}_N\,, \end{aligned} \tag{3.36}$$

for the expansion of the Sudakov exponents and the hard-virtual coefficients, respectively. A similar expansion is available for the soft-collinear coefficients C_{ab}. Other important ingredients

of the formalism are the mixed QCD-QED renormalization group equations (RGE), which include a double expansion of the corresponding β-functions [14].

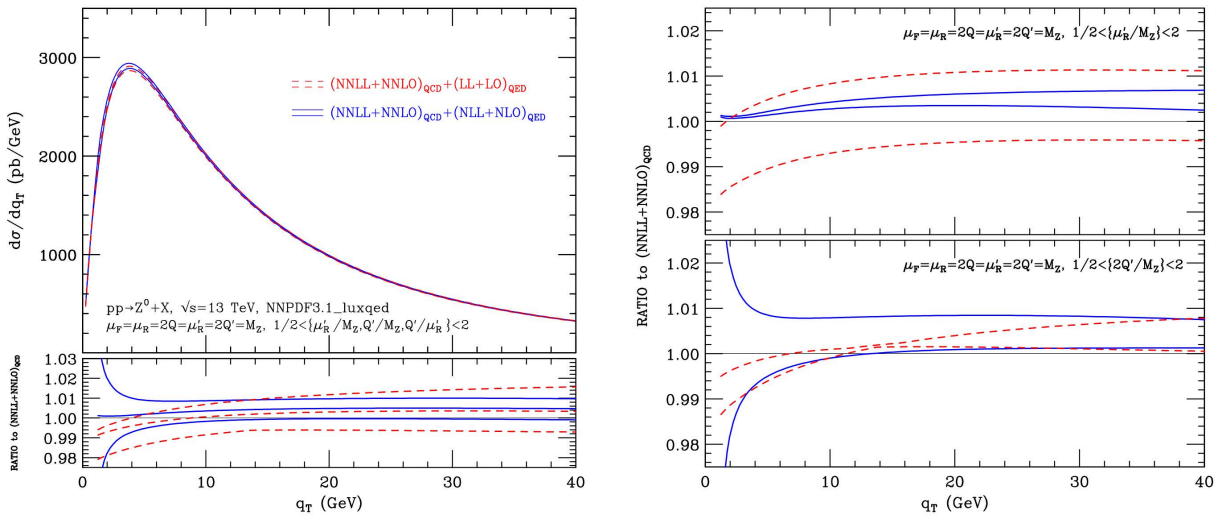

Fig. B.22: The q_T spectrum for Z boson production at the LHC with 13 TeV center-of-mass energy. In the left panel, we show the combination of NNLL+NNLO QCD contributions together with the LL (red dashed) and NLL'+NLO (blue solid) QED effects. We include the uncertainty bands that result from the full scale variation by a factor 2 (up and down). More details about scale uncertainties are shown in the right panel, where we modified independently the resummation (upper plot) and renormalization (lower plot) scales.

In order to test our formalism, we used Z boson production as a benchmark process. We started from the code `DYqT` [15] to compute the next-to-next-to-leading logarithmic QCD (NNLL) corrections properly matched to the fixed-order contribution (i.e. NNLO QCD in this case). In Fig. B.22, we show the combination of NNLL+NNLO QCD predictions for the q_T spectrum of the produced Z (in the narrow width approximation), together with the LL (red dashed) and mixed NLL'+NLO QED contributions (blue solid). The effects introduced by mixed QCD-QED terms reach the percent-level for $q_T \approx 20\,\text{GeV}$, when considering LHC kinematics at 13 TeV center-of-mass energy. However, the most noticeable consequence of introducing these corrections is the scale-dependence reduction. This means that our predictions are more stable when varying the electro-weak parameters or the factorization/renormalization/resummation scales.

3.5 Conclusions

In this brief document, we reviewed some of our recent efforts towards more precise phenomenological predictions for colliders. We centered the discussion into the inclusion of QED and mixed QCD-QED corrections to the evolution of PDFs (through the computation of novel splitting functions), QED fixed-order computations (using diphoton production as a benchmark) and mixed QCD-QED q_T-resummation (applied to Z boson production). In all these cases, the corrections constitute percent-level deviation from the dominant QCD one, but this could still be detected through an increased precision of the forthcoming experimental measurements (such as those provided by the FCC-ee). So, understanding how to extend the exposed frameworks to deal with even higher perturbative orders is crucial to match the quality of the experimental

data, allowing to detect any possible deviation from the Standard Model and discover new physical phenomena.

Acknowledgments

The work has been done in collaboration with D. de Florian, G. Rodrigo, L. Cieri and G. Ferrera.

References

[1] S. Catani, M. Grazzini, An NNLO subtraction formalism in hadron collisions and its application to Higgs boson production at the LHC, Phys. Rev. Lett. 98 (2007) 222002. arXiv:hep-ph/0703012, doi:10.1103/PhysRevLett.98.222002.

[2] S. Catani, L. Cieri, D. de Florian, G. Ferrera, M. Grazzini, Universality of transverse-momentum resummation and hard factors at the NNLO, Nucl. Phys. B881 (2014) 414–443. arXiv:1311.1654, doi:10.1016/j.nuclphysb.2014.02.011.

[3] G. Altarelli, G. Parisi, Asymptotic Freedom in Parton Language, Nucl. Phys. B126 (1977) 298–318. doi:10.1016/0550-3213(77)90384-4.

[4] D. de Florian, G. F. R. Sborlini, G. Rodrigo, QED corrections to the Altarelli–Parisi splitting functions, Eur. Phys. J. C76 (5) (2016) 282. arXiv:1512.00612, doi:10.1140/epjc/s10052-016-4131-8.

[5] D. de Florian, G. F. R. Sborlini, G. Rodrigo, Two-loop QED corrections to the Altarelli-Parisi splitting functions, JHEP 10 (2016) 056. arXiv:1606.02887, doi:10.1007/JHEP10(2016)056.

[6] S. Catani, M. Grazzini, A. Torre, Transverse-momentum resummation for heavy-quark hadroproduction, Nucl. Phys. B890 (2014) 518–538. arXiv:1408.4564, doi:10.1016/j.nuclphysb.2014.11.019.

[7] R. Bonciani, S. Catani, M. Grazzini, H. Sargsyan, A. Torre, The q_T subtraction method for top quark production at hadron colliders, Eur. Phys. J. C75 (12) (2015) 581. arXiv:1508.03585, doi:10.1140/epjc/s10052-015-3793-y.

[8] S. Catani, L. Cieri, D. de Florian, G. Ferrera, M. Grazzini, Diphoton production at hadron colliders: a fully-differential QCD calculation at NNLO, Phys. Rev. Lett. 108 (2012) 072001, [Erratum: Phys. Rev. Lett.117,no.8,089901(2016)]. arXiv:1110.2375, doi:10.1103/PhysRevLett.108.072001,10.1103/PhysRevLett.117.089901.

[9] S. Catani, L. Cieri, D. de Florian, G. Ferrera, M. Grazzini, Diphoton production at the LHC: a QCD study up to NNLO, JHEP 04 (2018) 142. arXiv:1802.02095, doi:10.1007/JHEP04(2018)142.

[10] G. F. R. Sborlini, Higher-order QED effects in hadronic processes, PoS EPS-HEP2017 (2017) 398. arXiv:1709.09596, doi:10.22323/1.314.0398.

[11] G. F. R. Sborlini, Including higher-order mixed QCD-QED effects in hadronic calculations, in: 53rd Rencontres de Moriond on QCD and High Energy Interactions (Moriond QCD 2018) La Thuile, Italy, March 17-24, 2018, 2018. arXiv:1805.06192.

[12] R. D. Ball, et al., Parton distributions from high-precision collider data, Eur. Phys. J. C77 (10) (2017) 663. arXiv:1706.00428, doi:10.1140/epjc/s10052-017-5199-5.

[13] V. Bertone, S. Carrazza, N. P. Hartland, J. Rojo, Illuminating the photon content of the proton within a global PDF analysis, SciPost Phys. 5 (1) (2018) 008. arXiv:1712.07053, doi:10.21468/SciPostPhys.5.1.008.

[14] L. Cieri, G. Ferrera, G. F. R. Sborlini, Combining QED and QCD transverse-momentum resummation for Z boson production at hadron colliders, JHEP 08 (2018) 165. arXiv:1805.11948, doi:10.1007/JHEP08(2018)165.

[15] G. Bozzi, S. Catani, G. Ferrera, D. de Florian, M. Grazzini, Transverse-momentum resummation: A Perturbative study of Z production at the Tevatron, Nucl. Phys. B815 (2009) 174–197. arXiv:0812.2862, doi:10.1016/j.nuclphysb.2009.02.014.

4 CoLoRFulNNLO at work: A determination of α_S

Authors: Adam Kardos, Stefan Kluth, Gábor Somogyi, Zoltán Trócsányi, Zoltán Tulipánt and Andrii Verbytskyi
Corresponding Author: Adam Kardos [kardos.adam@science.unideb.hu]

4.1 Introduction

The most precise determination of fundamental parameters of the Standard Model is very important. One such fundamental parameter is the strong coupling of QCD. Its importance can be gauged by taking a look at the various experiments and configurations where it was measured, for an up to date summary see Ref. [1]. The precise measurement of such a parameter is two-fold difficult. First, high quality data with small and well-controlled uncertainties are needed. Second, high precision calculations are needed from the theory side such that theoretical uncertainties are small as well.

In a theoretical prediction based on calculation in perturbation theory the uncertainty has two main sources: the omission of higher-order terms which are estimated by the renormalization scale and the numerical stability of the integrations. While the dependence on unphysical scales can be, in principle, decreased by including more and more higher-order contributions in the prediction the numerical uncertainty can be intrinsic to the method used to obtain the theoretical prediction. Beside this, the way of comparison of experiment with theory is also affected by another uncertainty. While an experiment measures color-singlet objects, hadrons, the predictions are made in QCD for colorful ones, partons. The assumption of local parton-hadron duality ensures a correspondence between these two up to non-perturbative effects. Non-perturbative effects are power corrections in nature going with some negative power of the collision energy. This means that for an accurate comparison 1) either these effects should be estimated and taken into account 2) or the experiment should have a high enough energy that these contributions become negligible compared to other effects 3) or an observable has to be chosen which is not sensitive to these effects.

To take into account these non-perturbative effects we have to choose from phenomenological [2,3] or analytical models [4]. It is worth to note that none of these models are derived from first principles hence there is still room for improvement. Non-perturbative effects derived from first principles would also be favored because these corrections are to be used in comparisons of predictions to experimental measurements. Currently phenomenological models use several parameters fitted to experimental data thus bias is introduced in the measurement of physical parameters. The calculation of non-perturbative corrections from first principles is also advocated because the only available analytical model seems to be ill-suited for the current precision of theoretical calculations as it was shown in Ref. [5].

In this report we show two approaches how the measurement of a physical parameter, the strong coupling, can be carried out with high precision. Because the used observables allow for such measurements these can be considered as interesting subjects to study in a future electron-positron collider.

4.2 Precision through higher orders

One possible approach to increase the precision of a measurement from the theoretical perspective is to select an observable and refine its prediction by including higher-order contributions

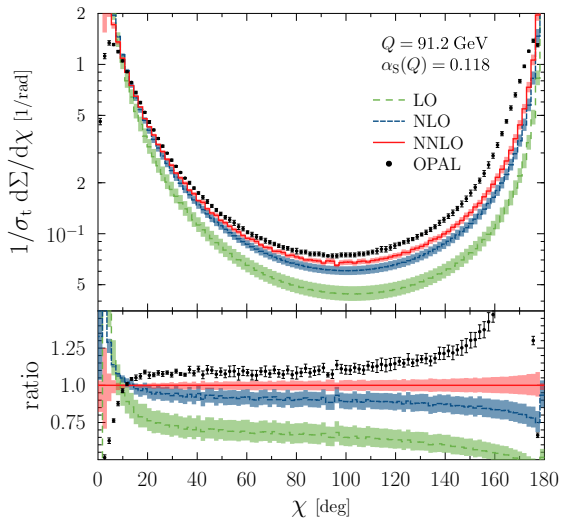

Fig. B.23: The fixed-order prediction for EEC in the first three orders of perturbation theory with theoretical uncertainties. The dots show the measurement by the OPAL collaboration [11]. On the lower panel we compared the predictions and the measurement to the NNLO result.

in fixed-order perturbation theory or by means of resummation. With the completion of the CoLoRFulNNLO subtraction method [6–8] for electron-positron collisions the next-to-next-to-leading order (NNLO) QCD prediction for energy-energy correlation (EEC) became available recently [9] for the first time. Matching this with predictions obtained by resumming leading (LL), next-to-leading (NLL) and next-to-next-to-leading logarithms (NNLL) in the back-to-back region [10] it was possible by matching the two calculations to arrive at the most precise theoretical prediction for this observable at NNLO+NNLL accuracy in QCD [5]. The energy-energy correlation is defined as a normalized energy-weighted sum of two-particle correlations:

$$\frac{1}{\sigma_t}\frac{d\Sigma(\chi)}{d\cos\chi} \equiv \frac{1}{\sigma_t}\int \sum_{i,j} \frac{E_i E_j}{Q^2} d\sigma_{e^+e^-\to ij+X}\,\delta(\cos\chi + \cos\theta_{ij})\,, \tag{4.37}$$

where Q is the center-of mass energy of the collision, σ_t is the corresponding total cross section, E_i is the energy of the ith particle, $\cos\theta_{ij}$ is the enclosed angle between the particles, i and j. The theoretical prediction for EEC in the first three orders of perturbation theory is depicted on Fig. B.23. The theoretical uncertainties were obtained from varying the renormalization scale between $m_Z/2$ and $2m_Z$. As can be seen from the lower panel even when using the highest precision prediction the difference between measurement and theory is sizable. This can be attributed to missing higher-order terms becoming important at the edge of phase space and missing hadronization corrections.

The behavior near $\chi = 0$ can be improved by including all-order results through resummation. In Ref. [12] we used modern Monte Carlo (MC) tools to extract such corrections for EEC. To do so we generated event samples both at the hadron and at the parton level and the ratio of these provided the hadron-to-parton ratio or H/P. Using this ratio and multiplying our parton-level predictions bin-by-bin we obtained our theoretical prediction at the hadron level. As MC tools we used `SHERPA2.2.4` [13] and `Herwig7.1.1` [14]. The exact setup of the MC tools is presented in Ref. [12].

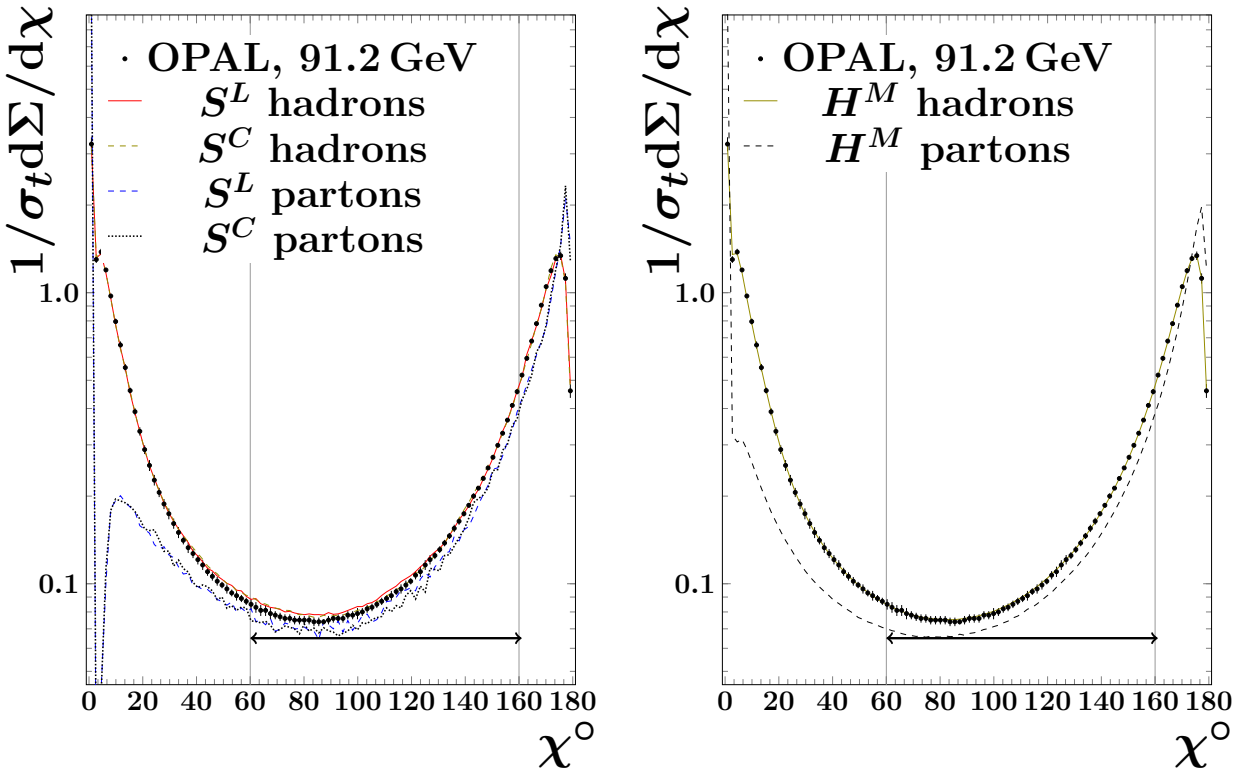

Fig. B.24: EEC distributions obtained with the two MC tools at the parton and hadron level at 91.2 GeV with corresponding OPAL data shown as well. Note that for these two plots a different χ definition was used: this time the back-to-back region corresponds to $\chi \to 180°$.

The value for the strong coupling was determined by fitting the predictions to 20 different data sets, for details see Tab. 1 of Ref. [12]. For illustrative purposes on Fig. B.24 we showed the predictions obtained with `SHERPA` and `Herwig` at the parton and hadron level. For `SHERPA` we used both the Lund (S^L) [3] and cluster (S^C) [2] hadronization models while in `Herwig` we used the built-in cluster model. On the figure we also indicated the range what was used in the actual fitting procedure.

To carry out the fitting the `MINUIT2` program [15] was used to minimize the quantity:

$$\chi^2(\alpha_S) = \sum_{\text{datasets}} \chi^2_{\text{dataset}}(\alpha_S) \tag{4.38}$$

with the $\chi^2(\alpha_S)$[§] quantity calculated as:

$$\chi^2(\alpha_S) = (\boldsymbol{D} - \boldsymbol{P}(\alpha_S))^T \underline{\underline{V}}^{-1} (\boldsymbol{D} - \boldsymbol{P}(\alpha_S)) \,, \tag{4.39}$$

where $\boldsymbol{D}$ is the vector of data points, $\boldsymbol{P}$ is the vector of predictions as functions of α_S and $\underline{\underline{V}}$ is the covariance matrix.

With the fitting procedure performed in the range between 60° and 160°. The resulting strong coupling NNLL+NNLO prediction is:

$$\alpha_S(m_Z) = 0.11750 \pm 0.00287 \tag{4.40}$$

[§]Not to be confused with the angle χ.

and at NNLL+NLO accuracy is:

$$\alpha_S(m_Z) = 0.12200 \pm 0.00535\,. \tag{4.41}$$

Notice the reduction of uncertainties as we go from NNLL+NLO to NNLL+NNLO.

4.3 Precision through small power corrections

As outlined in the introduction the current ways of taking into account the effect of non-perturbative contributions can raise concerns mainly because only phenomenological models are present for them. The other big concern is that these models rely on experimental results through tuned parameters. The best option without any model derived from first principles is to decrease these effects as much as possible. The idea is simple: if the non-perturbative contribution can be shrunk its large uncertainties will become smaller contribution to the final uncertainty of the extracted value of strong coupling.

In this section we focus on altering the definitions of existing observables to decrease the non-perturbative corrections. The most basic and most used observables in electron-positron collisions are the thrust (T) and the various jet masses. In their original definitions all of them incorporate all registered hadronic objects of the event or a given, well-defined region. Hence a natural way to modify these is to filter the tracks contributing to their value in an event. One possible way to remove tracks is by means of grooming [16–21]. In particular the soft drop [21] is a grooming when a part of the soft content of the event is removed according to some criteria.

In Ref. [22] soft-drop variants were defined for thrust, $\tau'_{\rm SD} = 1 - T'_{\rm SD}$, hemisphere jet mass, $e_2^{(2)}$ and narrow jet mass, ρ. As it was showed in the paper the non-perturbative corrections can be drastically decreased if soft drop is applied. The effect of soft drop turns out to be the most significant in the peak region of the distributions where the contribution from all-order resummation and non-perturbative effects is the greatest. This makes these observables promising candidates for strong coupling measurements at a future electron-positron collider. The application of these observables – although very interesting – is limited at LEP measurements due to the limited amount of data taken and because the soft-drop procedure inherently results in a decrease of cross section.

In our recent paper [23] we analyzed the proposed observables from the standpoint of perturbative behavior by calculating the NNLO QCD corrections to them and analyzing their dependence on the non-physical renormalization scale as an indicator of the size of neglected higher-order terms. The soft-drop versions of the observables listed above have two parameters related to soft drop: z_c and β [22]. This allows for optimization in order to minimize the decrease in cross section when the soft-drop procedure is applied.

On Fig. B.25 the soft-dropped thrust distribution is shown in the first three orders of QCD perturbation theory for a specific choice of the two soft-drop related parameters. On the right hand side of the same figure the K-factors are depicted for various parameter choices to illustrate the stability of the result. We found that the most stable perturbation prediction and moderate drop in cross section can be achieved when $(z_c, \beta) = (0.1, 0)$.

On Fig. B.26 the soft-dropped hemisphere jet mass is depicted in exactly the same way as the soft-dropped thrust on Fig. B.25. In this case it can be seen once more that the perturbative behavior stabilizes as going to higher orders in perturbation theory. This is the most pronounced at the left hand side of the peak where the NLO and NNLO predictions coincide. For this observable we found that the best choice for the soft-drop parameters is also $(z_c, \beta) = (0.1, 0)$.

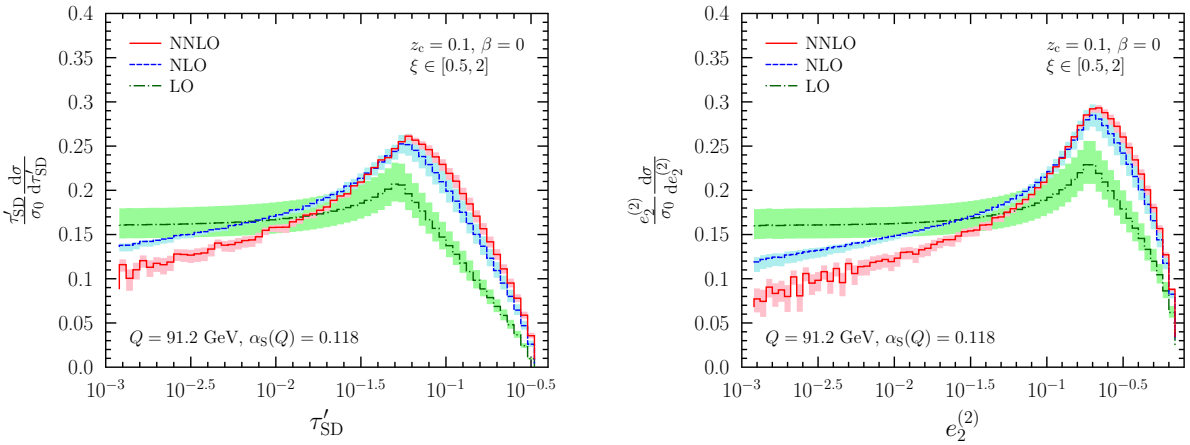

Fig. B.25: (L): Soft-dropped thrust distribution at the Z peak in the first three orders of perturbation theory, the bands represent the uncertainty coming from the variation of the renormalization scale between $Q/2$ and $2Q$. (R): The K-factors for the soft-dropped thrust distribution for various choices of the soft-drop parameters.

For the traditional versions of these observables the peak region is the one where the all-order resummed results and non-perturbative corrections are mandatory to have agreement with the experiment but for the soft-dropped versions neither the higher-order contributions nor the non-perturbative corrections are drastic. The minimal role of higher orders in perturbation theory can be seen from the perturbative stability of our results while the small size of non-perturbative corrections has been shown in Ref. [22]. These properties make the soft-dropped event shapes attractive observables for the extraction of the strong coupling.

4.4 Conclusions

A future electron-positron collider would be considered as a dream machine for many reasons. A machine of this type would allow for a precise tuning of collision energy, it would be without

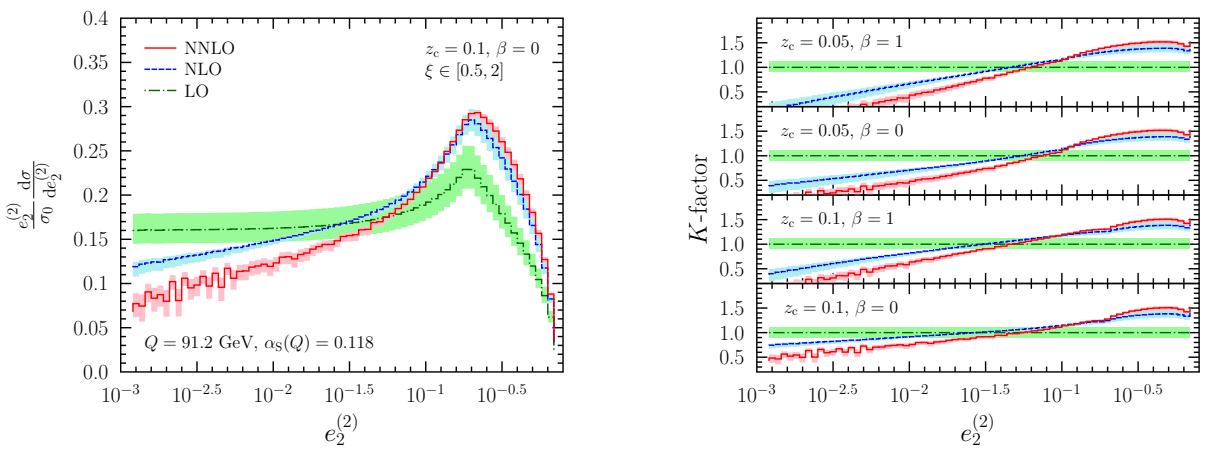

Fig. B.26: The same as Fig. B.25 but for the hemisphere jet mass.

any annoying underlying event and with colored partons in the initial state. Several possible measurements could be envisioned at such a machine but from the QCD point of view the determination of the strong coupling stands out. The strong coupling is a fundamental parameter of the standard model of particle physics so knowing its value is of key importance.

In this report we showed two possible ways to conduct such a measurement. First, by including higher-order corrections in the theoretical prediction and comparing this to the experimental result modeling non-perturbative effects with modern MC tools. Second, we showed modified versions of well-known observables defined in electron-positron collisions where non-perturbative corrections can be minimized hence diminishing the effects of their uncertainties on theoretical predictions. These observables seem to be promising candidates not just for strong coupling measurements but also for the purpose of testing the Standard Model further. Thus they should be seriously considered as important measurements at a future electron-positron facility.

Acknowledgements

A.K. is grateful to the organizers of the FCC-ee 2019 workshop held at CERN for the invitation to give a talk about recent advancements in QCD related to electron-positron colliders and for the warm atmosphere they created.

References

[1] S. Bethke, α_s 2016, Nucl. Part. Phys. Proc. 282-284 (2017) 149–152. doi:10.1016/j.nuclphysbps.2016.12.028.

[2] B. R. Webber, A QCD Model for Jet Fragmentation Including Soft Gluon Interference, Nucl. Phys. B238 (1984) 492–528. doi:10.1016/0550-3213(84)90333-X.

[3] B. Andersson, G. Gustafson, G. Ingelman, T. Sjostrand, Parton Fragmentation and String Dynamics, Phys. Rept. 97 (1983) 31–145. doi:10.1016/0370-1573(83)90080-7.

[4] Y. L. Dokshitzer, G. Marchesini, B. R. Webber, Nonperturbative effects in the energy energy correlation, JHEP 07 (1999) 012. arXiv:hep-ph/9905339, doi:10.1088/1126-6708/1999/07/012.

[5] Z. Tulipánt, A. Kardos, G. Somogyi, Energy–energy correlation in electron–positron annihilation at NNLL + NNLO accuracy, Eur. Phys. J. C77 (11) (2017) 749. arXiv:1708.04093, doi:10.1140/epjc/s10052-017-5320-9.

[6] G. Somogyi, Z. Trocsanyi, V. Del Duca, A Subtraction scheme for computing QCD jet cross sections at NNLO: Regularization of doubly-real emissions, JHEP 01 (2007) 070. arXiv:hep-ph/0609042, doi:10.1088/1126-6708/2007/01/070.

[7] G. Somogyi, Z. Trocsanyi, A Subtraction scheme for computing QCD jet cross sections at NNLO: Regularization of real-virtual emission, JHEP 01 (2007) 052. arXiv:hep-ph/0609043, doi:10.1088/1126-6708/2007/01/052.

[8] V. Del Duca, C. Duhr, A. Kardos, G. Somogyi, Z. Szőr, Z. Trócsányi, Z. Tulipánt, Jet production in the CoLoRFulNNLO method: event shapes in electron-positron collisions, Phys. Rev. D94 (7) (2016) 074019. arXiv:1606.03453, doi:10.1103/PhysRevD.94.074019.

[9] V. Del Duca, C. Duhr, A. Kardos, G. Somogyi, Z. Trócsányi, Three-Jet Production in Electron-Positron Collisions at Next-to-Next-to-Leading Order Accuracy, Phys. Rev. Lett. 117 (15) (2016) 152004. arXiv:1603.08927, doi:10.1103/PhysRevLett.117.152004.

[10] D. de Florian, M. Grazzini, The Back-to-back region in e+ e- energy-energy correlation, Nucl. Phys. B704 (2005) 387–403. arXiv:hep-ph/0407241, doi:10.1016/j.nuclphysb.2004.10.051.

[11] P. D. Acton, et al., A Determination of alpha-s (M (Z0)) at LEP using resummed QCD calculations, Z. Phys. C59 (1993) 1–20. doi:10.1007/BF01555834.

[12] A. Kardos, S. Kluth, G. Somogyi, Z. Tulipánt, A. Verbytskyi, Precise determination of $\alpha_S(M_Z)$ from a global fit of energy–energy correlation to NNLO+NNLL predictions, Eur. Phys. J. C78 (6) (2018) 498. arXiv:1804.09146, doi:10.1140/epjc/s10052-018-5963-1.

[13] T. Gleisberg, S. Hoeche, F. Krauss, M. Schonherr, S. Schumann, F. Siegert, J. Winter, Event generation with SHERPA 1.1, JHEP 02 (2009) 007. arXiv:0811.4622, doi:10.1088/1126-6708/2009/02/007.

[14] J. Bellm, et al., Herwig 7.0/Herwig++ 3.0 release note, Eur. Phys. J. C76 (4) (2016) 196. arXiv:1512.01178, doi:10.1140/epjc/s10052-016-4018-8.

[15] F. James, M. Roos, Minuit: A System for Function Minimization and Analysis of the Parameter Errors and Correlations, Comput. Phys. Commun. 10 (1975) 343–367. doi:10.1016/0010-4655(75)90039-9.

[16] J. M. Butterworth, A. R. Davison, M. Rubin, G. P. Salam, Jet substructure as a new Higgs search channel at the LHC, Phys. Rev. Lett. 100 (2008) 242001. arXiv:0802.2470, doi:10.1103/PhysRevLett.100.242001.

[17] D. Krohn, J. Thaler, L.-T. Wang, Jet Trimming, JHEP 02 (2010) 084. arXiv:0912.1342, doi:10.1007/JHEP02(2010)084.

[18] S. D. Ellis, C. K. Vermilion, J. R. Walsh, Recombination Algorithms and Jet Substructure: Pruning as a Tool for Heavy Particle Searches, Phys. Rev. D81 (2010) 094023. arXiv:0912.0033, doi:10.1103/PhysRevD.81.094023.

[19] S. D. Ellis, C. K. Vermilion, J. R. Walsh, Techniques for improved heavy particle searches with jet substructure, Phys. Rev. D80 (2009) 051501. arXiv:0903.5081, doi:10.1103/PhysRevD.80.051501.

[20] M. Dasgupta, A. Fregoso, S. Marzani, G. P. Salam, Towards an understanding of jet substructure, JHEP 09 (2013) 029. arXiv:1307.0007, doi:10.1007/JHEP09(2013)029.

[21] A. J. Larkoski, S. Marzani, G. Soyez, J. Thaler, Soft Drop, JHEP 05 (2014) 146. arXiv:1402.2657, doi:10.1007/JHEP05(2014)146.

[22] J. Baron, S. Marzani, V. Theeuwes, Soft-Drop Thrust, JHEP 08 (2018) 105. arXiv:1803.04719, doi:10.1007/JHEP08(2018)105.

[23] A. Kardos, G. Somogyi, Z. Trócsányi, Soft-drop event shapes in electron–positron annihilation at next-to-next-to-leading order accuracy, Phys. Lett. B786 (2018) 313–318. arXiv:1807.11472, doi:10.1016/j.physletb.2018.10.014.

5 Theoretical Luminosity Precision for the FCC-ee: Overview of the Path to 0.01%

Authors: Bennie F.L. Ward, Stanisław Jadach, Wiesław Płaczek, Maciej Skrzypek, and Scott A. Yost
Corresponding Author: Bennie F.L. Ward [BFL_Ward@baylor.edu]

We present an overview of the pathways to the required theoretical precision for the luminosity targeted by the FCC-ee precision studies. We put the discussion in context with a brief review of the situation at the time of LEP. We then present the current status and an overview of routes to the desired 0.01% targeted by the FCC-ee (as well as by the ILC).

We use the situation that existed at the end of LEP as our starting point. At the end of LEP, the error budget for the BHLUMI4.04 MC used by all LEP collaborations to simulate the luminosity process was calculated in Ref. [1]. For reference, we reproduce this result here in Table B.3. In this table, we show the published works upon which the various error estimates

	LEP1		LEP2	
Type of correction/error	1996	1999	1996	1999
(a) Missing photonic $\mathcal{O}(\alpha^2)$ [2,3]	0.10%	0.027%	0.20%	0.04%
(b) Missing photonic $\mathcal{O}(\alpha^3 L_e^3)$ [4]	0.015%	0.015%	0.03%	0.03%
(c) Vacuum polarization [5,6]	0.04%	0.04%	0.10%	0.10%
(d) Light pairs [7,8]	0.03%	0.03%	0.05%	0.05%
(e) Z and s-channel γ [9,10]	0.015%	0.015%	0.0%	0.0%
Total	0.11% [10]	0.061% [1]	0.25% [10]	0.12% [1]

Table B.3: Summary of the total (physical+technical) theoretical uncertainty for a typical calorimetric detector. For LEP1, the above estimate is valid for a generic angular range within 1°–3° (18–52 mrads), and for LEP2 energies up to 176 GeV and an angular range within 3°–6°. Total uncertainty is taken in quadrature. Technical precision included in (a).

are based as they are discussed in Ref. [1].

One way to address the 0.01% precision tag needed for the luminosity theory error for the FCC-ee is to develop the corresponding improved version of the BHLUMI. This problem is addressed recently in Ref. [11], wherein the path to 0.01% theory precision for the FCC-ee luminosity is presented in some detail. The results of this latter reference are shown in Table B.4, wherein we also present the current state of the art for completeness, as it is discussed in more detail in Ref. [11].

The key steps in arriving at Table B.4 are as follows. The errors associated with the photonic corrections in lines (a) and (b) in the LEP results in Table B.3 are due to effects which are known from Refs. [2–4] but which were not implemented into BHLUMI. In Table B.4 we show what these errors will become after these known results are included in BHLUMI as discussed in Ref. [11]. Similarly, in line (c) of Table B.3 the error is due to the uncertainty at the time of LEP on the hadronic contribution to the vacuum polarization for the photon at the respective momentum transfers for the luminosity process; in Table B.4 we show the improvement of this error that is expected for the FCC-ee as discussed in Refs. [12,16].

Continuing in this way, in line (d) in Table B.4 we show the expected [11] improvement, with reference to the LEP time for Table B.3, in the light pairs error for the FCC-ee . As we

Type of correction / Error	Update 2018	FCC-ee forecast
(a) Photonic $[\mathcal{O}(L_e\alpha^2)]$ $\mathcal{O}(L_e^2\alpha^3)$	0.027%	0.1×10^{-4}
(b) Photonic $[\mathcal{O}(L_e^3\alpha^3)]$ $\mathcal{O}(L_e^4\alpha^4)$	0.015%	0.6×10^{-5}
(c) Vacuum polariz.	0.014% [12]	0.6×10^{-4}
(d) Light pairs	0.010% [13, 14]	0.5×10^{-4}
(e) Z and s-channel γ exchange	0.090% [9]	0.1×10^{-4}
(f) Up-down interference	0.009% [15]	0.1×10^{-4}
(f) Technical Precision	(0.027)%	0.1×10^{-4}
Total	0.097%	1.0×10^{-4}

Table B.4: Anticipated total (physical+technical) theoretical uncertainty for a FCC-ee luminosity calorimetric detector with the angular range being 64–86 mrad (narrow), near the Z peak. Description of photonic corrections in square brackets is related to the 2nd column. The total error is summed in quadrature.

explain in Ref. [11], the complete matrix element for the additional real e^+e^- pair radiation should be used, because non-photonic graphs can contribute as much as 0.01% for the cut-off $z_{\rm cut} \sim 0.7$. This can be done with the MC generators developed for the $e^+e^- \to 4f$ processes for LEP2 physics - see Ref. [11] for further discussion. With known methods [11], the contributions of light quark pairs, muon pairs and non-leading, non-soft additional $e^+e^- + n\gamma$ corrections can be controlled such that the error on the pairs contribution is as given in line (d) for the FCC-ee. As noted, we also show the current state of the art [11] for this error in line(d) of Table B.4.

Turning to line (e) in Table B.4, we show the improvement of the error on the Z and s-channel γ exchange for the FCC-ee as well as its current state of the art. In Ref. [11], a detailed discussion is presented of all of the six interference and three additional squared modulus terms that result from the s-channel γ, s-channel Z, and t-channel Z exchange contributions to the amplitude for the luminosity process. It is shown that, if the predictions of `BHLUMI` for the luminosity measurement at FCC-ee are combined with the ones from `Bhwide` [17] for this Z and s-channel γ exchange contribution, then the error in the second column of line (e) of Table B.4 could be reduced to 0.01%. In order to reduce the uncertainty of this contribution practically to zero we would include these Z and γ_s exchanges within the CEEX [18] type matrix element at $\mathcal{O}(\alpha^1)$ in `BHLUMI`. Here, CEEX stands for coherent exclusive exponentiation which acts at the level of the amplitudes as compared the original Yennie–Frautschi–Suura [19](YFS) exclusive exponentiation (EEX) that is used in `BHLUMI`4.04 and that acts at the level of the squared amplitudes. It is expected to be enough to add the EW corrections to the LABH process in the form of effective couplings in the Born amplitudes. This leads to the error estimate shown in Table B.4 in line(e) for the FCC-ee.

For completeness, we note that for our discussion of the Z and s-channel γ exchanges we made in Ref. [11] a numerical study using `Bhwide` for the the calorimetric LCAL-type detector, as described in ref. [20], for the symmetric angular range 64–86 mrad without any cut on acoplanarity. The pure weak corrections were calculated with the `ALIBABA` EW library [21, 22]. The results, shown in Table B.5, were obtained for three values of the centre-of-mass (CM) energy: $E_{\rm CM} = M_Z$, $M_Z \pm 1\,{\rm GeV}$, where the latter two values have Z contributions that are close to maximal in size. The results in the second column for the total size of the Z and γ_s exchanges are consistent with our expectations as explained in ref. [11]: the contribution is positive below the Z peak where it reaches a size $\sim 0.64\%$, is close to zero near the peak, and

$E_{\rm CM}$ [GeV]	$\Delta_{\rm tot}$ [%]	$\delta^{\rm QED}_{\mathcal{O}(\alpha)}$ [%]	$\delta^{\rm QED}_{\rm h.o.}$ [%]	$\delta^{\rm weak}_{\rm tot}$ [%]
90.1876	+0.642 (12)	−0.152 (59)	+0.034 (38)	−0.005 (12)
91.1876	+0.041 (11)	+0.148 (59)	−0.035 (38)	+0.009 (12)
92.1876	−0.719 (13)	+0.348 (59)	−0.081 (38)	+0.039 (13)

Table B.5: Results from Bhwide for the Z and γ_s exchanges contribution to the FCC-ee luminosity with respect to the $\gamma_t \otimes \gamma_t$ process for the calorimetric LCAL-type detector [20] with the symmetric angular range 64–86 mrad; no acoplanarity cut was applied. MC errors are marked in brackets.

changes sign above the peak where it reaches a size $\sim -0.72\%$. The third column features the fixed-order (non-exponentiated) $\mathcal{O}(\alpha)$ QED correction and shows that it is sizeable and up to a half of the size of the Born level effect, with a sign that is opposite to that of the latter effect. The fourth column shows the size of the higher-order QED effects from YFS exponentiation, which also change their sign near the Z-peak, oppositely to the corresponding change of the $\mathcal{O}(\alpha)$ corrections. We see that the size of the former effects is about a quarter of that of the latter. The effects in the fourth column allow us to make a conservative estimate of the size of the missing higher-order QED effects in Bhwide using the big log factor $\gamma = \frac{\alpha}{\pi} \ln \frac{|\bar{t}|}{m_e^2} = 0.042$ of Section 4 of Ref. [11] and a safety factor of 2 of Ref. [9] together with the largest higher-order effect in Table B.5, 0.081%, as $0.081\% \times \gamma \times 2 \simeq 0.007\%$. The last column shows that the size of the pure weak corrections, as implemented within the $\mathcal{O}(\alpha)$ YFS exponentiation scheme, is at the level of 0.01% below and at M_Z and increases up to $\sim 0.04\%$ above M_Z. We may use the same factor as we did for the higher order corrections to estimate the size of the missing higher order pure weak corrections in Bhwide as $\sim 0.003\%$. Altogether, by adding the two estimates of its massing effects, we obtain a conservative estimate of 0.01% for the physical precision of Bhwide to justify our remarks above concerning the error in line (e) of Table B.4 that would result from the combination of the prediction of BHLUMI and that of Bhwide for this contribution.

In line (f) in Table B.4 we show the estimate of the error on the up-down interference between radiation from the e^- and e^+ lines. Unlike in LEP1, where it was negligible, for the FCC-ee this effect, calculated in Ref. [15] at $\mathcal{O}(\alpha^1)$, is 10 times larger and has to be included in the upgraded BHLUMI. Once this is done, the error estimate shown in line (f) for the FCC-ee obtains [11].

This brings us to the issue of the technical precision. In an ideal situation, in order to get the upgraded BHLUMIś technical precision at the level 10^{-5} for the total cross section and 10^{-4} for single differential distributions, one would need to compare it with another MC program developed independently, which properly implements the soft-photon resummation, LO corrections up to $\mathcal{O}(\alpha^3 L_e^3)$, and the second-order corrections with the complete $\mathcal{O}(\alpha^2 L_e)$. In principle, an extension of a program like BabaYaga [23–25], which is currently exact at NLO with a matched QED shower, to the level of NNLO for the hard process, while keeping the correct soft-photon resummation, would provide the best comparison to the upgraded BHLUMI to establish the technical precision of both programs at the 10^{-5} precision level[¶]. During the intervening time period, a very good test of the technical precision of the upgraded BHLUMI would follow from the comparison between its results with EEX and CEEX matrix elements; for, the basic multi-photon phase space integration module of BHLUMI was already well tested

[¶] The upgrade of the BHLUMI distributions will be relatively straightforward because its multi-photon phase space is exact [26] for any number of photons.

in Ref. [27] and such a test can be repeated at an even higher-precision level.

In summary, we conclude that, with the appropriate resources, the path to 0.01% precision for the FCC-ee luminosity (and the ILC luminosity) at the Z peak is open via an upgraded version of `BHLUMI`.

References

[1] B. F. L. Ward, S. Jadach, M. Melles, S. A. Yost, New results on the theoretical precision of the LEP/SLC luminosity, Phys. Lett. B450 (1999) 262–266. arXiv:hep-ph/9811245, doi:10.1016/S0370-2693(99)00104-5.

[2] S. Jadach, M. Melles, B. F. L. Ward, S. A. Yost, Exact results on $O(\alpha)$ corrections to the single hard bremsstrahlung process in low angle Bhabha scattering in the SLC/LEP energy regime, Phys. Lett. B377 (1996) 168–176. arXiv:hep-ph/9603248, doi:10.1016/0370-2693(96)00354-1.

[3] S. Jadach, M. Melles, B. F. L. Ward, S. A. Yost, New results on the precision of the LEP luminosity, Acta Phys. Polon. B30 (1999) 1745–1750.

[4] S. Jadach, B. F. L. Ward, Missing third order leading log corrections in the small angle Bhabha calculation, Phys. Lett. B389 (1996) 129–136. doi:10.1016/S0370-2693(96)01242-7.

[5] H. Burkhardt, B. Pietrzyk, Update of the hadronic contribution to the QED vacuum polarization, Phys. Lett. B356 (1995) 398–403. doi:10.1016/0370-2693(95)00820-B.

[6] S. Eidelman, F. Jegerlehner, Hadronic contributions to g-2 of the leptons and to the effective fine structure constant $\alpha(M_Z^2)$, Z. Phys. C67 (1995) 585–602. arXiv:hep-ph/9502298, doi:10.1007/BF01553984.

[7] S. Jadach, M. Skrzypek, B. F. L. Ward, Analytical results for low angle Bhabha scattering with pair production, Phys. Rev. D47 (1993) 3733–3741. doi:10.1103/PhysRevD.47.3733.

[8] S. Jadach, M. Skrzypek, B. F. L. Ward, Soft pairs corrections to low angle Bhabha scattering: YFS Monte Carlo approach, Phys. Rev. D55 (1997) 1206–1215. doi:10.1103/PhysRevD.55.1206.

[9] S. Jadach, W. Placzek, B. F. L. Ward, Precision calculation of the $\gamma - Z$ interference effect in the SLC/LEP luminosity process, Phys. Lett. B353 (1995) 349–361. doi:10.1016/0370-2693(95)00576-7.

[10] A. Arbuzov, et al., The Present theoretical error on the Bhabha scattering cross-section in the luminometry region at LEP, Phys. Lett. B383 (1996) 238–242. arXiv:hep-ph/9605239, doi:10.1016/0370-2693(96)00733-2.

[11] S. Jadach, W. Płaczek, M. Skrzypek, B. F. L. Ward, S. A. Yost, The path to 0.01% theoretical luminosity precision for the FCC-ee, Phys. Lett. B790 (2019) 314–321. arXiv:1812.01004, doi:10.1016/j.physletb.2019.01.012.

[12] F. Jegerlehner, $\alpha_{QED}(M_Z)$ and future prospects with low energy e^+e^- collider data FCC-ee Mini-Workshop, "Physics Behind Precision" *https://indico.cern.ch/event/469561/*.

[13] G. Montagna, M. Moretti, O. Nicrosini, A. Pallavicini, F. Piccinini, Light pair correction to Bhabha scattering at small angle, Nucl. Phys. B547 (1999) 39–59. arXiv:hep-ph/9811436, doi:10.1016/S0550-3213(99)00064-4.

[14] G. Montagna, M. Moretti, O. Nicrosini, A. Pallavicini, F. Piccinini, Light pair corrections

to small angle Bhabha scattering in a realistic set up at LEP, Phys. Lett. B459 (1999) 649–652. arXiv:hep-ph/9905235, doi:10.1016/S0370-2693(99)00729-7.

[15] S. Jadach, E. Richter-Was, B. F. L. Ward, Z. Was, Analytical $O(\alpha)$ distributions for Bhabha scattering at low angles, Phys. Lett. B253 (1991) 469–477. doi:10.1016/0370-2693(91)91754-J.

[16] F. Jegerlehner, Variations on Photon Vacuum Polarization, arXiv:1711.06089.

[17] S. Jadach, W. Placzek, B. F. L. Ward, BHWIDE 1.00: $O(\alpha)$ YFS exponentiated Monte Carlo for Bhabha scattering at wide angles for LEP-1/SLC and LEP-2, Phys. Lett. B390 (1997) 298–308. arXiv:hep-ph/9608412, doi:10.1016/S0370-2693(96)01382-2.

[18] S. Jadach, B. Ward, Z. Wąs, Coherent exclusive exponentiation for precision Monte Carlo calculations, Phys. Rev. D63 (2001) 113009. arXiv:hep-ph/0006359, doi:10.1103/PhysRevD.63.113009.

[19] D. R. Yennie, S. C. Frautschi, H. Suura, The infrared divergence phenomena and high-energy processes, Annals Phys. 13 (1961) 379–452. doi:10.1016/0003-4916(61)90151-8.

[20] S. Jadach, E. Richter-Was, B. F. L. Ward, Z. Was, QED multi - photon corrections to Bhabha scattering at low angles: Monte Carlo solution, Phys. Lett. B268 (1991) 253–262. doi:10.1016/0370-2693(91)90813-6.

[21] W. Beenakker, F. A. Berends, S. C. van der Marck, Large angle Bhabha scattering, Nucl. Phys. B349 (1991) 323–368. doi:10.1016/0550-3213(91)90328-U.

[22] W. Beenakker, F. A. Berends, S. C. van der Marck, Small angle Bhabha scattering, Nucl. Phys. B355 (1991) 281–294. doi:10.1016/0550-3213(91)90114-D.

[23] C. M. Carloni Calame, C. Lunardini, G. Montagna, O. Nicrosini, F. Piccinini, Large angle Bhabha scattering and luminosity at flavor factories, Nucl. Phys. B584 (2000) 459–479. arXiv:hep-ph/0003268, doi:10.1016/S0550-3213(00)00356-4.

[24] C. M. Carloni Calame, An Improved parton shower algorithm in QED, Phys. Lett. B520 (2001) 16–24. arXiv:hep-ph/0103117, doi:10.1016/S0370-2693(01)01108-X.

[25] G. Balossini, C. M. Carloni Calame, G. Montagna, O. Nicrosini, F. Piccinini, Matching perturbative and parton shower corrections to Bhabha process at flavour factories, Nucl. Phys. B758 (2006) 227–253. arXiv:hep-ph/0607181, doi:10.1016/j.nuclphysb.2006.09.022.

[26] S. Jadach, B. F. L. Ward, Z. Was, The precision Monte Carlo event generator KK for two- fermion final states in e^+e^- collisions, Comput. Phys. Commun. 130 (2000) 260–325, program source available from http://jadach.web.cern.ch/. arXiv:hep-ph/9912214.

[27] S. Jadach, B. F. L. Ward, Semianalytical third order calculations of the small angle Bhabha cross-sections, Acta Phys. Polon. B28 (1997) 1907–1979.

6 $e^+e^- \to \gamma\gamma$ at large angle for FCC-ee luminometry

Author: Carlo M. Carloni, Mauro Chiesa, Guido Montagna, Oreste Nicrosini, Fulvio Piccinini
Corresponding Author: Carlo M. Carloni [carlo.carloni.calame@pv.infn.it]

Abstract

We examine large-angle two photon production in e^+e^- annihilation as a possible process to monitor the luminosity of FCC-ee. We review the current status of the theoretical predictions and perform an exploratory phenomenological study of the next-to-leading and higher-order QED corrections using the Monte Carlo event generator BabaYaga@NLO. We also consider the one-loop weak corrections, that are necessary to meet the high-precision requirements of FCC-ee. Possible ways to approach the target theoretical accuracy are sketched.

6.1 Introduction

The successful accomplishment of the FCC-ee physics goals requires a detailed knowledge of the collider luminosity. The ambitious FCC-ee target is a luminosity measurement with a total error of the order of 10^{-4} (or even better) and calls for a major effort by both the experimental and theoretical community.

At FCC-ee, the standard luminosity process is expected to be small-angle Bhabha scattering, likewise at LEP. However, also the process of large-angle two photon production, i.e. $e^+e^- \to \gamma\gamma$, has been recently proposed as a possible alternative normalization process for FCC-ee operation [1–3]. Actually, it is a purely QED process at leading order at any energy, it receives QED corrections from the initial state only and does not contain at order α the contribution due to the vacuum polarization (in particular, hadronic loops), which enters at next-to-next-to-leading order (NNLO) only. On the other hand, the cross section of $e^+e^- \to \gamma\gamma$ is significantly smaller than that of small-angle Bhabha scattering but adequate everywhere at FCC-ee, with the exception of the running at the Z resonance. Moreover, the process is affected by a large background due to large-angle Bhabha scattering.

In spite of the above limitations, the possibility of using photon-pair production as a luminosity process at FCC-ee is an interesting option to be pursued. Contrarily to Bhabha scattering, which received a lot of attention over the past decades, there is a rather poor theoretical literature about $e^+e^- \to \gamma\gamma$ annihilation and the most recent phenomenological results refer to e^+e^- colliders of moderate energies [4–7]. Also the few available Monte Carlo (MC) generators [5, 7] are tailored for low-energy accelerators and need to be improved for the high-energy, high-precision requirements of FCC-ee.

In this contribution, we provide a first assessment of the current status of the theoretical accuracy for large-angle two photon production at FCC-ee energies. For that purpose, we use the MC program BabaYaga@nlo [5, 8–11], that includes next-to-leading-order (NLO) QED corrections matched to a QED Parton Shower (PS), and compute the one-loop weak corrections due to heavy boson exchange. QED corrections to $e^+e^- \to \gamma\gamma$ at order α were previously calculated time ago in [12–14] and NLO electroweak corrections were studied in [15–17]. A generator based on [14] was used at LEP for the analysis of photon-pair production at energies above the Z [18]. Here, we perform an exploratory phenomenological study of the QED corrections at NLO and evaluate the impact of higher-order contributions due to multiple

photon emission, by considering typical values for the c.m. energies of FCC-ee. Possible perspectives to achieve the target theoretical accuracy are briefly outlined.

6.2 Theoretical approach and numerical results

According to the theoretical formulation implemented in BabaYaga@nlo, the photonic corrections are computed by using a fully-exclusive QED PS matched to QED contributions at NLO. The matching of the PS ingredients with the NLO QED corrections is realized in such a way that its $O(\alpha)$ expansion reproduces the NLO cross section and exponentiation of the leading contributions due to soft and collinear radiation is preserved as in a pure PS algorithm. Various studies and comparisons with independent calculations [6, 11, 19] showed that this formulation enables a theoretical accuracy at the level of 0.1% (or slightly better) for the calculation of integrated cross sections.

To meet the high-precision requirements of FCC-ee, we also computed the one-loop weak corrections due to heavy boson exchange. The calculation was performed by treating the ultraviolet divergencies in dimensional regularization and using the computer program Recola [20], which internally adopts the Collier [21] library for the evaluation of one-loop scalar and tensor integrals. We used in our calculation the on-shell renormalization scheme, with complex mass values for the heavy boson masses [22].

In the following, we show a sample of numerical results obtained with the code BabaYaga@nlo. They refer to four canonical c.m. energy values, that are representative of the expected FCC-ee operation program (Z-pole, WW, ZH and $t\bar{t}$ tresholds)

$$\sqrt{s} = 91,\ 160,\ 240,\ 365 \text{ GeV} \tag{6.42}$$

To study the effects due to the QED corrections, we consider a simulation setup where we require at least two photons within the angular acceptance $20^\circ \leq \theta_\gamma \leq 160^\circ$ and with energy $E_\gamma \geq 0.25 \times \sqrt{s}$. In Tab. B.6 we examine the impact of the QED radiative corrections on the integrated cross sections, when considering the above kinematical cuts.

$\sqrt{s}$ (GeV)	LO (pb)	NLO (pb)	w h.o. (pb)
91	39.821	41.043 [+3.07%]	40.868(3) [−0.44%]
160	12.881	13.291 [+3.18%]	13.228(1) [−0.49%]
240	5.7250	5.9120 [+3.26%]	5.884(2) [−0.49%]
365	2.4752	2.5582 [+3.35%]	2.5436(2) [−0.59%]

Table B.6: The two photon production cross section at LO, NLO and with higher-order QED corrections, for four FCC-ee c.m. energies. The numbers in parenthesis are the relative contributions of NLO and higher-order QED corrections.

The photon-pair production cross section is shown according to different accuracy levels, i.e. at LO, NLO QED and including higher-order contributions due to multiple photon radiation. The numbers in parenthesis are the relative contributions due to NLO and higher-order QED corrections, respectively. It can be noticed that the NLO corrections are at a few percent level, while the higher-order contributions amount to about five per mille and reduce the effect due to $O(\alpha)$ corrections.

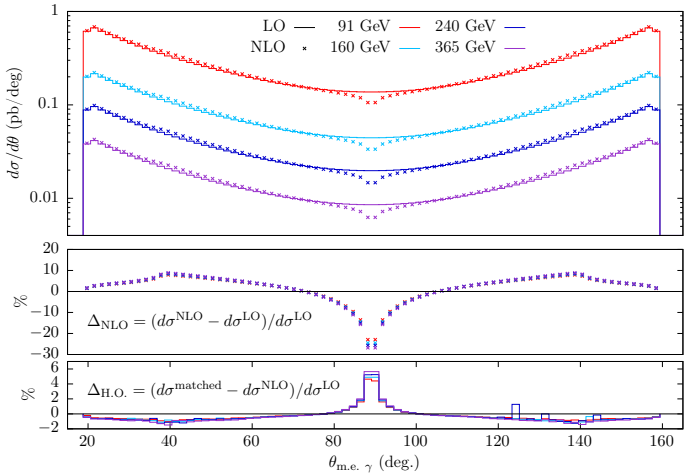

Fig. B.27: Upper panel: the angular distribution of the most energetic photon, for four FCC-ee c.m. energies. Lower panel: relative contributions of NLO and higher-order QED corrections.

A representative example of the effects due to QED corrections on the differential cross sections is given in Fig. B.27, which shows the angular distribution of the most energetic photon for the four energy points. One can see that the NLO corrections are particularly important in the central region, where they reach the 20-30% level, as mainly due to soft-photon radiation. This effect is partially compensated by the higher-order corrections, that amount to some percents in the same region.

We also preliminarily explored the contribution of one-loop weak corrections, to conclude that their size is at the per cent level, i.e. roughly as large as QED contributions beyond NLO. A more detailed investigation of their effects will be given elsewhere [23].

6.3 Summary and outlook

We have examined large-angle two photon production in e^+e^- annihilation as a possible process to monitor the luminosity at FCC-ee. We have assessed the present status of the theoretical accuracy through an exploratory phenomenological study of the radiative corrections to $e^+e^- \to \gamma\gamma$ annihilation at the c.m. energies of main interest. To this end, we have improved the theoretical content of the code BabaYaga@nlo, that includes exact NLO QED corrections matched to PS, by computing the weak corrections due to the presence of heavy bosons in the internal loops.

The accuracy of the present calculation can be estimated to be at the 0.1% level or slightly better. A first way to improve it is given by the calculation of NNLO fermion loop contributions accompanied by the computation of the same-order real pair corrections, along the lines described in [19, 24]. This should be sufficient to get close to an accuracy at the 10^{-4} level. Beyond that, a full calculation of NNLO QED corrections and, eventually, of two-loop weak contributions will be ultimately needed to reach the challenging frontier of the 10 ppm theoretical accuracy. These developments are by now under consideration.

References

[1] P. Janot, Determination of $\alpha_{QED}(M_Z)$ @ FCC-ee, talk at the *FCC-ee Physics meeting*, June 2015, CERN (2015).

[2] M. Dam, Luminosity measurements at FCC-ee, talk at the *FCC week*, April 2016, Rome (2016).

[3] C. M. Carloni Calame, $e^+e^- \to \gamma\gamma$ at large angle for FCC-ee luminometry, talk at the *11th FCC-ee workshop: Theory and Experiments*, January 2019, CERN (2019).

[4] A. B. Arbuzov, G. V. Fedotovich, E. A. Kuraev, N. P. Merenkov, V. D. Rushai, L. Trentadue, Large angle QED processes at e^+e^- colliders at energies below 3-GeV, JHEP 10 (1997) 001. arXiv:hep-ph/9702262, doi:10.1088/1126-6708/1997/10/001.

[5] G. Balossini, C. Bignamini, C. M. Carloni Calame, G. Montagna, O. Nicrosini, F. Piccinini, Photon pair production at flavour factories with per mille accuracy, Phys. Lett. B663 (2008) 209–213. arXiv:0801.3360, doi:10.1016/j.physletb.2008.04.007.

[6] S. Actis, et al., Quest for precision in hadronic cross sections at low energy: Monte Carlo tools vs. experimental data, Eur. Phys. J. C66 (2010) 585–686. arXiv:0912.0749, doi:10.1140/epjc/s10052-010-1251-4.

[7] S. I. Eidelman, G. V. Fedotovich, E. A. Kuraev, A. L. Sibidanov, Monte-Carlo Generator Photon Jets for the process $e^+e^- \to \gamma\gamma$, Eur. Phys. J. C71 (2011) 1597. arXiv:1009.3390, doi:10.1140/epjc/s10052-011-1597-2.

[8] C. M. Carloni Calame, C. Lunardini, G. Montagna, O. Nicrosini, F. Piccinini, Large angle Bhabha scattering and luminosity at flavor factories, Nucl. Phys. B584 (2000) 459–479. arXiv:hep-ph/0003268, doi:10.1016/S0550-3213(00)00356-4.

[9] C. M. Carloni Calame, An improved parton shower algorithm in QED, Phys. Lett. B520 (2001) 16–24. arXiv:hep-ph/0103117, doi:10.1016/S0370-2693(01)01108-X.

[10] C. M. Carloni Calame, G. Montagna, O. Nicrosini, F. Piccinini, The BABAYAGA event generator, Nucl. Phys. Proc. Suppl. 131 (2004) 48–55. arXiv:hep-ph/0312014, doi:10.1016/j.nuclphysbps.2004.02.008.

[11] G. Balossini, C. M. Carloni Calame, G. Montagna, O. Nicrosini, F. Piccinini, Matching perturbative and parton shower corrections to Bhabha process at flavour factories, Nucl. Phys. B758 (2006) 227–253. arXiv:hep-ph/0607181, doi:10.1016/j.nuclphysb.2006.09.022.

[12] F. A. Berends, R. Gastmans, Hard photon corrections for $e^+e^- \to \gamma\gamma$, Nucl. Phys. B61 (1973) 414–428. doi:10.1016/0550-3213(73)90372-6.

[13] S. I. Eidelman, E. A. Kuraev, e^+e^- annihilation into two and three photons at high-energy, Nucl. Phys. B143 (1978) 353–364. doi:10.1016/0550-3213(78)90030-5.

[14] F. A. Berends, R. Kleiss, Distributions for electron-positron annihilation into two and three photons, Nucl. Phys. B186 (1981) 22–34. doi:10.1016/0550-3213(81)90090-0.

[15] M. Capdequi-Peyranere, G. Grunberg, F. M. Renard, M. Talon, Weak interaction effects in $e^+e^- \to \gamma\gamma$, Nucl. Phys. B149 (1979) 243–263. doi:10.1016/0550-3213(79)90240-2.

[16] M. Bohm, T. Sack, Electroweak Radiative Corrections to $e^+e^- \to \gamma\gamma$, Z. Phys. C33 (1986) 157–165. doi:10.1007/BF01410463.

[17] J. Fujimoto, M. Igarashi, Y. Shimizu, Radiative Correction to $e^+e^- \to \gamma\gamma$ in Electroweak Theory, Prog. Theor. Phys. 77 (1987) 118. doi:10.1143/PTP.77.118.

[18] J. Alcaraz, et al., A combination of preliminary electroweak measurements and constraints on the standard model arXiv:hep-ex/0612034.

[19] C. Carloni Calame, H. Czyz, J. Gluza, M. Gunia, G. Montagna, O. Nicrosini, F. Piccinini, T. Riemann, M. Worek, NNLO leptonic and hadronic corrections to Bhabha scattering

and luminosity monitoring at meson factories, JHEP 07 (2011) 126. arXiv:1106.3178, doi:10.1007/JHEP07(2011)126.

[20] S. Actis, A. Denner, L. Hofer, J.-N. Lang, A. Scharf, S. Uccirati, RECOLA: REcursive Computation of One-Loop Amplitudes, Comput. Phys. Commun. 214 (2017) 140–173. arXiv:1605.01090, doi:10.1016/j.cpc.2017.01.004.

[21] A. Denner, S. Dittmaier, L. Hofer, Collier: a fortran-based Complex One-Loop LIbrary in Extended Regularizations, Comput. Phys. Commun. 212 (2017) 220–238. arXiv:1604.06792, doi:10.1016/j.cpc.2016.10.013.

[22] A. Denner, S. Dittmaier, The complex-mass scheme for perturbative calculations with unstable particles, Nucl. Phys. Proc. Suppl. 160 (2006) 22–26. arXiv:hep-ph/0605312, doi:10.1016/j.nuclphysbps.2006.09.025.

[23] C. M. Carloni Calame, M. Chiesa, G. Montagna, O. Nicrosini, F. Piccinini, in preparation.

[24] G. Montagna, M. Moretti, O. Nicrosini, A. Pallavicini, F. Piccinini, Light pair correction to Bhabha scattering at small angle, Nucl. Phys. B547 (1999) 39–59. arXiv:hep-ph/9811436, doi:10.1016/S0550-3213(99)00064-4.

7 Prospects for higher-order corrections to W-pair production near threshold in the EFT approach

Author: Christian Schwinn [schwinn@physik.rwth-aachen.de]

The precise measurement of the mass of the W-boson plays an essential role for precision tests of the Standard Model (SM) and indirect searches for new physics through global fits to electroweak observables. Cross-section measurements near the W-pair production threshold at a possible future e^-e^+ collider promise to reduce the experimental uncertainty to the level of 3 MeV at an International Linear Collider (ILC) [1, 2], while a high-luminosity circular collider offers a potential improvement to 0.5 MeV in case of the FCC-ee [3, 4] or 1 MeV at the CEPC [5]. At the point of highest sensitivity, an uncertainty of the cross-section measurement of 0.1% translates to an uncertainty of ~ 1.5 MeV on $M_{\rm W}$ [3]. Therefore a theoretical prediction for the cross section with an accuracy of $\Delta\sigma \sim 0.01\%$ at threshold is required to fully exploit the potential of a future circular e^-e^+ collider. Theory predictions using the double-pole approximation (DPA) [6] at next-to-leading order (NLO) [7–11] successfully described LEP2 results with an accuracy of better than 1% above threshold. An extension of the DPA to NNLO appears to be appropriate for a future e^-e^+ collider operating above the W-pair threshold, e.g. for the interpretation of anomalous triple-gauge-coupling measurements at $\sqrt{s} = 240$ GeV. However, the accuracy of the DPA at NLO degrades to 2-3% near threshold. In this region the combination of a full NLO calculation of four-fermion production [12, 13] with leading NNLO effects obtained using effective-field-theory (EFT) methods [14, 15] reduces the theory uncertainty of the total cross section below 0.3%; sufficient for the ILC target uncertainty but far above that of FCC-ee. This raises the question of the methods required to reach a theory accuracy $\sim 0.01\%$. In this contribution, this issue is addressed from the EFT point of view. The discussion is limited to the total cross section, where the EFT approach is best developed so far, although cuts on the W decay products can also be incorporated [15]. To reach the target accuracy, it will also be essential to have theoretical control of effects beyond the pure electroweak effects considered here. In particular it is assumed that next-to-leading logarithmic corrections $(\alpha/\pi)^2 \ln(m_{\rm e}^2/s)$ from collinear initial-state photon radiation (ISR), which have been estimated to be $\lesssim 0.1\%$ [12], will be resummed to all orders. QCD effects, which are important in particular for the fully hadronic decay modes, are only briefly considered. In Section 7.1 aspects of the EFT approach are reviewed from an updated perspective using insight into the factorization of soft, hard, and Coulomb corrections [16]. The NLO and leading NNLO results are summarized and compared to the NLO$^{\rm ee4f}$ calculation [12]. In Section 7.2 the structure of the EFT expansion and calculations of subsets of corrections are used to estimate the magnitude of the NNLO and leading N^{3}LO corrections and to assess if such calculations are sufficient to meet the FCC-ee target accuracy.

7.1 Effective-theory approach to W-pair production

In the EFT approach to four-fermion production near the W-pair production near threshold [14], the cross section is expanded simultaneously in the coupling, the W-decay width and the energy relative to the production threshold, which are taken to be of similar order and are denoted collectively by

$$\delta \sim v^2 \equiv \frac{(s - 4M_{\rm W}^2)}{M_{\rm W}^2} \sim \frac{\Gamma_{\rm W}}{M_{\rm W}} \sim \alpha. \tag{7.43}$$

An $\mathrm{N}^n\mathrm{LO}^{\mathrm{EFT}}$ calculation includes corrections up to $\mathcal{O}(\delta^n)$, whereas as usual $\mathrm{N}^n\mathrm{LO}$ refers to the $\mathcal{O}(\alpha^n)$ corrections. As discussed below, non-resonant and Coulomb corrections lead to odd powers of v, so that the expansion proceeds in half-integer powers of δ. The current state-of-the-art in the EFT is the calculation of the total cross section for the semi-leptonic final state $\mu^-\overline{\nu}_\mu \mathrm{u}\overline{\mathrm{d}}$ up to $\mathrm{NLO}^{\mathrm{EFT}}$ [14], which includes corrections of the order

$$\mathrm{NLO}^{\mathrm{EFT}} : v^2, \alpha, \alpha^2/v^2, \tag{7.44}$$

supplemented with the genuine $\mathcal{O}(\alpha^2, \alpha^3)$ corrections at the next order $\delta^{3/2}$ in the δ-expansion [15],

$$\mathrm{N}^{3/2}\mathrm{LO}^{\mathrm{EFT}} : \quad \alpha v, \quad \alpha^2/v, \quad \alpha^3/v^3. \tag{7.45}$$

In the following, aspects of these results and the EFT method are reviewed that are useful for the estimate of $\mathrm{NNLO}^{\mathrm{EFT}}$ corrections and the remaining uncertainty.

7.1.1 Expansion of the Born cross section

The total cross section $\mathrm{e}^-\mathrm{e}^+ \to 4f$ can be obtained from the imaginary part of the forward scattering amplitude $\mathrm{e}^-\mathrm{e}^+ \to \mathrm{e}^-\mathrm{e}^+$ where the Cutkosky-cuts are restricted to those with 4-fermion final states. Flavour specific final states can be selected accordingly. The expansion of the forward scattering amplitude in δ can be formulated in terms of an EFT [14, 17, 18], where the initial state leptons are described by soft-collinear effective theory [19], and the W bosons by a non-relativistic EFT. Similarly to the DPA [6], the cross section is decomposed into resonant and non-resonant contributions,

$$\sigma^{\mathrm{ee4f}}(s \approx 4M_{\mathrm{W}}^2) = \sigma_{\mathrm{res}}(s) + \sigma_{\text{non-res}}(s). \tag{7.46}$$

The EFT method allows a computation of the Born cross section as an expansion according to the counting (7.43), $\sigma^{\mathrm{ee4f}}_{\mathrm{Born}} = \sigma^{(0)}_{\mathrm{Born}} + \sigma^{(1/2)}_{\mathrm{Born}} + \ldots$. This is not necessary in practice since the full $\mathrm{e}^-\mathrm{e}^+ \to 4f$ Born cross section for arbitrary kinematics can be computed using automated Monte Carlo programs. However, the expansion serves as a test-case of the EFT method and provides useful input for the estimate of the accuracy of a future $\mathrm{NNLO}^{\mathrm{EFT}}$ calculation. The leading order resonant contribution to the cross section is given by the imaginary part of a one-loop EFT diagram with non-relativistic W-propagators denoted by dashed lines,

$$\sigma^{(0)}_{\mathrm{Born}}(s) = \sigma^{(0)}_{\mathrm{res}}(s) = \frac{1}{s}\mathrm{Im}\left[\quad\right] = \frac{\pi\alpha^2}{s_{\mathrm{W}}^4 s}\mathrm{Im}\left[-\sqrt{-\frac{\mathcal{E}_{\mathrm{W}}}{M_{\mathrm{W}}}}\right]. \tag{7.47}$$

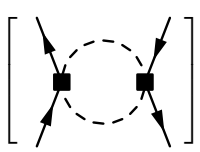

Here the complex energy variable $\mathcal{E}_{\mathrm{W}} \equiv \sqrt{s} - 2M_{\mathrm{W}} + \mathrm{i}\Gamma_{\mathrm{W}} \sim M_{\mathrm{W}}v^2$ has been introduced and $s_{\mathrm{W}} = \sin\theta_{\mathrm{W}}$ with the weak-mixing angle θ_{W}. A specific final state is selected by multiplying (7.47) by the LO branching ratios,

$$\sigma^{(0)}_{f_1\bar{f}_2 f_3\bar{f}_4} = \frac{\Gamma^{(0)}_{\mathrm{W}^-\to f_1\bar{f}_2}\Gamma^{(0)}_{\mathrm{W}^+\to f_3\bar{f}_4}}{\Gamma^2_{\mathrm{W}}}\sigma^{(0)}_{\mathrm{res}}. \tag{7.48}$$

The non-resonant contribution to the cross section arises from local four-electron operators,

$$\sigma_{\text{non-res}}(s) = \frac{1}{s}\mathrm{Im}\left[\quad\right] = \frac{\alpha^3}{s_{\mathrm{W}}^6 s}\mathcal{K}, \tag{7.49}$$

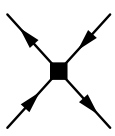

where the dimensionless constant $\mathcal{K} = \mathcal{K}^{(0)} + \frac{\alpha}{s_{\rm W}^2}\mathcal{K}^{(1)} + \dots$ is is computed from the forward-scattering amplitude in the full SM without self-energy resummation in the W-propagators. The first contribution is of order α^3 and arises from cut two-loop diagrams corresponding to squared tree diagrams of the $e^-e^+ \to W^\pm f\bar{f}$ processes. Hence, the leading non-resonant contribution $\sigma^{(1/2)}_{\text{non-res}} \equiv \sigma^{(1/2)}_{\text{Born}}$ is suppressed by $\alpha/v \sim \delta^{1/2}$ compared to the resonant LO cross section (7.47). For the final state $\mu^-\bar{\nu}_\mu u\bar{d}$, the explicit result is [14]*

$$\mathcal{K}^{(0)} = -4.25698. \tag{7.50}$$

The $\mathcal{O}(v^2)$ corrections in (7.44) originate from higher-order terms in the EFT expansion of the resonant Born cross section, $\sigma^{(1)}_{\text{Born}}$, and depend strongly on the centre-of-mass energy [14],

$$\sigma^{(1)}_{\text{Born}}(\sqrt{s} = 161\ \text{GeV}) = 8\% \times \sigma^{\text{ee4f}}_{\text{Born}}, \quad \sigma^{(1)}_{\text{Born}}(\sqrt{s} = 170\ \text{GeV}) = -8\% \times \sigma^{\text{ee4f}}_{\text{Born}}. \tag{7.51}$$

7.1.2 Radiative corrections

Including radiative corrections, the resonant cross section factorizes into hard, soft, and Coulomb functions [16],†

$$\sigma_{\text{res}}(s) = \text{Im}\left[\ C \quad C\ \right] = \frac{4\pi^2\alpha^2}{sM_{\rm W}^2 s_{\rm W}^4}\text{Im}\left[C^2\int d\omega W(\omega) G_C(0,0,\mathcal{E}_{\rm W}-\omega)\right]. \tag{7.52}$$

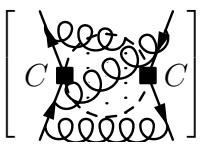

Here curly lines depict soft photons with momenta $(q^0, \vec{q}) \sim (\delta, \delta)$, while dotted lines denote potential (Coulomb) photons with $(q^0, \vec{q}) \sim (\delta, \sqrt{\delta})$. The Wilson coefficient $C = 1 + \frac{\alpha}{2\pi}C^{(1)}\dots$ is related to contributions of hard loop momenta $q \sim M_{\rm W}$ to the on-shell amplitudes $e^-e^+ \to W^-W^+$ evaluated at the production threshold. For the input parameters used in [14], the explicit value of the one-loop coefficient is

$$C^{(1)} = \text{Re}\, c^{(1,\text{fin})}_{p,LR} = -10.076. \tag{7.53}$$

The function $W(\omega)$ includes soft-photon effects, which decouple from the W bosons [21, 22] for the total cross section since soft radiation is only sensitive to the total (i.e. vanishing) electric charge of the produced system. This function is the QED-analog of the soft function for Drell-Yan production near partonic threshold [23, 24]. The leading Coulomb Green function at the origin,

$$G^{(0)}_{\rm C}(0,0;\mathcal{E}_{\rm W}) = -\frac{M_{\rm W}^2}{4\pi}\left\{\sqrt{-\frac{\mathcal{E}_{\rm W}}{M_{\rm W}}} + \frac{\alpha}{2}\ln\left(-\frac{\mathcal{E}_{\rm W}}{M_{\rm W}}\right) - \frac{\alpha^2\pi^2}{12}\sqrt{-\frac{M_{\rm W}}{\mathcal{E}_{\rm W}}} + \alpha^3\frac{\zeta(3)}{4}\frac{M_{\rm W}}{\mathcal{E}_{\rm W}} + \dots\right\}, \tag{7.54}$$

sums Coulomb exchange and is known to all orders (see e.g. [14]). At each order, the Coulomb corrections $\sim (\alpha/v)^n \sim \delta^{n/2}$ are parametrically enhanced over the remaining $\mathcal{O}(\alpha^n)$-corrections but do not have to be resummed to all orders due to the screening of the Coulomb singularity

*The value (7.50) is obtained by setting $s = 4M_{\rm W}^2$ in Eq. (37) in [14], where an additional s-dependence of $\mathcal{K}$ has been kept.

†This formula holds for the leading term in the expansion in v. Subleading terms result in a sum over Wilson coefficients and Green functions related to higher partial waves. In higher orders there are also soft corrections to the Coulomb function analogous to ultrasoft QCD corrections in $t\bar{t}$ production [20].

by Γ_W [25]. The convolution of the soft- and Coulomb functions results in logarithms of $\mathcal{E}_W \sim M_W v^2$, which can be resummed in analogy to threshold resummation at hadron colliders [24,26, 27]. However, for QED corrections $\alpha \log v$ is not enhanced, so this resummation is formally not necessary.[‡] Higher-order corrections to the non-resonant cross section (7.49) only arise through hard corrections to $\mathcal{K}$ while loop corrections in the EFT vanish.

The above ingredients provide results for massless initial-state electrons and could be used, in analogy to QCD predictions at hadron colliders, to define appropriate 'partonic' cross sections that are convoluted with corresponding electron structure functions resumming large mass-logarithms. Structure functions in such a scheme are known up to NNLO [29]. In the NLO$^{\rm EFT}$ calculation of [14], however, electron-mass effects have been treated by including collinear corrections and matching to the commonly used resummed structure functions [30] by subtracting double-counting contributions.

A useful result [15] to compute a class of higher-order effects of the form α^{n+1}/v^n is obtained from (7.52) by combining the all-order Coulomb Green function with one-loop hard and soft corrections and matching to ISR structure functions as discussed above:

$$\Delta\sigma^{\mathrm{C}\times[\mathrm{S+H}]_1}(s) = \frac{4\pi^2\alpha^2}{sM_W^2 s_W^4}\frac{\alpha}{\pi}\Bigg\{\left(\frac{9}{2}+\frac{\pi^2}{4}+C^{(1)}\right)\mathrm{Im}\, G_C(0,0;\mathcal{E}_W) + 2\,\mathrm{Im}\int_0^\infty \frac{dk}{k}\Big[G_C(0,0;\mathcal{E}_W-k) - G_C(0,0;\mathcal{E}_W)\theta(M_W-k)\Big]\Bigg\}. \tag{7.55}$$

Corrections of the same order α^{n+1}/v^n result from the NLO Green function [31] $G_C^{(1)}$, which includes the $\mathcal{O}(\alpha)$ correction to the Coulomb potential. In the G_μ input parameter scheme, the $\mathcal{O}(\alpha^2/v)$ correction reads [15]

$$\Delta G_C^{(1)}(0,0,\mathcal{E}_W) = -\frac{M_W^2}{4\pi}\frac{\alpha^2}{8\pi}\ln\Big(-\frac{\mathcal{E}_W}{M_W}\Big)\left\{-\frac{\beta_0}{2}\left[\ln\Big(-\frac{\mathcal{E}_W}{M_W}\Big)\right]+\Delta_{G_\mu}\right\}+\mathcal{O}(\alpha^3) \tag{7.56}$$

with the QED beta function with five quark flavours, $\beta_0 = -\frac{4}{3}\sum_{f\neq t} N_{C_f} Q_f^2 = -80/9$, and where the scheme-dependent constant $\Delta_{G_\mu} = 61.634$ is related to the quantity $\delta_{\alpha(M_Z)\to G_\mu} = \frac{\alpha}{4\pi}\left(\Delta_{G_\mu} + 2\beta_0 \ln\left(\frac{2M_W}{M_Z}\right)\right)$ used in [15]. The results (7.55) and (7.56) are the basis for computing examples of leading N^{3}LO corrections in Section 7.2.

7.1.3 NLO^{EFT} result

The genuine radiative corrections at NLO$^{\rm EFT}$ can be obtained by expanding the expression (7.55) to $\mathcal{O}(\alpha)$ relative to the leading order and adding the second order Coulomb correction from (7.54). A specific four-fermion final state is selected by multiplying the NLO correction with the LO branching ratios (7.48) and adding NLO decay corrections,

$$\Delta\sigma^{(1)}_{\rm decay} = \left(\frac{\Gamma^{(1,ew)}_{f_1\bar f_2}}{\Gamma^{(0)}_{f_1\bar f_2}} + \frac{\Gamma^{(1,ew)}_{f_3\bar f_4}}{\Gamma^{(0)}_{f_3\bar f_4}}\right)\sigma^{(0)}_{\rm res}, \tag{7.57}$$

with the one-loop electroweak corrections to the partial decay-widths, $\Gamma^{(1,ew)}_{f_i\bar f_j}$. For hadronic decay modes, also QCD corrections to the partial decay widths have to be included up to

[‡] An initial study obtained NLL effects of 0.1% [28], so the relevance for the FCC-ee may have to be revisited.

	$\sigma(e^-e^+ \to \mu^-\overline{\nu}_\mu u\bar{d}\, X)$(fb)			
$\sqrt{s}$ [GeV]	Born	NLO(EFT) [14]	ee4f [12]	DPA [12]
161	150.05(6)	104.97(6)	106.33(7)	103.15(7)
170	481.2(2)	373.74(2)	379.5(2)	376.9(2)

Table B.7: Comparison of the strict electroweak NLO results (without QCD corrections, second Coulomb correction and ISR resummation) in the EFT approach to the full NLO$^{\text{ee4f}}$ calculation and the DPA implementation of [11].

NNLO, using the counting $\alpha_s^2 \sim \alpha$. In table B.7 the $\mathcal{O}(\alpha)$-contributions of the NLO$^{\text{EFT}}$ result are compared to the NLO$^{\text{ee4f}}$ calculation in the full SM [12].[§] The differences are of the order

$$\Delta\sigma_{4\text{f}}^{(1)}(s) \equiv \sigma_{\text{NLO}}^{\text{ee4f}}(s) - \sigma_{\text{EFT}}^{(1)}(s) = \sigma_{\text{Born}}^{\text{ee4f}}(s) \times (0.9 - 1.2)\% \tag{7.58}$$

between $\sqrt{s} = 161$–170 GeV. Near threshold, the dominant source of this discrepancy is expected to be the $\mathcal{O}(\delta^{3/2})$ contribution from the $\mathcal{O}(\alpha)$ correction to the non-resonant cross section (7.49), which has not been computed in the EFT approach.[¶] Attributing the difference at $\sqrt{s} = 161$ GeV to this correction, one obtains

$$\mathcal{K}^{(1)} \approx 1.8, \tag{7.59}$$

indicating that the $\mathcal{O}(\alpha)$ corrections to the non-resonant contribution (7.50) are moderate, $|\mathcal{K}^{(1)}/\mathcal{K}^{(0)}| \approx 0.4$. Above threshold, $\mathcal{O}(\delta^{3/2})$ and $\mathcal{O}(\delta^2)$ corrections to the resonant cross section are expected to be important, which arise from the combination of $\mathcal{O}(\alpha/v, \alpha)$ corrections in the EFT with $\mathcal{O}(v^2)$ kinematic corrections and from $\mathcal{O}(\alpha)$ corrections to the Wilson coefficients of sub-leading production operators. Naive estimates using the $\mathcal{O}(v^2)$ expansion of the Born amplitude and the first Coulomb correction,

$$\sigma_{\alpha v}^{(3/2)}(s) \sim |\sigma_{\text{Born}}^{(1)}(s)|\sigma_C^{(1/2)}(s)/\sigma_{\text{Born}}^{(0)}(s), \qquad \sigma_{\alpha v^2}^{(2)}(s) \sim \frac{\alpha}{s_{\text{W}}^2}|\sigma_{\text{Born}}^{(1)}(s)|, \tag{7.60}$$

indicate that both corrections are $\sim 0.3\% \times \sigma_{\text{Born}}^{\text{ee4f}}$ at $\sqrt{s} = 170$ GeV, underestimating the discrepancy to the NLO$^{\text{ee4f}}$ calculation by a factor of two. To assess the accuracy of the EFT expansion, it would be interesting to calculate these corrections exactly and investigate if the difference to the NLO$^{\text{ee4f}}$ calculation could be reduced e.g. by resumming relativistic corrections to the W-propagators.

7.1.4 Leading NNLO corrections

In [15] those $\mathcal{O}(\delta^{3/2})$ corrections according to (7.45) have been computed that originate from genuine NNLO corrections in the usual counting in α. These consist of several classes: a) Interference of one-loop Coulomb corrections with soft and hard corrections (7.55), b) interference of one-loop Coulomb corrections with corrections to W-decay, obtained from (7.57) by replacing the LO cross section with the first Coulomb correction, c) interference of one-loop Coulomb corrections with NLO corrections to residues of W-propagators, d) radiative NLO corrections

[§]Note that here the updated results in the erratum to [12] are used.

[¶]For $e^-e^+ \to t\bar{t}$ a related calculation has been performed recently [32].

to the Coulomb potential (7.56). The third Coulomb correction from (7.54) contributes at the same order $\delta^{3/2}$. Care has been taken to avoid double-counting corrections already included in the NLO$^{\rm ee4f}$ calculation so the two results can be added to obtain the current best prediction for the total cross section near threshold. The numerical results are reproduced in Table B.8, together with the second Coulomb correction included in the NLO$^{\rm EFT}$ calculation. The results show that the leading, Coulomb enhanced two-loop corrections are of the order of 0.3%. The uncertainty due to the remaining, non-Coulomb enhanced NNLO corrections was estimated to be below the ILC target accuracy of $\Delta M_{\rm W} = 3$ MeV [15] but not sufficient for the FCC-ee.

7.2 Estimate of NNLO$^{\rm EFT}$ corrections and beyond

In this section the structure of the EFT expansion of the cross section and the ingredients for higher-order corrections reviewed in Section 7.1 are used to estimate the possible effects of a future NNLO$^{\rm EFT}$ calculation. Due to the counting (7.43), this includes also leading corrections beyond NNLO in the conventional perturbative expansion:

$$\text{NNLO}^{\rm EFT}: \quad v^4, \quad \alpha v^2, \quad \alpha^2 \quad \alpha^3/v^2, \quad \alpha^4/v^4. \tag{7.61}$$

The contributions of $\mathcal{O}(v^4, \alpha v^2)$ in (7.61) arise from kinematic corrections to the Born and NLO cross section in the full SM as discussed in Sections 7.1.1 and 7.1.3, respectively. The genuine $\mathcal{O}(\alpha^2)$ corrections are estimated in Section 7.2.1. A representative subset of the $\mathcal{O}(\alpha^3/v^2)$ corrections is computed in Section 7.2.2 and serves as an estimate of effects beyond a conventional NNLO calculation. The quadruple-Coulomb correction α^4/v^4 follows from the expansion of the known Coulomb Green function and is smaller than 0.001% and therefore negligible. Counting $\alpha \sim \alpha_s^2$, also QCD corrections to W self-energies and decay widths up to

$$\alpha\alpha_s^2, \quad \alpha_s^4 \tag{7.62}$$

are required. Currently the required $\mathcal{O}(\alpha_s^4)$ corrections for inclusive hadronic vector-boson decays are known [33], while mixed QCD-EW corrections are known up to $\mathcal{O}(\alpha\alpha_s)$ [34]. The uncertainty of a future NNLO$^{\rm EFT}$ calculation can be estimated by considering the impact of corrections at the next order in the δ-expansion, i.e.

$$\text{N}^{5/2}\text{LO}^{\rm EFT}: \quad \alpha v^3, \quad \alpha^2 v, \quad \alpha^3/v, \quad \alpha^4/v^3, \quad \alpha^5/v^5. \tag{7.63}$$

The contributions $\sim \alpha v^3$ are already included in the NLO$^{\rm ee4f}$ calculation. The fifth Coulomb correction $\sim \alpha^5/v^5$ is known but negligibly small. The corrections $\sim \alpha^4/v^3$ arise from the combination of $\mathcal{O}(\alpha)$ corrections with triple Coulomb exchange and are also expected to be negligible since the latter is $< 0.01\%$. Therefore the dominant genuine radiative corrections beyond NNLO$^{\rm EFT}$ are expected to be of order α^3/v. These arise from a combination of single Coulomb exchange and various sources of $\mathcal{O}(\alpha^2)$ corrections and are estimated in Section 7.2.3. Further contributions from triple Coulomb exchange combined with $\sim v^2$ kinematic corrections are again expected to be negligible. The $\mathcal{O}(\alpha^2)$ corrections to the non-resonant cross section (7.49) also provide $\sim \alpha^3/v$ corrections relative to the LO cross section, while corrections $\sim \alpha^2 v$ arise from a combination of single Coulomb exchange with kinematic corrections $\sim \alpha v^2$. Such non-resonant and kinematic corrections are estimated in Section 7.2.4. It is assumed throughout that large logarithms of $m_{\rm e}$ are absorbed in electron structure functions and only the uncertainty due to non-universal $\mathcal{O}(\alpha^2, \alpha^3)$ corrections is considered.

7.2.1 $\mathcal{O}(\alpha^2)$ corrections in the EFT

The most involved corrections of order α^2 in the EFT arise from hard two-loop corrections to the Wilson coefficients of production operators and to decay rates and from soft two-loop corrections to the forward-scattering amplitude. Additional corrections from higher-order potentials or the combination of double Coulomb exchange with kinematic corrections $\sim v^2$ are anticipated to be subdominant. The soft corrections for massless initial-state electrons can be extracted from the two-loop Drell-Yan soft function [23, 24] and converted to the electron-mass regulator scheme using the NNLO structure functions computed in [29]. We make no attempt here to estimate these soft corrections, which are formally of the same order as the hard corrections. This is supported by the NLO result, where hard corrections alone provide a reasonable order-of-magnitude estimate and soft corrections contribute less than 50% of the NLO corrections for $\sqrt{s} = 158$–170 GeV. The contribution of the NNLO Wilson coefficient of the production operator to the cross section reads

$$\sigma^{(2)}_{\text{hard}}(s) = \frac{\pi\alpha^2}{s_{\text{W}}^4 s}\text{Im}\left[-\sqrt{-\frac{\mathcal{E}_{\text{W}}}{M_{\text{W}}}}\left(\frac{\alpha}{\pi}\right)^2 C^{(2)}\right], \tag{7.64}$$

where the NNLO hard coefficient is defined in terms of the squared Wilson coefficient, $C^2 = 1 + \frac{\alpha}{\pi}C^{(1)} + \left(\frac{\alpha}{\pi}\right)^2 C^{(2)} + \ldots$. The computation of $C^{(2)}$ involves the two-loop amplitude for $\text{e}^-\text{e}^+ \to \text{W}^-\text{W}^+$ evaluated directly at threshold. Such a computation is beyond the current state-of-the art, which includes two-loop EW corrections to three-point functions [35, 36, 80], but presumably feasible before the operation of the FCC-ee. A naive estimate of the NNLO coefficient in terms of the the one-loop result (7.53),

$$C^{(2)} \sim (C^{(1)})^2, \tag{7.65}$$

suggests an effect on the cross section of

$$\Delta\sigma^{(2)}_{\text{hard}} \approx \sigma^{(0)}_{\text{res}} \times 0.06\%. \tag{7.66}$$

The NNLO corrections to W-boson decay give rise to the correction

$$\Delta\sigma^{(2)}_{\text{decay}} = \left(\frac{\Gamma^{(2,ew)}_{\mu^-\overline{\nu}_\mu}}{\Gamma^{(0)}_{\mu^-\overline{\nu}_\mu}} + \frac{\Gamma^{(2,ew)}_{\text{u}\overline{\text{d}}}}{\Gamma^{(0)}_{\text{u}\overline{\text{d}}}} + \frac{\Gamma^{(1,ew)}_{\mu^-\overline{\nu}_\mu}\Gamma^{(1,ew)}_{\text{u}\overline{\text{d}}}}{\Gamma^{(0)}_{\mu^-\overline{\nu}_\mu}\Gamma^{(0,ew)}_{\text{u}\overline{\text{d}}}}\right)\sigma^{(0)}_{\text{res}}. \tag{7.67}$$

The product of NLO corrections in the last term contributes a negligible 0.001% in the G_μ input parameter scheme. A naive estimate of the currently unknown $\mathcal{O}(\alpha^2)$ corrections to W decay suggests $\Gamma^{(2,ew)}_{f_i\overline{f}_j} \approx \frac{\alpha}{s_{\text{W}}^2}\Gamma^{(1,ew)}_{f_i\overline{f}_j} \sim 0.01\% \times \Gamma^{(0)}_{f_i\overline{f}_j}$, consistent with the size of the $\mathcal{O}(\alpha^2)$ corrections to Z decay [36, 80]. The estimates given in this subsection indicate that the combined non-Coulomb enhanced corrections of $\mathcal{O}(\alpha^2)$ are of the order of 0.1% and are therefore mandatory to reduce the uncertainty below $\Delta M_{\text{W}} \lesssim 1.5$ MeV.

7.2.2 Corrections of $\mathcal{O}(\alpha^3/v^2)$

The corrections of $\mathcal{O}(\alpha^3/v^2)$ involve a double-Coulomb exchange in combination with an $\mathcal{O}(\alpha)$ correction and arise from similar sources as the $\mathcal{O}(\alpha^2/v)$ corrections discussed in Section 7.1.4. The subclass of contributions arising from the combination of double Coulomb exchange with

	$\sigma(e^-e^+ \to \mu^-\bar{\nu}_\mu u\bar{d}\, X)$(fb)				
$\sqrt{s}$ [GeV]	$\mathcal{O}(\alpha^2/v^2)$	$\mathcal{O}(\alpha^2/v)$	$\mathcal{O}(\alpha^3/v^3)$	$\mathcal{O}(\alpha^3/v^2)\vert_{C_2\times[S+H]_1}$	$\mathcal{O}(\alpha^3/v^2)\vert_{C_2^{NLO}}$
158	0.151 [+0.245%]	−0.005 [−0.007%]	3.82×10^{-3} [+0.006%]	-3.82×10^{-3} [−0.006%]	5.38×10^{-3} [+0.009%]
161	0.437 [+0.284%]	0.137 [+0.089%]	9.92×10^{-3} [+0.006%]	-1.12×10^{-2} [−0.007%]	1.52×10^{-2} [+0.010%]
164	0.399 [+0.132%]	0.808 +[0.267%]	2.84×10^{-3} [+0.001%]	-7.62×10^{-3} [−0.003%]	1.97×10^{-2} [+0.007%]
167	0.303 [+0.074%]	1.286 [+0.315%]	9.43×10^{-4} [+0.000%]	-4.57×10^{-3} [−0.001%]	1.77×10^{-2} [+0.004%]
170	0.246 [+0.051%]	1.577 [+0.327%]	4.39×10^{-4} [+0.000%]	-3.12×10^{-3} [−0.001%]	1.56×10^{-2} [+0.003%]

Table B.8: Leading $\mathcal{O}(\alpha^2)$ corrections [15] (second and third column) and contributions to leading $\mathcal{O}(\alpha^3)$ corrections from triple-Coulomb exchange [15] (fourth column), interference of double-Coulomb exchange with soft and hard corrections (7.68) (fifth column), and double-Coulomb exchange with the NLO Coulomb potential (7.69) (sixth column). The relative correction is given with respect to the Born cross section without ISR improvement as quoted in [15].

soft and hard corrections is obtained by inserting the $\mathcal{O}(\alpha^2)$ term in the expansion of the Coulomb Green function (7.54) into (7.55), resulting in the contribution to the cross section

$$\Delta\sigma^{C_2\times[S+H]_1} = \frac{\alpha^2}{s_W^4 s}\frac{\alpha^3\pi^2}{12}\mathrm{Im}\left\{\sqrt{-\frac{M_W}{\mathcal{E}_W}}\left[\left(\frac{9}{2}+\frac{\pi^2}{4}+C^{(1)}\right)+2\ln\left(-\frac{4\mathcal{E}_W}{M_W}\right)\right]\right\}. \tag{7.68}$$

Corrections from the NLO Coulomb potential to double Coulomb exchange can be obtained by expanding the expression for the NLO Coulomb Green function [31] quoted in [37] and using the result for the Coulomb potential in the G_μ input parameter scheme [15], resulting in

$$\Delta\sigma^{C_2^{NLO}}(s) = \frac{\alpha^2}{s_W^4 s}\frac{\alpha^3}{24}\mathrm{Im}\left\{\sqrt{-\frac{M_W}{\mathcal{E}_W}}\left[\pi^2\left(-\beta_0\ln\left(-\frac{\mathcal{E}_W}{M_W}\right)+\Delta_{G_\mu}\right)-12\beta_0\zeta_3\right]\right\}. \tag{7.69}$$

The combination of double Coulomb exchange with NLO corrections to W-decay is obtained from (7.57) by replacing $\sigma_{res}^{(0)}$ with the second Coulomb correction. The resulting effect is at most 0.002%. Further corrections arise from corrections to the propagator residues and can be computed with current methods, but are beyond the scope of the present simple estimates. At $\mathcal{O}(\alpha^2/v)$, the corresponding corrections are of similar size as the mixed soft+hard/Coulomb corrections [15]. Therefore the predictions from (7.68) and (7.69), which are shown in Table B.8 together with the known two- and three-loop corrections [15], are expected to be representative for the the $\mathcal{O}(\alpha^3/v^2)$ corrections. They are of a similar order as the third Coulomb correction, and individually of the order $\approx 0.01\%$ near threshold. The sum of all $\mathcal{O}(\alpha^3/v^2)$ corrections may therefore be of the size few $\times\, 0.01\%$, indicating the need to go beyond a strict $\mathcal{O}(\alpha^2)$ calculation to reach the FCC-ee accuracy goal.

7.2.3 Radiative corrections of $\mathcal{O}(\alpha^3/v)$

Genuine three-loop corrections at $\mathcal{O}(\alpha^3/v)$ can arise from a combination of the first Coulomb correction and soft or hard $\mathcal{O}(\alpha^2)$ corrections, corrections from higher-order potentials to the Coulomb Green function or a combination of $\mathcal{O}(\alpha)$ hard/soft and potential corrections. One contribution in the latter class can be computed by inserting the NLO Green function (7.56) into the convolution with the $\mathcal{O}(\alpha)$ hard and soft corrections (7.55),

$$\hat{\sigma}^{\mathrm{C^{NLO}}\times[\mathrm{S+H}]_1}(s) = \frac{\alpha^2}{s s_{\mathrm{W}}^4}\frac{\alpha^3}{8\pi}\mathrm{Im}\Bigg\{\ln\Big(-\frac{\mathcal{E}_W}{M_W}\Big)\Bigg[-\frac{\beta_0}{3}\left(2\ln^2\Big(-\frac{\mathcal{E}_W}{M_W}\Big)+\pi^2\right)+\Delta_{G_\mu}\ln\Big(-\frac{\mathcal{E}_W}{M_W}\Big) + \left(\frac{9}{2}+\frac{\pi^2}{4}+C^{(1)}\right)\left(-\frac{\beta_0}{2}\ln\Big(-\frac{\mathcal{E}_W}{M_W}\Big)+\Delta_{G_\mu}\right)\Bigg]\Bigg\}. \tag{7.70}$$

The corrections to the cross section are given by

$$\Delta\sigma^{\mathrm{C^{NLO}}\times[\mathrm{S+H}]_1}(161\text{ GeV}) = -0.004\%\times\sigma_{\mathrm{LO}},\quad \Delta\sigma^{\mathrm{C^{NLO}}\times[\mathrm{s+H}]_1}(170\text{ GeV}) \approx -0.002\%\times\sigma_{\mathrm{LO}}. \tag{7.71}$$

A further indication for the magnitude of corrections at this order can be obtained from the combination of the NNLO hard coefficient with the first Coulomb correction,

$$\Delta\sigma^{\mathrm{C_1}\times\mathrm{H_2}} = -\frac{\pi\alpha^2}{s_{\mathrm{W}}^4 s}\frac{\alpha^3 C^{(2)}}{2\pi}\mathrm{Im}\left[\ln\left(-\frac{\mathcal{E}_{\mathrm{W}}}{M_{\mathrm{W}}}\right)\right], \tag{7.72}$$

and using the estimate (7.65) for the hard two-loop coefficient, which results in

$$\Delta\sigma^{\mathrm{C_1}\times\mathrm{H_2}}(161\text{ GeV}) \approx 0.005\%\times\sigma_{\mathrm{LO}},\quad \Delta\sigma^{\mathrm{C_1}\times\mathrm{H_2}}(170\text{ GeV} \approx 0.002\%\times\sigma_{\mathrm{LO}}. \tag{7.73}$$

These results indicate that the $\mathcal{O}(\alpha^3)$ corrections beyond $\mathrm{NNLO^{EFT}}$ are $\lesssim 0.01\%$. It is expected that the factorization (7.52) and the $\mathrm{N^3LO}$ Coulomb Green function [38] allow to compute all $\mathcal{O}(\alpha^3/v)$ corrections once the $\mathrm{NNLO^{EFT}}$ result is known, similarly to a related calculation for hadronic $\mathrm{t\bar{t}}$ production [39].

7.2.4 Non-resonant and kinematic $\mathcal{O}(\alpha^2)$ corrections

Kinematic $\mathcal{O}(\alpha^2 v)$ corrections and $\mathcal{O}(\alpha^2)$ corrections to the non-resonant cross section in (7.63) would be included in a full $\mathrm{NNLO^{ee4f}}$ calculation, which is far beyond current calculational methods. The comparison of the $\mathrm{NLO^{EFT}}$ and $\mathrm{NLO^{ee4f}}$ results in Section 7.1.3 indicate a well-behaved perturbative expansion of the non-resonant corrections (7.49) with coefficients $\mathcal{K}^{(i)}$ of order one, but a somewhat larger relevance of kinematic corrections above threshold. This suggests that the non-resonant and kinematic NNLO corrections are reasonably estimated by scaling the corresponding NLO corrections,

$$\Delta\sigma_{4\mathrm{f}}^{(2)}(s) = \sigma_{\mathrm{NNLO}}^{\mathrm{ee4f}}(s) - \sigma_{\mathrm{EFT}}^{(2)}(s) \approx \frac{\alpha}{s_{\mathrm{W}}^2}\left(\sigma_{\mathrm{NLO}}^{\mathrm{ee4f}}(s) - \sigma_{\mathrm{EFT}}^{(1)}(s)\right) = \sigma_{\mathrm{Born}}^{\mathrm{ee4f}}(s)\times(0.03-0.04)\% \tag{7.74}$$

between $\sqrt{s} = 161$–170 GeV. Therefore these effects must be under control to reach the desired accuracy for the FCC-ee. A calculation of the $\mathcal{O}(\alpha^2)$ non-resonant correction in the EFT involves a combination of $\mathcal{O}(\alpha^2)$ corrections to the processes $\mathrm{e^-e^+}\to\mathrm{W^\pm}f\bar{f}$ with $\mathcal{O}(\alpha)$ corrections for $\mathrm{e^-e^+}\to 4f$. Such a computation is beyond current capabilities, but may be possible before a full $\mathrm{NNLO^{ee4f}}$ calculation is available. A comparison of future NNLO calculations in the EFT and the conventional DPA may also allow to constrain these corrections.

7.3 Summary and outlook

The prospects of reducing the theoretical uncertainty of the total W-pair production cross section near threshold to the level of $\sim 0.01\%$ required to fully exploit the high statistics at a future circular e^-e^+ collider have been investigated within the EFT approach, building on results for the NLO and dominant NNLO corrections. The estimates in Section 7.2.1 suggest that $\mathcal{O}(\alpha^2)$ corrections beyond the leading Coulomb effects [15] are of the order

$$\Delta\sigma_{\rm NNLO} \approx 0.1\% \times \sigma_{\rm Born} \tag{7.75}$$

at threshold and are therefore mandatory to reach FCC-ee precision. In Sections 7.2.2 and 7.2.3 the dominant, Coulomb enhanced three-loop effects have been estimated to be of the order

$$\Delta\sigma_{\rm N^3LO} \approx \text{few} \times 0.01\% \times \sigma_{\rm Born} \tag{7.76}$$

based on computations or estimates of representative examples of $\mathcal{O}(\alpha^3/v^2, \alpha^3/v)$ effects. These corrections are either part of the $\text{NNLO}^{\rm EFT}$ result or can be computed once this result is available. The effect of the remaining $\mathcal{O}(\alpha^3)$ corrections without Coulomb enhancement is expected to be below the FCC-ee target accuracy. However, the accuracy of the $\text{NNLO}^{\rm EFT}$ calculation is limited by non-resonant and kinematic corrections. An extrapolation of the difference of the $\text{NLO}^{\rm EFT}$ and $\text{NLO}^{\rm ee4f}$ calculations suggests the magnitude

$$\Delta\sigma^{(2)}_{\rm 4f} \approx 0.03\% \times \sigma_{\rm Born}. \tag{7.77}$$

Related estimates $\Delta\sigma_{\rm N^3LO} \approx 0.02\%$ and $\Delta\sigma^{(\text{non-res})}_{\rm NNLO} \approx 0.016\%$ have been obtained using scaling arguments and an extrapolation of the accuracy of the DPA [40]. Our results suggest that a theory-induced systematic error of the mass measurement from a threshold scan of

$$\Delta M_{\rm W} = (0.15 - 0.60)\ \text{MeV} \tag{7.78}$$

should be achievable, where the lower value results from assuming the non-resonant corrections are under control. In addition to the corrections considered here, it is also essential to reduce the uncertainty from ISR corrections and QCD corrections for hadronic final states to the required accuracy. It would also be desirable to bring the precision for differential cross sections to a similar level as that of the total cross section.

Acknowledgements

I would like to thank M. Beneke for useful comments.

References

[1] H. Baer, et al., The International Linear Collider Technical Design Report - Volume 2: Physics (2013). arXiv:1306.6352.

[2] M. Baak, et al., Working Group Report: Precision Study of Electroweak Interactions, in: APS DPF Community Summer Study (Snowmass 2013), 2013. arXiv:1310.6708.

[3] P. Azzurri, et al., Physics Behind Precision (2017). arXiv:1703.01626.

[4] M. Mangano, et al., Future Circular Collider (2018). URL http://cds.cern.ch/record/2651294

[5] CEPC Conceptual Design Report: Volume 2 - Physics & Detector (2018). arXiv:1811.10545.

[6] A. Aeppli, G. J. van Oldenborgh, D. Wyler, Unstable particles in one loop calculations, Nucl. Phys. B428 (1994) 126–146. arXiv:hep-ph/9312212.

[7] S. Jadach, W. Placzek, M. Skrzypek, B. F. L. Ward, Z. Was, Exact $\mathcal{O}(\alpha)$ gauge invariant YFS exponentiated Monte Carlo for (un)stable W^+W^- production at and beyond LEP2 energies, Phys. Lett. B417 (1998) 326–336. arXiv:hep-ph/9705429.

[8] S. Jadach, W. Placzek, M. Skrzypek, B. F. L. Ward, Z. Was, The Monte Carlo event generator YFSWW3 version 1.16 for W pair production and decay at LEP2/LC energies, Comput. Phys. Commun. 140 (2001) 432–474. arXiv:hep-ph/0103163.

[9] W. Beenakker, F. A. Berends, A. P. Chapovsky, Radiative corrections to pair production of unstable particles: Results for $e^+e^- \to 4$ fermions, Nucl. Phys. B548 (1999) 3–59. arXiv:hep-ph/9811481.

[10] A. Denner, S. Dittmaier, M. Roth, D. Wackeroth, $\mathcal{O}(\alpha)$ corrections to $e^+e^- \to WW \to 4$ fermions $(+\gamma)$: First numerical results from RACOONWW, Phys. Lett. B475 (2000) 127–134. arXiv:hep-ph/9912261.

[11] A. Denner, S. Dittmaier, M. Roth, D. Wackeroth, Electroweak radiative corrections to $e^+e^- \to WW \to 4$ fermions in double-pole approximation: The RACOONWW approach, Nucl. Phys. B587 (2000) 67–117. arXiv:hep-ph/0006307.

[12] A. Denner, S. Dittmaier, M. Roth, L. H. Wieders, Complete electroweak $\mathcal{O}(\alpha)$ corrections to charged- current $e^+e^- \to$ 4fermion processes, Phys. Lett. B612 (2005) 223–232. arXiv:hep-ph/0502063.

[13] A. Denner, S. Dittmaier, M. Roth, L. H. Wieders, Electroweak corrections to charged-current $e^+e^- \to 4$ fermion processes: Technical details and further results, Nucl. Phys. B724 (2005) 247–294. arXiv:hep-ph/0505042.

[14] M. Beneke, P. Falgari, C. Schwinn, A. Signer, G. Zanderighi, Four-fermion production near the W pair production threshold, Nucl.Phys. B792 (2008) 89–135. arXiv:0707.0773, doi:10.1016/j.nuclphysb.2007.09.030.

[15] S. Actis, M. Beneke, P. Falgari, C. Schwinn, Dominant NNLO corrections to four-fermion production near the W-pair production threshold, Nucl.Phys. B807 (2009) 1–32. arXiv:0807.0102, doi:10.1016/j.nuclphysb.2008.08.006.

[16] M. Beneke, P. Falgari, C. Schwinn, Threshold resummation for pair production of coloured heavy (s)particles at hadron colliders, Nucl.Phys. B842 (2011) 414–474. arXiv:1007.5414, doi:10.1016/j.nuclphysb.2010.09.009.

[17] M. Beneke, A. P. Chapovsky, A. Signer, G. Zanderighi, Effective theory approach to unstable particle production, Phys. Rev. Lett. 93 (2004) 011602. arXiv:hep-ph/0312331.

[18] M. Beneke, A. P. Chapovsky, A. Signer, G. Zanderighi, Effective theory calculation of resonant high-energy scattering, Nucl. Phys. B686 (2004) 205–247. arXiv:hep-ph/0401002.

[19] C. W. Bauer, S. Fleming, D. Pirjol, I. W. Stewart, An effective field theory for collinear and soft gluons: Heavy to light decays, Phys. Rev. D63 (2001) 114020. arXiv:hep-ph/0011336.

[20] M. Beneke, Y. Kiyo, Ultrasoft contribution to heavy-quark pair production near threshold, Phys. Lett. B668 (2008) 143–147. arXiv:0804.4004, doi:10.1016/j.physletb.2008.08.031.

[21] V. S. Fadin, V. A. Khoze, A. D. Martin, Interference radiative phenomena in the production of heavy unstable particles, Phys. Rev. D49 (1994) 2247–2256.

[22] K. Melnikov, O. I. Yakovlev, Top near threshold: All alpha-s corrections are trivial, Phys. Lett. B324 (1994) 217–223. arXiv:hep-ph/9302311.

[23] A. V. Belitsky, Two-loop renormalization of Wilson loop for Drell-Yan production, Phys. Lett. B442 (1998) 307–314. arXiv:hep-ph/9808389.

[24] T. Becher, M. Neubert, G. Xu, Dynamical Threshold Enhancement and Resummation in Drell- Yan Production, JHEP 07 (2008) 030. arXiv:0710.0680, doi:10.1088/1126-6708/2008/07/030.

[25] V. S. Fadin, V. A. Khoze, A. D. Martin, A. Chapovsky, Coulomb effects in W+ W- production, Phys. Rev. D52 (1995) 1377–1385. arXiv:hep-ph/9501214, doi:10.1103/PhysRevD.52.1377.

[26] G. Sterman, Summation of Large Corrections to Short Distance Hadronic Cross-Sections, Nucl. Phys. B281 (1987) 310.

[27] S. Catani, L. Trentadue, Resummation of the QCD Perturbative Series for Hard Processes, Nucl. Phys. B327 (1989) 323.

[28] P. Falgari, W-pair production near threshold in unstable-particle effective theory, Ph.D. thesis, RWTH Aachen University, available at http://darwin.bth.rwth-aachen.de/opus3/volltexte/2009/2682/ (2008).

[29] J. Blümlein, A. De Freitas, W. van Neerven, Two-loop QED Operator Matrix Elements with Massive External Fermion Lines, Nucl. Phys. B855 (2012) 508–569. arXiv:1107.4638, doi:10.1016/j.nuclphysb.2011.10.009.

[30] M. Skrzypek, Leading logarithmic calculations of QED corrections at LEP, Acta Phys. Polon. B23 (1992) 135–172.

[31] M. Beneke, A. Signer, V. A. Smirnov, Top quark production near threshold and the top quark mass, Phys. Lett. B454 (1999) 137–146. arXiv:hep-ph/9903260, doi:10.1016/S0370-2693(99)00343-3.

[32] M. Beneke, A. Maier, T. Rauh, P. Ruiz-Femenia, Non-resonant and electroweak NNLO correction to the e^+e^- top anti-top threshold, JHEP 02 (2018) 125. arXiv:1711.10429, doi:10.1007/JHEP02(2018)125.

[33] P. A. Baikov, K. G. Chetyrkin, J. H. Kühn, Order $\alpha^4(s)$ QCD Corrections to Z and tau Decays, Phys. Rev. Lett. 101 (2008) 012002. arXiv:0801.1821, doi:10.1103/PhysRevLett.101.012002.

[34] D. Kara, Corrections of Order $\alpha\alpha_s$ to W Boson Decays, Nucl. Phys. B877 (2013) 683–718. arXiv:1307.7190, doi:10.1016/j.nuclphysb.2013.10.024.

[35] S. Actis, G. Passarino, C. Sturm, S. Uccirati, NNLO Computational Techniques: The Cases $H \to \gamma\gamma$ and $H \to gg$, Nucl. Phys. B811 (2009) 182–273. arXiv:0809.3667, doi:10.1016/j.nuclphysb.2008.11.024.

[36] A. Freitas, Higher-order electroweak corrections to the partial widths and branching ratios of the Z boson, JHEP 04 (2014) 070. arXiv:1401.2447, doi:10.1007/JHEP04(2014)070.

[37] M. Beneke, P. Falgari, S. Klein, C. Schwinn, Hadronic top-quark pair production with NNLL threshold resummation, Nucl.Phys. B855 (2012) 695–741. arXiv:1109.1536, doi:10.1016/j.nuclphysb.2011.10.021.

[38] M. Beneke, Y. Kiyo, P. Marquard, A. Penin, J. Piclum, M. Steinhauser, Next-to-Next-to-Next-to-Leading Order QCD Prediction for the Top Antitop S-Wave Pair Production Cross Section Near Threshold in e^+e^- Annihilation, Phys. Rev. Lett. 115 (19) (2015) 192001. arXiv:1506.06864, doi:10.1103/PhysRevLett.115.192001.

[39] J. Piclum, C. Schwinn, Soft-gluon and Coulomb corrections to hadronic top-quark pair production beyond NNLO, JHEP 03 (2018) 164. arXiv:1801.05788, doi:10.1007/

JHEP03(2018)164.

[40] S. Jadach, M. Skrzypek, QED challenges at FCC-ee precision measurements (2019). arXiv:1903.09895.

8 Perspectives of heavy-quarkonium production at FCC-ee

Authors: Zhi-Guo He and Bernd A. Kniehl
Corresponding Author: Bernd A. Kniehl [kniehl@desy.de]

Due to its non-relativistic nature, heavy quarkonium constituted by heavy quark-antiquark pairs ($Q\bar{Q} = b\bar{b}$ or $c\bar{c}$) is an ideal object to investigate both perturbative and nonpertative aspects of QCD. The non-relativistic QCD factorization formalism [1] built on the rigorous effective field theory [2] provides a powerful tool to systematically calculate heavy-quarkonium production and decay. In this formalism, the production of heavy quarkonium is factorized into the process dependent short-distance coefficients (SDCs) times supposedly universal long-distance matrix elements (LDMEs). The SDC describing the production of a $Q\bar{Q}$ pair in Fock state $n = {}^{2S+1}L_J^{[a]}$ with total spin S, orbital angular momentum L, and total angular momentum J can be calculated perturbatively as an expansion in α_s. The LDMEs related to the probability of Fock state n to evolve into the heavy meson are organized by the velocity scaling rules [3] of NRQCD, and their values can be determined by fitting to experimental data. Here, the velocity, v_Q, refers to the motion of heavy quark, Q, in the rest frame of the heavy meson. Although NRQCD has greatly improved our understanding of the heavy-quarkonium production mechanism, the long-standing "J/ψ polarization puzzle" has not been resolved yet. The SDCs for the relevant color singlet (CS) channel (${}^3S_1^{[1]}$) and the three color octet (CO) (${}^3S_1^{[8]}$, ${}^1S_0^{[8]}$, ${}^3P_J^{[8]}$) channels have been obtained by three groups independently, while the corresponding LDMEs were fitted to different sets of experimental data based on different considerations [4–6]. However, none of their predictions can explain both the J/ψ yield and polarization data at hadron colliders simultaneously. Recently, the universality of the NRQCD LDMEs was challenged by η_c hadroproduction data [7].

Compared to hadron colliders, in e^+e^- colliders, the production mechanism is simpler, the uncertainties in the theoretical calculations are smaller, and the convergence of perturbative calculations is faster. Moreover, on the experimental side, the much cleaner background makes it possible to study the production of other heavy quarkonia besides the J/ψ and Υ mesons, such as $\eta_{c,b}$ and $\chi_{c,b}$, and to study more production processes, like associated production of heavy quarkonium with a photon or a heavy-quark pair in detail. Therefore, heavy-quarkonium production in e^+e^- colliders plays an important role in testing NRQCD factorization, so as to help resolving the "J/ψ polarization puzzle." There are two ways to produce heavy quarkonium directly.* One is in e^+e^- annihilation and the other one in $\gamma\gamma$ collisions. We review heavy-quarkonium production, concentrating on the J/ψ case, by these two processes in Sections 8.1 and 8.2, respectively, and discuss the prospects of heavy-quarkonium production at the Fcc-ee beyond the current measurements carried at B factories and CERN LEP-II. Section 8.3 contains a summary and an outlook.

*Here, we mean production not through the decay of other heavy particles, like Z-boson, Higgs boson, or top quark.

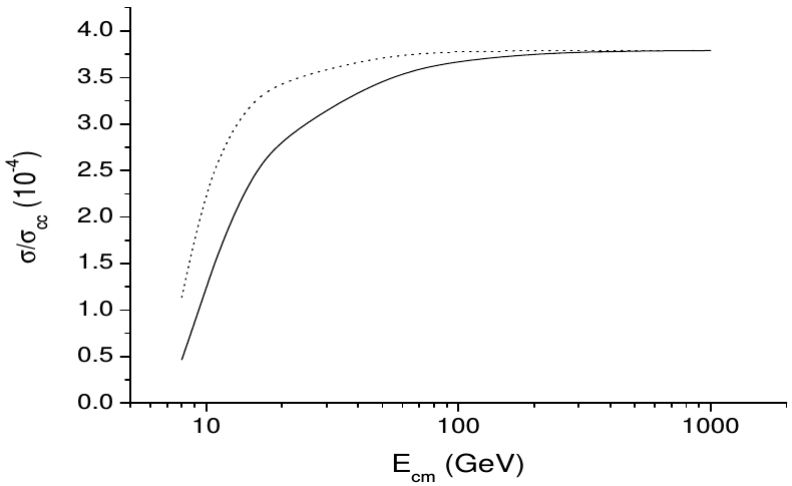

Fig. B.28: The cross section of $\sigma(e^+e^- \to J/\psi + c\bar{c} + X)$ normalized to $\sigma(e^+e^- \to c\bar{c} + X)$ at LO in NRQCD as function of the center-of-mass energy. The dotted line denotes the complete result, and the solid line denotes the fragmentation calculation [16].

8.1 Heavy-quarkonium production through e^+e^- annihilation

The total cross section for inclusive J/ψ production in e^+e^- annihilation was measured by the Babar [8], Belle [9], and CLEO [10] Collaborations at $\sqrt{s} = 10.6$ GeV yielding

$$\sigma(e^+e^- \to J/\psi + X) = \begin{cases} 2.5 \pm 0.21 \pm 0.21 \text{ pb} & \text{Babar} \\ 1.47 \pm 0.10 \pm 0.13 \text{ pb} & \text{Belle} \\ 1.9 \pm 0.2 \text{ pb} & \text{CLEO} \end{cases}$$

The NRQCD prediction at leading order (LO) is in the wide range of $0.8 - 1.7$ pb [11–14] including 0.3 pb from the CS mechanism. The Belle Collaboration further managed to discriminate the contributions due to the final states $J/\psi + c\bar{c} + X$ and $J/\psi + X_{\text{non}-c\bar{c}}$, and found that $\sigma(e^+e^- \to J/\psi + c\bar{c} + X) = 0.74 \pm 0.08^{+0.09}_{-0.08}$ pb and $\sigma(e^+e^- \to J/\psi + X_{\text{non}-c\bar{c}}) = 0.43 \pm 0.09 \pm 0.09$ pb [15]. Neither of these results is compatible with LO NRQCD predictions.

The LO NRQCD prediction for $\sigma(e^+e^- \to J/\psi + c\bar{c} + X)$ is about 0.15 pb, in which the CO contribution is negligible [16]. To solve the problem, both the next-to-leading-order (NLO) QCD [17] and relativistic corrections [18] were calculated. The relativistic correction was found to be less than one percent of the LO contribution. The effect of the NLO QCD correction is large. Its K factor is about 1.8 for $m_c = 1.5$ GeV and $\alpha_s = 0.26$. After including the feed-down contribution from $\psi(2S)$, the NRQCD prediction at NLO becomes $0.53^{+0.59}_{-0.23}$ pb and largely removes the discrepancy [17]. However, the theoretical prediction depends strongly on the chosen values of m_c and α_s. According to the design [19], the Fcc-ee will run at several beam energies. Measuring $J/\psi + c\bar{c}$ production at different energies will definitely help to improve our understanding of the parameter setting in the theoretical calculation.

At high energies, the predominant contribution to $J/\psi + c\bar{c}$ production comes from the fragmentation process. For heavy-quarkonium production, it is found that there are two types of fragmentation [20]: (1) single-parton fragmentation (SPF) and (2) double-parton fragmentation (DPF). At hadron colliders, experimentally, the $J/\psi + c\bar{c}$ final state is hard to detect and, theoretically, both SPF and DPF contribute, so that it is very difficult to study their properties separately.

In the e^+e^- annihilation process, only SPF contributes. Thus, the differential cross section in the fragmentation limit can be expressed as

$$d\sigma(e^+e^- \to J/\psi + c\bar{c}) = 2 \int d\sigma(e^+e^- \to c\bar{c}) D_{c\to J/\psi}(z) dz, \tag{8.79}$$

where

$$D_{c\to J/\psi}(z) = \frac{8\alpha_s^2}{27\pi} \frac{z(1-z)^2(5z^4 - 32z^3 + 72z^2 - 32z + 16)}{(2-z)^6} \frac{|R(0)|^2}{m_c^3}, \tag{8.80}$$

with $z = E_{J/\psi}/\sqrt{s}$ and $|R(0)|$ being the wave function of J/ψ at the origin [21].

At $\sqrt{s} = 10.6$ GeV, the fragmentation contribution can only account for 58% of the complete calculation [16]. The comparison between the complete calculation and the fragmentation approximation is shown in Fig. B.28. We observe that, only in the energy range of the Fcc-ee or even beyond, the fragmentation contribution provides a good approximation. On the other hand, the differential cross section of $e^+e^- \to Q\bar{Q}$ is known at $\mathcal{O}(\alpha_s^2)$ [22, 23]. By comparing experimental measurements with higher-order theoretical calculations, the fragmentation function at higher orders can also be extracted.

For $J/\psi + X_{\text{non}-c\bar{c}}$ production, in the CS contribution, the NLO QCD corrections [24] and relativistic corrections [25] are equally important. Their K factors are both around 1.2 [24, 25], and the cross section through NLO in QCD and v^2 becomes $\sigma(e^+e^- \to J/\psi + gg) \simeq 437$ fb for $\mu = \sqrt{s}/2$ and $m_c = 1.5$ GeV, which almost saturates the Belle measurement and leaves little room for the CO contribution [25]. The NLO QCD corrections to the CO channels ${}^1S_0^{[8]}$ and ${}^3P_J^{[8]}$ were also computed [26]. A lower bound on the CO contribution is obtained by using the LDMEs from Ref. [4], which yields 0.3 pb. Therefore, the total NRQCD prediction is larger than the Belle measurements, but does not conflict with the Babar and CLEO measurements if we assume that $\sigma(e^+e^- \to J/\psi + c\bar{c} + X)$ is similar in these three experiments. To understand the CO mechanism in e^+e^- annihilation, further analysis of $J/\psi + X_{\text{non}-c\bar{c}}$ production at 10.6 GeV and in the future at the Fcc-ee is necessary.

Besides charmonium, the production of bottomonium in e^+e^- annihilation is also of great interest. However, the collision energy at B factories is so close to the Υ production threshold that perturbative calculations are no longer reliable. Moreover, such a low energy is not sufficient to enable $\Upsilon + b\bar{b}$ production. At Fcc-ee, the collision energy is of order 10^2 GeV and, therefore, provides a unique opportunity to study $\Upsilon + X_{\text{non}-b\bar{b}}$ and $\Upsilon + b\bar{b}$ production in e^+e^- annihilation. Theoretically, the NRQCD prediction through NLO can be easily obtained from the known J/ψ calculation by changing the value of $\sqrt{s}$ and replacing m_c by m_b and the LDMEs of J/ψ by the ones of Υ.

8.2 Heavy-quarkonium production in $\gamma\gamma$ collisions

J/ψ photoproduction in $\gamma\gamma$ collisions ($e^+e^- \to e^+e^- J/\psi + X$) was measured by the DELPHI Collaboration at LEP-II [27,28]. The total cross section was found to be $\sigma(e^+e^- \to e^+e^- J/\psi + X) = (45 \pm 9 \pm 17)$ pb [28]. They also measured the transverse-momentum (p_T) distribution of the cross section. Since the higher excited states χ_{cJ} and ψ' can decay into J/ψ via radiative decays or hadronic transitions, their feed-down contributions should also be considered. In such processes, the $c\bar{c}$ pair can either be produced by photons directly (direct photoproduction) or via the light-quark and gluon content of the photons (resolved photoproduction), so that there are three channels: direct, single resolved, and double resolved, all of which contribute formally at the same order in the perturbative expansion and should be included.

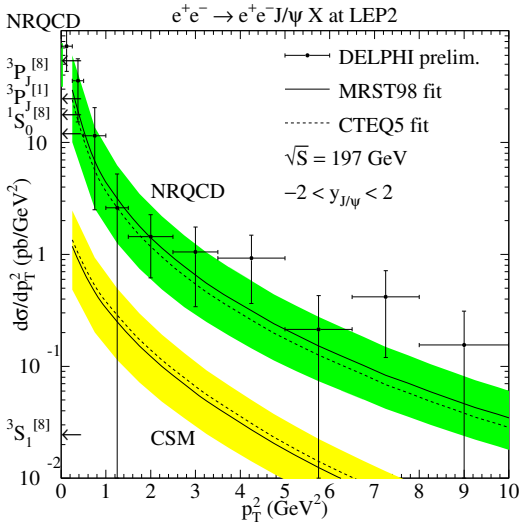

Fig. B.29: Comparison between NRQCD and CS model predictions of $d\sigma/dp_T^2$ as functions of p_T^2 for $\gamma\gamma \to J/\psi$ at LO [29] and DELPHI measurement at LEP-II. The solid and dashed lines are calculated with the MRST98 LO and CTEQ5 parton distribution functions, respectively. The bands indicate the theoretical uncertainties.

Working in the Weizsäcker-Williams approximation to describe the bremsstrahlung photons radiated off the $e^\pm$ beams and using the factorization theorems of the QCD parton model and NRQCD, the general formula for the differential cross section for the production of the heavy-quarkonium state H can be written as:

$$\frac{d\sigma(e^+e^- \to e^+e^-H+X)}{dx_1dx_2dx_adx_b} = \sum_{a,b,n} f_\gamma(x_1)f_\gamma(x_2)f_{a/\gamma}(x_a)f_{b/\gamma}(x_b) \times d\hat{\sigma}(a+b \to Q\bar{Q}(n)+X)\langle\mathcal{O}^H(n)\rangle, \tag{8.81}$$

where $f_\gamma(x)$ is the flux function of the photon in the $e^\pm$ beam, $f_{j/\gamma}(x)$ is $\delta(1-x)$ if $j=\gamma$ and otherwise the parton distribution function of parton j in the resolved photon, $d\hat{\sigma}(a+b \to Q\bar{Q}(n)+X)$ is the partonic cross section, and $\langle\mathcal{O}^H(n)\rangle$ is the NRQCD LDME.

In the LO calculation, both direct J/ψ production and the feed-down from χ_{cJ} for $J=0,1,2$ and ψ' are included [29]. For J/ψ (ψ') production through relative order $\mathcal{O}(v^4)$, the Fock states include $n = {}^3S_1^{[1,8]}, {}^1S_0^{[8]}, {}^3P_J^{[8]}$, and for χ_{cJ} production at LO in v^2 one needs $n = {}^3P_J^{[1]}, {}^3S_1^{[8]}$. As we see in Fig. B.29, the LO NRQCD prediction of $d\sigma/dp_T^2$, evaluated with the LDMEs from the LO fit to Tevatron data [30], agree very well with the DELPHI data, while the CS contribution itself lies far below the data, as the central values are about 16 times smaller. The total cross section in the range $1 \le p_T^2 \le 10$ GeV^2 measured by DELPHI is 6.4 ± 2.0 pb [27]. The NRQCD prediction is $4.7^{+1.9}_{-1.2}$ pb [29], which is also consistent with the DELPHI result within errors. However, the CS contribution is only $0.39^{+0.16}_{-0.09}$ pb [29]. The nice agreement between the NRQCD calculation and the experimental measurement for J/ψ photoproduction is one of the earliest pieces of evidence for the CO mechanism predicted by NRQCD.

In 2011, two groups independently obtained the complete NLO QCD corrections to J/ψ direct hadroproduction for the first time [31,32]. However, their LDMEs are different because

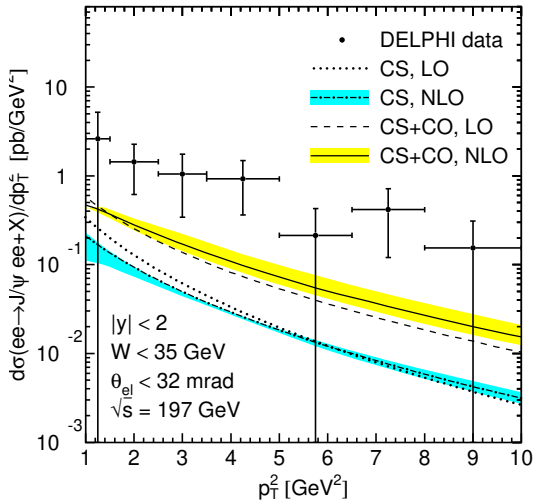

Fig. B.30: Comparison of LEP-II data on $\gamma\gamma \to J/\psi$ with NLO NRQCD predictions evaluated with LDMEs obtained via a global data analysis [4].

they fitted to data in different p_T ranges. To eliminate such problems and further check the universality of the NRQCD LDMEs at NLO, a global analysis to worldwide data including $\gamma\gamma$ collisions was carried out. The resulting three CO LDMEs, $\left\langle \mathcal{O}^{J/\psi}(^1S_0^{[8]}) \right\rangle = (4.97 \pm 0.44) \times 10^{-2}$ GeV^3, $\left\langle \mathcal{O}^{J/\psi}(^3S_1^{[8]}) \right\rangle = (2.24 \pm 0.59) \times 10^{-3}$ GeV^3, and $\left\langle \mathcal{O}^{J/\psi}(^3P_0^{[8]}) \right\rangle = (-1.61 \pm 0.20) \times 10^{-2}$ GeV^5, which obey the velocity scaling rules, were found to explain fairly well all the J/ψ yield data, except for the case of $\gamma\gamma$ collisions [4]. In contrast to situation at LO, the DELPHI data systematically overshoot the NLO NRQCD prediction, as may be seen in Fig. B.30. However, Figs. B.29 and B.30 indicate that the uncertainties in the experimental measurements are very large. There are only 36 ± 7 $J/\psi \to \mu^+\mu^-$ events in total (and 16 thereof in the region $p_T > 1$ GeV), collected with an integrated luminosity of 617 pb^{-1}. The integrated luminosity at Fcc-ee will reach the ab^{-1} level, which is more than three orders of magnitude larger than that of LEP-II. Measuring J/ψ production in $\gamma\gamma$ collisions at the Fcc-ee would not only serve as a cross check of the LEP-II results, but also provide results with high accuracy. Such a study could surely clarify the current conflict and deepen our understanding of the heavy-quarkonium production mechanism in $\gamma\gamma$ collisions.

Unlike the case of e^+e^- annihilation, $J/\psi{+}c\bar{c}{+}X$ production in $\gamma\gamma$ collisions is predicted to have a smaller cross section than $J/\psi{+}X_{\text{non}-c\bar{c}}$ production. While $\gamma\gamma \to J/\psi{+}X_{\text{non}-c\bar{c}}$ proceeds dominantly via single-resolved photoproduction, $\gamma\gamma \to J/\psi + c\bar{c} + X$ proceeds dominantly via direct photoproduction [33]. The total cross section in the region $p_T^{J/\psi} > 1$ GeV is predicted to be about $0.16 - 0.20$ pb depending on the chosen values of α_s and the CS LDME [33, 34]. Its NLO NRQCD correction has also been calculated, and the K factor is found to be 1.46, enhancing the total cross section in the region $p_T^{J/\psi} > 1$ GeV to become around $0.23 - 0.29$ pb, which is too small to be analyzed at LEP-II [34]. The cross section becomes larger as the e^+e^- collision energy increases. Based on the results in Ref. [34], we estimate the numbers of $J\psi + c\bar{c}$ events accumulated with the Fcc-ee at the ZZ and ZH thresholds each to be around 2×10^6, assuming the kinematic-cut conditions for the Fcc-ee to be the same as for LEP-II. Such large data samples should be enough to usefully study $J/\psi + c\bar{c} + X$ production in $\gamma\gamma$ collisions.

8.3 Summary and Outlook

The production mechanisms of heavy quarkonium, especially of the J/ψ meson, have not yet been fully understood within the framework of NRQCD factorization. We have discussed here two modes of J/ψ production at e^+e^- colliders, through e^+e^- annihilation and $\gamma\gamma$ collsions. In the e^+e^- annihilation case, for $J/\psi + c\bar{c} + X$ production, the NRQCD prediction and the Belle measurement agree within errors; however, for $J/\psi + X_{\text{non}-c\bar{c}}$ production, the Belle result favors the CS model prediction and is overshot by NRQCD predictions evaluated using any of the available LDME sets, although the latter are mutually inconsistent. We note that the NRQCD predictions seem to be compatible with the Babar and CLEO results. As for J/ψ production in $\gamma\gamma$ collisions, the NRQCD prediction can explain the LEP-II data, whose uncertainties are large, at LO, but fails once the NLO correction is included.

The FCC-ee will run at different energy points with considerable integrated luminosity, of $\mathcal{O}(\text{ab}^{-1})$ or even $\mathcal{O}(10^2\ \text{ab}^{-1})$ at the Z-boson peak [19], which will provide a perfect environment to judge the disagreements independently. Moreover, it can significantly enrich our knowledge of heavy-quarkonium production in e^+e^- collisions, especially by studying bottomonium production, the fragmentation function of $c \to J/\psi$, and $J/\psi + c\bar{c}$ production in $\gamma\gamma$ collisions.

References

[1] G. T. Bodwin, E. Braaten, G. P. Lepage, Rigorous QCD analysis of inclusive annihilation and production of heavy quarkonium, Phys. Rev. D51 (1995) 1125–1171, [Erratum: Phys. Rev.D55,5853(1997)]. arXiv:hep-ph/9407339, doi:10.1103/PhysRevD.55.5853, 10.1103/PhysRevD.51.1125.

[2] W. E. Caswell, G. P. Lepage, Effective Lagrangians for Bound State Problems in QED, QCD, and Other Field Theories, Phys. Lett. 167B (1986) 437–442. doi:10.1016/0370-2693(86)91297-9.

[3] G. P. Lepage, L. Magnea, C. Nakhleh, U. Magnea, K. Hornbostel, Improved nonrelativistic QCD for heavy quark physics, Phys. Rev. D46 (1992) 4052–4067. arXiv:hep-lat/9205007, doi:10.1103/PhysRevD.46.4052.

[4] M. Butenschoen, B. A. Kniehl, World data of J/psi production consolidate NRQCD factorization at NLO, Phys. Rev. D84 (2011) 051501. arXiv:1105.0820, doi:10.1103/PhysRevD.84.051501.

[5] K.-T. Chao, Y.-Q. Ma, H.-S. Shao, K. Wang, Y.-J. Zhang, J/ψ Polarization at Hadron Colliders in Nonrelativistic QCD, Phys. Rev. Lett. 108 (2012) 242004. arXiv:1201.2675, doi:10.1103/PhysRevLett.108.242004.

[6] B. Gong, L.-P. Wan, J.-X. Wang, H.-F. Zhang, Polarization for Prompt J/Ψ and $\Psi(2s)$ Production at the Tevatron and LHC, Phys. Rev. Lett. 110 (4) (2013) 042002. arXiv:1205.6682, doi:10.1103/PhysRevLett.110.042002.

[7] M. Butenschoen, Z.-G. He, B. A. Kniehl, η_c production at the LHC challenges nonrelativistic-QCD factorization, Phys. Rev. Lett. 114 (9) (2015) 092004. arXiv:1411.5287, doi:10.1103/PhysRevLett.114.092004.

[8] B. Aubert, et al., Measurement of J/ψ production in continuum e^+e^- annihilations near $\sqrt{s} = 10.6$ GeV, Phys. Rev. Lett. 87 (2001) 162002. arXiv:hep-ex/0106044, doi:10.1103/PhysRevLett.87.162002.

[9] K. Abe, et al., Production of prompt charmonia in e^+e^- annihilation at $\sqrt{s}$ is approximately 10.6-GeV, Phys. Rev. Lett. 88 (2002) 052001. arXiv:hep-ex/0110012, doi:10.1103/PhysRevLett.88.052001.

[10] R. A. Briere, et al., New measurements of υ_{1S} decays to charmonium final states, Phys. Rev. D70 (2004) 072001. arXiv:hep-ex/0407030, doi:10.1103/PhysRevD.70.072001.

[11] F. Yuan, C.-F. Qiao, K.-T. Chao, Prompt J/ψ production at e^+e^- colliders, Phys. Rev. D56 (1997) 321–328. arXiv:hep-ph/9703438, doi:10.1103/PhysRevD.56.321.

[12] F. Yuan, C.-F. Qiao, K.-T. Chao, Determination of color octet matrix elements from e^+e^- process at low-energies, Phys. Rev. D56 (1997) 1663–1667. arXiv:hep-ph/9701361, doi:10.1103/PhysRevD.56.1663.

[13] S. Baek, P. Ko, J. Lee, H. S. Song, Polarized J/Ψ production at CLEO, J. Korean Phys. Soc. 33 (1998) 97–101, [225(1998)]. arXiv:hep-ph/9804455.

[14] G. A. Schuler, Testing factorization of charmonium production, Eur. Phys. J. C8 (1999) 273–281, [,57(1998)]. arXiv:hep-ph/9804349, doi:10.1007/s100529900948.

[15] P. Pakhlov, et al., Measurement of the $e^+e^- \to J/\Psi + c\bar{c}$ cross section at $\sqrt{s} \sim 10.6$ GeV, Phys. Rev. D79 (2009) 071101. arXiv:0901.2775, doi:10.1103/PhysRevD.79.071101.

[16] K.-Y. Liu, Z.-G. He, K.-T. Chao, Inclusive charmonium production via double $c\bar{c}$ in e^+e^- annihilation, Phys. Rev. D69 (2004) 094027. arXiv:hep-ph/0301218, doi:10.1103/PhysRevD.69.094027.

[17] Y.-J. Zhang, K.-T. Chao, Double charm production $e^+e^- \to J/\Psi + c\bar{c}$ at B factories with next-to-leading order QCD correction, Phys. Rev. Lett. 98 (2007) 092003. arXiv:hep-ph/0611086, doi:10.1103/PhysRevLett.98.092003.

[18] Z.-G. He, Y. Fan, K.-T. Chao, Relativistic corrections to J/ψ exclusive and inclusive double charm production at B factories, Phys. Rev. D75 (2007) 074011. arXiv:hep-ph/0702239, doi:10.1103/PhysRevD.75.074011.

[19] M. Benedikt, A. Blondel, O. Brunner, M. Capeans Garrido, F. Cerutti, J. Gutleber, P. Janot, J. M. Jimenez, V. Mertens, A. Milanese, K. Oide, J. A. Osborne, T. Otto, Y. Papaphilippou, J. Poole, L. J. Tavian, F. Zimmermann, Future Circular Collider, Tech. Rep. CERN-ACC-2018-0057, CERN, Geneva, submitted for publication to Eur. Phys. J. ST. (Dec 2018).
URL http://cds.cern.ch/record/2651299

[20] Z.-B. Kang, J.-W. Qiu, G. Sterman, Heavy quarkonium production and polarization, Phys. Rev. Lett. 108 (2012) 102002. arXiv:1109.1520, doi:10.1103/PhysRevLett.108.102002.

[21] E. Braaten, K.-m. Cheung, T. C. Yuan, Z0 decay into charmonium via charm quark fragmentation, Phys. Rev. D48 (1993) 4230–4235. arXiv:hep-ph/9302307, doi:10.1103/PhysRevD.48.4230.

[22] J. Gao, H. X. Zhu, Electroweak prodution of top-quark pairs in e^+e^- annihilation at NNLO in QCD: the vector contributions, Phys. Rev. D90 (11) (2014) 114022. arXiv:1408.5150, doi:10.1103/PhysRevD.90.114022.

[23] J. Gao, H. X. Zhu, Top Quark Forward-Backward Asymmetry in e^+e^- Annihilation at Next-to-Next-to-Leading Order in QCD, Phys. Rev. Lett. 113 (26) (2014) 262001. arXiv:1410.3165, doi:10.1103/PhysRevLett.113.262001.

[24] Y.-Q. Ma, Y.-J. Zhang, K.-T. Chao, QCD correction to $e^+e^- \to J/\psi + gg$ at B Factories, Phys. Rev. Lett. 102 (2009) 162002. arXiv:0812.5106, doi:10.1103/PhysRevLett.102.

162002.

[25] Z.-G. He, Y. Fan, K.-T. Chao, Relativistic correction to $e^+e^- \to J/\Psi + gg$ at B factories and constraint on color-octet matrix elements, Phys. Rev. D81 (2010) 054036. arXiv:0910.3636, doi:10.1103/PhysRevD.81.054036.

[26] Y.-J. Zhang, Y.-Q. Ma, K. Wang, K.-T. Chao, QCD radiative correction to color-octet J/ψ inclusive production at B Factories, Phys. Rev. D81 (2010) 034015. arXiv:0911.2166, doi:10.1103/PhysRevD.81.034015.

[27] S. Todorova-Nova, (Some of) recent gamma gamma measurements from LEP, in: Multiparticle dynamics. Proceedings, 31st International Symposium, ISMD 2001, Datong, China, September 1-7, 2001, 2001, pp. 62–67. arXiv:hep-ph/0112050, doi:10.1142/9789812778048_0010.
URL http://www.slac.stanford.edu/econf/C010901

[28] J. Abdallah, et al., Study of inclusive J/Ψ production in two photon collisions at LEP-2 with the DELPHI detector, Phys. Lett. B565 (2003) 76–86. arXiv:hep-ex/0307049, doi:10.1016/S0370-2693(03)00660-9.

[29] M. Klasen, B. A. Kniehl, L. N. Mihaila, M. Steinhauser, Evidence for color octet mechanism from CERN LEP-2 $\gamma\gamma \to J/\psi + X$ data, Phys. Rev. Lett. 89 (2002) 032001. arXiv:hep-ph/0112259, doi:10.1103/PhysRevLett.89.032001.

[30] E. Braaten, B. A. Kniehl, J. Lee, Polarization of prompt J/ψ at the Tevatron, Phys. Rev. D62 (2000) 094005. arXiv:hep-ph/9911436, doi:10.1103/PhysRevD.62.094005.

[31] M. Butenschoen, B. A. Kniehl, Reconciling J/ψ production at HERA, RHIC, Tevatron, and LHC with NRQCD factorization at next-to-leading order, Phys. Rev. Lett. 106 (2011) 022003. arXiv:1009.5662, doi:10.1103/PhysRevLett.106.022003.

[32] Y.-Q. Ma, K. Wang, K.-T. Chao, $J/\psi(\psi')$ production at the Tevatron and LHC at $\mathcal{O}(\alpha_s^4 v^4)$ in nonrelativistic QCD, Phys. Rev. Lett. 106 (2011) 042002. arXiv:1009.3655, doi:10.1103/PhysRevLett.106.042002.

[33] R. Li, K.-T. Chao, Photoproduction of J/Ψ in association with a $c\bar{c}$ pair, Phys. Rev. D79 (2009) 114020. arXiv:0904.1643, doi:10.1103/PhysRevD.79.114020.

[34] Z.-Q. Chen, L.-B. Chen, C.-F. Qiao, NLO QCD Corrections for $J/\psi + c\bar{c}$ Production in Photon-Photon Collision, Phys. Rev. D95 (3) (2017) 036001. arXiv:1608.06231, doi:10.1103/PhysRevD.95.036001.

9 Vertex functions in QCD - preparation for beyond two loops

Author: J.A. Gracey [gracey@liverpool.ac.uk]

Abstract. We summarize the algorithm to determine the two loop off-shell 3-point vertex functions of QCD before outlining the steps required to extend the results to three and higher loops.

9.1 Introduction.

In our current generation of high energy particle accelerators involving hadron collisions, a major source of background is radiation derived from the strong sector. As this is governed by Quantum Chromodynamics (QCD) in order to quantify the background effects one has to carry out high loop order computations. There has been remarkable activity and progress in this direction since around the turn of the Millennium. The primary focus has been with the evaluation of on-shell n-point gluonic and fermionic amplitudes to several loop orders both analytically and numerically. Indeed such results have been crucial in ensuring that the Higgs particle was observed at CERN's LHC. However having information on the off-shell Green's functions such as the 3-point vertices of QCD is also important for theory as well as experiment. For instance, various articles in this direction have appeared over the years. A non-exhaustive set of references for ths status of 3- and 4-point functions at various external momenta configurations is [1–11]. There are various theoretical reasons for having such off-shell Green's functions. One is that knowing, say, the two loop off-shell vertex functions then higher loop n-point on-shell amplitudes could be modelled numerically. This could be an interim position in the absence of the technology to compute them fully explicitly. Such an approach is not uncommon. Equally in solving QCD beyond the perturbative limit analytically to probe deep infrared properties using the Schwinger-Dyson formalism, approximations have to be made in order to solve the infinite tower of Green's functions. Until recent years the validity of such approximations could not be fully quantified. However with explicit perturbative results, for instance, such error analyses have been possible. For instance one approximation in solving 2- and 3-point Schwinger-Dyson equations is to neglect the summed graphs deriving from the quartic gluon vertex. Work in this direction over a period of time, [12–16], has checked that such a step does not affect final results by more than a few percent. Equally the Schwinger-Dyson method has been applied to finding the behaviour of the vertex functions. While similar approximations have been made such analyses have to be consistent with explicit perturbative results where *no* approximation is made at a particular loop order to drop a subset of contributing graphs. As an aside lattice gauge theory calculations of vertex functions equally have to match on to perturbative results. Therefore in light of these different areas of activity there is a clear need to compute QCD n-point and specifically vertex functions off-shell as well as on-shell. For the former, which is the focus of this article, we will review the status of the two loop evaluation of the 3-point vertices as well as outline the algorithm to extend this to higher loop order. While the discussion will be technical by nature, we will pool together all the necessary ingredients for the goal to be obtained at three loops.

While it is not immediately obvious it is the case that the route to achieve this will involve higher level mathematics extracted for instance from an algebraic geometry approach. Indeed this also lies at the heart of on-shell amplitude computations. This technology has revolutionalized the programme of loop calculations. An example of this can be seen in the results for two loop off-shell vertex results of [17] where harmonic polylogarithms based on

a specific type of polynomials known as cyclotomic, [18], appeared. One corollary of such results is the possibility of effecting renormalization schemes other than the canonical $\overline{\rm MS}$ one which is universally accepted as the default scheme. Although it is the scheme with which one can carry out very high loop order calculations it is not a kinematic one and retains no data within the β-function, for instance, of the information on the subtraction point. In [19] the momentum subtraction scheme, denoted by MOM, was introduced and the R-ratio studied [20]. Extending [19] to the next order in [21] produced the three loop MOM renormalization group functions. This allowed for studies of physical quantities at a loop order where scheme effects were apparent, [22]. One consequence is that choosing alternative renormalization schemes could lead to a different way of estimating theory errors in measurements. In other words similar to an experiment estimating a measured quantity in different schemes the average of the result could be a more sound way of assessing truncation errors as an alternative to using values at different scales. With fully off-shell vertex functions, for instance, this idea can be extended beyond the symmetric point subtraction of the MOM case to have a region bounding the central value.

The article is organized as follows. The method used to evaluate 3-point off-shell vertex functions is discussed in the next section with reference to the triple gluon vertex. This forms the basis for higher loop computations with the algorithm being outlined in Section 3. Concluding remarks are made in Section 4.

9.2 Current status

At the outset it is worth reviewing aspects of the early QCD vertex evaluations. By this we mean that our focus will be on cases where there is *no* nullification of an extenal momentum. This is important since in the computation of the QCD β-function to very high loop order the extraction of the $\overline{\rm MS}$ coupling constant renormalization constant can be facilitated by setting the momentum of one of the external fields of the vertex function to zero. This is a mathematical shortcut since the ultraviolet divergence is not contaminated by any infrared ones. By contrast this infrared safe procedure does not produce the *correct* finite part of the vertex functions. So it is not an appropriate method for gaining insight into any aspect of the kinematic properties of the vertex functions themselves. To be more concrete in the discussion we will focus on the triple gluon vertex function of Figure B.31 which represents

$$\left\langle A^a_\mu(p_1) A^b_\nu(p_2) A^c_\sigma(-p_1-p_2) \right\rangle \;=\; f^{abc} \Sigma^{\rm ggg}_{\mu\nu\sigma}(p_1,p_2) \;=\; f^{abc} \sum_{k=1}^{14} \mathcal{P}^{\rm ggg}_{(k)\,\mu\nu\sigma}(p_1,p_2)\, \Sigma^{\rm ggg}_{(k)}(p_1,p_2) \tag{9.82}$$

where f^{abc} are the colour group stucture constants. The momenta p_i satisfy energy-momentum conservation

$$\sum_{n=1}^{3} p_i \;=\; 0 \tag{9.83}$$

and the underlying Lorentz invariants which the 3-point functions depend on are expressed in terms of two dimensionless variables, x and y, and one mass scale μ which are defined by

$$x \;=\; \frac{p_1^2}{p_3^2} \quad , \quad y \;=\; \frac{p_2^2}{p_3^2} \quad , \quad p_3^2 \;=\; -\,\mu^2 \tag{9.84}$$

and we assume that none of p_i^2 vanishes. In (9.82) we have decomposed the vertex into its 14 scalar amplitudes $\Sigma^{\rm ggg}_{(k)}(p_1,p_2)$ with respect to a basis of Lorentz tensors $\mathcal{P}^{\rm ggg}_{(k)\,\mu\nu\sigma}(p_1,p_2)$. With

this structure in mind for the other two 3-point vertices the full one loop vertex functions were studied in [19] in the early years following the discovery of asymptotic freedom.

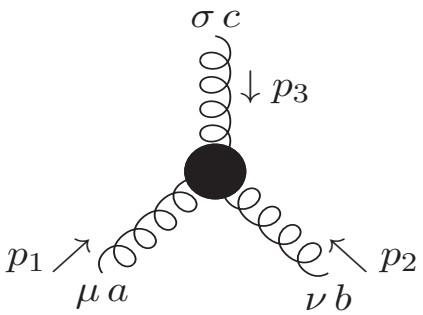

Fig. B.31: Triple gluon vertex function.

Two important main early papers which stand out are [19,23]. The former focused on the vertex functions at the fully symmetric subtraction point defined by $x = y = 1$ and introduced the MOM kinematic renormalization scheme known as MOM for momentum subtraction. Unlike the $\overline{\rm MS}$ scheme the renormalization is carried out at this specific symmetric point and the finite part of the vertex functions is absorbed into the renormalization constants. Therefore the β-functions contain kinematic data. The motivation of [19] was to study if the convergence of the perturbative series could be improved in this new scheme. The other article [23] was a systematic study of each fully off-shell 3-point vertex with a view to writing each in terms of amplitudes dictated by external gluons being transverse. As such it has served as the default vertex function convention where Schwinger-Dyson techniques are used to approximate other Green's functions. Consequently there have been a large number of one loop studies of the three 3-point vertices for different external momentum configurations as noted earlier. In some cases these studies have been at two loops but for the most part one or more external gluon legs were on-shell and quarks have been massless except in the case of [3, 7]. In the main the evaluation has been by standard quantum field theory techniques via Feynman graphs. However modern string inspired methods have been used [11, 24] for off-shell one loop vertex functions. The case where a gluon for example is on-shell has to be treated separately from the configuration introduced in (9.84) due to potential infrared singularities in taking the on-shell limit from the fully off-shell results.

Studies of the vertex functions for the special cases where one or more external line is on-shell has direct applications to experimental set-ups. One of the reasons why these were computed was in the main that the calculational tools for the off-shell case were not developed until much later. Several main components were necessary for this with the main breakthrough arriving in the form of the Laporta algorithm [25]. This is a procedure of relating scalar Feynman integrals of a particular n-point function at a specfied loop order to core or master integrals of r-point functions with $r \leq n$ and the same loop order. The connection between integrals being made via integration by parts. Then starting with the most complicated integral the relations derived from integration by parts could be solved algebraically. While clearly such a large set of equations contains a degree of redundancy the whole process can be encoded for a computer to handle this and several packages are publicly available to do so, [26–32]. The second breakthrough necessary to complete this task was the determination of the master integrals. For 3-point functions these had to be constructed by specialized methods [33–36] to

two loops as integration by parts had been exhausted by the Laporta algorithm. To have a flavour of the resultant mathematical structure the one loop master integral of Figure B.32 is for instance given by, [33–35],

$$I_1(x,y) \;=\; -\;\frac{1}{\mu^2}\left[\Phi_1(x,y) + \Psi_1(x,y)\epsilon + \left[\frac{\zeta(2)}{2}\Phi_1(x,y) + \chi_1(x,y)\right]\epsilon^2 \;+\; O(\epsilon^3)\right] \tag{9.85}$$

in $d = 4 - 2\epsilon$ dimensions where $\zeta(z)$ is the Riemann zeta function. Here the functions are related to polylogarithms $\mathrm{Li}_n(z)$. For instance

$$\Phi_1(x,y) \;=\; \frac{1}{\lambda}\left[2\mathrm{Li}_2(-\rho x) + 2\mathrm{Li}_2(-\rho y) + \ln\left(\frac{y}{x}\right)\ln\left(\frac{(1+\rho y)}{(1+\rho x)}\right) + \ln(\rho x)\ln(\rho y) + \frac{\pi^2}{3}\right] . \tag{9.86}$$

with

$$\rho(x,y) \;=\; \frac{2}{[1-x-y+\lambda(x,y)]} \quad , \quad \lambda(x,y) \;=\; [1-2x-2y+x^2-2xy+y^2]^{\frac{1}{2}} \tag{9.87}$$

with the other functions of (9.85) given in [33–35] too. While the $O(\epsilon)$ terms may not at first sight appear to be necessary they are required for various reasons. One is that at higher loops these one loop expressions are multiplied by the counterterms. So when a pole in ϵ multiplies a term which is $O(\epsilon)$ then that will contribute to the finite part of the vertex function at the next loop order. Accordingly one needs the master integrals to at least $O(\epsilon^2)$ at one loop for a three loop evaluation. We have indicated this since it could be the case that in the reduction using the Laporta algorithm a spurious pole in ϵ arises which we discuss later. This is not an uncommon occurrence but the latest Laporta algorithm packages have now tools to circumvent this possibility. These technical issues aside the full off-shell 3-point QCD vertex functions are available to two loops with more details provided in [17].

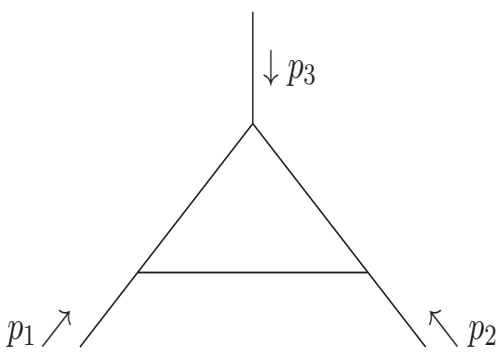

Fig. B.32: One loop 3-point master integral $I_1(x,y)$.

9.3 Three loop strategy

One of the reasons for detailing the formalism to carry out the two loop computations is that it points the way for higher loop corrections. On that basis we outline the next parts of the jigsaw to construct the three loop extension of [17]. First we assume the procedure of the general algorithm for the Green's functions is applied to obtain the three loop scalar amplitudes as

illustrated in (9.82). From these the large set of scalar Feynman integrals are assembled which have to be reduced to the master integrals. The Laporta algorithm can in principle be applied in the three loop case using one of the latest packages which have the built-in improvements such as the refined algebraic reduction of the KIRA package, [32]. However to speed the integration by parts procedure it is not inconceivable that a faster algorithm could be developed. For instance for many years the MINCER package served the multiloop community well for three loop massless 2-point graphs in four dimensions, [37, 38]. It implemented the star-triangle rule to produce an efficient code to evaluate even the heaviest fully gluonic three loop graphs. With the need for more precision experimentally the four loop FORCER package, [39, 40], has superseded MINCER in the journey to hit the latest precision benchmark. Each have been encoded in the symbolic manipulation language FORM, [41, 42]. With the increase in loop order the evaluation time for a Green's function increases. However the FORCER algorithm implements a *new* integration rule to handle an internal topology which has no three loop antecedents and hence is a purely four loop feature. We have mentioned this since FORCER like MINCER applies only to 2-point functions. However the same new rule should be applicable or adaptable to three loop 3-point functions since such a configuration emerges when one slices the vertex off a 2-point function where that vertex contains one of the external legs. The remaining graph would retain the internal topology of the 2-point four loop case. Therefore an adaptation of the new feature of FORCER could in principle be transferred to the 3-point case to provide an efficient alternative to the application of the Laporta algorithm for massless 3-point functions.

While such technology is already in effect in situ the main obstacle to the full implementation of a three loop evaluation is the determination of the required three loop master integrals. In recent years this field has advanced with progress having been made in understanding the mathematical properties of high order Feynman integrals. Examples of such articles include [43, 44] which provide novel procedures to compute Feynman graphs. The background to this is that there are a wide range of tools to evaluate a graph. One is to introduce the Schwinger parameter representation of each propagator and convert the L-loop d-dimensional spacetime integral into an integral over Schwinger parameters. The resulting integral has a large number of parameter integrations to be carried out and there is no guarantee that this can be achieved analytically. This is to be preferred over a numerical approach as the latter, if a Monte Carlo approach is used, could require a sizeable amount of computer resources to get a reasonable accuracy. In certain instances an analytic evaluation is possible and in essence uses algebraic geometry to produce an integration strategy. Such higher mathematics is relevant since the integrand contains polynomials of the parameters which represent higher dimensional geometries. Established mathematical theorems are then effected which determine which parameter integration order is to be used with the guiding principle being linear reducibility. By this we mean that after each parameter integration the polynomial degree reduces but the key to achieve this is to have the polynomial factor off a smaller polynomial involving only factors linear in the next variable to be integrated. It is this linearity which is key as it allows one to use the machinery of hyperlogarithms to carry out the integration over that Schwinger parameter. What was not immediately evident is if this proceduce could be iterated without obstruction and that when it terminates the value of the integral is found. It has now been shown that if an integral is linearly reducible, [45, 46], in the above sense there is at least one choice of integration order which allows the integral to be determined. While this is in essence the general current position it is known that to three loops the 3-point vertex master integrals are all linearly reducible. So in principle the required master integrals can be determined.

The actual practicalities of this have yet to be carried out. However several packages are available to assist with this task. For instance converting a scalar Feynman integral into Schwinger parameter representation via the underlying graphs polynomials is now a standard feature of integration packages such as in HYPERINT, [47]. This package is appropriate for an analytic determination since any evaluation can be written in various hyperlogarithm representations. It has features which allows one to find the order of integration over the parameter variables to ensure that there is no obstruction to the linear reducibility. In principle one can expand to several orders in the ϵ expansion in $d = 4 - 2\epsilon$ dimensions. However for terms beyond the leading few the parameter integration can become tedious especially for high loop order. Therefore a more appropriate strategy would be one where only the first term of the ϵ expansion of a master integral was required which would then require the Laporta reduction to be constrained to producing a basis of masters which is finite. There is a caveat with this due to the fact that one is using dimensional regularization which means that the reduction produces factors of rational polynomials in d. Such functions can include poles in $(d - 4)$ which are termed spurious poles. This is in the sense that while they correspond to a divergence it is not necessarily one due to the divergence of an actual graph. There are now ways to circumvent this which work hand in hand with another property of the beauty of computing in d-dimensions. This was analysed in depth in [48, 49] where it was shown that d-dimensional integrals can be related to the corresponding topology in $(d + 2)$-dimensions plus a sum of others which have the same core topology but with propagators missing. Such higher dimensional integrals can be incorporated in the Laporta reduction process and has been implemented in version 2.11 of the REDUZE package, [27]. The advantage is that with the increase in dimensionality in the higher dimensional integral, it is not as ultraviolet divergent as its lower dimensional counterpart. Thereby in principle one reduces the evaluation of the more difficult master integrals to finite higher dimensional ones which should therefore be more accessible to the HYPERINT package.

In summarizing the algorithm to extend the two loop QCD off-shell vertex functions it is worth noting that for the triple gluon vertex there will be 2382 three loop graphs to evaluate and 63992 at four loops. For both the other 3-point vertices the numbers of graphs in each case are the same and are 688 and 17311 respectively at three and four loops. So the evaluation of even just the three loop vertex functions will require a substantial amount of work and computing time. This would especially be the case at four loops without access to appropriate computers to build the necessary databases of integral relations. In the interim there is a potential alternative to gain some insight into or estimate of the three loop contributions. In the period between the early work of Celmaster and Gonsalves, [19], and its extension to the next order in [21] a method was developed in [9] where the vertex functions were computed at the fully symmetric point numerically at two loops in QCD. The approach was to apply a large momentum expansion of the vertex functions to very high order. This produced a set of 2-point integrals which were evaluated using MINCER, [37, 38]. Provided enough terms were computed the approximate value of the contributing graphs could be accurately estimated numerically. The stability and accuracy of the expansion could be checked by choosing different external momenta to play the role of the large momentum. What was remarkable when the analytic two loop expressions became available in [21], was how accurate the large momentum MINCER based expansion values were. The only major difference was for a colour group Casimir coefficient in one three loop MOM β-function which turned out to be of the order 0.01, [9]. The numerical coefficient was small and the expansion needed to a higher accuracy than was computationally available at the time of [9]. With the advances in symbolic manipulation such as the provision of the FORCER programme which is significantly more efficient than MINCER such an interim

numerical evaluation of the vertex functions would at least give information on the magnitude of the next order corrections. As a corollary it would provide the four loop MOM β-functions numerically.

9.4 Discussion

To recap we have reviewed recent results in the determination of the 3-point vertex functions of QCD at two loops. We have for the most part concentrated on the off-shell case and to achieve this would not have been possible without the earlier work on different external momentum configurations. While the two loop off-shell results followed a long time after the one loop case, the main reason for this was lack of the computational technology. The last decade has seen a revolution in this direction with the Laporta algorithm, [25], as well as a systematic way of computing master integrals from high level mathematics. Consequently the road to achieve the extension to three loops is in principle possible. One useful corollary of such a computation would be the extension of the renormalization group functions to four loops in kinematic schemes such as MOM. To go to higher orders beyond three this depends on whether the linear reducibility of four loop masters can be established. One case which we have not touched on is that of the 4-point functions. The technology to compute the full off-shell one loop amplitudes is already available. However the current situation is that the relevant two loop off-shell masters have not been computed. Moreover it has not been established if they are linearly reducible in order that the hyperlogarithm approach can be applied. This at present appears to be an open question for future work. Finally, including massive quarks in 3- and 4-point functions is another direction which needs consideration. However this is not straightforward at two loops since the 3-point masters with one mass scale and off-shell momentum configuration are not yet known.

References

[1] P. Pascual, R. Tarrach, Slavnov-Taylor Identities in Weinberg's Renormalization Scheme, Nucl. Phys. B174 (1980) 123, [Erratum: Nucl. Phys.B181,546(1981)]. doi:10.1016/0550-3213(80)90193-5,10.1016/0550-3213(81)90540-X.

[2] A. I. Davydychev, P. Osland, O. V. Tarasov, Three gluon vertex in arbitrary gauge and dimension, Phys. Rev. D54 (1996) 4087–4113, [Erratum: Phys. Rev.D59,109901(1999)]. arXiv:hep-ph/9605348, doi:10.1103/PhysRevD.59.109901,10.1103/PhysRevD.54.4087.

[3] A. I. Davydychev, P. Osland, L. Saks, Quark mass dependence of the one loop three gluon vertex in arbitrary dimension, JHEP 08 (2001) 050. arXiv:hep-ph/0105072, doi:10.1088/1126-6708/2001/08/050.

[4] M. Binger, S. J. Brodsky, The Form-factors of the gauge-invariant three-gluon vertex, Phys. Rev. D74 (2006) 054016. arXiv:hep-ph/0602199, doi:10.1103/PhysRevD.74.054016.

[5] A. I. Davydychev, P. Osland, O. V. Tarasov, Two loop three gluon vertex in zero momentum limit, Phys. Rev. D58 (1998) 036007. arXiv:hep-ph/9801380, doi:10.1103/PhysRevD.58.036007.

[6] A. I. Davydychev, P. Osland, On-shell two loop three gluon vertex, Phys. Rev. D59 (1999) 014006. arXiv:hep-ph/9806522, doi:10.1103/PhysRevD.59.014006.

[7] A. I. Davydychev, P. Osland, L. Saks, Quark gluon vertex in arbitrary gauge and dimension, Phys. Rev. D63 (2001) 014022. arXiv:hep-ph/0008171, doi:10.1103/PhysRevD.

63.014022.

[8] K. G. Chetyrkin, A. Retey, Three loop three linear vertices and four loop similar to MOM beta functions in massless QCD, arXiv:hep-ph/0007088.

[9] K. G. Chetyrkin, T. Seidensticker, Two loop QCD vertices and three loop MOM beta functions, Phys. Lett. B495 (2000) 74–80. arXiv:hep-ph/0008094, doi:10.1016/S0370-2693(00)01217-X.

[10] C. Kellermann, C. S. Fischer, The Running coupling from the four-gluon vertex in Landau gauge Yang-Mills theory, Phys. Rev. D78 (2008) 025015. arXiv:0801.2697, doi:10.1103/PhysRevD.78.025015.

[11] N. Ahmadiniaz, C. Schubert, A covariant representation of the Ball-Chiu vertex, Nucl. Phys. B869 (2013) 417–439. arXiv:1210.2331, doi:10.1016/j.nuclphysb.2012.12.019.

[12] A. Blum, M. Q. Huber, M. Mitter, L. von Smekal, Gluonic three-point correlations in pure Landau gauge QCD, Phys. Rev. D89 (2014) 061703. arXiv:1401.0713, doi:10.1103/PhysRevD.89.061703.

[13] A. L. Blum, R. Alkofer, M. Q. Huber, A. Windisch, Three-point vertex functions in Yang-Mills Theory and QCD in Landau gauge, EPJ Web Conf. 137 (2017) 03001. arXiv:1611.04827, doi:10.1051/epjconf/201713703001.

[14] M. Mitter, J. M. Pawlowski, N. Strodthoff, Chiral symmetry breaking in continuum QCD, Phys. Rev. D91 (2015) 054035. arXiv:1411.7978, doi:10.1103/PhysRevD.91.054035.

[15] R. Alkofer, C. S. Fischer, F. J. Llanes-Estrada, K. Schwenzer, The Quark-gluon vertex in Landau gauge QCD: Its role in dynamical chiral symmetry breaking and quark confinement, Annals Phys. 324 (2009) 106–172. arXiv:0804.3042, doi:10.1016/j.aop.2008.07.001.

[16] R. Alkofer, M. Mitter, The effect of an infrared divergent quark-antiquark interaction kernel on other Green functions, PoS ConfinementX (2012) 061. arXiv:1302.0307, doi:10.22323/1.171.0061.

[17] J. A. Gracey, Off-shell two-loop QCD vertices, Phys. Rev. D90 (2) (2014) 025014. arXiv:1406.0649, doi:10.1103/PhysRevD.90.025014.

[18] J. Ablinger, J. Blumlein, C. Schneider, Harmonic Sums and Polylogarithms Generated by Cyclotomic Polynomials, J. Math. Phys. 52 (2011) 102301. arXiv:1105.6063, doi:10.1063/1.3629472.

[19] W. Celmaster, R. J. Gonsalves, The Renormalization Prescription Dependence of the QCD Coupling Constant, Phys. Rev. D20 (1979) 1420. doi:10.1103/PhysRevD.20.1420.

[20] W. Celmaster, R. J. Gonsalves, Fourth Order QCD Contributions to the e+ e- Annihilation Cross-Section, Phys. Rev. D21 (1980) 3112. doi:10.1103/PhysRevD.21.3112.

[21] J. A. Gracey, Two loop QCD vertices at the symmetric point, Phys. Rev. D84 (2011) 085011. arXiv:1108.4806, doi:10.1103/PhysRevD.84.085011.

[22] J. A. Gracey, Momentum subtraction and the R ratio, Phys. Rev. D90 (9) (2014) 094026. arXiv:1410.6715, doi:10.1103/PhysRevD.90.094026.

[23] J. S. Ball, T.-W. Chiu, Analytic Properties of the Vertex Function in Gauge Theories. 2., Phys. Rev. D22 (1980) 2550, [Erratum: Phys. Rev.D23,3085(1981)]. doi:10.1103/physrevd.23.3085.2,10.1103/PhysRevD.22.2550.

[24] N. Ahmadiniaz, C. Schubert, Form factor decomposition of the off-shell four-gluon ampli-

tudes, PoS QCD-TNT-III (2013) 002. arXiv:1311.6829, doi:10.22323/1.193.0002.

[25] S. Laporta, High precision calculation of multiloop Feynman integrals by difference equations, Int. J. Mod. Phys. A15 (2000) 5087–5159. arXiv:hep-ph/0102033, doi:10.1016/S0217-751X(00)00215-7,10.1142/S0217751X00002157.

[26] C. Studerus, Reduze-Feynman Integral Reduction in C++, Comput. Phys. Commun. 181 (2010) 1293–1300. arXiv:0912.2546, doi:10.1016/j.cpc.2010.03.012.

[27] A. von Manteuffel, C. Studerus, Reduze 2 - Distributed Feynman Integral Reduction, arXiv:1201.4330.

[28] A. V. Smirnov, Algorithm FIRE – Feynman Integral REduction, JHEP 10 (2008) 107. arXiv:0807.3243, doi:10.1088/1126-6708/2008/10/107.

[29] R. N. Lee, Presenting LiteRed: a tool for the Loop InTEgrals REDuction, arXiv:1212.2685.

[30] R. N. Lee, LiteRed 1.4: a powerful tool for reduction of multiloop integrals, J. Phys. Conf. Ser. 523 (2014) 012059. arXiv:1310.1145, doi:10.1088/1742-6596/523/1/012059.

[31] C. Anastasiou, A. Lazopoulos, Automatic integral reduction for higher order perturbative calculations, JHEP 07 (2004) 046. arXiv:hep-ph/0404258, doi:10.1088/1126-6708/2004/07/046.

[32] P. Maierhoefer, J. Usovitsch, P. Uwer, Kira – A Feynman integral reduction program, Comput. Phys. Commun. 230 (2018) 99–112. arXiv:1705.05610, doi:10.1016/j.cpc.2018.04.012.

[33] A. I. Davydychev, Recursive algorithm of evaluating vertex type Feynman integrals, J. Phys. A25 (1992) 5587–5596.

[34] N. I. Usyukina, A. I. Davydychev, Some exact results for two loop diagrams with three and four external lines, Phys. Atom. Nucl. 56 (1993) 1553–1557, [Yad. Fiz.56N11,172(1993)]. arXiv:hep-ph/9307327.

[35] N. I. Usyukina, A. I. Davydychev, New results for two loop off-shell three point diagrams, Phys. Lett. B332 (1994) 159–167. arXiv:hep-ph/9402223, doi:10.1016/0370-2693(94)90874-5.

[36] T. G. Birthwright, E. W. N. Glover, P. Marquard, Master integrals for massless two-loop vertex diagrams with three offshell legs, JHEP 09 (2004) 042. arXiv:hep-ph/0407343, doi:10.1088/1126-6708/2004/09/042.

[37] S. G. Gorishnii, S. A. Larin, L. R. Surguladze, F. V. Tkachov, Mincer: Program for Multiloop Calculations in Quantum Field Theory for the Schoonschip System, Comput. Phys. Commun. 55 (1989) 381–408. doi:10.1016/0010-4655(89)90134-3.

[38] S. A. Larin, F. V. Tkachov, J. A. M. Vermaseren, The FORM version of MINCER, NIKHEF-H-91-18.

[39] T. Ueda, B. Ruijl, J. A. M. Vermaseren, Forcer: a FORM program for 4-loop massless propagators, PoS LL2016 (2016) 070. arXiv:1607.07318, doi:10.22323/1.260.0070.

[40] B. Ruijl, T. Ueda, J. A. M. Vermaseren, Forcer, a FORM program for the parametric reduction of four-loop massless propagator diagrams, arXiv:1704.06650.

[41] J. A. M. Vermaseren, New features of FORM, arXiv:math-ph/0010025.

[42] M. Tentyukov, J. A. M. Vermaseren, The Multithreaded version of FORM, Comput. Phys. Commun. 181 (2010) 1419–1427. arXiv:hep-ph/0702279, doi:10.1016/j.cpc.2010.04.009.

[43] F. Brown, On the decomposition of motivic multiple zeta values, arXiv:1102.1310.

[44] O. Schnetz, Numbers and Functions in Quantum Field Theory, Phys. Rev. D97 (8) (2018) 085018. arXiv:1606.08598, doi:10.1103/PhysRevD.97.085018.

[45] F. Brown, The Massless higher-loop two-point function, Commun. Math. Phys. 287 (2009) 925–958. arXiv:0804.1660, doi:10.1007/s00220-009-0740-5.

[46] F. C. S. Brown, On the periods of some Feynman integrals, arXiv:0910.0114.

[47] E. Panzer, Algorithms for the symbolic integration of hyperlogarithms with applications to Feynman integrals, Comput. Phys. Commun. 188 (2015) 148–166. arXiv:1403.3385, doi:10.1016/j.cpc.2014.10.019.

[48] O. V. Tarasov, Connection between Feynman integrals having different values of the space-time dimension, Phys. Rev. D54 (1996) 6479–6490. arXiv:hep-th/9606018, doi:10.1103/PhysRevD.54.6479.

[49] O. V. Tarasov, Generalized recurrence relations for two loop propagator integrals with arbitrary masses, Nucl. Phys. B502 (1997) 455–482. arXiv:hep-ph/9703319, doi:10.1016/S0550-3213(97)00376-3.

10 Effective field theory approach to QED corrections in flavour physics

Authors: Christoph Bobeth and Robert Szafron
Corresponding Author: Robert Szafron [robert.szafron@tum.de]

10.1 Introduction and motivation

Thanks to the accurate measurements performed at the low-energy facilities [1] and LHC, flavour physics of light quarks, especially the bottom quark, emerged on the precision frontier for tests of the standard model (SM) and in searches for new physics effects. On the theoretical side, short-distance perturbative higher-order QCD and electroweak corrections are under good control for many processes. Moreover, tremendous progress in lattice computations [2] allows achieving percent to even subpercent accuracy for long-distance nonperturbative quantities. This allows for the prediction of some key observables with unprecedented accuracy and in turn the determination of short-distance parameters like the elements of the quark-mixing matrix (CKM) in the framework of the SM. In view of these prospects, it is also desirable to improve the understanding and treatment of QED corrections, which are generally assumed to be small. Unfortunately not much new development has taken place in the evaluation of such corrections.

For the future e^+e^- machines, the proper computation of QED corrections will be particularly important because the large data samples allow for precision measurements that require their inclusion in theoretical predictions. We would like to advocate a framework for a proper and systematic treatment of QED effects based on the effective field theory (EFT) approach that exploits scale hierarchies present in processes involving mesons. In this spirit, QED corrections to $B_s \to \mu^+\mu^-$ have been recently analysed [3], revealing an unexpectedly large contribution owing to power enhancement. Such an effect cannot be found in the standard approach based on soft-photon approximation [4–6] as it requires a helicity flip induced by the photon. Further, the common assumption that hadrons are point-like objects neglects effects related to the structure of hadrons. It implies implicitly that the soft-photon approximation itself is performed in the framework of an EFT in which photons have virtuality below a typical hadronic binding scale $\Lambda_{\rm QCD} \sim \mathcal{O}(100\ \text{MeV})$ of partons in hadrons, below which they do not resolve the partonic structure of the hadrons. In consequence this approach can not address QED corrections due to virtualities above the scale $\Lambda_{\rm QCD}$. These observations are a motivation to scrutinise further QED corrections in flavour physics in the light of upcoming precise measurements and existing tensions in flavour measurements, in particular, related to tests of lepton flavour universality.

In addition to a systematic power counting, the EFT treatment offers the possibility of the all-order resummation of the corrections. This is particularly important for the mixed QCD-QED corrections owing to the size of the QCD coupling constant and the presence of large logarithmic corrections. While the soft-exponentiation theorem allows resumming leading QED effects related to ultrasoft photons that do not resolve the partonic structure of hadrons, not much is known about the resummation of the subleading logarithms in QED for photons with larger virtuality. Standard factorization theorems derived in QCD cannot be directly translated to QED, for in the QCD case, the mass effects related to light degrees of freedom are typically neglected. This is not the case in QED, where the lepton mass provides a cut-off for collinear divergences. Moreover, the fact that in QCD one can observe only color-singlet states

additionally simplifies the computations, while in QED, and more generally in the electroweak sector of the SM [7, 8], it is necessary to account for charged particles both in the final and initial states. As a result, the QED factorization theorems have not been explored intensively in the literature so far, but this gap should be filled before a precise e^+e^- collider becomes operational.

Power-corrections to the standard soft approximation may also play an important role in certain processes. Studies of power corrections in the QCD case gained recently much attention [9–15]. New tools based on soft-collinear EFT (SCET) developed to study processes with energetic quarks and gluons can, after certain modifications, be applied to improve the accuracy of electroweak corrections in future lepton colliders. This is particularly important in collider physics for regions of phase space where the perturbative approach breaks down due to the presence of large logarithmic enhancements and the next-to-soft effects become more important. Particularly interesting are mass-suppressed effects related to soft fermion exchange [16–18], whose consistent treatment in the SCET language is not yet fully known. Beyond applications to precision SM physics, the SCET framework may be necessary after possible discovery of new physics at the LHC [19, 20].

10.2 QED corrections in $B_q \to \ell^+\ell^-$

The decay of a neutral meson $B_q \to \ell^+\ell^-$ ($\ell = e, \mu, \tau$) is the first step in an investigation of QED effects in QCD bound states. Its purely leptonic final state and neutral initial state keep complications related to the nonperturbative nature of QCD to the necessary minimum. Yet as we shall see, even this simple example requires investigation of power corrections in SCET. The importance of this decay derives from the fact that it depends, at leading order (LO) in QED, only on the B_q-meson decay constant, which can be nowadays calculated with subpercent precision on the lattice [21], necessitating the inclusion of higher order QED corrections from all scales at this level. This decay has been observed for $\ell = \mu$ by LHCb [22, 23], CMS [24] and ATLAS [25]. The currently measured branching fraction for B_s decays of about $3 \cdot 10^{-9}$ is compatible with the latest SM predictions [3,26,27] and it is expected that the LHCb experiment will be able to measure the branching fraction with 5% accuracy with 50/fb (Run 4) around the year 2030 [28]. The FCC-ee running on the Z resonance is expected to provide with about $\mathcal{O}(10^3)$ reconstructed events [29] an even higher event yield compared to LHCb Run 4. This together with the cleaner hadronic environment at the FCC-ee should allow better control of backgrounds and also systematic uncertainties, such that one can expect improved accuracy. However, the gain in accuracy cannot be quantified without a dedicated study.

On the theory side, electroweak and QCD corrections above the scale $\mu_b \sim 5$ GeV of the order of the b-quark mass m_b are treated in the standard framework of weak EFT of the SM [30]. The effective Lagrangian is a sum of four-fermion and dipole operators

$$\mathcal{L}_{\Delta B=1} = \mathcal{N}_{\Delta B=1} \left[\sum_{i=1}^{10} C_i(\mu_b)\, Q_i \right] + \text{h.c.}\,, \tag{10.88}$$

with $\mathcal{N}_{\Delta B=1} \equiv 2\sqrt{2} G_F V_{tb} V_{tq}^*$ and covers in principle all weak decays of b hadrons. The pertinent operators relevant for $B_q \to \ell^+\ell^-$ ($q = d, s$) are

$$Q_7 = \frac{e}{(4\pi)^2} \big[\bar{q}\sigma^{\mu\nu}(m_b P_R + m_q P_L) b\big] F_{\mu\nu}\,,$$
$$Q_9 = \frac{\alpha_{em}}{4\pi} \big[\bar{q}\gamma^\mu P_L b\big] \sum_\ell \big[\bar{\ell}\gamma_\mu \ell\big]\,,$$

$$Q_{10} = \frac{\alpha_{em}}{4\pi}\Big[\bar{q}\gamma^\mu P_L b\Big]\sum_\ell\Big[\bar{\ell}\gamma_\mu\gamma_5\ell\Big]\,. \tag{10.89}$$

The matching $C_i(\mu_b)$ coefficients are computed at the electroweak scale $\mu_W \sim \mathcal{O}(100\text{ GeV})$ and evolved to the scale of $\mu_b \sim m_b$ with the renormalization group equation of the weak EFT.

Because the neutral B_q meson is a pseudoscalar and the SM interactions are mediated by axial and vector currents, the decay rate must vanish in the limit $m_\mu \to 0$, and therefore the decay amplitude is proportional to the muon mass. The hadronic matrix element at LO in QED is parameterized by a single decay constant f_{B_q}, defined by $\langle 0|\bar{q}\gamma^\mu\gamma_5 b|\bar{B}_q(p)\rangle = i f_{B_q} p^\mu$. The leading amplitude for $B_q \to \ell^+\ell^-$ is

$$i\mathcal{A} = m_\ell\, f_{B_q}\,\mathcal{N}\,C_{10}(\mu_b)\Big[\bar{\ell}\gamma_5\ell\Big], \qquad \Big(\mathcal{N} \equiv \mathcal{N}_{\Delta B=1}\frac{\alpha_{em}}{4\pi}\Big) \tag{10.90}$$

and the branching fraction is

$$\text{Br}^{(0)}_{q\ell} \equiv \text{Br}^{(0)}\Big[B_q \to \ell^+\ell^-\Big] = \frac{\tau_{B_q} m_{B_q}^3 f_{B_q}^2}{8\pi}\,|\mathcal{N}|^2\,\frac{m_\ell^2}{m_{B_q}^2}\sqrt{1-\frac{4m_\ell^2}{m_{B_q}^2}}\,|C_{10}|^2\,, \tag{10.91}$$

with m_{B_q} denoting the mass of the meson and τ_{B_q} its total lifetime. For neutral B_s mesons the mixing needs to be accounted for [31], thereby allowing for the measurement of related CP asymmetries to be discussed below. In this case, the above expression refers to the "instantaneous" branching fraction at time $t = 0$, which differs from the measured untagged time-integrated one by the factor $(1 - y_s^2)/(1 + y_s\mathcal{A}_{\Delta\Gamma})$, where $y_s = \Delta\Gamma_s/(2\Gamma_s)$ is related to the lifetime difference and $\mathcal{A}_{\Delta\Gamma}$ denotes the mass-eigenstate rate asymmetry. Concerning QED corrections, the above branching fraction refers to the "non-radiative" one prior to the inclusion of photon bremsstrahlung effects.

If one takes into account soft-photon radiation (both real and virtual) with energies smaller than the muon mass, the decay amplitude is dressed by the standard Yennie-Frautschi-Suura exponent [4, 32]

$$\text{Br}\Big[B_q \to \ell^+\ell^- + n\gamma\Big] = \text{Br}^{(0)}_{q\ell} \times \left(\frac{2E_{\text{max}}}{m_{B_q}}\right)^{2\frac{\alpha_{em}}{\pi}\left(\ln\frac{m_{B_q}^2}{m_\mu^2}-1\right)+\mathcal{O}(m_\mu)}. \tag{10.92}$$

This "photon-inclusive" branching fraction is based on eikonal approximation, in the limit when the total energy carried away by the n photons E_{max} is much smaller than the muon mass. QED corrections in the initial state are entirely neglected and photons are assumed to couple to leptons through eikonal currents

$$J^\mu(q) = e\sum_i Q_i\eta_i\frac{p_i^\mu}{p_i\cdot q}, \tag{10.93}$$

where $\eta = -1$ for incoming particles and $\eta = +1$ for outgoing particles. The sum runs over all charged particles with momenta p_i and charges Q_i. Eikonal currents are spin independent and thus they do not change helicity of the leptons.

In the experimental analysis [23–25] the signal is simulated fully inclusive of final-state radiation off the muons by applying PHOTOS [33] corresponding to a convolution of the E_{max}-depending exponential factor in the determination of the signal efficiency. On the other hand,

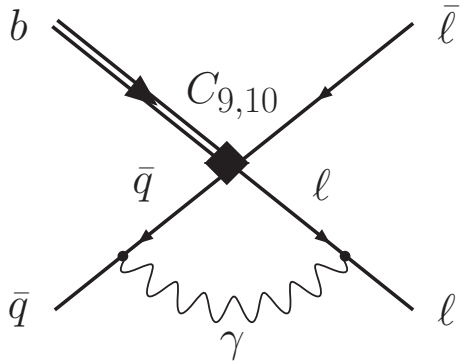

Fig. B.33: An example diagram that give rise to the power-enhanced QED correction. A photon can be either collinear with virtuality $k^2 \sim m_\mu^2$ or hard-collinear, $k^2 \sim m_\mu m_b$.

photon emission from the quarks (initial state) vanishes in the limit of small photon energies because it is infrared safe since the decaying meson is electrically neutral. Hence it can be neglected as long as the signal window is sufficiently small, in practice of $\mathcal{O}(60\text{ MeV})$ [34], and is effectively treated as negligible background on both, experimental and theory sides. In consequence, currently the experimental analyses provide the non-radiative branching fraction relying on the simulation with PHOTOS.

The limitations of the conventional approximation had missed the important effect responsible for the power-enhancement of QED corrections to the $B_s \to \mu^+\mu^-$ decay. Indeed, even when the cut on the real photon emission is much smaller than the muon mass, the virtual photons with virtualities of the order of muon mass or larger can resolve the structure of the meson whose typical size is of the order of $1/\Lambda_{\text{QCD}}$. In this case, the meson cannot be treated as a point-like object. Moreover, the eikonal approximation is not suitable for such photons as they can induce a helicity flip of the leptons. However, straightforward computation of the QED corrections is not possible, as it requires the evaluation of non-local time-ordered products of the $\mathcal{L}_{\Delta B=1}(0)$ Lagrangian with the electromagnetic current $j_{\text{QED}} = Q_q \bar{q}\gamma^\mu q$ such as

$$\langle 0| \int d^4x\, T\{j_{\text{QED}}(x), \mathcal{L}_{\Delta B=1}(0)\}|\bar{B}_q\rangle. \tag{10.94}$$

Currently this object is beyond the reach of lattice QCD, while the SCET approach allows to systematically expand this matrix element and reduce the nonperturbative quantities to universal ones at leading order.

Let us consider a diagram in Fig. B.33, where the photon is exchanged between the light quark and the lepton. There are two low energy scales in the diagram set by the external kinematics of the process $B_q \to \mu^+\mu^-$. One is the muon mass m_μ, which is related to the collinear scale. We parametrize the lepton momentum in terms of the light-cone coordinates as $p_\ell = (n_+p_\ell,\, n_-p_\ell,\, p_\ell^\perp) \sim m_b\,(1,\, \lambda_c^2,\, \lambda_c)$, where we introduced the small counting parameter $\lambda_c \sim m_\mu/m_b$. The second low energy scale is related to the typical size of the soft light-quark momentum $l_q \sim \Lambda_{\text{QCD}}$ and for counting purposes we introduce a $\lambda_s \sim \Lambda_{\text{QCD}}/m_b$. In the case of muons, it happens that numerically $\lambda_c \approx \lambda_s$ and below we equate them and do not distinguish among them. It turns out that there exists also a hard-collinear invariant constructed from the lepton and quark momentum $p_\ell \cdot l_q \sim \lambda m_b^2$, thus in addition to the collinear and soft regions we must also consider a hard-collinear region, where momenta scale like $k \sim m_b\left(1,\, \lambda,\, \lambda^{1/2}\right)$. This

non-trivial hierarchy of intermediate scales has to be properly accounted to evaluate the leading QED corrections, which can be done by subsequent matching on SCET_1 and SCET_2 [35] at the hard ($\sim m_b$) and hard-collinear scales, respectively.

The power enhancement is directly related to the interplay of collinear and hard-collinear scales. When the hard-collinear or collinear photon interacts with the soft quark, momentum conservation forces the quark to become hard-collinear. These modes can be integrated out perturbatively with the help of the EFT methods. In this case, we must first match the operators in eq. (10.89) on SCET_1 currents [36]. In SCET_1, we retain soft, collinear and hard-collinear modes, only the hard modes are integrated out. The leading SCET_1 operator contains a hard-collinear quark field which scales like $\lambda^{1/2}$ instead of the soft quark field with scaling $\lambda^{3/2}$. When we integrate out the hard-collinear modes, we must convert the hard-collinear quark field $\xi_C(x)$ to the soft quark field q_s. This is done with the help of power-suppressed Lagrangian [37]

$$\mathcal{L}^{(1)}_{\xi q} = \bar{q}_s(x_-)\, W^\dagger_{\xi C} i\not{D}_\perp\, \xi_C(x) - \bar{\xi}_C(x)\, i\overleftarrow{\not{D}}_\perp W_{\xi C}\, q_s(x_-),$$

where $W_{\xi C}$ is a collinear Wilson line carrying charge of the collinear field ξ_C. This Lagrangian insertion costs additional power of $\lambda^{1/2}$, but the resulting SCET_2 operators are sill power enhanced, when compared to the operators obtained without intermediate hard-collinear scale. The power-enhanced correction to the amplitude is [3]

$$\begin{aligned} i\Delta\mathcal{A} = {}& \frac{\alpha_{em}}{4\pi} Q_\ell Q_q\, m_\ell m_{B_q} f_{B_q} \mathcal{N} \left[\bar{\ell}(1+\gamma_5)\ell\right] \\ & \times \left\{ \int_0^1 du\, (1-u)\, C_9^{\mathrm{eff}}(u m_b^2) \int_0^\infty \frac{d\omega}{\omega}\, \phi_{B+}(\omega) \left[\ln\frac{m_b\omega}{m_\ell^2} + \ln\frac{u}{1-u} \right] \right. \\ & \left. - Q_\ell C_7^{\mathrm{eff}} \int_0^\infty \frac{d\omega}{\omega}\, \phi_{B+}(\omega) \left[\ln^2\frac{m_b\omega}{m_\ell^2} - 2\ln\frac{m_b\omega}{m_\ell^2} + \frac{2\pi^2}{3} \right] \right\}, \end{aligned} \tag{10.95}$$

where $\phi_{B+}(\omega)$ is the B_q-meson light-cone distribution amplitude (LCDA), which contains information about the nonperturbative structure of the meson. This virtual correction is by itself infrared finite as it modifies the exclusive decay rate. The power-enhancement manifest itself in eq. (10.95) as the inverse power of the ω variable that results from the decoupling of the hard-collinear quark modes

$$m_{B_q} \int_0^\infty \frac{d\omega}{\omega}\, \phi_{B+}(\omega)\, \ln^k\omega \sim \frac{m_{B_q}}{\Lambda_{\mathrm{QCD}}} \sim \frac{1}{\lambda}. \tag{10.96}$$

The ω may be interpreted as a momentum of the soft quark along the light-cone direction of the lepton and thus $\omega \sim \Lambda_{\mathrm{QCD}}$. The annihilation of the quark into leptons is a non-local process in the presence of the QED interactions and the virtual leptons with the wrong helicity can propagate over distances of the order of the meson size. Thus the helicity flip costs a factor $m_\ell/\Lambda_{\mathrm{QCD}}$ instead of typical suppression factor of m_ℓ/m_b present in the leading order amplitude.

The terms proportional to C_{10} cancel after the collinear and anti-collinear contributions are added, such that only C_9 contributes out of the semileptonic operators. The term $\propto C_7$ requires separate treatment since the convolution integral containing the hard matching coefficient exhibits an endpoint singularity. In addition, the collinear contribution has a rapidity-type divergence. There exist an additional contribution related to the soft region, which after a suitable rapidity regularization can be combined with the collinear one. When the convolution

integral is performed in dimensional regularization before taking the limit $d \to 4$, the total correction is finite and exhibits the double-logarithmic enhancement.

The numerical evaluation [3] of the power-enhanced correction (10.95) shows a partial cancellation of the terms $\propto C_9^{\text{eff}}$ and $\propto C_7^{\text{eff}}$. The final impact on the branching fraction $\text{Br}_{q\mu}^{(0)}$ is a decrease in the range of $(0.3 - 1.1)\%$ with a central value of 0.7%. Despite the cancellation, the overall correction is still sizeable compared to the natural size of a QED correction of $\alpha_{em}/\pi \sim 0.3\%$. The large uncertainties of the power-enhanced QED correction are due to the poorly known inverse moment λ_B and almost unknown inverse-logarithmic moments σ_1 and σ_2 of the B-meson LCDA. * The prediction for the muonic modes for the untagged time-integrated branching fractions for $B_s \to \mu^+\mu^-$ and $B_d \to \mu^+\mu^-$ are

$$\overline{\text{Br}}_{s\mu}^{(0)} = \binom{3.59}{3.65} \Bigg[1 \pm \binom{0.032}{0.011}_{f_{B_s}} \pm 0.031|_{\text{CKM}} \pm 0.011|_{m_t} \pm 0.012|_{\text{non-pmr}} \pm 0.006|_{\text{pmr}} \pm {}^{+0.003}_{-0.005}|_{\text{QED}}\Bigg] \cdot 10^{-9}, \tag{10.97}$$

$$\overline{\text{Br}}_{d\mu}^{(0)} = \binom{1.05}{1.02} \Bigg[1 \pm \binom{0.045}{0.014}_{f_{B_d}} \pm 0.046|_{\text{CKM}} \pm 0.011|_{m_t} \pm 0.012|_{\text{non-pmr}} \pm 0.003|_{\text{pmr}} \pm {}^{+0.003}_{-0.005}|_{\text{QED}}\Bigg] \cdot 10^{-10}, \tag{10.98}$$

where we group uncertainties: *i*) main parametric long-distance (f_{B_q}) and short-distance (CKM and m_t), *ii*) remaining non-QED parametric (τ_{B_q}, α_s) and non-QED non-parametric (μ_W, μ_b, higher order, see [26]) and *iii*) from the QED correction (λ_B and $\sigma_{1,2}$, see [3]). We provide here two values depending on the choice of the lattice calculation of f_{B_q} for $N_f = 2+1$ (upper) and $N_f = 2+1+1$ (lower) with averages from FLAG 2019 [2]. Note that the small uncertainties of the $N_f = 2+1+1$ results are currently dominated by a single group [21] and confirmation by other lattice groups in the future is desirable. It can be observed that in this case the largest uncertainties are due to CKM parameters, such that they can be determined provided the accuracy of the measurements at FCC-ee is at one-percent level. Still fairly large errors are due to the top-quark mass $m_t = (173.1 \pm 0.6)$ GeV, here assumed to be in the pole scheme, where an additional non-parametric uncertainty of 0.2% is included (in "non-pmr") for the conversion to the $\overline{\text{MS}}$ scheme. Further "non-pmr" contains a 0.4% uncertainty from μ_W variation and 0.5% further higher order uncertainty, all linearly added. For the CKM input we use [3, 27].

As mentioned above, for the B_s meson the mixing provides the opportunity to measure CP asymmetries in a time-dependent analysis

$$\frac{\Gamma[B_s(t) \to \mu_\lambda^+\mu_\lambda^-] - \Gamma[\bar{B}_s(t) \to \mu_\lambda^+\mu_\lambda^-]}{\Gamma[B_s(t) \to \mu_\lambda^+\mu_\lambda^-] + \Gamma[\bar{B}_s(t) \to \mu_\lambda^+\mu_\lambda^-]} = \frac{C_\lambda \cos(\Delta m_{B_s} t) + S_\lambda \sin(\Delta m_{B_s} t)}{\cosh(y_s t/\tau_{B_s}) + \mathcal{A}_{\Delta\Gamma}^\lambda \sinh(y_s t/\tau_{B_s})}, \tag{10.99}$$

where all quantities are defined in Ref. [31] and $|\mathcal{A}_{\Delta\Gamma}^\lambda|^2 + |C_\lambda|^2 + |S_\lambda|^2 = 1$ holds. For example, the mass-eigenstate rate asymmetry $\mathcal{A}_{\Delta\Gamma} = +1$ in the SM exactly, if only a pseudo-scalar amplitude exists, and is therefore assumed to be very sensitive to possible new flavour-changing interactions, with essentially no uncertainty from SM background. We now see that the QED correction of the SM itself generates a small "contamination" of the observable, given by [3]

$$\mathcal{A}_{\Delta\Gamma}^\lambda \approx 1 - 1.0 \cdot 10^{-5}, \qquad S_\lambda \approx -0.1\%, \qquad C_\lambda \approx \eta_\lambda\, 0.6\%, \tag{10.100}$$

*Throughout same numerical values as in [3] are used for B_s and B_d, neglecting $SU(3)$-flavour breaking effects.

where $\eta_{L/R} = \pm 1$. Present measurements [23] set only very weak constraints on the deviations of $A^{\lambda}_{\Delta\Gamma}$ from unity, and C_λ, S_λ have not yet been measured, [†] but the uncertainty in the B-meson LCDA is in principle a limiting factor for the precision with which new physics can be constrained from these observables. Also S_λ and C_λ deviate marginally from the leading order SM prediction of zero, but signals from new physics should be substantially larger to distinguish them from the SM QED correction.

A similar framework can be used to analyse QED corrections to $B^\pm \to \ell^\pm \nu_\ell$. In this case, power-enhancement does not arise due to the different chirality structure of the current and the presence of only one charged lepton in the final state [3]. QED corrections that depend on the meson structure are subleading in this case. The leading QED corrections for this process can be obtained from the usual soft photon approximation, where the charged meson is treated as a point-like charge.

10.3 Summary and outlook

The proper treatment of QED corrections in theoretical predictions is essential to the success of future e^+e^- colliders. In this document we have shown how this goal could be achieved in flavour physics for the example of a power-enhanced leading QED correction to the leptonic decays $B_q \to \mu^+\mu^-$ with $q = d, s$ [3] and provide updated predictions. A systematic expansion based on the appropriate EFTs must be implemented to cover dynamics from the hard scale $\mu_b \sim 5$ GeV over hard-collinear (SCET_1) and collinear scales (SCET_2) down to the ultrasoft scales $\mathcal{O}(10\,\mathrm{MeV})$. Further, the EFTs allow for a systematic resummation of the leading logarithmic corrections and they provide a field-theoretical definition of nonperturbative objects in the presence of QED, as for example generalised light-cone distribution amplitudes of the B-meson dressed by process-dependent Wilson lines [36]. The consistent evaluation of the QED corrections is thus a challenging task, but it can be accomplished with the help of effective field theory.

In the example at hand, the special numerical value of the muon mass and its proximity to the typical size of hadronic binding energies Λ_{QCD} gave rise to a special tower of EFTs. The application to the cases of electrons and taus requires additional considerations. Full theoretical control of QED corrections is also desirable for other decays that will allow future precision determinations of short-distance parameters. For example, an important class are exclusive $b \to u\ell\bar{\nu}_\ell$ and $b \to c\ell\bar{\nu}_\ell$ decays for the determination of CKM elements V_{ub} and V_{cb}, respectively. Due to the absence of resonant hadronic contributions, the only hadronic uncertainties from $B \to M$ form factors could become controllable with high accuracy in lattice calculations for large dilepton invariant masses, i.e. energetic leptons, which is also the preferred kinematic region for the tower of EFTs discussed here. Other interesting applications are observables that are predicted in the SM to vanish when restricting to the leading order in the weak operator product expansion but might be sensitive to nonstandard interactions. Then the QED corrections in the SM provide a background to the new physics searches, as in the example of $\mathcal{A}_{\Delta\Gamma}$ in $B_s \to \mu^+\mu^-$ given above. This concerns observables in the angular distributions of $B \to K^{(*)}\ell^+\ell^-$ as for example discussed in [38, 39].

[†] Note that C^λ requires the measurement of the muon helicity, whereas $\mathcal{A}^{\lambda}_{\Delta\Gamma}$ and S_λ can be determined also as averages over the muon helicity. Further $\mathcal{A}^{\lambda}_{\Delta\Gamma}$ can be measured without flavour-tagging, whereas it is required for S_λ and C_λ.

References

[1] A. J. Bevan, et al., The Physics of the B Factories, Eur. Phys. J. C74 (2014) 3026. arXiv:1406.6311, doi:10.1140/epjc/s10052-014-3026-9.

[2] S. Aoki, et al., FLAG Review 2019arXiv:1902.08191.

[3] M. Beneke, C. Bobeth, R. Szafron, Enhanced electromagnetic correction to the rare B-meson decay $B_{s,d} \to \mu^+\mu^-$, Phys. Rev. Lett. 120 (1) (2018) 011801. arXiv:1708.09152, doi:10.1103/PhysRevLett.120.011801.

[4] D. R. Yennie, S. C. Frautschi, H. Suura, The infrared divergence phenomena and high-energy processes, Annals Phys. 13 (1961) 379–452. doi:10.1016/0003-4916(61)90151-8.

[5] S. Weinberg, Infrared photons and gravitons, Phys. Rev. 140 (1965) B516–B524. doi:10.1103/PhysRev.140.B516.

[6] G. Isidori, Soft-photon corrections in multi-body meson decays, Eur. Phys. J. C53 (2008) 567–571. arXiv:0709.2439, doi:10.1140/epjc/s10052-007-0487-0.

[7] A. V. Manohar, W. J. Waalewijn, Electroweak Logarithms in Inclusive Cross Sections, JHEP 08 (2018) 137. arXiv:1802.08687, doi:10.1007/JHEP08(2018)137.

[8] B. Fornal, A. V. Manohar, W. J. Waalewijn, Electroweak Gauge Boson Parton Distribution Functions, JHEP 05 (2018) 106. arXiv:1803.06347, doi:10.1007/JHEP05(2018)106.

[9] D. Bonocore, E. Laenen, L. Magnea, L. Vernazza, C. D. White, Non-abelian factorisation for next-to-leading-power threshold logarithms, JHEP 12 (2016) 121. arXiv:1610.06842, doi:10.1007/JHEP12(2016)121.

[10] I. Moult, L. Rothen, I. W. Stewart, F. J. Tackmann, H. X. Zhu, Subleading Power Corrections for N-Jettiness Subtractions, Phys. Rev. D95 (7) (2017) 074023. arXiv:1612.00450, doi:10.1103/PhysRevD.95.074023.

[11] I. Moult, L. Rothen, I. W. Stewart, F. J. Tackmann, H. X. Zhu, N -jettiness subtractions for $gg \to H$ at subleading power, Phys. Rev. D97 (1) (2018) 014013. arXiv:1710.03227, doi:10.1103/PhysRevD.97.014013.

[12] M. Beneke, M. Garny, R. Szafron, J. Wang, Anomalous dimension of subleading-power N-jet operators, JHEP 03 (2018) 001. arXiv:1712.04416, doi:10.1007/JHEP03(2018)001.

[13] M. Beneke, M. Garny, R. Szafron, J. Wang, Anomalous dimension of subleading-power N-jet operators. Part II, JHEP 11 (2018) 112. arXiv:1808.04742, doi:10.1007/JHEP11(2018)112.

[14] I. Moult, I. W. Stewart, G. Vita, H. X. Zhu, First Subleading Power Resummation for Event Shapes, JHEP 08 (2018) 013. arXiv:1804.04665, doi:10.1007/JHEP08(2018)013.

[15] M. Beneke, A. Broggio, M. Garny, S. Jaskiewicz, R. Szafron, L. Vernazza, J. Wang, Leading-logarithmic threshold resummation of the Drell-Yan process at next-to-leading power, JHEP 03 (2019) 043. arXiv:1809.10631, doi:10.1007/JHEP03(2019)043.

[16] T. Liu, A. A. Penin, High-Energy Limit of QCD beyond the Sudakov Approximation, Phys. Rev. Lett. 119 (26) (2017) 262001. arXiv:1709.01092, doi:10.1103/PhysRevLett.119.262001.

[17] T. Liu, A. Penin, High-Energy Limit of Mass-Suppressed Amplitudes in Gauge Theories, JHEP 11 (2018) 158. arXiv:1809.04950, doi:10.1007/JHEP11(2018)158.

[18] A. A. Penin, High-Energy Limit of Quantum Electrodynamics beyond Sudakov Approximation, Phys. Lett. B745 (2015) 69–72, [Erratum: Phys. Lett.B771,633(2017)]. arXiv:1412.0671, doi:10.1016/j.physletb.2015.04.036,10.1016/j.physletb.

2017.05.069,10.1016/j.physletb.2015.10.035.

[19] S. Alte, M. König, M. Neubert, Effective Field Theory after a New-Physics Discovery, JHEP 08 (2018) 095. arXiv:1806.01278, doi:10.1007/JHEP08(2018)095.

[20] S. Alte, M. König, M. Neubert, Effective Theory for a Heavy Scalar Coupled to the SM via Vector-Like Quarksarxiv:1902.04593.

[21] A. Bazavov, et al., B- and D-meson leptonic decay constants from four-flavor lattice QCD, Phys. Rev. D98 (7) (2018) 074512. arXiv:1712.09262, doi:10.1103/PhysRevD.98.074512.

[22] R. Aaij, et al., Measurement of the $B_s^0 \to \mu^+\mu^-$ branching fraction and search for $B^0 \to \mu^+\mu^-$ decays at the LHCb experiment, Phys. Rev. Lett. 111 (2013) 101805. arXiv:1307.5024, doi:10.1103/PhysRevLett.111.101805.

[23] R. Aaij, et al., Measurement of the $B_s^0 \to \mu^+\mu^-$ branching fraction and effective lifetime and search for $B^0 \to \mu^+\mu^-$ decays, Phys. Rev. Lett. 118 (19) (2017) 191801. arXiv:1703.05747, doi:10.1103/PhysRevLett.118.191801.

[24] S. Chatrchyan, et al., Measurement of the $B_s \to \mu^+\mu^-$ branching fraction and search for $B^0 \to \mu^+\mu^-$ with the CMS Experiment, Phys. Rev. Lett. 111 (2013) 101804. arXiv:1307.5025, doi:10.1103/PhysRevLett.111.101804.

[25] M. Aaboud, et al., Study of the rare decays of B_s^0 and B^0 into muon pairs from data collected during the LHC Run 1 with the ATLAS detector, Eur. Phys. J. C76 (9) (2016) 513. arXiv:1604.04263, doi:10.1140/epjc/s10052-016-4338-8.

[26] C. Bobeth, M. Gorbahn, T. Hermann, M. Misiak, E. Stamou, M. Steinhauser, $B_{s,d} \to l^+l^-$ in the Standard Model with Reduced Theoretical Uncertainty, Phys. Rev. Lett. 112 (2014) 101801. arXiv:1311.0903, doi:10.1103/PhysRevLett.112.101801.

[27] A. Crivellin, et al., PSI/UZH Workshop: Impact of $B \to \mu^+\mu^-$ on New Physics Searches, arXiv:1803.10097.

[28] R. Aaij, et al., Implications of LHCb measurements and future prospects, Eur. Phys. J. C73 (4) (2013) 2373. arXiv:1208.3355, doi:10.1140/epjc/s10052-013-2373-2.

[29] A. Abada, et al., Future Circular Collider: Vol. 1 "Physics opportunities", http://inspirehep.net/record/1713706/files/CERN-ACC-2018-0056.pdf.

[30] A. J. Buras, Weak Hamiltonian, CP violation and rare decays, in: Probing the standard model of particle interactions. Proceedings, Summer School in Theoretical Physics, NATO Advanced Study Institute, 68th session, Les Houches, France, July 28-September 5, 1997. Pt. 1, 2, 1998, pp. 281–539. arXiv:hep-ph/9806471.

[31] K. De Bruyn, R. Fleischer, R. Knegjens, P. Koppenburg, M. Merk, A. Pellegrino, N. Tuning, Probing New Physics via the $B_s^0 \to \mu^+\mu^-$ Effective Lifetime, Phys. Rev. Lett. 109 (2012) 041801. arXiv:1204.1737, doi:10.1103/PhysRevLett.109.041801.

[32] A. J. Buras, J. Girrbach, D. Guadagnoli, G. Isidori, On the Standard Model prediction for $BR(B_{s,d} \to \mu^+\mu^-)$, Eur. Phys. J. C72 (2012) 2172. arXiv:1208.0934, doi:10.1140/epjc/s10052-012-2172-1.

[33] P. Golonka, Z. Was, PHOTOS Monte Carlo: A Precision tool for QED corrections in Z and W decays, Eur. Phys. J. C45 (2006) 97–107. arXiv:hep-ph/0506026, doi:10.1140/epjc/s2005-02396-4.

[34] Y. G. Aditya, K. J. Healey, A. A. Petrov, Faking $B_s \to \mu^+\mu^-$, Phys. Rev. D87 (2013) 074028. arXiv:1212.4166, doi:10.1103/PhysRevD.87.074028.

[35] M. Beneke, T. Feldmann, Factorization of heavy to light form-factors in soft collinear effective theory, Nucl. Phys. B685 (2004) 249–296. arXiv:hep-ph/0311335, doi:10.1016/j.nuclphysb.2004.02.033.

[36] M. Beneke, C. Bobeth, R. Szafron, QED corrections to $B_s \to \mu^+\mu^-$ in SCET [in preparation].

[37] M. Beneke, T. Feldmann, Multipole expanded soft collinear effective theory with non-Abelian gauge symmetry, Phys. Lett. B553 (2003) 267–276. arXiv:hep-ph/0211358, doi:10.1016/S0370-2693(02)03204-5.

[38] C. Bobeth, G. Hiller, G. Piranishvili, Angular distributions of $\bar{B} \to \bar{K}\ell^+\ell^-$ decays, JHEP 12 (2007) 040. arXiv:0709.4174, doi:10.1088/1126-6708/2007/12/040.

[39] F. Beaujean, C. Bobeth, S. Jahn, Constraints on tensor and scalar couplings from $B \to K\bar{\mu}\mu$ and $B_s \to \bar{\mu}\mu$, Eur. Phys. J. C75 (9) (2015) 456. arXiv:1508.01526, doi:10.1140/epjc/s10052-015-3676-2.

11 Top pair production and mass determination

Author: Andreas Maier [andreas.martin.maier@desy]

The mass of the top quark can be measured in a well-defined scheme and with unrivalled precision at a future electron-positron collider, like the FCC-ee. The most sensitive observable is the total production cross section for $b\bar{b}W^+W^-X$ final states near the top-pair production threshold. I review the state of the art in theory predictions for this quantity.

11.1 Introduction

The total cross section for inclusive $b\bar{b}W^+W^-X$ production can be measured with very high precision at a future high-energy electron-positron collider. Due to the potential for large integrated luminosity, the FCC-ee is especially well-suited for such a measurement. The line shape for centre-of-mass energies close to the top-antitop production threshold is highly sensitive to the mass of the top-quark, which allows its determination with unprecedented precision. Since the statistical uncertainty of the measurement is projected to be significantly below the current theory error [1, 2], it is crucial to continuously improve the theoretical prediction.

11.2 Effective theory framework

The $b\bar{b}W^+W^-X$ final state is mostly produced through the creation and decay of non-relativistic top-antitop pairs interacting predominantly via a colour Coulomb potential. The dynamics of this system are described by Potential Non-Relativistic Effective Field Theory (PNREFT) [3–5] combined with Unstable Particle Effective Field Theory [6, 7]. Within this framework, higher-order corrections can be treated systematically through a simultaneous expansion in the non-relativistic velocity v and the strong, electromagnetic, and top Yukawa couplings α_s, α, and y_t. We adopt the power counting $v \sim \alpha_s \sim \sqrt{\alpha} \sim y_t$ with the top-quark width $\Gamma_t \sim m_t\alpha$. Powers of α_s/v from the bound-state interaction are resummed to all orders in perturbation theory.

At leading order, the PNREFT Lagrangian is given by

$$\mathcal{L}_{\text{PNREFT, LO}} = \psi^\dagger\left(i\partial_0 + \frac{\vec{\partial}^2 + im_t\Gamma_t}{2m_t}\right)\psi + \mathcal{L}_{\text{anti-quark}} - \int d^3\vec{r}\,\Big[\psi^\dagger\psi\Big](\vec{x}+\vec{r})\frac{C_F\alpha_s}{r}\Big[\chi^\dagger\chi\Big](\vec{x})\,, \tag{11.101}$$

where ψ is the quark field and χ the antiquark field. The resulting top-pair propagator is the Green function of the Schrödinger equation with the colour Coulomb potential interaction. Its imaginary part is closely related to the resonant top-pair production cross section via the optical theorem.

11.3 Higher-order corrections

Higher-order corrections to the PNREFT Lagrangian are obtained by matching to the full Standard Model. In the first step, hard modes with large four-momenta $k \sim m_t$ are integrated out. This gives rise to a non-relativistic effective field theory with local effective vertices. These matching corrections are known to NNNLO in the QCD and Higgs sector [8–11] and to NNLO in the electroweak sector [12–16].

In the second matching step, also soft modes $k \sim m_t v$ and potential modes $k_0 \sim m_t v^2, \vec{k} \sim m_t v$ for gluons and light quarks are eliminated from the theory. The most challenging part is

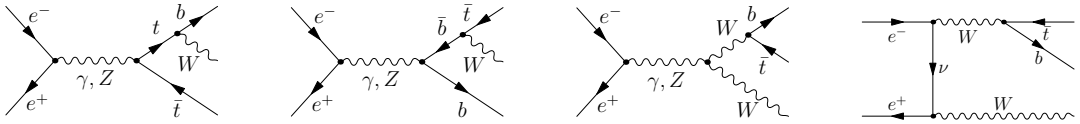

Fig. B.34: Nonresonant diagrams contributing to the $W^+b\bar{t}$ final state at NLO. The final state $W^-\bar{b}t$ follows from charge conjugation.

the calculation of the corrections to the static colour Coulomb potential to NNNLO, which was achieved in [17–19].

11.3.1 Resonant production

With the matched PNREFT Lagrangian, the resonant top-pair production cross section can be calculated including NNNLO QCD and Higgs effects and NNLO electroweak effects by computing corrections to the Green function to this order. The complete result for the QCD corrections was first presented for the S-wave contribution in [20] and for the P-wave contribution in [9] (see also [21]). Schematically, the known contributions to the top-pair production cross section can be written as

$$\sigma_{\text{res}} \sim \alpha^2 v \sum_{k=0}^{\infty} \left(\frac{\alpha_s}{v}\right)^k \times \begin{cases} 1 & \text{LO} \\ \alpha_s, v, \frac{\alpha}{v} & \text{NLO} \\ \alpha_s^2, \alpha_s v, v^2, \frac{\alpha}{v} \times \left\{\frac{\alpha}{v}, \alpha_s, v\right\}, y_t\sqrt{\alpha}, y_t^2 & \text{NNLO} \\ \alpha_s^{3-i} v^i, y_t^2 \times \left\{\frac{\alpha}{v}, \alpha_s, v\right\} & \text{NNNLO} \end{cases} . \tag{11.102}$$

11.3.2 Non-resonant production

Top quarks are unstable and the final state $b\bar{b}W^+W^-X$ can also be produced in non-resonant channels that do not involve the creation of a top-antitop pair near mass shell. According to Unstable Particle Effective Field Theory the full cross section is given by the sum of resonant and non-resonant contribution:

$$\sigma = \sigma_{\text{res}} + \sigma_{\text{non-res}} . \tag{11.103}$$

While non-resonant production is suppressed by one power of α, it does not suffer from the same phase space suppression as resonant production and therefore contributes with a factor of $\frac{\alpha}{v}$ relative to the leading-order cross section, i.e. at NLO. The diagrams at this order are shown in figure B.34; their contribution was first calculated in [22]. The NNLO non-resonant cross section was later computed in [16].

Virtual top quarks in the non-resonant channels are formally far off-shell with squared momenta $p_t^2 - m_t^2 \sim m_t^2 \gg m_t\Gamma_t$, so the width must not be resummed in the propagators. Since we integrate over the full phase space, endpoint divergences occur whenever $p_t^2 - m_t^2$ vanishes. At NNLO, this leads to poles proportional to $\frac{\Gamma_t}{\epsilon}$ in $4 - 2\epsilon$ dimensions. As usual in asymptotic expansions, these cancel against poles in a different expansion region. In this case, the corresponding poles appear in the form of finite-width divergences in the resonant cross section. A detailed account of the NNLO calculation including the arrangement of pole cancellations is given in [16].

11.3.3 Initial-state radiation

Formally, photonic corrections in the initial state are suppressed by one order in α and therefore contribute at NNLO according to our power counting. However, it is well known that these corrections are enhanced by logarithms of m_t over m_e, which have to be resummed to all orders. The resummed cross section is given by [23, 24]

$$\sigma(s) = \int_0^1 \mathrm{d}x_1 \int_0^1 \mathrm{d}x_2\, \Gamma_{ee}^{LL}(x_1)\Gamma_{ee}^{LL}(x_2)\hat{\sigma}(x_1x_2s) + \sigma_{\text{const}}^{\text{ISR}}(s)\,, \tag{11.104}$$

where $\Gamma_{ee}^{LL}(x)$ is a leading-logarithmic structure function, $\hat{\sigma}$ the "partonic" cross section without ISR resummation and $\sigma_{\text{const}}^{\text{ISR}}$ accounts for the non-logarithmic NNLO contribution.

11.4 Cross section predictions

The formulas for the cross section can be evaluated numerically with the code `QQbar_threshold` [25], which includes all aforementioned corrections. Figure B.35 shows the behaviour of the total cross section near threshold for a top-quark mass of $m_t(20\,\text{GeV}) = 171.5\,\text{GeV}$ in the potential-subtracted (PS) scheme [26] and input parameters $\Gamma_t = 1.33\,\text{GeV}$, $m_H = 125\,\text{GeV}$, $\alpha_s(m_Z) = 0.1177$, $\alpha(m_Z) = 1/128.944$. The uncertainty bands originate from a variation of the renormalisation scale between 50 and 350 GeV.

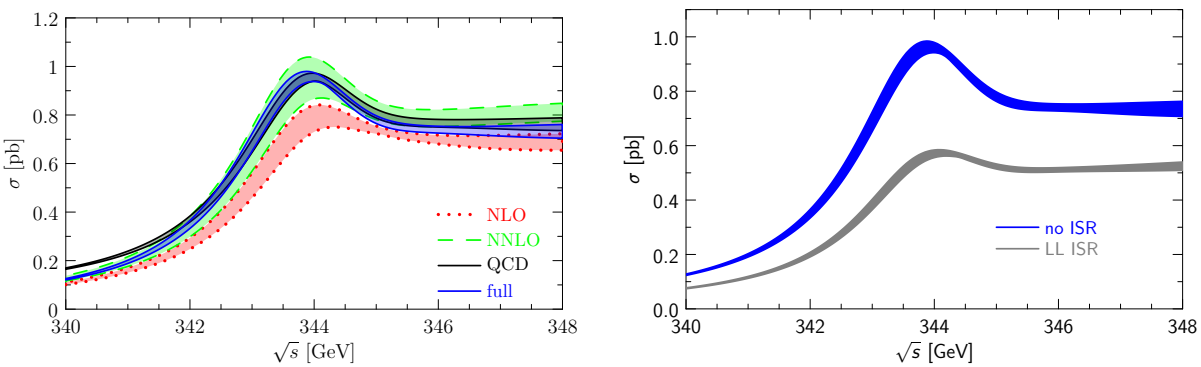

Fig. B.35: Total cross section for the process $e^+e^- \to$ at various orders in perturbation theory. Left: cross section without ISR from NLO to NNNLO with the pure NNNLO QCD result as comparison. Right: effect of ISR on the cross section.

Figure B.36 shows the effect of changing various parameters. The variation suggests that it should be possible to extract the top-quark width and mass in the PS scheme with an uncertainty of better than 100 MeV. The sensitivity to the top Yukawa coupling and the strong coupling is less pronounced and there is a considerable degeneracy between the two parameters. A precise knowledge of the strong coupling constant from other sources will be crucial to meaningfully constrain the Yukawa coupling. In any case, a dedicated experimental analysis will be needed to determine the exact precision with which the various top-quark properties can be extracted from a measurement of the cross section.

Acknowledgements

I thank the CERN theory group for their hospitality and support during the workshop.

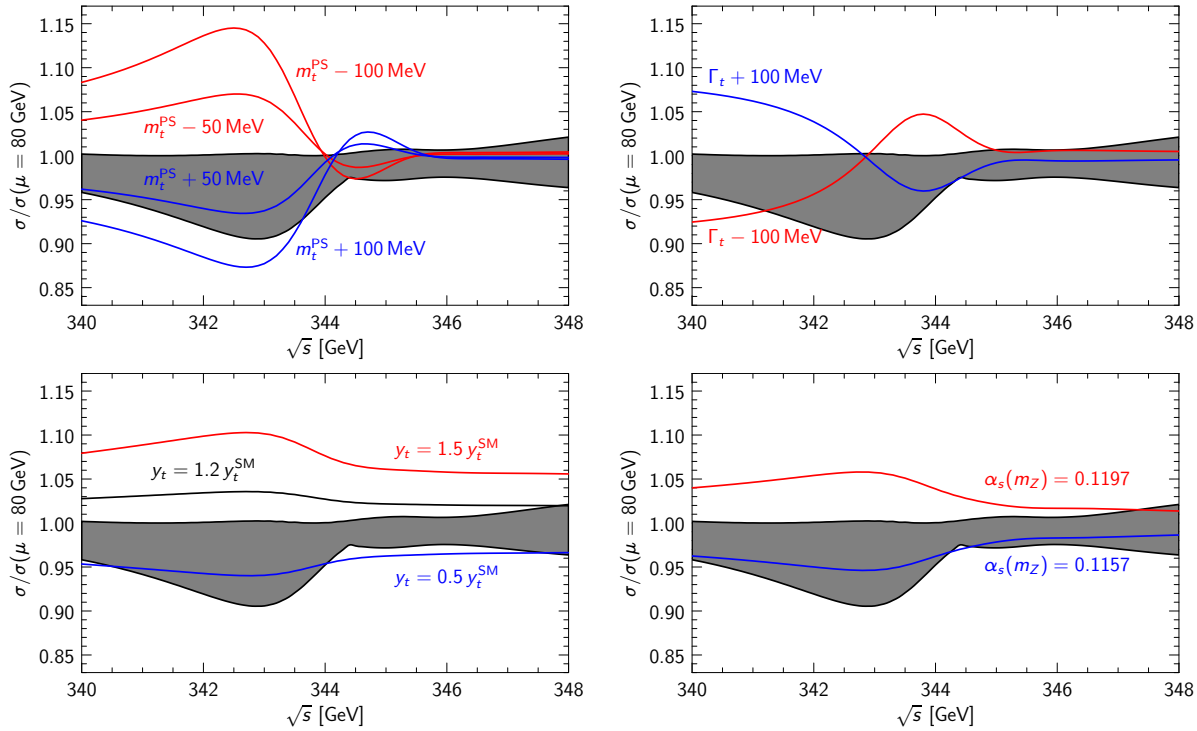

Fig. B.36: Sensitivity of the cross section to parameter variation. Top left: variation of the top-quark mass by up to ±100 MeV. Top right: variation of the top-quark width by up ±100 MeV. Bottom left: variation of the top Yukawa coupling. Bottom right: variation of the strong coupling constant.

References

[1] K. Seidel, F. Simon, M. Tesar, S. Poss, Top quark mass measurements at and above threshold at CLIC, Eur. Phys. J. C73 (8) (2013) 2530. arXiv:1303.3758, doi:10.1140/epjc/s10052-013-2530-7.

[2] F. Simon, Impact of Theory Uncertainties on the Precision of the Top Quark Mass in a Threshold Scan at Future e+e- Colliders, PoS ICHEP2016 (2017) 872. arXiv:1611.03399, doi:10.22323/1.282.0872.

[3] A. Pineda, J. Soto, Effective field theory for ultrasoft momenta in NRQCD and NRQED, Nucl. Phys. Proc. Suppl. 64 (1998) 428–432, [,428(1997)]. arXiv:hep-ph/9707481, doi:10.1016/S0920-5632(97)01102-X.

[4] M. Beneke, V. A. Smirnov, Asymptotic expansion of Feynman integrals near threshold, Nucl. Phys. B522 (1998) 321–344. arXiv:hep-ph/9711391, doi:10.1016/S0550-3213(98)00138-2.

[5] N. Brambilla, A. Pineda, J. Soto, A. Vairo, Potential NRQCD: An Effective theory for heavy quarkonium, Nucl. Phys. B566 (2000) 275. arXiv:hep-ph/9907240, doi:10.1016/S0550-3213(99)00693-8.

[6] M. Beneke, A. P. Chapovsky, A. Signer, G. Zanderighi, Effective theory approach to unstable particle production, Phys. Rev. Lett. 93 (2004) 011602. arXiv:hep-ph/0312331, doi:10.1103/PhysRevLett.93.011602.

[7] M. Beneke, A. P. Chapovsky, A. Signer, G. Zanderighi, Effective theory calculation of res-

onant high-energy scattering, Nucl. Phys. B686 (2004) 205–247. arXiv:hep-ph/0401002, doi:10.1016/j.nuclphysb.2004.03.016.

[8] D. Eiras, M. Steinhauser, Complete Higgs mass dependence of top quark pair threshold production to order alpha alpha(s), Nucl. Phys. B757 (2006) 197–210. arXiv:hep-ph/0605227, doi:10.1016/j.nuclphysb.2006.09.010.

[9] M. Beneke, J. Piclum, T. Rauh, P-wave contribution to third-order top-quark pair production near threshold, Nucl. Phys. B880 (2014) 414–434. arXiv:1312.4792, doi:10.1016/j.nuclphysb.2014.01.015.

[10] P. Marquard, J. H. Piclum, D. Seidel, M. Steinhauser, Three-loop matching of the vector current, Phys. Rev. D89 (3) (2014) 034027. arXiv:1401.3004, doi:10.1103/PhysRevD.89.034027.

[11] M. Beneke, A. Maier, J. Piclum, T. Rauh, Higgs effects in top anti-top production near threshold in e^+e^- annihilation, Nucl. Phys. B899 (2015) 180–193. arXiv:1506.06865, doi:10.1016/j.nuclphysb.2015.07.034.

[12] B. Grzadkowski, J. H. Kühn, P. Krawczyk, R. G. Stuart, Electroweak Corrections on the Toponium Resonance, Nucl. Phys. B281 (1987) 18–40. doi:10.1016/0550-3213(87)90245-8.

[13] R. J. Guth, J. H. Kühn, Top quark threshold and radiative corrections, Nucl. Phys. B368 (1992) 38–56. doi:10.1016/0550-3213(92)90196-I.

[14] A. H. Hoang, C. J. Reisser, Electroweak absorptive parts in NRQCD matching conditions, Phys. Rev. D71 (2005) 074022. arXiv:hep-ph/0412258, doi:10.1103/PhysRevD.71.074022.

[15] A. H. Hoang, C. J. Reisser, On electroweak matching conditions for top pair production at threshold, Phys. Rev. D74 (2006) 034002. arXiv:hep-ph/0604104, doi:10.1103/PhysRevD.74.034002.

[16] M. Beneke, A. Maier, T. Rauh, P. Ruiz-Femenia, Non-resonant and electroweak NNLO correction to the e^+e^- top anti-top threshold, JHEP 02 (2018) 125. arXiv:1711.10429, doi:10.1007/JHEP02(2018)125.

[17] C. Anzai, Y. Kiyo, Y. Sumino, Static QCD potential at three-loop order, Phys. Rev. Lett. 104 (2010) 112003. arXiv:0911.4335, doi:10.1103/PhysRevLett.104.112003.

[18] A. V. Smirnov, V. A. Smirnov, M. Steinhauser, Three-loop static potential, Phys. Rev. Lett. 104 (2010) 112002. arXiv:0911.4742, doi:10.1103/PhysRevLett.104.112002.

[19] R. N. Lee, A. V. Smirnov, V. A. Smirnov, M. Steinhauser, Analytic three-loop static potential, Phys. Rev. D94 (5) (2016) 054029. arXiv:1608.02603, doi:10.1103/PhysRevD.94.054029.

[20] M. Beneke, Y. Kiyo, P. Marquard, A. Penin, J. Piclum, M. Steinhauser, Next-to-Next-to-Next-to-Leading Order QCD Prediction for the Top Antitop S-Wave Pair Production Cross Section Near Threshold in e^+e^- Annihilation, Phys. Rev. Lett. 115 (19) (2015) 192001. arXiv:1506.06864, doi:10.1103/PhysRevLett.115.192001.

[21] A. A. Penin, A. A. Pivovarov, Analytical results for $e^+e^- \to t\bar{t}$ and $\gamma\gamma \to t\bar{t}$ observables near the threshold up to the next-to-next-to leading order of NRQCD, Phys. Atom. Nucl. 64 (2001) 275–293, [Yad. Fiz.64,323(2001)]. arXiv:hep-ph/9904278, doi:10.1134/1.1349450.

[22] M. Beneke, B. Jantzen, P. Ruiz-Femenia, Electroweak non-resonant NLO corrections to $e^+e^- \to W^+W^-b\bar{b}$ in the $t\bar{t}$ resonance region, Nucl. Phys. B840 (2010) 186–213. arXiv:

1004.2188, doi:10.1016/j.nuclphysb.2010.07.006.

[23] E. A. Kuraev, V. S. Fadin, On Radiative Corrections to e^+e^- Single Photon Annihilation at High-Energy, Sov. J. Nucl. Phys. 41 (1985) 466–472, [Yad. Fiz.41,733(1985)].

[24] V. S. Fadin, V. A. Khoze, Threshold Behavior of Heavy Top Production in e^+e^- Collisions, JETP Lett. 46 (1987) 525–529, [Pisma Zh. Eksp. Teor. Fiz.46,417(1987)].

[25] M. Beneke, Y. Kiyo, A. Maier, J. Piclum, Near-threshold production of heavy quarks with QQbar_threshold, Comput. Phys. Commun. 209 (2016) 96–115. arXiv:1605.03010, doi:10.1016/j.cpc.2016.07.026.

[26] M. Beneke, A Quark mass definition adequate for threshold problems, Phys. Lett. B434 (1998) 115–125. arXiv:hep-ph/9804241, doi:10.1016/S0370-2693(98)00741-2.

12 Higgs Boson Decays: Theoretical Status

Author: Michael Spira [Michael.Spira@psi.ch]

12.1 Introduction

The discovery of a Standard-Model-like Higgs boson at the LHC [1, 2] completed the theory of electroweak and strong interactions. The measured Higgs mass of (125.09 ± 0.24) GeV [3] ranges at the order of the weak scale. The existence of the Higgs boson [4–9] allows the Standard Model (SM) particles to be weakly interacting up to high-energy scales. This, however, is only possible for particular Higgs-boson couplings to all other particles so that with the knowledge of the Higgs-boson mass all its properties are uniquely fixed. The massive gauge bosons and fermions acquire mass through their interaction with the Higgs field that develops a finite vacuum expectation value in its ground state. The minimal model requires the introduction of one isospin doublet of the Higgs field and leads after spontaneous symmetry breaking to the existence of one scalar Higgs boson.

Since all Higgs couplings are fixed within the SM any meaningful approach to introduce variations requires to introduce effects beyond the SM (BSM). There two major branches pursued for this purpose: *(i)* the introduction of higher-dimension operators in terms of a general effective Lagrangian with dimension-6 operators providing the leading contributions for energy scales sufficiently below the novel cut-off scale of these operators and *(ii)* the introduction of specific BSM models with extended Higgs, gauge and fermion sectors. The extraction of BSM effects, however, strongly relies on the accuracy of the SM part as e.g. sketched in the basic decomposition of the SM-like Higgs boson decay widths as

$$\Gamma = \Gamma_{SM} + \Delta\Gamma_{BSM} \tag{12.105}$$

Any potential to extract the BSM effects $\Delta\Gamma_{BSM}$ is limited by the uncertainties $\delta\Gamma_{SM}$ of the SM part.

12.2 SM Higgs Boson Decays

The determination of the branching ratios of Higgs-boson decays thus necessitates the inclusion of the available higher-order corrections (for a recent overview see e.g. [10]) and a sophisticated estimate of the theoretical and parametric uncertainties.

(i) $H \to f\bar{f}$: The Higgs decay $H \to b\bar{b}$ is the dominant Higgs boson decay with a branching ratio of about 58%. The subleading fermionic decays $H \to \tau^+\tau^-$ and $H \to c\bar{c}$ reach branching ratios of about 6% and 3%, respectively. The rare decay $H \to \mu^+\mu^-$ will become visible at the HL-LHC and happens with about 0.02% probability [11]. The present status of the partial decay widths can be summarized in terms of the (factorized) expression

$$\Gamma(H \to f\overline{f}) = \frac{N_c G_F M_H}{4\sqrt{2}\pi}\; m_f^2\; (1 + \delta_{\rm QCD} + \delta_t + \delta_{mixed})\,(1 + \delta_{elw}) \tag{12.106}$$

where $N_c = 3(1)$ for quarks (leptons), G_F denotes the Fermi constant, M_H the Higgs mass and m_f the fermion mass. In general the pure QCD corrections $\delta_{\rm QCD}$ to the Higgs boson decays into quarks are known up to NLO including the full quark mass dependence [12–16] and up to N^{4}LO for the leading corrections with the leading mass effects [17–23]. The dominant part of

the QCD corrections can be absorbed in the running quark mass evaluated at the scale of the Higgs mass. The top-induced QCD corrections, which are related to interference effects between $H \to gg$ and $H \to q\bar{q}$, are known at NNLO in the limit of heavy top quarks and light bottom quarks [24–26]. In the case of leptons there are no QCD corrections ($\delta_{\rm QCD} = \delta_t = \delta_{mixed} = 0$). The electroweak corrections δ_{elw} are known at NLO exactly [27–30]. In addition the mixed QCD-elw. corrections range at the one-per-mille level if the factorized expression with respect to QCD and elw. corrections is used [31–35]. The public tool `Hdecay` [36, 37] neglects these mixed QCD-elw. corrections but includes all other corrections. The partial decay width of $H \to b\bar{b}$ is also known fully differential at N^{3}LO QCD [38–41].

(ii) $H \to W^{(*)}W^{(*)}, Z^{(*)}Z^{(*)}$: The branching ratios of SM Higgs boson decays into (off-shell) W and Z bosons amount to about 21% and 3%, respectively. Off-shell effects of the W and Z are important [42–44] and lead to the $H \to Z^*Z^{(*)} \to 4\ell^\pm$ decay as one of the discovery modes of the SM Higgs boson [1, 2]. The electroweak corrections to the full decay modes $H \to V^{(*)}V^{(*)} \to 4f$ ($V = W, Z$) have been calculated [27, 45–48]. The public tool `Prophecy4f` [47, 48] calculating the exclusive decay processes has been used in the experimental analyses. An improvement beyond the pure elw. corrections has been made by the proper matching to parton showers at NLO [49]. However, shower effects have not been relevant for the analyses performed so far.

(iii) $H \to gg$: The loop-induced Higgs decay into gluons reaches a branching ratio of about 8%. The decay is dominantly mediated by top and bottom-quark loops with the latter providing a 10%-contribution. The charm quark contributes at the level of about 2%. The two-loop QCD corrections are known including the exact quark mass dependences [50–52]. They enhance the partial decay width by about 70% and thus cannot be neglected in the decay profile of the Higgs boson. The NNLO, N^{3}LO and recently the N^{4}LO QCD corrections have been obtained for the top loops in the limit of heavy top quarks, i.e. the leading term of a heavy top-mass expansion [53–55]. The QCD corrections beyond NLO amount to less than 20% of the NLO QCD corrected partial decay width thus signaling perturbative convergence in spite of the large NLO corrections. The residual theoretical uncertainties have been estimated at the level of about 3% from the scale dependence of the QCD corrected partial decay width. The NLO elw. corrections have been calculated for the top-loop contributions first in the limit of heavy top quarks [33, 56, 57], then the electroweak corrections involving light fermion loops exactly [58–60] and finally the full electroweak corrections involving W, Z and top-loop contributions including the full virtual mass dependences by means of a numerical integration [61, 62]. They amount to about 5% for the SM Higgs mass value. The public tool `Hdecay` [36, 37] includes the NLO QCD results with the full quark mass dependences, the NNLO and N^{3}LO QCD corrections in the heavy-top limit and the full NLO elw. corrections in terms of a grid in the Higgs and top masses used for an interpolation.

(iv) $H \to \gamma\gamma$: The rare loop-induced Higgs decay into photons reaches a branching ratio of about 0.2%. The decay is dominantly mediated by W and top-quark loops with the W loops being dominant. The two-loop QCD corrections are known including the exact top mass dependences [52, 63–72]. They correct the partial decay width by a small amount of about 2%. The QCD corrections beyond NLO have been estimated in the limit of heavy top quarks to be in the per-mille range [73–75]. The NLO elw. corrections to the W and top-induced

contributions have been obtained by a numerical integration of the corresponding two-loop diagrams [62, 76–78]. They decrease the partial photonic branching ratio of the SM Higgs boson by about 2% thus nearly canceling against the QCD corrections by accident. The public tool `Hdecay` [36,37] includes the NLO QCD results with the full quark mass dependences and the full NLO elw. corrections in terms of a grid in the Higgs and top masses used for an interpolation, but neglects all corrections beyond NLO.

(v) $H \to Z\gamma$ and Dalitz decays: The rare loop-induced Higgs decay into a Z boson and photon reaches a branching ratio of less than 0.2%. The decay is dominantly mediated by W and top-quark loops with the W loops being dominant. The two-loop QCD corrections are known including the exact top mass dependences [79–81]. They correct the partial decay width by a small amount in the per-mille range and thus can safely be neglected. The electroweak corrections to this decay mode are unknown. However, the decay mode $H \to Z\gamma \to f\bar{f}\gamma$ is part of the more general Dalitz decays $H \to f\bar{f}\gamma$ [82–88]. The latter are described by the diagrams in Fig. B.37 where the Z-boson exchange appears in a part of the triangle diagrams. The resonant Z-boson exchange corresponds to the $H \to Z\gamma$ decay mode. The separation of

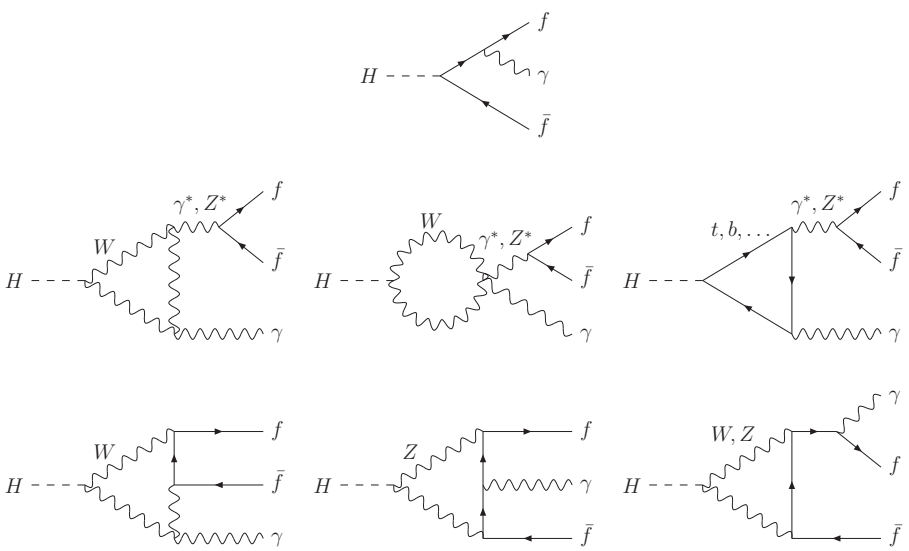

Fig. B.37: *Generic diagrams contributing to the Dalitz decays $H \to \gamma f\bar{f}$.*

this part, however, depends on the experimental strategy to reconstruct the Z boson in the final state. A first step for the reconstruction of the Z boson is to cut on the invariant mass of the final-state fermion pair. The corresponding distributions of the Dalitz decays are shown in Fig. B.38 for the three charged-lepton final states normalized to the partial width into photons with a cut $E_\gamma > 1$ GeV on the photon energy. For small invariant masses the photon conversion $H \to \gamma\gamma^* \to \gamma\ell^+\ell^-$ provides the dominant contribution, while for invariant masses around the Z-boson mass the Z-boson contribution $H \to \gamma Z^* \to \gamma f\bar{f}$ takes over the dominant role. At the end-point $q^2 \lesssim M_H^2$ of the spectrum the direct contribution determines the distributions. This rises with growing Yukawa coupling, i.e. it is largest for $H \to \gamma\tau^+\tau^-$ (where it dominates in the whole q^2-range)[‡]. For a clean separation of the $H \to \gamma\gamma$, $H \to \gamma\gamma^* \to \gamma\ell^+\ell^-$, $H \to Z\gamma$

[‡]It should be noted that the end point in the $e^+e^-\gamma$ case is 4–5 orders of magnitude smaller than the photon

and $H \to \ell^+\ell^-$ contributions appropriate cuts have to be implemented for the Dalitz decays. The low-q^2 part has to be attributed to $H \to \gamma\gamma$, the q^2-part around M_Z^2 to $H \to Z\gamma$ and the end-point region close to M_H^2 to the QED corrections to $H \to \ell^+\ell^-$. The public code `Hdecay` [36, 37] does not include the full Dalitz decays.

12.3 Uncertainties

The parametric errors are dominated by the uncertainties in the top, bottom and charm quark masses as well as the strong coupling α_s. We have used the $\overline{\rm MS}$ masses for the bottom and charm quark, $\overline{m}_b(\overline{m}_b) = (4.18 \pm 0.03)$ GeV and $\overline{m}_c(3\text{ GeV}) = (0.986 \pm 0.026)$ GeV, and the top quark pole mass $m_t = (172.5 \pm 1)$ GeV according to the conventions of the LHC Higgs Cross Section WG (HXSWG) [11]. The $\overline{\rm MS}$ bottom and charm masses are evolved from the input scale to the scale of the decay process with 4-loop accuracy in QCD. The strong coupling α_s is fixed by the input value at the Z-boson mass scale, $\alpha_s(M_Z) = 0.118 \pm 0.0015$. The total parametric uncertainty for each branching ratio has been derived from a quadratic sum of the individual impacts of the input parameters on the decay modes.

The theoretical uncertainties from missing higher orders in the perturbative expansion are summarized in Table B.9 for the individual partial decay processes along with the perturbative orders of the included QCD/elw. corrections [10, 11]. In order to be conservative the total parametric uncertainties are added linearly to the theoretical uncertainties. The final result for the branching ratios is shown in Fig. B.39 for the leading Higgs decay modes with branching ratio larger than 10^{-4} for the Higgs-mass range between 120 and 130 GeV. They have been obtained with `Prophecy4f` [47,48] for the decays $H \to WW, ZZ$ and `Hdecay` [36,37] for the other decay modes. The bands represent the total uncertainties of the individual branching ratios. For a Higgs mass $M_H = 125$ GeV the total uncertainty of the leading decay mode $H \to b\bar{b}$ amounts to less than 2%, since the bulk of it cancels out within the branching ratio. The uncertainty of $\Gamma(H \to b\bar{b})$, however, generates a significant increase of the uncertainties for the subleading decay modes. The total uncertainties of $BR(H \to WW/ZZ)$ and $BR(H \to \tau^+\tau^-/\mu^+\mu^-)$ amount to $\sim 2\%$, while the uncertainties of $BR(H \to gg)$ and $BR(H \to c\bar{c})$ range at $\sim 6-7\%$, of $BR(H \to \gamma\gamma)$ at $\sim 3\%$ and of $BR(H \to Z\gamma)$ at $\sim 7\%$. The total decay width of ~ 4.1 MeV can be predicted with $\sim 2\%$ total uncertainty.

and Z-exchange contributions thus making it impossible to determine the electron Yukawa coupling. The same conclusion is also valid for the reverse process $e^+e^- \to H\gamma$ so that the s-channel line-shape measurement proposed in Ref. [89] will not be sensitive to the electron Yukawa coupling but dominated by the loop-induced contribution with an additional photon.

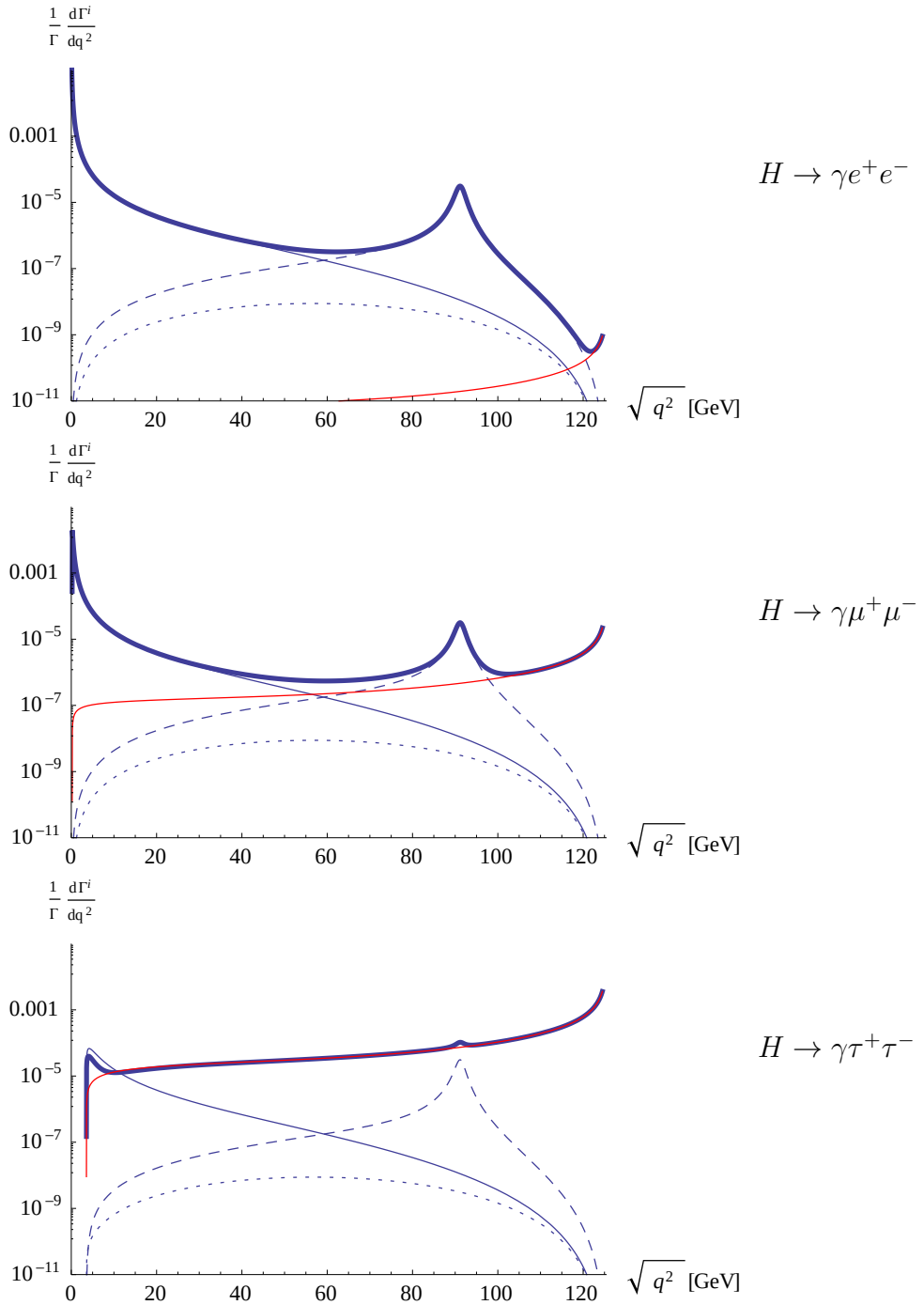

Fig. B.38: *The invariant mass distributions in* $\sqrt{q^2} = M_{\ell^+\ell^-}$ *of the Dalitz decays* $H \to \gamma + e^+e^-/\mu^+\mu^-/\tau^+\tau^-$ *normalized to* $\Gamma(H \to \gamma\gamma)$ *with a cut* $E_\gamma > 1$ *GeV on the photon energy. The red lines show the contribution of the tree diagrams, the thin solid lines denote the contribution of the photon conversion* $H \to \gamma\gamma^* \to \gamma\ell^+\ell^-$*, and the dashed line the contribution from the* Z^* *exchange diagrams, while the thick lines present the total contributions. The dotted lines denote the contribution from the box diagrams (in 't Hooft–Feynman gauge). From Ref. [88].*

Partial Width	**QCD**	**Electroweak**	**Total**	**on-shell Higgs**
$H \to b\bar{b}/c\bar{c}$	$\sim 0.2\%$	$\sim 0.5\%$	$\sim 0.5\%$	N^{4}LO / NLO
$H \to \tau^+\tau^-/\mu^+\mu^-$	—	$\sim 0.5\%$	$\sim 0.5\%$	— / NLO
$H \to gg$	$\sim 3\%$	$\sim 1\%$	$\sim 3\%$	N^{3}LO / NLO
$H \to \gamma\gamma$	$< 1\%$	$< 1\%$	$\sim 1\%$	NLO / NLO
$H \to Z\gamma$	$< 1\%$	$\sim 5\%$	$\sim 5\%$	LO / LO
$H \to WW/ZZ \to 4f$	$< 0.5\%$	$\sim 0.5\%$	$\sim 0.5\%$	NLO/NLO

Table B.9: *Estimated theoretical uncertainties from missing higher orders and the perturbative orders (QCD/elw.) of the results included in the analysis.*

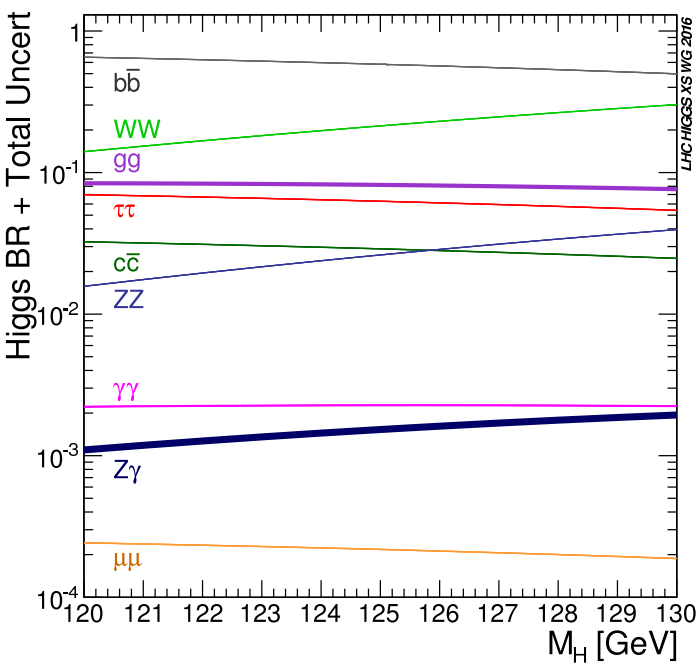

Fig. B.39: *Higgs boson branching ratios and their uncertainties for Higgs masses around 125 GeV. From Ref. [11].*

References

[1] G. Aad, et al., Observation of a new particle in the search for the Standard Model Higgs boson with the ATLAS detector at the LHC, Phys. Lett. B716 (2012) 1–29. arXiv:1207.7214, doi:10.1016/j.physletb.2012.08.020.

[2] S. Chatrchyan, et al., Observation of a new boson at a mass of 125 GeV with the CMS experiment at the LHC, Phys. Lett. B716 (2012) 30–61. arXiv:1207.7235, doi:10.1016/j.physletb.2012.08.021.

[3] G. Aad, et al., Measurements of the Higgs boson production and decay rates and constraints on its couplings from a combined ATLAS and CMS analysis of the LHC pp collision data at $\sqrt{s} = 7$ and 8 TeV, JHEP 08 (2016) 045. arXiv:1606.02266, doi:10.1007/JHEP08(2016)045.

[4] P. W. Higgs, Broken symmetries, massless particles and gauge fields, Phys. Lett. 12 (1964) 132–133. doi:10.1016/0031-9163(64)91136-9.

[5] P. W. Higgs, Broken Symmetries and the Masses of Gauge Bosons, Phys. Rev. Lett. 13 (1964) 508–509. doi:10.1103/PhysRevLett.13.508.

[6] F. Englert, R. Brout, Broken Symmetry and the Mass of Gauge Vector Mesons, Phys. Rev. Lett. 13 (1964) 321–323. doi:10.1103/PhysRevLett.13.321.

[7] G. S. Guralnik, C. R. Hagen, T. W. B. Kibble, Global Conservation Laws and Massless Particles, Phys. Rev. Lett. 13 (1964) 585–587. doi:10.1103/PhysRevLett.13.585.

[8] P. W. Higgs, Spontaneous Symmetry Breakdown without Massless Bosons, Phys. Rev. 145 (1966) 1156–1163. doi:10.1103/PhysRev.145.1156.

[9] T. W. B. Kibble, Symmetry breaking in nonAbelian gauge theories, Phys. Rev. 155 (1967) 1554–1561. doi:10.1103/PhysRev.155.1554.

[10] M. Spira, Higgs Boson Production and Decay at Hadron Colliders, Prog. Part. Nucl. Phys. 95 (2017) 98–159. arXiv:1612.07651, doi:10.1016/j.ppnp.2017.04.001.

[11] D. de Florian, et al., Handbook of LHC Higgs Cross Sections: 4. Deciphering the Nature of the Higgs Sector, arXiv:1610.07922, doi:10.23731/CYRM-2017-002.

[12] E. Braaten, J. P. Leveille, Higgs Boson Decay and the Running Mass, Phys. Rev. D22 (1980) 715. doi:10.1103/PhysRevD.22.715.

[13] N. Sakai, Perturbative QCD Corrections to the Hadronic Decay Width of the Higgs Boson, Phys. Rev. D22 (1980) 2220. doi:10.1103/PhysRevD.22.2220.

[14] T. Inami, T. Kubota, Renormalization Group Estimate of the Hadronic Decay Width of the Higgs Boson, Nucl. Phys. B179 (1981) 171–188. doi:10.1016/0550-3213(81)90253-4.

[15] M. Drees, K.-I. Hikasa, Note on QCD Corrections to Hadronic Higgs Decay, Phys. Lett. B240 (1990) 455, [Erratum: Phys. Lett.B262,497(1991)]. doi:10.1016/0370-2693(90)91130-4.

[16] M. Drees, K.-I. Hikasa, Heavy Quark Thresholds in Higgs Physics, Phys. Rev. D41 (1990) 1547. doi:10.1103/PhysRevD.41.1547.

[17] S. G. Gorishnii, A. L. Kataev, S. A. Larin, The Width of Higgs Boson Decay Into Hadrons: Three Loop Corrections of Strong Interactions, Sov. J. Nucl. Phys. 40 (1984) 329–334, [Yad. Fiz.40,517(1984)].

[18] S. G. Gorishnii, A. L. Kataev, S. A. Larin, L. R. Surguladze, Corrected Three Loop QCD Correction to the Correlator of the Quark Scalar Currents and $\Gamma_{tot}(H^0 \to \text{Hadrons})$, Mod. Phys. Lett. A5 (1990) 2703–2712. doi:10.1142/S0217732390003152.

[19] S. G. Gorishnii, A. L. Kataev, S. A. Larin, L. R. Surguladze, Scheme dependence of the next to next-to-leading QCD corrections to $\Gamma_{tot}(H^0 \to \text{hadrons})$ and the spurious QCD infrared fixed point, Phys. Rev. D43 (1991) 1633–1640. doi:10.1103/PhysRevD.43.1633.

[20] A. L. Kataev, V. T. Kim, The Effects of the QCD corrections to $\Gamma(H^0 \to b\bar{b})$, Mod. Phys. Lett. A9 (1994) 1309–1326. doi:10.1142/S0217732394001131.

[21] L. R. Surguladze, Quark mass effects in fermionic decays of the Higgs boson in $\mathcal{O}(\alpha_s^2)$ perturbative QCD, Phys. Lett. B341 (1994) 60–72. arXiv:hep-ph/9405325, doi:10.1016/0370-2693(94)01253-9.

[22] K. G. Chetyrkin, Correlator of the quark scalar currents and $\Gamma_{tot}(H \to \text{hadrons})$ at $\mathcal{O}(\alpha_s^3)$ in pQCD, Phys. Lett. B390 (1997) 309–317. arXiv:hep-ph/9608318, doi:10.1016/S0370-2693(96)01368-8.

[23] K. Melnikov, Two loop $\mathcal{O}(N_f\alpha_s^2)$ correction to the decay width of the Higgs boson to two massive fermions, Phys. Rev. D53 (1996) 5020–5027. arXiv:hep-ph/9511310, doi:10.1103/PhysRevD.53.5020.

[24] K. G. Chetyrkin, A. Kwiatkowski, Second order QCD corrections to scalar and pseudoscalar Higgs decays into massive bottom quarks, Nucl. Phys. B461 (1996) 3–18. arXiv:hep-ph/9505358, doi:10.1016/0550-3213(95)00616-8.

[25] S. A. Larin, T. van Ritbergen, J. A. M. Vermaseren, The Large top quark mass expansion for Higgs boson decays into bottom quarks and into gluons, Phys. Lett. B362 (1995) 134–140. arXiv:hep-ph/9506465, doi:10.1016/0370-2693(95)01192-S.

[26] A. Primo, G. Sasso, G. Somogyi, F. Tramontano, Exact Top Yukawa corrections to Higgs boson decay into bottom quarks, Phys. Rev. D99 (5) (2019) 054013. arXiv:1812.07811, doi:10.1103/PhysRevD.99.054013.

[27] J. Fleischer, F. Jegerlehner, Radiative Corrections to Higgs Decays in the Extended Weinberg-Salam Model, Phys. Rev. D23 (1981) 2001–2026. doi:10.1103/PhysRevD.23.2001.

[28] D. Yu. Bardin, B. M. Vilensky, P. K. Khristova, Calculation of the Higgs boson decay width into fermion pairs, Sov. J. Nucl. Phys. 53 (1991) 152–158, [Yad. Fiz.53,240(1991)].

[29] A. Dabelstein, W. Hollik, Electroweak corrections to the fermionic decay width of the standard Higgs boson, Z. Phys. C53 (1992) 507–516. doi:10.1007/BF01625912.

[30] B. A. Kniehl, Radiative corrections for $H \to$ f anti-f (γ) in the standard model, Nucl. Phys. B376 (1992) 3–28. doi:10.1016/0550-3213(92)90065-J.

[31] B. A. Kniehl, M. Spira, Two loop $\mathcal{O}(\alpha_s G_F m_t^2)$ correction to the $H \to b\bar{b}$ decay rate, Nucl. Phys. B432 (1994) 39–48. arXiv:hep-ph/9410319, doi:10.1016/0550-3213(94)90592-4.

[32] A. Kwiatkowski, M. Steinhauser, Corrections of order $\mathcal{O}(G_F\alpha_s m_t^2)$ to the Higgs decay rate $\Gamma(H \to b\bar{b})$, Phys. Lett. B338 (1994) 66–70, [Erratum: Phys. Lett.B342,455(1995)]. arXiv:hep-ph/9405308, doi:10.1016/0370-2693(94)01527-J, 10.1016/0370-2693(94)91345-5.

[33] K. G. Chetyrkin, B. A. Kniehl, M. Steinhauser, Virtual top quark effects on the $H \to b\bar{b}$ decay at next-to-leading order in QCD, Phys. Rev. Lett. 78 (1997) 594–597. arXiv:hep-ph/9610456, doi:10.1103/PhysRevLett.78.594.

[34] L. Mihaila, B. Schmidt, M. Steinhauser, $\Gamma(H \to b\bar{b})$ to order $\alpha\alpha_s$, Phys. Lett. B751 (2015) 442–447. arXiv:1509.02294, doi:10.1016/j.physletb.2015.10.078.

[35] E. Chaubey, S. Weinzierl, Two-loop master integrals for the mixed QCD-electroweak cor-

rections for $H \to b\bar{b}$ through a $Ht\bar{t}$-coupling, arXiv:1904.00382.

[36] A. Djouadi, J. Kalinowski, M. Spira, HDECAY: A Program for Higgs boson decays in the standard model and its supersymmetric extension, Comput. Phys. Commun. 108 (1998) 56–74. arXiv:hep-ph/9704448, doi:10.1016/S0010-4655(97)00123-9.

[37] A. Djouadi, J. Kalinowski, M. Mühlleitner, M. Spira, HDECAY: Twenty$_{++}$ years after, Comput. Phys. Commun. 238 (2019) 214–231. arXiv:1801.09506, doi:10.1016/j.cpc.2018.12.010.

[38] C. Anastasiou, F. Herzog, A. Lazopoulos, The fully differential decay rate of a Higgs boson to bottom-quarks at NNLO in QCD, JHEP 03 (2012) 035. arXiv:1110.2368, doi:10.1007/JHEP03(2012)035.

[39] V. Del Duca, C. Duhr, G. Somogyi, F. Tramontano, Z. Trócsányi, Higgs boson decay into b-quarks at NNLO accuracy, JHEP 04 (2015) 036. arXiv:1501.07226, doi:10.1007/JHEP04(2015)036.

[40] G. Ferrera, G. Somogyi, F. Tramontano, Associated production of a Higgs boson decaying into bottom quarks at the LHC in full NNLO QCD, Phys. Lett. B780 (2018) 346–351. arXiv:1705.10304, doi:10.1016/j.physletb.2018.03.021.

[41] R. Mondini, M. Schiavi, C. Williams, N^{3}LO predictions for the decay of the Higgs boson to bottom quarks, arXiv:1904.08960.

[42] T. G. Rizzo, Decays of Heavy Higgs Bosons, Phys. Rev. D22 (1980) 722. doi:10.1103/PhysRevD.22.722.

[43] W.-Y. Keung, W. J. Marciano, Higgs Scalar Decays: $H \to W^{\pm}X$, Phys. Rev. D30 (1984) 248. doi:10.1103/PhysRevD.30.248.

[44] R. N. Cahn, The Higgs Boson, Rept. Prog. Phys. 52 (1989) 389. doi:10.1088/0034-4885/52/4/001.

[45] B. A. Kniehl, Radiative corrections for $H \to ZZ$ in the standard model, Nucl. Phys. B352 (1991) 1–26. doi:10.1016/0550-3213(91)90126-I.

[46] D. Yu. Bardin, P. K. Khristova, B. M. Vilensky, Calculation of the Higgs boson decay widths into boson pairs, Sov. J. Nucl. Phys. 54 (1991) 833–844, [Yad. Fiz.54,1366(1991)].

[47] A. Bredenstein, A. Denner, S. Dittmaier, M. M. Weber, Precise predictions for the Higgs-boson decay $H \to WW/ZZ \to 4$ leptons, Phys. Rev. D74 (2006) 013004. arXiv:hep-ph/0604011, doi:10.1103/PhysRevD.74.013004.

[48] A. Bredenstein, A. Denner, S. Dittmaier, M. M. Weber, Radiative corrections to the semileptonic and hadronic Higgs-boson decays $H \to WW/ZZ \to 4$ fermions, JHEP 02 (2007) 080. arXiv:hep-ph/0611234, doi:10.1088/1126-6708/2007/02/080.

[49] S. Boselli, C. M. Carloni Calame, G. Montagna, O. Nicrosini, F. Piccinini, Higgs boson decay into four leptons at NLOPS electroweak accuracy, JHEP 06 (2015) 023. arXiv:1503.07394, doi:10.1007/JHEP06(2015)023.

[50] T. Inami, T. Kubota, Y. Okada, Effective Gauge Theory and the Effect of Heavy Quarks in Higgs Boson Decays, Z. Phys. C18 (1983) 69–80. doi:10.1007/BF01571710.

[51] A. Djouadi, M. Spira, P. M. Zerwas, Production of Higgs bosons in proton colliders: QCD corrections, Phys. Lett. B264 (1991) 440–446. doi:10.1016/0370-2693(91)90375-Z.

[52] M. Spira, A. Djouadi, D. Graudenz, P. M. Zerwas, Higgs boson production at the LHC, Nucl. Phys. B453 (1995) 17–82. arXiv:hep-ph/9504378, doi:10.1016/0550-3213(95)00379-7.

[53] K. G. Chetyrkin, B. A. Kniehl, M. Steinhauser, Hadronic Higgs decay to order α_s^4, Phys. Rev. Lett. 79 (1997) 353–356. arXiv:hep-ph/9705240, doi:10.1103/PhysRevLett.79.353.

[54] P. A. Baikov, K. G. Chetyrkin, Top Quark Mediated Higgs Boson Decay into Hadrons to Order α_s^5, Phys. Rev. Lett. 97 (2006) 061803. arXiv:hep-ph/0604194, doi:10.1103/PhysRevLett.97.061803.

[55] F. Herzog, B. Ruijl, T. Ueda, J. A. M. Vermaseren, A. Vogt, On Higgs decays to hadrons and the R-ratio at N^{4}LO, JHEP 08 (2017) 113. arXiv:1707.01044, doi:10.1007/JHEP08(2017)113.

[56] A. Djouadi, P. Gambino, Leading electroweak correction to Higgs boson production at proton colliders, Phys. Rev. Lett. 73 (1994) 2528–2531. arXiv:hep-ph/9406432, doi:10.1103/PhysRevLett.73.2528.

[57] K. G. Chetyrkin, B. A. Kniehl, M. Steinhauser, Three loop $\mathcal{O}(\alpha_s^2 G_F m_t^2)$ corrections to hadronic Higgs decays, Nucl. Phys. B490 (1997) 19–39. arXiv:hep-ph/9701277, doi:10.1016/S0550-3213(97)00051-5.

[58] U. Aglietti, R. Bonciani, G. Degrassi, A. Vicini, Two loop light fermion contribution to Higgs production and decays, Phys. Lett. B595 (2004) 432–441. arXiv:hep-ph/0404071, doi:10.1016/j.physletb.2004.06.063.

[59] U. Aglietti, R. Bonciani, G. Degrassi, A. Vicini, Two-loop electroweak corrections to Higgs production in proton-proton collisions, in: TeV4LHC Workshop: 2nd Meeting Brookhaven, Upton, New York, February 3-5, 2005, 2006. arXiv:hep-ph/0610033.

[60] G. Degrassi, F. Maltoni, Two-loop electroweak corrections to Higgs production at hadron colliders, Phys. Lett. B600 (2004) 255–260. arXiv:hep-ph/0407249, doi:10.1016/j.physletb.2004.09.008.

[61] S. Actis, G. Passarino, C. Sturm, S. Uccirati, NLO Electroweak Corrections to Higgs Boson Production at Hadron Colliders, Phys. Lett. B670 (2008) 12–17. arXiv:0809.1301, doi:10.1016/j.physletb.2008.10.018.

[62] S. Actis, G. Passarino, C. Sturm, S. Uccirati, NNLO Computational Techniques: The Cases $H \to \gamma\gamma$ and $H \to gg$, Nucl. Phys. B811 (2009) 182–273. arXiv:0809.3667, doi:10.1016/j.nuclphysb.2008.11.024.

[63] H.-Q. Zheng, D.-D. Wu, First order QCD corrections to the decay of the Higgs boson into two photons, Phys. Rev. D42 (1990) 3760–3763. doi:10.1103/PhysRevD.42.3760.

[64] A. Djouadi, M. Spira, J. J. van der Bij, P. M. Zerwas, QCD corrections to gamma gamma decays of Higgs particles in the intermediate mass range, Phys. Lett. B257 (1991) 187–190. doi:10.1016/0370-2693(91)90879-U.

[65] S. Dawson, R. P. Kauffman, QCD corrections to $H \to \gamma\gamma$, Phys. Rev. D47 (1993) 1264–1267. doi:10.1103/PhysRevD.47.1264.

[66] A. Djouadi, M. Spira, P. M. Zerwas, Two photon decay widths of Higgs particles, Phys. Lett. B311 (1993) 255–260. arXiv:hep-ph/9305335, doi:10.1016/0370-2693(93)90564-X.

[67] K. Melnikov, O. I. Yakovlev, Higgs $\to$ two photon decay: QCD radiative correction, Phys. Lett. B312 (1993) 179–183. arXiv:hep-ph/9302281, doi:10.1016/0370-2693(93)90507-E.

[68] M. Inoue, R. Najima, T. Oka, J. Saito, QCD corrections to two photon decay of the Higgs boson and its reverse process, Mod. Phys. Lett. A9 (1994) 1189–1194. doi:10.1142/

S0217732394001003.

[69] J. Fleischer, O. V. Tarasov, V. O. Tarasov, Analytical result for the two loop QCD correction to the decay H $\to 2\gamma$, Phys. Lett. B584 (2004) 294–297. arXiv:hep-ph/0401090, doi:10.1016/j.physletb.2004.01.063.

[70] R. Harlander, P. Kant, Higgs production and decay: Analytic results at next-to-leading order QCD, JHEP 12 (2005) 015. arXiv:hep-ph/0509189, doi:10.1088/1126-6708/2005/12/015.

[71] C. Anastasiou, S. Beerli, S. Bucherer, A. Daleo, Z. Kunszt, Two-loop amplitudes and master integrals for the production of a Higgs boson via a massive quark and a scalar-quark loop, JHEP 01 (2007) 082. arXiv:hep-ph/0611236, doi:10.1088/1126-6708/2007/01/082.

[72] U. Aglietti, R. Bonciani, G. Degrassi, A. Vicini, Analytic Results for Virtual QCD Corrections to Higgs Production and Decay, JHEP 01 (2007) 021. arXiv:hep-ph/0611266, doi:10.1088/1126-6708/2007/01/021.

[73] M. Steinhauser, Corrections of $\mathcal{O}(\alpha_s^2)$ to the decay of an intermediate mass Higgs boson into two photons, in: The Higgs puzzle - what can we learn from LEP-2, LHC, NLC and FMC? Proceedings, Ringberg Workshop, Tegernsee, Germany, December 8-13, 1996, 1996, pp. 177–185. arXiv:hep-ph/9612395.

[74] C. Sturm, Higher order QCD results for the fermionic contributions of the Higgs-boson decay into two photons and the decoupling function for the $\overline{\rm MS}$ renormalized fine-structure constant, Eur. Phys. J. C74 (8) (2014) 2978. arXiv:1404.3433, doi:10.1140/epjc/s10052-014-2978-0.

[75] P. Maierhöfer, P. Marquard, Complete three-loop QCD corrections to the decay $H \to \gamma\gamma$, Phys. Lett. B721 (2013) 131–135. arXiv:1212.6233, doi:10.1016/j.physletb.2013.02.040.

[76] A. Djouadi, P. Gambino, B. A. Kniehl, Two loop electroweak heavy fermion corrections to Higgs boson production and decay, Nucl. Phys. B523 (1998) 17–39. arXiv:hep-ph/9712330, doi:10.1016/S0550-3213(98)00147-3.

[77] G. Degrassi, F. Maltoni, Two-loop electroweak corrections to the Higgs-boson decay $H \to \gamma\gamma$, Nucl. Phys. B724 (2005) 183–196. arXiv:hep-ph/0504137, doi:10.1016/j.nuclphysb.2005.06.027.

[78] G. Passarino, C. Sturm, S. Uccirati, Complete Two-Loop Corrections to $H \to \gamma\gamma$, Phys. Lett. B655 (2007) 298–306. arXiv:0707.1401, doi:10.1016/j.physletb.2007.09.002.

[79] M. Spira, A. Djouadi, P. M. Zerwas, QCD corrections to the $HZ\gamma$ coupling, Phys. Lett. B276 (1992) 350–353. doi:10.1016/0370-2693(92)90331-W.

[80] R. Bonciani, V. Del Duca, H. Frellesvig, J. M. Henn, F. Moriello, V. A. Smirnov, Next-to-leading order QCD corrections to the decay width $H \to Z\gamma$, JHEP 08 (2015) 108. arXiv:1505.00567, doi:10.1007/JHEP08(2015)108.

[81] T. Gehrmann, S. Guns, D. Kara, The rare decay $H \to Z\gamma$ in perturbative QCD, JHEP 09 (2015) 038. arXiv:1505.00561, doi:10.1007/JHEP09(2015)038.

[82] A. Abbasabadi, D. Bowser-Chao, D. A. Dicus, W. W. Repko, Radiative Higgs boson decays $H \to$ fermion anti-fermion γ, Phys. Rev. D55 (1997) 5647–5656. arXiv:hep-ph/9611209, doi:10.1103/PhysRevD.55.5647.

[83] A. Abbasabadi, W. W. Repko, Higgs boson decay into Z bosons and a photon, JHEP 08 (2006) 048. arXiv:hep-ph/0602087, doi:10.1088/1126-6708/2006/08/048.

[84] A. Abbasabadi, W. W. Repko, A Note on the rare decay of a Higgs boson into photons and a Z boson, Phys. Rev. D71 (2005) 017304. arXiv:hep-ph/0411152, doi:10.1103/PhysRevD.71.017304.

[85] D. A. Dicus, W. W. Repko, Calculation of the decay $H \to e\bar{e}\gamma$, Phys. Rev. D87 (7) (2013) 077301. arXiv:1302.2159, doi:10.1103/PhysRevD.87.077301.

[86] L.-B. Chen, C.-F. Qiao, R.-L. Zhu, Reconstructing the 125 GeV SM Higgs Boson Through $\ell\bar{\ell}\gamma$, Phys. Lett. B726 (2013) 306–311. arXiv:1211.6058, doi:10.1016/j.physletb.2013.08.050.

[87] G. Passarino, Higgs Boson Production and Decay: Dalitz Sector, Phys. Lett. B727 (2013) 424–431. arXiv:1308.0422, doi:10.1016/j.physletb.2013.10.052.

[88] Y. Sun, H.-R. Chang, D.-N. Gao, Higgs decays to $\gamma\ell^+\ell^-$ in the standard model, JHEP 05 (2013) 061. arXiv:1303.2230, doi:10.1007/JHEP05(2013)061.

[89] S. Jadach, R. A. Kycia, Lineshape of the Higgs boson in future lepton colliders, Phys. Lett. B755 (2016) 58–63. arXiv:1509.02406, doi:10.1016/j.physletb.2016.01.065.

Chapter C

Methods and Tools

1 Heritage projects, archivization and re-usability concerns

Authors: Swagato Banerjee, Marcin Chrzaszcz, Zbigniew Was, Jakub Zaremba
Corresponding Author: Zbigniew Was [z.was@cern.ch]

FCC is a long term project. In many respects novel, and new calculations including simulation programs will be appearing in the forthcoming years. However, many of the approaches developed for the previous experiments, in particular LEP will be useful, either directly as a tools or as a means to prepare substantial benchmarks. Also programs which will be prepared for Belle II, especially in domain of τ, B and D resonance physics will continue to be valuable tools. Such programs and projects will undoubtedly evolve in the mean time, but one can expect that ready to use versions will be available when the need will arrive. Then only interfaces will need to be archived solely for the FCC need. In some cases the whole projects will require long term archivization. Before we will explain some attempts on archivization of some example projects, such as τ decays, radiative corrections in decays or electroweak corrections, let us mention general possible approaches.

There are many tools helpful to manage software projects: development and archivization. However, archivization-development tools become obsolete and code history, necessarily for future extensions and validation may become lost and therefore it is important to ensure proper migration from one archivization-development to the other. In addition, very stable solutions belong to repositories outside of authors responsibility and specifically targeting long term of archivization.

Library of CPC http://www.cpc.cs.qub.ac.uk/ serve such purpose, also the CERN web pages like the one used for TAUOLA [1] or PHOTOS [2] may offer necessary facility too.

Issues arrive if parts of the code is prepared with automated code development tools. If those tools (i.e. other programs) are not published, the programs prepared with their help are of limited help for future applications, especially if extensions are needed.

The interfaces between segments of the code can be of a different type. Comfort offered on solutions based on some tools is indisputable, but can be overshadowed if such tool evolves in unsuitable time. We have experienced minor, but at inconvenient moments for our project evolution difficulties due to ROOT library [3] new versions. By hand intervention on our side, and change of the work routine was necessary [4]. Because many of software development projects of phenomenology represent fraction of the total effort and often involved people may not be immediately available, this may represent a major inconvenience.

1.1 Common tools for all FCC design studies

As already mentioned it is of crucial importance to have a common software platform with all the repositories. In FCC this effort has begun with creation of twiki page: https://twiki.cern.ch/twiki/bin/view/FCC/CommonTools, where different MC generators are available. This

collection should be extended with documentation of programs, links to available original `git` repositories, etc. Everybody is welcome to link or put there related codes or results to be used in future software.

Presently it includes three sections:

- FccComputing, section containing installation procedure of the FCCee software is described.
- FccGenerators, section with different MC generators. Currently Tauola, Higgsline, KKMC and Bhabha generators are presented.
- FccSoftware, section with various examples of running the simulations in FCC framework.

Below we will present shortly currently available generators and discuss their preservation.

1.1.1 Tauola

The τ decays phenomenology, rely to a large degree on experimental data. This is because of complexity of experimental analyzes on one side and on difficulty for phenomenology modelling decays where intermediate resonances used in hadronic currents are broad and perturbative QCD description is only in part suitable. Background analysis for multi-dimensional distributions is a problem. Collaborations are hesitant to enable outside use of their matrix element parametrizations, because the may be unsuitable for other, than internally collaboration studied, distributions. Nevertheless, if they become available it is worthwhile to store them in publicly available repositories. In Ref. [5] parametrizations developed for Aleph and Cleo were archived, together with the original one, useful for technical test of Tauola algorithm. In [6] thanks to discussion with BaBar community extension of Tauola with multi-channel capacity easy to manipulate by users was prepared. Resulting default parametrization equivalent to that work was archived in [7]. In that reference, framework for work with C++ currents and for Belle II was prepared. Hopefully it may provide way for feed back code at FCC time. Smooth transition period for evolution from partly Fortan to fully C++ code is envisaged in this solution.

1.1.2 Photos and Tauola Universal interface

The code for these projects is at a time in C++. Archivization of the up to date variants is assured thanks to CERN special accounts and web pages [1, 2]. Some versions are archived in CPC. References [8, 9] The main issue for the project is fast evolution of event format HepMC [10], and specially the way how other projects use that format to write down generated events. Also, long term archivization effort may suffer because of evolution of configuration and makefile arrangements.

1.1.3 EvtGen

The decays of heavy flavoured hadrons provide huge constrains on Beyond Standard Model physics [11]. FCCee due to runs on the Z pole will be also a heavy flavour factory. The decays of such mesons and hadrons are modeled with the `EvtGen` package [12]. The package consists of various models, which are constantly being updated with the theory predictions, such as form factors and amplitude calculations. Currently the main developers of `EvtGen` are involved in LHCb collaboration, however the package is made publicly available [13] via git repository. It was recently extended to describe the decays of spin 1/2 particles. The project is written in

C++ and interference's the HepMC format [10]. It is also possible to interface is with `Tauola`, `Pythia` and `Photos` packages.

1.1.4 Electroweak corrections

The `KKMC` code is published and archived with ref. [14], Its electroweak correction library, used until today is also published and archived: `Dizet` version `6.21` [15,16]. At present, only `Dizet` version 6.42 [17,18] was available for the `KKMC` electroweak sector upgrade. This version of `Dizet` was missing updates due to the photonic vacuum polarization, e.g. as provided in refs. [19,20]. We could do it ourselves because `Dizet` version 6.42 is well documented. But some versions of `Dizet` which exist still at present, may become not available some time. In fact it was difficult for us to get an access and we decided to retreat to version 6.42. This point to necessity for the code maintenance, even if at a certain time authors may become not anymore available.

Anyway, this `Dizet` version 6.42 [17,18] with updates from refs. [19,20] is prepared as a facility for the electroweak tables used in `KKMC` [14].

The tables prepared by one program to be used by other one is not only the method to enhance speed of the calculation. Interpolation of values enable technical regularization of the functions. Technical instabilities at the phase space edges can be regulated.

The tables can be used by other programs which understand the format. In this way, for example `TauSpinner` package [9,21] can be used for graphical presentation for different variants of `Dizet` and of its initialization as natural continuation of work [22] for LHC or similar activity for FCC.

This limit substantially burden for interfaces. Archivization of the projects is only partly assured by the CPC publications. Most up to date versions are available by the user webpages, which sometimes are not available or may become non available.

References

[1] Tauola, http://tauolapp.web.cern.ch/tauolapp/TAUOLA/TauSpinner/examples/Dizet-example.

[2] Photos, http://photospp.web.cern.ch/photospp/.

[3] R. Brun, F. Rademakers, ROOT: An object oriented data analysis framework, Nucl. Instrum. Meth. A389 (1997) 81–86. doi:10.1016/S0168-9002(97)00048-X.

[4] We had to modified code of our projects due to changes of Root library: in July 2002 and now again for the changes introduced with Root release 6.

[5] P. Golonka, B. Kersevan, T. Pierzchala, E. Richter-Was, Z. Was, M. Worek, The Tauola photos F environment for the TAUOLA and PHOTOS packages: Release. 2., Comput. Phys. Commun. 174 (2006) 818–835. arXiv:hep-ph/0312240, doi:10.1016/j.cpc.2005.12.018.

[6] Z. Was, P. Golonka, TAUOLA as tau Monte Carlo for future applications, Nucl. Phys. Proc. Suppl. 144 (2005) 88–94, [,88(2004)]. arXiv:hep-ph/0411377, doi:10.1016/j.nuclphysbps.2005.02.012.

[7] M. Chrzaszcz, T. Przedzinski, Z. Was, J. Zaremba, TAUOLA of τ lepton decays-framework for hadronic currents, matrix elements and anomalous decays, Comput. Phys. Commun. 232 (2018) 220–236. arXiv:1609.04617, doi:10.1016/j.cpc.2018.05.017.

[8] N. Davidson, T. Przedzinski, Z. Was, PHOTOS interface in C++: Technical and Physics Documentation, Comput. Phys. Commun. 199 (2016) 86–101. arXiv:1011.0937, doi:10.1016/j.cpc.2015.09.013.

[9] N. Davidson, G. Nanava, T. Przedzinski, E. Richter-Was, Z. Was, Universal Interface of TAUOLA Technical and Physics Documentation, Comput. Phys. Commun. 183 (2012) 821–843. arXiv:1002.0543, doi:10.1016/j.cpc.2011.12.009.

[10] M. Dobbs, J. B. Hansen, The HepMC C++ Monte Carlo event record for High Energy Physics, Comput. Phys. Commun. 134 (2001) 41–46. doi:10.1016/S0010-4655(00)00189-2.

[11] J. Aebischer, W. Altmannshofer, D. Guadagnoli, M. Reboud, P. Stangl, D. M. Straub, B-decay discrepancies after Moriond 2019, arXiv:1903.10434.

[12] Evtgen, https://evtgen.hepforge.org/.

[13] Evtgen, https://phab.hepforge.org/source/evtgen.

[14] S. Jadach, B. F. L. Ward, Z. Was, The Precision Monte Carlo event generator K K for two fermion final states in e+ e- collisions, Comput. Phys. Commun. 130 (2000) 260–325. arXiv:hep-ph/9912214, doi:10.1016/S0010-4655(00)00048-5.

[15] D. Yu. Bardin, M. S. Bilenky, T. Riemann, M. Sachwitz, H. Vogt, Dizet: A Program Package for the Calculation of Electroweak One Loop Corrections for the Process $e^+e^- \to f^+f^-$ Around the Z^0 Peak, Comput. Phys. Commun. 59 (1990) 303–312. doi:10.1016/0010-4655(90)90179-5.

[16] D. Yu. Bardin, P. Christova, M. Jack, L. Kalinovskaya, A. Olchevski, S. Riemann, T. Riemann, ZFITTER v.6.21: A Semianalytical program for fermion pair production in e+ e- annihilation, Comput. Phys. Commun. 133 (2001) 229–395. arXiv:hep-ph/9908433, doi:10.1016/S0010-4655(00)00152-1.

[17] A. Andonov, A. Arbuzov, D. Bardin, S. Bondarenko, P. Christova, L. Kalinovskaya, V. Kolesnikov, R. Sadykov, Standard SANC Modules, Comput. Phys. Commun. 181 (2010) 305–312. arXiv:0812.4207, doi:10.1016/j.cpc.2009.10.004.

[18] A. Akhundov, A. Arbuzov, S. Riemann, T. Riemann, The ZFITTER project, Phys. Part. Nucl. 45 (3) (2014) 529–549. arXiv:1302.1395, doi:10.1134/S1063779614030022.

[19] H. Burkhardt, B. Pietrzyk, Low energy hadronic contribution to the QED vacuum polarization, Phys. Rev. D72 (2005) 057501. arXiv:hep-ph/0506323, doi:10.1103/PhysRevD.72.057501.

[20] F. Jegerlehner, Variations on Photon Vacuum PolarizationarXiv:1711.06089.

[21] Z. Czyczula, T. Przedzinski, Z. Was, TauSpinner Program for Studies on Spin Effect in tau Production at the LHC, Eur. Phys. J. C72 (2012) 1988. arXiv:1201.0117, doi:10.1140/epjc/s10052-012-1988-z.

[22] E. Richter-Was, Z. Was, The TauSpinner approach for electroweak corrections in LHC Z to ll observables, arXiv:1808.08616.

2 Scalar 1-loop Feynman integrals in arbitrary space-time dimension d – an update

Authors: Tord Riemann, Johann Usovitsch
Corresponding Author: Tord Riemann [tordriemann@gmail.com]

2.1 Introduction

The study and use of analyticity of scattering amplitudes was founded by R. Eden, P. Landshoff, D. Olive and J. Polkinghorn in their famous book "The Analytic S-Matrix" in 1966 [1]. Indeed, already in 1969 J. Schwinger quotes: "One of the most remarkable discoveries in elementary particle physics has been that of the complex plane," "... the theory of functions of complex variables plays the role not of a mathematical tool, but of a fundamental description of nature inseperable from physics. ..." [2].

It took many years to make the use of analyticity and unitarity, together with renormalizability and gauge invariance of quantum field theory a practical tool for the calculation of cross sections at real colliders. When the analysis of LEP 1 data, around 1989, was prepared it became evident that the S-matrix language helps to efficiently sort the various perturbative contributions of the Standard Model.

The scattering amplitude for the reaction $e^+e^- \to (Z,\gamma) \to f\bar{f}$ at LEP energies depends on two variables s and $\cos\theta$, and the integrated cross section may be described by an analytical function of s with a simple pole, describing mass and width of the Z resonance:

$$A = \frac{R}{s - M_Z^2 + iM_Z\Gamma_Z} + \sum_{i=0}^{\infty} a_i (s - M_Z^2 + iM_Z\Gamma_Z)^i. \tag{2.1}$$

Here, position $s_0 = M_Z^2 - iM_Z\Gamma_Z$ and residue R of the pole as well as the background expansion are of interest. The analytic form of (2.1) has to be respected when deriving a Z amplitude at multiloop accuracy; see [3] and the references therein.

Shortly after the work by Eden et al., physical amplitudes were proposed to be considered also as complex functions of space-time dimension d (dimensional regularization), in C. Bollini and J. Giambiagi, "Dimensional Renormalization: The Number of Dimensions as a Regularizing Parameter" (1972) [4] and G. 't Hooft and M. Veltman, "Regularization and renormalization of gauge fields" (1972) [5].

In perturbative calculations with dimensional regularization, Feynman integrals I are complex functions of the space-time dimension $d = 4 - 2\varepsilon$. In fact, they are meromorphic functions of d and may be expanded in Laurent series around poles at *e.g.* $d_s = 4+2N_0, N_0 \geq 0$. Be J_n an n-point one-loop Feynman integral as shown in figure C.1:

$$J_n \equiv J_n(d; \{p_i p_j\}, \{m_i^2\}) = \int \frac{d^d k}{i\pi^{d/2}} \frac{1}{D_1^{\nu_1} D_2^{\nu_2} \cdots D_n^{\nu_n}} \tag{2.2}$$

with

$$D_i \;=\; \frac{1}{(k+q_i)^2 - m_i^2 + i\epsilon} \tag{2.3}$$

and

$$\nu \;=\; \sum_{i=1}^{n} \nu_i, \qquad \sum_{e=1}^{n} p_e = 0. \tag{2.4}$$

The Feynman integrals are analytical functions of d everywhere with exclusion of isolated singular points d_s, where they behave not worse than

$$\frac{A_s}{(d-d_s)^{N_s}}. \tag{2.5}$$

In physics applications, we need the Feynman integrals at a potentially singular point, $d = 4$, so that the general behaviour of them at non-singular points is not in the original focus. Nevertheless, the question arises:

Can we determine the general d-dependence of a Feynman integral?

For one-loop integrals, the question has been answered recently, in K.H. Phan, T. Riemann, "Scalar 1-loop Feynman integrals as meromorphic functions in space-time dimension d" (2018) [6].

At the begin of systematic cross-section calculations in d dimensions, there are two seminal papers on 1-loop Feynman integrals in dimensional regularization: Passarino, Veltman (Feb. 1978), "One Loop Corrections for e^+e^- Annihilation into $\mu^+\mu^-$ in the Weinberg Model" [7] and 't Hooft, Veltman (Nov. 1978), "Scalar oneloop integrals" [8]. Later, many improvements and generalizations were introduced in various respects.

We see several reasons to study the d-dependence of one-loop Feynman integrals and will discuss them shortly in the next subsection.

2.2 Interests in the *d*-dependence of one-loop Feynman integrals

2.2.1 Interest from mathematical physics

There is a general interest to know the Feynman integrals as meromorphic functions of space-time dimension d, and the easiest case is that of one loop. Early attempts, for the massless case, trace back to E. Boos and A. Davydychev (1986), "A Method of the Evaluation of the Vertex Type Feynman Integrals" [9]. The general one-loop integrals were tackled systematically by O. Tarasov et al. since the nineteen nineties; see e.g. [10–13] and references therein. In J. Fleischer, F. Jegerlehner, O. Tarasov (2003), "A new hypergeometric representation of one loop scalar integrals in d dimensions" [14, 15], the class of generalized hypergeometric functions for massive one-loop Feynman integrals with unit indices was determined and studied with a novel approach based on dimensional difference equations:

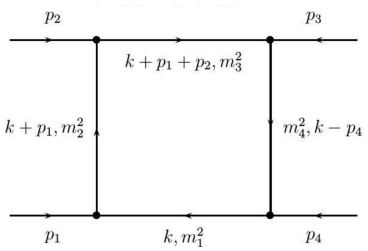

Fig. C.1: *One-loop Feynman integral.*

– ${}_2F_1$ Gauss hypergeometric functions are needed for self-energies;
– F_1 Appell functions are needed for vertices;
– F_S Lauricella-Saran functions are needed for boxes.

Finally, the correct, general massive one-loop one- to four-point functions with unit indices at arbitrary kinematics were determined by K.H. Phan and T.R. (2018) in [6], where also the numerics of the generalized hypergeometric functions was worked out.

2.2.2 Interest from tensor reductions of n-point functions in higher space-time dimensions

For many-particle calculations, there appear at certain kinematical configurations p_i inverse Gram determinants $1/G(p_i)$ from tensor reductions. These terms $1/G(p_i)$ may diverge, because Gram determinants can exactly vanish: $G(p_i) \equiv 0$. One may perform tensor reductions so that no inverse Gram determinants appear. But then one has to calculate scalar 1-loop integrals in higher dimensions, $D = 4 + 2n - 2\epsilon, n > 0$. See [16, 17]. In fact, one introduces new scalar integrals [16]. Let us take as an example a rank-5 tensor of an n-point function:

$$\begin{aligned} I_n^{\mu\,\nu\,\lambda\,\rho\,\sigma} &= \int \frac{d^dk}{i\pi^{d/2}} \; \frac{k^\mu\, k^\nu\, k^\lambda\, k^\rho\, k^\sigma}{\prod_{j=1}^n c_j} \\ &= -\sum_{i,j,k,l,m=1}^{n} q_i^\mu\, q_j^\nu\, q_k^\lambda\, q_l^\rho\, q_m^\sigma\, n_{ijklm}\; I^{[d+]^5}_{n,ijklm} \\ &\quad + \frac{1}{2}\sum_{i,j,k=1}^{n} g^{[\mu\nu} q_i^\lambda q_j^\rho q_k^{\sigma]}\, n_{ijk}\, I^{[d+]^4}_{n,ijk} - \frac{1}{4}\sum_{i=1}^{n} g^{[\mu\nu} g^{\lambda\rho} q_i^{\sigma]}\; I^{[d+]^3}_{n,i}. \end{aligned} \tag{2.6}$$

The integrals $I^{[d+]^l}_{n,ab\ldots}$ are special cases of $I^{[d+]^l,s}_{n,ab\ldots}$, defined in $[d+]^l = 4 - 2\varepsilon + 2l$ dimensions, by shrinking line s and raising the powers of propagators (indices) $a, b, \ldots$.

At this step, the tensor integral is represented by scalar integrals with higher space-time dimensions and higher propagator powers. The publicly available Feynman integral libraries deliver, though, ordinary scalar integrals in $d = 4 - 2\varepsilon$ dimensions and with unit propagator powers. With the usual integration-by-parts reduction technique [18, 19] one may shift indices, i.e. reduce propagator powers to unity:

$$\nu_j \mathbf{j}^+ I_5 = \frac{1}{\binom{0}{0}_5} \sum_{k=1}^{5} \binom{0j}{0k}_5 \left[d - \sum_{i=1}^{5} \nu_i (\mathbf{k}^- \mathbf{i}^+ + 1) \right] I_5. \tag{2.7}$$

The operators $\mathbf{i}^\pm, \mathbf{j}^\pm, \mathbf{k}^\pm$ act by shifting the indices ν_i, ν_j, ν_k by ± 1.

After this step, one has yet to deal with scalar functions in $d = 4-2\varepsilon+2l$ dimensions. This may be further reduced by applying dimensional reduction formulas invented by O. Tarasov (1996) [10, 13]. Shift of dimension and index:

$$\nu_j \left(\mathbf{j}^+ I_5^{[d+]} \right) = \frac{1}{()_5} \left[-\binom{j}{0}_5 + \sum_{k=1}^{5} \binom{j}{k}_5 \mathbf{k}^- \right] I_5, \tag{2.8}$$

and also shift of only dimension:

$$(d - \sum_{i=1}^{5} \nu_i + 1) I_5^{[d+]} = \frac{1}{()_5} \left[\binom{0}{0}_5 - \sum_{k=1}^{5} \binom{0}{k}_5 \mathbf{k}^- \right] I_5. \tag{2.9}$$

The procedure is elegant, but it introduces in both cases inverse powers of potentially vanishing Gram determinants. As a consequence, one has finally to treat in sophisticated ways their numerical implications.

At this stage one might try an alternative: Perform the reductions of tensor functions to scalar ones with unit indices, but allowing for the use of higher space-time dimensions. This avoids the vanishing inverse Gram problem, but introduces the need of a library of scalar Feynman integrals in higher dimensions. This idea makes it attractive to derive an algorithm allowing the systematic calculation of scalar one- to n-point functions in arbitrary dimensions, and to implement a numerical solution for that.

To be a bit more definite, we quote here some unpublished formulae from [17, 20]. The following reduction of a 5-point tensor in terms of tensor coefficients E^s_{ijklm}, with line s skipped from the 5-point integral, may be used as a starting point:

$$I_5^{\mu\,\nu\,\lambda\rho\sigma} = \sum_{s=1}^{5}\left[\sum_{i,j,k,l,m=1}^{5} q_i^\mu q_j^\nu q_k^\lambda q_l^\rho q_m^\sigma E^s_{ijklm} + \sum_{i,j,k=1}^{5} g^{[\mu\nu} q_i^\lambda q_j^\rho q_k^{\sigma]} E^s_{00ijk} + \sum_{i=1}^{5} g^{[\mu\nu} g^{\lambda\rho} q_i^{\sigma]} E^s_{0000i}\right]. \tag{2.10}$$

The tensor coefficients E^s_{ijklm} are expressed in terms of integrals $I^{[d+]^l,s}_{4,i\cdots}$, e.g.:

$$E^s_{ijklm} = -\frac{1}{\binom{0}{0}_5}\left\{\left[\binom{0l}{sm}_5 n_{ijk} I^{[d+]^4,s}_{4,ijk} + (i\leftrightarrow l) + (j\leftrightarrow l) + (k\leftrightarrow l)\right] + \binom{0s}{0m}_5 n_{ijkl} I^{[d+]^4,s}_{4,ijkl}\right\}. \tag{2.11}$$

No factors $1/G_5 = \binom{}{}_5$ appear. Now, in a next step, one may avoid the appearance of inverse sub-Gram determinants $()_4$. Further, the complete dependence on the indices i of the tensor coefficients can be shifted into the integral's pre-factors with signed minors. One can say that the indices *decouple* from the integrals. As an example, we reproduce the 4-point part of $I^{[d+]^4}_{4,ijkl}$:

$$\begin{aligned}
n_{ijkl} I^{[d+]^4}_{4,ijkl} &= \frac{\binom{0}{i}}{\binom{0}{0}}\frac{\binom{0}{j}}{\binom{0}{0}}\frac{\binom{0}{k}}{\binom{0}{0}}\frac{\binom{0}{l}}{\binom{0}{0}} d(d+1)(d+2)(d+3) I_4^{[d+]^4} \\
&+ \frac{\binom{0i}{0j}\binom{0}{k}\binom{0}{l} + \binom{0i}{0k}\binom{0}{j}\binom{0}{l} + \binom{0j}{0k}\binom{0}{i}\binom{0}{l} + \binom{0i}{0l}\binom{0}{j}\binom{0}{k} + \binom{0j}{0l}\binom{0}{i}\binom{0}{k} + \binom{0k}{0l}\binom{0}{i}\binom{0}{j}}{\binom{0}{0}^3} \\
&\times\ d(d+1) I_4^{[d+]^3} \\
&+ \frac{\binom{0i}{0l}\binom{0j}{0k} + \binom{0j}{0l}\binom{0i}{0k} + \binom{0k}{0l}\binom{0i}{0j}}{\binom{0}{0}^2} I_4^{[d+]^2} \quad + \quad \cdots
\end{aligned} \tag{2.12}$$

In (2.12), one has to understand the 4-point integrals to carry the corresponding index s of (2.10) and the signed minors are $\binom{0}{k} \to \binom{0s}{ks}_5$ etc. We arrived at:
✓ No scalar 5-point integrals in higher dimensions.
✓ No inverse Gram determinants $()_5$.
✓ The 4-point integrals are without indices.
† Scalar 4-point integrals in higher dimensions appear: $I_4^{[d+]^2,s}$ etc.
† Inverse 4-point Gram determinants $\binom{0}{0}_5 \equiv ()_4$ appear.

2.2.3 Interest from multi-loop calculations

Higher-order loop calculations need higher-order contributions from ϵ-expansions of one-loop terms, typically stemming from the expansions

$$\frac{1}{d-4} = -\frac{1}{2\epsilon} \tag{2.13}$$

and

$$\Gamma(\epsilon) = \frac{a_1}{\epsilon} + a_0 + a_1\epsilon + \cdots \tag{2.14}$$

A seminal paper on the ε-terms of one-loop functions is U. Nierste, D. Müller, M. Böhm, (1992), "Two loop relevant parts of D-dimensional massive scalar one loop integrals" [21]. A general analytical solution of the problem of determining the general ε-expansion of Feynman integrals is unsolved so far, even for the one-loop case. Though, see the series of papers by G. Passarino et al. [22–25]. The determination of one-loop Feynman integrals as meromorphic functions of d might be a useful preparatory step for determining the pole expansion in d around e.g. $d = 4$.

2.2.4 Interest from Mellin-Barnes representations

A powerful approach to arbitrary Feynman integrals is based on Mellin-Barnes representations [26, 27]. One-loop integrals with variable, in general non-integer indices are needed in the context of the *loop-by-loop Mellin-Barnes approach* to multi-loop integrals. Details may be found in the literature on the Mathematica package AMBRE [28–35], and in references therein.

A crucial technical problem of the Mellin-Barnes representations arises from the rising number of dimensions of these representations with a rising number of physical scales. We will detail this in subsection 2.3.1. So there is an unresolved need of low-dimensional one-loop MB-integrals, with arbitrary indices.

2.3 Mellin-Barnes representations for one-loop Feynman integrals

There are two numerical MB-approaches advocated.

2.3.1 AMBRE

There are several ways to take advantage of Mellin-Barnes representations for the calculation of Feynman integrals. One approach is the replacement of massive propagators by Mellin-Barnes integrals over massless propagators, invented by N. Usyukina (1975) [36]. Another approach transforms the Feynman parameter representation with Mellin-Barnes representations into multiple complex path integrals, invented in 1999 by V. Smirnov for planar diagrams [26] and B. Tausk for non-planar diagrams [27]. This approach implies "automatically" a general solution of the infra-red problem and has been worked out in the AMBRE approach [28, 32, 34, 35, 37].

The general definitions for a multi-loop Feynman integral are:

$$J_n^L \equiv J_n^L(d; \{p_i p_j\}, \{m_i^2\}) = \int \prod_{j=1}^{L} \frac{d^d k_j}{i\pi^{d/2}} \frac{1}{D_1^{\nu_1} D_2^{\nu_2} \cdots D_n^{\nu_n}} \tag{2.15}$$

with

$$D_i = \left(\sum_{l=1}^{L} a_{il} k_l + \sum_{e=1}^{E} b_{ie} p_e \right)^2 - m_i^2 + i\delta, \; a_{il}, \; b_{ie} \in \{-1, 0, 1\}, \tag{2.16}$$

where m_i are the masses, p_e the external momenta, k_l the loop momenta, $i\delta$ the Feynman prescription and finally ν_i the complex variables.

With the following Feynman trick we get a really neat parametric representation:

$$\frac{(-1)^\nu}{\prod\limits_{j=1}^{n}(-D_j^{\nu_j})} = \frac{(-1)^\nu\Gamma(\nu)\left(\prod\limits_{j=1}^{n}\int\limits_{\{x_j\geq 0\}}\frac{dx_j\,x_j^{\nu_j-1}}{\Gamma(\nu_j)}\right)\delta(1-\sum\limits_{j=1}^{n}x_j)}{(-k_l^\mu M_{ll'}k_{l'\mu}+2k_l^\mu Q_{l\mu}+J-i\delta)^\nu},\quad \nu=\sum_{j=1}^{n}\nu_j, \tag{2.17}$$

where

$$M_{ll'} = \sum_{j=1}^{n} a_{jl}a_{jl'}x_j \tag{2.18}$$

is an $L\times L$ symmetric matrix,

$$Q_l^\nu = -\sum_{j=1}^{n} x_j a_{jl}\sum_{e=1}^{E} b_{je}p_e^\nu \tag{2.19}$$

is a vector with L components and

$$J = -\sum_{j=1}^{n} x_j\left(\sum_{e=1}^{E} b_{je}p_e^\mu \sum_{e'=1}^{E} p_{e'}^\nu b_{je'}g_{\mu\nu} - m_j^2\right), \tag{2.20}$$

where x_j are the Feynman parameters introduced with the Feynman trick. The metric tensor is $g_{\mu\nu}=\mathrm{diag}(1,-1,\ldots,-1)$.

The Feynman integral can now be written in the Feynman parameter integral representation:

$$J_n^L = (-1)^\nu\Gamma(\nu-LD/2)\left(\prod_{j=1}^{n}\int\limits_{\{x_j\geq 0\}}\frac{dx_j\,x_j^{\nu_j-1}}{\Gamma(\nu_j)}\right)\delta(1-\sum_{j=1}^{n}x_j)\frac{U(x)^{\nu-(L+1)D/2}}{F(x)^{\nu-LD/2}}, \tag{2.21}$$

where

$$U(x) = \det M, \tag{2.22}$$

$$F(x) = U(x)(Q_l^\mu M_{ll'}^{-1}Q_{l'\mu}+J-i\delta). \tag{2.23}$$

From these definitions it follows that the functions $F(x)$ and $U(x)$ are homogeneous in the Feynman parameters x_i. The function $U(x)$ is of degree L and the function $F(x)$ is of degree $L+1$. The functions $U(x)$ and $F(x)$ are also known as Symanzik polynomials.

At one loop level the definition of the Feynman integral simplifies drastically and gives many insights straight away which we will bring to light in this work:

$$J_n \equiv J_n(d;\{p_ip_j\},\{m_i^2\}) = \int\frac{d^dk}{i\pi^{d/2}}\frac{1}{D_1^{\nu_1}D_2^{\nu_2}\cdots D_n^{\nu_n}} \tag{2.24}$$

with propagators depending only on one loop momenta:

$$D_i = \frac{1}{(k+q_i)^2-m_i^2+i\epsilon}, \tag{2.25}$$

with

$$q_i = \sum_{e=1}^{i} p_e. \tag{2.26}$$

We assume here for brevity

$$\nu_i \;=\; 1, \quad \sum_{e=1}^{n} p_e = 0. \tag{2.27}$$

If we take the argument of the Dirac delta function to be $1 - \sum_{j=1}^{n} x_j$ the Feynman parameter representation for one-loop Feynman integrals simplifies to:

$$J_n \;=\; (-1)^n \Gamma\left(n - d/2\right) \int_0^1 \prod_{i=1}^{n} dx_i \delta\left(1 - \sum_{j=1}^{n} x_j\right) \frac{1}{F_n(x)^{n-d/2}}. \tag{2.28}$$

Here, the F-function is the second Symanzik polynomial, which is just of second degree in the Feynman parameters:

$$F_n(x) \;=\; \frac{1}{2} \sum_{i,j} x_i Y_{ij} x_j - i\epsilon. \tag{2.29}$$

The Y_{ij} are elements of the Cayley matrix $Y = (Y_{ij})$,

$$Y_{ij} = Y_{ji} \;=\; m_i^2 + m_j^2 - (q_i - q_j)^2. \tag{2.30}$$

Gram and Cayley determinants were introduced by Melrose (1965) [38]; see also [13]. The $(n-1) \times (n-1)$ dimensional Gram determinant $G_n \equiv G_{12\cdots n}$ is

$$G_n = - \begin{vmatrix} (q_1 - q_n)^2 & (q_1 - q_n)(q_2 - q_n) & \dots & (q_1 - q_n)(q_{n-1} - q_n) \\ (q_1 - q_n)(q_2 - q_n) & (q_2 - q_n)^2 & \dots & (q_2 - q_n)(q_{n-1} - q_n) \\ \vdots & \vdots & \ddots & \vdots \\ (q_1 - q_n)(q_{n-1} - q_n) & (q_2 - q_n)(q_{n-1} - q_n) & \dots & (q_{n-1} - q_n)^2 \end{vmatrix}. \tag{2.31}$$

The $2^n G_n$ equals notationally the G_{n-1} of [13]. Evidently, the Gram determinant G_n is independent of the propagator masses.

The Cayley determinant $\Delta_n = \lambda_{12\dots n}$ is composed of the Y_{ij} introduced in (2.30):

$$\text{Cayley determinant}: \quad \Delta_n = \lambda_n \equiv \lambda_{12\dots n} \;=\; \begin{vmatrix} Y_{11} & Y_{12} & \dots & Y_{1n} \\ Y_{12} & Y_{22} & \dots & Y_{2n} \\ \vdots & \vdots & \ddots & \vdots \\ Y_{1n} & Y_{2n} & \dots & Y_{nn} \end{vmatrix}. \tag{2.32}$$

We also define the modified Cayley determinant

$$\text{modified Cayley determinant}: \quad ()_n \;=\; \begin{vmatrix} 0 & 1 & 1 & \dots & 1 \\ 1 & Y_{11} & Y_{12} & \dots & Y_{1n} \\ 1 & Y_{12} & Y_{22} & \dots & Y_{2n} \\ \vdots & \vdots & \vdots & \ddots & \vdots \\ 1 & Y_{1n} & Y_{2n} & \dots & Y_{nn} \end{vmatrix}. \tag{2.33}$$

The determinants Δ_n, $()_n$ and G_n are evidently independent of a common shifting of the momenta q_i.

One may use Mellin-Barnes integrals [39],

$$\frac{1}{(1+z)^\lambda} = \frac{1}{2\pi i}\int\limits_{-i\infty}^{+i\infty} ds\, \frac{\Gamma(-s)\,\Gamma(\lambda+s)}{\Gamma(\lambda)}\, z^s = {}_2F_1\left[\begin{array}{c} \lambda, b\,; \\ b\,; \end{array} -z\right], \tag{2.34}$$

in order to split the sum $F_n(x)$ in (2.29) into a product, getting nested MB-integrals to be calculated. For some mathematics behind the derivation, see the corollary at p. 289 in [40]). Eqn. (2.34) is valid if $|\mathrm{Arg}(z)| < \pi$. The integration contour has to be chosen such that the poles of $\Gamma(-s)$ and $\Gamma(\lambda+s)$ are well-separated. The right hand side of (2.34) is identified as Gauss' hypergeometric function.

There are $N_n = \frac{1}{2}n(n+1)$ different Y_{ij} for n-point functions, leading to $N_n = [\frac{1}{2}n(n+1)-1]$ dimensional Mellin-Barnes integrals when splitting the sum in (2.29) into a product:

- $N_3 = 5$ MB-dimensions for the most general massive vertices;
- $N_4 = 9$ MB-dimensions for the most general massive box integrals;
- $N_5 = 14$ MB-dimensions for the most general massive pentagon integrals.

The introduction of N_n-dimensional MB-integrals allows to perform the x-integrations. The MB-integrations have to be performed afterwards, and this raises some mathematical problems with rising integral dimensions. This is, for Mellin-Barnes integrals numerical applications, one of the most important limiting factors.

For further details of this approach, we refer to the quoted literature on AMBRE and MBnumerics.

2.3.2 MBOneLoop

A completely different approach was initiated in [6, 41]. The idea is based on rewriting the F-function in (2.28) by exploring the factor $\delta(1-\sum x_i)$ which makes the n-fold x-integration to be an integral over an $(n-1)$-simplex.

The δ-function allows for the elimination of x_n, just one of the x_i, which creates linear terms in the remaining x_i-variables in the F-function:

$$F_n(x) = x^T G_n x + 2H_n^T x + K_n. \tag{2.35}$$

The $F_n(x)$ may be re-cast back into a bilinear form by shifts $x \to (x-y)$,

$$F_n(x) = (x-y)^T G_n (x-y) + r_n - i\varepsilon = \Lambda_n(x) + r_n - i\varepsilon = \Lambda_n(x) + R_n. \tag{2.36}$$

As a result, there is a separation of F into a homogeneous part $\Lambda_n(x)$,

$$\Lambda_n(x) = (x-y)^T G_n (x-y), \tag{2.37}$$

and an inhomogeneity R_n,

$$R_n = r_n - i\varepsilon = K_n - H_n^T G_n^{-1} H_n - i\varepsilon = -\frac{\lambda_n}{g_n} - i\varepsilon = -\frac{\left(\begin{array}{c} 0 \\ 0 \end{array}\right)_n}{()_n}. \tag{2.38}$$

It is only this inhomogeneity $R_n = r_n - i\varepsilon$ who carries the $i\varepsilon$-prescription. The $(n-1)$ components y_i of the shift vector y appearing here in $F_n(x)$ are:

$$y_i = -\left(G_n^{-1} K_n\right)_i, \quad i \neq n. \tag{2.39}$$

The following relations are also valid:

$$y_i = \frac{\partial r_n}{\partial m_i^2} = -\frac{1}{g_n}\frac{\partial \lambda_n}{\partial m_i^2} = -\frac{\partial_i \lambda_n}{g_n} = \frac{2}{g_n}\begin{pmatrix} 0 \\ i \end{pmatrix}_n, \quad i = 1 \cdots n. \tag{2.40}$$

One further notation has been introduced in (2.40), namely that of *co-factors of the modified Cayley matrix*, also called signed minors in e.g. [38, 42]:

$$\begin{pmatrix} j_1 & j_2 & \cdots j_m \\ k_1 & k_2 & \cdots k_m \end{pmatrix}_n. \tag{2.41}$$

The signed minors are determinants, labeled by those rows $j_1, j_2, \cdots j_m$ and columns $k_1, k_2, \cdots k_m$ which have been discarded from the definition of the modified Cayley determinant $()_n$, with a sign convention:

$$\begin{aligned} \text{sign}\begin{pmatrix} j_1 & j_2 & \cdots j_m \\ k_1 & k_2 & \cdots k_m \end{pmatrix}_n &= (-1)^{j_1+j_2+\cdots+j_m+k_1+k_2+\cdots+k_m} \times \texttt{Signature}[j_1, j_2, \cdots j_m] \\ &\quad \times \texttt{Signature}[k_1, k_2, \cdots k_m]. \end{aligned} \tag{2.42}$$

Here, `Signature` (defined like the Wolfram Mathematica command) gives the sign of permutations needed to place the indices in increasing order. The Cayley determinant is a signed minor of the modified Cayley determinant,

$$\Delta_n = \lambda_n = \begin{pmatrix} 0 \\ 0 \end{pmatrix}_n. \tag{2.43}$$

For later use, we introduce also

$$y_n = 1 - \sum_{i-1}^{n-1} y_i \equiv \frac{\partial r_n}{\partial m_n^2}. \tag{2.44}$$

The auxiliary condition $\sum_i^n y_i = 1$ is fulfilled. Further, the notations for the F-function are finally independent of the choice of the variable which was eliminated by the use of the δ-function in the integrand of (2.28). And the inhomogeneity R_n is the only variable carrying the causal $i\epsilon$-prescription, while e.g. $\Lambda(x)$ and the y_i are by definition real quantities. The R_n may be expressed by the ratio of the Cayley determinant (2.32) and the Gram determinant (2.31),

$$R_n = r_{1\cdots n} - i\epsilon = -\frac{\lambda_{1\ldots n}}{g_{1\ldots n}} - i\epsilon. \tag{2.45}$$

One may use the Mellin-Barnes relation (2.34) in order to decompose the integrand of J_n given in (2.28) as follows:

$$J_n \sim \int dx \, \frac{1}{[F(x)]^{n-\frac{d}{2}}} \equiv \int dx \, \frac{1}{[\Lambda_n(x) + R_n]^{n-\frac{d}{2}}} \equiv \int dx \, \frac{R_n^{-(n-\frac{d}{2})}}{[1 + \frac{\Lambda_n(x)}{R_n}]^{n-\frac{d}{2}}}$$

$$= \int dx \; \frac{R_n^{-(n-\frac{d}{2})}}{2\pi i} \int\limits_{-i\infty}^{+i\infty} ds \; \frac{\Gamma(-s)\,\Gamma(n-\frac{d}{2}+s)}{\Gamma(n-\frac{d}{2})} \left[\frac{\Lambda_n(x)}{R_n}\right]^s, \quad (2.46)$$

for $|\mathrm{Arg}(\Lambda_n/R_n)| < \pi$. The condition always applies. Further, the integration path in the complex s-plane separates the poles of $\Gamma(-s)$ and $\Gamma(n-\frac{d}{2}+s)$.
As a result of (2.46), the Feynman parameter integral of J_n becomes homogeneous:

$$\begin{aligned} \kappa_n &= \int dx \; \left[\frac{\Lambda_n(x)}{R_n}\right]^s \\ &= \prod_{j=1}^{n-1} \int_0^{1-\sum_{i=j+1}^{n-1} x_i} dx_j \; \left[\frac{\Lambda_n(x)}{R_n}\right]^s \equiv \int dS_{n-1} \; \left[\frac{\Lambda_n(x)}{R_n}\right]^s. \end{aligned} \quad (2.47)$$

In order to reformulate this integral, one may introduce the differential operator $\hat{P}_n$ [43, 44],

$$\frac{\hat{P}_n}{s} \left[\frac{\Lambda_n(x)}{R_n}\right]^s \equiv \sum_{i=1}^{n-1} \frac{1}{2s}(x_i - y_i) \frac{\partial}{\partial x_i} \left[\frac{\Lambda_n(x)}{R_n}\right]^s = \left[\frac{\Lambda_n(x)}{R_n}\right]^s, \quad (2.48)$$

into (2.47):

$$K_n = \frac{1}{s} \int dS_{n-1} \; \hat{P}_n \left[\frac{\Lambda_n(x)}{R_n}\right]^s = \frac{1}{2s} \sum_{i=1}^{n-1} \prod_{k=1}^{n-1} \int_0^{u_k} dx'_k \; (x_i - y_i) \frac{\partial}{\partial x_i} \left[\frac{\Lambda_n(x)}{R_n}\right]^s. \quad (2.49)$$

After performing now one of the x-integrations – by partial integration, eliminating this way the corresponding differential, and applying a Barnes relation [45] (item 14.53 at page 290 of [46]), one arrives at a recursion relation in the number of internal lines n:

$$\begin{aligned} J_n(d, \{q_i, m_i^2\}) &= \frac{-1}{2\pi i} \int\limits_{-i\infty}^{+i\infty} ds \frac{\Gamma(-s)\Gamma(\frac{d-n+1}{2}+s)\Gamma(s+1)}{2\Gamma(\frac{d-n+1}{2})} \left(\frac{1}{R_n}\right)^s \\ &\quad \times \sum_{k=1}^{n} \left(\frac{1}{R_n} \frac{\partial r_n}{\partial m_k^2}\right) \mathbf{k}^- J_n(d+2s; \{q_i, m_i^2\}). \end{aligned} \quad (2.50)$$

The operator $\mathbf{k}^-$, introduced in (2.7), will reduce an n-point Feynman integral J_n to a sum of $(n-1)$-point integrals J_{n-1} by shrinking propagators D_k from the original n-point integral. The starting term is the 1-point function, or tadpole,

$$J_1(d; m^2) = \int \frac{d^d k}{i\pi^{d/2}} \frac{1}{k^2 - m^2 + i\varepsilon} = -\frac{\Gamma(1-d/2)}{R_1^{1-d/2}}, \quad (2.51)$$

$$R_1 = m^2 - i\varepsilon. \quad (2.52)$$

The cases $G_n = 0$ and $\lambda_n = r_n = 0$ are discussed in subsection 2.5.

Eq. (2.50) is the master integral for one-loop n-point functions in space-time dimension d, representing them by n integrals over $(n-1)$-point functions with a shifted dimension $d+2s$. The recursion was first published in [41]. It implies a series of Mellin-Barnes representations for arbitrary massive one-loop n-point integrals with Mellin-Barnes integral dimensions $n-1$. This linear rise of the MB-dimension is highly advantageous compared to the number of MB-integral dimensions in the AMBRE approach (rising as n^2 with the number n of scales).

Based on (2.50), one has now several opportunites to proceed:

– (i) Evaluate the MB-integral in a direct numerical way.
– (ii) Derive ε-expansions for the Feynman integrals.
– (iii) Apply the Cauchy theorem for deriving sums and determine analytical expressions in terms of known special functions.

The first approach is based on AMBRE/MBOneLoop, the middle one is not yet finished, and the last approach was applied in [41] for massive vertex integrals and in [6] also for massive box integrals.

Few comments are at hand:

– Any 4-point integral e.g. is in the recursion a 3-fold Mellin-Barnes integral. While, with AMBRE, one gets for e.g. box integrals up to 9-fold MB-integrals.
– Euklidean and Minkoswkian integrals converge equally good. See J. Usovitsch's talk at LL2018 [47, 48].
– There appear no numerical problems due to vanishing Gram determinants. See for few details table C.6 and [49].

2.4 The basic scalar one-loop functions

2.4.1 Massive two-point functions

From the recursion relation (2.50), taken at $n = 2$ and using the expression (2.51) with $d \to d + 2s$ for the one-point functions under the integral, one gets the following Mellin-Barnes representation:

$$J_2(d; q_1, m_1^2, q_2, m_2^2) = \frac{e^{\epsilon\gamma_E}}{2\pi i} \int_{-i\infty}^{+i\infty} ds \, \frac{\Gamma(-s)\,\Gamma\left(\frac{d-1}{2}+s\right)\,\Gamma(s+1)}{2\,\Gamma\left(\frac{d-1}{2}\right)} R_2^s \times \left[\frac{1}{r_2}\frac{\partial r_2}{\partial m_2^2}\frac{\Gamma\left(1-\frac{d+2s}{2}\right)}{(m_1^2)^{1-\frac{d+2s}{2}}} + (m_1^2 \leftrightarrow m_2^2)\right]. \tag{2.53}$$

One may close the integration contour of the MB-integral in (2.53) to the right, apply the Cauchy theorem and collect the residua originating from two series of zeros of arguments of Γ-functions at $s = m$ and $s = m - d/2 - 1$ for $m \in \mathbb{N}$. The first series stems from the MB-integration kernel, the other one from the dimensionally shifted 1-point functions. And then one may sum up analytically in terms of Gauss' hypergeometric functions.

The 2-point function, with $R_2 \equiv R_{12}$, becomes:

$$\begin{aligned} J_2(d; Q^2, m_1^2, q_2, m_2^2) = & -\frac{\Gamma\left(2-\frac{d}{2}\right)}{(d-2)}\frac{\Gamma\left(\frac{d}{2}-1\right)}{\Gamma\left(\frac{d}{2}\right)}\frac{\partial_2 R_2}{R_2} \\ & \left[(m_1^2)^{\frac{d}{2}-1}\,{}_2F_1\left[\begin{matrix}1, \frac{d}{2}-\frac{1}{2}\,; \\ \frac{d}{2}\,;\end{matrix} \frac{m_1^2}{R_2}\right] + \frac{R_2^{\frac{d}{2}-1}}{\sqrt{1-\frac{m_1^2}{R_2}}}\sqrt{\pi}\frac{\Gamma\left(\frac{d}{2}\right)}{\Gamma\left(\frac{d}{2}-\frac{1}{2}\right)}\right] \\ & + \; (m_1^2 \leftrightarrow m_2^2). \end{aligned} \tag{2.54}$$

The representation (2.54) is valid for $\left|\frac{m_1^2}{r_{12}}\right| < 1$, $\left|\frac{m_2^2}{r_{12}}\right| < 1$ and $\mathcal{R}\mathrm{e}(\frac{d-2}{2}) > 0$. The result is in agreement with Eqn. (53) of of Tarasov et al. (2003) [15].

The iterative determination of higher-point functions proceeds analogously. Closing the integration contours to the right or to the left will cover different kinematical regions in the invariants R_n.

2.4.2 Massive three-point functions

The Mellin-Barnes integral for the massive vertex is a sum of three terms [50]:

$$J_3 = J_{123} + J_{231} + J_{312}, \tag{2.55}$$

using the representation for e.g. J_{123}

$$\begin{aligned} J_{123}(d,\{q_i,m_i^2\}) &= -\frac{e^{\epsilon\gamma_E}}{2\pi i}\int\limits_{-i\infty}^{+i\infty} ds\, \frac{\Gamma(-s)\,\Gamma(\frac{d-2+2s}{2})\Gamma(s+1)}{2\,\Gamma(\frac{d-2}{2})} R_3^{-s} \\ &\times \frac{1}{r_3}\frac{\partial r_3}{\partial m_3^2}\, J_2(d+2s;q_1,m_1^2,q_2,m_2^2). \end{aligned} \tag{2.56}$$

After applying the Cauchy theorem and summing up, one gets an analytical representation. The integrated massive vertex has been published in [41]. We quote here the representation given in [6]:

$$\begin{aligned} J_{123} &= \Gamma\left(2-\frac{d}{2}\right)\frac{\partial_3 r_3}{r_3}\frac{\partial_2 r_2}{r_2}\frac{r_2}{2\sqrt{1-m_1^2/r_2}} \\ &\left[-R_2^{d/2-2}\frac{\sqrt{\pi}}{2}\frac{\Gamma\left(\frac{d}{2}-1\right)}{\Gamma\left(\frac{d}{2}-\frac{1}{2}\right)}\,{}_2F_1\left[\begin{matrix}\frac{d-2}{2},1;\\ \frac{d-1}{2};\end{matrix}\frac{R_2}{R_3}\right] + R_3^{d/2-2}\,{}_2F_1\left[\begin{matrix}1,1;\\ 3/2;\end{matrix}\frac{R_2}{R_3}\right]\right] \\ &+ \Gamma\left(2-\frac{d}{2}\right)\frac{\partial_3 r_3}{r_3}\frac{\partial_2 r_2}{r_2}\frac{m_1^2}{4\sqrt{1-m_1^2/r_2}} \\ &\left[+\frac{2(m_1^2)^{d/2-2}}{d-2}F_1\left(\frac{d-2}{2};1,\frac{1}{2};\frac{d}{2};\frac{m_1^2}{R_3},\frac{m_1^2}{R_2}\right) - R_3^{d/2-2}F_1\left(1;1,\frac{1}{2};2;\frac{m_1^2}{R_3},\frac{m_1^2}{R_2}\right)\right] \\ &+ (m_1^2 \leftrightarrow m_2^2), \end{aligned}$$

with the short notations

$$R_3 = R_{123}, R_2 = R_{12}, \tag{2.57}$$

etc. For $d \to 4$, the bracket expressions vanish so that their product with the prefactor $\Gamma(2-d/2)$ stays finite in this limit, as it must come out for a massive vertex function. For some numerics see tables C.1 and C.2 and C.3 and C.4.

2.4.3 Massive four-point functions

Finally we reproduce the box integral, as a three-dimensional Mellin-Barnes representation:

$$J_4(d;\{p_i^2\},s,t,\{m_i^2\}) = \left(\frac{-1}{4\pi i}\right)^4 \frac{1}{\Gamma(\frac{d-3}{2})} \sum_{k_1,k_2,k_3,k_4=1}^{4} D_{k_1k_2k_3k_4}\left(\frac{1}{r_4}\frac{\partial r_4}{\partial m_{k_4}^2}\right)$$

Table C.1: *Numerics for a vertex, $d = 4 - 2\epsilon$. Input quantities suggest that, according to Eqn. (73) in [15], one has to set $b_3 = 0$. Although b_3 of [15] deviates from our vanishing value, it has to be set to zero, $b_3 \to 0$. The results of both calculations for J_3 agree for this case.*

$[p_i^2]$, $[m_i^2]$	[+100, +200, +300], [10, 20, 30]	
G_{123}	-160000	
λ_{123}	-8860000	
m_i^2/r_{123}	-0.180587, -0.361174, -0.541761	
m_i^2/r_{12}	-0.97561, -1.95122, -2.92683	
m_i^2/r_{23}	-0.39801, -0.79602, -1.19403	
m_i^2/r_{31}	-0.180723, -0.361446, -0.542169	
$\sum J$-terms [15]	$(0.019223879 - 0.007987267\ i)$	
$\sum b_3$-terms (TR)	0	
J_3 (TR)	$(0.019223879 - 0.007987267\ i)$	
b_3-term [15]	$(-0.089171509 + 0.069788641\ i)$	(0.022214414)/eps
$b_3 + \sum J$-terms	$(-0.012307377 - 0.009301346\ i)$	
J_3 (OT)	$\sum J$-terms, b_3-term $\to 0$, OK	
MB suite		
(-1)×fiesta3 [51]	$-(0.012307 + 0.009301\ i)$	$+ (8 * 10^{-6} + 0.00001\ i) \pm (1+i)10^{-4}$)
LoopTools [52]	$0.0192238790286 - 0.00798726725497\ i$	

$$\left(\frac{1}{r_{k_3k_2k_1}}\frac{\partial r_{k_3k_2k_1}}{\partial m_{k_3}^2}\right)\left(\frac{1}{r_{k_2k_1}}\frac{\partial r_{k_2k_1}}{\partial m_{k_2}^2}\right)(m_{k_1}^2)^{d/2-1} \tag{2.58}$$
$$\int_{-i\infty}^{+i\infty} dz_4 \int_{-i\infty}^{+i\infty} dz_3 \int_{-i\infty}^{+i\infty} dz_2 \left(\frac{m_{k_1}^2}{R_4}\right)^{z_4}\left(\frac{m_{k_1}^2}{R_{k_3k_2k_1}}\right)^{z_3}\left(\frac{m_{k_1}^2}{R_{k_2k_1}}\right)^{z_2}$$
$$\Gamma(-z_4)\Gamma(z_4+1)\frac{\Gamma(z_4+\frac{d-3}{2})}{\Gamma(z_4+\frac{d-2}{2})}\Gamma(-z_3)\Gamma(z_3+1)\frac{\Gamma(z_3+z_4+\frac{d-2}{2})}{\Gamma(z_3+z_4+\frac{d-1}{2})}$$
$$\Gamma(z_2+z_3+z_4+\frac{d-1}{2})\Gamma(-z_2-z_3-z_4-\frac{d+2}{2})\Gamma(-z_2)\Gamma(z_2+1).$$

The representation (2.58) can be treated by the Mathematica packages MB and MBnumerics of the MBsuite, replacing AMBRE by a derivative of MBnumerics: MBOneLoop [47,54]. For numerical examples, see table C.5.

After applying the Cauchy theorem and summing the residues, we get [6, 55] :

$$J_4 = J_{1234} + J_{2341} + J_{3412} + J_{4123}, \tag{2.59}$$

with $R_4 = R_{1234}, R_3 = R_{123}, R_2 = R_{12}$ etc.:

$$J_{1234} = \Gamma\left(2-\frac{d}{2}\right)\frac{\partial_4 r_4}{r_4}\Bigg\{$$
$$\left[\frac{b_{123}}{2}\left(-R_3^{d/2-2}\,{}_2F_1\left[\begin{matrix}\frac{d-3}{2},1;\\ \frac{d}{2}-1;\end{matrix}\frac{R_2}{R_3}\right]+R_4^{d/2-2}\sqrt{\pi}\frac{\Gamma\left(\frac{d}{2}-1\right)}{\Gamma\left(\frac{d}{2}-\frac{3}{2}\right)}\,{}_2F_1(d\to 4)\right)\right]$$

Table C.2: *Numerics for a vertex, $d = 4 - 2\epsilon$. Input quantities suggest that, according to eq. (73) in [15], one has to set $b_3 = 0$. Further, we have set in the numerics for eq. (75) of [15] that the root of the Gram determinant is $\sqrt{-g_{123} + i\,\varepsilon}$, what looks counter-intuitive for a "momentum"-like function. Both results agree if we do not set Tarasov's $b_3 \to 0$. Table courtesy [53].*

$[p_i^2]$, $[m_i^2]$	$[-100, +200, -300]$, $[10, 20, 30]$	
G_{123}	480000	
λ_3	-19300000	
m_i^2/r_3	0.248705, 0.497409, 0.746114	
m_i^2/r_{12}	0.248447, 0.496894, 0.745342	
m_i^2/r_{23}	-0.39801, -0.79602, -1.19403	
m_i^2/r_{31}	0.104895, 0.20979, 0.314685	
$\sum J$-terms	$(-0.012307377 - 0.056679689\ i)$	$(0.012825498\ i)$/eps
$\sum b_3$-terms	$(0.047378343\ i)$	$(-0.012825498\ i)$/eps
J_3(TR)	$(-0.012307377 - 0.009301346\ i)$	
b_3-term	$(0.047378343\ i)$	$(-0.012825498\ i)$/eps
b_3+$\sum J$-terms	$(-0.012307377 - 0.009301346\ i)$	
J_3(OT)	$\sum J$-terms, b_3-term$\to$0, gets wrong!	
MB suite		
(-1)*fiesta3	$-(0.012307 + 0.009301\ i)$	$(8 * 10^{-6} + 0.00001\ i) \pm (1 + i)10^{-4}$)
LoopTools/FF, ϵ^0	$-0.01230737736778 - 0.009301346170\ i$	

$$
\begin{aligned}
&+\left[+\frac{R_2^{d/2-2}}{d-3}F_1\left(\frac{d-3}{2};1,\frac{1}{2};\frac{d-1}{2};\frac{R_2}{R_4},\frac{R_2}{R_3}\right)-R_4^{d/2-2}F_1\left(d\to 4\right)\right]\\
&+\frac{m_1^2}{8}\frac{\Gamma\left(\frac{d}{2}-1\right)}{\Gamma\left(\frac{d}{2}-\frac{3}{2}\right)}\frac{\partial_3 r_3}{r_3}\frac{\partial_2 r_2}{r_2}\frac{r_3}{r_3-m_1^2}\frac{r_2}{r_2-m_1^2}\\
&\Big[-(m_1^2)^{d/2-2}\frac{\Gamma\left(\frac{d}{2}-3/2\right)}{\Gamma\left(\frac{d}{2}\right)}F_S(d/2-3/2,1,1,1,1,d/2,d/2,d/2,d/2,\frac{m_1^2}{R_4},\frac{m_1^2}{m_1^2-R_3},\frac{m_1^2}{m_1^2-R_2})\\
&+R_4^{d/2-2}\sqrt{\pi}F_S(d\to 4)\Big]\quad+\quad(m_1^2\leftrightarrow m_2^2)\Big\}. \qquad (2.60)
\end{aligned}
$$

For $d \to 4$, all three contributions in square brackets approach zero, so that the massive J_4 gets finite in this limit, as it should do. Table C.5 contains numerical examples.

2.5 The cases of vanishing Cayley determinant $\lambda_n = 0$ and of vanishing Gram determinant $G_n = 0$

We refer here to two important special cases, where the general derivations cannot be applied.

In the case of vanishing Cayley determinant, $\lambda_n = 0$, we cannot introduce the inhomogeneity $R_n = -\lambda_n/G_n$ into the Symanzik polynomial F_n. Let us assume that it is $G_n \neq 0$, so that $r_n = 0$. A useful alternative representation to (2.50) is known from the literature, see e.g.

Table C.3: *Numerics for a vertex in space-time dimension* $d = 4 - 2\epsilon$. *Causal* $\varepsilon = 10^{-20}$. *Agreement with [15]. Table courtesy [53].*

p_i^2 m_i^2	$-100,-200,-300$ 10,20,30	
G_{123} λ_{123} m_i^2/r_{123} m_i^2/r_{12} m_i^2/r_{23} m_i^2/r_{31} $\sum J$-terms	-160000 15260000 0.104849, 0.209699, 0.314548 0.248447, 0.496894, 0.745342 0.133111, 0.266223, 0.399334 0.104895, 0.20979, 0.314685 $(0.0933877 - 0\ i)$	$-(0.0222144 - 0\ i)/\text{eps}$
$\sum b$-terms J_3(TR)	-0.101249 $(-0.00786155 - 0\ i)$	$+0.0222144/\text{eps}$
b_3 b_3+J-terms	$(-0.101249 + 0\ i)$ $(-0.007861546 + 0\ i)$	$(0.0222144 + 0\ i)/\text{eps}$
J_3(OT)	b_3+J-terms $\rightarrow$ OK	
MB suite	$-0.007862014,\ 5.002549159 * 10^{-6},\ 0$	
(-1)*fiesta3	-0.007862	$6 * 10^{-6} + 6 * 10^{-6}\ i \pm (1+i)10^{-10}$
LoopTools/FF, ϵ^0	-0.00786154613229082290	

Eqn. (3) in [15]:

$$J_n(d) \;=\; \frac{1}{d-n-1}\sum_{k=1}^{n}\frac{\partial_k\lambda_n}{G_n}\mathbf{k}^-J_n(d-2). \tag{2.61}$$

Another special case is a vanishing Gram determinant, $G_n = 0$. Here, again one may use Eqn. (3) of [15] and the result is (for $\lambda_n \neq 0$):

$$J_n(d) \;=\; -\sum_{k=1}^{n}\frac{\partial_k\lambda_n}{2\lambda_n}\mathbf{k}^-J_n(d). \tag{2.62}$$

The representation was, for the special case of the vertex function, also given in Eqn. (46) of [60].

For the vertex function, a general study of the special cases has been carried through in [61].

2.6 Example: A massive 4-point function with vanishing Gram determinant

As a very interesting, non-trivial example we had re-studied the numerics of a massive 4-point function with a small or vanishing Gram determinant [47, 50, 54, 62]. The original example has been taken from Appendix C of [17].

The sample outcome is shown in Table C.6. The new iterative Mellin-Barnes representations deliver very precise numerical results for e.g. box functions, including cases of small or vanishing Gram determinants. The software used is MBOneLoop [63].

The notational correspondences are e.g.:

$J_4(12 - 2\epsilon, 1, 5, 1, 1) \rightarrow I^{[d+]^4}_{4,2222} = D_{1111}$.

Table C.4: *Numerics for a vertex in space-time dimension $d = 4 - 2\epsilon$. Causal $\varepsilon = 10^{-20}$. Input quantities suggest that, according to eq. (73) in [15], one has to set $b_3 = 0$. Agreement due to setting $b_3 = 0$ there. Table courtesy [53].*

p_i^2 m_i^2	+100, −200, +300 10, 20, 30	
G_{123} λ_{123} m_i^2/r_{123} m_i^2/r_{12} m_i^2/r_{23} m_i^2/r_{31} $\sum J$-terms	480000 4900000 −0.979592, −1.95918, −2.93878 -0.97561, −1.95122, −2.92683 0.133111, 0.266223, 0.399334 −0.180723, −0.361446, −0.542169 $(0.006243624 - 0.018272524\ i)$	
$\sum b_3$-terms J_3(TR)	0 $(0.006243624 - 0.018272524\ i)$	
b_3-term b_3+$\sum J$-terms	$(0.040292491 + 0.029796253\ i)$ $(-0.012307377 - 0.009301346\ i)$	$(-0.012825498\ i)$/eps $(4 * 10^{-18} - 6 * 10^{-18}\ i)$/eps
J_3(OT)	$\sum J$-terms, b_3-term→0, OK	
MB suite		
(-1)*fiesta3	$-(-0.006322 + 0.014701\ i)$	$+ (0.000012 + 0.000014\ i) \pm (1 + i)10^{-2}$
LoopTools/FF, ϵ^0	$0.00624362477277 - 0.0182725240487\ i$	

2.7 Calculation of Gauss hypergeometric function ${}_2F_1$, Appell function F_1, and Saran function F_S at arbitrary kinematics

There is little known about the precise numerical calculation of generalized hypergeometric functions at arbitrary arguments. Numerical calculations of specific Gauss hypergeometric functions ${}_2F_1$, Appell functions F_1 (Eqn. (1) of [64]), and Lauricella-Saran functions F_S (Eqn. (2.9) of [65]) are needed for the scalar one-loop Feynman integrals:

$$ {}_2F_1(a,b;c;x) = \sum_{k=0}^{\infty} \frac{(a)_k (b)_k}{k!\ (c)_k}\ x^k, \tag{2.63} $$

$$ F_1(a;b,b';c;y,z) = \sum_{m,n=0}^{\infty} \frac{(a)_{m+n} (b)_m (b')_n}{m!\ n!\ (c)_{m+n}}\ y^m z^n, \tag{2.64} $$

$$ F_S(a_1,a_2,a_2;b_1,b_2,b_3;c,c,c;x,y,z) = \sum_{m,n,p=0}^{\infty} \frac{(a_1)_m (a_2)_{n+p} (b_1)_m (b_2)_n (b_3)_p}{m!\ n!\ p!\ (c)_{m+n+p}}\ x^m y^n z^p. \tag{2.65} $$

The $(a)_k$ is the Pochhammer symbol. The specific cases needed here are discussed in the appendices of [6]. Here, we repeat only few definitions.

One approach to the numerics of ${}_2F_1$, F_1, and F_S may be based on Mellin-Barnes representations. For the Gauss function ${}_2F_1$ and the Appell function F_1, Mellin-Barnes representations are known since a while. See Eqn. (1.6.1.6) in [66],

$$ {}_2F_1(a,b;c;z) = \frac{1}{2\pi i}\ \frac{\Gamma(c)}{\Gamma(a)\Gamma(b)} \int_{-i\infty}^{+i\infty} ds\ (-z)^s\ \frac{\Gamma(a+s)\Gamma(b+s)\Gamma(-s)}{\Gamma(c+s)}, \tag{2.66} $$

Table C.5: *Comparison of the box integral J_4 defined in (2.60) with the LoopTools function* `D0`$(p_1^2, p_2^2, p_3^2, p_4^2, (p_1+p_2)^2, (p_2+p_3)^2, m_1^2, m_2^2, m_3^2, m_4^2)$ *[56, 57] at $m_2^2 = m_3^2 = m_4^2 = 0$. Further numerical references are the packages K.H.P_D0 (PHK, unpublished) and MBOneLoop [58, 59]. External invariants: $(p_1^2 = \pm 1, p_2^2 = \pm 5, p_3^2 = \pm 2, p_4^2 = \pm 7, s = \pm 20, t = \pm 1)$.*
Table from Phan, Riemann, PLB 2019 [6], licence: https://creativecommons.org/licenses/by/4.0/.

$(p_1^2, p_2^2, p_3^2, p_4^2, s, t)$	4-point integral
$(-,-,-,-,-,-)$	$d = 4, \quad m_1^2 = 100$
J_4	0.00917867
LoopTools	0.0091786707
MBOneLoop	0.0091786707
$(+,+,+,+,+,+)$	$d = 4, \quad m_1^2 = 100$
J_4	$-0.0115927 - 0.00040603\ i$
LoopTools	$-0.0115917 - 0.00040602\ i$
MBOneLoop	$-0.0115917369 - 0.0004060243\ i$
$(-,-,-,-,-,-)$	$d = 5, \quad m_1^2 = 100$
J_4	0.00926895
K.H.P_D0	0.00926888
MBOneLoop	0.0092689488
$(+,+,+,+,+,+)$	$d = 5, \quad m_1^2 = 100$
J_4	$-0.00272889 + 0.0126488\ i$
K.H.P_D0	(–)
MBOneLoop	$-0.0027284242 + 0.0126488134\ i$
$(-,-,-,-,-,-)$	$d = 5, \quad m_1^2 = 100 - 10\ i$
J_4	$0.00920065 + 0.000782308\ i$
K.H.P_D0	$0.0092006 \quad + 0.000782301\ i$
MBOneLoop	$0.0092006481 + 0.0007823090\ i$
$(+,+,+,+,+,+)$	$d = 5, \quad m_1^2 = 100 - 10\ i$
J_4	$-0.00398725 + 0.012067\ i$
K.H.P_D0	$-0.00398723 + 0.012069\ i$
MBOneLoop	$-0.0039867702 + 0.0120670388\ i$

and Eqn. (10) in [64], which is a two-dimensional MB-integral:

$$F_1(a;b,b';c;x,y) = \frac{1}{2\pi i}\,\frac{\Gamma(c)}{\Gamma(a)\Gamma(b')}\int_{-i\infty}^{+i\infty} dt\ (-y)^t\ {}_2F_1(a+t,b;c+t,x)\frac{\Gamma(a+t)\Gamma(b'+t)\Gamma(-t)}{\Gamma(c+t)}. \tag{2.67}$$

For the Lauricella-Saran function F_S, the following, new, three-dimensional MB-integral was given in [6]:

$$F_S(a_1,a_2,a_2;b_1,b_2,b_3;c,c,c;x,y,z) = \frac{1}{2\pi i}\,\frac{\Gamma(c)}{\Gamma(a_1)\Gamma(b_1)}\int_{-i\infty}^{+i\infty} dt(-x)^t\ \frac{\Gamma(a_1+t)\Gamma(b_1+t)\Gamma(-t)}{\Gamma(c+t)}$$
$$\times\ F_1(a_2;b_2,b_3;c+t;y,z). \tag{2.68}$$

Table C.6: *The Feynman integral* $J_4(12-2\epsilon,1,5,1,1)$ *compared to numbers from [17]. The* $I^{[d+]^4}_{4,2222}$ *is the scalar integral where propagator 2 has index* $\nu_2 = 1+(1+1+1+1) = 5$*, the others have index 1. The integral corresponds to* D_{1111} *in notations of LoopTools [56]. For* $x = 0$*, the Gram determinant vanishes. We see an agreement of about 10 to 11 relevant digits. The deviations of the two calculations seem to stem from a limited accuracy of the Pade approximations used in [17]. Table courtesy [54, 62].*

x	value for $4! \times \; J_4(12-2\epsilon,1,5,1,1)$	
0	$(2.05969289730 + 1.55594910118i)10^{-10}$	[J. Fleischer, T. Riemann, 2010]
0	$(2.05969289730 + 1.55594910118\ i)10^{-10}$	MBOneLoop+Kira+MBnumerics
10^{-8}	$(2.05969289342 + 1.55594909187\ i)10^{-10}$	[J. Fleischer, T. Riemann, 2010]
10^{-8}	$(2.05969289363 + 1.55594909187\ i)10^{-10}$	MBOneLoop+Kira+MBnumerics
10^{-4}	$(2.05965609497 + 1.55585605343\ i)10^{-10}$	[J. Fleischer, T. Riemann, 2010]
10^{-4}	$(2.05965609489 + 1.55585605343\ i)10^{-10}$	MBOneLoop+Kira+MBnumerics

The numerics of the Gauss hypergeometric function is generally known in all detail.

For the Appell function F_1, the numerical mean value integration of the one-dimensional integral representation of [67] may be advocated, being quoted in Eqn. (9) of [64]:

$$F_1(a;b,b';c;x,y) = \frac{\Gamma(c)}{\Gamma(a)\Gamma(c-a)} \int_0^1 du \frac{u^{a-1}(1-u)^{c-a-1}}{(1-xu)^b(1-yu)^{b'}}. \tag{2.69}$$

We need three specific cases, taken at $d \geq 4$. For vertices e.g.,

$$F_1^v(d) \equiv F_1\left(\frac{d-2}{2};1,\frac{1}{2};\frac{d}{2};x_c,y_c\right) = \frac{1}{2}(d-2)\int_0^1 \frac{du\ u^{\frac{d}{2}-2}}{(1-x_cu)\sqrt{1-y_cu}}. \tag{2.70}$$

Integrability is violated at $u=0$ if not $\Re e(d) > 2$. The stability of numerics is well controlled as exemplified in Table C.7.

For the calculation of the 4-point Feynman integrals, one needs additionally the Lauricella-Saran function F_S [65]. Saran defines F_S as a three-fold sum (2.65), see Eqn. (2.9) in [65]. He derives a 3-fold integral representation in Eqn. (2.15) and a 2-fold integral in Eqn. (2.16). We recommend to use the following representation, derived at p. 304 of [65]:

$$\begin{aligned} &F_S(a_1,a_2,a_2;b_1,b_2,b_3;c,c,c,x,y,z) \\ &= \frac{\Gamma(c)}{\Gamma(a_1)\Gamma(c-a_1)} \int_0^1 dt \frac{t^{c-a_1-1}(1-t)^{a_1-1}}{(1-x+tx)^{b_1}} F_1(a_2;b_2,b_3;c-a_1;ty,tz). \end{aligned} \tag{2.71}$$

For the box integrals one needs the specific case

$$\begin{aligned} F_S^b(d) &= F_S\left(\frac{d-3}{2},1,1;1,1,\frac{1}{2};\frac{d}{2},\frac{d}{2},\frac{d}{2},x_c,y_c,z_c\right) \\ &= \frac{\Gamma(\frac{d}{2})}{\Gamma(\frac{d-3}{2})\Gamma(\frac{3}{2})} \int_0^1 dt \frac{\sqrt{t}(1-t)^{\frac{d-5}{2}}}{(1-x_c+x_ct)} F_1(1;1,\frac{1}{2};\frac{3}{2};y_ct,z_ct). \end{aligned} \tag{2.72}$$

Table C.7: *The Appell function F_1 of the massive vertex integrals as defined in (2.70). As a proof of principle, only the constant term of the expansion in $d = 4 - 2\varepsilon$ is shown, $F_1(1; 1, \frac{1}{2}; 2; x, y)$. Upper values from geberal numerics of appendices of [6] , lower values from setting $d = 4$ and use of analytical formulae. Table courtesy from [6] under licence* http://creativecommons.org/licenses/by/4.0/.

$x - i\varepsilon_x$	$y - i\varepsilon_y$	$F_1(1; 1, \frac{1}{2}; 2; x, y)$	
$+11.1 - 10^{-12}i$	$+12.1 - 10^{-12}i$	-0.1750442480735	$-0.0542281294732\ i$
		$-0.17504424807351877884498289912$	$-0.05422812947330402788209764 1167\ i$
$+11.1 - 10^{-12}i$	$+12.1 + 10^{-12}i$	$+1.7108545293244$	$+0.0542281294732\ i$
		$+1.71085452932433557134838204175$	$+0.05422812947148217381589270924\ i$
$+11.1 + 10^{-12}i$	$+12.1 - 10^{-12}i$	$+1.7108545304114$	$-0.0542281294732\ i$
		$+1.71085452932433557134838204175$	$-0.05422812947148217381589270924\ i$
$+11.1 + 10^{-12}\ i$	$+12.1 + 10^{-12}\ i$	-0.1750442480735	$+0.0542281294733\ i$
		$-0.17504424807351877884498289912$	$+0.05422812947330402788209764 1167\ i$
$+12.1 - 10^{-15}\ i$	$+11.1 - 10^{-15}\ i$	-0.1700827166484	$-0.0518684846037\ i$
$+12.1 - 10^{-10}\ i$	$+11.1 - 10^{-15}\ i$	$-0.17008271664800058101165749279$	$-0.05186848460465674976556525621\ i$
$+12.1 - 10^{-15}\ i$	$+11.1 + 10^{-15}\ i$	-0.1700827166484	$-1.7544202909955\ i$
		$-0.17008271664844025647268817399$	$-1.75442029099557688735842562038\ i$
$+12.1 + 10^{-15}\ i$	$+11.1 - 10^{-15}\ i$	-0.1700827166484	$+1.7544202909955\ i$
		$-0.17008271664844025647268817399$	$+1.75442029099557688735842562038\ i$
$+12.1 + 10^{-15}\ i$	$+11.1 + 10^{-15}\ i$	-0.1700827166484	$+0.0518684846037\ i$
$+12.1 - 10^{-10}\ i$	$+11.1 - 10^{-15}\ i$	$-0.17008271664800058101165749279$	$+0.05186848460465674976556525621\ i$
$+11.1 - 10^{-15}\ i$	-12.1	-0.0533705146518	$-0.1957692111557\ i$
		$-0.05337051465189944473349401152$	$-0.19576921115573398538892083 3693\ i$
$+11.1 + 10^{-15}\ i$	-12.1	-0.0533705146518	$+0.1957692111557\ i$
		$-0.05337051465189944473349401152$	$+0.19576921115573398538892083 3693\ i$
-11.1	$+12.1 - 10^{-12}\ i$	$+0.1060864084662$	$-0.1447440700082i$
		$+0.10608640847651064287133527599$	$-0.14474407002133340716734961 9088\ i$
-11.1	$+12.1 + 10^{-12}\ i$	$+0.1060864084662$	$+0.1447440700082i$
		$+0.10608640847651064287133527599$	$+0.14474407002133340716734961 9088\ i$
-12.1	-11.1	$+0.122456767687224028$	
		$+0.12245676768722402506513395161$	

Eqn. (2.72) is valid if $\Re e(d) > 3$.

Acknowledgement
We would like to thank J. Gluza for a careful reading of the manuscript.

References

[1] R. J. Eden, P. V. Landshoff, D. I. Olive, J. C. Polkinghorn, "The Analytic S-Matrix" (Cambridge University Press, Cambridge, 1966).

[2] J. Schwinger, Particles, sources, and fields. Volume 1 (Reading, Mass., 1970). Quote from section 1-4.

[3] A. Blondel, J. Gluza, S. Jadach, P. Janot, T. Riemann (eds.), Standard Model Theory for the FCC-ee: The Tera-Z, report on the mini workshop on precision EW and QCD calculations for the FCC studies: methods and techniques, CERN, Geneva, Switzerland, January 12-13, 2018; subm. as CERN Yellow Report. arXiv:1809.01830.

[4] C. G. Bollini, J. J. Giambiagi, Dimensional Renormalization: The Number of Dimensions as a Regularizing Parameter, Nuovo Cim. B12 (1972) 20–26. doi:10.1007/BF02895558.

[5] G. 't Hooft, M. J. G. Veltman, Regularization and Renormalization of Gauge Fields, Nucl. Phys. B44 (1972) 189–213. doi:10.1016/0550-3213(72)90279-9.

[6] K. H. Phan, T. Riemann, Scalar 1-loop Feynman integrals as meromorphic functions in space-time dimension d, Phys. Lett. B791 (2019) 257–264. arXiv:1812.10975, doi:10.1016/j.physletb.2019.02.044.

[7] G. Passarino, M. Veltman, One loop corrections for e^+e^- annihilation into $\mu^+\mu^-$ in the Weinberg model, Nucl. Phys. B160 (1979) 151. doi:10.1016/0550-3213(79)90234-7.

[8] G. 't Hooft, M. Veltman, Scalar one loop integrals, Nucl. Phys. B153 (1979) 365–401. doi:10.1016/0550-3213(79)90605-9.

[9] E. E. Boos, A. I. Davydychev, A Method of the Evaluation of the Vertex Type Feynman Integrals, Moscow Univ. Phys. Bull. 42N3 (1987) 6–10, [Vestn. Mosk. Univ. Fiz. Astron.28N3,8(1987)]. http://www.higgs.de/~davyd/preprints/bd_vmu.pdf.

[10] O. Tarasov, Connection between Feynman integrals having different values of the space-time dimension, Phys. Rev. D54 (1996) 6479–6490. arXiv:hep-th/9606018, doi:10.1103/PhysRevD.54.6479.

[11] O. Tarasov, Generalized recurrence relations for two loop propagator integrals with arbitrary masses, Nucl. Phys. B502 (1997) 455–482. arXiv:hep-ph/9703319, doi:10.1016/S0550-3213(97)00376-3.

[12] O. V. Tarasov, Reduction of Feynman graph amplitudes to a minimal set of basic integrals, Acta Phys. Polon. B29 (1998) 2655, http://www.actaphys.uj.edu.pl/fulltext?series=Reg&vol=29&page=2655. arXiv:hep-ph/9812250.

[13] J. Fleischer, F. Jegerlehner, O. V. Tarasov, Algebraic reduction of one loop Feynman graph amplitudes, Nucl. Phys. B566 (2000) 423–440. arXiv:hep-ph/9907327, doi:10.1016/S0550-3213(99)00678-1.

[14] O. Tarasov, Application and explicit solution of recurrence relations with respect to space-time dimension, Nucl. Phys. Proc. Suppl. 89 (2000) 237. arXiv:hep-ph/0102271, doi:10.1016/S0920-5632(00)00849-5.

[15] J. Fleischer, F. Jegerlehner, O. Tarasov, A new hypergeometric representation of one loop scalar integrals in d dimensions, Nucl. Phys. B672 (2003) 303. arXiv:hep-ph/0307113, doi:10.1016/j.nuclphysb.2003.09.004.

[16] A. I. Davydychev, A simple formula for reducing Feynman diagrams to scalar integrals, Phys. Lett. B263 (1991) 107–111, http://www.higgs.de/~davyd/preprints/tensor1.pdf. doi:10.1016/0370-2693(91)91715-8.

[17] J. Fleischer, T. Riemann, A complete algebraic reduction of one-loop tensor Feynman integrals, Phys. Rev. D83 (2011) 073004. arXiv:1009.4436, doi:10.1103/PhysRevD.83.073004.

[18] F. V. Tkachov, A Theorem on Analytical Calculability of Four Loop Renormalization Group Functions, Phys. Lett. 100B (1981) 65–68. doi:10.1016/0370-2693(81)90288-4.

[19] K. Chetyrkin, F. Tkachov, Integration by parts: The algorithm to calculate β functions in 4 loops, Nucl. Phys. B192 (1981) 159–204. doi:10.1016/0550-3213(81)90199-1.

[20] J. Fleischer, J. Gluza, A. Almasy, T. Riemann, Replacing 1-loop tensor reduction by contractions, talk held by T.R. at 11^{th} International Symposium on Radiative Corrections - Applications of Quantum Field Theory to Phenomenology - RADCOR 2013, 22 - 27 Sep 2013, Lumley Castle, UK, unpublished. See (11) and following equations. Slides: https://conference.ippp.dur.ac.uk/event/341/session/8/contribution/56/material/slides/0.pdf.

[21] U. Nierste, D. Müller, M. Böhm, Two loop relevant parts of D-dimensional massive scalar one loop integrals, Z. Phys. C57 (1993) 605–614. doi:10.1007/BF01561479.

[22] G. Passarino, An approach toward the numerical evaluation of multiloop Feynman diagrams, Nucl. Phys. B619 (2001) 257–312. arXiv:hep-ph/0108252, doi:10.1016/S0550-3213(01)00528-4.

[23] A. Ferroglia, G. Passarino, M. Passera, S. Uccirati, The frontier of multi-loop Feynman diagrams: (Semi-) numerical techniques, Nucl. Phys. Proc. Suppl. 117 (2003) 206, [,206(2002)]. doi:10.1016/S0920-5632(03)90526-3.

[24] A. Ferroglia, G. Passarino, S. Uccirati, M. Passera, A frontier in multi-scale multi-loop integrals: The algebraic-numerical method, Nucl. Instrum. Meth. A502 (2003) 391–395. doi:10.1016/S0168-9002(03)00450-9.

[25] A. Ferroglia, M. Passera, G. Passarino, S. Uccirati, All purpose numerical evaluation of one loop multileg Feynman diagrams, Nucl. Phys. B650 (2003) 162–228. arXiv:hep-ph/0209219, doi:10.1016/S0550-3213(02)01070-2.

[26] V. A. Smirnov, Analytical result for dimensionally regularized massless on shell double box, Phys. Lett. B460 (1999) 397–404. arXiv:hep-ph/9905323, doi:10.1016/S0370-2693(99)00777-7.

[27] J. Tausk, Nonplanar massless two loop Feynman diagrams with four on-shell legs, Phys. Lett. B469 (1999) 225–234. arXiv:hep-ph/9909506, doi:10.1016/S0370-2693(99)01277-0.

[28] J. Gluza, K. Kajda, T. Riemann, AMBRE: A Mathematica package for the construction of Mellin-Barnes representations for Feynman integrals, Comput. Phys. Commun. 177 (2007) 879–893. arXiv:0704.2423, doi:10.1016/j.cpc.2007.07.001.

[29] J. Gluza, K. Kajda, T. Riemann, V. Yundin, New results for loop integrals: AMBRE, CSectors, hexagon, PoS ACAT08 (2008) 124, https://pos.sissa.it/070/124/pdf. arXiv:0902.4830, doi:10.22323/1.070.0124.

[30] K. Kajda, I. Dubovyk, AMBRE 2.2 (12 Sep 2015), a Mathematica package representing Feynman integrals by Mellin-Barnes integrals, available at http://prac.us.edu.pl/~gluza/ambre/, [68].

[31] J. Gluza, K. Kajda, T. Riemann, V. Yundin, News on Ambre and CSectors, Nucl. Phys. Proc. Suppl. 205-206 (2010) 147–151. arXiv:1006.4728, doi:10.1016/j.nuclphysbps.2010.08.034.

[32] I. Dubovyk, J. Gluza, T. Riemann, Non-planar Feynman diagrams and Mellin-Barnes representations with *AMBRE* 3.0, J. Phys. Conf. Ser. 608 (1) (2015) 012070. doi:10.1088/1742-6596/608/1/012070.

[33] I. Dubovyk, J. Gluza, T. Riemann, J. Usovitsch, Numerical integration of massive two-loop Mellin-Barnes integrals in Minkowskian regions, PoS LL2016 (2016) 034, https://pos.sissa.it/260/034/pdf. arXiv:1607.07538.

[34] J. Usovitsch, Numerical evaluation of Mellin-Barnes integrals in Minkowskian regions and their application to two-loop bosonic electroweak contributions to the weak mixing angle of the $Zb\bar{b}$-vertex, Ph.D. thesis, Humboldt-Universität zu Berlin, Mathematisch-Naturwissenschaftliche Fakultät (2018). doi:http://dx.doi.org/10.18452/19484.

[35] I. Dubovyk, Mellin-Barnes representations for multiloop Feynman integrals with applications to 2-loop electroweak Z boson studies, PhD thesis, Universität Hamburg, to be submitted.

[36] N. I. Usyukina, On a Representation for Three Point Function, Teor. Mat. Fiz. 22 (1975) 300–306, http://www.mathnet.ru/php/getFT.phtml?jrnid=tmf&paperid=3683&what=fullt&option_lang=eng. doi:10.1007/BF01037795.

[37] Krzysztof Kajda, *Multipoint Feynman diagrams at the one loop level* (PhD thesis, University of Silesia, Katowice, Poland, 3 Sep 2009).

[38] D. B. Melrose, Reduction of Feynman diagrams, Nuovo Cim. 40 (1965) 181–213. doi:10.1007/BF028329.

[39] E. W. Barnes, Proc. London Math. Soc. (1908) **s2-6 (1)**: 141-177. doi:10.1112/plms/s2-6.1.141.

[40] E. Whittaker, G. Watson, A course of modern analysis, Cambridge University Press, 1927.

[41] K. H. Phan, J. Blümlein, T. Riemann, Scalar one-loop vertex integrals as meromorphic functions of space-time dimension d, Acta Phys. Polon. B48 (2017) 2313. arXiv:1711.05510, doi:10.5506/APhysPolB.48.2313.

[42] T. Regge, G. Barucchi, On the properties of Landau curves, Nuovo Cim. 34 (1964) 106. doi:10.1007/BF02725874.

[43] I. Bernshtein, Modules over a ring of differential operators. Moscow State University, translated from Funktsional'nyi Analiz i Ego Prilozheniya, Vol. 5, pp. 1-16, April 1971. Available at http://www.math1.tau.ac.il/~bernstei/Publication_list/publication_texts/bernstein-mod-dif-FAN.pdfdoi:10.1007/BF01076413.

[44] V.A. Golubeva and V.Z. Énol'skii, The differential equations for the Feynman amplitude of a single-loop graph with four vertices, Mathematical Notes of the Academy of Sciences of the USSR 23 (1978) 63. doi:10.1007/BF01104888, available at http://www.mathnet.ru/links/c4b9d8a15c8714d3d8478d1d7b17609b/mzm8124.pdf.

[45] E. W. Barnes, A new development of the theory of the hypergeometric functions, Proc. Lond. Math. Soc. (2) 6 (1908) 141–177. doi:10.1112/plms/s2-6.1.141.

[46] G. N. Watson, A treatise on the theory of Bessel functions, Cambridge University Press 1922, https://www.forgottenbooks.com/de/download/ATreatiseontheTheoryofBesselFunctions_10019747.pdf.

[47] J. Usovitsch, I. Dubovyk and T. Riemann, MBnumerics: Numerical integration of Mellin-Barnes integrals in physical regions [48]. Slides of talk held by J.U. at LL2018 at https://indico.desy.de/indico/event/16613/session/4/contribution/22/material/slides/0.pdf.

[48] J. Usovitsch, I. Dubovyk, T. Riemann, MBnumerics: Numerical integration of Mellin-Barnes integrals in physical regions, PoS LL2018 (2018) 046, https://pos.sissa.it/303/046/pdf. arXiv:1810.04580, doi:10.22323/1.303.0046.

[49] J. Usovitsch and T. Riemann, New approach to Mellin-Barnes integrals for massive one-loop Feynman integrals, section E.6 in [3]. arXiv:1809.01830.

[50] T. Riemann, Scalar 1-loop Feynman integrals in arbitrary space-time dimension D, slides of talk held at 14^{th} Workshop on Calculations for Modern and Future Colliders (CALC2018), July 22 - August 1, 2018, JINR, Dubna, Russia, https://indico.jinr.ru/conferenceOtherViews.py?showSession=all&showDate=all&view=standard&fr=no&confId=418. Slides: http://indico.jinr.ru/getFile.py/access?contribId=77&sessionId=5&resId=0&materialId=slides&confId=418.

[51] A. V. Smirnov, FIESTA 3: cluster-parallelizable multiloop numerical calculations in physical regions, Comput. Phys. Commun. 185 (2014) 2090–2100. arXiv:1312.3186, doi:10.1016/j.cpc.2014.03.015.

[52] T. Hahn, M. Perez-Victoria, Automatized one-loop calculations in four and D dimensions, Comput. Phys. Commun. 118 (1999) 153–165; http://www.feyn-arts.% de/looptools. arXiv:hep-ph/9807565.

[53] K. H. Phan, J. Blümlein, T. Riemann, Scalar one-loop vertex integrals as meromorphic functions of space-time dimension d [41], slides of talk held by T.R. at 41st International Conference of Theoretical Physics: Matter to the Deepest: Podlesice, Poland, September 4-8, 2017. http://indico.if.us.edu.pl/event/4/contribution/32/material/slides/0.pdf.

[54] J. Usovitsch, Numerical evaluation of Mellin-Barnes integrals in Minkowskian regions, slides of talk held at FCC-ee Mini workshop Precision EW and QCD calculations for the FCC studies: Methods and techniques, 12-13 January 2018, CERN, Geneva, Switzerland, https://indico.cern.ch/event/669224/overview. slides: https://indico.cern.ch/event/669224/contributions/2805454/attachments/1581984/2500208/Usovitsch.pdf.

[55] T. Riemann, et al., Scalar one-loop Feynman integrals in arbitrary space-time dimension. Talk held at LL2018, April 29 to May 4, 2018, St. Goar, Germany. Unpublished, slides: https://indico.desy.de/indico/event/16613/session/12/contribution/24/material/slides/0.pdf.

[56] T. Hahn, M. Perez-Victoria, Automatized one loop calculations in four-dimensions and D-dimensions, Comput. Phys. Commun. 118 (1999) 153–165. arXiv:hep-ph/9807565, doi:10.1016/S0010-4655(98)00173-8.

[57] G. van Oldenborgh, FF: A package to evaluate one loop Feynman diagrams, Comput. Phys. Commun. 66 (1991) 1–15. doi:10.1016/0010-4655(91)90002-3.

[58] J. Usovitsch, I. Dubovyk, T. Riemann, The MBnumerics project, section E.2 in [3]. arXiv:1809.01830.

[59] T. Riemann, 1-loop Feynman integrals at arbitrary space-time d, slides of talk held at 11^{th} FCC-ee workshop: Theory and Experiments, 8 - 11 January 2019, CERN, Geneva, Switzerland, https://indico.cern.ch/event/766859/contributions/3252618/attachments/1776255/2887926/riemann11FCCeeWS2019.pdf.

[60] G. Devaraj, R. G. Stuart, Reduction of one-loop tensor form-factors to scalar integrals: A general scheme, Nucl. Phys. B519 (1998) 483–513. arXiv:hep-ph/9704308, doi:10.

1016/S0550-3213(98)00035-2.

[61] K. H. Phan, D. T. Tran, One-loop three-point Feynman integrals with Appell F_1 hypergeometric functions. arXiv:1904.07430.

[62] J. Usovitsch and T. Riemann, New approach to Mellin-Barnes representations for massive one-loop Feynman integrals, section E.6 in [3].

[63] J. Usovitsch, MBOneLoop, a Mathematica/Fortran package for the numerical calculation of multiple MB-integral representations for one-loop Feynman integrals at arbitrary kinematics, to be published at http://prac.us.edu.pl/~gluza/ambre/.

[64] P. Appell, Sur les fonctions hypergéométriques de plusieurs variables, les polynômes d'Hermite et autres fonctions sphériques dans l'hyperespace, Mémorial des sciences mathématiques, fascicule 3 (1925), p. 82. http://www.numdam.org/item?id=MSM_1925__3__1_0.

[65] S. Saran, Transformation of certain hypergeometric functions of three variables, Acta Math. 93 (1955) 293. doi:10.1007/BF02392525.

[66] L. Slater, Generalized hypergeometric functions, Cambridge University Press, Cambridge, 1966, https://onlinelibrary.wiley.com/doi/pdf/10.1002/zamm.19660460536#accessDenialLayout.

[67] E. Picard, Sur une extension aux fonctions de deux variables du problème de Riemann relatif aux fonctions hypergéométriques. Annales scientifiques de l'É.N.S. 2 e série 10, 305-322 (1881). http://www.numdam.org/item?id=ASENS_1881_2_10__305_0.

[68] J. Gluza, K. Kajda, T. Riemann, V. Yundin, Numerical evaluation of tensor Feynman integrals in Euclidean kinematics, Eur. Phys. J. C71 (2011) 1516. arXiv:1010.1667, doi:10.1140/epjc/s10052-010-1516-y.

3 NNLO corrections in 4 dimensions

Author: Roberto Pittau [pittau@ugr.es]

3.1 Introduction

Currently, four-dimensional techniques applied to higher order calculations are under active investigation [1–8]. The main motivation for this is the need of simplifying perturbative calculations necessary to cope with the precision requirements of the future LHC and FCC experiments.

In this contribution, I review the FDR approach [9] to the computation of NNLO corrections in 4 dimensions. In particular, I describe how fully inclusive NNLO final state quark-pair corrections [10]

$$\sigma^{NNLO} = \sigma_B + \sigma_V + \sigma_R \qquad \text{with} \qquad \begin{cases} \sigma_B = \int d\Phi_n \sum_{\text{spin}} |A_n^{(0)}|^2 \\ \sigma_V = \int d\Phi_n \sum_{\text{spin}} \left\{ A_n^{(2)} (A_n^{(0)})^* + A_n^{(0)} (A_n^{(2)})^* \right\} \\ \sigma_R = \int d\Phi_{n+2} \sum_{\text{spin}} \left\{ A_{n+2}^{(0)} (A_{n+2}^{(0)})^* \right\} \end{cases} \tag{3.73}$$

are computed in FDR by directly enforcing gauge invariance and unitarity in the definition of the regularized UV and IR divergent integrals. The IR divergent parts of the amplitudes are depicted in Fig. C.2 and $d\Phi_m := \delta\left(P - \sum_{i=1}^m p_i\right) \prod_{i=1}^m d^4 p_i \delta_+(p_i^2)$.

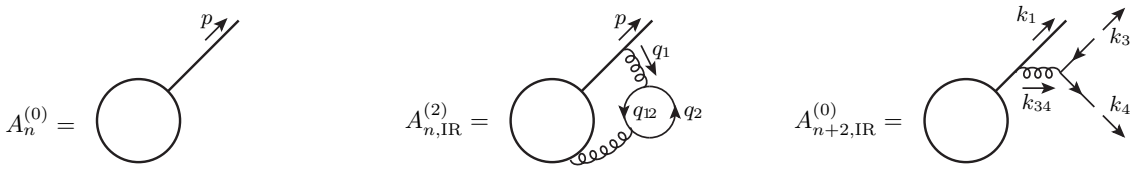

(a) (b) (c)

Fig. C.2: The lowest order amplitude (a), the IR divergent final-state virtual quark-pair correction (b) and the IR divergent real component (c). The empty circle stands for the emission of $n-1$ particles. Additional IR finite corrections are created if the gluons with momenta q_1 and k_{34} are emitted by off-shell particles contained in the empty circle.

In Sec. 3.2, I recall the basics of FDR. The next Sections deal with its use in the contest of the calculation of σ^{NNLO} in Eq. (3.73).

3.2 FDR integration and loop integrals

The main idea of FDR can be sketched out with the help of a simple one-dimensional example [11]. More details can be found in the relevant literature [9, 10, 12–16]. Let's assume one needs to define the UV divergent integral

$$I = \lim_{\Lambda\to\infty} \int_0^\Lambda dx \frac{x}{x+M}, \tag{3.74}$$

where M stands for a physical energy scale. FDR identifies the UV divergent pieces in terms of integrands which do not depend on M, the so called FDR vacua, and separates them by

rewriting

$$\frac{x}{x+M} = 1 - \frac{M}{x} + \frac{M^2}{x(x+M)}. \tag{3.75}$$

The first term in the r.h.s. of Eq. (3.75) is the vacuum responsible for the linear $\mathcal{O}(\Lambda)$ UV divergence of I and $1/x$ generates its $\ln\Lambda$ behavior. By *definition* of FDR integration, both divergent contributions need to be subtracted from Eq. (3.74). The subtraction of the $\mathcal{O}(\Lambda)$ piece is performed over the full integration domain $[0,\Lambda]$, while the logarithmic divergence is removed over the interval $[\mu_R,\Lambda]$ only. The arbitrary separation scale $\mu_R \neq 0$ is needed to keep a-dimensional and finite the arguments of the logarithms appearing in the subtracted and finite parts. Thus

$$I_{\rm FDR} := I - \lim_{\Lambda\to\infty}\left(\int_0^\Lambda dx - \int_{\mu_R}^\Lambda dx\frac{M}{x}\right) = M\ln\frac{M}{\mu_R}. \tag{3.76}$$

The advantage of the definition in Eq. (3.76) is twofold:

- the UV cutoff Λ is traded for μ_R, which is interpreted, right away, as the renormalization scale;
- other than logarithmic UV divergences never contribute.

The use of Eq. (3.76) is inconvenient in practical calculations due to the explicit appearance of μ_R in the integration interval. An equivalent definition is obtained by adding an auxiliary unphysical scale μ to x,

$$x \to \bar{x} := x + \mu, \tag{3.77}$$

and introducing an integral operator $\int_0^\infty[dx]$ defined in such a way that it annihilates the FDR vacua before integration. Thus

$$I_{\rm FDR} = \int_0^\infty[dx]\frac{\bar{x}}{\bar{x}+M} = \int_0^\infty[dx]\left(1 - \frac{M}{\bar{x}} + \frac{M^2}{\bar{x}(\bar{x}+M)}\right) := M^2\lim_{\mu\to 0}\int_0^\infty dx\frac{1}{\bar{x}(\bar{x}+M)}\bigg|_{\mu=\mu_R} \tag{3.78}$$

where $\mu \to 0$ is an asymptotic limit. Note that, in order to keep the structure of the subtracted terms as in Eq. (3.75), the replacement $x \to \bar{x}$ must be performed in *both numerator and denominator* of the integrated function.

This strategy can be extended to more dimensions and to integrands which are rational functions of the integration variables, as is the case of multi-loop integrals. For instance, typical two-loop integrals contributing to $\sigma_V(\gamma^* \to jets)$ and $\sigma_V(H \to b\bar{b} + jets)$ are

$$K_1 := \int[d^4q_1][d^4q_2]\frac{1}{\bar{q}_1^2\bar{D}_1\bar{D}_2\bar{q}_2^2\bar{q}_{12}^2}, \qquad K_2^{\rho\sigma\alpha\beta} := \int[d^4q_1][d^4q_2]\frac{q_2^\rho q_2^\sigma q_1^\alpha q_1^\beta}{\bar{q}_1^4\bar{D}_1\bar{D}_2\bar{q}_2^2\bar{q}_{12}^2}, \tag{3.79}$$

where $q_{12} := q_1 + q_2$, $\bar{D}_{1,2} = \bar{q}_1^2 + 2(q_1\cdot p_{1,2})$, $p_{1,2}^2 = 0$, and $\bar{q}_i^2 := q_i^2 - \mu^2$ $(i = 1, 2, 12)$, in the same spirit of Eq. (3.77).

FDR integration keeps shift invariance in any of the loop integration variables and the possibility of cancelling reconstructed denominators, e.g.

$$\int[d^4q_1][d^4q_2]\frac{\bar{q}_1^2}{\bar{q}_1^4\bar{D}_1\bar{D}_2\bar{q}_2^2\bar{q}_{12}^2} = K_1. \tag{3.80}$$

Since, instead, $\int [d^4q_1][d^4q_2] \frac{q_1^2}{\bar{q}_1^4 \bar{D}_1 \bar{D}_2 \bar{q}_2^2 \bar{q}_{12}^2} \neq K_1$, this last property is maintained only if the replacement $q_i^2 \to \bar{q}_i^2$ is also performed in the numerator of the loop integrals whenever q_i^2 is generated by Feynman rules. This is called *global prescription* (GP), often denoted by $q_i^2 \overset{\text{GP}}{\to} \bar{q}_i^2$.

GP and shift invariance guarantee results which do not depend on the chosen gauge [12, 14]. Nevertheless, unitarity should also be maintained. This requires that any given UV divergent sub-diagram produce the same result when computed/manipulated separately or when embedded in the full diagram. Such a requirement is called *sub-integration consistency* (SIC) [15]. Enforcing SIC in the presence of IR divergent integrals, such as those in Eq. (3.79), needs extra care. In fact, the IR treatments of σ_V and σ_R should match with each other. In the next Sections I describe how this is achieved in the computation of the observable in Eq. (3.73).

3.3 Keeping unitarity in the virtual component

Any integral contributing to σ_V has the form

$$I_V = \int [d^4q_1][d^4q_2] \frac{N_V}{\bar{D}\bar{q}_2^2\bar{q}_{12}^2}, \tag{3.81}$$

where $\bar{D}$ collects all q_2-independent propagators and N_V is the numerator of the corresponding Feynman diagram. I_V can be sub-divergent or globally divergent for large values of the integration momenta. For example, K_1 in Eq. (3.79) only diverges when $q_2 \to \infty$, while K_2 also when $q_{1,2} \to \infty$. This means that FDR prescribes the subtraction of a *global vacuum* (GV) involving both integration variables in K_2, while the *sub-vacuum* (SV) developed when $q_2 \to \infty$ should be removed from both K_1 and K_2. In addition, IR infinities are generated by the on-shell conditions $p_{1,2}^2 = 0$. Even though IR divergences are automatically regulated when barring the loop denominators, a careful SIC preserving treatment is necessary in order not to spoil unitarity. Since the only possible UV sub-divergence is produced by the quark loop in Fig. C.2-(b), this is accomplished as follows [10]:

- one does not apply GP to the contractions $g_{\rho\sigma}q_2^\rho q_2^\sigma$ when $g_{\rho\sigma}$ refers to indices external to the UV divergent sub-diagram;
- one replaces back everywhere $\bar{q}_1^2 \to q_1^2$ *after* GV subtraction.

The external indices entering the calculation of σ_V in Eq. (3.73) are denoted by $\hat{\rho}$ and $\hat{\sigma}$ in Fig. C.3-(a,b). Using this convention, one can rephrase the first rule as follows: $g_{\rho\sigma}q_2^\rho q_2^\sigma =$

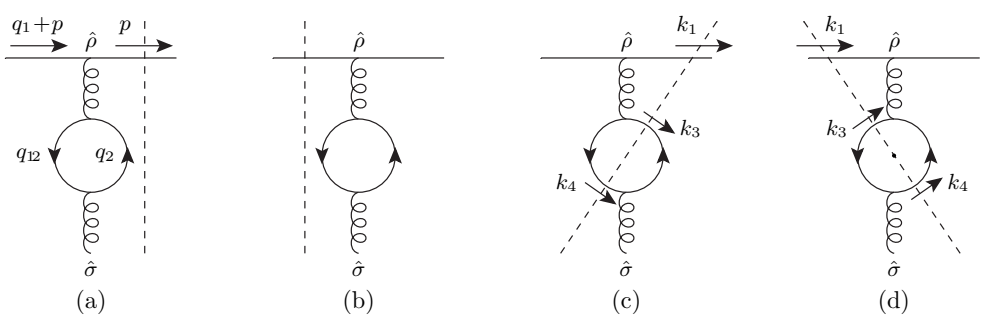

Fig. C.3: Virtual and real cuts contributing to the IR divergent parts of σ_V (a,b) and σ_R (c,d).

$q_2^2 \overset{\rm GP}{\to} \bar{q}_2^2$, but $g_{\hat{\rho}\hat{\sigma}} q_2^\rho q_2^\sigma := \hat{q}_2^2 \overset{\rm GP}{\to} q_2^2$, which gives, for instance,

$$
\begin{aligned}
g_{\rho\sigma} K_2^{\rho\sigma\alpha\beta} &\overset{\rm GP}{\to} \bar{K}_2^{\alpha\beta} = \int [d^4q_1] \frac{q_1^\alpha q_1^\beta}{\bar{q}_1^4 \bar{D}_1 \bar{D}_2} \int [d^4q_2] \frac{1}{\bar{q}_{12}^2} = 0, \text{ but} \\
g_{\hat{\rho}\hat{\sigma}} K_2^{\rho\sigma\alpha\beta} &\overset{\rm GP}{\to} \hat{K}_2^{\alpha\beta} = \int [d^4q_1][d^4q_2] \frac{q_2^2 q_1^\alpha q_1^\beta}{\bar{q}_1^4 \bar{D}_1 \bar{D}_2 \bar{q}_2^2 \bar{q}_{12}^2} \neq 0,
\end{aligned}
\tag{3.82}
$$

where $\bar{K}_2^{\alpha\beta}$ vanishes because the shift $q_2 \to q_2 - q_1$ makes it proportional to the sub-vacuum $1/\bar{q}_2^2$, which is annihilated by the $\int [d^4q_2]$ operator. It can be shown [10, 15] that integrals such as $\hat{K}_2^{\alpha\beta}$ generate the unitarity restoring logarithms missed by $\bar{K}_2^{\alpha\beta}$.

As for the second rule, it states that a GV subtraction is needed first. In the case of $\hat{K}_2^{\alpha\beta}$, this is achieved by rewriting $\frac{1}{\bar{D}_1} = \frac{1}{\bar{q}_1^2} - \frac{2(q_1 \cdot p_1)}{D_1 \bar{q}_1^2}$. The first term gives a scaleless integral, annihilated by $\int [d^4q_1][d^4q_2]$, so that

$$
\hat{K}_2^{\alpha\beta} = -2 \int [d^4q_1][d^4q_2] \frac{(q_1 \cdot p_1) q_2^2 q_1^\alpha q_1^\beta}{\bar{q}_1^6 \bar{D}_1 \bar{D}_2 \bar{q}_2^2 \bar{q}_{12}^2},
\tag{3.83}
$$

which is now only sub-divergent when $q_2 \to \infty$, as is K_1 in Eq. (3.79). After that, the replacement $\bar{q}_1^2 \to q_1^2$ produces

$$
K_1 \to \tilde{K}_1 = \int d^4q_1 [d^4q_2] \frac{1}{q_1^2 D_1 D_2 \bar{q}_2^2 \bar{q}_{12}^2}, \;\; \hat{K}_2^{\alpha\beta} \to \tilde{K}_2^{\alpha\beta} = -2 \int d^4q_1 [d^4q_2] \frac{(q_1 \cdot p_1) q_2^2 q_1^\alpha q_1^\beta}{q_1^6 D_1 D_2 \bar{q}_2^2 \bar{q}_{12}^2}.
\tag{3.84}
$$

All two-loop integrals I_V in Eq. (3.81) should be treated in this way. In the case of the N_F part of $\sigma_V(\gamma^* \to jets)$ and $\sigma_V(H \to b\bar{b} + jets)$ this produces three master integrals, which can be computed as described in Appendix D of [10].

After loop integration, σ_V contains logarithms of μ^2 of both UV and IR origin. The former should be replaced by logarithms of μ_R^2, as dictated by Eq. (3.78), while the latter compensate the IR behavior of σ_R. To disentangle the two cases, it is convenient to renormalize σ_V first. This means expressing the bare strong coupling constant $a^0 := \alpha_S^0/4\pi$ and the bare bottom Yukawa coupling y_b^0 in terms of $a := \alpha_S^{\overline{\rm MS}}(s)/4\pi$ and y_b extracted from the the bottom pole mass m_b. The relevant relations in terms of $L := \ln \mu^2/(p_1 - p_2)^2$ and $L'' := \ln \mu^2/m_b^2$ are as follows [10]

$$
a^0 = a\left(1 + a\delta_a^{(1)}\right), \;\; y_b^0 = y_b\left(1 + a\delta_y^{(1)} + a^2\left(\delta_y^{(2)} + \delta_a^{(1)}\delta_y^{(1)}\right)\right),
\tag{3.85}
$$

with

$$
\delta_a^{(1)} = \frac{2}{3} N_F L, \;\; \delta_y^{(1)} = -C_F\left(3L'' + 5\right), \;\; \delta_y^{(2)} = C_F N_F\left(L''^2 + \frac{13}{3} L'' + \frac{2}{3}\pi^2 + \frac{151}{18}\right).
\tag{3.86}
$$

After renormalization, the remaining μ^2s are the IR ones.

3.4 Keeping unitarity in the real component

The integrands in σ_R of Eq. (3.73) are represented in Fig. C.3-(c,d). They are of the form

$$
J_R = \frac{N_R}{S s_{34}^\alpha s_{134}^\beta}, \;\; s_{i\ldots j} := (k_i + \ldots + k_j)^2, \;\; 0 \le \alpha, \beta \le 2,
\tag{3.87}
$$

where N_R is the numerator of the amplitude squared and S collects the remaining propagators. Depending on the value of α and β, J_R becomes infrared divergent when integrated over Φ_{n+2}. These IR singularities must be regulated consistently with the SIC preserving treatment of σ_V described in Sec. 3.3.

The changes $q_2^2 \overset{\text{GP}}{\to} \bar{q}_2^2$ and $q_{12}^2 \overset{\text{GP}}{\to} \bar{q}_{12}^2$ in the virtual cuts of Fig. C.3-(a,b) imply the Cutkosky relation

$$\frac{1}{(\bar{q}_2^2 + i0^+)(\bar{q}_{12}^2 + i0^+)} \leftrightarrow \left(\frac{2\pi}{i}\right)^2 \delta_+(\bar{k}_3^2)\delta_+(\bar{k}_4^2), \tag{3.88}$$

with $\bar{k}_{3,4}^2 := k_{3,4}^2 - \mu^2$. Hence, one replaces in Eq. (3.73) $\Phi_{n+2} \to \tilde{\Phi}_{n+2}$, where the phase-space $\tilde{\Phi}_{n+2}$ is such that $k_3^2 = k_4^2 = \mu^2$ and $k_i^2 = 0$ when $i \neq 3, 4$. In [10] it is proven that SV subtraction in σ_V does not alter Eq. (3.88). Analogously, the correspondence between cuts (a) and (d)

$$\frac{1}{(q_1 + p)^2 + i0^+} \leftrightarrow \frac{2\pi}{i}\delta_+(k_1^2) \tag{3.89}$$

is not altered by GV subtraction. Finally, k_3^2, k_4^2 and $(k_3 + k_4)^2 = s_{34}$ in N_R of Eq. (3.87) should be treated using the same prescriptions imposed on q_2^2, q_{12}^2 and q_1^2 in N_V of Eq. (3.81), respectively. This means replacing

$$k_{3,4}^2 \to \bar{k}_{3,4}^2 = 0, \quad (k_3 \cdot k_4) = \frac{1}{2}\left(s_{34} - k_3^2 - k_4^2\right) \to \frac{1}{2}(s_{34} - \bar{k}_3^2 - \bar{k}_4^2) = \frac{1}{2}s_{34}, \tag{3.90}$$

where the last equalities are induced by the delta functions in Eq. (3.88). These changes should be performed everywhere in N_R except in contractions induced by the external indices $\hat{\rho}$ and $\hat{\sigma}$ in cuts (c,d). In this case

$$g_{\hat{\rho}\hat{\sigma}} k_{3,4}^\rho k_{3,4}^\sigma \to k_{3,4}^2 = \mu^2, \quad g_{\hat{\rho}\hat{\sigma}} k_3^\rho k_4^\sigma \to (k_3 \cdot k_4) = \frac{s_{34} - 2\mu^2}{2}. \tag{3.91}$$

In the case of the N_F part of $\sigma_R(\gamma^* \to jets)$ and $\sigma_R(H \to b\bar{b} + jets)$, integrating J_R over $\tilde{\Phi}_4$ and taking the asymptotic $\mu \to 0$ limit produces the phase-space integrals reported in Appendix E of [10].

3.5 Results and conclusions

Using the approach outlined in Sec. 3.3 and Sec. 3.4 one reproduces the known $\overline{\text{MS}}$ results for the N_F components of $\sigma^{\text{NNLO}}(H \to b\bar{b} + jets)$ and $\sigma^{\text{NNLO}}(\gamma^* \to jets)$ [10]

$$\begin{aligned}
\sigma^{\text{NNLO}}(H \to b\bar{b} + jets) &= \Gamma_{\text{BORN}}(y_b^{\overline{\text{MS}}}(M_H))\left\{1 + a^2 C_F N_F \left(8\zeta_3 + \frac{2}{3}\pi^2 - \frac{65}{2}\right)\right\}, \\
\sigma^{\text{NNLO}}(\gamma^* \to jets) &= \sigma_{\text{BORN}}\left\{1 + a^2 C_F N_F \left(8\zeta_3 - 11\right)\right\}.
\end{aligned} \tag{3.92}$$

This shows, for the first time, that a fully four-dimensional framework to compute NNLO quark-pair corrections can be constructed based on the requirement of preserving gauge invariance and unitarity. The basic principles leading to a consistent treatment of all the pieces contributing to the NNLO results in Eq. (3.92) are expected to remain valid also when considering more complicated environments. A general four-dimensional NNLO procedure including initial state IR singularities is currently under investigation.

References

[1] R. A. Fazio, P. Mastrolia, E. Mirabella, W. J. Torres Bobadilla, On the Four-Dimensional Formulation of Dimensionally Regulated Amplitudes, Eur. Phys. J. C74 (12) (2014) 3197. arXiv:1404.4783, doi:10.1140/epjc/s10052-014-3197-4.

[2] O. A. Battistel, A. L. Mota, M. C. Nemes, Consistency conditions for 4-D regularizations, Mod. Phys. Lett. A13 (1998) 1597–1610. doi:10.1142/S0217732398001686.

[3] A. L. Cherchiglia, M. Sampaio, M. C. Nemes, Systematic Implementation of Implicit Regularization for Multi-Loop Feynman Diagrams, Int. J. Mod. Phys. A26 (2011) 2591–2635. arXiv:1008.1377, doi:10.1142/S0217751X11053419.

[4] R. J. Hernandez-Pinto, G. F. R. Sborlini, G. Rodrigo, Towards gauge theories in four dimensions, JHEP 02 (2016) 044. arXiv:1506.04617, doi:10.1007/JHEP02(2016)044.

[5] G. F. R. Sborlini, F. Driencourt-Mangin, R. Hernandez-Pinto, G. Rodrigo, Four-dimensional unsubtraction from the loop-tree duality, JHEP 08 (2016) 160. arXiv:1604.06699, doi:10.1007/JHEP08(2016)160.

[6] G. F. R. Sborlini, F. Driencourt-Mangin, G. Rodrigo, Four-dimensional unsubtraction with massive particles, JHEP 10 (2016) 162. arXiv:1608.01584, doi:10.1007/JHEP10(2016)162.

[7] F. Driencourt-Mangin, G. Rodrigo, G. F. R. Sborlini, W. J. Torres Bobadilla, Universal four-dimensional representation of $H \to \gamma\gamma$ at two loops through the Loop-Tree Duality, JHEP 02 (2019) 143. arXiv:1901.09853, doi:10.1007/JHEP02(2019)143.

[8] R. Runkel, Z. Szor, J. P. Vesga, S. Weinzierl, Causality and loop-tree duality at higher loops.arXiv:1902.02135.

[9] R. Pittau, A four-dimensional approach to quantum field theories, JHEP 11 (2012) 151. arXiv:1208.5457, doi:10.1007/JHEP11(2012)151.

[10] B. Page, R. Pittau, NNLO final-state quark-pair corrections in four dimensions.arXiv:1810.00234.

[11] R. Pittau, Matching electroweak fermion loops onto the Fermi theory without higher dimensional operators.arXiv:1902.01767.

[12] A. M. Donati, R. Pittau, Gauge invariance at work in FDR: $H \to \gamma\gamma$, JHEP 04 (2013) 167. arXiv:1302.5668, doi:10.1007/JHEP04(2013)167.

[13] R. Pittau, QCD corrections to $H \to gg$ in FDR, Eur. Phys. J. C74 (1) (2014) 2686. arXiv:1307.0705, doi:10.1140/epjc/s10052-013-2686-1.

[14] A. M. Donati, R. Pittau, FDR, an easier way to NNLO calculations: a two-loop case study, Eur. Phys. J. C74 (2014) 2864. arXiv:1311.3551, doi:10.1140/epjc/s10052-014-2864-9.

[15] B. Page, R. Pittau, Two-loop off-shell QCD amplitudes in FDR, JHEP 11 (2015) 183. arXiv:1506.09093, doi:10.1007/JHEP11(2015)183.

[16] A. Blondel, et al., Standard Model Theory for the FCC-ee: The Tera-Z, in: Mini Workshop on Precision EW and QCD Calculations for the FCC Studies : Methods and Techniques CERN, Geneva, Switzerland, January 12-13, 2018, 2018. arXiv:1809.01830.

4 Unsubtractions at NNLO

Authors: J. Jesús Aguilera-Verdugo, Félix Driencourt-Mangin, Judith Plenter, Selomit Ramírez-Uribe, Germán Rodrigo, Germán F. R. Sborlini, William J. Torres Bobadilla, Szymon Tracz
Corresponding Author: Germán Rodrigo [german.rodrigo@csic.es]

4.1 Introduction

Computations in perturbative Quantum Field Theory (pQFT) feature several aspects which, although intrinsically non-physical, are traditionally successfully eluded by modifying the dimensions of the space-time. Closed loops in pQFT implicitly extrapolate the validity of the Standard Model (SM) to infinite energies – equivalent to zero distance–, much above the Planck scale. We should expect this to be a legitimate procedure if the loop scattering amplitudes that contribute to the physical observables are either suppressed at very high energies, or if there is a way to suppress / renormalise their contribution in this limit. In gauge theories like QCD, massless particles can be emitted with zero energy, and pQFT treats the quantum state with N external partons as different from the quantum state with emission of extra massless particles at zero energy, while these two states are physically identical. In addition, partons can be emitted in exactly the same direction, or in other words at zero distance. All these unphysical features have a price and lead to the emergence of infinities in the four dimensions of the space-time.

In Dimensional Regularization (DREG) [1–5], the infinities are replaced by explicit poles in $1/\varepsilon$, with $d = 4 - 2\varepsilon$, through integration of the loop momenta and the phase-space of real radiation. Then, the $1/\varepsilon$ ultraviolet (UV) singularities of the virtual contributions are removed by renormalisation, and the infrared (IR) soft and collinear singularities are subtracted. The general idea of subtraction [6–18] consists of introducing counter-terms which mimic the local IR behaviour of the real components and that can easily be integrated analytically in d-dimensions. In this way, the integrated form is combined with the virtual component whilst the unintegrated counter-term cancels the IR poles originated from the phase-space integration of the real-radiation contribution.

Although this procedure efficiently transforms the theory into a calculable and well-defined mathematical framework, a big effort needs to be invested in evaluating loop and phase-space integrals in arbitrary space-time dimensions, which are particularly difficult at higher perturbative orders. In view of the highly challenging demands imposed by the expected accuracy attainable at the LHC and future colliders, like the FCC, there has been a recent interest in the community to define perturbative methods directly in $d = 4$ space-time dimensions in order to avoid the complexity of working in a non-physical multidimensional space [19]. Examples of those methods are the four-dimensional formulation (FDF) [20] of the four-dimensional helicity scheme, the six-dimensional formalism (SDF) [21], implicit regularisation (IREG) [22, 23], and four-dimensional regularisation / renormalisation (FDR) [24, 25] *. In this section, we review the four-dimensional unsubtraction (FDU) [26–28] method, which is based on the loop-tree duality (LTD) [29–36]. The idea behind FDU is to exploit a suitable mapping of momenta between the virtual and real kinematics in such a way that the summation over the degenerate soft and collinear quantum states is performed locally at integrand level without the necessity to introduce IR subtractions, whereas the UV singularities are locally suppressed at very high

*R. Pittau, see Section 3

energies, e.g. at two loops [35]. The method should improve the efficiency of Monte Carlo event generators because it simultaneously describes real and virtual contributions.

Finally, LTD is also a powerful framework to analyse the singular structure of scattering amplitudes directly in the loop momentum space, which is particularly interesting to charaterise unitarity thresholds and anomalous thresholds for specific kinematical configurations [36].

4.2 The Loop-Tree Duality

The LTD representation of a one-loop scattering amplitude is given by

$$\mathcal{A}^{(1)}(\{p_n\}_N) \;=\; -\int_\ell \mathcal{N}(\ell,\{p_n\}_N)\otimes G_D(\alpha)\;, \tag{4.93}$$

where $G_D(\alpha)=\sum_{i\in\alpha}\tilde{\delta}\,(q_i)\prod_{j\neq i}G_D(q_i;q_j)$, and $\mathcal{N}(\ell,\{p_n\}_N)$ the numerator of the integrand, which depends on the loop momentum ℓ and the external momenta $\{p_n\}_N$. The delta function $\tilde{\delta}\,(q_i)=\imath 2\pi\,\theta(q_{i,0})\,\delta(q_i^2-m_i^2)$ sets on-shell the internal propagator with momentum $q_i=\ell+k_i$ and selects its positive energy mode, $q_{i,0}>0$. At one-loop, $\alpha=\{1,\cdots,N\}$ labels all the internal momenta, and Eq.(4.93) is the sum of N single-cut dual amplitudes. The dual propagators,

$$G_D(q_i;q_j)=\frac{1}{q_j^2-m_j^2-\imath 0\,\eta\cdot k_{ji}}\;, \tag{4.94}$$

differ from the usual Feynman propagators only by the imaginary prescription that now depends on $\eta\cdot k_{ji}$, with $k_{ji}=q_j-q_i$. The dual propagators are implicitly linear in the loop momentum due to the on-shell conditions. With $\eta=(1,\mathbf{0})$, which is equivalent to integrating out the energy component of the loop momentum, the remaining integration domain is Euclidean.

At two-loops the corresponding dual representation is [31, 35]

$$\begin{aligned}\mathcal{A}^{(2)}(\{p_n\}_N) \;=\; &\int_{\ell_1}\int_{\ell_2}\mathcal{N}(\ell_1,\ell_2,\{p_n\}_N)\otimes\big[G_D(\alpha_1)\,G_D(\alpha_2\cup\alpha_3)+G_D(-\alpha_2\cup\alpha_1)G_D(\alpha_3)\\ &-\;G_D(\alpha_1)\,G_F(\alpha_2)\,G_D(\alpha_3)\big]\;.\end{aligned} \tag{4.95}$$

Now, the internal momenta are $q_i=\ell_1+k_i$, $q_j=\ell_2+k_j$ and $q_k=\ell_1+\ell_2+k_k$, and are classified into three different sets, with $i\in\alpha_1$, $j\in\alpha_2$ and $k\in\alpha_3$ (see Fig. C.4). The minus sign in front of α_2 indicates that the momenta in α_2 are reversed to hold a momentum flow consistent with α_1. The dual representation in Eq. (4.95) spans over the sum of all possible double-cut contributions, with each of the two cuts belonging to a different set. In general, at higher orders, LTD transforms any loop integral or loop scattering amplitude into a sum of tree-level like objects that are constructed by setting on-shell a number of internal loop propagators equal to the number of loops.

Explicit LTD representations of the scattering amplitude describing the decay $H\to\gamma\gamma$ have been presented at one- [34] and two-loops [35].

4.3 Four-Dimensional Unsubtraction

It is interesting to note that although in Eqs. (4.93) and (4.95) the on-shell loop three-momenta are unrestricted, all the IR and physical threshold singularities of the dual amplitudes are restricted to a compact region [32, 36], as discussed in Section 4.4. This is essential to define the Four-Dimensional Unsubtraction (FDU) [26–28] algorithm, namely, to establish a mapping

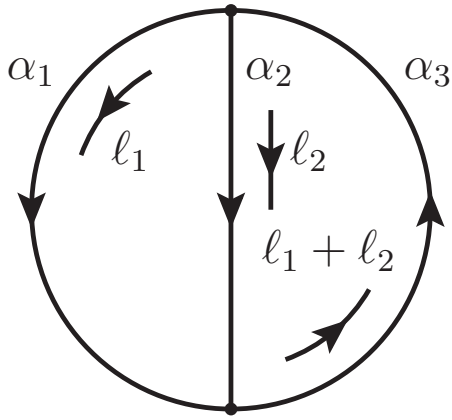

Fig. C.4: Momentum flow of a two-loop Feynman diagram.

between the real and virtual kinematics in order to locally cancel the IR singularities without the need for subtraction counter-terms.

In the FDU approach, the cross-section at next-to-leading order (NLO) is constructed, as usual, from the renormalised one-loop virtual correction with N external partons and the exclusive real cross-section with $N+1$ partons

$$\sigma^{\mathrm{NLO}} = \int_N d\sigma_{\mathrm{V}}^{(1,\mathrm{R})} + \int_{N+1} d\sigma_{\mathrm{R}}^{(1)} \ , \tag{4.96}$$

integrated over the corresponding phase-space, $\int_N$ and $\int_{N+1}$. The virtual contribution is obtained from its LTD representation

$$\int_N d\sigma_{\mathrm{V}}^{(1,\mathrm{R})} = \int_{(N,\vec{\ell})} 2\,\mathrm{Re}\,\langle \mathcal{M}_N^{(0)} | \left(\sum_i \mathcal{M}_N^{(1)}(\tilde{\delta}(q_i)) \right) - \mathcal{M}_{\mathrm{UV}}^{(1)}(\tilde{\delta}(q_{\mathrm{UV}})) \rangle \, \hat{\mathcal{O}}(\{p_n\}_N) \ , \tag{4.97}$$

where $\mathcal{M}_N^{(0)}$ is the N-leg scattering amplitude at leading order (LO), and $\mathcal{M}_N^{(1)}(\tilde{\delta}(q_i))$ is the dual representation of the unrenormalised one-loop scattering amplitude with the internal momentum q_i set on-shell. The integral is weighted with the explicit observable function $\hat{\mathcal{O}}(\{p_n\}_N)$. The expression includes appropriate counter-terms, $\mathcal{M}_{\mathrm{UV}}^{(1)}(\tilde{\delta}(q_{\mathrm{UV}}))$, that implement renormalisation by subtracting the UV singularities locally, as discussed in Ref. [27, 28], including UV singularities of degree higher than logarithmic that integrate to zero.

By means of an appropriate mapping between the real and virtual kinematics [27, 28]:

$$\{p_r'\}_{N+1} \to (q_i, \{p_n\}_N) \ , \tag{4.98}$$

the real phase-space is rewritten in terms of the virtual phase-space and the loop three-momentum

$$\int_{N+1} = \int_{(N,\vec{\ell})} \sum_i \mathcal{J}_i(q_i)\, \mathcal{R}_i(\{p_r'\}_{N+1}) \ , \tag{4.99}$$

where $\mathcal{J}_i(q_i)$ is the Jacobian of the transformation with q_i on-shell, and $\mathcal{R}_i(\{p_j'\}_{N+1})$ defines a complete partition of the real phase-space

$$\sum_i \mathcal{R}_i(\{p_r'\}_{N+1}) = 1 \ . \tag{4.100}$$

As the result, the NLO cross-section is cast into a single integral in the Born/virtual phase-space and the loop three-momentum

$$\begin{aligned}\sigma^{\rm NLO} &= \int_{(N,\vec{\ell})} \Bigg[2\,{\rm Re}\,\langle \mathcal{M}_N^{(0)}| \Bigg(\sum_i \mathcal{M}_N^{(1)}(\tilde{\delta}(q_i)) \Bigg) - \mathcal{M}_{\rm UV}^{(1)}(\tilde{\delta}(q_{\rm UV}))\rangle\, \hat{\mathcal{O}}(\{p_n\}_N) \\ &+ \sum_i \mathcal{J}_i(q_i)\, \mathcal{R}_i(\{p'_r\}_{N+1})\, |\mathcal{M}_{N+1}^{(0)}(\{p'_r\}_{N+1})|^2\, \hat{\mathcal{O}}(\{p'_r\}_{N+1}) \Bigg] \,, \end{aligned} \tag{4.101}$$

and exhibits a smooth four-dimensional limit in such a way that it can be evaluated directly in four space-time dimensions. Explicit computations have been presented in Refs. [27, 28] with both massless and massive final-state quarks. More important, with suitable mappings in Eq. (4.98) conveniently describing the quasi-collinear configurations also the transition from the massive [28] to the massless configuration [27] is smooth.

The extension of FDU to next-to-next-to-leading order (NNLO) is obvious, the total cross-section consists of three contributions

$$\sigma^{\rm NNLO} = \int_N d\sigma_{\rm VV}^{(2,{\rm R})} + \int_{N+1} d\sigma_{\rm VR}^{(2,{\rm R})} + \int_{N+2} d\sigma_{\rm RR}^{(2)} \,, \tag{4.102}$$

where the double virtual cross-section $d\sigma_{\rm VV}^{(2,{\rm R})}$ receives contributions from the interference of the two-loop with the Born scattering amplitudes, and the square of the one-loop scattering amplitude with N external partons, the virtual-real cross-section $d\sigma_{\rm VR}^{(2,{\rm R})}$ includes the contributions from the interference of one-loop and tree-level scattering amplitudes with one extra external particle, and the double real cross-section $d\sigma_{\rm RR}^{(2)}$ are tree-level contributions with emission of two extra particles. The LTD representation of the two-loop scattering amplitude, $\langle \mathcal{M}_N^{(0)}|\mathcal{M}_N^{(2)}(\tilde{\delta}(q_i,q_j))\rangle$, is obtained from Eq. (4.95), while the two loop momenta of the squared one-loop amplitude are independent and generate dual contributions of the type $\langle \mathcal{M}_N^{(1)}(\tilde{\delta}(q_i))|\mathcal{M}_N^{(1)}(\tilde{\delta}(q_j))\rangle$. In both cases, there are two independent loop three-momenta and N external momenta, with which to reconstruct the kinematics of the tree-level corrections entering $d\sigma_{\rm RR}^{(2)}$ and the one-loop corrections in $d\sigma_{\rm VR}^{(2,{\rm R})}$:

$$\{p''_r\}_{N+2} \to (q_i, q_j, \{p_n\}_N) \,, \qquad (q'_k, \{p'_s\}_{N+1}) \to (q_i, q_j, \{p_n\}_N) \,, \tag{4.103}$$

in such a way that all the contributions to the NNLO cross-section are cast into a single phase-space integral

$$\sigma^{\rm NNLO} = \int_{(N,\vec{\ell}_1,\vec{\ell}_2)} d\sigma^{\rm NNLO} \,. \tag{4.104}$$

Explicit applications of FDU at NNLO are currently under investigation.

4.4 Unitarity Thresholds and Anomalous Thresholds

An essential feature for FDU to work is to proof that all the IR singularities of the dual amplitudes are restricted to a compact region of the loop three-momenta. This has recently been proven at higher orders in Ref. [36], thus extending the one-loop analysis of Ref. [32], and also analysing the case of anomalous thresholds. The location of the singularities of the dual amplitudes in the loop three-momentum space are encoded at one-loop through the set of conditions

$$\lambda_{ij}^{\pm\pm} = \pm q_{i,0}^{(+)} \pm q_{j,0}^{(+)} + k_{ji,0} \to 0 \,. \tag{4.105}$$

where $q_{r,0}^{(+)} = \sqrt{\vec{q}_r^{\,2} + m_r^2}$, with $r \in \{i, j\}$, are the on-shell loop energies. There are indeed only two independent solutions. The limit $\lambda_{ij}^{++} \to 0$ describes the causal unitarity threshold, and determines that $q_{r,0}^{(+)} < |k_{ji,0}|$, where $k_{ji,0}$ depends on the external momenta only and is therefore bounded. For massless partons, it also describes soft and collinear singularities. The other potential singularity occurs for $\lambda_{ij}^{+-} \to 0$, but this is a non-causal or unphysical threshold and it cancels locally in the forest defined by the sum of all the on-shell dual contributions. For this to happen, the dual prescription of the dual propagators plays a central role. Finally, anomalous thresholds are determined by overlapping causal unitarity thresholds, e.g. λ_{ij}^{++} and $\lambda_{ik}^{++} \to 0$ simultaneously.

At two loops, the location of the singularities is determined by the set of conditions

$$\lambda_{ijk}^{\pm\pm\pm} = \pm q_{i,0}^{(+)} \pm q_{j,0}^{(+)} \pm q_{k,0}^{(+)} + k_{k(ij),0} \to 0 \ , \tag{4.106}$$

where $k_{k(ij)} = q_k - q_i - q_j$ depends on external momenta only, with $i \in \alpha_1$, $j \in \alpha_2$ and $k \in \alpha_3$. Now, the unitarity threshold is defined by the limit $\lambda_{ijk}^{+++} \to 0$ (or $\lambda_{ijk}^{---} \to 0$) with $q_{r,0}^{(+)} \leq |k_{k(ij),0}|$ and $r \in \{i, j, k\}$, and the potential singularities at $\lambda_{ijk}^{++-} \to 0$ and $\lambda_{ijk}^{+--} \to 0$ cancel locally in the forest of all the dual contributions. Again, the anomalous thresholds are determined by the simultaneous contribution of unitarity thresholds. The generalization of Eq. (4.106) to higher orders is straitforward.

4.5 Conclusions

The bottleneck in higher order perturbative calculations is not only the evaluation of multi-loop Feynman diagrams, but also the gathering of all the quantum corrections from different loop orders (and thus different number of final-state partons). In order to match the expected experimental accuracy at the LHC, particularly in the high luminosity phase, and at future colliders new theoretical efforts are still needed to overcome the current precision frontier. LTD is also a powerful framework to analyse comprehensively the emergence of anomalous thresholds at higher orders.

References

[1] C. G. Bollini, J. J. Giambiagi, Dimensional Renormalization: The Number of Dimensions as a Regularizing Parameter, Nuovo Cim. B12 (1972) 20–26. doi:10.1007/BF02895558.

[2] G. 't Hooft, M. J. G. Veltman, Regularization and Renormalization of Gauge Fields, Nucl. Phys. B44 (1972) 189–213. doi:10.1016/0550-3213(72)90279-9.

[3] G. M. Cicuta, E. Montaldi, Analytic renormalization via continuous space dimension, Lett. Nuovo Cim. 4 (1972) 329–332. doi:10.1007/BF02756527.

[4] J. F. Ashmore, A Method of Gauge Invariant Regularization, Lett. Nuovo Cim. 4 (1972) 289–290. doi:10.1007/BF02824407.

[5] K. G. Wilson, Quantum field theory models in less than four-dimensions, Phys. Rev. D7 (1973) 2911–2926. doi:10.1103/PhysRevD.7.2911.

[6] Z. Kunszt, D. E. Soper, Calculation of jet cross-sections in hadron collisions at order α_s^3, Phys. Rev. D46 (1992) 192–221. doi:10.1103/PhysRevD.46.192.

[7] S. Frixione, Z. Kunszt, A. Signer, Three jet cross-sections to next-to-leading order, Nucl. Phys. B467 (1996) 399–442. arXiv:hep-ph/9512328, doi:10.1016/0550-3213(96)00110-1.

[8] S. Catani, M. H. Seymour, The Dipole formalism for the calculation of QCD jet cross-sections at next-to-leading order, Phys. Lett. B378 (1996) 287–301. arXiv:hep-ph/9602277, doi:10.1016/0370-2693(96)00425-X.

[9] S. Catani, M. H. Seymour, A General algorithm for calculating jet cross-sections in NLO QCD, Nucl. Phys. B485 (1997) 291–419, [Erratum: Nucl. Phys.B510,503(1998)]. arXiv:hep-ph/9605323, doi:10.1016/S0550-3213(96)00589-5, 10.1016/S0550-3213(98)81022-5.

[10] A. Gehrmann-De Ridder, T. Gehrmann, E. W. N. Glover, Antenna subtraction at NNLO, JHEP 09 (2005) 056. arXiv:hep-ph/0505111, doi:10.1088/1126-6708/2005/09/056.

[11] S. Catani, M. Grazzini, An NNLO subtraction formalism in hadron collisions and its application to Higgs boson production at the LHC, Phys. Rev. Lett. 98 (2007) 222002. arXiv:hep-ph/0703012, doi:10.1103/PhysRevLett.98.222002.

[12] M. Czakon, A novel subtraction scheme for double-real radiation at NNLO, Phys. Lett. B693 (2010) 259–268. arXiv:1005.0274, doi:10.1016/j.physletb.2010.08.036.

[13] P. Bolzoni, G. Somogyi, Z. Trocsanyi, A subtraction scheme for computing QCD jet cross sections at NNLO: integrating the iterated singly-unresolved subtraction terms, JHEP 01 (2011) 059. arXiv:1011.1909, doi:10.1007/JHEP01(2011)059.

[14] R. Boughezal, C. Focke, X. Liu, F. Petriello, W-boson production in association with a jet at next-to-next-to-leading order in perturbative QCD, Phys. Rev. Lett. 115 (6) (2015) 062002. arXiv:1504.02131, doi:10.1103/PhysRevLett.115.062002.

[15] J. Gaunt, M. Stahlhofen, F. J. Tackmann, J. R. Walsh, N-jettiness Subtractions for NNLO QCD Calculations, JHEP 09 (2015) 058. arXiv:1505.04794, doi:10.1007/JHEP09(2015)058.

[16] V. Del Duca, C. Duhr, A. Kardos, G. Somogyi, Z. Szor, Z. Trocsanyi, Z. Tulipant, Jet production in the CoLoRFulNNLO method: event shapes in electron-positron collisions, Phys. Rev. D94 (7) (2016) 074019. arXiv:1606.03453, doi:10.1103/PhysRevD.94.074019.

[17] F. Caola, K. Melnikov, R. Röntsch, Nested soft-collinear subtractions in NNLO QCD computations, Eur. Phys. J. C77 (4) (2017) 248. arXiv:1702.01352, doi:10.1140/epjc/s10052-017-4774-0.

[18] L. Magnea, E. Maina, G. Pelliccioli, C. Signorile-Signorile, P. Torrielli, S. Uccirati, Local Analytic Sector Subtraction at NNLO, JHEP 12 (2018) 107. arXiv:1806.09570, doi:10.1007/JHEP12(2018)107.

[19] C. Gnendiger, et al., To d, or not to d: recent developments and comparisons of regularization schemes, Eur. Phys. J. C77 (7) (2017) 471. arXiv:1705.01827, doi:10.1140/epjc/s10052-017-5023-2.

[20] R. A. Fazio, P. Mastrolia, E. Mirabella, W. J. Torres Bobadilla, On the Four-Dimensional Formulation of Dimensionally Regulated Amplitudes, Eur. Phys. J. C74 (12) (2014) 3197. arXiv:1404.4783, doi:10.1140/epjc/s10052-014-3197-4.

[21] Z. Bern, A. De Freitas, L. J. Dixon, H. L. Wong, Supersymmetric regularization, two loop QCD amplitudes and coupling shifts, Phys. Rev. D66 (2002) 085002. arXiv:hep-ph/0202271, doi:10.1103/PhysRevD.66.085002.

[22] O. A. Battistel, A. L. Mota, M. C. Nemes, Consistency conditions for 4-D regularizations, Mod. Phys. Lett. A13 (1998) 1597–1610. doi:10.1142/S0217732398001686.

[23] H. G. Fargnoli, A. P. Baeta Scarpelli, L. C. T. Brito, B. Hiller, M. Sampaio, M. C. Nemes, A. A. Osipov, Ultraviolet and Infrared Divergences in Implicit Regularization: A

Consistent Approach, Mod. Phys. Lett. A26 (2011) 289–302. arXiv:1001.1543, doi:10.1142/S0217732311034773.

[24] A. M. Donati, R. Pittau, FDR, an easier way to NNLO calculations: a two-loop case study, Eur. Phys. J. C74 (2014) 2864. arXiv:1311.3551, doi:10.1140/epjc/s10052-014-2864-9.

[25] B. Page, R. Pittau, NNLO final-state quark-pair corrections in four dimensions, Eur. Phys. J. C79 (4) (2019) 361. arXiv:1810.00234, doi:10.1140/epjc/s10052-019-6865-6.

[26] R. J. Hernández-Pinto, G. F. R. Sborlini, G. Rodrigo, Towards gauge theories in four dimensions, JHEP 02 (2016) 044. arXiv:1506.04617, doi:10.1007/JHEP02(2016)044.

[27] G. F. R. Sborlini, F. Driencourt-Mangin, R. Hernández-Pinto, G. Rodrigo, Four-dimensional unsubtraction from the loop-tree duality, JHEP 08 (2016) 160. arXiv:1604.06699, doi:10.1007/JHEP08(2016)160.

[28] G. F. R. Sborlini, F. Driencourt-Mangin, G. Rodrigo, Four-dimensional unsubtraction with massive particles, JHEP 10 (2016) 162. arXiv:1608.01584, doi:10.1007/JHEP10(2016)162.

[29] S. Catani, T. Gleisberg, F. Krauss, G. Rodrigo, J.-C. Winter, From loops to trees by-passing Feynman's theorem, JHEP 09 (2008) 065. arXiv:0804.3170, doi:10.1088/1126-6708/2008/09/065.

[30] I. Bierenbaum, S. Catani, P. Draggiotis, G. Rodrigo, A Tree-Loop Duality Relation at Two Loops and Beyond, JHEP 10 (2010) 073. arXiv:1007.0194, doi:10.1007/JHEP10(2010)073.

[31] I. Bierenbaum, S. Buchta, P. Draggiotis, I. Malamos, G. Rodrigo, Tree-Loop Duality Relation beyond simple poles, JHEP 03 (2013) 025. arXiv:1211.5048, doi:10.1007/JHEP03(2013)025.

[32] S. Buchta, G. Chachamis, P. Draggiotis, I. Malamos, G. Rodrigo, On the singular behaviour of scattering amplitudes in quantum field theory, JHEP 11 (2014) 014. arXiv:1405.7850, doi:10.1007/JHEP11(2014)014.

[33] S. Buchta, G. Chachamis, P. Draggiotis, G. Rodrigo, Numerical implementation of the loop–tree duality method, Eur. Phys. J. C77 (5) (2017) 274. arXiv:1510.00187, doi:10.1140/epjc/s10052-017-4833-6.

[34] F. Driencourt-Mangin, G. Rodrigo, G. F. R. Sborlini, Universal dual amplitudes and asymptotic expansions for $gg \to H$ and $H \to \gamma\gamma$ in four dimensions, Eur. Phys. J. C78 (3) (2018) 231. arXiv:1702.07581, doi:10.1140/epjc/s10052-018-5692-5.

[35] F. Driencourt-Mangin, G. Rodrigo, G. F. R. Sborlini, W. J. Torres Bobadilla, Universal four-dimensional representation of $H \to \gamma\gamma$ at two loops through the Loop-Tree Duality, JHEP 02 (2019) 143. arXiv:1901.09853, doi:10.1007/JHEP02(2019)143.

[36] J. J. Aguilera-Verdugo, F. Driencourt-Mangin, J. Plenter, S. Ramírez-Uribe, G. Rodrigo, G. F. R. Sborlini, W. J. Torres Bobadilla, S. Tracz, Causality, unitarity thresholds, anomalous thresholds and infrared singularities from the loop-tree duality at higher ordersarXiv:1904.08389.

5 Numerics for elliptic Feynman integrals

Authors: Christian Bogner, Ina Hönemann, Kirsten Tempest, Armin Schweitzer, Stefan Weinzierl
Corresponding Author: Stefan Weinzierl [weinzierl@uni-mainz.de]

The Standard Model involves several heavy particles: the Z- and W-bosons, the Higgs boson and the top quark. Precision studies of these particles require on the theoretical side quantum corrections at the two-loop order and beyond. It is a well-known fact that starting from two-loops Feynman integrals with massive particles can no longer be expressed in terms of multiple polylogarithms. This raises immediately the following question. What is the larger class of functions needed to express the relevant Feynman integrals? For single-scale two-loop Feynman integrals related to a single elliptic curve we have by now the answer: They are expressed as iterated integrals of modular forms [1]. This brings us to a second question: Is there an efficient method to evaluate these functions numerically in the full kinematic range? In this contribution we review how this can be done. This review is mainly based on [2,3].

Efficient numerical evaluation methods rely on three ingredients: (i) an (iterated) integral representation, used to transform the arguments into the region of convergence, (ii) a (nested) sum representation defined in the region of convergence, which can be truncated and gives a numerical approximation and (iii) methods, which accelerate the convergence of the truncated series. Let us illustrate this strategy for the numerical evaluation of the dilogarithm [4], defined by

$$\mathrm{Li}_2(x) = \int\limits_0^x \frac{dt_1}{t_1} \int\limits_0^{t_1} \frac{dt_2}{1-t_2} = \sum_{n=1}^{\infty} \frac{x^n}{n^2}. \tag{5.107}$$

The power series expansion can be evaluated numerically, provided $|x| < 1$. Using the functional equations

$$\mathrm{Li}_2(x) = -\mathrm{Li}_2\left(\frac{1}{x}\right) - \frac{\pi^2}{6} - \frac{1}{2}\left(\ln(-x)\right)^2, \qquad \mathrm{Li}_2(x) = -\mathrm{Li}_2(1-x) + \frac{\pi^2}{6} - \ln(x)\ln(1-x),$$

any argument of the dilogarithm can be mapped into the region $|x| \leq 1$ and $-1 \leq \mathrm{Re}(x) \leq 1/2$. The numerical computation can be accelerated by using an expansion in $z = -\ln(1-x)$ and the Bernoulli numbers B_i:

$$\mathrm{Li}_2(x) = \sum_{i=0}^{\infty} B_i \frac{z^{i+1}}{(i+1)!}. \tag{5.108}$$

Multiple polylogarithms are defined for $z_k \neq 0$ by [5–7]

$$G(z_1,...,z_k;y) = \int\limits_0^y \frac{dy_1}{y_1 - z_1} \int\limits_0^{y_1} \frac{dy_2}{y_2 - z_2} ... \int\limits_0^{y_{k-1}} \frac{dy_k}{y_k - z_k}. \tag{5.109}$$

This represents multiple polylogarithms as iterated integrals. Alternatively, we may define multiple polylogarithms through a nested sum

$$\mathrm{Li}_{m_1,...,m_k}(x_1,...,x_k) = \sum_{n_1>n_2>...>n_k>0} \frac{x_1^{n_1}}{{n_1}^{m_1}} \cdots \frac{x_k^{n_k}}{{n_k}^{m_k}}. \tag{5.110}$$

With the short-hand notation

$$G_{m_1,...,m_k}(z_1,...,z_k;y) = G(\underbrace{0,...,0}_{m_1-1},z_1,...,z_{k-1},\underbrace{0...,0}_{m_k-1},z_k;y), \tag{5.111}$$

where all z_j for $j = 1,...,k$ are assumed to be non-zero. The two notations are related by

$$\mathrm{Li}_{m_1,...,m_k}(x_1,...,x_k) = (-1)^k G_{m_1,...,m_k}\left(\frac{1}{x_1},\frac{1}{x_1x_2},...,\frac{1}{x_1...x_k};1\right). \tag{5.112}$$

The numerical evaluation of multiple polylogarithms follows the same strategy [8]: Using the integral representation one transforms all arguments into a region, where the sum representation gives a converging power series expansion. In addition, the Hölder convolution is used to accelerate the convergence of the series expansion. The Hölder convolution reads (with $z_1 \neq 1$ and $z_k \neq 0$)

$$G\left(z_1,...,z_k;1\right) = \sum_{j=0}^{k}(-1)^j\, G\left(1-z_j,1-z_{j-1},...,1-z_1;\frac{1}{2}\right) G\left(z_{j+1},...,z_k;\frac{1}{2}\right). \tag{5.113}$$

Multiple polylogarithms are a special case of iterated integrals. Let us briefly review Chen's definition of iterated integrals [9]: Let M be a n-dimensional manifold and

$$\gamma \;:\; [0,1] \to M \tag{5.114}$$

a path with start point $x_i = \gamma(0)$ and end point $x_f = \gamma(1)$. Suppose further that ω_1, ..., ω_k are differential 1-forms on M. Let us write

$$f_j\left(\lambda\right) d\lambda = \gamma^* \omega_j \tag{5.115}$$

for the pull-backs to the interval $[0,1]$. For $\lambda \in [0,1]$ the k-fold iterated integral of ω_1, ..., ω_k along the path γ is defined by

$$I_\gamma\left(\omega_1,...,\omega_k;\lambda\right) = \int\limits_0^\lambda d\lambda_1 f_1\left(\lambda_1\right) \int\limits_0^{\lambda_1} d\lambda_2 f_2\left(\lambda_2\right) ... \int\limits_0^{\lambda_{k-1}} d\lambda_k f_k\left(\lambda_k\right). \tag{5.116}$$

For multiple polylogarithms we have $\omega_j = d\ln(\lambda - z_j)$. A second special case is given by iterated integrals of modular forms [10]:

$$\omega_j = 2\pi i\; f_j\left(\tau\right)\; d\tau, \tag{5.117}$$

where $f_j(\tau)$ is a modular form. This type of iterated integrals occurs in physics for the equal-mass sunrise integral [1, 11–14] and the the kite integral [15, 16]. A physical application is the two-loop electron self-energy in quantum electrodynamics, if the mass of the electron is not neglected [3, 17]. This is a single-scale problem and we set $x = p^2/m^2$. In all these examples the complication is related to the equal-mass sunrise integral, which cannot be expressed in terms of multiple polylogarithms. This is related to the fact, that the system of differential equations for this Feynman integral contains an irreducible second-order differential operator [18–20]

$$L = x\left(x-1\right)\left(x-9\right)\frac{d^2}{dx^2} + \left(3x^2-20x+9\right)\frac{d}{dx} + x - 3. \tag{5.118}$$

Let ψ_1 and ψ_2 be two independent solutions of the homogeneous equation

$$L\,\psi \;=\; 0. \tag{5.119}$$

ψ_1 and ψ_2 can be taken as the periods of the elliptic curve

$$E \;:\; w^2 - z\,(z+4)\left[z^2 + 2\,(1+x)\,z + (1-x)^2\right] \;=\; 0. \tag{5.120}$$

One defines the modulus k and the complementary modulus k' by

$$k^2 \;=\; \frac{16\sqrt{x}}{(1+\sqrt{x})^3\,(3-\sqrt{x})}, \qquad k'^2 \;=\; 1-k^2. \tag{5.121}$$

In a neighbourhood of $x = 0$ the periods may be taken as

$$\psi_{1,0} \;=\; \frac{4K\,(k)}{(1+\sqrt{x})^{\frac{3}{2}}\,(3-\sqrt{x})^{\frac{1}{2}}}, \qquad \psi_{2,0} \;=\; \frac{4iK\,(k')}{(1+\sqrt{x})^{\frac{3}{2}}\,(3-\sqrt{x})^{\frac{1}{2}}}. \tag{5.122}$$

The complete elliptic integral $K(k)$ can be computed efficiently from the arithmetic-geometric mean

$$K\,(k) \;=\; \frac{\pi}{2\,\mathrm{agm}\,(k',1)}. \tag{5.123}$$

The periods ψ_1 and ψ_2 generate a lattice. Any other basis of the lattice gives again two independent solutions of the homogeneous differential equation (5.119). It is a standard convention to normalise one basis vector of the lattice to one: $(\psi_2, \psi_1) \to (\tau, 1)$ where $\tau = \psi_2/\psi_1$ and $\mathrm{Im}\tau > 0$. Let us now consider a change of basis:

$$\begin{pmatrix} \psi_2' \\ \psi_1' \end{pmatrix} = \gamma \begin{pmatrix} \psi_2 \\ \psi_1 \end{pmatrix}, \qquad \gamma = \begin{pmatrix} a & b \\ c & d \end{pmatrix}. \tag{5.124}$$

The transformation should be invertible and preserve $\mathrm{Im}(\psi_2'/\psi_1') > 0$, therefore $\gamma \in \mathrm{SL}_2\,(\mathbb{Z})$. In terms of τ and τ' this yields

$$\tau' = \frac{a\tau + b}{c\tau + d}. \tag{5.125}$$

This is a modular transformation and we write $\tau' = \gamma(\tau)$. Let us denote the complex upper half plane by $\mathbb{H}$. A meromorphic function $f : \mathbb{H} \to \mathbb{C}$ is a modular form of modular weight k for $\mathrm{SL}_2(\mathbb{Z})$, if (i) f transforms under Möbius transformations as $f\,(\tau') = (c\tau + d)^k \cdot f(\tau)$ for all $\gamma \in \mathrm{SL}_2(\mathbb{Z})$, (ii) f is holomorphic on $\mathbb{H}$, and (iii) f is holomorphic at infinity. Furthermore, one defines modular forms for congruence subgroups $\Gamma \subset \mathrm{SL}_2(\mathbb{Z})$ by requiring property (i) only for $\gamma \in \Gamma$ (plus holomorphicity on $\mathbb{H}$ and at the cusps). Relevant to us will be the congruence subgroup $\Gamma_1(6)$, defined by

$$\Gamma_1(6) \;=\; \left\{ \begin{pmatrix} a & b \\ c & d \end{pmatrix} \in \mathrm{SL}_2(\mathbb{Z}) : a, d \equiv 1 \bmod 6,\; c \equiv 0 \bmod 6 \right\}. \tag{5.126}$$

With $\psi_{1,0}$ and $\psi_{2,0}$ defined by eq. (5.122) we set

$$\tau_0 \;=\; \frac{\psi_{2,0}}{\psi_{1,0}}, \qquad q_0 \;=\; e^{2i\pi\tau_0}. \tag{5.127}$$

We then change the variable from x to τ_0 (or q_0) [12]. The differential equation for the master integrals $\vec{I}$ relevant to the two-loop electron self-energy reads then

$$\frac{d}{d\tau_0}\vec{I} \;=\; \varepsilon\, A(\tau_0)\, \vec{I}, \tag{5.128}$$

where $A(\tau_0)$ is an ε-independent matrix whose entries are modular forms for $\Gamma_1(6)$ [1, 14]. It follows immediately that all master integrals can be expressed in terms of iterated integrals of modular forms.

Let us now discuss how to evaluate numerically iterated integrals of modular forms in an efficient way. The essential point is that modular forms have a q-expansion. Using

$$2\pi i\, d\tau_0 \;=\; \frac{dq_0}{q_0} \tag{5.129}$$

we may integrate term-by-term and obtain the q_0-expansion of the master integrals. Truncating the q_0-series to the desired accuracy gives a polynomial in q_0. This needs to be done only once and for all. The resulting polynomial can then be evaluated for different values of q_0 (or x) numerically. Note that the conversion from x to q_0 is also fast, since the complete elliptic integrals can be computed efficiently with the help of the arithmetic-geometric mean. Let us give an example. One finds for the ε^2-term of the sunrise integral [3]

$$\begin{aligned} I_6^{(2)} = & \\ & 3\,\mathrm{Cl}_2\left(\frac{2\pi}{3}\right) - 3\sqrt{3}\left[q_0 - \frac{5}{4}\,q_0^2 + q_0^3 - \frac{11}{16}\,q_0^4 + \frac{24}{25}\,q_0^5 - \frac{5}{4}\,q_0^6 + \frac{50}{49}\,q_0^7 - \frac{53}{64}\,q_0^8 + q_0^9\right] + \mathcal{O}\left(q_0^{10}\right). \end{aligned} \tag{5.130}$$

We have $q_0 = 0$ for $x = 0$ and eq. (5.130) gives a fast convergent series in a neighbourhood of $x = 0$. We are interested in evaluating the master integrals in the full kinematic range $x \in \mathbb{R}$. This raises the question for which values $x \in \mathbb{R}$ do the q_0-series for the master integrals converge? Or phrased differently, for which values $x \in \mathbb{R}$ do we have $|q_0| < 1$? It turns out that we have $|q_0| < 1$ for $x \in \mathbb{R}\backslash\{1, 9, \infty\}$, corresponding to $p^2 \in \mathbb{R}\backslash\{m^2, 9m^2, \infty\}$ [2]. Thus the q_0-series for the master integrals converge for all real values of x except three points. Let us stress that the q_0-series give the correct real and imaginary part of the master integrals, as specified by Feynman's $i\delta$-prescription. In order to cover the three remaining points $x \in \{1, 9, \infty\}$, we recall that the periods ψ_1 and ψ_2 are not uniquely determined. By using four different choices for the pair of periods (ψ_1, ψ_2), we may define q_0, q_1, q_9 and q_∞ such that (i) the integration kernels are modular forms of $\Gamma_1(6)$ and (ii) $q_j = 0$ for $x = j$ [3]. This gives expansions around all singular points of the system of differential equations or – phrased differently – around all cusps of $\Gamma_1(6)$. In particular, there is always a choice such that $|q_j| \lessapprox 0.163$ for all real values of x. Truncation of the q-series to order $\mathcal{O}(q^{30})$ gives for the finite part of the two-loop electron self-energy a relative precision better than 10^{-20} for all real values p^2/m^2.

Although we focussed on the two-loop electron self-energy, we expect the methods discussed here to be applicable to any single-scale Feynman integral related to a single elliptic curve. This is a significant step beyond Feynman integrals evaluating to multiple polylogarithms and puts single-scale Feynman integrals related to a single elliptic curve on the same level of understanding as Feynman integrals evaluating to multiple polylogarithms. With the ongoing research on Feynman integrals beyond multiple polylogarithms [1, 2, 11–16, 20–50] we may expect more results – and in particular on multi-scale Feynman integrals beyond multiple polylogarithms – to be coming soon.

References

[1] L. Adams, S. Weinzierl, Feynman integrals and iterated integrals of modular forms, Commun. Num. Theor. Phys. 12 (2018) 193–251. arXiv:1704.08895, doi:10.4310/CNTP.2018.v12.n2.a1.

[2] C. Bogner, A. Schweitzer, S. Weinzierl, Analytic continuation and numerical evaluation of the kite integral and the equal mass sunrise integral, Nucl. Phys. B922 (2017) 528–550. arXiv:1705.08952, doi:10.1016/j.nuclphysb.2017.07.008.

[3] I. Hönemann, K. Tempest, S. Weinzierl, Electron self-energy in QED at two loops revisited, Phys. Rev. D98 (11) (2018) 113008. arXiv:1811.09308, doi:10.1103/PhysRevD.98.113008.

[4] G. 't Hooft, M. J. G. Veltman, Scalar One Loop Integrals, Nucl. Phys. B153 (1979) 365–401. doi:10.1016/0550-3213(79)90605-9.

[5] A. Goncharov, Multiple polylogarithms, cyclotomy and modular complexes, Math. Res. Letters 5 (1998) 497, available at http://www.math.uiuc.edu/K-theory/0297.

[6] J. M. Borwein, D. M. Bradley, D. J. Broadhurst, P. Lisonek, Special values of multiple polylogarithms, Trans. Amer. Math. Soc. 353:3 (2001) 907. arXiv:math.CA/9910045.

[7] S. Moch, P. Uwer, S. Weinzierl, Nested sums, expansion of transcendental functions and multi-scale multi-loop integrals, J. Math. Phys. 43 (2002) 3363–3386. arXiv:hep-ph/0110083.

[8] J. Vollinga, S. Weinzierl, Numerical evaluation of multiple polylogarithms, Comput. Phys. Commun. 167 (2005) 177. arXiv:hep-ph/0410259.

[9] K.-T. Chen, Iterated path integrals, Bull. Amer. Math. Soc. 83 (1977) 831–879.

[10] F. Brown, Multiple Modular Values and the relative completion of the fundamental group of $M_{1,1}$, arXiv:1407.5167.

[11] S. Laporta, E. Remiddi, Analytic treatment of the two loop equal mass sunrise graph, Nucl. Phys. B704 (2005) 349–386. arXiv:hep-ph/0406160, doi:10.1016/j.nuclphysb.2004.10.044.

[12] S. Bloch, P. Vanhove, The elliptic dilogarithm for the sunset graph, J. Numb. Theor. 148 (2015) 328–364. arXiv:1309.5865.

[13] L. Adams, C. Bogner, S. Weinzierl, The iterated structure of the all-order result for the two-loop sunrise integral, J. Math. Phys. 57 (3) (2016) 032304. arXiv:1512.05630, doi:10.1063/1.4944722.

[14] L. Adams, S. Weinzierl, The ε-form of the differential equations for Feynman integrals in the elliptic case, Phys. Lett. B781 (2018) 270–278. arXiv:1802.05020, doi:10.1016/j.physletb.2018.04.002.

[15] E. Remiddi, L. Tancredi, Differential equations and dispersion relations for Feynman amplitudes. The two-loop massive sunrise and the kite integral, Nucl. Phys. B907 (2016) 400–444. arXiv:1602.01481, doi:10.1016/j.nuclphysb.2016.04.013.

[16] L. Adams, C. Bogner, A. Schweitzer, S. Weinzierl, The kite integral to all orders in terms of elliptic polylogarithms, J. Math. Phys. 57 (12) (2016) 122302. arXiv:1607.01571, doi:10.1063/1.4969060.

[17] A. Sabry, Fourth order spectral functions for the electron propagator, Nucl. Phys. 33 (1962) 401–430.

[18] D. J. Broadhurst, J. Fleischer, O. Tarasov, Two loop two point functions with masses:

Asymptotic expansions and Taylor series, in any dimension, Z.Phys. C60 (1993) 287–302. arXiv:hep-ph/9304303, doi:10.1007/BF01474625.

[19] S. Müller-Stach, S. Weinzierl, R. Zayadeh, Picard-Fuchs equations for Feynman integrals, Commun.Math.Phys. 326 (2014) 237–249. arXiv:1212.4389, doi:10.1007/s00220-013-1838-3.

[20] L. Adams, E. Chaubey, S. Weinzierl, Simplifying differential equations for multi-scale Feynman integrals beyond multiple polylogarithms, Phys. Rev. Lett. 118 (14) (2017) 141602. arXiv:1702.04279, doi:10.1103/PhysRevLett.118.141602.

[21] S. Müller-Stach, S. Weinzierl, R. Zayadeh, A second-order differential equation for the two-loop sunrise graph with arbitrary masses, Commun. Num. Theor. Phys. 6 (2012) 203–222. arXiv:1112.4360.

[22] L. Adams, C. Bogner, S. Weinzierl, The two-loop sunrise graph with arbitrary masses, J. Math. Phys. 54 (2013) 052303. arXiv:1302.7004.

[23] E. Remiddi, L. Tancredi, Schouten identities for Feynman graph amplitudes; The Master Integrals for the two-loop massive sunrise graph, Nucl.Phys. B880 (2014) 343–377. arXiv:1311.3342, doi:10.1016/j.nuclphysb.2014.01.009.

[24] L. Adams, C. Bogner, S. Weinzierl, The two-loop sunrise graph in two space-time dimensions with arbitrary masses in terms of elliptic dilogarithms, J. Math. Phys. 55 (2014) 102301. arXiv:1405.5640.

[25] S. Bloch, M. Kerr, P. Vanhove, A Feynman integral via higher normal functions, Compos. Math. 151 (2015) 2329–2375. arXiv:1406.2664, doi:10.1112/S0010437X15007472.

[26] L. Adams, C. Bogner, S. Weinzierl, The two-loop sunrise integral around four space-time dimensions and generalisations of the Clausen and Glaisher functions towards the elliptic case, J. Math. Phys. 56 (7) (2015) 072303. arXiv:1504.03255, doi:10.1063/1.4926985.

[27] M. Søgaard, Y. Zhang, Elliptic Functions and Maximal Unitarity, Phys. Rev. D91 (8) (2015) 081701. arXiv:1412.5577, doi:10.1103/PhysRevD.91.081701.

[28] S. Bloch, M. Kerr, P. Vanhove, Local mirror symmetry and the sunset Feynman integral, Adv. Theor. Math. Phys. 21 (2017) 1373–1453. arXiv:1601.08181, doi:10.4310/ATMP.2017.v21.n6.a1.

[29] L. Tancredi, Integration by parts identities in integer numbers of dimensions. A criterion for decoupling systems of differential equations, Nucl. Phys. B901 (2015) 282–317. arXiv:1509.03330, doi:10.1016/j.nuclphysb.2015.10.015.

[30] A. Primo, L. Tancredi, On the maximal cut of Feynman integrals and the solution of their differential equations, Nucl. Phys. B916 (2017) 94–116. arXiv:1610.08397, doi:10.1016/j.nuclphysb.2016.12.021.

[31] R. Bonciani, V. Del Duca, H. Frellesvig, J. M. Henn, F. Moriello, V. A. Smirnov, Two-loop planar master integrals for Higgs→ 3 partons with full heavy-quark mass dependence, JHEP 12 (2016) 096. arXiv:1609.06685, doi:10.1007/JHEP12(2016)096.

[32] A. von Manteuffel, L. Tancredi, A non-planar two-loop three-point function beyond multiple polylogarithms, JHEP 06 (2017) 127. arXiv:1701.05905, doi:10.1007/JHEP06(2017)127.

[33] J. Ablinger, J. Blümlein, A. De Freitas, M. van Hoeij, E. Imamoglu, C. G. Raab, C. S. Radu, C. Schneider, Iterated Elliptic and Hypergeometric Integrals for Feynman Diagrams, J. Math. Phys. 59 (6) (2018) 062305. arXiv:1706.01299, doi:10.1063/1.4986417.

[34] A. Primo, L. Tancredi, Maximal cuts and differential equations for Feynman integrals. An

application to the three-loop massive banana graph, Nucl. Phys. B921 (2017) 316–356. arXiv:1704.05465, doi:10.1016/j.nuclphysb.2017.05.018.

[35] E. Remiddi, L. Tancredi, An Elliptic Generalization of Multiple Polylogarithms, Nucl. Phys. B925 (2017) 212–251. arXiv:1709.03622, doi:10.1016/j.nuclphysb.2017.10.007.

[36] J. L. Bourjaily, A. J. McLeod, M. Spradlin, M. von Hippel, M. Wilhelm, The Elliptic Double-Box Integral: Massless Amplitudes Beyond Polylogarithms, Phys. Rev. Lett. 120 (12) (2018) 121603. arXiv:1712.02785, doi:10.1103/PhysRevLett.120.121603.

[37] M. Hidding, F. Moriello, All orders structure and efficient computation of linearly reducible elliptic Feynman integrals, JHEP 01 (2019) 169. arXiv:1712.04441, doi:10.1007/JHEP01(2019)169.

[38] J. Broedel, C. Duhr, F. Dulat, L. Tancredi, Elliptic polylogarithms and iterated integrals on elliptic curves. Part I: general formalism, JHEP 05 (2018) 093. arXiv:1712.07089, doi:10.1007/JHEP05(2018)093.

[39] J. Broedel, C. Duhr, F. Dulat, L. Tancredi, Elliptic polylogarithms and iterated integrals on elliptic curves II: an application to the sunrise integral, Phys. Rev. D97 (11) (2018) 116009. arXiv:1712.07095, doi:10.1103/PhysRevD.97.116009.

[40] J. Broedel, C. Duhr, F. Dulat, B. Penante, L. Tancredi, Elliptic symbol calculus: from elliptic polylogarithms to iterated integrals of Eisenstein series, JHEP 08 (2018) 014. arXiv:1803.10256, doi:10.1007/JHEP08(2018)014.

[41] L. Adams, E. Chaubey, S. Weinzierl, Planar Double Box Integral for Top Pair Production with a Closed Top Loop to all orders in the Dimensional Regularization Parameter, Phys. Rev. Lett. 121 (14) (2018) 142001. arXiv:1804.11144, doi:10.1103/PhysRevLett.121.142001.

[42] L. Adams, E. Chaubey, S. Weinzierl, Analytic results for the planar double box integral relevant to top-pair production with a closed top loop, JHEP 10 (2018) 206. arXiv:1806.04981, doi:10.1007/JHEP10(2018)206.

[43] J. Broedel, C. Duhr, F. Dulat, B. Penante, L. Tancredi, Elliptic Feynman integrals and pure functions, JHEP 01 (2019) 023. arXiv:1809.10698, doi:10.1007/JHEP01(2019)023.

[44] J. L. Bourjaily, A. J. McLeod, M. von Hippel, M. Wilhelm, Bounded Collection of Feynman Integral Calabi-Yau Geometries, Phys. Rev. Lett. 122 (3) (2019) 031601. arXiv:1810.07689, doi:10.1103/PhysRevLett.122.031601.

[45] J. L. Bourjaily, A. J. McLeod, M. von Hippel, M. Wilhelm, Rationalizing Loop Integration, JHEP 08 (2018) 184. arXiv:1805.10281, doi:10.1007/JHEP08(2018)184.

[46] M. Besier, D. Van Straten, S. Weinzierl, Rationalizing roots: an algorithmic approach, arXiv:1809.10983.

[47] P. Mastrolia, S. Mizera, Feynman Integrals and Intersection Theory, JHEP 02 (2019) 139. arXiv:1810.03818, doi:10.1007/JHEP02(2019)139.

[48] J. Ablinger, J. Blümlein, P. Marquard, N. Rana, C. Schneider, Automated Solution of First Order Factorizable Systems of Differential Equations in One Variable, Nucl. Phys. B939 (2019) 253–291. arXiv:1810.12261, doi:10.1016/j.nuclphysb.2018.12.010.

[49] H. Frellesvig, F. Gasparotto, S. Laporta, M. K. Mandal, P. Mastrolia, L. Mattiazzi, S. Mizera, Decomposition of Feynman Integrals on the Maximal Cut by Intersection Numbersarxiv:1901.11510.

[50] J. Broedel, C. Duhr, F. Dulat, B. Penante, L. Tancredi, Elliptic polylogarithms and Feyn-

man parameter integrals, arXiv:1902.09971.

6 Numerical Multi-loop Calculations: Sector Decomposition & QMC Integration in pySecDec

Authors: Sophia Borowka, Gudrun Heinrich, Stephan Jahn, Stephen P. Jones, Matthias Kerner, Johannes Schlenk
Corresponding Author: Stephen Philip Jones [s.jones@cern.ch]

The FCC-ee will allow the experimental uncertainties on several important observables, such as the Electroweak Pseudo-Observables (EWPOs), to be reduced by up to two orders of magnitude compared to the previous generation LEP/SLC experiments [1, 2]. In order to be able to best exploit this unprecedented boost in precision, it is necessary also for theoretical predictions to be known with sufficient accuracy. In practice, this means that very high order perturbative corrections to electroweak precision observables and other processes will be required both in the Standard Model (SM) and potentially also in BSM scenarios.

One of the key challenges for computing perturbative corrections is our ability to compute the Feynman integrals that appear in these multi-loop corrections. There has been very significant progress in this direction in recent years ranging from purely analytic approaches [3–17] to semi-analytic approaches based on expansions [18–23] and also via purely numerical methods [24–32].

So far, the method of sector decomposition has already proved to be useful for computing the complete electroweak two-loop corrections to Z-boson production and decay [33], which is of direct relevance to the FCC-ee, as well as several processes of significant interest at the LHC [34–37] and also BSM corrections [38, 39]. The latter calculations were based on SecDec 3 [40]. Another code based on sector decomposition, Fiesta [41–43], has also been used successfully in various multi-loop calculations, for example for numerical checks of recent evaluations of four-loop three-point functions [13–16].

In this contribution we will briefly describe the essential aspects of this method and provide a short update regarding some of the recent developments [26, 44] that have enabled state of the art predictions to be made using this technique.

In Section 6.1 we will introduce the method of sector decomposition as we use it for computing Feynman integrals and describe how it leads to integrals that are suitable for numerical evaluation. In Section 6.2 we will discuss a particular type of Quasi-Monte-Carlo integration that allows us to efficiently numerically integrate the sector decomposed loop integrals. Finally, in Section 6.3 we will give a short outlook for the field of numerical multi-loop calculations.

6.1 Feynman Integrals & Sector Decomposition

A general scalar Feynman integral I in $D = 4 - 2\epsilon$ dimension with L loops and N propagators P_j, each raised to a power ν_j, can be written in momentum space as

$$I = \int_{-\infty}^{\infty} \prod_{l=1}^{L} \left[\mathrm{d}^D k_l\right] \frac{1}{\prod_{j=1}^{N} P_j^{\nu_j}}, \quad \text{where} \quad \left[\mathrm{d}^D k_l\right] = \frac{\mu^{4-D}}{i\pi^{\frac{D}{2}}} \mathrm{d}^D k_l, \qquad P_j = (q_j - m_j^2 + i\delta), \quad (6.131)$$

and q_j are linear combinations of external momenta p_i and loop momenta k_l. After introducing Feynman parameters the momentum integrals can be performed straightforwardly and the

integral can be recast in the following form

$$I = (-1)^{N_\nu} \frac{\Gamma(N_\nu - LD/2)}{\prod_{j=1}^{N} \Gamma(\nu_j)} \int_0^\infty \prod_{j=1}^{N} \mathrm{d}x_j \; x_j^{\nu_j - 1} \delta(1 - \sum_{i=1}^{N} x_i) \frac{\mathcal{U}^{N_\nu - (L+1)D/2}(\vec{x})}{\mathcal{F}^{N_\nu - LD/2}(\vec{x}, s_{ij})}, \tag{6.132}$$

where the momentum integrals have been replaced by an N-fold parameter integral. Here $\mathcal{U}$ and $\mathcal{F}$ are the 1st and 2nd Symanzik polynomials, they are homogeneous polynomials in the Feynman parameters of degree L and $L+1$, respectively, and $N_\nu = \sum_j \nu_j$. The above procedure can be extended to support also Feynman integrals with tensor numerators. There are 3 possibilities for poles in the dimensional regulator ϵ to arise:

1. The overall $\Gamma(N_\nu - LD/2)$ can diverge, resulting in a single UV pole,
2. $\mathcal{U}(\vec{x})$ vanishes for some $x = 0$ and has a negative exponent, resulting in a UV subdivergence,
3. $\mathcal{F}(\vec{x}, s_{ij})$ vanishes on the boundary and has a negative exponent, giving rise to an IR divergence.

After integrating out the δ-distribution and extracting a common factor of $(-1)^{N_\nu}\Gamma(N_\nu - LD/2)$ we are faced with integrals of the form

$$I_i = \int_0^1 \prod_{j=1}^{N-1} \mathrm{d}x_j x_j^{\nu_j - 1} \frac{\mathcal{U}_i(\vec{x})^{\mathrm{expo}\mathcal{U}(\epsilon)}}{\mathcal{F}_i(\vec{x}, s_{ij})^{\mathrm{expo}\mathcal{F}(\epsilon)}}. \tag{6.133}$$

The sector decomposition algorithm(s) aim to factorise, via integral transforms, the polynomials $\mathcal{U}_i$ and $\mathcal{F}_i$ (or more generally any product of polynomials $\mathcal{P}(\{x_j\})$) as products of a monomial and a polynomial with non-zero constant term, explicitly

$$\mathcal{P}(\{x_j\}) \to \prod_j x_j^{\alpha_j} \left(c + p(\{x_j\})\right), \tag{6.134}$$

where $\{x_j\}$ is the set of Feynman parameters, c is a constant and the polynomial p has no constant term. After this procedure, singularities in ϵ resulting from the region where one or more $x_j \to 0$ can appear only from the monomials $x_j^{\alpha_j}$. In this factorised form, the integrand can now be expanded in ϵ and the coefficients of the expansion can be numerically integrated, for an overview see [25].

If we consider only integrals for which the Mandelstam variables and masses can be chosen such that the $\mathcal{F}$ polynomial is positive semidefinite (i.e. with a Euclidean region), the above procedure is sufficient to render the integrals numerically integrable[†]. However, not all integrals of interest have a Euclidean region in this sense. Consider, for example, the three-point function depicted in Figure C.5 which appears in the two-loop electroweak corrections to the $Zb\bar{b}$ vertex [48, 49]. The $\mathcal{F}$ polynomial is given by,

$$\begin{aligned} \mathcal{F}/m_Z^2 = {} & x_3^2 x_5 + x_3^2 x_4 + x_2 x_3 x_5 + x_2 x_3 x_4 + x_1 x_3 x_5 + x_1 x_3 x_4 \\ & + x_1 x_3^2 + x_1 x_2 x_3 + x_0 x_3 x_4 + x_0 x_3^2 + x_0 x_2 x_3 \\ & - x_1 x_2 x_4 - x_0 x_1 x_5 - x_0 x_1 x_4 - x_0 x_1 x_2 - x_0 x_1 x_3. \end{aligned} \tag{6.135}$$

[†]In the physical region such integrals may still require the integration contour to be deformed into the complex-plane in accordance with the causal $i\delta$ Feynman prescription [45–47].

where m_Z is the Z-boson mass and x_j are the Feynman parameters. Note that the massive propagator has the same mass as the external Z-boson which gives rise to terms in the $\mathcal{F}$ polynomial of differing sign regardless of the value chosen for m_Z.

After sector decomposition, integrals for which the $\mathcal{F}$ polynomial is not positive semidefinite can diverge not only as some $x_j \to 0$ but also as some $x_j \to 1$. One solution for dealing with such integrals is to split the integration domain in each Feynman parameter and then map the integration boundaries back to the unit hypercube such that the divergences at $x_j \to 1$ are mapped to divergences at $x_j \to 0$. Sector decomposition can then resolve the singularities at $x_j \to 0$ as usual. Such a splitting procedure was introduced in earlier versions of SecDec [50, 51], and also in Fiesta [42, 43].

However, prior to pySecDec [44], integrals were always split at $x_j = 1/2$ and, as shown in Ref. [52], this can again lead to problems if the $\mathcal{F}$ polynomial vanishes at this point (which happens to be the case for the polynomial in Eq. 6.135). The proposed solution in [52] was therefore to split the integrals at a random point, such that, if one run produces a problematic result, it is always possible to re-run the code and avoid a problematic split.

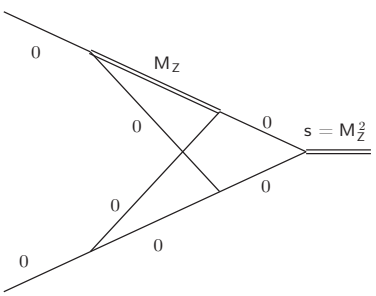

Fig. C.5: A $Zb\bar{b}$ vertex diagram with no Euclidean region and which can give rise to poorly convergent numerical integrals after sector decomposition. Figure taken from [49].

Alternatively, it is often possible to avoid having to evaluate such problematic integrals, as well as integrals that have poor numerical convergence properties, through the use of integration by parts identities (IBPs) [53, 54]. In particular, it is usually possible to express Feynman integrals in terms of a sum of (quasi-)finite integrals[‡] with rational coefficients [55,56]. Typically, choosing a basis of (quasi-)finite integrals leads to significantly improved numerical properties, see for example [57]. The choice of a quasi-finite basis proved advantageous for the numerical evaluation of the $gg \to HH$ and $gg \to Hg$ amplitudes [34–36].

6.2 QMC Integration

The numerical integration of the sector decomposed finite integrals can be a computationally intensive process. One of the most widely used tools for numerical integration is the Cuba package [58, 59] which implements several different numerical integration routines relying on pseudo-random sampling, quasi-random sampling or cubature rules.

[‡]Here, quasi-finite integrals are integrals for which the overall $\Gamma(N_\nu - LD/2)$ can give rise to poles in ϵ but for which no poles arise from the integration over the $\mathcal{U}$ and $\mathcal{F}$ polynomials.

In the last few years, it was found that a particular type of Quasi-Monte-Carlo (QMC) integration based on Rank-1 Shifted Lattice (R1SL) rules has particularly good convergence properties for the numerical integration of Feynman parametrised integrals [60–62]. An unbiased R1SL estimate $\bar{Q}_{n,m}[f]$ of the integral $I[f]$ can be obtained from the following (QMC) cubature rule [63]:

$$I[f] \approx \bar{Q}_{n,m}[f] \equiv \frac{1}{m} \sum_{k=0}^{m-1} Q_n^{(k)}[f], \qquad Q_n^{(k)}[f] \equiv \frac{1}{n} \sum_{i=0}^{n-1} f\left(\left\{\frac{i\mathbf{z}}{n} + \mathbf{\Delta}_k\right\}\right). \tag{6.136}$$

Here, the estimate of the integral depends on the number of lattice points n and the number of random shifts m. The generating vector $\mathbf{z} \in \mathbb{Z}^d$ is a fixed d-dimensional vector of integers coprime to n. The shift vectors $\mathbf{\Delta}_k \in [0,1)^d$ are d-dimensional vectors with components consisting of independent, uniformly distributed random real numbers in the interval $[0,1)$. Finally, the curly brackets indicate that the fractional part of each component is taken, such that all arguments of f remain in the interval $[0,1)$. An unbiased estimate of the mean-square error due to the numerical integration can be obtained by computing the variance of the different random shifts $Q_n^{(k)}[f]$.

The latest version of pySecDec provides a public implementation of a R1SL (QMC) integrator. The implementation is capable of performing numerical integration also on multiple CUDA compatible Graphics Processing Units (GPUs), which can accelerate the evaluation of the integrand significantly. The integrator, which is distributed as a header-only C++ library, can also be used as a standalone integration package [26]. The generating vectors distributed with the package are generated using the component-by-component (CBC) construction [64].

6.3 Summary and Outlook

We have presented new developments for the numerical calculation of multi-loop integrals, focusing on the sector decomposition approach in combination with Quasi-Monte-Carlo (QMC) integration. We described a new feature present in pySecDec, which allows to calculate integrals with special (non-Euclidean) kinematic configurations as they occur e.g. in electroweak two-loop corrections, which previously had shown poor convergence in SecDec 3. We also described a QMC integrator, developed in conjunction with pySecDec as well as for standalone usage, which can lead to considerably more accurate results in a given time compared to standard Monte Carlo integration. This integrator is also capable of utilising CUDA compatible Graphics Processing Units (GPUs).

In view of the need for high-precision calculations with many mass scales at future colliders, as they occur for example in electroweak corrections, numerical methods are a promising approach, and are being actively developed to best utilise recent progress in computing hardware. Several further developments towards the automation of numerical multi-loop calculations, with sector decomposition as an ingredient, could be envisaged. For example, to provide boundary conditions for numerical solutions to differential equations, along the lines of [29, 65], or for automated asymptotic expansions similar to [20, 66], or aiming at fully numerical evaluations of both virtual and real corrections.

Acknowledgements

We would like to thank Tom Zirke for his contributions to earlier versions of the code and Oliver Schulz for providing GPU computing support.

References

[1] G. S. Abrams, et al., Initial Measurements of Z Boson Resonance Parameters in e+ e- Annihilation, Phys. Rev. Lett. 63 (1989) 724. doi:10.1103/PhysRevLett.63.724.

[2] S. Schael, et al., Electroweak Measurements in Electron-Positron Collisions at W-Boson-Pair Energies at LEP, Phys. Rept. 532 (2013) 119–244. arXiv:1302.3415, doi:10.1016/j.physrep.2013.07.004.

[3] S. Badger, C. Bronnum-Hansen, H. B. Hartanto, T. Peraro, First look at two-loop five-gluon scattering in QCD, Phys. Rev. Lett. 120 (9) (2018) 092001. arXiv:1712.02229, doi:10.1103/PhysRevLett.120.092001.

[4] S. Abreu, F. Febres Cordero, H. Ita, B. Page, M. Zeng, Planar Two-Loop Five-Gluon Amplitudes from Numerical Unitarity, Phys. Rev. D97 (11) (2018) 116014. arXiv:1712.03946, doi:10.1103/PhysRevD.97.116014.

[5] T. Gehrmann, J. M. Henn, N. A. Lo Presti, Pentagon functions for massless planar scattering amplitudes, JHEP 10 (2018) 103. arXiv:1807.09812, doi:10.1007/JHEP10(2018)103.

[6] S. Abreu, F. Febres Cordero, H. Ita, B. Page, V. Sotnikov, Planar Two-Loop Five-Parton Amplitudes from Numerical Unitarity, JHEP 11 (2018) 116. arXiv:1809.09067, doi:10.1007/JHEP11(2018)116.

[7] S. Abreu, J. Dormans, F. Febres Cordero, H. Ita, B. Page, Analytic Form of Planar Two-Loop Five-Gluon Scattering Amplitudes in QCD, Phys. Rev. Lett. 122 (8) (2019) 082002. arXiv:1812.04586, doi:10.1103/PhysRevLett.122.082002.

[8] S. Abreu, L. J. Dixon, E. Herrmann, B. Page, M. Zeng, The two-loop five-point amplitude in $\mathcal{N} = 4$ super-Yang-Mills theoryarXiv:1812.08941.

[9] D. Chicherin, T. Gehrmann, J. M. Henn, P. Wasser, Y. Zhang, S. Zoia, All master integrals for three-jet production at NNLOarXiv:1812.11160.

[10] D. Chicherin, J. M. Henn, P. Wasser, T. Gehrmann, Y. Zhang, S. Zoia, Analytic result for a two-loop five-particle amplitude, Phys. Rev. Lett. 122 (2019) 121602. arXiv:1812.11057, doi:10.1103/PhysRevLett.122.121602.

[11] J. Broedel, C. Duhr, F. Dulat, B. Penante, L. Tancredi, Elliptic polylogarithms and Feynman parameter integrals, arXiv:1902.09971.

[12] H. Frellesvig, F. Gasparotto, S. Laporta, M. K. Mandal, P. Mastrolia, L. Mattiazzi, S. Mizera, Decomposition of Feynman Integrals on the Maximal Cut by Intersection Numbers, arXiv:1901.11510.

[13] R. N. Lee, A. V. Smirnov, V. A. Smirnov, M. Steinhauser, Four-loop quark form factor with quartic fundamental colour factor, JHEP 02 (2019) 172. arXiv:1901.02898, doi:10.1007/JHEP02(2019)172.

[14] R. Brüser, A. Grozin, J. M. Henn, M. Stahlhofen, Matter dependence of the four-loop QCD cusp anomalous dimension: from small angles to all angles, arXiv:1902.05076.

[15] J. M. Henn, T. Peraro, M. Stahlhofen, P. Wasser, Matter dependence of the four-loop cusp anomalous dimensionarXiv:1901.03693.

[16] A. von Manteuffel, R. M. Schabinger, Planar master integrals for four-loop form factorsarXiv:1903.06171.

[17] J. Blümlein, C. Schneider, Analytic computing methods for precision calculations in quantum field theory, Int. J. Mod. Phys. A33 (17) (2018) 1830015. arXiv:1809.02889,

doi:10.1142/S0217751X18300156.

[18] S. Borowka, T. Gehrmann, D. Hulme, Systematic approximation of multi-scale Feynman integrals, JHEP 08 (2018) 111. arXiv:1804.06824, doi:10.1007/JHEP08(2018)111.

[19] J. Davies, G. Mishima, M. Steinhauser, D. Wellmann, Double Higgs boson production at NLO in the high-energy limit: complete analytic results, JHEP 01 (2019) 176. arXiv:1811.05489, doi:10.1007/JHEP01(2019)176.

[20] G. Mishima, High-Energy Expansion of Two-Loop Massive Four-Point Diagrams, JHEP 02 (2019) 080. arXiv:1812.04373, doi:10.1007/JHEP02(2019)080.

[21] F. Caola, J. M. Lindert, K. Melnikov, P. F. Monni, L. Tancredi, C. Wever, Bottom-quark effects in Higgs production at intermediate transverse momentum, JHEP 09 (2018) 035. arXiv:1804.07632, doi:10.1007/JHEP09(2018)035.

[22] R. Bonciani, G. Degrassi, P. P. Giardino, R. Gröber, Analytical Method for Next-to-Leading-Order QCD Corrections to Double-Higgs Production, Phys. Rev. Lett. 121 (16) (2018) 162003. arXiv:1806.11564, doi:10.1103/PhysRevLett.121.162003.

[23] R. Gröber, A. Maier, T. Rauh, Reconstruction of top-quark mass effects in Higgs pair production and other gluon-fusion processes, JHEP 03 (2018) 020. arXiv:1709.07799, doi:10.1007/JHEP03(2018)020.

[24] T. Binoth, G. Heinrich, An automatized algorithm to compute infrared divergent multi-loop integrals, Nucl. Phys. B585 (2000) 741–759. arXiv:hep-ph/0004013.

[25] G. Heinrich, Sector Decomposition, Int. J. Mod. Phys. A23 (2008) 1457–1486. arXiv:0803.4177, doi:10.1142/S0217751X08040263.

[26] S. Borowka, G. Heinrich, S. Jahn, S. P. Jones, M. Kerner, J. Schlenk, A GPU compatible quasi-Monte Carlo integrator interfaced to pySecDec, Comp. Phys. Comm.arXiv:1811.11720, doi:10.1016/j.cpc.2019.02.015.

[27] M. Czakon, Automatized analytic continuation of Mellin-Barnes integrals, Comput.Phys.Commun. 175 (2006) 559–571. arXiv:hep-ph/0511200, doi:10.1016/j.cpc.2006.07.002.

[28] J. Usovitsch, I. Dubovyk, T. Riemann, MBnumerics: Numerical integration of Mellin-Barnes integrals in physical regions, PoS LL2018 (2018) 046. arXiv:1810.04580.

[29] M. K. Mandal, X. Zhao, Evaluating multi-loop Feynman integrals numerically through differential equations, JHEP 03 (2019) 190. arXiv:1812.03060, doi:10.1007/JHEP03(2019)190.

[30] X. Liu, Y.-Q. Ma, C.-Y. Wang, A Systematic and Efficient Method to Compute Multi-loop Master Integrals, Phys. Lett. B779 (2018) 353–357. arXiv:1711.09572, doi:10.1016/j.physletb.2018.02.026.

[31] F. Driencourt-Mangin, G. Rodrigo, G. F. R. Sborlini, W. J. Torres Bobadilla, Universal four-dimensional representation of $H \to \gamma\gamma$ at two loops through the Loop-Tree Duality, JHEP 02 (2019) 143. arXiv:1901.09853, doi:10.1007/JHEP02(2019)143.

[32] R. Runkel, Z. Szor, J. P. Vesga, S. Weinzierl, Causality and loop-tree duality at higher loops, Phys. Rev. Lett. 122 (2019) 111603. arXiv:1902.02135, doi:10.1103/PhysRevLett.122.111603.

[33] I. Dubovyk, A. Freitas, J. Gluza, T. Riemann, J. Usovitsch, Complete electroweak two-loop corrections to Z boson production and decay, Phys. Lett. B783 (2018) 86–94. arXiv:1804.10236, doi:10.1016/j.physletb.2018.06.037.

[34] S. Borowka, N. Greiner, G. Heinrich, S. Jones, M. Kerner, J. Schlenk, U. Schubert, T. Zirke, Higgs Boson Pair Production in Gluon Fusion at Next-to-Leading Order with Full Top-Quark Mass Dependence, Phys. Rev. Lett. 117 (1) (2016) 012001, [Erratum: Phys. Rev. Lett.117,no.7,079901(2016)]. arXiv:1604.06447, doi:10.1103/PhysRevLett.117.079901,10.1103/PhysRevLett.117.012001.

[35] S. Borowka, N. Greiner, G. Heinrich, S. P. Jones, M. Kerner, J. Schlenk, T. Zirke, Full top quark mass dependence in Higgs boson pair production at NLO, JHEP 10 (2016) 107. arXiv:1608.04798, doi:10.1007/JHEP10(2016)107.

[36] S. P. Jones, M. Kerner, G. Luisoni, Next-to-Leading-Order QCD Corrections to Higgs Boson Plus Jet Production with Full Top-Quark Mass Dependence, Phys. Rev. Lett. 120 (16) (2018) 162001. arXiv:1802.00349, doi:10.1103/PhysRevLett.120.162001.

[37] G. Heinrich, S. P. Jones, M. Kerner, G. Luisoni, L. Scyboz, Probing the trilinear Higgs boson coupling in di-Higgs production at NLO QCD including parton shower effects, arXiv:1903.08137.

[38] G. Buchalla, M. Capozi, A. Celis, G. Heinrich, L. Scyboz, Higgs boson pair production in non-linear Effective Field Theory with full m_t-dependence at NLO QCD, JHEP 09 (2018) 057, [JHEP18,057(2020)]. arXiv:1806.05162, doi:10.1007/JHEP09(2018)057.

[39] S. Borowka, T. Hahn, S. Heinemeyer, G. Heinrich, W. Hollik, Momentum-dependent two-loop QCD corrections to the neutral Higgs-boson masses in the MSSM, Eur.Phys.J. C74 (2014) 2994. arXiv:1404.7074, doi:10.1140/epjc/s10052-014-2994-0.

[40] S. Borowka, G. Heinrich, S. P. Jones, M. Kerner, J. Schlenk, T. Zirke, SecDec-3.0: numerical evaluation of multi-scale integrals beyond one loop, Comput. Phys. Commun. 196 (2015) 470–491. arXiv:1502.06595, doi:10.1016/j.cpc.2015.05.022.

[41] A. Smirnov, M. Tentyukov, Feynman Integral Evaluation by a Sector decomposiTion Approach (FIESTA), Comput.Phys.Commun. 180 (2009) 735–746. arXiv:0807.4129, doi:10.1016/j.cpc.2008.11.006.

[42] A. V. Smirnov, FIESTA 3: cluster-parallelizable multiloop numerical calculations in physical regions, Comput.Phys.Commun. 185 (2014) 2090–2100. arXiv:1312.3186, doi:10.1016/j.cpc.2014.03.015.

[43] A. V. Smirnov, FIESTA4: Optimized Feynman integral calculations with GPU support, Comput. Phys. Commun. 204 (2016) 189–199. arXiv:1511.03614, doi:10.1016/j.cpc.2016.03.013.

[44] S. Borowka, G. Heinrich, S. Jahn, S. P. Jones, M. Kerner, J. Schlenk, T. Zirke, pySecDec: a toolbox for the numerical evaluation of multi-scale integrals, Comput. Phys. Commun. 222 (2018) 313–326. arXiv:1703.09692, doi:10.1016/j.cpc.2017.09.015.

[45] D. E. Soper, Techniques for QCD calculations by numerical integration, Phys. Rev. D62 (2000) 014009. arXiv:hep-ph/9910292.

[46] T. Binoth, J. P. Guillet, G. Heinrich, E. Pilon, C. Schubert, An algebraic / numerical formalism for one-loop multi-leg amplitudes, JHEP 10 (2005) 015. arXiv:hep-ph/0504267.

[47] Z. Nagy, D. E. Soper, Numerical integration of one-loop Feynman diagrams for N-photon amplitudes, Phys. Rev. D74 (2006) 093006. arXiv:hep-ph/0610028.

[48] J. Fleischer, A. V. Kotikov, O. L. Veretin, Analytic two loop results for selfenergy type and vertex type diagrams with one nonzero mass, Nucl. Phys. B547 (1999) 343–374. arXiv:hep-ph/9808242, doi:10.1016/S0550-3213(99)00078-4.

[49] I. Dubovyk, A. Freitas, J. Gluza, T. Riemann, J. Usovitsch, 30 years, some 700 integrals,

and 1 dessert, or: Electroweak two-loop corrections to the $Z\bar{b}b$ vertex, PoS LL2016 (2016) 075. arXiv:1610.07059.

[50] J. Carter, G. Heinrich, SecDec: A general program for sector decomposition, Comput.Phys.Commun. 182 (2011) 1566–1581. arXiv:1011.5493, doi:10.1016/j.cpc.2011.03.026.

[51] S. Borowka, J. Carter, G. Heinrich, Numerical Evaluation of Multi-Loop Integrals for Arbitrary Kinematics with SecDec 2.0, Comput.Phys.Commun. 184 (2013) 396–408. arXiv:1204.4152, doi:10.1016/j.cpc.2012.09.020.

[52] S. Jahn, Numerical evaluation of multi-loop integrals, PoS LL2018 (2018) 019. doi:10.22323/1.303.0019.

[53] F. V. Tkachov, A Theorem on Analytical Calculability of Four Loop Renormalization Group Functions, Phys. Lett. 100B (1981) 65–68. doi:10.1016/0370-2693(81)90288-4.

[54] K. G. Chetyrkin, F. V. Tkachov, Integration by Parts: The Algorithm to Calculate beta Functions in 4 Loops, Nucl. Phys. B192 (1981) 159–204. doi:10.1016/0550-3213(81)90199-1.

[55] E. Panzer, Feynman integrals and hyperlogarithms, Ph.D. thesis, Humboldt U., Berlin, Inst. Math. (2015). arXiv:1506.07243, doi:10.18452/17157.

[56] A. von Manteuffel, E. Panzer, R. M. Schabinger, A quasi-finite basis for multi-loop Feynman integrals, JHEP 02 (2015) 120. arXiv:1411.7392, doi:10.1007/JHEP02(2015)120.

[57] A. von Manteuffel, R. M. Schabinger, Numerical Multi-Loop Calculations via Finite Integrals and One-Mass EW-QCD Drell-Yan Master Integrals, JHEP 04 (2017) 129. arXiv:1701.06583, doi:10.1007/JHEP04(2017)129.

[58] T. Hahn, CUBA: A library for multidimensional numerical integration, Comput. Phys. Commun. 168 (2005) 78–95. arXiv:hep-ph/0404043, doi:10.1016/j.cpc.2005.01.010.

[59] T. Hahn, Concurrent Cuba, J. Phys. Conf. Ser. 608 (1) (2015) 012066. arXiv:1408.6373, doi:10.1088/1742-6596/608/1/012066.

[60] Z. Li, J. Wang, Q.-S. Yan, X. Zhao, Efficient Numerical Evaluation of Feynman Integral, Chinese Physics C 40, No. 3 (2016) 033103. arXiv:1508.02512, doi:10.1088/1674-1137/40/3/033103.

[61] E. de Doncker, A. Almulihi, F. Yuasa, High-speed evaluation of loop integrals using lattice rules, J. Phys. Conf. Ser. 1085 (5) (2018) 052005. doi:10.1088/1742-6596/1085/5/052005.

[62] E. D. Doncker, A. Almulihi, F. Yuasa, Transformed lattice rules for feynman loop integrals on GPUs, Journal of Physics: Conference Series 1136 (2018) 012002. doi:10.1088/1742-6596/1136/1/012002.

[63] J. Dick, F. Y. Kuo, I. H. Sloan, High-dimensional integration: The quasi-monte carlo way, Acta Numerica 22 (2013) 133–288.

[64] D. Nuyens, R. Cools, Fast algorithms for component-by-component construction of rank-1 lattice rules in shift-invariant reproducing kernel hilbert spaces, Mathematics of Computation 75 (254) (2006) 903–920.

[65] M. Czakon, Tops from Light Quarks: Full Mass Dependence at Two-Loops in QCD, Phys.Lett. B664 (2008) 307–314. arXiv:0803.1400, doi:10.1016/j.physletb.2008.05.028.

[66] B. Jantzen, A. V. Smirnov, V. A. Smirnov, Expansion by regions: revealing potential

and Glauber regions automatically, Eur. Phys. J. C72 (2012) 2139. arXiv:1206.0546, doi:10.1140/epjc/s10052-012-2139-2.

7 Analytics from Numerics: 5-Point QCD Amplitudes at Two Loops

Authors: Samuel Abreu, Jerry Dormans, Fernando Febres Cordero, Harald Ita and Ben Page
Corresponding Author: Ben Page [bpage@ipht.fr]

7.1 Introduction

The operation of the Large Hadron Collider (LHC) has been a great success with Run 1 culminating in the discovery of the Higgs boson by the ATLAS and CMS experiments in 2012. In Run 2, the LHC experiments have moved towards performing high precision measurements with uncertainties reaching below percent level for certain observables. Looking forward to the Future Circular Collider with electron beams (FCC-ee), which will operate in the experimentally much cleaner environment of electron-positron initial states, there will be an even more dramatic increase in experimental precision. In order to exploit the precision measurements, the theory community will need to provide high-precision predictions that match the experimental uncertainties. This requires the development of efficient ways to compute these corrections, breaking through the current computational bottlenecks.

In these proceedings, we discuss the calculation of a key component in making such predictions—the loop amplitude. Specifically, we discuss the computation of an independent set of analytic two-loop five-gluon helicity amplitudes in the leading-color approximation. These amplitudes are an ingredient for the phenomenologically relevant description of three-jet production at next-to-next-to-leading order (NNLO) for hadron colliders. Nonetheless, the methods we present are completely general and can also be applied to predictions for electron-positron collisions.

The first two-loop five-gluon amplitude to be computed was the one with all helicities positive in the leading-color approximation, initially numerically [1] and subsequently analytically [2,3]. In the last few years, a flurry of activity in this field led to the numerical calculation of all five-gluon [4, 5], and then all five-parton amplitudes [6, 7] in the leading-color approximation. The combination of numerical frameworks with finite-field techniques with a view to the reconstruction of the rational functions appearing in final results was first introduced to our field in ref. [8], and an algorithm applicable to multi-scale calculations was presented in ref. [9]. Inspired by these ideas, the four-gluon amplitudes were analytically reconstructed from floating-point evaluations [10]. The first application involving multiple scales was the single-minus two-loop five-gluon amplitude [11]. In these proceedings, we describe the calculation of the full set of independent five-gluon amplitudes in the leading-color approximation [12]. These results were obtained by analytical reconstruction techniques, starting from numerical results obtained in the framework of two-loop numerical unitarity [5, 7, 10, 13]. Since this talk was given, the remaining five-parton amplitudes have also become available [14], and all two-loop amplitudes for three-jet production at NNLO in QCD are now known analytically in the leading-color approximation.[§]

These proceedings are organized as follows. In section 7.2 we describe the amplitudes

[§] The approach taken in ref. [14] is very similar to the one described here. We refer the reader to the results presented in ref. [14] for more compact expressions for the five-gluon amplitudes and further improvements in the methodology.

under consideration and the numerical unitarity framework employed for their evaluation. Section 7.3 describes the objects we will be computing and the simplifications that are performed to allow for an efficient functional reconstruction. The implementation and the results are presented in section 7.4 and we conclude in section 7.5.

7.2 Amplitudes

We discuss the computation of the two-loop five-gluon amplitudes in QCD. The calculation is performed in the leading-color approximation where there is a single partial amplitude. The bare amplitude can be perturbatively expanded as

$$\begin{aligned}\mathcal{A}(\{p_i,h_i\}_{i=1,\ldots,5})\Big|_{\text{leading color}} = \sum_{\sigma\in S_5/Z_5} \text{Tr}\left(T^{a_{\sigma(1)}}T^{a_{\sigma(2)}}T^{a_{\sigma(3)}}T^{a_{\sigma(4)}}T^{a_{\sigma(5)}}\right)\\ g_0^3\left(\mathcal{A}^{(0)}+\lambda\mathcal{A}^{(1)}+\lambda^2\mathcal{A}^{(2)}+\mathcal{O}(\lambda^3)\right).\end{aligned} \tag{7.137}$$

Here, $\lambda = N_c g_0^2/(4\pi)^2$, g_0 is the bare QCD coupling and S_5/Z_5 is the set of all non-cyclic permutations of five indices. The amplitudes $\mathcal{A}^{(k)}$ appearing in the expansion of eq. (7.137) depend on the momenta $p_{\sigma(i)}$ and the helicities $h_{\sigma(i)}$ and these proceedings focus on the calculation of $\mathcal{A}^{(2)}$ in the 't Hooft-Veltman scheme of dimensional regularization with $D = 4 - 2\epsilon$.

The first step in the analytic reconstruction procedure is the numerical evaluation of the amplitude. We evaluate the amplitudes in the framework of two-loop numerical unitarity [5, 7, 10, 13]. The integrands of the amplitudes $\mathcal{A}^{(2)}$ are parametrized with a decomposition in terms of master integrands and surface terms. Upon integration, the former yield the master integrals while the latter vanish. Labelling the loop momenta by ℓ_l, the parametrization we use is given by

$$\mathcal{A}^{(2)}(\ell_l) = \sum_{\Gamma\in\Delta}\sum_{i\in M_\Gamma\cup S_\Gamma} c_{\Gamma,i}\frac{m_{\Gamma,i}(\ell_l)}{\prod_{j\in P_\Gamma}\rho_j}, \tag{7.138}$$

with Δ being the set of all propagator structures Γ, P_Γ the associated set of propagators, and M_Γ and S_Γ denoting the corresponding sets of master integrands and surface terms, respectively. If the master integrals are known, the evaluation of the amplitude reduces to the determination of master coefficients $c_{\Gamma,i}$ with $i \in M_\Gamma$. In numerical unitarity, this is achieved by solving a linear system which is generated by sampling on-shell values of the loop momenta ℓ_l^Γ belonging to the algebraic variety of P_Γ. In this limit the leading contribution to eq. (7.137) factorizes into products of tree amplitudes

$$\sum_{\text{states}}\prod_{i\in T_\Gamma}\mathcal{A}_i^{\text{tree}}(\ell_l^\Gamma) = \sum_{\substack{\Gamma'\geq\Gamma,\\ i\,\in\, M_{\Gamma'}\cup S_{\Gamma'}}}\frac{c_{\Gamma',i}\,m_{\Gamma',i}(\ell_l^\Gamma)}{\prod_{j\in(P_{\Gamma'}\setminus P_\Gamma)}\rho_j(\ell_l^\Gamma)}\,. \tag{7.139}$$

The tree amplitudes associated to vertices in the diagram corresponding to Γ are denoted by T_Γ and the sum is over the physical states of each internal line of Γ. On the right hand side, the sum is performed over all propagator structures Γ' such that $P_\Gamma \subseteq P_{\Gamma'}$. At two-loops, subleading contributions appear which cannot be described by a factorization theorem in the on-shell limit. In practice, this complication is eliminated by constructing a larger system of equations as described for instance in ref. [15]. For a given (rational) phase-space point, we solve the linear system in eq. (7.139) by using finite-field arithmetic. This allows to obtain exact results for the master integral coefficients in a very efficient manner.

Once the coefficients $c_{\Gamma,i}$ are known, the amplitude can be decomposed into a linear combination of master integrals $\mathcal{I}_{\Gamma,i}$ according to

$$\mathcal{A}^{(2)} = \sum_{\Gamma\in\Delta}\sum_{i\in M_\Gamma} c_{\Gamma,i}\mathcal{I}_{\Gamma,i}\,, \tag{7.140}$$

with

$$\mathcal{I}_{\Gamma,i} = \int d^D l_l \frac{m_{\Gamma,i}(l_l)}{\prod_{j\in P_\Gamma}\rho_j}\,. \tag{7.141}$$

For planar massless five-point scattering at two loops, the basis of master integrals is known in analytic form [16, 17].

7.3 Simplifications for Functional Reconstruction

Functional reconstruction techniques allow one to reconstruct rational functions from numerical data, preferably in a finite field to avoid issues related to loss of precision [8, 9]. By choosing an appropriate set of variables, such as momentum twistors [18], we can guarantee that the coefficients $c_{\Gamma,i}$ in eq. (7.140) are rational. The specific parametrization we use is [9]

$$\begin{aligned}
&s_{12} = x_4,\quad s_{23} = x_2x_4,\quad s_{34} = x_4\left(\frac{(1+x_1)x_2}{x_0} + x_1(x_3-1)\right),\\
&s_{45} = x_3x_4,\quad s_{51} = x_1x_4(x_0 - x_2 + x_3)\,,\\
&\mathrm{tr}_5 = 4\,i\,\varepsilon(p_1,p_2,p_3,p_4)\\
&\quad = x_4^2\left(x_2(1+2x_1) + x_0x_1(x_3-1) - \frac{x_2(1+x_1)(x_2-x_3)}{x_0}\right),
\end{aligned} \tag{7.142}$$

where $s_{ij} = (p_i+p_j)^2$ with the indices defined cyclically. One could in principle reconstruct the rational master integral coefficients. However, the difficulty of the reconstruction is governed by the complexity of the function under consideration. The amplitude $\mathcal{A}^{(2)}$ of eq. (7.140) contains a lot of redundant information, and to improve the efficiency of the reconstruction it is thus beneficial to remove this redundancy. Furthermore, while eq. (7.140) provides a decomposition in terms of master integrals in dimensional regularization, after expanding the master integrals in ϵ there can be new linear relations between the different terms in the Laurent expansion in ϵ. We thus expect cancellations between the different coefficients $c_{\Gamma,i}$. In this section we discuss how we address these issues and define the object we reconstruct.

We start by expressing the Laurent expansion of the master integrals in eq. (7.141) in terms of a basis B of so-called pentagon functions $h_i \in B$ [17]. That is, we rewrite the amplitudes as

$$\mathcal{A}^{(2)} = \sum_{i\in B}\sum_{k=-4}^{0} \epsilon^k\,\tilde{c}_{k,i}(\vec{x})h_i(\vec{x}) + \mathcal{O}(\epsilon), \tag{7.143}$$

where $\vec{x} = \{x_0, x_1, x_2, x_3, x_4\}$ and the $\tilde{c}_{k,i}(\vec{x})$ are rational functions of the twistor variables. All linear relations between master integrals that appear after expansion in ϵ are resolved in such a decomposition.

Next, we recall that the singularity structure of two-loop amplitudes is governed by lower-loop amplitudes [19–22]. One can thus exploit this knowledge to subtract the pole structure

from the amplitudes in order to obtain a finite remainder that contains the new two-loop information. There is freedom in how to define the remainders, as they are only constrained by removing the poles of the amplitudes. For helicity amplitudes which vanish at tree-level, $\mathcal{A}^{(k)}_{\pm++++}$, we use

$$\mathcal{R}^{(2)}_{\pm++++} = \bar{\mathcal{A}}^{(2)}_{\pm++++} + S_\epsilon \bar{\mathcal{A}}^{(1)}_{\pm++++} \sum_{i=1}^{5} \frac{(-s_{i,i+1})^{-\epsilon}}{\epsilon^2} + \mathcal{O}(\epsilon), \tag{7.144}$$

where $S_\epsilon = (4\pi)^\epsilon e^{-\epsilon\gamma_E}$. The $\bar{\mathcal{A}}^{(k)}$ denote amplitudes normalized to remove any ambiguity related to overall phases. In the case of amplitudes that vanish at tree level, we normalize to the leading order in ϵ of the (finite) one-loop amplitude. For the MHV amplitudes, $\mathcal{A}^{(k)}_{-\mp\pm++}$, which we normalize to the corresponding tree amplitude, we define

$$\begin{aligned}\mathcal{R}^{(2)}_{-\mp\pm++} = \bar{\mathcal{A}}^{(2)}_{-\mp\pm++} &- \left(\frac{5\,\tilde{\beta}_0}{2\epsilon} + \mathbf{I}^{(1)}\right) S_\epsilon \bar{\mathcal{A}}^{(1)}_{-\mp\pm++} \\ &+ \left(\frac{15\,\tilde{\beta}_0^2}{8\epsilon^2} + \frac{3}{2\epsilon}\left(\tilde{\beta}_0 \mathbf{I}^{(1)} - \tilde{\beta}_1\right) - \mathbf{I}^{(2)}\right) S_\epsilon^2 + \mathcal{O}(\epsilon)\,,\end{aligned} \tag{7.145}$$

where $\tilde{\beta}_i$ are the coefficients of the QCD β-function divided by N_c^{i+1}. $\mathbf{I}^{(1)}$ and $\mathbf{I}^{(2)}$ are the standard Catani operators at leading color. Precise expressions for the operators in our conventions can be found in appendix B of ref. [7]. We note that for both eq. (7.144) and (7.145) we require one-loop amplitudes expanded up to order ϵ^2. By expressing the one-loop amplitudes and the Catani operators in the basis of pentagon functions, the remainder can be expressed in the same way,

$$\mathcal{R}^{(2)} = \sum_{i \in B} r_i(\vec{x})\, h_i(\vec{x})\,. \tag{7.146}$$

We observe that the coefficients $r_i(\vec{x})$ are rational functions of lower total degree than the $\tilde{c}_{k,i}(\vec{x})$ of eq. (7.143).

As a further simplification we investigate the pole structure of the coefficients $r_i(\vec{x})$. The alphabet determines the points in phase space where the pentagon functions have logarithmic singularities, and as such provides a natural candidate to describe the pole structure of the coefficients. We use the alphabet A determined in ref. [17] to build an ansatz for the denominator structure of the $r_i(\vec{x})$,

$$r_i(\vec{x}) = \frac{n_i(\vec{x})}{\prod_{j \in A} w_j(\vec{x})^{q_{ij}}}\,. \tag{7.147}$$

We then reconstruct the remainder on a slice $\vec{x}(t) = \vec{a}\cdot t + \vec{b}$ where all the twistor variables depend on a single parameter t and $\vec{a}$ and $\vec{b}$ are random vectors of finite field values. This reconstruction in one variable is drastically simpler than the full multivariate reconstruction. In addition, the maximal degree in t on the slice corresponds to the total degree in $\vec{x}$. We determine the exponents q_{ij} by matching the ansatz on the univariate slice and check its validity on a second slice. Having determined the denominators of the rational coefficients r_i, the reconstruction reduces to the much simpler polynomial reconstruction of the numerators $n_i(\vec{x})$.

The last simplification we implement is a change of basis in the space of pentagon functions. Amplitudes are expected to simplify in specific kinematic configurations where the pentagon functions degenerate into a smaller basis, which requires relations between the different

coefficients. This motivates the search for (helicity-dependent) bases with coefficients of lower total degree. To find them we construct linear combinations of coefficients

$$\sum_{i\in B} a_{i,k} r_i(\vec{x}) = \frac{N_k(\vec{x}, a_{i,k})}{\prod_{j\in A} w_j(\vec{x})^{q'_{kj}}}\,, \tag{7.148}$$

and solve for phase-space independent $a_{i,k}$ such that the numerators $N_k(\vec{x}, a_{i,k})$ factorize a subset of the $w_j \in A$. This can be performed on univariate slices by only accepting solutions which are invariant over multiple slices. The matrix $a_{i,k}$ allows to change to a new basis B' in the space of special functions, in which remainders can be decomposed as in eq. (7.146), with coefficients $r'_i(\vec{x})$ whose numerators $n'_i(\vec{x})$ are polynomials of lower total degree than those of eq. (7.147).

7.4 Implementation and Results

The master integral coefficients of the one- and two-loop amplitudes are computed using numerical unitarity in a finite-field. They are combined with the corresponding master integrals, expressed in terms of pentagon functions, and the known pole structure is subtracted to obtain the finite remainders as a linear combination of pentagon functions. After a rotation in the space of pentagon functions and multiplication by the predetermined denominator factors, we obtain numerical samples for the numerators $n'_i(\vec{x})$ in a finite-field. These samples are used to analytically reconstruct the $n'_i(\vec{x})$ with the algorithm of [9], which we slightly modified to allow a more efficient parallelization. The above steps were implemented in a flexible C++ framework, which was used to reconstruct the analytic form of the two-loop remainders of a basis of five-gluon helicity amplitudes (the other helicities can be obtained by parity and charge conjugation). Two finite fields of cardinality $O(2^{31})$ were necessary for the rational reconstruction by means of the Chinese remainder theorem.

Table C.8 shows the impact of the simplifications discussed in the previous section for each helicity. In the most complicated case, the $g^-g^+g^-g^+g^+$ helicity amplitude, we must reconstruct a polynomial of degree 53. This required 250000 numerical evaluations, with 4.5 minutes per evaluation.

The results that we provide contain the one-loop amplitudes in terms of master integrals and the two-loop remainders in terms of pentagon functions. The one-loop master integrals are provided in terms of pentagon functions up to order ϵ^2. The combined size of the expressions amounts to 45 MB without attempting any simplification (we refer the reader to [14] for more compact expressions). These expressions can be combined to construct the full analytic expression for the two-loop five-gluon leading-color amplitudes in the euclidean region. We validated our expressions by reproducing all the target benchmark values available in the literature [1–5, 7, 11].

7.5 Conclusion

In these proceedings we have presented the recent computation of the analytic form of the leading-color contributions to the two-loop five-gluon scattering amplitudes in pure Yang-Mills theory. This computation was undertaken in a novel way, made possible by a collection of mature tools. The amplitude is first numerically reduced to a basis of master integrals with the two-loop numerical unitarity approach, where the coefficients take finite-field values [5, 7, 10, 13]. This allows to numerically calculate a finite remainder, expressed in terms of pentagon functions [17]. The generation of these numerical samples is driven by a functional reconstruction

helicity	$\tilde{c}_{k,i}(t)$	$r_i(t)$	$n'_i(t)$	w_j's in denominator
$++++-$	t^{34}/t^{28}	t^{10}/t^{4}	t^{10}	3
$-+++-$	t^{50}/t^{42}	t^{35}/t^{28}	t^{35}	14
$--++-$	t^{70}/t^{65}	t^{50}/t^{45}	t^{40}	17
$-+-+-$	t^{84}/t^{82}	t^{68}/t^{66}	t^{53}	20

Table C.8: Each t^n/t^d denotes the total degree of numerator (n) and denominator (d) of the most complex coefficient for each helicity amplitude in the decomposition of eq. (7.143) (second column) or eq. (7.146) (third column). The fourth column lists the highest polynomial we reconstruct. The final column lists the number of letters $w_j(\vec{x})$ that contribute in the denominator of eq. (7.147).

algorithm [9] which determines the analytic form of the pentagon-function coefficients from a series of evaluations. A key step in efficiently implementing this strategy was to utilize physical information to simplify the analytic form of the objects we reconstruct, and hence reduce the required number of evaluations. First, we reconstruct the finite remainder, which removes redundant information related to lower loop contributions. Second, we decompose the remainder in terms of pentagon functions to account for relations between different master integrals after expansion in the dimensional regulator. Next, we exploit the knowledge of the singularity structure of the pentagon functions to efficiently establish the denominators of the coefficient functions. Finally, we find a basis of pentagon functions with coefficients of lower degree by exploiting their reconstruction on a univariate slice.

These techniques show a great deal of potential for future calculations. Indeed, they have very recently been used to obtain the full set of leading color contributions to the five-parton scattering amplitudes [14]. We foresee further applications to processes with a higher number of scales and loops such as the ones required for a future lepton collider in the near future.

References

[1] S. Badger, H. Frellesvig, Y. Zhang, A Two-Loop Five-Gluon Helicity Amplitude in QCD, JHEP 12 (2013) 045. arXiv:1310.1051, doi:10.1007/JHEP12(2013)045.

[2] T. Gehrmann, J. M. Henn, N. A. Lo Presti, Analytic form of the two-loop planar five-gluon all-plus-helicity amplitude in QCD, Phys. Rev. Lett. 116 (6) (2016) 062001, [Erratum: Phys. Rev. Lett.116,no.18,189903(2016)]. arXiv:1511.05409, doi:10.1103/PhysRevLett.116.189903,10.1103/PhysRevLett.116.062001.

[3] D. C. Dunbar, W. B. Perkins, Two-loop five-point all plus helicity Yang-Mills amplitude, Phys. Rev. D93 (8) (2016) 085029. arXiv:1603.07514, doi:10.1103/PhysRevD.93.085029.

[4] S. Badger, C. Brønnum-Hansen, H. B. Hartanto, T. Peraro, First look at two-loop five-gluon scattering in QCD, Phys. Rev. Lett. 120 (9) (2018) 092001. arXiv:1712.02229, doi:10.1103/PhysRevLett.120.092001.

[5] S. Abreu, F. Febres Cordero, H. Ita, B. Page, M. Zeng, Planar Two-Loop Five-Gluon Amplitudes from Numerical Unitarity, Phys. Rev. D97 (11) (2018) 116014. arXiv:1712.03946, doi:10.1103/PhysRevD.97.116014.

[6] S. Badger, C. Brønnum-Hansen, T. Gehrmann, H. B. Hartanto, J. Henn, N. A. Lo Presti,

T. Peraro, Applications of integrand reduction to two-loop five-point scattering amplitudes in QCD, in: 14th DESY Workshop on Elementary Particle Physics: Loops and Legs in Quantum Field Theory 2018 (LL2018) St Goar, Germany, April 29-May 4, 2018, 2018. arXiv:1807.09709.

[7] S. Abreu, F. Febres Cordero, H. Ita, B. Page, V. Sotnikov, Planar Two-Loop Five-Parton Amplitudes from Numerical Unitarity, JHEP 11 (2018) 116. arXiv:1809.09067, doi:10.1007/JHEP11(2018)116.

[8] A. von Manteuffel, R. M. Schabinger, A novel approach to integration by parts reduction, Phys. Lett. B744 (2015) 101–104. arXiv:1406.4513, doi:10.1016/j.physletb.2015.03.029.

[9] T. Peraro, Scattering amplitudes over finite fields and multivariate functional reconstruction, JHEP 12 (2016) 030. arXiv:1608.01902, doi:10.1007/JHEP12(2016)030.

[10] S. Abreu, F. Febres Cordero, H. Ita, M. Jaquier, B. Page, M. Zeng, Two-Loop Four-Gluon Amplitudes from Numerical Unitarity, Phys. Rev. Lett. 119 (14) (2017) 142001. arXiv:1703.05273, doi:10.1103/PhysRevLett.119.142001.

[11] S. Badger, C. Brønnum-Hansen, H. B. Hartanto, T. Peraro, Analytic helicity amplitudes for two-loop five-gluon scattering: the single-minus case, JHEP 01 (2019) 186. arXiv:1811.11699, doi:10.1007/JHEP01(2019)186.

[12] S. Abreu, J. Dormans, F. Febres Cordero, H. Ita, B. Page, Analytic Form of the Planar Two-Loop Five-Gluon Scattering Amplitudes in QCD, arXiv:1812.04586.

[13] H. Ita, Towards a Numerical Unitarity Approach for Two-loop Amplitudes in QCD, PoS LL2016 (2016) 080. arXiv:1607.00705.

[14] S. Abreu, J. Dormans, F. Febres Cordero, H. Ita, B. Page, V. Sotnikov, Analytic Form of the Planar Two-Loop Five-Parton Scattering Amplitudes in QCD, arXiv:1904.00945.

[15] S. Abreu, F. Febres Cordero, H. Ita, M. Jaquier, B. Page, Subleading Poles in the Numerical Unitarity Method at Two Loops, Phys. Rev. D95 (9) (2017) 096011. arXiv:1703.05255, doi:10.1103/PhysRevD.95.096011.

[16] C. G. Papadopoulos, D. Tommasini, C. Wever, The Pentabox Master Integrals with the Simplified Differential Equations approach, JHEP 04 (2016) 078. arXiv:1511.09404, doi:10.1007/JHEP04(2016)078.

[17] T. Gehrmann, J. M. Henn, N. A. L. Presti, Pentagon functions for massless planar scattering amplitudesarXiv:1807.09812.

[18] A. Hodges, Eliminating spurious poles from gauge-theoretic amplitudes, JHEP 05 (2013) 135. arXiv:0905.1473, doi:10.1007/JHEP05(2013)135.

[19] S. Catani, The Singular behavior of QCD amplitudes at two loop order, Phys. Lett. B427 (1998) 161–171. arXiv:hep-ph/9802439, doi:10.1016/S0370-2693(98)00332-3.

[20] G. F. Sterman, M. E. Tejeda-Yeomans, Multi-loop amplitudes and resummation, Phys. Lett. B552 (2003) 48–56. arXiv:hep-ph/0210130, doi:10.1016/S0370-2693(02)03100-3.

[21] T. Becher, M. Neubert, Infrared singularities of scattering amplitudes in perturbative QCD, Phys. Rev. Lett. 102 (2009) 162001, [Erratum: Phys. Rev. Lett.111,no.19,199905(2013)]. arXiv:0901.0722, doi:10.1103/PhysRevLett.102.162001,10.1103/PhysRevLett.111.199905.

[22] E. Gardi, L. Magnea, Factorization constraints for soft anomalous dimensions in QCD scattering amplitudes, JHEP 03 (2009) 079. arXiv:0901.1091, doi:10.1088/1126-6708/

2009/03/079.

8 Recent developments in Kira

Authors: Philipp Maierhöfer, Johann Usovitsch
Corresponding Author: Johann Usovitsch [usovitsj@maths.tcd.ie]

In this section we report on the recent progress made in the development of the Feynman integral reduction program `Kira`. The development is focused on algorithmic improvements that are essential to extend the range of feasible high precision calculations for present and future colliders like the FCC-ee.

8.1 Introduction

`Kira` [1] implements Laporta's algorithm [2] to reduce Feynman integrals to a basis of master integrals. In this approach, large systems of integration-by-parts [3] and Lorentz invariance [4] identities, and symmetry relations, are generated and solved by a variant of Gaussian elimination, systematically expressing complicated integrals in terms of simpler integrals wrt. a given complexity criterion. Though alternative reduction techniques have been proposed and applied to specific problems, see e.g. [5–8], to date programs based on Laporta's algorithm [9–11] pose the only general purpose tools suited for large scale applications. Since these reduction programs constitute one of the bottlenecks of high precision predictions, their continous improvement is crucial to meet the increasing demand for such calculations.

A key element of `Kira` is its equation selector to extract a linearly independent system of equations, discarding equations that are not required to fully reduce all integrals requested by the user. The selector is based on Gaussian elimination using modular arithmetic on the coefficients.

8.2 Improved symmetrisation

The detection of symmetry relations between sectors within and across topologies received a performance boost due to the implementation of the algorithm described in [12]. In this approach, a canonical form of the integrand of each sector is constructed, so that a one-to-one comparison of the representations can be done. Additionally, the combinatorial complexity of the loop momentum shift finder to determine the mapping prescriptions of equivalent sectors has been reduced. Furthermore, the detection of trivial sectors received a significant speed-up by employing `Kira`'s IBP solver instead of the less optimised previous linear solver.

As an example, the "cube topology" shown in Fig. C.6, i.e. the 5-loop vacuum bubble with 12 propagators of equal mass and the symmetry of a cube, can now be analysed in less than 10 minutes on a state-of-the-art desktop computer.

8.3 Parallel simplification algorithms for coefficients

Algebraic simplifications with Fermat

To simplify multivariate rational functions in masses and kinematic quantities, which appear as coefficients in the Gaussian elimination steps, `Kira` relies on the program `Fermat` [13]. In almost all cases, the runtime for the reduction is dominated by those algebraic simplifications. It turns out that, when a new coefficient is constructed from several (often thousands of) known coefficients, combining them naïvely and simplifying them in one step results in an avoidable performance penalty. Instead, `Kira` recursively combines coefficients pairwise, choosing the pairs based on the size of their string representations. Besides the improved performance, this

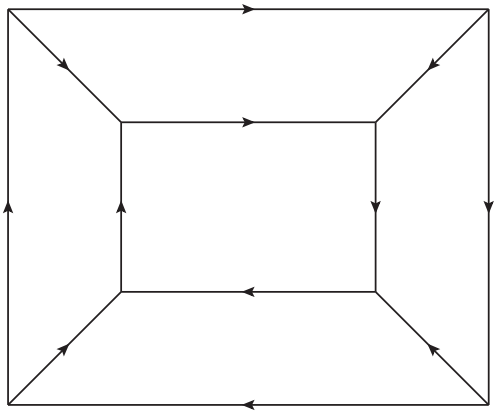

Fig. C.6: The cube topology is the 5-loop vacuum bubble with 12 propagators of equal mass and octahedral symmetry. The high symmetry of 48 equivalent propagator permutations in the top-level sector makes this topology an ideal candidate for symmetrisation benchmarks.

strategy also offers new possibilities for the parallelisation, since the pairwise combinations can be evaluated by different `Fermat` instances.

In the Gaussian back substitution, one can restrict a solver to calculate only the coefficients of a specific master integral. This allows the user to parallelise the reduction across several machines and merge the results in a final step.

Algebraic reconstruction over integers

An alternative algorithm to simplify the coefficients is given by algebraic reconstruction over integers, introduced in [7, 14, 15]. This strategy is based on sampling the rational functions by setting kinematic invariants and masses to integer values repeatedly. Each sample can be evaluated rather quickly, but the number of samples required to reconstruct the simplified result increases with the degree of the numerator and denominator of the rational function, the number of invariants involved, and the number of invariants over which is sampled. Of course, the sample can again be evaluated in parallel, leading to the potential for massive parallelisation on dozens of CPU cores. An implementation of this algorithm is available in `Kira 1.2` and is continuously improved and extended. Furthermore, `Kira` automatically decides which simplification strategy, i.e. algebraic reconstruction or `Fermat`, is expected to be more efficient in each case. The criteria for these decisions are subject to investigation and offer room for future improvements.

Algebraic reconstruction over finite integer fields

Instead of sampling rational functions over integers, it is also possible to reconstruct them from samples over finite integer fields. Mapping coefficients to a finite field limits the size of each coefficient and with that the complexity of each operation. Choosing the module as a word-size prime, numerical operations on coefficients correspond to the native arithmetic capabilities of the employed CPU, allowing for high performance sampling of the coefficients. A reconstruction algorithm for multivariate rational functions was first presented in [16]. Recently, the library `FireFly` [17] became available, implementing a similar algorithm. `FireFly` has been combined with `Kira` to use it for Feynman integral reduction, calculating the samples with `Kira`'s finite integer Gaussian elimination. An independent implementation is available in `FIRE 6` [11].

In the sampling over (arbitrary-size) integers described above, whenever a coefficient is

required to proceed with the reduction, the solver needs to wait until that coefficient has been reconstructed. Using finite integers, the entire solver can be parallelised, opening the possibility to distribute solvers over different machines. The reconstructor can then collect the samples from the solvers and finish the calculation when a sufficient number of samples is available. The finite integer reconstruction is expected to become publicly available in a future `Kira` release in combination with `FireFly`.

8.4 Basis choice

It is well known that the reduction time strongly depends on the choice of the master integrals. In a convenient basis, the reduction coefficients tend to become much simpler than e.g. in the basis that follows directly from the integral ordering. In this respect, uniformly transcendental bases [18], finite bases [19], or finite uniformly transcendental bases [20] present interesting candidates to study the impact of the basis choice on the reduction performance. These special choices involve linear combinations of integrals as basis elements that we call "master equations".

In `Kira`, integrals are represented by integer "weights" in such a way that they obey the imposed integral ordering. Choosing a specific basis of master integrals is already possible. To this end, the weights are modified so that the preferred basis integrals are regarded as simpler than all other integrals. In the presence of master equations, a new kind objects must be introduced, representing the master equation instead of a particular integral. With an appropriate bookkeeping, the implementation becomes straight forward and will soon be available in a `Kira` release.

8.5 Conclusions

The complexity of precision calculations needed to match the accuracy of the FCC-ee experiment demands for integral reduction tools beyond the state-of-the-art capabilities. For example, the computation of pseudo observables at the Z-boson resonance, involving reductions of 3-loop Feynman diagrams with up to five scales, will be necessary to reach the accuracy that may be achieved with the FCC-ee [21]. We expect that Feynman integral reduction programs based on Laporta's algorithm will continue to play a key role in such calculations. E.g. by harnessing the potential of rational reconstruction, basis choices, and large-scale parallelisation, we are convinced that `Kira` will keep up with the arising technical challenges.

References

[1] P. Maierhöfer, J. Usovitsch, P. Uwer, Kira—A Feynman integral reduction program, Comput. Phys. Commun. 230 (2018) 99–112. arXiv:1705.05610, doi:10.1016/j.cpc.2018.04.012.

[2] S. Laporta, High precision calculation of multiloop Feynman integrals by difference equations, Int.J.Mod.Phys. A15 (2000) 5087–5159. arXiv:hep-ph/0102033, doi:10.1016/S0217-751X(00)00215-7.

[3] K. G. Chetyrkin, F. V. Tkachov, Integration by Parts: The Algorithm to Calculate beta Functions in 4 Loops, Nucl. Phys. B192 (1981) 159–204. doi:10.1016/0550-3213(81)90199-1.

[4] T. Gehrmann, E. Remiddi, Differential equations for two loop four point functions, Nucl. Phys. B580 (2000) 485–518. arXiv:hep-ph/9912329, doi:10.1016/S0550-3213(00)00223-6.

[5] A. V. Smirnov, V. A. Smirnov, Applying Grobner bases to solve reduction problems for Feynman integrals, JHEP 01 (2006) 001. arXiv:hep-lat/0509187, doi:10.1088/1126-6708/2006/01/001.

[6] R. N. Lee, LiteRed 1.4: a powerful tool for reduction of multiloop integrals, J. Phys. Conf. Ser. 523 (2014) 012059. arXiv:1310.1145, doi:10.1088/1742-6596/523/1/012059.

[7] K. J. Larsen, Y. Zhang, Integration-by-parts reductions from unitarity cuts and algebraic geometry, Phys. Rev. D93 (4) (2016) 041701. arXiv:1511.01071, doi:10.1103/PhysRevD.93.041701.

[8] D. A. Kosower, Direct Solution of Integration-by-Parts Systems, Phys. Rev. D98 (2) (2018) 025008. arXiv:1804.00131, doi:10.1103/PhysRevD.98.025008.

[9] C. Anastasiou, A. Lazopoulos, Automatic integral reduction for higher order perturbative calculations, JHEP 07 (2004) 046. arXiv:hep-ph/0404258, doi:10.1088/1126-6708/2004/07/046.

[10] A. von Manteuffel, C. Studerus, Reduze 2 - Distributed Feynman Integral ReductionarXiv:1201.4330.

[11] A. V. Smirnov, F. S. Chuharev, FIRE6: Feynman Integral REduction with Modular ArithmeticarXiv:1901.07808.

[12] A. Pak, The Toolbox of modern multi-loop calculations: novel analytic and semi-analytic techniques, J. Phys. Conf. Ser. 368 (2012) 012049. arXiv:1111.0868, doi:10.1088/1742-6596/368/1/012049.

[13] R. H. Lewis, Computer Algebra System FermatarXiv:http://www.bway.net/lewis.

[14] J. Böhm, A. Georgoudis, K. J. Larsen, M. Schulze, Y. Zhang, Complete sets of logarithmic vector fields for integration-by-parts identities of Feynman integrals, Phys. Rev. D98 (2) (2018) 025023. arXiv:1712.09737, doi:10.1103/PhysRevD.98.025023.

[15] J. Böhm, A. Georgoudis, K. J. Larsen, H. Schönemann, Y. Zhang, Complete integration-by-parts reductions of the non-planar hexagon-box via module intersections, JHEP 09 (2018) 024. arXiv:1805.01873, doi:10.1007/JHEP09(2018)024.

[16] T. Peraro, Scattering amplitudes over finite fields and multivariate functional reconstruction, JHEP 12 (2016) 030. arXiv:1608.01902, doi:10.1007/JHEP12(2016)030.

[17] J. Klappert, F. Lange, Reconstructing Rational Functions with `FireFly`arXiv:1904.00009.

[18] J. M. Henn, Multiloop integrals in dimensional regularization made simple, Phys. Rev. Lett. 110 (2013) 251601. arXiv:1304.1806, doi:10.1103/PhysRevLett.110.251601.

[19] E. Panzer, Feynman integrals and hyperlogarithms, Ph.D. thesis, Humboldt U., Berlin, Inst. Math. (2015). arXiv:1506.07243, doi:10.18452/17157.

[20] R. M. Schabinger, Constructing multi-loop scattering amplitudes with manifest singularity structure, arXiv:1806.05682.

[21] A. Blondel, et al., Standard Model Theory for the FCC-ee: The Tera-Z, in: Mini Workshop on Precision EW and QCD Calculations for the FCC Studies : Methods and Techniques CERN, Geneva, Switzerland, January 12-13, 2018, 2018. arXiv:1809.01830.

9 Precision Monte Carlo simulations with WHIZARD

Authors: Simon Braß, Wolfgang Kilian, Thorsten Ohl, Jürgen Reuter, Vincent Rothe, Pascal Stienemeier
Corresponding Author: Jürgen Reuter [juergen.reuter@desy.de]

The precision physics programs of FCC-ee demands for a precise simulation of all Standard Model (SM) processes and possible beyond the SM (BSM) signals in a state-of-the-art way by means of Monte Carlo (MC) techniques. As a standard tool for e^+e^- simulations, the multi-purpose event generator WHIZARD [1, 2] has been used: this generator has been originally developed for the TESLA project, and later on been used e.g. for the ILC Technical Design Report [3,4]. The WHIZARD package has a modular structure which serves a modern unit-test driven software development and guarantees a high level of maintainability and extendability. WHIZARD comes with its own fully general tree-level matrix-element generator for the hard process, O'Mega [5]. It generates amplitudes in a recursive way based on the graph-theoretical concepts of directed acyclical graphs (DAGs), thereby avoiding all redundancies. The matrix elements are generated either as compilable modern Fortran code or as bytecode instructions interpreted by a virtual machine [6]. For QCD, WHIZARD uses the color-flow formalism [7]. Matrix elements support all kinds of particles and interactions up to spin-2. A large number of BSM models is hard-coded, particularly the MSSM and NMSSM [8, 9]. General BSM models can be loaded from a Lagrangian level tool, using the interface to FeynRules [10]; from the version 2.8.0 of WHIZARD on (early summer 2019) a full-fledged interface to the general UFO format will be available. One of the biggest assets of WHIZARD is its general phase-space parameterization which uses a heuristic based on the dominating sub-processes, which allows to integrate and simulate processes with up to 10 fermions in the final state. The integration is based on an adaptive multi-channel algorithm, called VAMP [11]. Recently, this multi-channel adaptive integration has been enhanced to a parallelized version using the MPI3 protocol showing speedups of up to 100 [12], while a first physics study using this MPI parallelized integration and event generation has been published in [13].

WHIZARD allows to describe all the necessary ingredients for a high-precision e^+e^- event simulation: the CIRCE1/CIRCE2 modules [14] simulate the spectrum of beamstrahlung (including beam energy spectra) that comes from the classical electromagnetic radiation due to extreme space charge densities of highly collimated bunches for high-luminosity running. This takes care of a precise description of the peaks of the luminosity spectra and a smooth mapping of the tail that does not lead to artificial spikes and kinks in differential distributions. For the beam setup, WHIZARD furthermore allows to correctly describe polarized beams with arbitrary polarization settings and fractions, asymmetric beams and crossing angles. QED initial-state radiation (ISR) is convoluted in a collinear approximation according to a resummation of soft photons to all orders and hard-collinear photons up to third order [15]. While this will give a correct normalization of the cross section to the given QED order, one explicit ISR photon per beam will be inserted into the event record. A special handler generates transverse momentum according to a physical p_T distribution and boosts the complete events accordingly. This treatment is available also for the photon beam components according to the Weizsäcker-Williams spectrum (equivalent photon approximation, EPA).

The MC generator WHIZARD offers a vast functionality which cannot be given full justice here, e.g. automatic generation of decays, factorized processes including full spin correlations (which can also be switched off for case studies), specification of the helicity of decaying res-

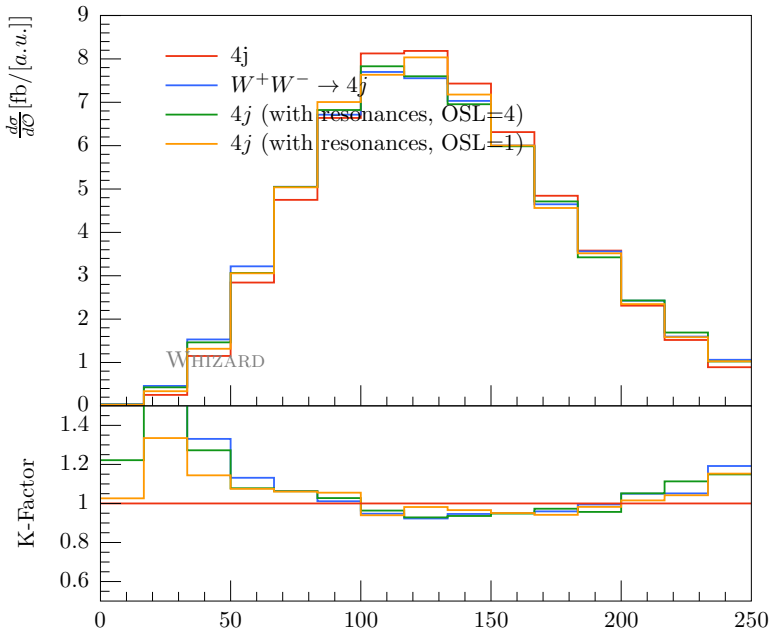

Fig. C.7: Energy distribution of photons in $e^+e^- \to jjjj$ after parton shower and hadronization. Full amplitudes without resonance histories (red), factorized process $e^+e^- \to W^+W^- \to (jj)(jj)$ (blue), and full process with resonance histories and different Breit-Wigner settings (green and orange, respectively).

onances, preset branching ratios, etc. WHIZARD supports all used HEP event formats, like StdHEP, LHE, HepMC, LCIO, and various ASCII formats. It allows easy reweighting of event samples. WHIZARD has its own two QCD parton shower algorithms, a k_T-ordered shower and an analytic parton shower [16], and ships with the final version of PYTHIA6 [17] for showering and hadronization. The event records are directly interfaced and exchanged, and the framework has been validated with the full LEP data set by the Linear Collider Generator Group in a setup similar to the FCC-ee. Recently, we added a corresponding interface for an externally linked PYTHIA8 [18] which uses again direct communcation between the event records of WHIZARD and PYTHIA. This offers to use all the machinery for QCD jet matching and merging from PYTHIA inside WHIZARD. WHIZARD also directly interfaces Fastjet [19] for jet clustering. One important feature of WHIZARD is the proper resonance matching of hadronically decaying resonances, e.g. in the process $e^+e^- \to jjjj$. This is predominantly WW production ($\sim$80%), followed by ZZ production ($\lesssim$ 20%) and the QCD four-jet continuum. When simulating full quantum theoretical amplitudes for four-jet production, the parton shower does not know intermediate resonances because of the full coherence of the process, and hence does not preserve the resonance mass of the hadronic Ws. WHIZARD allows to automatically determine underlying resonance histories, evaluates their approximate rates and inserts according to these rates resonance histories for final-state jets. Fig. C.7 shows for the process $e + e^- \to jjjj$ the photon energy distribution after hadronization and hadronic decays. The central line in the inset (red) shows the full process which disagrees with LEP data, while the blue line shows the factorized process $e^+e^- \to W^+W^- \to (jj)(jj)$ (where the shower program knows the resonance history) and the resonance-matched processes (green and orange). These correctly reproduce the data using full matrix elements, thereby allowing different handles on how far to take into account

Breit-Wigner tails of resonances. This kind of matching has now been validated for six-jet processes including $H \to b\bar{b}$.

Finally, we comment on the NLO QCD capabilities of WHIZARD: WHIZARD has completed its final validation phase for lepton collider QCD NLO corrections, and v3.0.0 will be released (approximately end of 2019) when proton collider processes are also completely validated. For NLO QCD corrections, WHIZARD uses the Frixione-Kunszt-Signer subtraction (FKS) formalism [20] where automatically for all processes real and integrated subtraction terms are generated. WHIZARD also implements the resonance-aware variant [21]. Virtual multi-leg one-loop matrix elements are included from one-loop providers like GoSam [22], OpenLoops [23,24], and RECOLA [25,26]. First proof-of-princple NLO calculations have been done for electroweak corrections [27,28] in lepton collisions, while NLO QCD have been implemented for LHC processes first [29,30]. The automatized FKS subtraction has been tested and published in the study of off-shell $t\bar{t}$ and $t\bar{t}H$ processes in lepton collisions in [31]. The complete validation of the automatized NLO QCD setup will be available after the v3.0.0 release of WHIZARD [32]. WHIZARD allows to generate fixed-order NLO events for differential distributions at NLO QCD using weighted events, but also to automatically do POWHEG-matched and -damped events [33,34]. Decays at NLO QCD are treated in the same set-up as scattering processes.

The scan of the top threshold is a crucial component of the FCC-ee physics program. In order to determine systematic uncertainties from e.g. the event selection, WHIZARD allows to simulate at the completely exclusive final-state $e^+e^- \to W^+bW^-\bar{b}$ matching the continuum NLO QCD calculation to the NRQCD threshold NLL resummation [35]. This simulation is available via a specific top-threshold model inside WHIZARD.

References

[1] W. Kilian, T. Ohl, J. Reuter, WHIZARD: Simulating Multi-Particle Processes at LHC and ILC, Eur. Phys. J. C71 (2011) 1742. arXiv:0708.4233, doi:10.1140/epjc/s10052-011-1742-y.

[2] Whizard, http://whizard.hepforge.org.

[3] H. Baer, T. Barklow, K. Fujii, Y. Gao, A. Hoang, S. Kanemura, J. List, H. E. Logan, A. Nomerotski, M. Perelstein, et al., The International Linear Collider Technical Design Report - Volume 2: Physics, arXiv:1306.6352.

[4] H. Abramowicz, et al., The International Linear Collider Technical Design Report - Volume 4: Detectors, arXiv:1306.6329.

[5] M. Moretti, T. Ohl, J. Reuter, O'Mega: An Optimizing matrix element generator, (2001) 1981–2009arXiv:hep-ph/0102195.

[6] B. Chokoufe Nejad, T. Ohl, J. Reuter, Simple, parallel virtual machines for extreme computations, Comput. Phys. Commun. 196 (2015) 58–69. arXiv:1411.3834, doi:10.1016/j.cpc.2015.05.015.

[7] W. Kilian, T. Ohl, J. Reuter, C. Speckner, QCD in the Color-Flow Representation, JHEP 10 (2012) 022. arXiv:1206.3700, doi:10.1007/JHEP10(2012)022.

[8] T. Ohl, J. Reuter, Clockwork SUSY: Supersymmetric Ward and Slavnov-Taylor identities at work in Green's functions and scattering amplitudes, Eur. Phys. J. C30 (2003) 525–536. arXiv:hep-th/0212224, doi:10.1140/epjc/s2003-01301-7.

[9] K. Hagiwara, W. Kilian, F. Krauss, T. Ohl, T. Plehn, D. Rainwater, J. Reuter, S. Schu-

mann, Supersymmetry simulations with off-shell effects for CERN LHC and ILC, Phys. Rev. D73 (2006) 055005. arXiv:hep-ph/0512260, doi:10.1103/PhysRevD.73.055005.

[10] N. D. Christensen, C. Duhr, B. Fuks, J. Reuter, C. Speckner, Introducing an interface between WHIZARD and FeynRules, Eur. Phys. J. C72 (2012) 1990. arXiv:1010.3251, doi:10.1140/epjc/s10052-012-1990-5.

[11] T. Ohl, Vegas revisited: Adaptive Monte Carlo integration beyond factorization, Comput. Phys. Commun. 120 (1999) 13–19. arXiv:hep-ph/9806432, doi:10.1016/S0010-4655(99)00209-X.

[12] S. Brass, W. Kilian, J. Reuter, Parallel Adaptive Monte Carlo Integration with the Event Generator WHIZARD, Eur. Phys. J. C79 (4) (2019) 344. arXiv:1811.09711, doi:10.1140/epjc/s10052-019-6840-2.

[13] A. Ballestrero, et al., Precise predictions for same-sign W-boson scattering at the LHC, Eur. Phys. J. C78 (8) (2018) 671. arXiv:1803.07943, doi:10.1140/epjc/s10052-018-6136-y.

[14] T. Ohl, CIRCE version 1.0: Beam spectra for simulating linear collider physics, Comput. Phys. Commun. 101 (1997) 269–288. arXiv:hep-ph/9607454, doi:10.1016/S0010-4655(96)00167-1.

[15] M. Skrzypek, S. Jadach, Exact and approximate solutions for the electron nonsinglet structure function in QED, Z. Phys. C49 (1991) 577–584. doi:10.1007/BF01483573.

[16] W. Kilian, J. Reuter, S. Schmidt, D. Wiesler, An Analytic Initial-State Parton Shower, JHEP 04 (2012) 013. arXiv:1112.1039, doi:10.1007/JHEP04(2012)013.

[17] T. Sjostrand, S. Mrenna, P. Z. Skands, PYTHIA 6.4 Physics and Manual, JHEP 05 (2006) 026. arXiv:hep-ph/0603175, doi:10.1088/1126-6708/2006/05/026.

[18] T. Sjostrand, S. Mrenna, P. Z. Skands, A Brief Introduction to PYTHIA 8.1, Comput. Phys. Commun. 178 (2008) 852–867. arXiv:0710.3820, doi:10.1016/j.cpc.2008.01.036.

[19] M. Cacciari, G. P. Salam, G. Soyez, FastJet User Manual, Eur. Phys. J. C72 (2012) 1896. arXiv:1111.6097, doi:10.1140/epjc/s10052-012-1896-2.

[20] S. Frixione, Z. Kunszt, A. Signer, Three jet cross-sections to next-to-leading order, Nucl. Phys. B467 (1996) 399–442. arXiv:hep-ph/9512328, doi:10.1016/0550-3213(96)00110-1.

[21] T. Jezo, P. Nason, On the Treatment of Resonances in Next-to-Leading Order Calculations Matched to a Parton Shower, JHEP 12 (2015) 065. arXiv:1509.09071, doi:10.1007/JHEP12(2015)065.

[22] G. Cullen, et al., G*OSAM*-2.0: a tool for automated one-loop calculations within the Standard Model and beyond, Eur. Phys. J. C74 (8) (2014) 3001. arXiv:1404.7096, doi:10.1140/epjc/s10052-014-3001-5.

[23] F. Cascioli, P. Maierhofer, S. Pozzorini, Scattering Amplitudes with Open Loops, Phys. Rev. Lett. 108 (2012) 111601. arXiv:1111.5206, doi:10.1103/PhysRevLett.108.111601.

[24] F. Buccioni, S. Pozzorini, M. Zoller, On-the-fly reduction of open loops, Eur. Phys. J. C78 (1) (2018) 70. arXiv:1710.11452, doi:10.1140/epjc/s10052-018-5562-1.

[25] S. Actis, A. Denner, L. Hofer, J.-N. Lang, A. Scharf, S. Uccirati, RECOLA: REcursive Computation of One-Loop Amplitudes, Comput. Phys. Commun. 214 (2017) 140–173. arXiv:1605.01090, doi:10.1016/j.cpc.2017.01.004.

[26] A. Denner, J.-N. Lang, S. Uccirati, Recola2: REcursive Computation of One-Loop Amplitudes 2, Comput. Phys. Commun. 224 (2018) 346–361. arXiv:1711.07388, doi:10.1016/j.cpc.2017.11.013.

[27] W. Kilian, J. Reuter, T. Robens, NLO Event Generation for Chargino Production at the ILC, Eur. Phys. J. C48 (2006) 389–400. arXiv:hep-ph/0607127, doi:10.1140/epjc/s10052-006-0048-y.

[28] T. Robens, J. Kalinowski, K. Rolbiecki, W. Kilian, J. Reuter, (N)LO Simulation of Chargino Production and Decay, Acta Phys. Polon. B39 (2008) 1705–1714. arXiv:0803.4161.

[29] T. Binoth, N. Greiner, A. Guffanti, J. Reuter, J. P. Guillet, T. Reiter, Next-to-leading order QCD corrections to pp –> b anti-b b anti-b + X at the LHC: the quark induced case, Phys. Lett. B685 (2010) 293–296. arXiv:0910.4379, doi:10.1016/j.physletb.2010.02.010.

[30] N. Greiner, A. Guffanti, T. Reiter, J. Reuter, NLO QCD corrections to the production of two bottom-antibottom pairs at the LHC, Phys. Rev. Lett. 107 (2011) 102002. arXiv:1105.3624, doi:10.1103/PhysRevLett.107.102002.

[31] B. Chokoufe Nejad, W. Kilian, J. M. Lindert, S. Pozzorini, J. Reuter, C. Weiss, NLO QCD predictions for off-shell $t\bar{t}$ and $t\bar{t}H$ production and decay at a linear collider, JHEP 12 (2016) 075. arXiv:1609.03390, doi:10.1007/JHEP12(2016)075.

[32] S. Brass, B. Chokoufe Nejad, W. Kilian, J. Reuter, V. Rothe, P. Stienemeier, C. Weiss, Automatized NLO QCD simulations with WHIZARD, in preparation.

[33] B. Chokoufe Nejad, W. Kilian, J. Reuter, C. Weiss, Matching NLO QCD Corrections in WHIZARD with the POWHEG scheme, PoS EPS-HEP2015 (2015) 317. arXiv:1510.02739, doi:10.22323/1.234.0317.

[34] J. Reuter, B. Chokoufe, A. Hoang, W. Kilian, M. Stahlhofen, T. Teubner, C. Weiss, Automation of NLO processes and decays and POWHEG matching in WHIZARD, J. Phys. Conf. Ser. 762 (1) (2016) 012059. arXiv:1602.06270, doi:10.1088/1742-6596/762/1/012059.

[35] F. Bach, B. C. Nejad, A. Hoang, W. Kilian, J. Reuter, M. Stahlhofen, T. Teubner, C. Weiss, Fully-differential Top-Pair Production at a Lepton Collider: From Threshold to Continuum, JHEP 03 (2018) 184. arXiv:1712.02220, doi:10.1007/JHEP03(2018)184.

10 FCC Tau Polarization

Authors: Swagato Banerjee and Zbigniew Was
Corresponding Author: Zbigniew Was [z.was@cern.ch]

SM parameters, such as the τ polarization can be measured very precisely in τ decays. The phenomenology is quite similar to that of measurement of the A_{FB} parameter of the SM [21]. Details of τ decay spectrum as well a good understanding of associated uncertainty play an important role in this measurement of polarization, because the spin of the τ lepton is not measured directly.

The distribution of hadronic final state products in decays of a τ lepton needs to be evaluated to understand the sub-structure of the vertex. One of the important effect is related to bremsstrahlung, because signature of every decay mode needs to take into account the final state configurations with accompanying photons. Corresponding virtual corrections cancel the bulk of these effects and specialized programs such as PHOTOS [1, 2] are useful.

Corresponding effects can be sizable, and even during early step of LEP preparations it was found [3] that the corresponding corrections affect the slope of π spectrum in $\tau^- \to \pi^-\nu$, for example. That translates to 0.013 effect on τ idealized observable A_{pol}. For more discussion and essential experimental context see [4].

However, not all of final state photons can be associated with bremsstrahlung. For example, in the cascade decay $\tau^- \to \pi^-\omega\nu$, a subsequent decay of $\omega \to \pi^0\gamma$ contributes to the final state $\tau^- \to \pi^-\pi^0\gamma\nu$ coincides with the radiative corrections to final state of the $\tau^- \to \rho^-\nu$ decay channel. In this case, the photon originates from the $\omega \to \pi^0\gamma$ decay and is of non-QED bremsstrahlung origin.

The branching fractions for the $\tau^- \to \pi^-\omega\nu$ decay, and for the $\omega \to \pi^0\gamma$ decay are 0.02 and 0.08, respectively [5]. Thus, the resulting decay channel $\tau^- \to \pi^-\pi^0\gamma\nu$ contributes 0.0015 of all τ decays.

Such contributions and subsequent changes of the hadronic decay energy spectrum in τ decays need to be understood for each spin sensitive channel. Resulting deformation of $\tau^- \to \rho^-\nu$ decay spectra may mimic the contribution of the τ polarization can be obtained from a future high precision data analysis at the Belle II experiment.

This is the case when one of the τ decay channels mimic bremsstrahlung correction for the other one. The dynamics of the low energy strong interactions is difficult to obtain from a perturbative calculation.

Another hint of non-point-like nature of the τ vertex was explained in the corrections to the π energy spectra in the $\tau^- \to \pi^-\nu$ decay channel [6, 7]. Although at the lowest order, the spectrum is fully determined by the Lorentz structure of the vertex, the real and virtual photonic corrections play an important role in the level of precision under discussion. The dominant part of the effects of the QED bremsstrahlung from point-like sources can be seen in the Fig. 3 of [7], where the effects induced by hadronic resonances also play an important role.

The Belle II experiment is expected to collect 10^{11} τ lepton decays with 50 ab^{-1} of data, and the detector is extremely well-suited to study τ lepton physics. The backgrounds can be well controlled in an electron-positron collider environment. We can expect that the τ decay spectra can be measured without large degradation due to a highly granular electromagnetic calorimeter with large fiducial coverage, as explained in the Belle II technical design report [8].

References

[1] E. Barberio, Z. Was, PHOTOS: A Universal Monte Carlo for QED radiative corrections. Version 2.0, Comput. Phys. Commun. 79 (1994) 291–308. doi:10.1016/0010-4655(94)90074-4.

[2] N. Davidson, T. Przedzinski, Z. Was, PHOTOS interface in C++: Technical and Physics Documentation, Comput. Phys. Commun. 199 (2016) 86–101. arXiv:1011.0937, doi:10.1016/j.cpc.2015.09.013.

[3] F. Boillot, Z. Was, Uncertainties in τ Polarization Measurement at SLC/LEP and QED/-Electroweak Radiative Corrections, Z. Phys. C43 (1989) 109. doi:10.1007/BF02430616.

[4] LEP Electroweak Working Group, Precision Electroweak Measurements and Constraints on the Standard Model, arXiv:1012.2367.

[5] M. Tanabashi, et al., Review of Particle Physics, Phys. Rev. D98 (3) (2018) 030001. doi:10.1103/PhysRevD.98.030001.

[6] R. Decker, M. Finkemeier, Radiative corrections to the decay tau $\to$ pi (K) tau-neutrino, Phys. Lett. B316 (1993) 403–406. arXiv:hep-ph/9307372, doi:10.1016/0370-2693(93)90345-I.

[7] R. Decker, M. Finkemeier, Radiative corrections to the decay tau $\to$ pi tau-neutrino, Nucl. Phys. Proc. Suppl. 40 (1995) 453–461. arXiv:hep-ph/9411316, doi:10.1016/0920-5632(95)00170-E.

[8] T. Abe, et al., Belle II Technical Design Report, arXiv:1011.0352.

11 Electron-positron annihilation processes in MCSANCee

Authors: Andrej Arbuzov, Serge Bondarenko, Yahor Dydyshka, Lidia Kalinovskaya, Leonid Rumyantsev, Renat Sadykov, Vitaly Yermolchyk
Corresponding Author: Andrej Arbuzov [arbuzov@theor.jinr.ru]

The Monte Carlo even generator `MCSANCee` is used to estimate the significance of polarization effects in one-loop electroweak radiative corrections. The electron-positron annihilation processes $e^+e^- \to \mu^-\mu^+$ ($\tau^-\tau^+$, ZH) were considered taking into account conditions of future colliders.

11.1 Introduction

Radiative corrections with effects due to polarization of the initial particles will play an important role in the high-precision program at the $\texttt{FCC}_{ee}$. `MCSANCee` is a Monte Carlo generator of unweighted events for polarized e^+e^- scattering and annihilation [processes with complete one-loop electroweak (EW) corrections. The generator uses the adaptive Monte Carlo algorithm `mFOAM` [1], which is a part of the `ROOT` [2] framework.

The SANC computer system is capable to calculate cross-sections of general Standard Model (SM) processes with up to three final state particles [3, 4]. By using the SANC system, we calculated electroweak radiative corrections at the one-loop level to the polarized Bhabha scattering [5, 6] which is the basic normalization process at e^+e^- colliders. For processes

$$e^+e^- \to \mu^-\mu^+ \ (\tau^-\tau^+, \ ZH) \tag{11.149}$$

we made a few upgrades of the standard procedures in the SANC system. We investigated the effect of the polarization degrees of initial particles to the differential cross-sections. We found that the EW corrections to the total cross-section range from -18 percent to $+69$ percent. when the centre-of-mass energy $\sqrt{s}$ varies in the set 250 GeV, 500 Gev, and 1 TeV .

11.2 Cross-section structure

The cross-section of a generic $2 \to 2(\gamma)$ process $e^+e^- \to X_3X_4(\gamma)$
$(X_3X_4 = \mu^-\mu^+, \tau^-\tau^+, ZH)$ reads

$$\sigma_{P_{e^-}P_{e^+}} = \frac{1}{4}\sum_{\chi_1,\chi_2}(1+\chi_1 P_{e^-})(1+\chi_2 P_{e^+})\sigma_{\chi_1\chi_2},$$

where $\chi_i = -1(+1)$ corresponds to lepton with left (right) helicity state.

The cross-section at the one-loop level can be divided into four parts:

$$\sigma^{1-\text{loop}} = \sigma^{\text{Born}} + \sigma^{\text{virt}}(\lambda) + \sigma^{\text{soft}}(\lambda,\omega) + \sigma^{\text{hard}}(\omega),$$

where σ^{Born} is the Born level cross-section, σ^{virt} is the virtual (loop) contribution, σ^{soft} is due to soft photon emission, σ^{hard} is due to hard photon emission (with energy $E_\gamma > \omega$). Auxiliary parameters λ ("photon mass") and ω cancel out after summation.

We treat all contributions using the helicity amplitudes (HA) approach:

$$\sigma^{\text{Part}}_{\chi_1\chi_2} = \frac{1}{2s}\sum_{\chi_i, i\geq 3}\left|\mathcal{H}^{\text{Part}}_{\chi_1\chi_2\chi_3\ldots}\right|^2 d\text{LIPS}, \tag{11.150}$$

where Part $\in$ {Born, virt, hard}, and dLIPS is a volume element of the Lorentz-invariant phase space.

The soft photon contribution is factorized in front of the Born-level cross-section:

$$d\sigma^{\rm soft}_{\chi_1\chi_2} = d\sigma^{\rm Born}_{\chi_1\chi_2} \cdot \frac{\alpha}{2\pi} K^{soft}(\omega, \lambda).$$

11.3 Numerical results and comparison

The following input parameters are used for numerical estimates and comparisons below

$$\begin{aligned}
&\alpha^{-1}(0) = 137.03599976,\\
&M_W = 80.4514958 \text{ GeV}, \quad M_Z = 91.1876 \text{ GeV}, \quad \Gamma_Z = 2.49977 \text{ GeV},\\
&m_e = 0.51099907 \text{ MeV}, \quad m_\mu = 0.105658389 \text{ GeV}, \quad m_\tau = 1.77705 \text{ GeV},\\
&m_d = 0.083 \text{ GeV}, \quad m_s = 0.215 \text{ GeV}, \quad m_b = 4.7 \text{ GeV},\\
&m_u = 0.062 \text{ GeV}, \quad m_c = 1.5 \text{ GeV}, \quad m_t = 173.8 \text{ GeV}.
\end{aligned}$$

The following simple cuts are imposed

$$\begin{aligned}
&|\cos\theta| < 0.9,\\
&E_\gamma > 1 \text{ GeV} \quad \text{(for comparison of hard Bremsstrahlung)}.
\end{aligned}$$

Tuned comparison of our results for polarized Born and hard Bremsstrahlung with the results `WHIZARD` [7], and `CalcHEP` [8] programs shows an agreement within statistical errors. Unpolarized *soft + virtual* contribution agree with the results of [9] for $e^+e^- \to \mu^+\mu^-(\tau^+\tau^-)$ and with the ones of the `GRACE` system [10]. For $e^+e^- \to ZH$ we found an agreement with the results of the `GRACE` system [10] and with the ones give in paper [11].

The integrated cross-sections of processes (11.149) and the relative corrections δ are given in the Tables C.9 [12], and C.10 [13] for various energies and beam polarization degrees.

In these Tables we summarize the estimation of the Born and one-loop cross-sections in pb and the relative corrections δ in percent of the processes $e^+e^- \to \mu^+\mu^-, (\tau^+\tau^-, ZH)$ for the set (0, 0; -0.8, 0; -0.8, -0.6; -0.8, +0.6) of longitudinal polarizations P_{e^+} and P_{e^-} of the positron and electron beams, respectively. The energy values 250, 500, and 1000 GeV were taken. The relative correction δ is defined as

$$\delta = \frac{\sigma^{\text{1-loop}} - \sigma^{\text{Born}}}{\sigma^{\text{Born}}} \cdot 100\%. \tag{11.151}$$

11.4 Conclusion

As can be seen from the Tables C.9 and C.10 the difference between values δ for polarization degrees of initial particles (0, 0) and (-0.8, 0; -0.8, -0.6; -0.8, +0.6) amounts a significant value: 6-20 %.

In assessing theoretical uncertainties for future e^+e^- colliders, it is necessary to achieve the accuracy of approximately 10^{-4} for many observables. Estimating the value δ at different

Table C.9: Processes $e^+e^- \to \mu^+\mu^-$ and $e^+e^- \to \tau^+\tau^-$: Born vs 1-loop.

P_{e^-},	P_{e^+}	$\sigma^{\rm Born}_{\mu^+\mu^-}$, pb	$\sigma^{\rm 1-loop}_{\mu^+\mu^-}$, pb	δ,%	$\sigma^{\rm Born}_{\tau^+\tau^-}$, pb	$\sigma^{\rm 1-loop}_{\tau^+\tau^-}$, pb	δ,%
$\sqrt{s} = 250$ GeV							
0,	0	1.417(1)	2.397(1)	69.1(1)	1.417(1)	2.360(1)	66.5(1)
−0.8,	0	1.546(1)	2.614(1)	69.1(1)	1.546(1)	2.575(1)	66.5(1)
−0.8,	−0.6	0.7690(2)	1.301(1)	69.2(1)	0.7692(1)	1.298(1)	68.8(1)
−0.8,	+0.6	2.323(1)	3.927(1)	69.1(1)	2.324(1)	3.850(1)	65.7(1)
$\sqrt{s} = 500$ GeV							
0,	0	0.3436(1)	0.4696(1)	36.7(1)	0.3436(1)	0.4606(1)	34.0(3)
−0.8,	0	0.3716(1)	0.4953(1)	33.3(1)	0.3715(1)	0.4861(1)	30.8(1)
−0.8,	−0.6	0.1857(1)	0.2506(1)	35.0(1)	0.1857(1)	0.2466(1)	32.8(1)
−0.8,	+0.6	0.5575(1)	0.7399(1)	32.7(1)	0.5575(1)	0.7257(1)	30.1(1)
$\sqrt{s} = 1000$ GeV							
0,	0	0.08535(1)	0.1163(1)	36.2(1)	0.08534(2)	0.1134(1)	33.6(1)
−0.8,	0	0.09213(1)	0.1212(1)	31.6(1)	0.09213(1)	0.11885(2)	29.0(1)
−0.8,	−0.6	0.04608(1)	0.06169(1)	33.9(1)	0.04608(1)	0.06067(1)	31.7(1)
−0.8,	+0.6	0.1382(1)	0.1807(1)	30.8(1)	0.1382(1)	0.1770(1)	28.1(1)

Table C.10: Process $e^+e^- \to ZH$: Born vs 1-loop.

P_{e^-},	P_{e^+}	$\sigma^{\rm Born}_{ZH}$, pb	$\sigma^{\rm 1-loop}_{ZH}$, pb	δ,%
$\sqrt{s} = 250$ GeV				
0,	0	205.64(1)	186.6(1)	-9.24(1)
−0.8,	0	242.55(1)	201.5(1)	-16.94(1)
−0.8,	−0.6	116.16(1)	100.8(1)	-13.25(1)
−0.8,	+0.6	368.93(1)	302.2(1)	-18.10(1)
$\sqrt{s} = 500$ GeV				
0,	0	51.447(1)	57.44(1)	11.65(1)
−0.8,	0	60.680(1)	62.71(1)	3.35(2)
−0.8,	−0.6	29.061(1)	31.25(1)	7.54(1)
−0.8,	+0.6	92.299(1)	94.17(2)	2.03(2)
$\sqrt{s} = 1000$ GeV				
0,	0	11.783(1)	12.92(1)	9.68(1)
−0.8,	0	13.898(1)	13.91(1)	0.10(2)
−0.8,	−0.6	6.6559(1)	6.995(1)	5.09(2)
−0.8,	+0.6	21.140(1)	20.83(1)	-1.47(2)

degrees of polarization of the initial states, we see that taking into account beam polarization is crucial.

Further development of the process library of the Monte-Carlo generator `MCSANCee` involves $e^+e^- \to \gamma\gamma$ (plus cross-symmetric processes) and ("W fusion") $e^+e^- \to \nu_e\nu_e H$. We have started the work on introduction of higher-order corrections, as well as on the implementation of multiphoton emission contributions.

References

[1] S. Jadach, P. Sawicki, mFOAM-1.02: A Compact version of the cellular event generator FOAM, Comput. Phys. Commun. 177 (2007) 441–458. arXiv:physics/0506084, doi:10.1016/j.cpc.2007.02.112.

[2] ROOT, Data Analysis Framework, https://root.cern.ch.

[3] A. Andonov, A. Arbuzov, D. Bardin, S. Bondarenko, P. Christova, L. Kalinovskaya, G. Nanava, W. von Schlippe, SANCscope - v.1.00, Comput. Phys. Commun. 174 (2006) 481–517, [Erratum: Comput. Phys. Commun.177,623(2007)]. arXiv:hep-ph/0411186, doi:10.1016/j.cpc.2005.12.006,10.1016/j.cpc.2007.06.010.

[4] A. Arbuzov, D. Bardin, S. Bondarenko, P. Christova, L. Kalinovskaya, U. Klein, V. Kolesnikov, L. Rumyantsev, R. Sadykov, A. Sapronov, Update of the MCSANC Monte Carlo integrator, v. 1.20, JETP Lett. 103 (2) (2016) 131–136. arXiv:1509.03052, doi:10.1134/S0021364016020041.

[5] D. Bardin, Y. Dydyshka, L. Kalinovskaya, L. Rumyantsev, A. Arbuzov, R. Sadykov, S. Bondarenko, One-loop electroweak radiative corrections to polarized Bhabha scattering, Phys. Rev. D98 (1) (2018) 013001. arXiv:1801.00125, doi:10.1103/PhysRevD.98.013001.

[6] A. Blondel, et al., Standard Model Theory for the FCC-ee: The Tera-Z, in: Mini Workshop on Precision EW and QCD Calculations for the FCC Studies : Methods and Techniques CERN, Geneva, Switzerland, January 12-13, 2018, 2018. arXiv:1809.01830.

[7] W. Kilian, T. Ohl, J. Reuter, WHIZARD: Simulating Multi-Particle Processes at LHC and ILC, Eur. Phys. J. C71 (2011) 1742. arXiv:0708.4233, doi:10.1140/epjc/s10052-011-1742-y.

[8] A. Belyaev, N. D. Christensen, A. Pukhov, CalcHEP 3.4 for collider physics within and beyond the Standard Model, Comput. Phys. Commun. 184 (2013) 1729–1769. arXiv:1207.6082, doi:10.1016/j.cpc.2013.01.014.

[9] A. Lorca, T. Riemann, An Integrated tool for loop calculations: aITALC, Comput. Phys. Commun. 174 (2006) 71–82. arXiv:hep-ph/0412047, doi:10.1016/j.cpc.2005.09.003.

[10] G. Belanger, F. Boudjema, J. Fujimoto, T. Ishikawa, T. Kaneko, K. Kato, Y. Shimizu, Automatic calculations in high energy physics and Grace at one-loop, Phys. Rept. 430 (2006) 117–209. arXiv:hep-ph/0308080, doi:10.1016/j.physrep.2006.02.001.

[11] A. Denner, S. Dittmaier, Electroweak radiative corrections to $e^-\gamma \to e^-Z$, Nucl. Phys. B398 (1993) 265–284. doi:10.1016/0550-3213(93)90109-3.

[12] R. Sadykov, MCSANCee generator with one-loop electroweak corrections for processes with polarized e^+e^- beams, aCAT 2019 — https://indico.cern.ch/event/708041/contributions/3266626/attachments/1810462/2956579/ACAT19_Sadykov.pdf (2019).

[13] S. Bondarenko, Ya. Dydyshka, L. Kalinovskaya, L. Rumyantsev, R. Sadykov, V. Yermolchyk, One-loop electroweak radiative corrections to polarized $e^+e^- \to ZH$ arXiv:

1812.10965.

Chapter D

SMEFT

1 CoDEx : BSM physics being realised as an SMEFT

Authors: Supratim Das Bakshi, Joydeep Chakrabortty, Sunando Kumar Patra
Corresponding Author: Supratim Das Bakshi [sdbakshi13@gmail.com]

Program Summary
Program Title: `CoDEx`
Version: `1.0.0`
Licensing provisions: `CC By 4.0`
Programming language: `Wolfram Language®`
Mathematica® Version: `10 +`
URL: https://effexteam.github.io/CoDEx
Send BUG reports and Questions: effex.package@gmail.com

1.1 Introduction

In spite of the non-observation of any new resonances after the discovery of the Standard Model (SM)-Higgs like particle, which announces the success of the SM, we have enough reason to believe the existence of theories beyond it (BSM), with the SM as a part. As any such theory will affect the electro-weak and the Higgs sector, and the sensitivity of these precision observables are bound to increase in near future, indirect estimation of allowed room left for BSM using Standard Model Effective Field Theory (SMEFT) is well-motivated.

Provided that the S-matrix can be expanded perturbatively in the inverse powers of the ultraviolet scale (Λ^{-1}), and the resultant series is convergent, we can integrate out heavy degrees of freedom and the higher mass dimensional operators capture their impact through – $\sum_i (1/\Lambda^{d_i-4}) C_i \mathcal{O}_i$, where d_i is the operator mass dimension (> 5), and C_i, a function of BSM parameters, is the corresponding Wilson coefficient. Among different choices of operator bases, we restrict ourselves to `"SILH"` [1, 2] and `"Warsaw"` [3–6] bases. All WCs are computed at the cut-of scale Λ, usually identified as the mass of the heavy field. The truncation the $1/\Lambda$ series depends on the experimental precision of the observables [7]. Already, there have been quite a progress in building packages and libraries in the literature, [8–13].

One can justifiably question the validity of choosing to use SMEFT over the full BSM Lagrangian and the answer lies in the trade-off between the computational challenge of the full BSM and precision of the observables. The choice of Λ ensures the convergence of M_Z/Λ series. Using the anomalous dimension matrix (γ) (which is basis dependent), the SMEFT WCs $C_i(\Lambda)$ (computed at Λ), are evolved to $C_i(M_Z)$, some of which are absent at the Λ scale as the matrix γ contains non-zero off-diagonal elements. See [4–6, 14] regarding the running of the SMEFT operators. We need to choose only those 'complete' bases, in which the precision observables are defined.

CoDEx, a *Mathematica*® package [15], in addition to integrating out the heavy field propagator(s) from tree and 1-loop processes and generating SMEFT operators up to dimension-6, provides the WCs as a function of BSM parameters. In this draft, we briefly discuss the underlying principle of **CoDEx**, and give one illustrative example of the work-flow. Details about downloading, installation, and detailed documentation of the functions are available in the website: https://effexteam.github.io/CoDEx.

1.2 The package, in detail

CoDEx is a Wilson coefficient calculator which is developed in Mathematica environment. The algorithm of this code is based on the "Covariant Derivative Expansion" method discussed in [16–30]. Each and every detail about this package can be found here :https://effexteam.github.io/CoDEx. The main functions based on which this program works are captured in Table D.1. Here, we have demonstrated the working methodology of **CoDEx** with an explicit example.

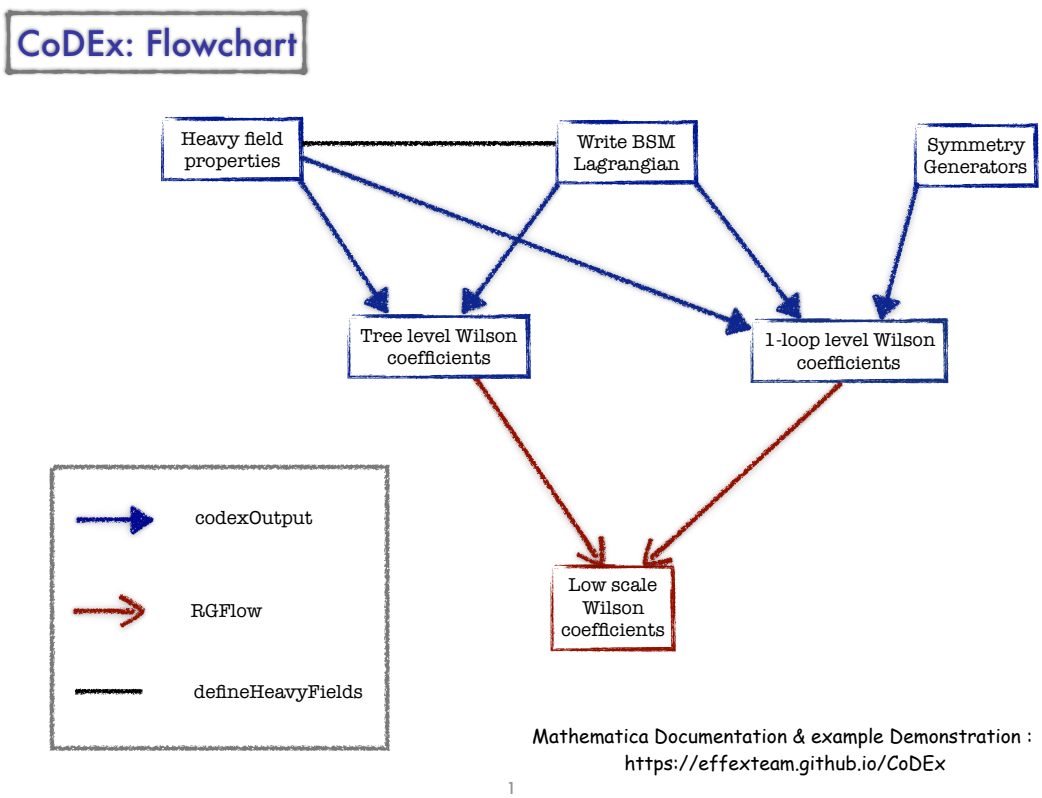

Fig. D.1: Flow-chart demonstrates the working principle of CoDEx

1.2.1 Detailed example: Electro-weak $SU(2)_L$ Triplet Scalar with hypercharge $Y = 1$

Here, we have demonstrated the work-flow of **CoDEx** with the help of a complete analysis of a representative model.

$$\mathcal{L}_{BSM} = \mathcal{L}_{SM} + Tr[(\mathcal{D}_\mu\Delta)^\dagger(\mathcal{D}^\mu\Delta)] - m_\Delta^2 Tr[\Delta^\dagger\Delta] + \mathcal{L}_Y - V(H,\Delta), \tag{1.1}$$

Table D.1: Main functions provided by CoDEx

Function	*Details*
CoDExHelp	Opens the **CoDEx** guide, with all help files listed.
treeOutput	Calculates WCs generated from tree level processes.
loopOutput	Calculates WCs generated from 1-loop processes.
codexOutput	Generic function for WCs calculation with choices for level, bases etc. given with **OptionValue**s.
defineHeavyFields	Creates representation of heavy fields. Use the output to construct BSM Lagrangian.
texTable	Given a **List**, returns the LaTeX output of a tabular environment, displayed and/or copied to clipboard.*
formPick	Applied on a list of WCs from a specific operator basis, reformats the output in the specified style.
RGFlow	RG Flow of WCs of dim. 6 operators in "Warsaw" basis, from matching scale to a lower (arbitrary) scale.
initializeLoop	Prepares the Isospin and Color symmetry generators for a specific model with a specific heavy field content. loopOutput can only be run after this step is done.

where,

$$V(H,\Delta) = \zeta_1 (H^\dagger H) Tr[\Delta^\dagger \Delta] + \zeta_2 (H^\dagger \tau^i H) Tr[\Delta^\dagger \tau^i \Delta] + [\mu (H^T i\sigma^2 \Delta^\dagger H) + h.c.], \tag{1.2}$$

$$\text{and} \quad \mathcal{L}_Y = y_\Delta L^T C i\tau^2 \Delta L + h.c. \tag{1.3}$$

Here, the heavy field is Δ. Once this heavy field, Δ, is integrated out using **CoDEx**, the effective operators upto dimension-6 for both bases are generated. The effective operators and their respective Wilson coefficients are listed in Table D.2-D.4. Below we have appended the exact steps one needs to follow to run the code and compute the desired results.

1. First, load the package:

```
In[1]:= Needs["CoDEx"]
```

2. We have to define the field Δ as:

```
fields =
{
{fieldName, components, colorDim, isoDim,
hyperCharge, spin,mass}
};
```

We follow the convention in above line.

```
In[2]:= fieldewcts=
        {
        {hf,3,1,3,1,0,m_Δ}
        };

In[3]:= hfvecst2ss=defineHeavyFields[fieldewcts];

In[4]:= δ=hfvecst2ss[[1,1]]

Out[4]= {hf[1,1]+i ihf[1,1],hf[1,2]+i ihf[1,2],hf[1,3]+i ihf[1,3]}
```

3. Now, we will build the Lagrangian after defining the heavy field. We need to provide only those terms that contain the heavy fields. The kinetic terms (covariant derivative and mass terms) of the heavy field will not play any role in this construction, and thus can be ignored. The Lagrangian is written in the following way:

```
In[5]:= Δ=∑_i^3 δ[[i]] PauliMatrix[i];

In[6]:= Δc =i tau[2].Δ;

In[7]:= V=ζ1 dag[H].H Tr[dag[Δ].Δ]
            +ζ2 ∑_i^3 dag[H].tau[i].H Tr[dag[Δ].tau[i].Δ]
            +μ H.(i tau[2].dag[Δ]).H
            +μ dag[H].(-i Δ.tau[2]).hermitianConjugate[H];

In[8]:= lyukawa=Expand[yΣ ∑_i^2 ∑_j^2 hermitianConjugate[lepb[1][[i]]].
                  gamma[0].chargeC.(Δc[[i,j]] lep[1][[j]])
                  +yΣ ∑_i^2 ∑_j^2 lepb[1][[i]].gamma[0].
                  (dag[Δc][[i,j]] dag[chargeC].lep[1][[j]])];

In[9]:= Lpotent2ss=Expand[lyukawa-V];
```

```
In[10]:= initializeLoop["t2ss",fieldt2ss]

Out[10]= Check the documentation page CoDExParafernalia for details.

  » Isospin Symmetry Generators for the field 'hf' are
    isot2ss[1,a] = tauadj[a]

  » Color Symmetry Generators for the field 'hf' are colt2ss[1,a] = 0
```

(See the documentation of **initializeLoop** for details.)

```
In[13]:= wcT2SSwar=codexOutput[Lpotent2ss,fieldt2ss,model→"t2ss"];
         formPick["Warsaw","Detailed2",wcT2SSwar,FontSize→Medium,
         FontFamily→"Times New Roman",Frame→All]
```

4. The operators can be generated in both "SILH" and "Warsaw" bases along with their respective Wilson coefficients. This output can be exported into a LaTeX format as well, see Table D.3.

```
In[14]:= wcT2SSsilh=codexOutput[Lpotent2ss,fieldt2ss,model→"t2ss",
         operBasis→"SILH"];
         formPick["SILH","Detailed2",wcT2SSsilh,FontSize→Medium,
         FontFamily→"Times New Roman",Frame→All]
```

Output of this can be found in Table D.2.

```
In[15]:= wcT2SSdim5=codexOutput[Lpotent2ss,fieldt2ss,model→"t2ss",
                    operBasis→"Dim5"];
         formPick["Dim5","Detailed2",wcT2SSdim5,FontSize→Medium,
         FontFamily→"Times New Roman",Frame→All]
```

Output of this can be found in Table D.4.

5. The RG evolution of these WCs can be performed only in "Warsaw" basis as this is the complete one using **RGFlow** as:

```
In[16]:= RGFlow[wcT2SSwar,m,μ]
```

Let us consider that the **CoDEx** output which is the WCs at the high scale is generated, and saved as:

```
In[17]:= wcT2SSwar={{"qH",-ζ1^3/(4 m_Δ^2 π^2)-ζ1 ζ2^2/(32 m_Δ^2 π^2)-ζ1 μ^2/m_Δ^4-ζ2 μ^2/(4 m_Δ^4)},
                    {"qHbox",ζ2^2/(192 m_Δ^2 π^2)+μ^2/(2 m_Δ^4)},
         {"qHD",ζ1^2/(4 m_Δ^2 π^2)+ζ2^2/(96 m_Δ^2 π^2)-2 μ^2/m_Δ^4},{"qHW",gW^2 ζ1/(48 m_Δ^2 π^2)},
         {"qHWB",-gW gY ζ2/(48 m_Δ^2 π^2)},{"qll[1,1,1,1]",yΣ^2/(4 m_Δ^2)},{"qW",gW^3/(1440 m_Δ^2 π^2)}}
```

Table D.2: Effective operators and Wilson Coefficients in "SILH" basis for Complex Triplet Scalar (Y=1) model.

O_{2B}	$\frac{g_Y^2}{160\pi^2 m_\Delta^2}$
O_{2W}	$\frac{g_W^2}{240\pi^2 m_\Delta^2}$
O_{3W}	$\frac{g_W^2}{240\pi^2 m_\Delta^2}$
O_6	$-\frac{\zeta_1\mu^2}{m_\Delta^4} - \frac{\zeta_2\mu^2}{4m_\Delta^4} - \frac{\zeta_1^3}{4\pi^2 m_\Delta^2} - \frac{\zeta_2^2\zeta_1}{32\pi^2 m_\Delta^2}$
$O_{\rm BB}$	$\frac{\zeta_1}{32\pi^2 m_\Delta^2}$
O_H	$\frac{\zeta_1^2}{8\pi^2 m_\Delta^2} + \frac{\mu^2}{2m_\Delta^4}$
O_R	$\frac{\zeta_2^2}{96\pi^2 m_\Delta^2} + \frac{\mu^2}{m_\Delta^4}$
O_T	$\frac{\zeta_2^2}{192\pi^2 m_\Delta^2} - \frac{\mu^2}{2m_\Delta^4}$
$O_{\rm WB}$	$-\frac{\zeta_2}{96\pi^2 m_\Delta^2}$
$O_{\rm WW}$	$\frac{\zeta_1}{48\pi^2 m_\Delta^2}$

Once we declare the matching scale (high scale) as the mass of the heavy particle ('`m`'), we need to recall the function `RGFlow` to generate the WCs at low scale as:

In[18]:=
```
floRes1 = RGFlow[wcT2SSwar,m,μ]
```

Out[18]=
```
{{qW, gW^3/(1440 m_Δ^2 π^2) + 29 gW^5 Log[μ/m]/(46080 m_Δ^2 π^4)},{qH, -ζ1^3/(4 m_Δ^2 π^2) - ζ1 ζ2^2/(32 m_Δ^2 π^2) - ζ1 μ^2/m_Δ^4 - ζ2 μ^2/(4 m_Δ^4) - 3 gW^6 ζ1 Log[μ/m]/(256 m_Δ^2 π^4)
- gW^4 gY^2 ζ1 Log[μ/m]/(256 m_Δ^2 π^4) - 3 gW^2 ζ1^2 Log[μ/m]/(32 m_Δ^2 π^4) - 3 gW^4 ζ1^2 Log[μ/m]/(256 m_Δ^2 π^4) + 3 gY^2 ζ1^2 Log[μ/m]/(32 m_Δ^2 π^4)
- 3 gW^2 gY^2 ζ1^2 Log[μ/m]/(128 m_Δ^2 π^4) - 3 gY^4 ζ1^2 Log[μ/m]/(256 m_Δ^2 π^4) + 27 gW^2 ζ1^3 Log[μ/m]/(128 m_Δ^2 π^4) + 9 gY^2 ζ1^3 Log[μ/m]/(128 m_Δ^2 π^4)
+ gW^4 gY^2 ζ2 Log[μ/m]/(256 m_Δ^2 π^4) + gW^2 gY^4 ζ2 Log[μ/m]/(256 m_Δ^2 π^4) - gW^2 ζ2^2 Log[μ/m]/(256 m_Δ^2 π^4) - gW^4 ζ2^2 Log[μ/m]/(2048 m_Δ^2 π^4) + gY^2 ζ2^2 Log[μ/m]/(256 m_Δ^2 π^4)
- gW^2 gY^2 ζ2^2 Log[μ/m]/(1024 m_Δ^2 π^4) - gY^4 ζ2^2 Log[μ/m]/(2048 m_Δ^2 π^4) + 27 gW^2 ζ1 ζ2^2 Log[μ/m]/(1024 m_Δ^2 π^4)
+ 9 gY^2 ζ1 ζ2^2 Log[μ/m]/(1024 m_Δ^2 π^4) + 3 gW^4 ζ1 λ Log[μ/m]/(64 m_Δ^2 π^4) - gW^2 gY^2 ζ2 λ Log[μ/m]/(64 m_Δ^2 π^4) + 5 gW^2 ζ2^2 λ Log[μ/m]/(1152 m_Δ^2 π^4)
+ 3 gW^2 μ^2 Log[μ/m]/(4 m_Δ^4 π^2) + 3 gW^4 μ^2 Log[μ/m]/(32 m_Δ^4 π^2) - 3 gY^2 μ^2 Log[μ/m]/(4 m_Δ^4 π^2)
+ 3 gW^2 gY^2 μ^2 Log[μ/m]/(16 m_Δ^4 π^2) + 3 gY^4 μ^2 Log[μ/m]/(32 m_Δ^4 π^2) + 27 gW^2 ζ1 μ^2 Log[μ/m]/(32 m_Δ^4 π^2)
+ 9 gY^2 ζ1 μ^2 Log[μ/m]/(32 m_Δ^4 π^2) + 27 gW^2 ζ2 μ^2 Log[μ/m]/(128 m_Δ^4 π^2) + 9 gY^2 ζ2 μ^2 Log[μ/m]/(128 m_Δ^4 π^2) + 5 gW^2 λ μ^2 Log[μ/m]/(12 m_Δ^4 π^2)},
{qHbox, ζ2^2/(192 m_Δ^2 π^2) + μ^2/(2 m_Δ^4) + 5 gY^2 ζ1^2 Log[μ/m]/(192 m_Δ^2 π^4) - gW^2 ζ2^2 Log[μ/m]/(768 m_Δ^2 π^4)
+ gY^2 ζ2^2 Log[μ/m]/(1536 m_Δ^2 π^4) - gW^2 μ^2 Log[μ/m]/(8 m_Δ^4 π^2) - gY^2 μ^2 Log[μ/m]/(4 m_Δ^4 π^2)},
```

Table D.3: Effective operators and Wilson Coefficients in "Warsaw" basis for Complex Triplet Scalar (Y=1) model.

Q_H	$-\frac{\zeta_1\mu^2}{m_\Delta^4} - \frac{\zeta_2\mu^{\ 2}}{4m_\Delta^4} - \frac{\zeta_1^3}{4\pi^2 m_\Delta^2} - \frac{\zeta_2^2\zeta_1}{32\pi^2 m_\Delta^2}$
$Q_{H\Box}$	$\frac{\zeta_2^2}{192\pi^2 m_\Delta^2} + \frac{\mu^2}{2m_\Delta^4}$
$Q_{\rm HD}$	$\frac{\zeta_1^2}{4\pi^2 m_\Delta^2} + \frac{\zeta_2^2}{96\pi^2 m_\Delta^2} - \frac{2\mu^{\ 2}}{m_\Delta^4}$
$Q_{\rm HW}$	$\frac{\zeta_1 g_W^2}{48\pi^2 m_\Delta^2}$
$Q_{\rm HWB}$	$-\frac{\zeta_2 g_W g_Y}{48\pi^2\ m_\Delta^2}$
$Q_{\rm ll}$	$\frac{y_\Delta^2}{4m_\Delta^2}$
Q_W	$\frac{g_W^3}{1440\pi^2 m_\Delta^2}$

Table D.4: Mass dimenion-5 Effective operators and Wilson Coefficients for Complex Triplet Scalar (Y=1) model.

Dimension-5 operator	Wilson Coefficient
$llHH$	$\frac{y_\Delta^2}{m_\Delta}$

$$\{qHD, \frac{\zeta 1^2}{4\ m_\Delta{}^2\ \pi^2} + \frac{\zeta 2^2}{96\ m_\Delta{}^2\ \pi^2} - \frac{2\ \mu^2}{m_\Delta{}^4} + \frac{9\ gW^2\ \zeta 1^2\ Log[\frac{\mu}{m}]}{128\ m_\Delta{}^2\ \pi^4} - \frac{5\ gY^2\ \zeta 1^2\ Log[\frac{\mu}{m}]}{384\ m_\Delta{}^2\ \pi^4}$$
$$+ \frac{3\ gW^2\ \zeta 2^2\ Log[\frac{\mu}{m}]}{1024\ m_\Delta{}^2\ \pi^4} + \frac{5\ gY^2\ \zeta 2^2\ Log[\frac{\mu}{m}]}{3072\ m_\Delta{}^2\ \pi^4} - \frac{9\ gW^2\ \mu^2\ Log[\frac{\mu}{m}]}{16\ m_\Delta{}^4\ \pi^2} + \frac{5\ gY^2\ \mu^2\ Log[\frac{\mu}{m}]}{16\ m_\Delta{}^4\ \pi^2}\},$$
$$\{qHW, \frac{gW^2\ \zeta 1}{48\ m_\Delta{}^2\ \pi^2} - \frac{gW^6\ Log[\frac{\mu}{m}]}{1536\ m_\Delta{}^2\ \pi^4} - \frac{53\ gW^4\ \zeta 1\ Log[\frac{\mu}{m}]}{4608\ m_\Delta{}^2\ \pi^4}$$
$$- \frac{gW^2\ gY^2\ \zeta 1\ Log[\frac{\mu}{m}]}{512\ m_\Delta{}^2\ \pi^4} - \frac{gW^2\ gY^2\ \zeta 2\ Log[\frac{\mu}{m}]}{768\ m_\Delta{}^2\ \pi^4}\}, \{qHB, -\frac{gW^2\ gY^2\ \zeta 2\ Log[\frac{\mu}{m}]}{256\ m_\Delta{}^2\ \pi^4}\},$$
$$\{qHWB, -\frac{gW\ gY\ \zeta 2}{48\ m_\Delta{}^2\ \pi^2} + \frac{gW^5\ gY\ Log[\frac{\mu}{m}]}{7680\ m_\Delta{}^2\ \pi^4} + \frac{gW^3\ gY\ \zeta 1\ Log[\frac{\mu}{m}]}{384\ m_\Delta{}^2\ \pi^4} - \frac{gW^3\ gY\ \zeta 2\ Log[\frac{\mu}{m}]}{576\ m_\Delta{}^2\ \pi^4} - \frac{19\ gW\ gY^3\ \zeta 2\ Log[\frac{\mu}{m}]}{2304\ m_\Delta{}^2\ \pi^4}\},$$
$$\{qeH[1,1], \frac{3\ gW^4\ \zeta 1\ Log[\frac{\mu}{m}]\ Yu^\dagger[e]}{256\ m_\Delta{}^2\ \pi^4} - \frac{3\ gW^2\ \zeta 1^2\ Log[\frac{\mu}{m}]\ Yu^\dagger[e]}{128\ m_\Delta{}^2\ \pi^4}$$
$$+ \frac{3\ gY^2\ \zeta 1^2\ Log[\frac{\mu}{m}]\ Yu^\dagger[e]}{128\ m_\Delta{}^2\ \pi^4} + \frac{gW^2\ gY^2\ \zeta 2\ Log[\frac{\mu}{m}]\ Yu^\dagger[e]}{256\ m_\Delta{}^2\ \pi^4}$$
$$+ \frac{gW^2\ \zeta 2^2\ Log[\frac{\mu}{m}]\ Yu^\dagger[e]}{9216\ m_\Delta{}^2\ \pi^4} + \frac{gY^2\ \zeta 2^2\ Log[\frac{\mu}{m}]\ Yu^\dagger[e]}{1024\ m_\Delta{}^2\ \pi^4} + \frac{7\ gW^2\ \mu^2\ Log[\frac{\mu}{m}]\ Yu^\dagger[e]}{24\ m_\Delta{}^4\ \pi^2} - \frac{3\ gY^2\ \mu^2\ Log[\frac{\mu}{m}]\ Yu^\dagger[e]}{16\ m_\Delta{}^4\ \pi^2}\},$$
$$\{quH[1,1], \frac{3\ gW^4\ \zeta 1\ Log[\frac{\mu}{m}]\ Yu^\dagger[u]}{512\ m_\Delta{}^2\ \pi^4} - \frac{3\ gW^2\ \zeta 1^2\ Log[\frac{\mu}{m}]\ Yu^\dagger[u]}{128\ m_\Delta{}^2\ \pi^4}$$
$$+ \frac{3\ gY^2\ \zeta 1^2\ Log[\frac{\mu}{m}]\ Yu^\dagger[u]}{128\ m_\Delta{}^2\ \pi^4} + \frac{gW^2\ gY^2\ \zeta 2\ Log[\frac{\mu}{m}]\ Yu^\dagger[u]}{768\ m_\Delta{}^2\ \pi^4} + \frac{gW^2\ \zeta 2^2\ Log[\frac{\mu}{m}]\ Yu^\dagger[u]}{9216\ m_\Delta{}^2\ \pi^4}$$
$$+ \frac{gY^2\ \zeta 2^2\ Log[\frac{\mu}{m}]\ Yu^\dagger[u]}{1024\ m_\Delta{}^2\ \pi^4} + \frac{7\ gW^2\ \mu^2\ Log[\frac{\mu}{m}]\ Yu^\dagger[u]}{24\ m_\Delta{}^4\ \pi^2} - \frac{3\ gY^2\ \mu^2\ Log[\frac{\mu}{m}]\ Yu^\dagger[u]}{16\ m_\Delta{}^4\ \pi^2}\},$$
$$\{qdH[1,1], \frac{3\ gW^4\ \zeta 1\ Log[\frac{\mu}{m}]\ Yu^\dagger[d]}{512\ m_\Delta{}^2\ \pi^4} - \frac{3\ gW^2\ \zeta 1^2\ Log[\frac{\mu}{m}]\ Yu^\dagger[d]}{128\ m_\Delta{}^2\ \pi^4}$$
$$+ \frac{3\ gY^2\ \zeta 1^2\ Log[\frac{\mu}{m}]\ Yu^\dagger[d]}{128\ m_\Delta{}^2\ \pi^4} - \frac{gW^2\ gY^2\ \zeta 2\ Log[\frac{\mu}{m}]\ Yu^\dagger[d]}{768\ m_\Delta{}^2\ \pi^4} + \frac{gW^2\ \zeta 2^2\ Log[\frac{\mu}{m}]\ Yu^\dagger[d]}{9216\ m_\Delta{}^2\ \pi^4}$$

We have provided the flexibility to the users to reformat, save, and/or export all these WCs corresponding to the effective operators at the electro-weak scale (μ) to LaTeX, using **formPick**. We have also provided an illustrative example:

In[19]:=
```
formPick["Warsaw","Detailed2",floRes1,Frame→All,
         FontSize→Medium,FontFamily→"Times New Roman"]
```

Out[19]=

Q_W	$\epsilon^{abc} W_\rho^{a,\mu} W_\mu^{b,\nu} W_\nu^{c,\rho}$	$\frac{29 {g_W}^5 \log\left(\frac{\mu}{m_\Delta}\right)}{46080\pi^4 m_\Delta^2} + \frac{{g_W}^3}{1440\pi^2 m_\Delta^2}$
$\vdots$	$\vdots$	$\vdots$
Q_{ld}	$(\bar{l}\gamma_\mu\ \mathrm{l})(\bar{d}\gamma_\mu\ \mathrm{d})$	$\frac{{g_Y}^2 {y_\Sigma}^2 \log\left(\frac{\mu}{m_\Delta}\right)}{48\pi^2 m_\Delta^2}$

Acknowledgements

S. DasBakshi would like to thank the organizers of the 11th FCC-ee workshop: Theory and Experiments, CERN for the invitation and providing the opportunity to present this work.

References

[1] G. F. Giudice, C. Grojean, A. Pomarol, R. Rattazzi, The Strongly-Interacting Light Higgs, JHEP 06 (2007) 045. arXiv:hep-ph/0703164, doi:10.1088/1126-6708/2007/06/045.

[2] R. Contino, M. Ghezzi, C. Grojean, M. Muhlleitner, M. Spira, Effective Lagrangian for a light Higgs-like scalar, JHEP 07 (2013) 035. arXiv:1303.3876, doi:10.1007/JHEP07(2013)035.

[3] B. Grzadkowski, M. Iskrzynski, M. Misiak, J. Rosiek, Dimension-Six Terms in the Standard Model Lagrangian, JHEP 10 (2010) 085. arXiv:1008.4884, doi:10.1007/JHEP10(2010)085.

[4] E. E. Jenkins, A. V. Manohar, M. Trott, Renormalization Group Evolution of the Standard Model Dimension Six Operators I: Formalism and lambda Dependence, JHEP 10 (2013) 087. arXiv:1308.2627, doi:10.1007/JHEP10(2013)087.

[5] E. E. Jenkins, A. V. Manohar, M. Trott, Renormalization Group Evolution of the Standard Model Dimension Six Operators II: Yukawa Dependence, JHEP 01 (2014) 035. arXiv:1310.4838, doi:10.1007/JHEP01(2014)035.

[6] R. Alonso, E. E. Jenkins, A. V. Manohar, M. Trott, Renormalization Group Evolution of the Standard Model Dimension Six Operators III: Gauge Coupling Dependence and Phenomenology, JHEP 04 (2014) 159. arXiv:1312.2014, doi:10.1007/JHEP04(2014)159.

[7] R. J. Furnstahl, N. Klco, D. R. Phillips, S. Wesolowski, Quantifying truncation errors in effective field theory, Phys. Rev. C92 (2) (2015) 024005. arXiv:1506.01343, doi:10.1103/PhysRevC.92.024005.

[8] B. Gripaios, D. Sutherland, DEFT: A program for operators in EFTarXiv:1807.07546.

[9] A. Falkowski, B. Fuks, K. Mawatari, K. Mimasu, F. Riva, V. Sanz, Rosetta: an operator basis translator for Standard Model effective field theory, Eur. Phys. J. C75 (12) (2015) 583. arXiv:1508.05895, doi:10.1140/epjc/s10052-015-3806-x.

[10] A. Celis, J. Fuentes-Martin, A. Vicente, J. Virto, DsixTools: The Standard Model Effective Field Theory Toolkit, Eur. Phys. J. C77 (6) (2017) 405. arXiv:1704.04504, doi:10.1140/epjc/s10052-017-4967-6.

[11] J. C. Criado, MatchingTools: a Python library for symbolic effective field theory calculations, Comput. Phys. Commun. 227 (2018) 42–50. arXiv:1710.06445, doi:10.1016/j.cpc.2018.02.016.

[12] J. Aebischer, J. Kumar, D. M. Straub, Wilson: a Python package for the running and matching of Wilson coefficients above and below the electroweak scalearXiv:1804.05033.

[13] J. Aebischer, et al., WCxf: an exchange format for Wilson coefficients beyond the Standard Model, Comput. Phys. Commun. 232 (2018) 71–83. arXiv:1712.05298, doi:10.1016/j.cpc.2018.05.022.

[14] J. D. Wells, Z. Zhang, Renormalization group evolution of the universal theories EFT, JHEP 06 (2016) 122. arXiv:1512.03056, doi:10.1007/JHEP06(2016)122.

[15] S. Das Bakshi, J. Chakrabortty, S. K. Patra, CoDEx: Wilson coefficient calculator con-

necting SMEFT to UV theory, Eur. Phys. J. C79 (1) (2019) 21. arXiv:1808.04403, doi:10.1140/epjc/s10052-018-6444-2.

[16] M. K. Gaillard, The Effective One Loop Lagrangian With Derivative Couplings, Nucl. Phys. B268 (1986) 669–692. doi:10.1016/0550-3213(86)90264-6.

[17] O. Cheyette, Derivative Expansion of the Effective Action, Phys. Rev. Lett. 55 (1985) 2394. doi:10.1103/PhysRevLett.55.2394.

[18] B. Henning, X. Lu, H. Murayama, How to use the Standard Model effective field theory, JHEP 01 (2016) 023. arXiv:1412.1837, doi:10.1007/JHEP01(2016)023.

[19] B. Henning, X. Lu, H. Murayama, One-loop Matching and Running with Covariant Derivative Expansion, JHEP 01 (2018) 123. arXiv:1604.01019, doi:10.1007/JHEP01(2018)123.

[20] S. A. R. Ellis, J. Quevillon, T. You, Z. Zhang, Mixed heavy–light matching in the Universal One-Loop Effective Action, Phys. Lett. B762 (2016) 166–176. arXiv:1604.02445, doi:10.1016/j.physletb.2016.09.016.

[21] J. Fuentes-Martin, J. Portoles, P. Ruiz-Femenia, Integrating out heavy particles with functional methods: a simplified framework, JHEP 09 (2016) 156. arXiv:1607.02142, doi:10.1007/JHEP09(2016)156.

[22] F. del Aguila, Z. Kunszt, J. Santiago, One-loop effective lagrangians after matching, Eur. Phys. J. C76 (5) (2016) 244. arXiv:1602.00126, doi:10.1140/epjc/s10052-016-4081-1.

[23] B. Henning, X. Lu, T. Melia, H. Murayama, 2, 84, 30, 993, 560, 15456, 11962, 261485, ...: Higher dimension operators in the SM EFT, JHEP 08 (2017) 016. arXiv:1512.03433, doi:10.1007/JHEP08(2017)016.

[24] A. Drozd, J. Ellis, J. Quevillon, T. You, The Universal One-Loop Effective Action, JHEP 03 (2016) 180. arXiv:1512.03003, doi:10.1007/JHEP03(2016)180.

[25] J. D. Wells, Z. Zhang, Effective theories of universal theories, JHEP 01 (2016) 123. arXiv:1510.08462, doi:10.1007/JHEP01(2016)123.

[26] L. Lehman, A. Martin, Low-derivative operators of the Standard Model effective field theory via Hilbert series methods, JHEP 02 (2016) 081. arXiv:1510.00372, doi:10.1007/JHEP02(2016)081.

[27] R. Huo, Effective Field Theory of Integrating out Sfermions in the MSSM: Complete One-Loop Analysis, Phys. Rev. D97 (7) (2018) 075013. arXiv:1509.05942, doi:10.1103/PhysRevD.97.075013.

[28] R. Huo, Standard Model Effective Field Theory: Integrating out Vector-Like Fermions, JHEP 09 (2015) 037. arXiv:1506.00840, doi:10.1007/JHEP09(2015)037.

[29] C.-W. Chiang, R. Huo, Standard Model Effective Field Theory: Integrating out a Generic Scalar, JHEP 09 (2015) 152. arXiv:1505.06334, doi:10.1007/JHEP09(2015)152.

[30] L. Lehman, A. Martin, Hilbert Series for Constructing Lagrangians: expanding the phenomenologist's toolbox, Phys. Rev. D91 (2015) 105014. arXiv:1503.07537, doi:10.1103/PhysRevD.91.105014.

[31] M. Schunter, Textableform, Version 1.0, teichstr, 1, 2018.
URL http://library.wolfram.com/infocenter/MathSource/2720/

Chapter E

BSM

1 (Triple) Higgs-coupling imprints at future lepton colliders

Authors: Julien Baglio, Cédric Weiland
Corresponding Author: Julien Baglio [julien.baglio@uni-tuebingen.de]

1.1 Triple Higgs coupling studies in an EFT framework

The measurement of the triple Higgs coupling is one of the major goals of the future colliders. The direct measurement at lepton colliders relies on the production of Higgs boson pairs in two main channels, $e^+e^- \to ZHH$ which is dominant at centre-of-mass energies below 1 TeV and maximal at around 500 GeV, and $e^+e^- \to HH\nu_e\bar{\nu}_e$ that becomes dominant for high-energy colliders. This direct measurement requires to be at least at a centre-of-mass energy of 500 GeV, and is hence only possible at future linear colliders such as the International Linear Collider (ILC) operating at 500 GeV or 1 TeV [1], or the Compact LInear Collider (CLIC) operating at 1.4 TeV (stage 2) or 3 TeV (stage 3) [2]. The SM triple Higgs coupling sensitivity is estimated to be $\delta\kappa_\lambda = (\lambda_{HHH}/\lambda^{\rm SM}_{HHH} - 1) \sim 28\%$ at the 500 GeV ILC with a luminosity of 4 ab^{-1} [3, 4] and $\delta\kappa_\lambda \sim 13\%$ at the CLIC when combining the 1.4 TeV run with 2.5 ab^{-1} of data and the 3 TeV run with 5 ab^{-1} of data [5].

Still, circular-lepton-collider projects such as the Circular Electron Positron Collider (CEPC) [6] or the FCC-ee [7, 8], that run at energies below 500 GeV (not to mention the ILC or the CLIC running at lower energies), can provide a way to constraint the triple Higgs coupling [9]. Since the work of Ref. [10] that proposed for the first time to use precision measurements to constrain the triple Higgs coupling, in particular the measurements in single Higgs production at lepton colliders, there have been studies of the combination of single and double Higgs production observables not only at lepton but also at hadron colliders [11–14]. The analyses use the framework of the Standard Model Effective Field Theory (SMEFT). According to the latest ECFA report [15] the combination of HL-LHC projections [16] with ILC exclusive single-Higgs data gives $\delta\kappa_\lambda = 26\%$ at 68% CL, while with FCC-ee (at 250 or 365 GeV) it goes down to $\delta\kappa_\lambda = 19\%$ and with CEPC we get $\delta\kappa_\lambda = 17\%$. We will present in more details the results of Refs. [12, 13] that demonstrate how important the combination of the LHC results with an analysis at lepton colliders is, and show the potential of the FCC-ee*.

Fig. E.1 (left) displays the latest experimental results available at the 13 TeV LHC for the search of non-resonance Higgs pair production and the 95% CL limits on the triple Higgs coupling, which have been presented in Ref. [17]. The results constraint $\delta\kappa_\lambda$ in the range $[-6.0 : 11.1]$. We can compare them to the projections at the HL-LHC with 3 ab^{-1} presented in the HL-HE LHC report [16] in an SMEFT framework, using a differential analysis in the channel $pp \to HH$. Compared to the projection in Ref. [12], which also included single Higgs data in the channels $pp \to W^\pm H, ZH, t\bar{t}H$, there is a substantial improvement thanks to the

*Julien Baglio thanks Christophe Grojean for his very useful inputs in this subsection.

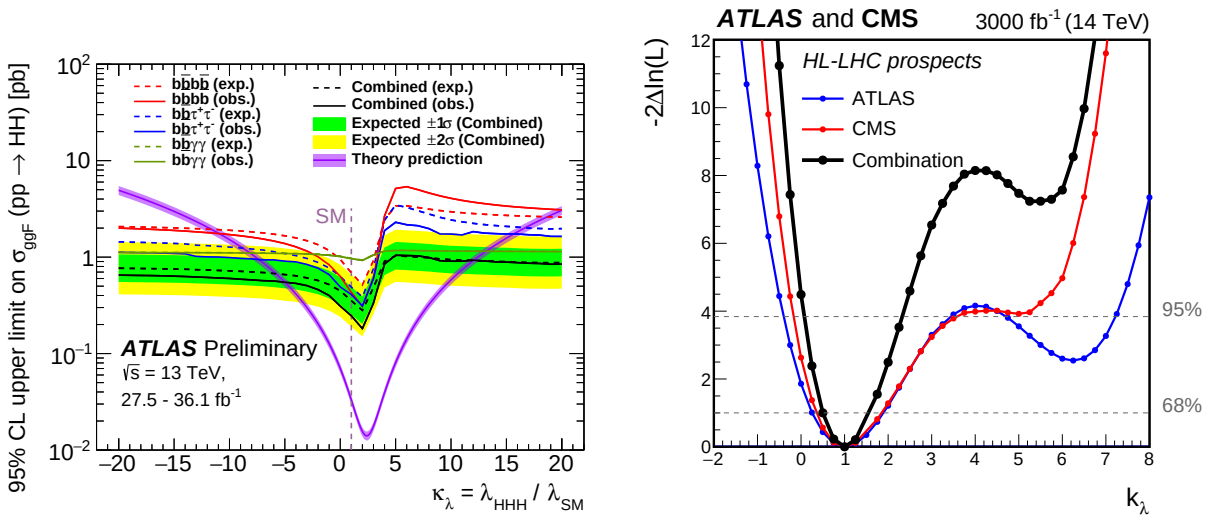

Fig. E.1: Left: Latest experimental bounds on the triple Higgs coupling from the ATLAS collaboration at the 13 TeV LHC, combining $b\bar{b}b\bar{b}$, $b\bar{b}\tau^+\tau^-$, and $b\bar{b}\gamma\gamma$ final states. Taken from Ref. [17]. Right: Minimum negative-log-likelihood distribution of κ_λ at the HL-LHC with 3 ab^{-1} of data including differential observables in Higgs pair production, with ATLAS (blue), CMS (red), and ATLAS+CMS (black) projected results. Figure taken from Ref. [16].

experimental differential analysis. We have $-0.5 \leq \delta\kappa_\lambda \leq 0.5$ at 68% CL and $-0.9 \leq \delta\kappa_\lambda \leq 1.3$ at 95% CL. The degeneracy observed in Ref. [12] with a second minimum at $\delta\kappa_\lambda \sim 5$ is now excluded at 4σ.

The combination with data from lepton colliders removes the second minimum even more drastically and only the SM minimum is left at $\delta\kappa_\lambda = 0$ [13], in particular when data from 250 GeV and 350-365 GeV centre-of-mass energies is combined [13]. This is shown in Fig. E.2 where two setups are compared, the combination of HL-LHC data with circular lepton colliders (FCC-ee or CEPC) data on the left-hand side, and the combination of HL-LHC data with the ILC data on the right-hand side. In both cases the lepton-collider data consists of measurements in the channels $e^+e^- \to W^+W^-, ZH, \nu_e\bar{\nu}_e H$. The second minimum disappears completely even with a relatively low integrated luminosity of $\mathcal{L} = 200$ fb^{-1} at 350 GeV combined to the data at 250 GeV. Note that the FCC-ee (or CEPC), thanks to its much higher luminosity in the 250 GeV run, is doing significantly better than the ILC.

1.2 Probing heavy neutral leptons via Higgs couplings

Since the confirmation of neutrino oscillations in 1998 by the Super-Kamiokande experiment [18], it has been established that at least two neutrinos have a non-zero mass [19]. This experimental fact cannot be accounted for in the SM and requires new physics. One of the simplest extensions is the addition of new heavy, neutral leptons that are gauge singlets and mix with the active neutrinos to generate the light neutrino masses. An appealing model, allowing for these new fermionic states to be in the GeV to a few TeV range while having Yukawa couplings of order one, is the inverse seesaw (ISS) model [20–22], in which a nearly conserved lepton-number symmetry [23,24] is introduced, naturally explaining the smallness of the mass of the lightest neutrino states while allowing for large couplings between the heavy neutrinos and the Higgs boson, leading to a rich phenomenology. In this view the very precise

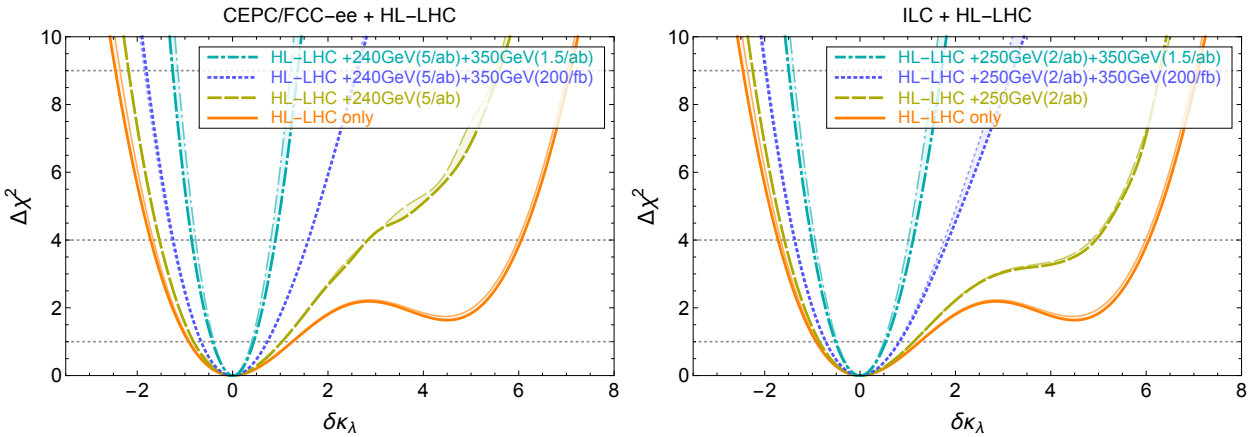

Fig. E.2: $\Delta\chi^2$ distributions for a global fit of the parameter $\delta\kappa_\lambda$ at circular lepton colliders (left) or at the ILC (right), combined with HL-LHC data. The different lines compare the different centre-of-mass energies and luminosity scenarios. Figures taken from Ref. [13].

study of the Higgs sector at lepton colliders can offer a unique opportunity to test low-scale seesaw mechanisms such as the ISS.

Heavy neutral leptons in the GeV regime

We begin with the GeV regime. In these low-scale seesaw models the mixing between the active and the sterile neutrinos leads to modified couplings of neutrinos to the W, Z, and Higgs bosons. This naturally leads to the idea of using precision measurements of the Higgs boson branching fractions into gauge bosons in order to test the mass range $M_N < M_H$ where M_N is the mass of the heavy neutrino states, M_H is the mass of the Higgs boson. As $H \to NN$ is allowed, the invisible Higgs decay width is modified and hence the branching fraction $\mathrm{BR}(H \to W^+W^-)$ is modified via the modified total decay width Γ_H. According to an analysis in 2015 [25] the FCC-ee could be the most competitive lepton collider to test this option, as demonstrated in Fig. E.3. In particular, the experimental sensitivity to $\mathrm{BR}(H \to W^+W^-)$ is expected to be 0.9% at the FCC-ee, compared to 1.3% at the CEPC operating at 240 GeV [26] and 6.4% at the ILC operating at 250 GeV [1][†].

Probing heavy neutral leptons in the multi-TeV regime

Since the coupling of the heavy neutral leptons to the Higgs boson can be quite large in low-scale seesaw models for masses M_N of a few TeV, it is also very appealing to use again Higgs properties to probe a mass regime of $M_N \sim \mathcal{O}(1 - 10\ \mathrm{TeV})$.

Off-diagonal couplings of the Higgs boson to heavy neutral leptons will induce charged-lepton-flavour-violating (cLFV) decays [28]. In particular, simplified formulae were provided in Ref. [29], showing that cLFV Higgs decays exhibit a different functional dependence on seesaw parameters than cLFV radiative decays. They thus provide complementary observables to search for heavy neutral leptons. In a typical low-scale seesaw model like the ISS, the predicted branching fractions can be as large as $\mathrm{BR}(H \to \tau\mu) \sim 10^{-5}$ and it could even reach $\mathrm{BR}(H \to \tau\mu) \sim 10^{-2}$ in a supersymmetric model [30] thus being well within the reach of a Higgs

[†]The latest analysis at the ILC, using a luminosity of 500 fb^{-1}, states that a precision of 4.1% can be achieved [27].

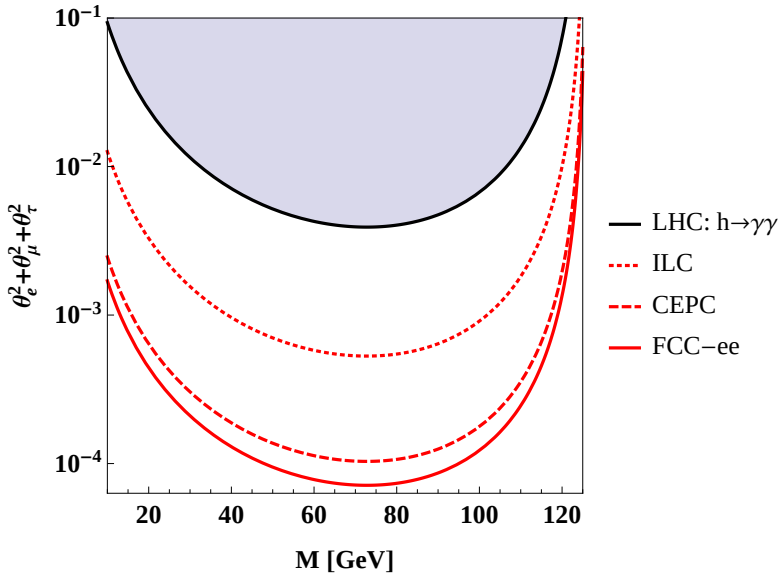

Fig. E.3: Estimated sensitivities on the heavy sterile neutrino properties from the decay $H \to W^+W^-$, assuming 10 years of data taking. The black line denotes the bound from the LHC coming from $H \to \gamma\gamma$ with up to 2015 data. Taken from Ref. [25].

factory like the FCC-ee. However, Higgs observables are uniquely sensitive to diagonal couplings as well and this was studied in particular in Refs. [31,32] using the triple Higgs coupling and in Ref. [33] using a direct physical observable, the production cross section $\sigma(e^+e^- \to W^+W^-H)$. Taking into account all theoretical and experimental constraints that were available, the three studies have found sizeable effects.

In the triple Higgs coupling studies the one-loop corrections to λ_{HHH}, defined as the physical triple Higgs coupling after electroweak symmetry breaking, are studied. The calculation is performed in the on-shell scheme and compares the SM prediction to the prediction in low-scale seesaw models (specifically the ISS in Ref. [32]). Representative one-loop diagrams involving the new heavy neutral leptons are given in Fig. E.4 and details of the calculation and analytical formulae can be found in the original articles. The results are given in terms of deviations with respect to the tree-level value λ^0_{HHH} and to the renormalised one-loop value in the SM $\lambda^{1,\mathrm{SM}}_{HHH}$ of the triple Higgs coupling,

$$\begin{aligned} \Delta^{(1)}\lambda_{HHH} &= \frac{1}{\lambda^0}\left(\lambda^1_{HHH} - \lambda^0\right) , \\ \Delta^{\mathrm{BSM}} &= \frac{1}{\lambda^{1,\mathrm{SM}}_{HHH}}\left(\lambda^1_{HHH} - \lambda^{1,\mathrm{SM}}_{HHH}\right) . \end{aligned} \tag{1.1}$$

with λ^1_{HHH} being the one-loop renormalised triple Higgs coupling in the low-scale seesaw model considered. The constraints from low-energy neutrino observables are implemented via the μ_X-parametrisation, see Ref. [29] for more details as well as the appendix A of Ref. [32] for terms beyond the lowest order in the seesaw expansion. All relevant theoretical and experimental bounds are taken into account and the most stringent constraint comes from the global fit to electroweak precision observables and lepton universality tests [34].

Fig. E.5 displays the results of the analysis in the plane $M_R - |Y_\nu|$ where M_R is the seesaw scale and $|Y_\nu|$ is the magnitude of the Yukawa coupling between the heavy neutral leptons and

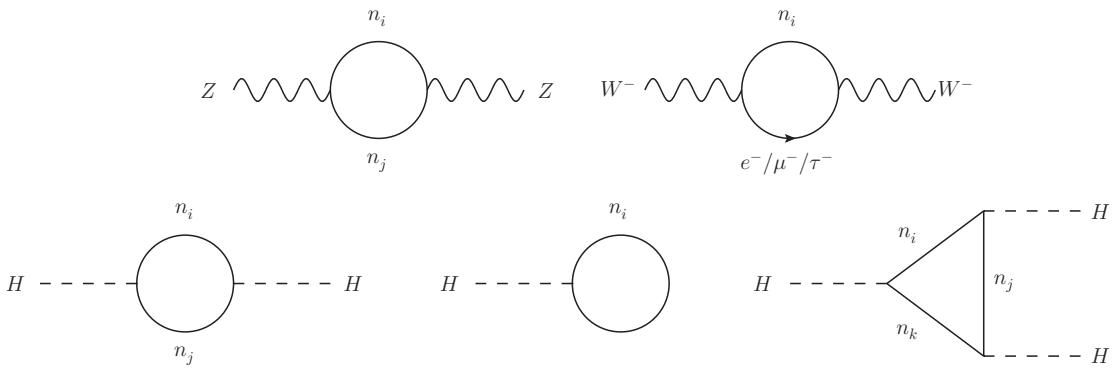

Fig. E.4: Representative Feynman diagrams for the one-loop corrections to λ_{HHH} involving the neutrinos in the ISS model.

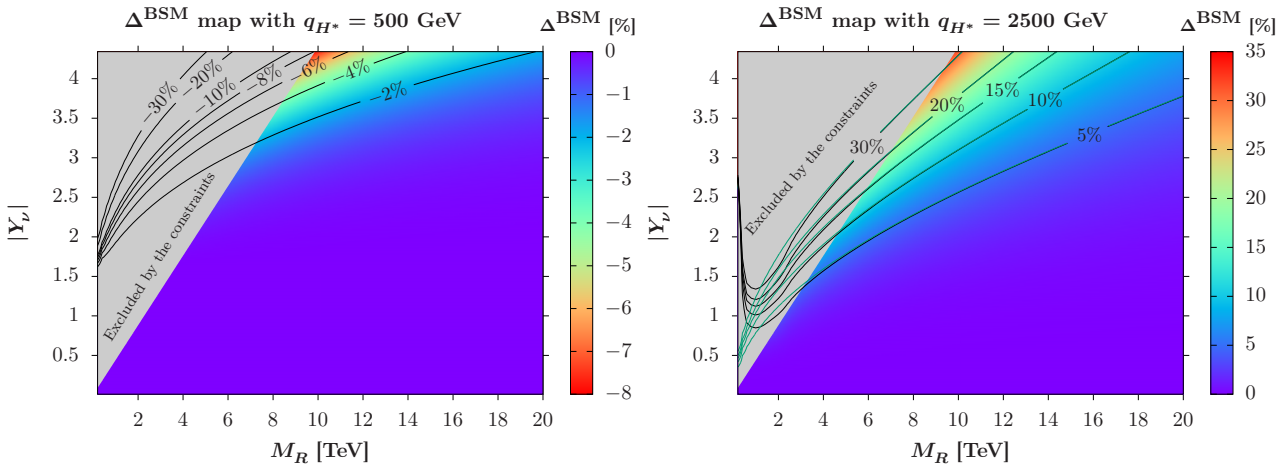

Fig. E.5: Contour maps of the heavy neutral lepton correction $\Delta^{\rm BSM}$ to the triple Higgs coupling λ_{HHH} (in %) as a function of the heavy neutral lepton parameters M_R (in TeV) and $|Y_\nu|$ at a fixed off-shell Higgs momentum $q_{H^*} = 500$ GeV (left) and $q_{H^*} = 2500$ GeV (right). The details of the spectrum are given in Ref. [32]. The grey area is excluded by the constraints on the model and the green lines on the right figure are contour lines that correspond to our approximate formula while the black lines correspond to the full calculation.

the Higgs boson. For an off-shell Higgs momentum of $q_{H^*} = 500$ GeV splitting into two on-shell Higgs bosons, sizeable deviations can be obtained, up to $\Delta^{\rm BSM} \simeq -8\%$. Compared to the expected sensitivity of $\sim 10\%$ at the ILC at 1 TeV with 5 ab^{-1} [35] or to the FCC-hh sensitivity of $\sim 5\%$ when two experiments were to be combined [36], the deviation can be probed and hence test masses of order $\mathcal{O}(10$ TeV). In the case of the FCC-hh, as the hadronic centre-of-mass energy is large, the case $q_{H^*} = 2500$ GeV is even more interesting with a deviation up to $\Delta^{\rm BSM} \simeq +35\%$, leading to a larger coverage of the parameter space and the possibility to test the model at the 3 TeV CLIC where the sensitivity to λ_{HHH} is expected to be of order 13% [5]. The triple Higgs coupling λ_{HHH} is a viable new (pseudo-) observable for the neutrino sector in order to constraint mass models, and might also be used in the context of the FCC-ee in an indirect way in $e^+e^- \to ZH$ at the 2-loop order, given the expected sensitivity the FCC-ee is supposed to reach in this channel. Studies remain to be done in this context.

The study presented in Ref. [33] considered a more direct observable, the production

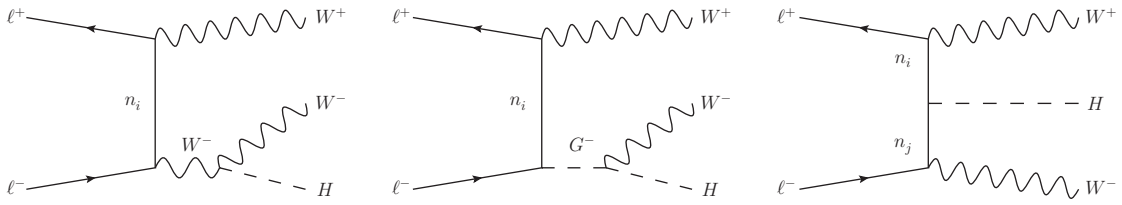

Fig. E.6: ISS neutrino contributions to the process $\ell^+\ell^- \to W^+W^-H$ in the Feynman-'t Hooft gauge. Mirror diagrams cam be obtained by flipping all the electric charges and the indices i, j run from 1 to 9.

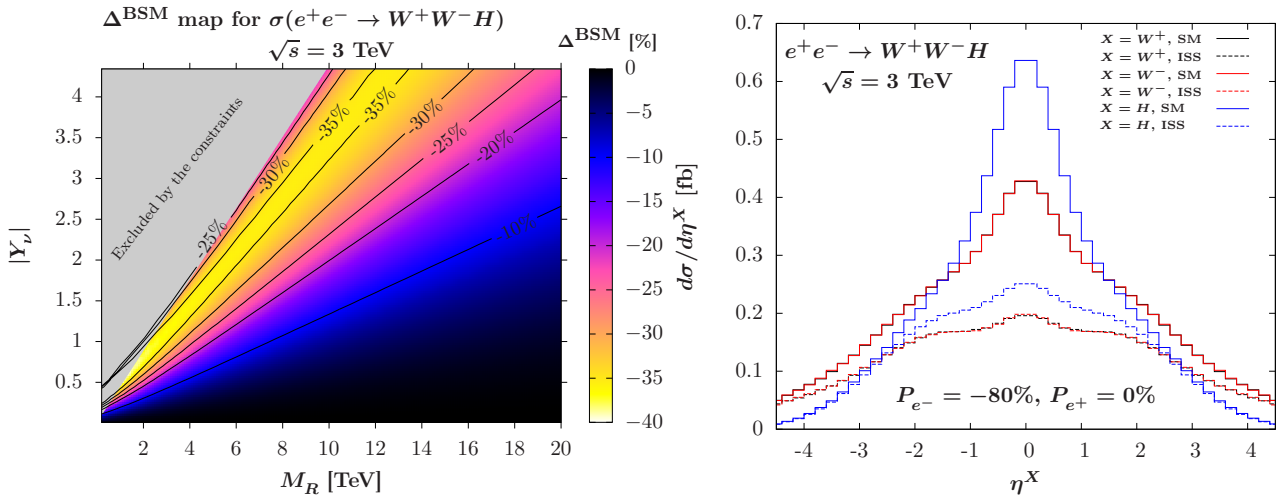

Fig. E.7: Left: Contour map of the neutrino corrections $\Delta^{\rm BSM}$ at the 3 TeV CLIC, using a -80% polarised electron beam, as a function of the seesaw scale M_R and $|Y_\nu|$. Right: Pseudo-rapidity distributions of the W^+ (black), W^- (red) and Higgs (blue) bosons. The solid curves stand for the SM predictions while the dashed curves stand for the ISS predictions, for the benchmark scenario described in the text. Figures taken from Ref. [33].

cross section $\sigma(e^+e^- \to W^+W^-H)$ at lepton colliders. The setup is the same as in Refs. [32] albeit with an updated global fit using NuFIT 3.0 [37] to explain neutrino oscillations. The representative diagrams in the Feynman-'t Hooft gauge are displayed in Fig. E.6 with the contributions of the heavy neutral leptons in the t–channel.

The deviation $\Delta^{\rm BSM}$ stands now for the comparison between the total cross section $\sigma(e^+e^- \to W^+W^-H)$ calculated in the ISS model and in the SM, $\Delta^{\rm BSM} = (\sigma^{\rm ISS} - \sigma^{\rm SM})/\sigma^{\rm SM}$. Using the CLIC baseline for the polarisation of the beams [2] with an unpolarised positron beam, $P_{e^+} = 0$, and a polarised electron beam, $P_{e^-} = -80\%$, the contour map at 3 TeV in the same $M_R - |Y_\nu|$ plane is presented in the left-hand side of Fig. E.7. Again the grey area is excluded by the constraints that mostly originate from the global fit [34]. The process $e^+e^- \to W^+W^-H$ exhibits sizeable negative deviations, of at least -20%. Note that the full results can be approximated within 1% for $M_R > 3$ TeV by the simple formulae presented in Ref. [33]. Compared to the left-hand side of Fig. E.5 the coverage of the parameter space is here much larger. Optimised cuts can also be chosen to enhance the deviation, such as the cuts $|\eta_{H/W^\pm}| < 1$ and $E_H > 1$ TeV (see the right-hand side of Fig. E.7 for the η distributions) that push the corrections down to -66% while keeping an ISS cross section at a reasonable level: 0.14 fb, to be compared to 1.23 fb before cuts. This has been studied for a benchmark

scenario with $|Y_\nu| = 1$ and heavy neutrinos in the range 2.4-8.6 TeV. The results means that this observable has a great potential that needs to be checked in a detailed sensitivity analysis. In the context of the FCC-ee, a similar observable could be chosen to test the effects of heavy neutral leptons in the same mass range, albeit at the one-loop level, namely the production cross section $\sigma(e^+e^- \to ZH)$.

1.3 Conclusions

This contribution has presented the current status of the triple Higgs coupling measurements at the LHC and the prospects for future lepton colliders. As combined studies in an EFT framework using precision measurements in single Higgs observables, as well as direct Higgs pair production, have shown, lepton colliders are able to completely remove the degeneracy in the measurement of the triple Higgs coupling beyond the 4σ level, and the combination of data collected at a centre-of-mass energy of 250 GeV with data collected at energies of at least 350 GeV is of crucial importance with very high precision measurements in single Higgs physics. Opportunities offered by the Higgs sector to test neutrino mass models at future lepton colliders have also been presented. The FCC-ee is very competitive to test the heavy-sterile-neutrino option in the GeV regime. As far as the TeV regime for the heavy-neutrino scale is concerned, studies in the literature have shown that the CLIC and ILC at high energies could offer new avenues in the Higgs sector via precision measurements of the triple Higgs coupling as well as of the production cross section of a pair of W bosons in association with a Higgs boson. In the same spirit the FCC-ee may well offer new opportunities in the same mass-regime via precision calculations at one- and two-loops for the ZH production cross section, that remain to be studied.

References

[1] H. Baer, T. Barklow, K. Fujii, Y. Gao, A. Hoang, S. Kanemura, J. List, H. E. Logan, A. Nomerotski, M. Perelstein, et al., The International Linear Collider Technical Design Report - Volume 2: PhysicsarXiv:1306.6352.

[2] M. J. Boland, et al., Updated baseline for a staged Compact Linear ColliderarXiv:1608.07537, doi:10.5170/CERN-2016-004.

[3] C. F. Dürig, Measuring the Higgs Self-coupling at the International Linear Collider, Ph.D. thesis, Hamburg U., Hamburg (2016).
URL http://bib-pubdb1.desy.de/search?cc=Publication+Database&of=hd&p=reportnumber:DESY-THESIS-2016-027

[4] T. Barklow, K. Fujii, S. Jung, M. E. Peskin, J. Tian, Model-Independent Determination of the Triple Higgs Coupling at e+e- Colliders, Phys. Rev. D97 (5) (2018) 053004. arXiv:1708.09079, doi:10.1103/PhysRevD.97.053004.

[5] H. Abramowicz, et al., Higgs physics at the CLIC electron-positron linear collider, Eur. Phys. J. C77 (7) (2017) 475. arXiv:1608.07538, doi:10.1140/epjc/s10052-017-4968-5.

[6] M. Dong, G. Li, CEPC Conceptual Design Report: Volume 2 - Physics & DetectorarXiv:1811.10545.

[7] A. Abada, et al., Future Circular Collider: Vol. 1 “Physics opportunities”, http://inspirehep.net/record/1713706/files/CERN-ACC-2018-0056.pdf.

[8] M. Benedikt, A. Blondel, O. Brunner, M. Capeans Garrido, F. Cerutti, J. Gutleber, P. Janot, J. M. Jimenez, V. Mertens, A. Milanese, K. Oide, J. A. Osborne, T. Otto, Y. Papaphilippou, J. Poole, L. J. Tavian, F. Zimmermann, Future Circular Collider, Tech. Rep. CERN-ACC-2018-0057, CERN, Geneva, submitted for publication to Eur. Phys. J. ST. (Dec 2018).
URL http://cds.cern.ch/record/2651299

[9] A. Blondel, P. Janot, Future strategies for the discovery and the precise measurement of the Higgs self couplingarXiv:1809.10041.

[10] M. McCullough, An Indirect Model-Dependent Probe of the Higgs Self-Coupling, Phys. Rev. D90 (1) (2014) 015001, [Erratum: Phys. Rev.D92,no.3,039903(2015)]. arXiv:1312.3322, doi:10.1103/PhysRevD.90.015001,10.1103/PhysRevD.92.039903.

[11] G. Degrassi, M. Fedele, P. P. Giardino, Constraints on the trilinear Higgs self coupling from precision observables, JHEP 04 (2017) 155. arXiv:1702.01737, doi:10.1007/JHEP04(2017)155.

[12] S. Di Vita, C. Grojean, G. Panico, M. Riembau, T. Vantalon, A global view on the Higgs self-coupling, JHEP 09 (2017) 069. arXiv:1704.01953, doi:10.1007/JHEP09(2017)069.

[13] S. Di Vita, G. Durieux, C. Grojean, J. Gu, Z. Liu, G. Panico, M. Riembau, T. Vantalon, A global view on the Higgs self-coupling at lepton colliders, JHEP 02 (2018) 178. arXiv:1711.03978, doi:10.1007/JHEP02(2018)178.

[14] F. Maltoni, D. Pagani, X. Zhao, Constraining the Higgs self-couplings at e^+e^- colliders, JHEP 07 (2018) 087. arXiv:1802.07616, doi:10.1007/JHEP07(2018)087.

[15] J. de Blas, et al., Higgs Boson Studies at Future Particle CollidersarXiv:1905.03764.

[16] M. Cepeda, et al., Higgs Physics at the HL-LHC and HE-LHCarXiv:1902.00134.

[17] The ATLAS collaboration, Combination of searches for Higgs boson pairs in *pp* collisions at 13 TeV with the ATLAS experiment, ATLAS-CONF-2018-043.

[18] Y. Fukuda, et al., Evidence for oscillation of atmospheric neutrinos, Phys. Rev. Lett. 81 (1998) 1562–1567. arXiv:hep-ex/9807003, doi:10.1103/PhysRevLett.81.1562.

[19] I. Esteban, M. C. Gonzalez-Garcia, A. Hernandez-Cabezudo, M. Maltoni, T. Schwetz, Global analysis of three-flavour neutrino oscillations: synergies and tensions in the determination of θ_{23}, δ_{CP}, and the mass ordering, JHEP 01 (2019) 106. arXiv:1811.05487, doi:10.1007/JHEP01(2019)106.

[20] R. N. Mohapatra, Mechanism for Understanding Small Neutrino Mass in Superstring Theories, Phys. Rev. Lett. 56 (1986) 561–563. doi:10.1103/PhysRevLett.56.561.

[21] R. N. Mohapatra, J. W. F. Valle, Neutrino Mass and Baryon Number Nonconservation in Superstring Models, Phys. Rev. D34 (1986) 1642, [,235(1986)]. doi:10.1103/PhysRevD.34.1642.

[22] J. Bernabeu, A. Santamaria, J. Vidal, A. Mendez, J. W. F. Valle, Lepton Flavor Nonconservation at High-Energies in a Superstring Inspired Standard Model, Phys. Lett. B187 (1987) 303–308. doi:10.1016/0370-2693(87)91100-2.

[23] J. Kersten, A. Yu. Smirnov, Right-Handed Neutrinos at CERN LHC and the Mechanism of Neutrino Mass Generation, Phys. Rev. D76 (2007) 073005. arXiv:0705.3221, doi:10.1103/PhysRevD.76.073005.

[24] K. Moffat, S. Pascoli, C. Weiland, Equivalence between massless neutrinos and lepton number conservation in fermionic singlet extensions of the Standard ModelarXiv:1712.07611.

[25] S. Antusch, O. Fischer, Testing sterile neutrino extensions of the Standard Model at future lepton colliders, JHEP 05 (2015) 053. arXiv:1502.05915, doi:10.1007/JHEP05(2015)053.

[26] M. Ruan, Higgs Measurement at e^+e^- Circular Colliders, Nucl. Part. Phys. Proc. 273-275 (2016) 857–862. arXiv:1411.5606, doi:10.1016/j.nuclphysbps.2015.09.132.

[27] M. Pandurović, Physics Potential for the Measurement of $\sigma(HZ) \times BR(H \to WW^*)$ at the 250 GeV ILC, in: International Workshop on Future Linear Colliders (LCWS 2018) Arlington, Texas, USA, October 22-26, 2018, 2019. arXiv:1902.08032.

[28] A. Pilaftsis, Lepton flavor nonconservation in H0 decays, Phys. Lett. B285 (1992) 68–74. doi:10.1016/0370-2693(92)91301-O.

[29] E. Arganda, M. J. Herrero, X. Marcano, C. Weiland, Imprints of massive inverse seesaw model neutrinos in lepton flavor violating Higgs boson decays, Phys. Rev. D91 (1) (2015) 015001. arXiv:1405.4300, doi:10.1103/PhysRevD.91.015001.

[30] E. Arganda, M. J. Herrero, X. Marcano, C. Weiland, Enhancement of the lepton flavor violating Higgs boson decay rates from SUSY loops in the inverse seesaw model, Phys. Rev. D93 (5) (2016) 055010. arXiv:1508.04623, doi:10.1103/PhysRevD.93.055010.

[31] J. Baglio, C. Weiland, Heavy neutrino impact on the triple Higgs coupling, Phys. Rev. D94 (1) (2016) 013002. arXiv:1603.00879, doi:10.1103/PhysRevD.94.013002.

[32] J. Baglio, C. Weiland, The triple Higgs coupling: A new probe of low-scale seesaw models, JHEP 04 (2017) 038. arXiv:1612.06403, doi:10.1007/JHEP04(2017)038.

[33] J. Baglio, S. Pascoli, C. Weiland, W^+W^-H production at lepton colliders: a new hope for heavy neutral leptons, Eur. Phys. J. C78 (10) (2018) 795. arXiv:1712.07621, doi:10.1140/epjc/s10052-018-6279-x.

[34] E. Fernandez-Martinez, J. Hernandez-Garcia, J. Lopez-Pavon, Global constraints on heavy neutrino mixing, JHEP 08 (2016) 033. arXiv:1605.08774, doi:10.1007/JHEP08(2016)033.

[35] K. Fujii, et al., Physics Case for the International Linear Collider, arXiv:1506.05992.

[36] H.-J. He, J. Ren, W. Yao, Probing new physics of cubic Higgs boson interaction via Higgs pair production at hadron colliders, Phys. Rev. D93 (1) (2016) 015003. arXiv:1506.03302, doi:10.1103/PhysRevD.93.015003.

[37] I. Esteban, M. C. Gonzalez-Garcia, M. Maltoni, I. Martinez-Soler, T. Schwetz, Updated fit to three neutrino mixing: exploring the accelerator-reactor complementarity, JHEP 01 (2017) 087. arXiv:1611.01514, doi:10.1007/JHEP01(2017)087.

2 Exotic Higgs decays (and Long-Lived Particles) at future colliders

Author: José Francisco Zurita [jose.zurita@kit.edu]

2.1 Exotic Higgs decays: motivations and signatures

The theoretical motivations and the large breadth of signatures for Exotic Higgs decays have been thoroughly reviewed in [1]. They were first consider as a discovery mode of new Physics in the context of Hidden Valley scenario [2–4]. In the last few years Exotic Higgs decays have been revisited, as they arise ubiquitiously in models of Neutral Naturalness, such as Twin Higgs [5], Folded Supersymmetry [6], Fraternal Twin Higgs [7], Hyperbolic Higgs [8] and Singlet Scalar Top Partners [9].

A simple proxy model for Hidden Valleys is obtained via a Higgs portal setup,

$$\mathcal{L} \supset \frac{1}{2}\Big(\partial_\mu \phi\Big)^2 - \frac{1}{2}M^2\phi^2 - A|H|^2\phi - \frac{1}{2}\kappa|H|^2\phi^2 - \frac{1}{6}\mu\phi^3 - \frac{1}{24}\phi^4 - \frac{1}{2}\lambda_H|H|^4\,. \tag{2.2}$$

The fields H and ϕ mix, depending on κ and A, giving rise to physical states $h(125)$ and $X(m_X)$. Note that the phenomenology is fully encapsulated by three free parameters: $m_X, c\tau(X) \equiv c\tau$ and $Br(h \to XX)$. We will assume that the $h \to XX$ is always kinematically open. Existing constraints on the $h(125)$ properties imply that currently the room for an exotic Higgs branching ratio, $Br(h \to XX)$ is below about 10 %. Since the mixing controls the X decay widths, a small mixing naturally gives rise to particles that travel a macroscopic distance $c\tau \gtrsim$ mm before decaying. Exotic Higgs decays are then encompassed within the larger class of "Long-Lived Particles" (LLP) signatures. For concreteness we review LLPs in the next subsection.

It is worth stressing that the HL-LHC will produce about 10^8 Higgs bosons, while the CEPC and FCC-ee (240) will only give about 10^6. Hence there is a trade-off between the clean environment provided by the collider and the corresponding production cross section. This already tell us that future electron-positron colliders might probe exotic Higgs Branching fractions down to 10^{-5}, while at the HL-LHC one could in principle go down to 10^{-6} or even 10^{-7}, depending on the visibility of the target final state.

2.2 Long-Lived Particles (LLPs)

Long-Lived Particles are Beyond Standard Model States with macroscopic lifetimes ($\gtrsim$ ns). These are theoretically well motivated in extensions of the SM trying to solve the fundamental problems of the SM, such as dark matter, neutrino masses). A comprehensive overview of the theoretical motivations for LLPs can be found in Ref. [10] while a signature driven document was put forward by the LLP@LHC Community in Ref [11].

In a nutshell, to obtain a macroscopic lifetime (or a very narrow width) one is lead to one of three choices: a large mass hierarchy (e.g: muon decay), a compressed spectra (e.g: neutron lifetime) and feeble interactions. The latter is the one that concerns Exotic Higgs decays.

In the last few years there have been several proposed detectors targeting neutral LLPs, such as MATHUSLA [12], FASER [13], CODEX-b [14] and AL3X [15]. Exotic Higgs decays constitutes a major theoretical motivation in the design of such experiments, that can probe the difficult phase-space regions where the standard triggers and object reconstruction became inefficient. These shortcomings will be detailed in the next subsection.

2.3 Exotic Higgs decays vis-à-vis current LHC data

Since in the simplest scenarios the X particle decays like a SM Higgs boson of m_X, what occurs is that the predominant decays are into $b\bar{b}$ pairs, if the channel is open. In that case the existing programme of LHC searches for displaced hadronic vertexes (see e.g [16–18]) can cover part of the parameter space. We display the current coverage in the $c\tau - m_X$ plane in Fig E.8. We

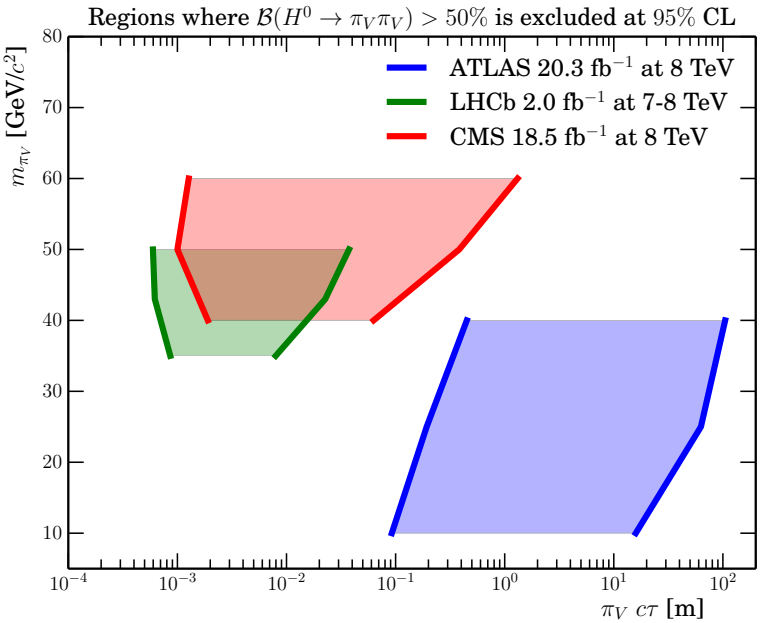

Fig. E.8: Reach of the ATLAS [16], CMS [17] and LHCb [18] studies for $X \to jj$, where X is taken to be a dark pion π_V of the Hidden Valley scenario. This model is in one-to-one correspondence with the one described in Section 2.1. The shaded regions show where $Br(H \to XX) > 50\%$ is excluded. Note that the area to the lower left can not be probed by current searches. Plot taken from the supplementary material of Ref. [18].

immediately see that the current LHC data is not able to cover the region of short lifetimes ($c\tau \lesssim 10$ cm) and low masses ($m_X < 35$ GeV). Low masses for X imply lower boosts, so the soft jets of the event will not pass the typical H_T or $p_T(j)$ trigger thresholds used by ATLAS and CMS [‡]. As a sample the reported trigger efficiency of CMS for $m_X = 50$ GeV and $c\tau = 30$ mm is about 2 %. The other limitation correspond to low lifetimes, which is limited by the vertex resolution. Hence the shortcomings of pp machines can be targeted, instead, with a collider providing better angular resolution, lower p_T thresholds and more accurate vertexing, which happens at both e^-p and e^+e^- machines. We stress that additional data will not alter these picture, and the low $c\tau$ and low m_X region would continue to be extremely hard to probe.

2.4 Future experiments: HL-LHC, FCC, CEPC, LHeC

Proton-proton colliders

We show in Fig E.9 (taken from [19] the expected reach at the HL-LHC ($\sqrt{s} = 14$TeV and total integrated luminosity of 3 ab^{-1}) and at the FCC-hh ($\sqrt{s} = 100$TeV and total integrated luminosity of 3 ab^{-1}) for an scalar mass of $m_X = 30$ GeV. The curves indicate different choices

[‡]It is worth noting that LHCb has the capability to trigger directly on displaced vertexes.

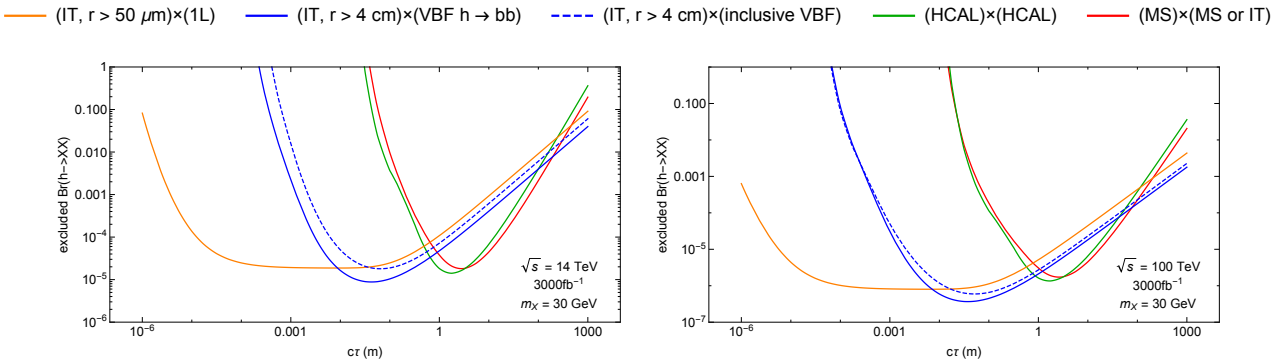

Fig. E.9: Sensitivities of the displaced searches for exotic Higgs decays at the HL-LHC (left) and FCC-hh (right), in the $c\tau - Br(h \to XX)$ plane, for $m_X = 30$ GeV. The curves correspond to the use of different triggers and different assumptions about the reconstruction of the displaced vertexes. Plot taken from Ref [19].

of triggers and of reconstruction capabilities of the displaced vertex. In particular, the orange curve corresponds to one displaced vertex in the Inner Tracker with an impact parameter of 50μm, which poses an interesting experimental challenge and thus should be regarded as an optimistic case. The blue curve corresponds to the realistic case of using VBF, $h \to b\bar{b}$ triggers down to an impact parameter of 4 cm.

We see that one can cover lifetimes as short as a millimeter (or even one micron for the optimistic scenario), while the probed exotic branching ratios can reach down to 10^{-5} (10^{-6}) for the HL-LHC (FCC-hh), for the benchmark case of $m_X = 30$ GeV. As discussed before, lower masses would suffer from a poor trigger efficiency, which opens a window of opportunity for both electron-proton and electron-positron colliders.

Electron-proton colliders

The reach on Exotic Higgs decays for future electron proton collider is displayed in Fig E.10. We see that the electron-proton colliders, due to their better resolution can test masses down to 5 GeV for exotic branching fractions of about 10^{-4}. This mass range is almost impossible to probe at the LHC, because of the overwhelming multi-jet background. We also note that electron-proton colliders provide a smaller luminosity [§]. Hence electron-proton colliders provide a window of opportunity to overcome the gaps in coverage discussed for the proton-proton colliders.

Electron-positron colliders

Finally, we take a look into the $e^+ - e^-$ case. A detailed analysis was carried out in Ref [23], and here we briefly summarize the most salient points. This study considers the Higgs-strahlung process $e^+e^- \to hZ$ with leptonic decays of the Z-boson for both the FCC-ee [24] and the CEPC [25, 26]. A set of basic selection cuts allows to achieve a zero-background regime for the

[§]During a 25 year run period of the Future Circular Collider (FCC), the proton-proton incarnation (FCC-hh) is expected to collect 15-30 ab^{-1}1 while the electron-proton version will collect only 1 ab^{-1} [20].

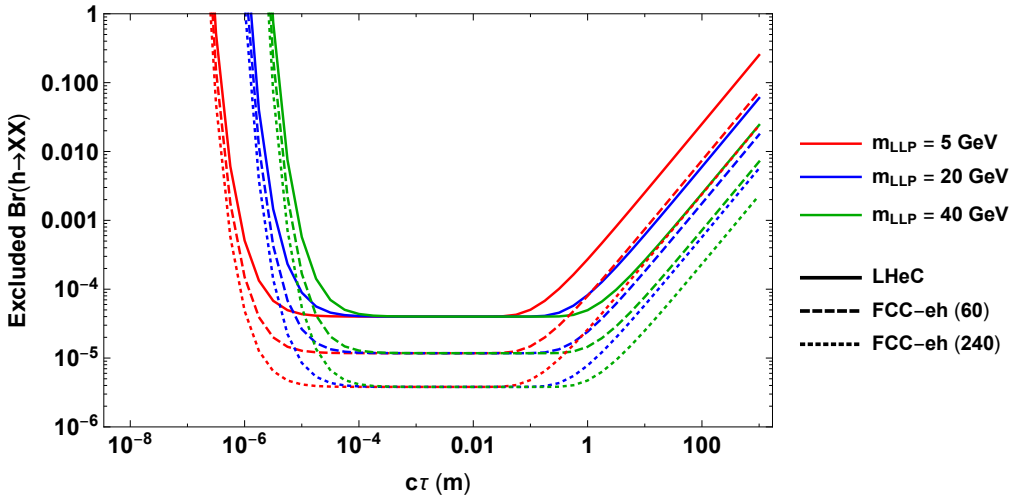

Fig. E.10: Reach of the future electron-proton colliders: LHeC (solid), FCC-eh (60) and FCC-eh (240). The LHeC would collider a 7 TeV proton from the LHC against a 50 GeV electron beam, while for the FCC-eh we a 50 TeV proton beam will collide against a 60 GeV (design case) and 240 GeV beam (optimistic scenario). Taken from Refs. [21, 22].

irreducible SM processes [¶]. Two different strategies are pursued: the large mass and the long-lifetime regime. The main difference between the two is on the requirements on the minimal distance between the displaced vertexes. The results are shown in Fig E.11.

One immediately sees that the e^+e^- colliders can test exotic branching fractions down to 5×10^{-5}. Moreover, they can go low in mass down to a few GeV, and they can also probe decay lengths down a μm, where the proton-proton colliders would be ineffective.

2.5 Conclusions

In this contribution I have summarized the existing studies on exotic Higgs decays at current and future collliders. While the proton-proton machines would in principle be the best option due to their larger energies and luminosities, we have also seen that the phase space regions where the LHC and FCC-hh lose steam, namely, low X masses and low lifetimes provide a unique window of opportunity for both e^-p and e^+e^- colliders. The latter two kind of machines have been only recently studied, and thus there is naturally a lot of room for improvement. We also stress that these kind of studies can help to optimize the detector design of future colliders.

[¶]Backgrounds from particles originating away from the interaction point (e.g: beam halo, cosmic muons, cavern radiation) are not considered.

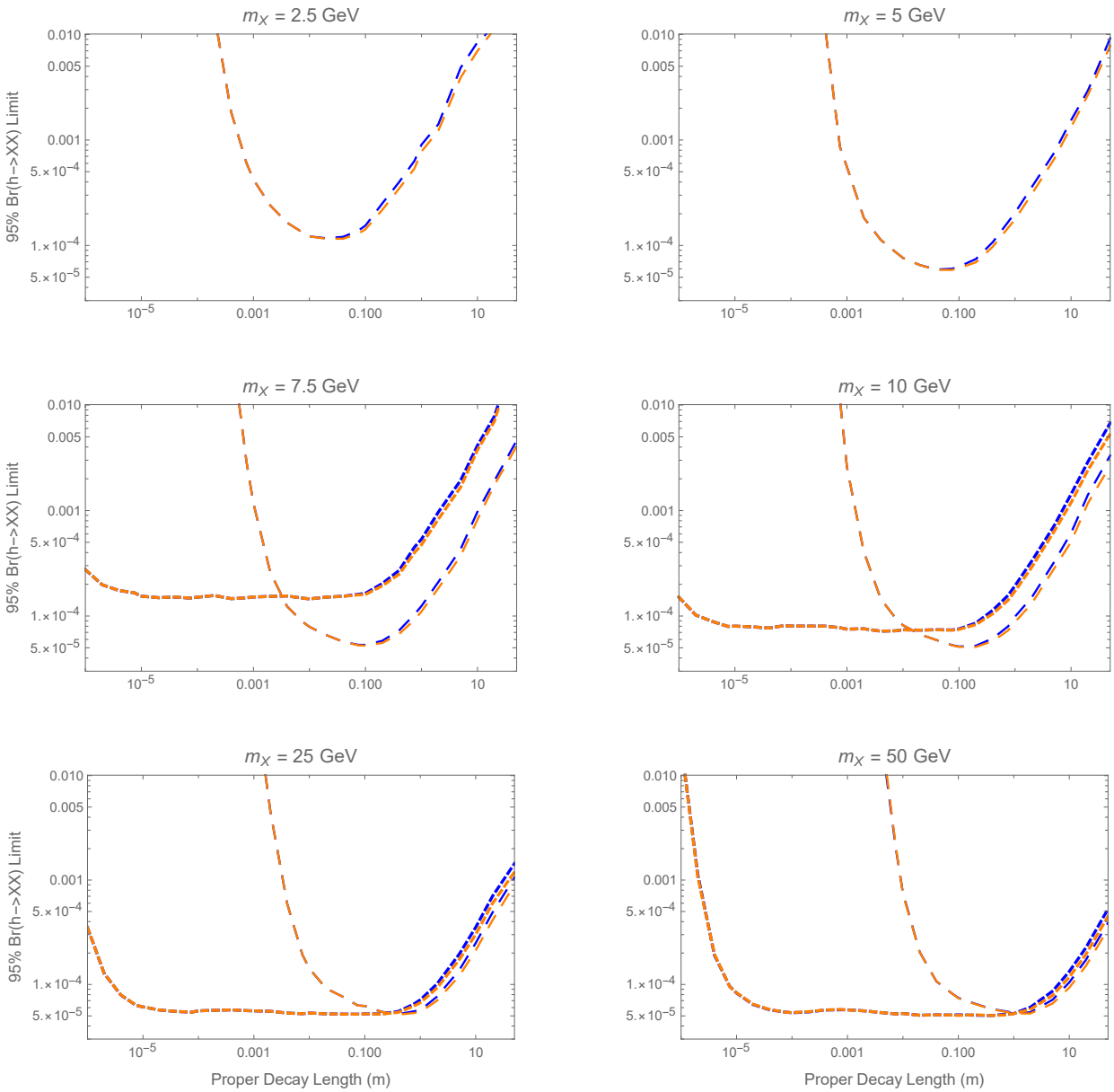

Fig. E.11: FCC-ee (blue) and CEPC (orange) limits on the exotic branching ratio $h \to XX$ at the 95 % C. L. The 'long-lifetime' analysis is shown with larger dashes, while smaller dashes correspond to the 'large mass' study. Taken from Ref [23].

References

[1] D. Curtin, et al., Exotic decays of the 125 GeV Higgs boson, Phys. Rev. D90 (7) (2014) 075004. arXiv:1312.4992, doi:10.1103/PhysRevD.90.075004.

[2] M. J. Strassler, K. M. Zurek, Echoes of a hidden valley at hadron colliders, Phys. Lett. B651 (2007) 374–379. arXiv:hep-ph/0604261, doi:10.1016/j.physletb.2007.06.055.

[3] M. J. Strassler, K. M. Zurek, Discovering the Higgs through highly-displaced vertices, Phys. Lett. B661 (2008) 263–267. arXiv:hep-ph/0605193, doi:10.1016/j.physletb.2008.02.008.

[4] M. J. Strassler, Possible effects of a hidden valley on supersymmetric phenomenologyarXiv:hep-ph/0607160.

[5] Z. Chacko, H.-S. Goh, R. Harnik, The Twin Higgs: Natural electroweak breaking from mirror symmetry, Phys. Rev. Lett. 96 (2006) 231802. arXiv:hep-ph/0506256, doi:10.1103/PhysRevLett.96.231802.

[6] G. Burdman, Z. Chacko, H.-S. Goh, R. Harnik, Folded supersymmetry and the LEP paradox, JHEP 02 (2007) 009. arXiv:hep-ph/0609152, doi:10.1088/1126-6708/2007/02/009.

[7] N. Craig, A. Katz, M. Strassler, R. Sundrum, Naturalness in the Dark at the LHC, JHEP 07 (2015) 105. arXiv:1501.05310, doi:10.1007/JHEP07(2015)105.

[8] T. Cohen, N. Craig, G. F. Giudice, M. Mccullough, The Hyperbolic Higgs, JHEP 05 (2018) 091. arXiv:1803.03647, doi:10.1007/JHEP05(2018)091.

[9] H.-C. Cheng, L. Li, E. Salvioni, C. B. Verhaaren, Singlet Scalar Top Partners from Accidental Supersymmetry, JHEP 05 (2018) 057. arXiv:1803.03651, doi:10.1007/JHEP05(2018)057.

[10] D. Curtin, et al., Long-Lived Particles at the Energy Frontier: The MATHUSLA Physics CasearXiv:1806.07396.

[11] J. Alimena, et al., Searching for long-lived particles beyond the Standard Model at the Large Hadron ColliderarXiv:1903.04497.

[12] J. P. Chou, D. Curtin, H. J. Lubatti, New Detectors to Explore the Lifetime Frontier, Phys. Lett. B767 (2017) 29–36. arXiv:1606.06298, doi:10.1016/j.physletb.2017.01.043.

[13] J. L. Feng, I. Galon, F. Kling, S. Trojanowski, ForwArd Search ExpeRiment at the LHC, Phys. Rev. D97 (3) (2018) 035001. arXiv:1708.09389, doi:10.1103/PhysRevD.97.035001.

[14] V. V. Gligorov, S. Knapen, M. Papucci, D. J. Robinson, Searching for Long-lived Particles: A Compact Detector for Exotics at LHCb, Phys. Rev. D97 (1) (2018) 015023. arXiv:1708.09395, doi:10.1103/PhysRevD.97.015023.

[15] V. V. Gligorov, S. Knapen, B. Nachman, M. Papucci, D. J. Robinson, Leveraging the ALICE/L3 cavern for long-lived particle searches, Phys. Rev. D99 (1) (2019) 015023. arXiv:1810.03636, doi:10.1103/PhysRevD.99.015023.

[16] G. Aad, et al., Search for massive, long-lived particles using multitrack displaced vertices or displaced lepton pairs in pp collisions at $\sqrt{s} = 8$ TeV with the ATLAS detector, Phys. Rev. D92 (7) (2015) 072004. arXiv:1504.05162, doi:10.1103/PhysRevD.92.072004.

[17] V. Khachatryan, et al., Search for Long-Lived Neutral Particles Decaying to Quark-Antiquark Pairs in Proton-Proton Collisions at $\sqrt{s} = 8$ TeV, Phys. Rev. D91 (1) (2015) 012007. arXiv:1411.6530, doi:10.1103/PhysRevD.91.012007.

[18] R. Aaij, et al., Updated search for long-lived particles decaying to jet pairs, Eur. Phys. J. C77 (12) (2017) 812. arXiv:1705.07332, doi:10.1140/epjc/s10052-017-5178-x.

[19] D. Curtin, C. B. Verhaaren, Discovering Uncolored Naturalness in Exotic Higgs Decays, JHEP 12 (2015) 072. arXiv:1506.06141, doi:10.1007/JHEP12(2015)072.

[20] M. Mangano, P. Azzi, M. Benedikt, A. Blondel, D. A. Britzger, A. Dainese, M. Dam, J. de Blas, D. d'Enterria, O. Fischer, C. Grojean, J. Gutleber, C. Gwenlan, C. Helsens, P. Janot, M. Klein, U. Klein, M. P. Mccullough, S. Monteil, J. Poole, M. Ramsey-Musolf, C. Schwanenberger, M. Selvaggi, F. Zimmermann, T. You, Future Circular Collider, Tech. Rep. CERN-ACC-2018-0056, CERN, Geneva, submitted for publication to Eur. Phys. J. C. (Dec 2018).
URL https://cds.cern.ch/record/2651294

[21] D. Curtin, K. Deshpande, O. Fischer, J. Zurita, New Physics Opportunities for Long-Lived Particles at Electron-Proton Colliders, JHEP 07 (2018) 024. arXiv:1712.07135, doi:10.1007/JHEP07(2018)024.

[22] D. Curtin, K. Deshpande, O. Fischer, J. Zurita, Probing BSM physics with electron-proton colliders, PoS DIS2018 (2018) 090. arXiv:1805.12533, doi:10.22323/1.316.0090.

[23] S. Alipour-Fard, N. Craig, M. Jiang, S. Koren, Long Live the Higgs Factory: Higgs Decays to Long-Lived Particles at Future Lepton CollidersarXiv:1812.05588.

[24] M. Bicer, et al., First Look at the Physics Case of TLEP, JHEP 01 (2014) 164. arXiv:1308.6176, doi:10.1007/JHEP01(2014)164.

[25] M. Dong, G. Li, CEPC Conceptual Design Report: Volume 2 - Physics & DetectorarXiv:1811.10545.

[26] CEPC Conceptual Design Report: Volume 1 - AcceleratorarXiv:1809.00285.

3 Precision Predictions for Higgs decays in the (N)MSSM

Authors: Florian Domingo, Sven Heinemeyer, Sebastian Paßehr, Georg Weiglein
Corresponding Author: Sven Heinemeyer [Sven.Heinemeyer@cern.ch]

3.1 Introduction

The signal that was discovered in the Higgs searches at ATLAS and CMS at a mass of $\sim$ 125 GeV [1–3] is, within the current theoretical and experimental uncertainties, compatible with the properties of the Higgs boson predicted within Standard-Model (SM) of particle physics. No conclusive signs of physics beyond the SM have been reported so far. However, the measurements of Higgs signal strengths for the various channels leave considerable room for Beyond Standard Model (BSM) interpretations. Consequently, the investigation of the precise properties of the discovered Higgs boson will be one of the prime goals at the LHC and beyond. While the mass of the observed particle is already known with excellent accuracy [4, 5], significant improvements of the information about the couplings of the observed state are expected from the upcoming runs of the LHC [3,6–9] and even more so from the high-precision measurements at a future e^+e^- collider [10–18]. For the accurate study of the properties of the Higgs boson, precise predictions for the various partial decay widths, the branching ratios (BRs) and the Higgs-boson production cross sections along with their theoretical uncertainties are indispensable.

Motivated by the "Hierarchy Problem", Supersymmetry (SUSY)-inspired extensions of the SM play a prominent role in the investigations of possible new physics. As such, the Minimal Supersymmetric Standard Model (MSSM) [19, 20] or its singlet extension, the Next-to-MSSM (NMSSM) [21, 22], have been the object of many studies in the last decades. Despite this attention, these models are not yet prepared for an era of precision tests as the uncertainties at the level of the Higgs-mass calculation [23–25] are about one order of magnitude larger than the experimental uncertainty. At the level of the decays, the theoretical uncertainty arising from unknown higher-order corrections has been estimated for the case of the Higgs boson of the SM (where the Higgs mass is treated as a free input parameter) in Refs. [26, 27] and updated in Ref. [28]: depending on the channel and the Higgs mass, it typically falls in the range of $\sim$ 0.5–5%. To our knowledge, no similar analysis has been performed in SUSY-inspired models (or other BSM models), but one can expect the uncertainties from missing higher-order corrections to be larger in general—with many nuances depending on the characteristics of the Higgs state and the considered point in parameter space: we provide some discussion of this issue at the end of this paper. In addition, parametric uncertainties that are induced by the experimental errors of the input parameters should be taken into account as well. For the case of the SM decays those parametric uncertainties have been discussed in the references above. In the SUSY case the parametric uncertainties induced by the (known) SM input parameters can be determined in the same way as for the SM, while the dependence on unknown SUSY parameters can be utilised for setting constraints on those parameters. While still competitive today, the level of accuracy of the theoretical predictions of Higgs-boson decays in SUSY models should soon become outclassed by the achieved experimental precision (in particular at future e^+e^- colliders) on the decays of the observed Higgs signal. Without comparable accuracy of the theoretical predictions, the impact of the exploitation of the precision data will be diminished—either in terms of further constraining the parameter space or of interpreting deviations from the SM results. Further efforts towards improving the theoretical accuracy are

therefore necessary in order to enable a thorough investigation of the phenomenology of these models. Besides the decays of the SM-like state at 125 GeV of a SUSY model—where the goal is clearly to reach an accuracy that is comparable to the case of the SM—it is also of interest to obtain reliable and accurate predictions for the decays of the other Higgs bosons in the spectrum. The decays of the non-SM-like Higgs bosons can be affected by large higher-order corrections as a consequence of either large enhancement factors or a suppression of the lowest-order contribution. Confronting accurate predictions with the available search limits yields important constraints on the parameter space. Here we review the evaluation of the decays of the neutral Higgs bosons of the $\mathbb{Z}_3$-conserving NMSSM into SM particles as presented in [29].

The current work focussing on NMSSM Higgs decays is part of the effort for developing a version of `FeynHiggs` [23, 30–37] dedicated to the NMSSM [38, 39]. The general methodology relies on a Feynman-diagrammatic calculation of radiative corrections, which employs `FeynArts` [40,41], `FormCalc` [42] and `LoopTools` [42]. The implementation of the renormalization scheme within the NMSSM [39] has been done in such a way that the result in the MSSM limit of the NMSSM exactly coincides with the MSSM result obtained from `FeynHiggs` without any further adjustments of parameters.

3.2 Higgs decays to SM particles in the $\mathcal{CP}$-violating NMSSM

In this section, we review the technical aspects of our calculation of the Higgs decays. Our notation and the renormalization scheme that we employ for the $\mathbb{Z}_3$-conserving NMSSM in the general case of complex parameters were presented in Sect. 2 of [39], and we refer the reader to this article for further details.

3.2.1 Decay amplitudes for a physical (on-shell) Higgs state – Generalities

3.2.1.1 On-shell external Higgs leg

In this article, we consider the decays of a physical Higgs state, i.e. an eigenstate of the inverse propagator matrix for the Higgs fields evaluated at the corresponding pole eigenvalue. The connection between such a physical state and the tree-level Higgs fields entering the Feynman diagrams is non-trivial in general since the higher-order contributions induce mixing among the Higgs states and between the Higgs states and the gauge bosons (as well as the associated Goldstone bosons). The LSZ reduction fully determines the (non-unitary) transition matrix $\mathbf{Z}^{\text{mix}}$ between the loop-corrected mass eigenstates and the lowest-order states. Then, the amplitude describing the decay of the physical state h_i^{phys} (we shall omit the superscript 'phys' later on), into e.g. a fermion pair $f\bar{f}$, relates to the amplitudes in terms of the tree-level states h_j^0 according to (see below for the mixing with gauge bosons and Goldstone bosons):

$$\mathcal{A}[h_i^{\text{phys}} \to f\bar{f}\,] = Z_{ij}^{\text{mix}}\, \mathcal{A}[h_j^0 \to f\bar{f}\,]\,. \tag{3.3}$$

Here, we characterize the physical Higgs states according to the procedure outlined in [39] (see also [32, 43, 44]):

- the Higgs self-energies include full one-loop and leading $\mathcal{O}(\alpha_t\alpha_s, \alpha_t^2)$ two-loop corrections (with two-loop effects obtained in the MSSM approximation via the publicly available code `FeynHiggs`[‖]);

[‖] The Higgs masses in `FeynHiggs` could be computed with additional improvements such as additional fixed-order results [45, 46] or the resummation of large logarithms for very heavy SUSY particles [33–35]. For simplicity we do not take such refinements into account in the present article.

- the pole masses correspond to the zeroes of the determinant of the inverse-propagator matrix;
- the (5×5) matrix $\mathbf{Z}^{\text{mix}}$ is obtained in terms of the solutions of the eigenvector equation for the effective mass matrix evaluated at the poles, and satisfying the appropriate normalization conditions (see Sect. 2.6 of [39]).

In correcting the external Higgs legs by the full matrix $\mathbf{Z}^{\text{mix}}$—instead of employing a simple diagrammatic expansion—we resum contributions to the transition amplitudes that are formally of higher loop order. This resummation is convenient for taking into account numerically relevant leading higher-order contributions. It can in fact be crucial for the frequent case where radiative corrections mix states that are almost mass-degenerate in order to properly describe the resonance-type effects that are induced by the mixing. On the other hand, care needs to be taken to avoid the occurrence of non-decoupling terms when Higgs states are well-separated in mass, since higher-order effects can spoil the order-by-order cancellations with vertex corrections.

We stress that all public tools, with the exception of `FeynHiggs`, neglect the full effect of the transition to the physical Higgs states encoded within $\mathbf{Z}^{\text{mix}}$, and instead employ the unitary approximation $\mathbf{U}^0$ neglecting external momenta (which is in accordance with leading-order or QCD-improved leading-order predictions). We refer the reader to [32, 39, 44] for the details of the definition of $\mathbf{U}^0$ or $\mathbf{U}^m$ (another unitary approximation) as well as a discussion of their impact at the level of Higgs decay widths.

3.2.1.2 Higgs–electroweak mixing

For the mass determination, we do not take into account contributions arising from the mixing of the Higgs fields with the neutral Goldstone or Z bosons since these corrections enter at the sub-dominant two-loop level (contributions of this kind can also be compensated by appropriate field-renormalization conditions [47]). We note that, in the $\mathcal{CP}$-conserving case, only external $\mathcal{CP}$-odd Higgs components are affected by such a mixing. Yet, at the level of the decay amplitudes, the Higgs mixing with the Goldstone and Z bosons enters already at the one-loop order (even if the corresponding self-energies are cancelled by an appropriate field-renormalization condition, this procedure would still provide a contribution to the $h_i f \bar{f}$ counterterm). Therefore, for a complete one-loop result of the decay amplitudes it is in general necessary to incorporate Higgs–Goldstone and Higgs–Z self-energy transition diagrams [43, 48, 49]. In the following, we evaluate such contributions to the decay amplitudes in the usual diagrammatic fashion (as prescribed by the LSZ reduction) with the help of the `FeynArts` modelfile for the $\mathcal{CP}$-violating NMSSM [39]. The corresponding one-loop amplitudes (including the associated counterterms) will be symbolically denoted as $\mathcal{A}^{1\text{L}}_{G/Z}$. These amplitudes can be written in terms of the self-energies $\Sigma_{h_i G/Z}$ with Higgs and Goldstone/Z bosons in the external legs. In turn, these self-energies are connected by a Slavnov–Taylor identity (see e.g. App. A of [50]):**

$$\begin{aligned} 0 = {} & M_Z\, \Sigma_{h_i G}\left(p^2\right) + \mathrm{i}\, p^2\, \Sigma_{h_i Z}\left(p^2\right) + M_Z \left(p^2 - m_{h_i}^2\right) f\left(p^2\right) \\ & - \frac{e}{2\, s_{\text{w}}\, c_{\text{w}}} \sum_j \left[(U_n)_{i1}(U_n)_{j4} - (U_n)_{i2}(U_n)_{j5} - (U_n)_{j1}(U_n)_{i4} + (U_n)_{j2}(U_n)_{i5}\right] T_{h_j}\,, \end{aligned} \tag{3.4a}$$

**We denote the imaginary unit by i.

$$f\left(p^2\right) \equiv -\frac{\alpha}{16\,\pi\,s_\mathrm{w}\,c_\mathrm{w}} \sum_j \left[(U_n)_{i1}(U_n)_{j4} - (U_n)_{i2}(U_n)_{j5} - (U_n)_{j1}(U_n)_{i4} + (U_n)_{j2}(U_n)_{i5}\right] \times \left[c_\beta\,(U_n)_{j1} + s_\beta\,(U_n)_{j2}\right] B_0\left(p^2, m_{h_j}^2, M_Z^2\right), \tag{3.4b}$$

where the T_{h_i} correspond to the tadpole terms of the Higgs potential, and $(U_n)_{ij}$ are the elements of the transition matrix between the gauge- and tree-level mass-eigenstate bases of the Higgs bosons—the notation is introduced in Sect. 2.1 of [39]. Similar relations in the MSSM are also provided in Eqs. (127) of [43]. We checked this identity at the numerical level.

3.2.1.3 Inclusion of one-loop contributions

The wave function normalization factors contained in $\mathbf{Z}^\mathrm{mix}$ together with the described treatment of the mixing with the Goldstone and Z bosons ensure the correct on-shell properties of the external Higgs leg in the decay amplitude, so that no further diagrams correcting this external leg are needed. Moreover, the SM fermions and gauge bosons are also treated as on-shell particles in our renormalization scheme. Beyond the transition to the loop-corrected states incorporated by $\mathbf{Z}^\mathrm{mix}$, we thus compute the decay amplitudes at the one-loop order as the sum of the tree-level contribution $\mathcal{A}^\mathrm{tree}$ (possibly equal to zero), the Higgs–electroweak one-loop mixing $\mathcal{A}^\mathrm{1L}_{G/Z}$ and the (renormalized) one-loop vertex corrections $\mathcal{A}^\mathrm{1L}_\mathrm{vert}$ (including counterterm contributions)—we note that each of these pieces of the full amplitude is separately ultraviolet-finite. In the example of the $f\bar{f}$ decay, the amplitudes with a tree-level external Higgs field h_j^0—on the right-hand side of (3.3)—thus symbolically read:

$$\mathcal{A}[h_j^0 \to f\bar{f}\,] = \mathcal{A}^\mathrm{tree}[h_j^0 \to f\bar{f}\,] + \mathcal{A}^\mathrm{1L}_{G/Z}[h_j^0 \to f\bar{f}\,] + \mathcal{A}^\mathrm{1L}_\mathrm{vert}[h_j^0 \to f\bar{f}\,]\,. \tag{3.5}$$

All the pieces on the right-hand side of this equation are computed with the help of `FeynArts` [40,41], `FormCalc` [42] and `LoopTools` [42], according to the prescriptions that are encoded in the modelfile for the $\mathcal{CP}$-violating NMSSM. However, we use a specific treatment for some of the contributions, such as QED and QCD one-loop corrections to Higgs decays into final state particles that are electrically and/or color charged, or include certain higher-order corrections. We describe these channel-specific modifications in the following subsections.

3.2.1.4 Goldstone-boson couplings

The cubic Higgs–Goldstone-boson vertices can be expressed as

$$\begin{aligned}\mathcal{L} \ni -\frac{1}{\sqrt{2}\,v}\Bigg\{ &\sum_j m_{h_j}^2 \left[\cos\beta\,(U_n)_{j1} + \sin\beta\,(U_n)_{j2}\right] h_j^0 \left[G^+G^- + \tfrac{1}{2}\left(G^0\right)^2\right] \\ &+ \left[\sum_j \left(m_{H^\pm}^2 - m_{h_j}^2\right)\left(\sin\beta\left[(U_n)_{j1} + \mathrm{i}\,(U_n)_{j4}\right] - \cos\beta\left[(U_n)_{j2} - \mathrm{i}\,(U_n)_{j5}\right]\right) h_j^0 H^+ G^- + \mathrm{h.\,c.}\right] \\ &+ \frac{1}{2}\sum_{j,\,k}\left(m_{h_k}^2 - m_{h_j}^2\right)\left[(U_n)_{j1}(U_n)_{k4} - (U_n)_{j2}(U_n)_{k5} - (j \leftrightarrow k)\right] h_j^0 h_k^0 G^0\Bigg\}\,. \end{aligned} \tag{3.6}$$

The doublet vacuum expectation value (vev), $v = M_W\,s_\mathrm{w}/\sqrt{2\,\pi\,\alpha}$, is expressed in terms of the gauge-boson masses M_W and M_Z $\left(s_\mathrm{w} = \sqrt{1 - M_W^2/M_Z^2}\right)$, as well as the electromagnetic coupling α. The symbol $m_{h_j}^2$, $(j = 1,\ldots,5)$, represents the tree-level mass squared of the neutral Higgs state h_j^0, and $m_{H^\pm}^2$ the mass squared of the charged Higgs state.

The use of the tree-level couplings of (3.6) together with a physical (loop-corrected) external Higgs leg $h_i = \sum_j Z_{ij}^{\text{mix}} h_j^0$ is potentially problematic regarding the gauge properties of the matrix elements. The structure of the gauge theory and its renormalization indeed guarantee that the gauge identities are observed at the order of the calculation (one loop). However, the evaluation of Feynman amplitudes is not protected against a violation of the gauge identities at the (incomplete) two-loop order. We detected such gauge-violating effects of two-loop order at several points in our calculation of the neutral-Higgs decays, e.g. :

- the Ward identity in $h_i \to \gamma\gamma$ is not satisfied (see also Ref. [51]);
- infrared (IR) divergences of the virtual corrections in $h_i \to W^+W^-$ do not cancel their counterparts in the bremsstrahlung process $h_i \to W^+W^-\gamma$ (see also Ref. [52]);
- computing $h_i \to f\bar{f}$ in an R_ξ gauge entails non-vanishing dependence of the amplitudes on the electroweak gauge-fixing parameters ξ_Z and ξ_W.

As these gauge-breaking effects could intervene with sizable and uncontrolled numerical impact, it is desirable to add two-loop order terms restoring the gauge identities at the level of the matrix elements. Technically, there are different possible procedures to achieve this: one would amount to replace the kinematic Higgs masses that appear in Higgs–gauge-boson couplings by tree-level Higgs masses; we prefer the alternative procedure consisting in changing the Higgs–Goldstone-boson couplings of (3.6): for the Higgs mass associated to the external Higgs leg the loop-corrected Higgs mass M_{h_i} is used instead of the tree-level one. This is actually the form of the Higgs–Goldstone-boson couplings that would be expected in an effective field theory of the physical Higgs boson h_i. Using the definition of Z_{ij}^{mix} as an eigenvector of the loop-corrected mass matrix for the eigenvalue $M_{h_i}^2$—see Sect. 2.6 of [39]—one can verify that the effective Higgs–Goldstone-boson vertices employing the physical Higgs mass differ from their tree-level counterparts by a term of one-loop order (proportional to the Higgs self-energies) so that the alteration of the one-loop amplitudes is indeed of two-loop order. Employing this shift of the Higgs–Goldstone couplings cures the gauge-related issues that we mentioned earlier.

Another issue with gauge invariance appears in connection with the amplitudes $\mathcal{A}_{G/Z}^{1\text{L}}$. The Goldstone and Z-boson propagators generate denominators with pole M_Z^2 (or $\xi_Z M_Z^2$ in an R_ξ gauge): in virtue of the Slavnov–Taylor identity of Eq. (3.4a) these terms should cancel one another in the total amplitude at the one-loop order—we refer the reader to Sect. 4.3 of [43] for a detailed discussion. However, the term $(p^2 - M_Z^2)^{-1}$ multiplying $f(p^2)$ of Eq. (3.4a) only vanishes if $p^2 = m_{h_i}^2$: if we employ $p^2 = M_{h_i}^2$ (the loop-corrected Higgs mass), the cancellation is spoilt by a term of two-loop order. In order to address this problem, we re-define $\mathcal{A}_{G/Z}^{1\text{L}}$ by adding a two-loop term:

$$\tilde{\mathcal{A}}_{G/Z}^{1\text{L}}[h_i \to f\bar{f}\,] \equiv Z_{ij}^{\text{mix}} \cdot \mathcal{A}_{G/Z}^{1\text{L}}[h_j^0 \to f\bar{f}\,] + \frac{\Gamma_{Gf\bar{f}}^{\text{tree}}}{M_{h_i}^2} \sum_{j,k} \hat{\Sigma}_{h_j h_k}\left(M_{h_i}^2\right) \cdot Z_{ik}^{\text{mix}} \frac{f\left(M_{h_i}^2\right) \xi_Z M_Z^2}{M_{h_i}^2 - \xi_Z M_Z^2}, \quad (3.7)$$

where $\Gamma_{Gf\bar{f}}^{\text{tree}}$ represents the tree-level vertex of the neutral Goldstone boson with the fermion f (in the particular example of a Higgs decay into $f\bar{f}$). Then, it is straightforward to check that $\tilde{\mathcal{A}}_{G/Z}^{1\text{L}}$ is gauge-invariant. The transformation of Eq. (3.7) can also be interpreted as a two-loop shift re-defining $\Sigma_{h_i Z}$, so that it satisfies a generalized Slavnov–Taylor identity of the form of Eq. (3.4a), but applying to a physical (loop-corrected) Higgs field, with the term $\left(p^2 - m_{h_i}^2\right) f(p^2)$ of Eq. (3.4a) replaced by $\left(p^2 - M_{h_i}^2\right) f(p^2)$.

3.2.1.5 Numerical input in the one-loop corrections

As usual, the numerical values of the input parameters need to reflect the adopted renormalization scheme, and the input parameters corresponding to different schemes differ from each other by shifts of the appropriate loop order (at the loop level there exists some freedom to use a numerical value of an input parameter that differs from the tree-level value by a one-loop shift, since the difference induced in this way is of higher order). Concerning the input values of the relevant light quark masses, we follow in our evaluation the choice of `FeynHiggs` and employ $\overline{\text{MS}}$ quark masses with three-loop QCD corrections evaluated at the scale of the mass of the decaying Higgs, $m_q^{\overline{\text{MS}}}(M_{h_i})$, in the loop functions and the definition of the Yukawa couplings. In addition, the input value for the pole top mass is converted to $m_t^{\overline{\text{MS}}}(m_t)$ using up to two-loop QCD and one-loop top Yukawa/electroweak corrections (corresponding to the higher-order corrections included in the Higgs-boson mass calculation). Furthermore, the $\tan\beta$-enhanced contributions are always included in the defining relation between the bottom Yukawa coupling and the bottom mass (and similarly for all other down-type quarks). Concerning the Higgs vev appearing in the relation between the Yukawa couplings and the fermion masses, we parametrize it in terms of $\alpha(M_Z)$. Finally, the strong coupling constant employed in SUSY-QCD diagrams is set to the scale of the supersymmetric particles entering the loop. We will comment on deviations from these settings if needed.[††]

3.2.2 Higgs decays into SM fermions

Our calculation of the Higgs decay amplitudes into SM fermions closely follows the procedure outlined in the previous subsection. However, we include the QCD and QED corrections separately, making use of analytical formulae that are well-documented in the literature [54, 55]. We also employ an effective description of the Higgs–$b\bar{b}$ interactions in order to resum potentially large effects for large values of $\tan\beta$. Below, we comment on these two issues and discuss further the derivation of the decay widths for this class of channels.

3.2.2.1 Tree-level amplitude

At the tree level, the decay $h_j^0 \to f\bar{f}$ is determined by the Yukawa coupling Y_f and the decomposition of the tree-level state h_j^0 in terms of the Higgs-doublet components:

$$\begin{aligned}\mathcal{A}^{\text{tree}}[h_j^0 \to f\bar{f}\,] = &-\mathrm{i}\,\frac{Y_f}{\sqrt{2}}\,\bar{u}_f(p_f)\Big\{\delta_{f,\,d_k/e_k}(U_n)_{j1} + \delta_{f,\,u_k}(U_n)_{j2} \\ &\qquad - \mathrm{i}\,\gamma_5\left[\delta_{f,\,d_k/e_k}(U_n)_{j4} + \delta_{f,\,u_k}(U_n)_{j5}\right]\Big\}\,v_f\Big(p_{\bar{f}}\Big) \\ \equiv &-\mathrm{i}\,\bar{u}_f(p_f)\left\{g^S_{h_j ff} - \gamma_5\,g^P_{h_j ff}\right\}v_f\Big(p_{\bar{f}}\Big)\,.\end{aligned} \tag{3.8}$$

The δ-s are Kronecker symbols selecting the appropriate Higgs matrix element for the fermionic final state, $u_k = u, c, t$, $d_k = d, s, b$ or $e_k = e, \mu, \tau$. We have written the amplitude in the Dirac-fermion convention, separating the scalar piece $g^S_{h_j ff}$ (first two terms between curly brackets in the first line) from the pseudoscalar one $g^P_{h_j ff}$ (last two terms). The fermion and antifermion spinors are denoted as $\bar{u}_f(p_f)$ and $v_f(p_{\bar{f}})$, respectively.

[††] Possibly large contributions by electroweak double-logarithms of Sudakov type as well as the corresponding counterparts in fermionic Higgs decays with additional real radiation of gauge bosons are investigated in a separate article [53].

3.2.2.2 Case of the $b\bar{b}$ final state: $\tan\beta$-enhanced corrections

In the case of a decay to $b\bar{b}$ (and analogously for down-type quarks of first and second generation, but with smaller numerical impact), the loop contributions that receive a $\tan\beta$ enhancement may have a sizable impact, thus justifying an effective description of the Higgs–$b\bar{b}$ vertex that provides a resummation of large contributions [43, 56–62]. We denote the neutral components of $\mathcal{H}_1$ and $\mathcal{H}_2$ from Eq. (2.2) of [39] by H_d^0 and H_u^0, respectively. The large $\tan\beta$-enhanced effects arise from contributions to the $(H_u^0)^*\,\bar{b}\,P_L\,b$ operator—$P_{L,R}$ are the left- and right-handed projectors in the Dirac description of the b spinors—and can be parametrized in the following fashion:

$$\mathcal{L}^{\text{eff}} = -Y_b\,\bar{b}\left[H_d^0 + \frac{\Delta_b}{\tan\beta}\left(\frac{\lambda}{\mu_{\text{eff}}}\,S\,H_u^0\right)^*\right] P_L\,b + \text{h.c.} \equiv -\sum_j g_{h_j bb}^{L\,\text{eff}}\,h_j^0\,\bar{b}\,P_L\,b + \text{h. c.} \tag{3.9}$$

Here, Δ_b is a coefficient that is determined via the calculation of the relevant ($\tan\beta$-enhanced) one-loop diagrams to the Higgs–$b\bar{b}$ vertex, involving gluino–sbottom, chargino–stop and neutralino–sbottom loops.[‡‡] The symbol μ_{eff} represents the effective μ term that is generated when the singlet field acquires a vev. The specific form of the operator, $(S\,H_u^0)^*\,\bar{b}\,P_L\,b$, is designed so as to preserve the $\mathbb{Z}_3$ symmetry, and it can be shown that this operator is the one that gives rise to leading contributions to the $\tan\beta$-enhanced effects. We evaluate Δ_b at a scale corresponding to the arithmetic mean of the masses of the contributing SUSY particles: this choice is consistent with the definition of Δ_b employed for the Higgs-mass calculation.

From the parametrization of (3.9), one can derive the non-trivial relation between the 'genuine' Yukawa coupling Y_b and the effective bottom mass m_b: $Y_b = \frac{m_b}{v_1(1+\Delta_b)}$. Then, the effective couplings of the neutral Higgs fields to $b\bar{b}$ read:

$$g_{h_j bb}^{L\,\text{eff}} = \frac{m_b}{\sqrt{2}\,v_1\,(1+\Delta_b)}\left\{(U_n)_{j1} + \mathrm{i}\,(U_n)_{j4} + \frac{\Delta_b}{\tan\beta}\left((U_n)_{j2} - \mathrm{i}\,(U_n)_{j5} + \tfrac{\lambda^* v_2}{\mu_{\text{eff}}^*}\left[(U_n)_{j3} - \mathrm{i}\,(U_n)_{j6}\right]\right)\right\}. \tag{3.10}$$

This can be used to substitute $\mathcal{A}^{\text{tree}}[h_j^0 \to b\bar{b}]$ in (3.5) by:

$$\mathcal{A}^{\text{eff}}[h_j^0 \to b\bar{b}] = -\mathrm{i}\,\bar{u}_b(p_b)\left[g_{h_j bb}^{L\,\text{eff}}\,P_L + g_{h_j bb}^{L\,\text{eff}\,*}\,P_R\right] v_b(p_{\bar{b}})\,, \tag{3.11}$$

where this expression resums the effect of $\tan\beta$-enhanced corrections to the $h_j^0 b\bar{b}$ vertex. However, if one now adds the one-loop amplitude $\mathcal{A}_{\text{vert}}^{\text{1L}}$, the one-loop effects associated with the $\tan\beta$-enhanced contributions would be included twice. To avoid this double counting, the terms that are linear in Δ_b in (3.10) need to be subtracted. Employing the 'subtraction' couplings

$$g_{h_j bb}^{L\,\text{sub}} = \frac{m_b\,\Delta_b}{\sqrt{2}\,v_1}\left\{(U_n)_{j1} + \mathrm{i}\,(U_n)_{j4} - \frac{1}{\tan\beta}\left((U_n)_{j2} - \mathrm{i}\,(U_n)_{j5} + \frac{\lambda^* v_u}{\mu_{\text{eff}}^*}\left[(U_n)_{j3} - \mathrm{i}\,(U_n)_{j6}\right]\right)\right\} \tag{3.12}$$

we define the following 'tree-level' amplitude for the Higgs decays into bottom quarks:

$$\mathcal{A}^{\text{tree}}[h_j^0 \to b\bar{b}] = \mathcal{A}^{\text{eff}}[h_j^0 \to b\bar{b}] + \mathcal{A}^{\text{sub}}[h_j^0 \to b\bar{b}]\,, \tag{3.13a}$$

$$\mathcal{A}^{\text{sub}}[h_j^0 \to b\bar{b}] \equiv -\mathrm{i}\,\bar{u}_b(p_b)\left[g_{h_j bb}^{L\,\text{sub}}\,P_L + g_{h_j bb}^{L\,\text{sub}\,*}\,P_R\right] v_b(p_{\bar{b}})\,. \tag{3.13b}$$

[‡‡] Two-loop corrections to Δ_b have also been studied in [63, 64].

3.2.2.3 QCD and QED corrections

The inclusion of QCD and QED corrections requires a proper treatment of IR effects in the decay amplitudes. The IR-divergent parts of the virtual contributions by gluons or photons in $\mathcal{A}^{\text{1L}}_{\text{vert}}$ are cancelled by their counterparts in processes with radiated photons or gluons. We employ directly the QCD and QED correction factors that are well-known analytically (see below) and therefore omit the Feynman diagrams involving a photon or gluon propagator when computing with `FeynArts` and `FormCalc` the one-loop corrections to the $h^0_j f\bar{f}$ vertex and to the fermion-mass and wave-function counterterms. The QCD- and QED-correction factors applying to the fermionic decays of a $\mathcal{CP}$-even Higgs state were derived in [54]. The $\mathcal{CP}$-odd case was addressed later in [55]. In the $\mathcal{CP}$-violating case, it is useful to observe that the $h_j f\bar{f}$ scalar and pseudoscalar operators do not interfere, so that the $\mathcal{CP}$-even and $\mathcal{CP}$-odd correction factors can be applied directly at the level of the amplitudes—although they were obtained at the level of the squared amplitudes:

$$\mathcal{A}^{\text{tree+QCD/QED}}[h^0_j \to f\bar{f}\,] = -\mathrm{i}\,\frac{m_f^{\overline{\text{MS}}}(M_{h_i})}{m_f}\,\bar{u}_f(p_f)\left\{g^S_{h_j ff}\,c_S - \gamma_5\,g^P_{h_j ff}\,c_P\right\}v_f\left(p_{\bar{f}}\right), \tag{3.14a}$$

$$c_{S,P} = \sqrt{1 + c^{\text{QED}}_{S,P} + c^{\text{QCD}}_{S,P}}\,, \tag{3.14b}$$

$$c^{\text{QED}}_{S,P} \equiv \frac{\alpha}{\pi}\,Q_f^2\,\Delta_{S,P}\left(\sqrt{1-\tfrac{4\,m_f^2}{M_{h_i}^2}}\right), \tag{3.14c}$$

$$c^{\text{QCD}}_{S,P} \equiv \frac{\alpha_s(M_{h_i})}{\pi}\,C_2(f)\left[\Delta_{S,P}\left(\sqrt{1-\tfrac{4\,m_f^2}{M_{h_i}^2}}\right) + 2 + 3\log\left(\frac{M_{h_i}}{m_f}\right)\right]. \tag{3.14d}$$

Here, Q_f is the electric charge of the fermion f, $C_2(f)$ is equal to $4/3$ for quarks and equal to 0 for leptons, M_{h_i} corresponds to the kinematic (pole) mass in the Higgs decay under consideration and the functions $\Delta_{S,P}$ are explicated in e.g. Sect. 4 of [65]. In the limit of $M_{h_i} \gg m_f$, both $\Delta_{S,P}$ reduce to $\left[-3\log\left(M_{h_i}/m_f\right) + \frac{9}{4}\right]$. As noticed already in [54], the leading logarithm in the QCD-correction factor can be absorbed by the introduction of a running $\overline{\text{MS}}$ fermion mass in the definition of the Yukawa coupling Y_f. Therefore, it is motivated to factorize $m_f^{\overline{\text{MS}}}(M_{h_i})$, with higher orders included in the definition of the QCD beta function.

The QCD (and QED) correction factors generally induce a sizable shift of the tree-level width of as much as $\sim 50\%$. While these effects were formally derived at the one-loop order, we apply them over the full amplitudes (without the QCD and QED corrections), i.e. we include the one-loop vertex amplitude without QCD/QED corrections $\mathcal{A}^{\text{1Lwo. QCD/QED}}_{\text{vert}}$ and $\mathcal{A}^{\text{1L}}_{G/Z}$ in the definitions of the couplings $g^{S,P}_{h_j ff}$ that are employed in (3.14)—we will use the notation $g^{S,P\,\text{1L}}_{h_j ff}$ below. The adopted factorization corresponds to a particular choice of the higher-order contributions beyond the ones that have been explicitly calculated.

3.2.2.4 Decay width

Putting together the various pieces discussed before, we can express the decay amplitude at the one-loop order as:

$$\mathcal{A}[h_i \to f\bar{f}\,] = -\mathrm{i}\,\frac{m_f^{\overline{\text{MS}}}(M_{h_i})}{m_f}\,Z^{\text{mix}}_{ij}\,\bar{u}_f(p_f)\left\{g^{S\,\text{1L}}_{h_j ff}\,c_S - \gamma_5\,g^{P\,\text{1L}}_{h_j ff}\,c_P\right\}v_f\left(p_{\bar{f}}\right), \tag{3.15a}$$

$$-\,\mathrm{i}\,\bar{u}_f(p_f)\left\{g^{S\,\text{1L}}_{h_j ff} - \gamma_5\,g^{P\,\text{1L}}_{h_j ff}\right\}v_f\left(p_{\bar{f}}\right) \equiv \left(\mathcal{A}^{\text{tree}} + \mathcal{A}^{\text{1Lwo. QCD/QED}}_{\text{vert}} + \mathcal{A}^{\text{1L}}_{G/Z}\right)\left[h_j \to f\bar{f}\,\right]. \tag{3.15b}$$

Summing over spinor and color degrees of freedom, the decay width is then obtained as:

$$\Gamma\Big[h_i \to f\bar{f}\Big] = \frac{1}{16\,\pi\,M_{h_i}}\sqrt{1-\frac{4m_f^2}{M_{h_i}^2}}\sum_{\substack{\text{polarization,}\\ \text{color}}}\Big|\mathcal{A}[h_i^{\text{phys.}} \to f\bar{f}\,]\Big|^2\,. \tag{3.16}$$

At the considered order, we could dismiss the one-loop squared terms in $\Big|\mathcal{A}[h_i \to f\bar{f}\,]\Big|^2$. However, in order to tackle the case where the contributions from irreducible one-loop diagrams are numerically larger than the tree-level amplitude, we keep the corresponding squared terms in the expression above (it should be noted that the QCD and QED corrections have been stripped off from the one-loop amplitude that gets squared). The approach of incorporating the squared terms should give a reliable result in a situation where the tree-level result is significantly suppressed, since the other missing contribution at this order consisting of the tree-level amplitude times the two-loop amplitude would be suppressed due to the small tree-level result. In such a case, however, the higher-order uncertainties are expected to be comparatively larger than in the case where one-loop effects are subdominant to the tree level.

The kinematic masses of the fermions are easily identified in the leptonic case. For decays into top quarks the 'pole' mass m_t is used, while for all other decays into quarks we employ the $\overline{\text{MS}}$ masses evaluated at the scale of the Higgs mass $m_q^{\overline{\text{MS}}}(M_{h_i})$. We note that these kinematic masses have little impact on the decay widths, as long as the Higgs state is much heavier. In the NMSSM, however, singlet-like Higgs states can be very light, in which case the choice of an $\overline{\text{MS}}$ mass is problematic. Yet, in this case the Higgs state is typically near threshold so that the free-parton approximation in the final state is not expected to be reliable. Our current code is not properly equipped to address decays directly at threshold independently of the issue of running kinematic masses. Improved descriptions of the hadronic decays of Higgs states close to the $b\bar{b}$ threshold or in the chiral limit have been presented in e.g. [66–71].

3.2.3 Decays into SM gauge bosons

Now we consider Higgs decays into the gauge bosons of the SM. Almost each of these channels requires a specific processing in order to include higher-order corrections consistently or to deal with off-shell effects.

3.2.3.1 Decays into electroweak gauge bosons

Higgs decays into on-shell W-s and Z-s can be easily included at the one-loop order in comparable fashion to the fermionic decays. However, the notion of WW or ZZ final states usually includes contributions from off-shell gauge bosons as well, encompassing a wide range of four-fermion final states. Such off-shell effects mostly impact the decays of Higgs bosons with a mass below the WW or ZZ thresholds. Instead of a full processing of the off-shell decays at one-loop order, we pursue two distinct evaluations of the decay widths in these channels.

Our first approach is that already employed in `FeynHiggs` for the corresponding decays in the MSSM. It consists in exploiting the precise one-loop results of `Prophecy4f` for the SM-Higgs decays into four fermions [72–74]. For an (N)MSSM Higgs boson h_i, the SM decay width is thus evaluated at the mass M_{h_i} and then rescaled by the squared ratio of the tree-level couplings to gauge bosons for h_i and an SM Higgs boson H_{SM} ($V = W, Z$):

$$\Gamma[h_i \to VV] = \Gamma^{\text{SM}}[H_{\text{SM}}(M_{h_i}) \to VV]\left|\mathcal{R}_{ij}\cdot\frac{g_{h_jVV}^{\text{NMSSM}}}{g_{HVV}^{\text{SM}}}\right|^2, \tag{3.17a}$$

$$\frac{g^{\text{NMSSM}}_{h_j VV}}{g^{\text{SM}}_{HVV}} \equiv \cos\beta\,(U_n)_{j1} + \sin\beta\,(U_n)_{j2}\,, \tag{3.17b}$$

where $\Gamma[h_i \to VV]$ represents the decay width of the physical Higgs state h_i in the NMSSM, while $\Gamma^{\text{SM}}[H_{\text{SM}}(M_{h_i}) \to VV]$ denotes the decay width of an SM-Higgs boson with the mass M_{h_i}. The matrix elements $\mathcal{R}_{ij}$ reflect the connection between the tree-level Higgs states and the physical states. This role is similar to $\mathbf{Z}^{\text{mix}}$. However, decoupling in the SM limit of the model yields the additional condition that the ratio in (3.17a) reduces to 1 in this limit for the SM-like Higgs boson of the NMSSM. For this reason, `FeynHiggs` employs the matrix $\mathbf{U}^m$ (or $\mathbf{U}^0$) as a unitary approximation of $\mathbf{Z}^{\text{mix}}$—see Sect. 2.6 of [39]. An alternative choice consists in using $X_{ij} \equiv Z^{\text{mix}}_{ij} \Big/ \sqrt{\sum_k |Z^{\text{mix}}_{ik}|^2}$. However, the difference of the widths when employing $\mathbf{U}^0$, $\mathbf{U}^m$, $\mathbf{Z}^{\text{mix}}$ or $\mathbf{X} \equiv (X_{ij})$ corresponds to effects of higher order, which should be regarded as part of the higher-order uncertainty. The rescaling of the one-loop SM width should only be applied for the SM-like Higgs of the NMSSM, where this implementation of the $h_i \to VV$ widths is expected to provide an approximation that is relatively close to a full one-loop result incorporating all NMSSM contributions. However, for the other Higgs states of the NMSSM one-loop contributions beyond the SM may well be dominant. Actually, the farther the quantity $[\mathcal{R}_{ij} \cdot (U_n)_{j2}] \big/ [\mathcal{R}_{ij} \cdot (U_n)_{j1}]$ departs from $\tan\beta$, the more inaccurate the prediction based on SM-like radiative corrections becomes.

Our second approach consists in a one-loop calculation of the Higgs decay widths into on-shell gauge bosons (see [52] for the MSSM case), including tree-level off-shell effects. This evaluation is meant to address the case of heavy Higgs bosons at the full one-loop order. The restriction to on-shell kinematics is justified above the threshold for electroweak gauge-boson production (off-shell effects at the one-loop level could be included via a numerical integration over the squared momenta of the gauge bosons in the final state—see [75, 76] for a discussion in the MSSM). For details of our implementation see [29], with the noteworthy feature that contributions from Higgs–electroweak mixing $\mathcal{A}^{\text{1L}}_{G/Z}$ vanish. In the case of the W^+W^- final state, the QED IR-divergences are regularized with a photon mass and cancel with bremsstrahlung corrections: soft and hard bremsstrahlung are included according to [77, 78] (see also [52]). We stress that the exact cancellation of the IR-divergences is only achieved through the replacement of the $h_i G^+ G^-$ coupling by the expression in terms of the kinematical Higgs mass (see [29] for more details). This fact had already been observed by [52]. In order to extend the validity of the calculation below threshold, we process the Born-order term separately, applying an off-shell kinematic integration over the squared external momentum of the gauge bosons—see e.g. Eq. (37) in [79]. Thus, this evaluation is performed at tree level below threshold and at full one-loop order (for the on-shell case) above threshold. The vanishing on-shell kinematical factor multiplying the contributions of one-loop order ensures the continuity of the prediction at threshold. Finally, we include the one-loop squared term in the calculation. Indeed, as we will discuss later on, the tree-level contribution vanishes for a decoupling doublet, meaning that the Higgs decays to WW/ZZ can be dominated by one-loop effects. To this end, the infrared divergences of two-loop order are regularized in an ad-hoc fashion—which appears compulsory as long as the two-loop order is incomplete—making use of the one-loop real radiation and estimating the logarithmic term in the imaginary part of the one-loop amplitude.

3.2.3.2 Radiative decays into gauge bosons

Higgs decays into photon pairs, gluon pairs or γZ appear at the one-loop level—i.e. $\mathcal{A}^{\text{tree}} = 0$ for all these channels. We compute the one-loop order using the `FeynArts` modelfile, although

the results are well-known analytically in the literature—see e.g. [51] or Sect. III of [80] ([79] for the MSSM). The electromagnetic coupling in these channels is set to the value $\alpha(0)$ corresponding to the Thomson limit.

The use of tree-level Higgs–Goldstone couplings together with loop-corrected kinematic Higgs masses M_{h_i} in our calculation would induce an effective violation of Ward identities by two-loop order terms in the amplitude: we choose to restore the proper gauge structure by re-defining the Higgs–Goldstone couplings in terms of the kinematic Higgs mass M_{h_i} (see [29] for more details). Since our calculation is restricted to the leading—here, one-loop—order, the transition of the amplitude from tree-level to physical Higgs states is performed via $\mathbf{U}^m$ or $\mathbf{X}$ instead of $\mathbf{Z}^{\text{mix}}$ in order to ensure the appropriate behavior in the decoupling limit.

Leading QCD corrections to the diphoton Higgs decays have received substantial attention in the literature. A frequently used approximation for this channel consists in multiplying the amplitudes driven by quark and squark loops by the factors $[1-\alpha_s(M_{h_i})/\pi]$ and $[1+8\,\alpha_s(M_{h_i})/(3\,\pi)]$, respectively—see e.g. [81]. However, these simple factors are only valid in the limit of heavy quarks and squarks (compared to the mass of the decaying Higgs boson). More general analytical expressions can be found in e.g. [82]. In our calculation, we apply the correction factors $\left[1+C^S(\tau_q)\,\alpha_s(M_{h_i})/\pi\right]$ and $\left[1+C^P(\tau_q)\,\alpha_s(M_{h_i})/\pi\right]$ to the contributions of the quark q to the $\mathcal{CP}$-even and the $\mathcal{CP}$-odd $h_i\gamma\gamma$ operators, respectively, and $\left[1+C(\tau_{\tilde{Q}})\,\alpha_s(M_{h_i})/\pi\right]$ to the contributions of the squark $\tilde{Q}$ (to the $\mathcal{CP}$-even operator). Here, τ_X denotes the ratio $\left[4\,m_X^2(M_{h_i}/2)/M_{h_i}^2\right]$. The coefficients $C^{S,P}$ and C are extracted from [83] and [84]. In order to obtain a consistent inclusion of the $\mathcal{O}(\alpha_s)$ corrections, the quark and squark masses m_X entering the one-loop amplitudes or the correction factors are chosen as defined in Eq. (5) of [83] and in Eq. (12) of [84] (rather than $\overline{\text{MS}}$ running masses).

The QCD corrections to the digluon decays include virtual corrections but also gluon and light-quark radiation. They are thus technically defined at the level of the squared amplitudes. In the limit of heavy quarks and squarks, the corrections are known beyond NLO—see the discussion in [79] for a list of references. The full dependence in mass was derived at NLO in [83,84], for both quark and squark loops. In our implementation, we follow the prescriptions of Eqs. (51), (63) and (67) of [79] in the limit of light radiated quarks and heavy particles in the loop. For consistency, the masses of the particles in the one-loop amplitude are taken as pole masses. Effects beyond this approximation can be sizable, as evidenced by Fig. 20 of [83] and Fig. 12 of [84]. As the $\mathcal{CP}$-even and $\mathcal{CP}$-odd Higgs–gg operators do not interfere, it is straightforward to include both correction factors in the $\mathcal{CP}$-violating case. Finally, we note that parts of the leading QCD corrections to $h_i \to gg$ are induced by the real radiation of quark–antiquark pairs. In the case of the heavier quark flavors (top, bottom and possibly charm), the channels are experimentally well-distinguishable from gluonic decays. Therefore, the partial widths related to these corrections could be attached to the Higgs decays into quarks instead [85]. The resolution of this ambiguity would involve a dedicated experimental analysis of the kinematics of the gluon radiation in $h_i \to gq\bar{q}$ (collinear or back-to-back emission).

The QCD corrections to the quark loops of an SM-Higgs decay into γZ have been studied in [86–88], but we do not consider them here.

3.3 Discussion concerning the remaining theoretical uncertainties

Below, we provide a summary of the main sources of theoretical uncertainties from unknown higher-order corrections applying to our calculation of the NMSSM Higgs decays. We do not

discuss here the parametric theoretical uncertainties arising from the experimental errors of the input parameters. For the experimentally known SM-type parameters the induced uncertainties can be determined in the same way as for the SM case (see e.g. Ref. [26]). The dependence on the unknown SUSY parameters, on the other hand, is usually not treated as a theoretical uncertainty but rather exploited for setting indirect constraints on those parameters.

3.3.1 Higgs decays into quarks ($h_i \to q\bar{q}$, $q = c, b, t$)

In our evaluation, these decays have been implemented at full one-loop order, i.e. at QCD, electroweak and SUSY next-to-leading order (NLO). In addition, leading QCD logarithmic effects have been resummed within the parametrization of the Yukawa couplings in terms of a running quark mass at the scale of the Higgs mass. The Higgs propagator-type corrections determining the mass of the considered Higgs particle as well as the wave function normalization at the external Higgs leg of the process contain full one-loop and dominant two-loop contributions.

For an estimate of the remaining theoretical uncertainties, several higher-order effects should be taken into account:

- First, we should assess the magnitude of the missing QCD NNLO (two-loop) effects. We stress that there should be no large logarithms associated to these corrections, since these are already resummed through the choice of running parameters and the renormalization scale. For the remaining QCD pieces, we can directly consider the situation in the SM. In the case of the light quarks, the QCD contributions of higher order have been evaluated and amount to $\sim 4\%$ at $m_H = 120\,\text{GeV}$ (see e.g. Ref. [89]). For the top quark, the uncertainty due to missing QCD NNLO effects was estimated to 5% [26].
- Concerning the electroweak corrections, the numerical analysis in [29] suggests that the one-loop contribution is small—at the percent level—for an SM-like Higgs, which is consistent with earlier estimates in the SM [26]. For the heavy Higgs states, the numerical analysis in [29] indicates a larger impact of such effects—at the level of $\sim 10\%$ in the considered scenario. Assuming that the electroweak NNLO corrections are comparable to the squared one-loop effects, our estimate for pure electroweak higher orders in decays of heavy Higgs states reaches the percent level. In fact, for multi-TeV Higgs bosons, the electroweak Sudakov logarithms may require a resummation (see [53]). Furthermore, mixed electroweak–QCD contributions are expected to be larger than the pure electroweak NNLO corrections, adding a few more percent to the uncertainty budget. For light Higgs states, the electroweak effects are much smaller since the Sudakov logarithms remain of comparatively modest size.
- Finally, the variations with the squark masses in the numerical analysis in [29] for the heavy doublet states show that the one-loop SUSY effects could amount to 5–10% for a sub-TeV stop/sbottom spectrum. In such a case, the two-loop SUSY and the mixed QCD/electroweak–SUSY corrections may reach the percent level. On the other hand, for very heavy squark spectra, we expect to recover an effective singlet-extended Two-Higgs-Doublet model (an effective SM if the heavy doublet and singlet states also decouple) at low energy. However, all the parameters of this low-energy effective field theory implicitly depend on the SUSY radiative effects, since unsuppressed logarithms of SUSY origin generate terms of dimension ≤ 4—e.g. in the Higgs potential or the Higgs couplings to SM fermions. On the other hand, the explicit dependence of the Higgs decay widths on SUSY higher-order corrections is suppressed for a large SUSY scale. In this case, the

uncertainty from SUSY corrections reduces to a parametric effect, that of the matching between the NMSSM and the low-energy lagrangian—e.g. in the SM-limit, the uncertainty on the mass prediction for the SM-like Higgs continues to depend on SUSY logarithms and would indirectly impact the uncertainty on the decay widths.

Considering all these higher-order effects together, we conclude that the decay widths of the SM-like Higgs should be relatively well controlled (up to $\sim 5\%$), while those of a heavy Higgs state could receive sizable higher-order contributions, possibly adding up to the level of $\sim 10\%$.

3.3.2 Higgs decays into leptons

Here, QCD corrections appear only at two-loop order in the Higgs propagator-type corrections as well as in the counterterms of the electroweak parameters and only from three-loop order onwards in the genuine vertex corrections. Thus, the theory uncertainty is expected to be substantially smaller than in the case of quark final states. For an SM-like Higgs, associated uncertainties were estimated to be below the percent level [28]. For heavy Higgs states, however, electroweak one-loop corrections are enhanced by Sudakov logarithms (see [53]) and reach the $\sim 10\%$ level for Higgs masses of the order of 1 TeV, so that the two-loop effects could amount to a few percent. In addition, light staus may generate a sizable contribution of SUSY origin, where the unknown corrections are of two-loop electroweak order.

3.3.3 Higgs decays into WW/ZZ

The complexity of these channels is illustrated by our presentation of two separate estimates, expected to perform differently in various regimes.

- In the SM, the uncertainty of `Prophecy4f` in the evaluation of these channels was assessed at the sub-percent level below 500 GeV, but up to $\sim 15\%$ at 1 TeV [26]. For an SM-like Higgs, our numerical analysis in [29] shows that the one-loop electroweak corrections are somewhat below 10%, making plausible a sub-percent uncertainty on the results employing `Prophecy4f`. On the other hand, the assumption that the decay widths for an NMSSM Higgs boson can be obtained through a simple rescaling of the result for the width in the SM by tree-level couplings, is in itself a source of uncertainties. We expect this approximation to be accurate only in the limit of a decoupling SM-like composition of the NMSSM Higgs boson. If these SM-like characteristics are altered through radiative corrections of SUSY origins or NMSSM-Higgs mixing effects—both of which may still reach the level of several percent in a phenomenologically realistic setup—the uncertainty on the rescaling procedure for the decay widths should be of corresponding magnitude.
- In the case of heavier states, our numerical analysis in [29] indicate that the previous procedure is unreliable in the mass range $\gtrsim 500$ GeV. In particular, for heavy doublets in the decoupling limit, radiative corrections dominate over the—then vanishing—tree-level amplitude, shifting the widths by orders of magnitude. In such a case, our one-loop calculation captures only the leading order and one can expect sizable contributions at the two-loop level: as discussed in the numerical analysis in [29], shifting the quark masses between pole and $\overline{\text{MS}}$ values—two legitimate choices at the one-loop order that differ in the treatment of QCD two-loop contributions—results in modifications of the widths of order $\sim 50\%$. On the other hand, one expects the decays of a decoupling heavy doublet into electroweak gauge bosons to remain a subdominant channel, so that a less accurate prediction may be tolerable. It should be noted, however, that the magnitude of the

corresponding widths is sizably enhanced by the effects of one-loop order, which may be of interest regarding their phenomenological impact.

3.3.4 Radiative decays into gauge bosons

As these channels appear at the one-loop order, our (QCD-corrected) results represent (only) an improved leading-order evaluation. Yet the situation is contrasted:

- In the SM, the uncertainty on a Higgs decay into $\gamma\gamma$ was estimated at the level of 1% in Ref. [26]: however, the corresponding calculation includes both QCD NLO and electroweak NLO corrections. In our case, only QCD NLO corrections (with full mass dependence) are taken into account. The comparison with `NMSSMCALC` in [29] provides us with a lower bound on the magnitude of electroweak NLO and QCD NNLO effects: both evaluations are at the same order but differ by a few percent. The uncertainty on the SUSY contribution should be considered separately, as light charginos or sfermions could have a sizable impact. In any case, we expect the accuracy of our calculation to perform at the level of $\gtrsim 4\%$.
- In the case of the Higgs decays into gluons, for the SM prediction—including QCD corrections with full mass dependence and electroweak two-loop effects—an uncertainty of 3% from QCD effects and 1% from electroweak effects was estimated in [26]. In our case, the QCD corrections are only included in the heavy-loop approximation, and NLO electroweak contributions have not been considered. Consequently, the uncertainty budget should settle above the corresponding estimate for the SM quoted above. In the case of heavy Higgs bosons, the squark spectrum could have a significant impact on the QCD two-loop corrections, as exemplified in Fig. 5 of [84].
- For $h_i \to \gamma Z$, QCD corrections are not available so far, so that the uncertainty should be above the $\sim 5\%$ estimated in the SM [26].

3.3.5 Additional sources of uncertainty from higher orders

For an uncertainty estimate, the following effects apply to essentially all channels and should be considered as well:

- The mixing in the Higgs sector plays a central role in the determination of the decay widths. Following the treatment in `FeynHiggs`, we have considered $\mathbf{Z}^{\text{mix}}$ in all our one-loop evaluations, as prescribed by the LSZ reduction. Most public codes consider a unitary approximation in the limit of the effective scalar potential ($\mathbf{U}^0$, in our notation). The analysis of [39] and our most recent analysis in [29]—employing $\mathbf{U}^m$, a more reliable unitary approximation than $\mathbf{U}^0$—indicate that the different choices of mixing matrices may affect the Higgs decays by a few percent (and far more in contrived cases). However, even the use of $\mathbf{Z}^{\text{mix}}$ is of course subject to uncertainties from unknown higher-order corrections. While the Higgs propagator-type corrections determining the mass of the considered Higgs boson and the wave function normalization contain corrections up to the two-loop order, the corresponding prediction for the mass of the SM-like Higgs still has an uncertainty at the level of about 2%, depending on the SUSY spectrum.
- In this paper, we confined ourselves to the evaluation of the Higgs decay widths into SM particles and did not consider the branching ratios. For the latter an implementation

at the full one-loop order of many other two-body decays, relevant in particular for the heavy Higgs states, would be desirable, which goes beyond the scope of the present analysis. Furthermore, in order to consider the Higgs branching ratios at the one-loop order, we would have to consider three-body widths at the tree level, for instance $h_i \to b\bar{b}Z$, since these are formally of the same magnitude as the one-loop effects for two-body decays [53]. In addition, these three-body decays—typically real radiation of electroweak and Higgs bosons—exhibit Sudakov logarithms that would require resummation in the limit of heavy Higgs states [53].

– At decay thresholds, the approximation of free particles in the final state is not sufficient, and a more accurate treatment would require the evaluation of final-state interactions. Several cases have been discussed in e.g. [69, 71, 90].

In this discussion we did not attempt to provide a quantitative estimate of the remaining theoretical uncertainties from unknown higher-order corrections, as such an estimate would in any case sensitively depend on the considered region in parameter space. Instead, we have pointed out the various sources of higher-order uncertainties remaining at the level of our state-of-the-art evaluation of the Higgs decays into SM particles in the NMSSM. For a decoupling SM-like Higgs boson one would ideally expect that the level of accuracy of the predictions approaches the one achieved in the SM. However, even in this limit, missing NNLO pieces—that are known for the SM, but not for the NMSSM—give rise to a somewhat larger theoretical uncertainty in the NMSSM. Furthermore, uncertainties of parametric nature (for instance from the theoretical prediction of the Higgs-boson mass) need to be taken into account as well. For heavy Higgs states, the impact of electroweak Sudakov logarithms and SUSY corrections add to the theoretical uncertainty to an extent that is strongly dependent on the details of the spectrum and the characteristics of the Higgs state (see [53]). For a decoupling doublet at $\sim 1\,\text{TeV}$, an uncertainty of ~ 5–15% may be used as a guideline for the fermionic and radiative decays, while the uncertainty may be as large as $\sim 50\%$ in $h_i \to WW/ZZ$.

References

[1] G. Aad, et al., Observation of a new particle in the search for the Standard Model Higgs boson with the ATLAS detector at the LHC, Phys. Lett. B716 (2012) 1–29. arXiv:1207.7214, doi:10.1016/j.physletb.2012.08.020.

[2] S. Chatrchyan, et al., Observation of a new boson at a mass of 125 GeV with the CMS experiment at the LHC, Phys. Lett. B716 (2012) 30–61. arXiv:1207.7235, doi:10.1016/j.physletb.2012.08.021.

[3] G. Aad, et al., Measurements of the Higgs boson production and decay rates and constraints on its couplings from a combined ATLAS and CMS analysis of the LHC pp collision data at $\sqrt{s} = 7$ and 8 TeV, JHEP 08 (2016) 045. arXiv:1606.02266, doi:10.1007/JHEP08(2016)045.

[4] G. Aad, et al., Combined Measurement of the Higgs Boson Mass in pp Collisions at $\sqrt{s} = 7$ and 8 TeV with the ATLAS and CMS Experiments, Phys. Rev. Lett. 114 (2015) 191803. arXiv:1503.07589, doi:10.1103/PhysRevLett.114.191803.

[5] A. M. Sirunyan, et al., Measurements of properties of the Higgs boson decaying into the four-lepton final state in pp collisions at $\sqrt{s} = 13$ TeV, JHEP 11 (2017) 047. arXiv:1706.09936, doi:10.1007/JHEP11(2017)047.

[6] The CMS Phase II Upgrade Scope Document, CERN Document Server, see: CERN-LHCC-2015-019.

[7] ATLAS Phase-II Upgrade Scoping Document, CERN Document Server, see: CERN-LHCC-2015-020.

[8] M. Testa, Prospects on Higgs Physics at the HL-LHC for ATLAS, see: ATLAS Higgs HL-LHC (2017).

[9] M. Cepeda, HIGGS @ HL-LHC, see: CMS Higgs HL-LHC (2017).

[10] H. Baer, T. Barklow, K. Fujii, Y. Gao, A. Hoang, S. Kanemura, J. List, H. E. Logan, A. Nomerotski, M. Perelstein, et al., The International Linear Collider Technical Design Report - Volume 2: PhysicsarXiv:1306.6352.

[11] K. Fujii, et al., Physics Case for the International Linear ColliderarXiv:1506.05992.

[12] K. Fujii, et al., The Potential of the ILC for Discovering New ParticlesarXiv:1702.05333.

[13] A. Arbey, et al., Physics at the e+ e- Linear Collider, Eur. Phys. J. C75 (8) (2015) 371. arXiv:1504.01726, doi:10.1140/epjc/s10052-015-3511-9.

[14] M. Bicer, et al., First Look at the Physics Case of TLEP, JHEP 01 (2014) 164. arXiv:1308.6176, doi:10.1007/JHEP01(2014)164.

[15] F. An, et al., Precision Higgs Physics at CEPC, Chin. Phys. C43 (4) (2019) 043002. arXiv:1810.09037, doi:10.1088/1674-1137/43/4/043002.

[16] A. Abada, et al., Future Circular Collider: Vol. 1 "Physics opportunities", http://inspirehep.net/record/1713706/files/CERN-ACC-2018-0056.pdf.

[17] M. Benedikt, A. Blondel, O. Brunner, M. Capeans Garrido, F. Cerutti, J. Gutleber, P. Janot, J. M. Jimenez, V. Mertens, A. Milanese, K. Oide, J. A. Osborne, T. Otto, Y. Papaphilippou, J. Poole, L. J. Tavian, F. Zimmermann, Future Circular Collider, Tech. Rep. CERN-ACC-2018-0057, CERN, Geneva, submitted for publication to Eur. Phys. J. ST. (Dec 2018).
URL http://cds.cern.ch/record/2651299

[18] The FCC CDR, the four volumes of the FCC CDR and the contributions to the European Strategy can be found on the FCC-CDR webpage https://fcc-cdr.web.cern.ch/.

[19] H.-P. Nilles, Supersymmetry, Supergravity and Particle Physics, Phys. Rept. 110 (1984) 1–162. doi:10.1016/0370-1573(84)90008-5.

[20] H. E. Haber, G. L. Kane, The Search for Supersymmetry: Probing Physics Beyond the Standard Model, Phys. Rept. 117 (1985) 75–263. doi:10.1016/0370-1573(85)90051-1.

[21] U. Ellwanger, C. Hugonie, A. M. Teixeira, The Next-to-Minimal Supersymmetric Standard Model, Phys. Rept. 496 (2010) 1–77. arXiv:0910.1785, doi:10.1016/j.physrep.2010.07.001.

[22] M. Maniatis, The Next-to-Minimal Supersymmetric extension of the Standard Model reviewed, Int. J. Mod. Phys. A25 (2010) 3505–3602. arXiv:0906.0777, doi:10.1142/S0217751X10049827.

[23] G. Degrassi, S. Heinemeyer, W. Hollik, P. Slavich, G. Weiglein, Towards high precision predictions for the MSSM Higgs sector, Eur. Phys. J. C28 (2003) 133–143. arXiv:hep-ph/0212020, doi:10.1140/epjc/s2003-01152-2.

[24] F. Staub, P. Athron, U. Ellwanger, R. Gröber, M. Mühlleitner, P. Slavich, A. Voigt, Higgs mass predictions of public NMSSM spectrum generators, Comput. Phys. Commun. 202 (2016) 113–130. arXiv:1507.05093, doi:10.1016/j.cpc.2016.01.005.

[25] P. Drechsel, R. Gröber, S. Heinemeyer, M. M. Muhlleitner, H. Rzehak, G. Weiglein, Higgs-Boson Masses and Mixing Matrices in the NMSSM: Analysis of On-Shell Calculations, Eur. Phys. J. C77 (6) (2017) 366. arXiv:1612.07681, doi:10.1140/epjc/s10052-017-4932-4.

[26] A. Denner, S. Heinemeyer, I. Puljak, D. Rebuzzi, M. Spira, Standard Model Higgs-Boson Branching Ratios with Uncertainties, Eur. Phys. J. C71 (2011) 1753. arXiv:1107.5909, doi:10.1140/epjc/s10052-011-1753-8.

[27] J. R. Andersen, et al., Handbook of LHC Higgs Cross Sections: 3. Higgs PropertiesarXiv:1307.1347, doi:10.5170/CERN-2013-004.

[28] D. de Florian, et al., Handbook of LHC Higgs Cross Sections: 4. Deciphering the Nature of the Higgs SectorarXiv:1610.07922, doi:10.23731/CYRM-2017-002.

[29] F. Domingo, S. Heinemeyer, S. Paßehr, G. Weiglein, Decays of the neutral Higgs bosons into SM fermions and gauge bosons in the $\mathcal{CP}$-violating NMSSM, Eur. Phys. J. C78 (11) (2018) 942. arXiv:1807.06322, doi:10.1140/epjc/s10052-018-6400-1.

[30] S. Heinemeyer, W. Hollik, G. Weiglein, The Masses of the neutral CP - even Higgs bosons in the MSSM: Accurate analysis at the two loop level, Eur. Phys. J. C9 (1999) 343–366. arXiv:hep-ph/9812472, doi:10.1007/s100529900006.

[31] S. Heinemeyer, W. Hollik, G. Weiglein, FeynHiggs: A Program for the calculation of the masses of the neutral CP even Higgs bosons in the MSSM, Comput. Phys. Commun. 124 (2000) 76–89. arXiv:hep-ph/9812320, doi:10.1016/S0010-4655(99)00364-1.

[32] M. Frank, T. Hahn, S. Heinemeyer, W. Hollik, H. Rzehak, G. Weiglein, The Higgs Boson Masses and Mixings of the Complex MSSM in the Feynman-Diagrammatic Approach, JHEP 02 (2007) 047. arXiv:hep-ph/0611326, doi:10.1088/1126-6708/2007/02/047.

[33] T. Hahn, S. Heinemeyer, W. Hollik, H. Rzehak, G. Weiglein, High-Precision Predictions for the Light CP -Even Higgs Boson Mass of the Minimal Supersymmetric Standard Model, Phys. Rev. Lett. 112 (14) (2014) 141801. arXiv:1312.4937, doi:10.1103/PhysRevLett.112.141801.

[34] H. Bahl, W. Hollik, Precise prediction for the light MSSM Higgs boson mass combining effective field theory and fixed-order calculations, Eur. Phys. J. C76 (9) (2016) 499. arXiv:1608.01880, doi:10.1140/epjc/s10052-016-4354-8.

[35] H. Bahl, S. Heinemeyer, W. Hollik, G. Weiglein, Reconciling EFT and hybrid calculations of the light MSSM Higgs-boson mass, Eur. Phys. J. C78 (1) (2018) 57. arXiv:1706.00346, doi:10.1140/epjc/s10052-018-5544-3.

[36] H. Bahl, T. Hahn, S. Heinemeyer, W. Hollik, S. Paßehr, H. Rzehak, G. Weiglein, Precision calculations in the MSSM Higgs-boson sector with FeynHiggs 2.14arXiv:1811.09073.

[37] See: www.feynhiggs.de.

[38] P. Drechsel, L. Galeta, S. Heinemeyer, G. Weiglein, Precise Predictions for the Higgs-Boson Masses in the NMSSM, Eur. Phys. J. C77 (1) (2017) 42. arXiv:1601.08100, doi:10.1140/epjc/s10052-017-4595-1.

[39] F. Domingo, P. Drechsel, S. Paßehr, On-Shell neutral Higgs bosons in the NMSSM with complex parameters, Eur. Phys. J. C77 (8) (2017) 562. arXiv:1706.00437, doi:10.1140/epjc/s10052-017-5104-2.

[40] J. Kublbeck, M. Bohm, A. Denner, Feyn Arts: Computer Algebraic Generation of Feynman Graphs and Amplitudes, Comput. Phys. Commun. 60 (1990) 165–180. doi:10.1016/0010-4655(90)90001-H.

[41] T. Hahn, Generating Feynman diagrams and amplitudes with FeynArts 3, Comput. Phys. Commun. 140 (2001) 418–431. arXiv:hep-ph/0012260, doi:10.1016/S0010-4655(01)00290-9.

[42] T. Hahn, M. Perez-Victoria, Automatized one loop calculations in four-dimensions and D-dimensions, Comput. Phys. Commun. 118 (1999) 153–165. arXiv:hep-ph/9807565, doi:10.1016/S0010-4655(98)00173-8.

[43] K. E. Williams, H. Rzehak, G. Weiglein, Higher order corrections to Higgs boson decays in the MSSM with complex parameters, Eur. Phys. J. C71 (2011) 1669. arXiv:1103.1335, doi:10.1140/epjc/s10052-011-1669-3.

[44] E. Fuchs, G. Weiglein, Breit-Wigner approximation for propagators of mixed unstable states, JHEP 09 (2017) 079. arXiv:1610.06193, doi:10.1007/JHEP09(2017)079.

[45] S. Paßehr, G. Weiglein, Two-loop top and bottom Yukawa corrections to the Higgs-boson masses in the complex MSSM, Eur. Phys. J. C78 (3) (2018) 222. arXiv:1705.07909, doi:10.1140/epjc/s10052-018-5665-8.

[46] S. Borowka, S. Paßehr, G. Weiglein, Complete two-loop QCD contributions to the lightest Higgs-boson mass in the MSSM with complex parameters, Eur. Phys. J. C78 (7) (2018) 576. arXiv:1802.09886, doi:10.1140/epjc/s10052-018-6055-y.

[47] W. Hollik, E. Kraus, M. Roth, C. Rupp, K. Sibold, D. Stockinger, Renormalization of the minimal supersymmetric standard model, Nucl. Phys. B639 (2002) 3–65. arXiv:hep-ph/0204350, doi:10.1016/S0550-3213(02)00538-2.

[48] K. E. Williams, G. Weiglein, Precise predictions for $h_a \to h_b h_c$ decays in the complex MSSM, Phys. Lett. B660 (2008) 217–227. arXiv:0710.5320, doi:10.1016/j.physletb.2007.12.049.

[49] A. C. Fowler, G. Weiglein, Precise Predictions for Higgs Production in Neutralino Decays in the Complex MSSM, JHEP 01 (2010) 108. arXiv:0909.5165, doi:10.1007/JHEP01(2010)108.

[50] N. Baro, F. Boudjema, A. Semenov, Automatised full one-loop renormalisation of the MSSM. I. The Higgs sector, the issue of tan(beta) and gauge invariance, Phys. Rev. D78 (2008) 115003. arXiv:0807.4668, doi:10.1103/PhysRevD.78.115003.

[51] R. Benbrik, M. Gomez Bock, S. Heinemeyer, O. Stal, G. Weiglein, L. Zeune, Confronting the MSSM and the NMSSM with the Discovery of a Signal in the two Photon Channel at the LHC, Eur. Phys. J. C72 (2012) 2171. arXiv:1207.1096, doi:10.1140/epjc/s10052-012-2171-2.

[52] P. González, S. Palmer, M. Wiebusch, K. Williams, Heavy MSSM Higgs production at the LHC and decays to WW,ZZ at higher orders, Eur. Phys. J. C73 (3) (2013) 2367. arXiv:1211.3079, doi:10.1140/epjc/s10052-013-2367-0.

[53] F. Domingo, S. Paß ehr, Electroweak corrections to the fermionic decays of heavy Higgs bosons.

[54] E. Braaten, J. P. Leveille, Higgs Boson Decay and the Running Mass, Phys. Rev. D22 (1980) 715. doi:10.1103/PhysRevD.22.715.

[55] M. Drees, K.-i. Hikasa, NOTE ON QCD CORRECTIONS TO HADRONIC HIGGS DECAY, Phys. Lett. B240 (1990) 455, [Erratum: Phys. Lett.B262,497(1991)]. doi:10.1016/0370-2693(90)91130-4.

[56] T. Banks, Supersymmetry and the Quark Mass Matrix, Nucl. Phys. B303 (1988) 172–188. doi:10.1016/0550-3213(88)90222-2.

[57] L. J. Hall, R. Rattazzi, U. Sarid, The Top quark mass in supersymmetric SO(10) unification, Phys. Rev. D50 (1994) 7048–7065. arXiv:hep-ph/9306309, doi:10.1103/PhysRevD.50.7048.

[58] R. Hempfling, Yukawa coupling unification with supersymmetric threshold corrections, Phys. Rev. D49 (1994) 6168–6172. doi:10.1103/PhysRevD.49.6168.

[59] M. Carena, M. Olechowski, S. Pokorski, C. E. M. Wagner, Electroweak symmetry breaking and bottom - top Yukawa unification, Nucl. Phys. B426 (1994) 269–300. arXiv:hep-ph/9402253, doi:10.1016/0550-3213(94)90313-1.

[60] M. Carena, D. Garcia, U. Nierste, C. E. M. Wagner, Effective Lagrangian for the $\bar{t}bH^+$ interaction in the MSSM and charged Higgs phenomenology, Nucl. Phys. B577 (2000) 88–120. arXiv:hep-ph/9912516, doi:10.1016/S0550-3213(00)00146-2.

[61] H. Eberl, K. Hidaka, S. Kraml, W. Majerotto, Y. Yamada, Improved SUSY QCD corrections to Higgs boson decays into quarks and squarks, Phys. Rev. D62 (2000) 055006. arXiv:hep-ph/9912463, doi:10.1103/PhysRevD.62.055006.

[62] J. Baglio, R. Gröber, M. Mühlleitner, D. T. Nhung, H. Rzehak, M. Spira, J. Streicher, K. Walz, NMSSMCALC: A Program Package for the Calculation of Loop-Corrected Higgs Boson Masses and Decay Widths in the (Complex) NMSSM, Comput. Phys. Commun. 185 (12) (2014) 3372–3391. arXiv:1312.4788, doi:10.1016/j.cpc.2014.08.005.

[63] D. Noth, M. Spira, Higgs Boson Couplings to Bottom Quarks: Two-Loop Supersymmetry-QCD Corrections, Phys. Rev. Lett. 101 (2008) 181801. arXiv:0808.0087, doi:10.1103/PhysRevLett.101.181801.

[64] D. Noth, M. Spira, Supersymmetric Higgs Yukawa Couplings to Bottom Quarks at next-to-next-to-leading Order, JHEP 06 (2011) 084. arXiv:1001.1935, doi:10.1007/JHEP06(2011)084.

[65] A. Dabelstein, Fermionic decays of neutral MSSM Higgs bosons at the one loop level, Nucl. Phys. B456 (1995) 25–56. arXiv:hep-ph/9503443, doi:10.1016/0550-3213(95)00523-2.

[66] M. Drees, K.-i. Hikasa, Heavy Quark Thresholds in Higgs Physics, Phys. Rev. D41 (1990) 1547. doi:10.1103/PhysRevD.41.1547.

[67] E. Fullana, M.-A. Sanchis-Lozano, Hunting a light CP-odd non-standard Higgs boson through its tauonic decay at a (Super) B factory, Phys. Lett. B653 (2007) 67–74. arXiv:hep-ph/0702190, doi:10.1016/j.physletb.2007.06.078.

[68] D. McKeen, Constraining Light Bosons with Radiative Upsilon(1S) Decays, Phys. Rev. D79 (2009) 015007. arXiv:0809.4787, doi:10.1103/PhysRevD.79.015007.

[69] F. Domingo, U. Ellwanger, Reduced branching ratio for $H \to AA \to 4\tau$ from $A - \eta_b$ mixing, JHEP 06 (2011) 067. arXiv:1105.1722, doi:10.1007/JHEP06(2011)067.

[70] M. J. Dolan, F. Kahlhoefer, C. McCabe, K. Schmidt-Hoberg, A taste of dark matter: Flavour constraints on pseudoscalar mediators, JHEP 03 (2015) 171, [Erratum: JHEP07,103(2015)]. arXiv:1412.5174, doi:10.1007/JHEP07(2015)103,10.1007/JHEP03(2015)171.

[71] F. Domingo, Decays of a NMSSM CP-odd Higgs in the low-mass region, JHEP 03 (2017) 052. arXiv:1612.06538, doi:10.1007/JHEP03(2017)052.

[72] A. Bredenstein, A. Denner, S. Dittmaier, M. M. Weber, Precise predictions for the Higgs-boson decay $H \to WW/ZZ \to 4$ leptons, Phys. Rev. D74 (2006) 013004. arXiv:hep-ph/0604011, doi:10.1103/PhysRevD.74.013004.

[73] A. Bredenstein, A. Denner, S. Dittmaier, M. M. Weber, Precision calculations for the Higgs decays $H \to ZZ/WW \to 4leptons$, Nucl. Phys. Proc. Suppl. 160 (2006) 131–135, [,131(2006)]. arXiv:hep-ph/0607060, doi:10.1016/j.nuclphysbps.2006.09.104.

[74] A. Bredenstein, A. Denner, S. Dittmaier, M. M. Weber, Radiative corrections to the semileptonic and hadronic Higgs-boson decays $H \to WW/ZZ \to 4$ fermions, JHEP 02 (2007) 080. arXiv:hep-ph/0611234, doi:10.1088/1126-6708/2007/02/080.

[75] W. Hollik, J.-H. Zhang, Radiative corrections to $h^0 \to WW^*/ZZ^* \to 4$ leptons in the MSSMarXiv:1011.6537.

[76] W. Hollik, J.-H. Zhang, Radiative Corrections to $H^0 \to WW/ZZ$ in the MSSM, Phys. Rev. D84 (2011) 055022. arXiv:1109.4781, doi:10.1103/PhysRevD.84.055022.

[77] B. A. Kniehl, Radiative corrections for $H \to W^+W^-$ (γ) in the standard model, Nucl. Phys. B357 (1991) 439–466. doi:10.1016/0550-3213(91)90476-E.

[78] B. A. Kniehl, Higgs phenomenology at one loop in the standard model, Phys. Rept. 240 (1994) 211–300. doi:10.1016/0370-1573(94)90037-X.

[79] M. Spira, Higgs Boson Production and Decay at Hadron Colliders, Prog. Part. Nucl. Phys. 95 (2017) 98–159. arXiv:1612.07651, doi:10.1016/j.ppnp.2017.04.001.

[80] G. Belanger, V. Bizouard, G. Chalons, Boosting Higgs boson decays into gamma and a Z in the NMSSM, Phys. Rev. D89 (9) (2014) 095023. arXiv:1402.3522, doi:10.1103/PhysRevD.89.095023.

[81] J. S. Lee, A. Pilaftsis, M. Carena, S. Y. Choi, M. Drees, J. R. Ellis, C. E. M. Wagner, CPsuperH: A Computational tool for Higgs phenomenology in the minimal supersymmetric standard model with explicit CP violation, Comput. Phys. Commun. 156 (2004) 283–317. arXiv:hep-ph/0307377, doi:10.1016/S0010-4655(03)00463-6.

[82] U. Aglietti, R. Bonciani, G. Degrassi, A. Vicini, Analytic Results for Virtual QCD Corrections to Higgs Production and Decay, JHEP 01 (2007) 021. arXiv:hep-ph/0611266, doi:10.1088/1126-6708/2007/01/021.

[83] M. Spira, A. Djouadi, D. Graudenz, P. M. Zerwas, Higgs boson production at the LHC, Nucl. Phys. B453 (1995) 17–82. arXiv:hep-ph/9504378, doi:10.1016/0550-3213(95)00379-7.

[84] M. Muhlleitner, M. Spira, Higgs Boson Production via Gluon Fusion: Squark Loops at NLO QCD, Nucl. Phys. B790 (2008) 1–27. arXiv:hep-ph/0612254, doi:10.1016/j.nuclphysb.2007.08.011.

[85] A. Djouadi, M. Spira, P. M. Zerwas, QCD corrections to hadronic Higgs decays, Z. Phys. C70 (1996) 427–434. arXiv:hep-ph/9511344, doi:10.1007/s002880050120.

[86] M. Spira, A. Djouadi, P. M. Zerwas, QCD corrections to the H Z gamma coupling, Phys. Lett. B276 (1992) 350–353. doi:10.1016/0370-2693(92)90331-W.

[87] R. Bonciani, V. Del Duca, H. Frellesvig, J. M. Henn, F. Moriello, V. A. Smirnov, Next-to-leading order QCD corrections to the decay width $H \to Z\gamma$, JHEP 08 (2015) 108. arXiv:1505.00567, doi:10.1007/JHEP08(2015)108.

[88] T. Gehrmann, S. Guns, D. Kara, The rare decay $H \to Z\gamma$ in perturbative QCD, JHEP 09 (2015) 038. arXiv:1505.00561, doi:10.1007/JHEP09(2015)038.

[89] P. A. Baikov, K. G. Chetyrkin, J. H. Kuhn, Scalar correlator at O(alpha(s)**4), Higgs decay into b-quarks and bounds on the light quark masses, Phys. Rev. Lett. 96 (2006) 012003. arXiv:hep-ph/0511063, doi:10.1103/PhysRevLett.96.012003.

[90] U. Haisch, J. F. Kamenik, A. Malinauskas, M. Spira, Collider constraints on light pseudoscalars, JHEP 03 (2018) 178. arXiv:1802.02156, doi:10.1007/JHEP03(2018)178.

Acknowledgements

Results by *A. Arbuzov, S. Bondarenko, Ya. Dydyshka, L. Kalinovskaya, L. Rumyantsev, R. Sadykov, V. Yermolchyk* are obtained in the framework of state's task N 3.9696.2017/8.9 of the Ministry of Education and Science of Russia.
The work of *J. Baglio* is supported by the Institutional Strategy of the University of Tübingen (DFG, ZUK 63) and the Carl-Zeiss foundation. *C. Weiland* received financial support from the European Research Council under the European Union's Seventh Framework Programme (FP/2007-2013)/ERC Grant NuMass Agreement No. 617143, and he is also supported in part by the U.S. Department of Energy under contract DE-FG02-95ER40896 and in part by the PITT PACC. Their work has been done in collaboration with S. Pascoli.
S.D. Bakshi acknowledges the financial support by IIT Kanpur and an Arepalli-Karumuri travel grant for attending this conference at CERN.
S. Borowka gratefully acknowledges financial support by the ERC Starting Grant "MathAm" (39568).
The work of *J. Chakrabortty* is supported by the Department of Science and Technology, Government of India, under the Grant IFA12/PH/34 (INSPIRE Faculty Award), the Science and Engineering Research Board, Government of India, under the agreement SERB/PHY/2016348 (Early Career Research Award), and by a Initiation Research Grant, agreement no. IITK/-PHY/2015077 of IIT Kanpur.
The work of *J. Gluza* is supported in part by the Polish National Science Centre, grant number 2017/25/B/ST2/01987 and by international mobilities for research activities of the University of Hradec Králové, CZ.02.2.69/0.0/0.0/16_027/0008487.
The work of *J.A. Gracey* was supported by a DFG Mercator Fellowship.
The work of *S. Heinemeyer* is supported in part by the MEINCOP Spain under contract FPA2016-78022-P, in part by the Spanish Agencia Estatal de Investigacion (AEI) and the EU Fondo Europeo de Desarrollo Regional (FEDER) through the project FPA2016-78645-P, in part by the AEI through the grant IFT Centro de Excelencia Severo Ochoa SEV-2016-0597, and by the "Spanish Red Consolider Multidark" FPA2017- 90566-REDC.
The work of *M. Chrzaszcz, Z. Was* and *J. Zaremba* is partly supported by the Polish National Science Center grant 2016/23/B/ST2/03927 and the CERN FCC Design Study Programme.
The work of *S. Jadach, M. Skrzypek* and *Z. Was* is partly supported by the Polish National Science Center grant 2016/23/B/ST2/03927 and the CERN FCC Design Study Programme.
A. Kardos acknowledges financial support from the Premium Postdoctoral Fellowship program of the Hungarian Academy of Sciences. This work was supported by grant K 125105 of the National Research, Development and Innovation Fund in Hungary.
M. Kerner acknowledges supported by the Swiss National Science Foundation (SNF) under grant number 200020-175595
P. Maierhöfer acknowledges support by the state of Baden-Württemberg through bwHPC and the German Research Foundation (DFG) through grant no. INST 39/963-1 FUGG.
The work of *J.J. Aguilera-Verdugo, F. Driencourt-Mangin, J. Plenter, S. Ramírez-Uribe, G. Rodrigo, G.F.R. Sborlini, W.J. Torres Bobadilla* and *S. Tracz* was supported by the Spanish Government (Agencia Estatal de Investigacion) and ERDF funds from European Commission (Grants No. FPA2017-84445-P and SEV-2014-0398), by Generalitat Valenciana (Grant No. PROMETEO/2017/053) and by Consejo Superior de Investigaciones Científicas (Grant No. PIE-201750E021). *J. Plenter* acknowledges support from the "la Caixa" Foundation (ID

100010434, LCF/BQ/IN17/11620037), and from the European Union's H2020-MSCA Grant Agreement No. 713673, SR from CONACYT, *J.J. Aguilera-Verdugo* from Generalitat Valenciana (GRISOLIAP/2018/101) and *W.J. Torres Bobadilla* from the Spanish Government (FJCI-2017-32128).
The work of *R. Pittau* was supported by the MECD project FPA2016-78220-C3-3-P.
The work of *T. Riemann* is funded by Deutsche Rentenversicherung Bund. He is supported in part by a 2015 Alexander von Humboldt Honorary Research Scholarship of the Foundation for Polish Sciences (FNP) and by the Polish National Science Centre (NCN) under the Grant Agreement 2017/25/B/ST2/01987. Support of participation at the workshop from the FCC group is acknowledged.
The work of *R. Szafron* was supported by the DFG Sonderforschungsbereich/Transregio 110 "Symmetries and the Emergence of Structure in QCD".
The research of *J. Schlenk* was supported by the European Union through the ERC Advanced Grant MC@NNLO (340983).
C. Schwinn acknowledges support by the Heisenberg Programme of the DFG and a fellowship of the Collaborative Research Centre SFB 676 „Particles, Strings, and the Early Universe" at Hamburg University.
J. Usovitsch has received funding from the European Research Council (ERC) under the European Union's Horizon 2020 research and innovation programme under grant agreement No 647356 (CutLoops).
The report was partly supported by COST (European Cooperation in Science and Technology) Action CA16201 PARTICLEFACE and the CERN FCC design study programme.